NOVA SCHOOL OF SCIENCE & TECHNOLOGY

DEPARTAMENT OF CHEMISTRY

EXPLOITING THE POTENTIAL OF SURFACE ACTIVE IONIC LIQUIDS: FLUORINATED IONIC LIQUIDS MEET BIOMOLECULES

MARGARIDA LOURENÇO FERREIRA

Master in Biochemistry for Health

DOCTORATE IN SUSTAINABLE CHEMISTRY

NOVA University Lisbon

June, 2022

DEPARTAMENT OF CHEMISTRY

EXPLOITING THE POTENTIAL OF SURFACE ACTIVE IONIC LIQUIDS: FLUORINATED IONIC LIQUIDS MEET BIOMOLECULES

MARGARIDA LOURENÇO FERREIRA

Master in Biochemistry for Health

Adviser: Ana Belén Pereiro Estévez, Senior Researcher, NOVA School of Science and Technology

Co-advisers: João Miguel Mendes de Araújo, Auxiliar Investigator, NOVA School of Science and Technology

Lourdes Vega Fernández, Full Professor, Khalifa University

Examination Committee:

Chair: José Paulo Barbosa Mota, Full Professor, NOVA School of Science and Technology

Rapporteurs: Ana María Soto Campos, Full Professor, Universidade de Santiago de Compostela

Margarida Costa Gomes, Research Professor, Ecole Normale Supérieure de Lyon

Adviser: Ana Belén Pereiro Estévez, Senior Researcher, NOVA School of Science and Technology

Members: Ana Rita Cruz Duarte, Associate Professor with Habilitation, NOVA School of Science and Technology

José Paulo Barbosa Mota, Full Professor, NOVA School of Science and Technology

DOCTORATE IN SUSTAINABLE CHEMISTRY

NOVA University Lisbon
June, 2022

Exploiting the Potential of Surface Active Ionic Liquids: Fluorinated Ionic Liquids meet Biomolecules

À minha família, obrigada pelo apoio incondicional.

ACKNOWLEDGEMENTS

At the beginning of this journey, I could not be more far of imagine how it would be difficult and worthy. I have dedicated all my efforts in the last years to obtain this degree and in order to do it, I have been supported by a lot of generous people that I need to express my sincere gratitude.

First, I would like to thank my supervisors, Dr. Ana B. Pereiro, Dr. João M.M. Araújo and Prof. Dr. Lourdes F. Vega for guiding me with their insightful discussions, advice, and encouragement, especially during the challenging times of this dissertation. I want to thank you for being an example of dedication and motivation, for the support and patience, and for the opportunities you have given me to improve my skills and knowledge and let me grow as a researcher and a person.

I would like to acknowledge the Fundação para a Ciência e Tecnologia for the financial support through the grants SFRH/BD/130965/2017 and COVID/BD/151919/2021 and the host institutions, NOVA School of Science and Associated Laboratory for Green Chemistry (LAQV - REQUIMTE) for providing the infrastructures, equipment, services, and resources to develop this project, and to the people that I have the opportunity to encounter in these institutions that have always been very helpful and available for solve several problems. I also want to acknowledge Khalifa University for the resources and facilities offered during the short-term internship that I had the opportunity to take during this project.

I want to thank all the co-authors of the scientific articles that are a result of this doctoral thesis, for the opportunity to collaborate and learn with them, which has contributed to the development of my critical and scientific thinking.

I want to express my gratitude to all the colleagues with I cross paths in the Alternative Fluids for Green Chemistry Laboratory and have shared several good science moments in the last years, particularly to Eduardo Sosa, Maria André, Ana Joyce Coutinho and Ana Luísa Oliveira. I also want to thank the colleagues that I had the pleasure to meet in Abu Dhabi for making me feel very welcome in a country with a completely different and remarkable culture and lifestyle.

Num tom mais pessoal quero agradecer a todos os meus amigos e família, que me apoiaram ao longo desta caminhada e me deram força e motivação nos momentos mais desafiantes e que vou levar sempre comigo.

Agradeço à Isabela por todas as longas conversas sobre ciência, as incertezas da vida, por me ajudares a relativizar muitos medos e inseguranças e por me teres apoiado sempre durante estes anos. Aos meus amigos do grupo dos Seca Adegas, pelos jantares e cafezadas

que me ajudaram sempre a ultrapassar as piores fases, especialmente à Daniela, Joana e Ricardo, por toda a paciência a ouvir-me e pelas palavras de apoio e amizade. À Catarina, por me ouvires e estares sempre presente, por todas as conversas sobre tudo, por me obrigares a desligar do trabalho, e principalmente pela amizade desde que Évora nos uniu. À minha Mimi, por seres a melhor ouvinte, pelo apoio constante, pela amizade, e por acreditares sempre em mim e naquilo que consigo fazer (ainda mais do que eu), obrigada por tudo e por estares sempre presente. À Joana, que esteve sempre comigo no lab e fora dele, apoiou-me e partilhou comigo os melhores anos da minha vida, motivando-me sempre a ser e a fazer melhor. Tornaste-te numa mãe incrível do nosso Matheus e espero que continuemos sempre juntas até sermos velinhas. À Nicole, por ter sido o apoio fundamental ao longo destes anos e que contribui muito para o trabalho que está nesta tese e para o meu sucesso. Quero agradecer-te por toda a ajuda e as horas intermináveis de discussões sobre ciência, por me ajudares a evoluir como pessoa e cientista, e por estares sempre a amparar as minhas derrotas e a celebrar as minhas vitórias. Agradeço-te por todos os conselhos e conversas sobre a vida, pela interajuda, mas acima de tudo pela amizade e o companheirismo e por me teres conseguido aturar quase 24/7 durante os últimos 7 anos. A saga continua no Lumiar, porque o destino assim o quer, e dificilmente te vais ver livre de mim porque com família é assim!

Este trabalho é sem dúvida dedicado à minha família. Ao Zé, por seres o meu porto seguro, por me ajudares todos os dias a ser melhor, pela paciência que tens comigo, pelo amor e amizade, pelo positivismo e segurança que me transmites todos os dias, por me ajudares a acreditar em mim. Ao meu sobrinho Gaspar, que nasceu quando eu comecei esta aventura e me permitiu crescer como ser humano, descobrir uma nova forma de amor, e com a sua ingenuidade de criança me ajudou a ultrapassar os piores momentos desta caminhada. Ao meu cunhado Herculano, por todas as conversas sobre a vida que me motivaram neste caminho. À minha irmã Daniela, que é sem dúvida a minha melhor amiga, confidente e ouvinte, que eu sei que me dirá sempre o que pensa, mesmo que não seja isso que eu queira ouvir, e que me apoia incondicionalmente em todas as coisas que eu me proponho fazer. Por último e muito especial, agradeço do fundo do coração aos meus pais Luís e Raquel, pois foram eles que me deram todas as oportunidades para alcançar os meus objetivos, que trabalharam a vida toda para que eu pudesse estudar e tivesse uma vida melhor e que por isso são a principal razão de eu ter chegado até aqui, incentivando-me a ser melhor pessoa e apoiando-me sempre sem nunca questionar as minhas decisões. Vou fazer sempre o meu melhor para que se possam orgulhar de mim.

"Life is not easy for any of us. But what of that? We must have perseverance and above all confidence in ourselves. We must believe that we are gifted for something, and that this thing must be attained." (Marie Curie)

ABSTRACT

Proteins are macromolecules constituting all the living organisms, being classified as versatile biopolymers, with the widest biological activities. Thus, they have a high impact in different fields, such as the biochemical, biotechnological, chemical, pharmaceutical, and food industries. However, their industrial applications depend on costly downstream processes to yield proteins with high purity, stability, and activity. Moreover, the biological activity of proteins depends on the preservation of the three-dimensional structure, which is determined by the delicate balance between their interactions with compounds in the surrounding environment. To surpass these challenges, ionic liquids (ILs) have emerged in the biological field as an improved asset due to the possibility to design task-specificity materials by selecting the anions and cations composing their structure, and fine-tuning their properties. The surface-active ionic liquids (SAILs) are a highly recognized family of ILs with improved surfactant behaviour. SAILs can be used in the stabilization, extraction, separation, crystallization, and development of protein delivery systems. However, there is still a great lack of knowledge about the interactions between SAILs and proteins, essential information to guide the selection of the best compounds for these bottom-line applications.

In this doctoral thesis, fluorinated ionic liquids (FILs), an enhanced family of SAILs, were used to study the interactions between IL-proteins with the aim to develop FIL-based systems for the separation, extraction, and proteins delivery systems. To begin, a review of the literature was performed to understand FILs properties. These compounds grant augmented solubilization mechanisms due to the rich self-aggregation behaviour and can be designed to be completely miscible in aqueous solutions with negligible toxicity, which aids their performance in the biological field. Furthermore, the soft-Statistical Associating Fluid Theory Equation of State (soft-SAFT EoS) was used to model FILs in an intuitive, robust, and reliable way. A straightforward methodology was implemented using soft-SAFT EoS to compute the thermophysical properties of FILs and their mixtures with various solutes. In addition, it was investigated the influence of the structural features of FILs in their self-aggregation behaviour in aqueous solutions. In the end, the impact of the FILs on the solubility, stability, and interaction with different proteins was evaluated. The results of this thesis comprise a proof of concept of the feasibility of FILs-based systems for biological, biochemical, and pharmaceutical applications.

Keywords: Fluorinated Ionic Liquids, Equations of State, Aggregation Behaviour, Proteins, Interactions.

RESUMO

As proteínas são macromoléculas que constituem os organismos vivos, sendo classificadas como biopolímeros versáteis, com as mais diversas atividades biológicas. Por isso têm um elevado impacto nas indústrias bioquímica, biotecnológica, química, farmacêutica e alimentícia. No entanto, as suas aplicações industriais dependem de processos de purificação muito dispendiosos para produzir proteínas com alta pureza, estabilidade e atividade. Adicionalmente, a atividade biológica depende da preservação da estrutura tridimensional, que é determinada pelo equilíbrio delicado entre as interações com os compostos no ambiente circundante. Para transpor estes problemas, os líquidos iónicos (LIs) surgiram no campo biológico como um recurso aprimorado porque permite projetar materiais para aplicações específicas, através da seleção dos aniões e catiões que constituem a estrutura dos LIs, customizando as suas propriedades. Os líquidos iónicos tensioativos (LITs) são uma família de LIs com comportamento surfactante. LITs podem ser usados na estabilização, extração, separação, cristalização e desenvolvimento de sistemas de entrega de proteínas. No entanto, ainda existe uma grande falta de conhecimento sobre as interações entre os LITs e as proteínas, o que é essencial para se poder selecionar os melhores LITs para as aplicações biológicas.

Nesta tese de doutoramento, uma família de LITs, os líquidos iónicos fluorados (LIFs), foram usados para estudar as interações entre LIs e proteínas com o objetivo de desenvolver sistemas para a separação, extração e sistemas de entrega de proteínas. Para isso, foi realizada uma revisão da literatura para compreender as propriedades dos LIFs. Estes compostos têm mecanismos de solubilização superiores devido ao comportamento de auto-agregação, podendo ser completamente miscíveis em soluções aquosas com reduzida toxicidade, o que permite o seu uso em aplicações biológicas. Além disso, uma equação de estado sustentada na teoria estatística do fluído associante (soft-SAFT EoS) foi usada para modelação dos LIFs de uma forma intuitiva, robusta e confiável. Uma metodologia simplificada foi implementada usando a soft-SAFT EoS para calcular as propriedades termofísicas dos LIFs e das suas misturas com vários solutos. Posteriormente, a influência das características estruturais dos LIFs no seu comportamento de auto-agregação em soluções aquosas foi investigada. Por fim, foi avaliado o impacto dos LIFs na solubilidade, estabilidade e interação com diferentes proteínas. Os resultados desta tese constituem uma prova de conceito da exequibilidade de sistemas baseados em LIFs para aplicações biológicas, bioquímicas e farmacêuticas.

Palavras chave: Líquidos Iónicos Fluorados, Equações de Estado, Comportamento Agregativo, Proteínas, Interações.

TABLE OF CONTENTS

LIST OF FIGURES

LIST OF TABLES

ACRONYMS AND ABBREVIATIONS

DNA	Deoxyribonucleic acid
RNA	Ribonucleic acid
AA	Amino acid
DMSO	Dimethyl sulfoxide
DDSs	Drug delivery systems
APIs	Active pharmaceutical ingredients
SAILs	Surface-active ionic liquids
CAC	Critical aggregation concentration
CMC	Critical micellar concentration
BSA	Bovine serum albumin
LYS	Lysozyme
Cyt C	Cytochrome C
FILs	Fluorinated ionic liquids
GB1	B1 immunoglobulin binding domain of streptococcal protein G
BSLA	*Bacillus Subtilis* lipase A
IFN-α 2b	Interferon-alpha 2b
PFCs	Perfluorocarbons
PFAs	Perfluoroalkyl acids
F-gases	Fluorinated greenhouse gases
GWP	Global warming potential
Caco-2	Human colon carcinoma cells
HepG2	Human hepatocellular carcinoma cells
EA.hy926	Human umbilical vein cells
HaCaT	Human keratinocyte cells

EC_{50}	Half maximal effective concentration
HIV	Human immunodeficiency virus
AGC	Artificial gas carrier
CD	Circular dichroism
DLS	Dynamic light scattering
TEM	Transmission electron microscopy
SEM	Scanning electron microscopy
ITC	Isothermal titration calorimetry
GHGs	Greenhouse gases
HFCs	Hydrofluorocarbons
DESs	Deep eutectic solvents
HBA	Hydrogen-bond acceptor
HBD	hydrogen-bond donor
VLE	Vapour-liquid equilibria
LLE	Liquid-liquid equilibria
SLE	Solid-liquid equilibria
NRTL	Non-random two-liquid model
EoS	Equation of state
SAFT	Statistical Associating Fluid Theory
SILMs	Supported ionic liquid membranes
PCILs	Proton conducting ionic liquids
HFOs	Hydrofluoroolefins
CILPMs	Composite ionic liquid–polymer membranes
TPT1	Wertheim's first-order thermodynamic perturbation theory
LJ	Lennard-Jones
DGT	Density Gradient Theory

UFF	Universal Force Field
AAD	Absolute average deviations
FCs	Fluorinated compounds
MS	Molecular simulations
CFCs	Chlorofluorocarbons
HCFCs	Hydrochlorofluorocarbons
EU	European Union
OH-FILs	FILs functionalized with a hydroxyl group
DSC	Differential Scanning Calorimeter
TGA	Thermogravimetric analysis
FVT	Free-Volume Theory
NMR	Nuclear Magnetic Resonance
SDS-PAGE	Sodium dodecyl sulfate–polyacrylamide gel electrophoresis
HPLC	High performance liquid chromatography
BCA	Bicinchoninic acid
COSY	Correlated spectroscopy
NOE	Nuclear overhauser effect
NOESY	Nuclear overhauser effect spectroscopy
hNOE	Heteronuclear overhauser effect
HOESY	Heteronuclear overhauser effect spectroscopy
DOSY	Diffusion-ordered spectroscopy
PFGSE	Pulsed field gradient spin echo
SE	Stokes-Einstein equation
SASA	Solvent-accessible surface area
DSMZ	Deutsche sammlung von mikroorganismen und zellkulturen
ECACC	European collection of cell culture

FBS	Fetal bovine serum
RPMI	Roswell Park Memorial Institute medium
MEM	Minimum essential media
MEM-NEAA	Minimum essential media nonessential amino acids
STEM	Scanning transmission electron microscopy
EDS	Energy-dispersive X-ray spectroscopy
UV-vis	Ultraviolet-visible spectroscopy
PdI	Polydispersity index
ISO	International standards organizations
MST	Microscale thermophoresis

CHEMICAL FORMULAE

$[C_nC_1Im]^+$	1-Alkyl-3-methylimidazolium
$[C_1C_1Im]^+$	1,3-Dimethylimidazolium
$[C_2C_1Im]^+$	1-Ethyl-3-methylimidazolium
$[C_3C_1Im]^+$	1-Propyl-3-methylimidazolium
$[C_4C_1Im]^+$	1-Butyl-3-methylimidazolium
$[C_5C_1Im]^+$	1-Pentyl-3-methylimidazolium
$[C_6C_1Im]^+$	1-Hexyl-3-methylimidazolium
$[C_7C_1Im]^+$	1-Heptyl-3-methylimidazolium
$[C_8C_1Im]^+$	1-Octyl-1-methylimidazolium
$[C_9C_1Im]^+$	1-Nonyl-3-methylimidazolium
$[C_{10}C_1Im]^+$	1-Decyl-3-methylimidazolium
$[C_{12}C_1Im]^+$	1-Dodecyl-3-methylimidazolium
$[C_{14}C_1Im]^+$	1-Tetradecyl-3-methylimidazolium
$[C_{16}C_1Im]^+$	1-Hexadecyl-3-methylimidazolium
$[C_{18}C_1Im]^+$	1-Octadecyl-3-methylimidazolium
$[C_{2(OH)}C_1Im]^+$	1-(2-Hydroxyethyl)-3-methylimidazolium
$[C_4C_nIm]^+$	1-Butyl-3-alkylimidazolium
$[C_1CO_2C_2C_1Im]^+$	3-Methyl-1-(ethoxycarbonylmethyl)imidazolium
$[C_{12}AC_1Im]^+$	3-(2-(dodecylamino)-2-oxoethyl)1-methyl-1H-imidazol-3-ium
$[C_{12}EC_1Im]^+$	3-methyl-1-dodecyloxy carbonyl methylimidazolium
$[C_{12}\text{-}4,C_{12}Im]^+$	1,4-Bis(3-dodecylimidazolium1-yl)butane
$[C_n\text{-}s\text{-}C_nIm]^+$	1,s-Bis(3-alkylimidazolium-1-yl)ethane
$[C_2(C_mF_{2m+1})C_1Im]^+$	1-Methyl-3-ethyl(perfluoroalkyl)imidazolium
$[C_2(C_6F_{13})C_1Im]^+$	1-Methyl-3-(3,3,4,4,5,5,6,6,7,7,8,8,8-tridecafluorooctyl)imidazolium

$[C_2(C_4F_9)C_1Im]^+$	1-Methyl-3-(3,3,4,4,5,5,6,6,6-nonafluorohexyl)methylimidazolium
$[C_nC_1py]$	1-Alkyl-3-methylpyridinium
$[C_2C_1py]^+$	1-Ethyl-3-methylpyridinium
$[C_3C_1py]^+$	1-Propyl-3-methylpyridinium
$[C_4C_1py]^+$	1-Butyl-3-methylpyridinium
$[C_6C_1py]^+$	1-Hexyl-3-methylpyridinium
$[C_8C_1py]^+$	1-Octyl-3-methylpyridinium
$[C_npy]^+$	1-Alkylpyridinium
$[C_2py]^+$	1-Ethylpyridinium
$[C_3py]^+$	1-Propylpyridinium
$[C_4py]^+$	1-Butylpyridinium
$[C_5py]^+$	1-Pentylpyridinium
$[C_6py]^+$	1-Hexylpyridinium
$[C_8py]^+$	1-Octylpyridinium
$[C_{10}py]^+$	1-Decylpyridinium
$[C_{12}py]^+$	1-Dodecylpyridinium
$[C_{16}py]^+$	Hexadecylpyridinium
$[C_nC_1pyr]^+$	1-Alkyl-1-methylpyrrolidinium
$[C_2C_1pyr]^+$	1-Ethyl-1-methylpyrrolidinium
$[C_4C_1pyr]^+$	1-Butyl-1-methylpyrrolidinium
$[C_1CO_2C_2C_1pyr]^+$	3-Methyl-1-(ethoxycarbonylmethyl)pyrrolidinium
$[C_{2(O)1(4F)}C_1pyr]^+$	N-((2,2,3,3,4,4,5,5-octafluoropentoxy)ethyl)-N-methylpyrrolidinium
$[C_{2(O)1(4F)}C_1pip]^+$	N-((2,2,3,3,4,4,5,5-octafluoropentoxy)ethyl)-N-methylpiperidinium
$[P_{4444}]^+$	Tetrabutylphosphonium
$[P_{44414}]^+$	Tributyltetradecylphosphonium

$[P_{66614}]^+$	Trihexyltetradecylphosphonium
$[P_{4442(6F)}]^+$	Tributyl-(3,3,4,4,5,5,6,6,7,7,8,8,8-tridecafluorooctyl)-phosphonium
$[N_{1112(OH)}]^+$	Choline, cholinium or (2-hydroxyethyl)trimethylammonium
$[N_{0222}]^+$	Triethylammonium
$[N_{11110}]^+$	Trimethyldecylammonium
$[N_{11112}]^+$	Dodecyltrimethylammonium
$[N_{11114}]^+$	Myristyltrimethylammonium
$[N_{11116}]^+$	Cetyltrimethylammonium or hexadecyltrimethylammonium
$[N_{1888}]^+$	Methyl-trioctylammonium
$[N_{2228}]^+$	Triethyloctylammonium
$[N_{4444}]^+$	Tetrabutylammonium
$[N_{11Bz16}]^+$	Benzyl-n-hexadecyldimethylammonium
$[N_{111010}]^+$	Didecyldimethylammonium
$[N_{11121(C7H7)}]^+$	Benzyldodecyldimethylammonium
$[N_{2212(O)1(4F)}]^+$	N,N-diethyl-N-methyl-N-((2,2,3,3,4,4,5,5-octafluoropentoxy)ethyl)-N-ammonium
$[NBEA]^+$	N-butylethanolammonium
$[TBEA]^+$	Tert-butylethanolammonium
$[ProC_3]^+$	L-proline propyl ester
$[Caf]^+$	Caffeine
Cl^-	Chloride
Br^-	Bromide
$[BF_4]^-$	Tetrafluoroborate
$[PF_6]^-$	Hexafluorophosphate
$[SCN]^-$	Thiocyanate
$[C_1CO_2]^-$	Acetate

$[C_{13}CO_2]^-$	Tetradecanoate
$[C_8SO_4]^-$	Octylsulfate
$[C_{12}SO_4]^-$	Dodecylsulfate
$[CF_3SO_3]^-$	Trifluoromethanesulfonate
$[C_4F_9SO_3]^-$	Perfluorobutanesulfonate
$[C_6F_{13}SO_3]^-$	Perfluorohexanesulfonate
$[C_8F_{17}SO_3]^-$	Perfluorooctanesulfonate
$[C_nF_{2n+1}SO_3]^-$	Perfluoroalkylsulfonate
$[CF_3CO_2]^-$	Trifluoroacetate
$[C_4F_9CO_2]^-$	Perfluoropentanoate
$[C_7F_{15}CO_2]^-$	Pentadecafluorooctanoate
$[C_8F_{17}CO_2]^-$	Perfluorononanoate
$[C_nF_{2n+1}CO_2]^-$	Perfluoroalkyl carboxylate
$[N(CF_3SO_2)_2]^-$	Bis(trifluoromethylsulfonyl)imide
$[N(C_2F_5SO_2)_2]^-$	Bis(pentaethylsulfonyl)imide
$[N(C_4F_9SO_2)_2]^-$	Bis(nonafluorobutanesulfonyl)imide
$[N(C_nF_{2n+1}SO_2)_2]^-$	Bis(perfluoroalkylsulfonyl)imide
$[C_2FAP]^-$	Tris(pentafluoroethyl)trifluorophosphate
$[C_4FAP]^-$	Tris(nonafluorobutyl)trifluorophosphate
$[C_mFAP]^-$	Tris(perfluoroalkyl)trifluorophosphate
$[AOT]^-$	1,4-bis(2- ethylhexyl)sulfosuccinate
$[Lau]^-$	Laurate
$[Pal]^-$	Palmitate
$[LS]^-$	Lauryl sulfate
$[Sar]^-$	Lauryl sarcosinate
$[Doc]^-$	Deoxycholate

$[FAs]^-$	Fatty acids
PEG	Poly(ethylene glycol)
DBS	Dodecylbenzenesulfonate
$[C_4F_9SO_3H]$	Nonafluoro-1-butanesulfonic acid
$[C_4F_9CO_2H]$	n-Perfluoropentanoic acid
SF_6	Sulphur hexafluoride
R-32	Difluoromethane
R-125	Pentafluoroethane
R-134a	1,1,1,2-Tetrafluoroethane
R-23	Trifluoromethane
R-152a	1,1-Difluoroethane
R-14 or CF_4	Tetrafluoromethane
R-116 or C_2F_6	Hexafluoroethane
R-218 or C_3F_8	Octafluoropropane
R-143a	1,1,1-Trifluoroethane
R-1234yf	2,3,3,3-Tetrafluoropropene
CO_2	Carbon dioxide
O_2	Oxygen
N_2	Nitrogen
H_2	Hydrogen
C_8F_{18}	Perfluorooctane
$C_{10}F_{18}$	Perfluorodecalin
CH_4	Methane
C_2H_6	Ethane
C_3H_8	Propane
C_3H_6	Propene

CH_3OH	Methanol
H_2O	Water
NF_3	Nitrogen trifluoride
NaH_2PO_4	Sodium dihydrogen phosphate anhydrous
$NaH_3C_2O_2$	Sodium acetate anhydrous
KH_2PO_4	Potassium dihydrogen phosphate
NaCl	Sodium chloride
HCl	Hydrochloric acid
KCl	Potassium chloride

SYMBOLS

pI	Isoelectric point
$P_{o/w}$	1-Octanol/water partition coefficients
T	Temperature
T_m	Melting temperature
T_{onset}	Onset or decomposition temperature
$T_{s\text{-}s}$	Solid-solid transition temperature
T_{start}	Start temperature
T_g	Glass transition temperature
ρ	Density
η	Viscosity
η_0	Dilute gas term
$\Delta\eta$	Dense liquid term
γ	Surface tension
H_C	Henry constant
$\Delta_{sol}G_m^0$	Molar Gibbs energy
$\Delta_{sol}H_m^0$	Molar enthalpy
$\Delta_{sol}S_m^0$	Molar entropy
A^{res}	Residual contribution of Helmholtz free energy
A^{id}	Ideal contribution of Helmholtz free energy
A^{ref}	Reference term
A^{chain}	Chain term
A^{assoc}	Association term
A^{polar}	Polar term
η	Size binary parameter

ξ	Energy binary parameter
m	Chain length
σ	Segment diameter
ε	Dispersive energy
ε^{HB}	Site-site association energy
κ^{HB}	Site-site volume of association
Q	Quadrupole moment
x	Molar fraction
w	Mass fraction
$a_0(\rho)$	Helmholtz free energy density
c	Influence parameter
$\mathbf{M_w}$	Molecular weight
k_B	Boltzmann constant
k_T	Isothermal compressibility
μ	Fugacity
P	Pressure
$\Delta_{dis}H$	Enthalpy of dissolution
$\Delta_{dis}S$	Entropy of dissolution
δ_H	Hildebrand solubility parameter
$\Delta_{vap}U$	Energy of vaporization
v	Molar volume
$\Delta_{vap}H$	Enthalpy of vaporization
R	Universal gas constant
a	Proportionality between the energy barrier and the density
B	Free-volume overlap
L_v	Length parameter

n_D	Refractive index
k	Ionic conductivity
a_e	Electronic polarizability
R_m	Molar polarizability
N_A	Avogadro's constant
ε_0	Dielectric constant
V_m	Molar volume
f_m	Free volume
α	Degree of ionization
β	Degree of counterion binding
ΔG^0_{agg}	Standard Gibbs free energy of aggregation
^1H	Hydrogen
^{19}F	Fluorine
δ	Pulsed gradient length
Δ	Diffusion time
g	Gradient strength
D	Self-diffusion coefficient
I	NMR signal dependent
I_0	NMR signal in the absence of an applied magnetic field
q	Gradient for the spatial encoding and decoding of the nuclear spin
γ	Gyromagnetic ratio
k_{exch}	Exchange rate
r_H	Hydrodynamic radius
r_{vd}	van der Waals radius
ΔH	Enthalpy
Γ_{max}	Maximum surface excess concentration

A_{mim}	Minimum area
Π_{CAC}	Parameter of reduce the surface tension
ΔG_{ad}^{0}	Standard free energy of adsorption
P	critical packing parameter
V_0	Volume occupied by the hydrophobic chains in the aggregate core
l_c	Critical chain length
n_c	Number of carbon atoms
θ	Contact angle
λ	Wavelength
F	Fluorescence intensity
K	Stern-Volmer quenching constant
$[Q]$	Quencher concentration
k_q	Biomolecular quenching constant
τ_0	Unquenched lifetime
K_d	Equilibrium dissociation constant
F_{norm}	Normalized fluorescence

CHAPTER 1

GENERAL INTRODUCTION

1.1 Proteins: *status quo*, challenges, and applications

The complex cellular functions that occur in all living organisms depend on the interplay between several biomolecules, such as deoxyribonucleic acid (DNA), ribonucleic acid (RNA), proteins, and peptides, which are considered valuable biopolymers in many fields. Fundamentally, the DNA carries the genetic material of an organism and the RNA the information to proteins synthesis, whereas proteins have almost uncountable functional properties, making them the building blocks of life. Proteins can function as: (i) enzymes, participating in the catalysis of complex biochemical reactions; (ii) contractile assemblies, contributing to the mechanical motion of different biological processes; (iii) structure makers, constituting the bones, muscles, hair, skin, nails, among others; (iv) transporters and storage units of compounds with high biological importance, such as ions, gases, lipids, and nutrients; (v) hormones, acting as chemical messengers for the regulation of several biological reactions; (vi) defenders, having a key role in the immune response to pathogens triggering diseases; (vii) regulators of the organism fluids pH, growth and repairment of the tissues; (viii) suppliers of energy; among others [1]. The versatility of the biological functionality of proteins has boosted an increasing demand for these compounds in multiple usages and has enhanced the search for technologies to manufacture synthetic biomolecules (such as recombinant proteins), using polymerization processes to develop biomaterials with enhanced properties compared to the natural ones [2] Therefore, proteins can have almost infinite usages in a vast amount of fields, such as in the biochemical, biotechnological, chemical, pharmaceutical, and food industries [3–5].

The properties of both synthetic and natural proteins are defined by their structural features. The structure of the proteins is primarily composed of a sequence of amino acid (AA) residues linked by peptide (covalent) bonds, known as polypeptide chain (see Figure 1.1.1a). Each AA is constituted by an amino group and a carboxyl group. Therefore, the properties of a protein are determined by the individual characteristics of the AAs sidechains (polar, charged (positive or negative), hydrophobic, and aromatic natures), comprising a total of 20 different types of amino acids that can constitute the polypeptide chain. The number, molecular weight, and frequency of the type of AAs composing the structure of the proteins will dictate their nature, physicochemical properties, and size. In the protein's native form, the polypeptide chain folds into specific patterns, named secondary structure, commonly occurring in three different conformations: α-helix, β-sheet, and loop or turn (see Figure 1.1.1b). Hence, the rearrangement in the space of the folded segments in several conformations results in the three-dimensional structure of the protein (tertiary structure, see Figure 1.1.1c). In the cases of proteins that have more than one polypeptide chain, multimeric units are

formed and classified as the quaternary structure, indicating the spatial assembly of those chains to one another (see Figure 1.1.1d) [1,6–8].

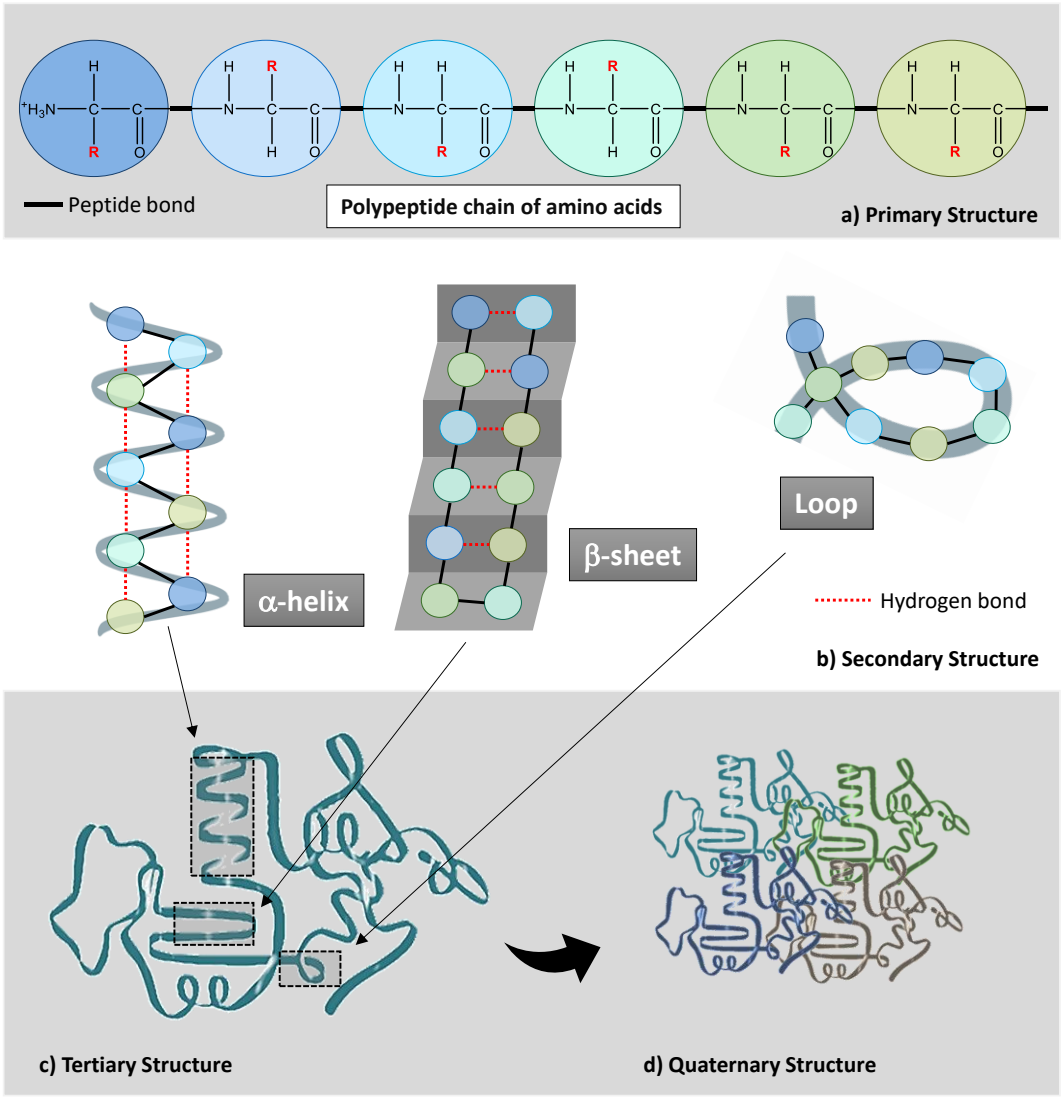

Figure 1.1.1 Representation of the different protein structure features where: a) is the primary structure composed of a polypeptide chain of amino acid residues covalently interacting through peptide bonds; b) is the secondary structure that can be constituted by the α-helix, β-sheet and loops that are formed through hydrogen bonding between the amino acid residues; c) is the tertiary structure that corresponds to the three-dimensional conformation of the protein; and d) is the quaternary structure that corresponds to a multi-subunit complex composed of more than one polypeptide chains. Adapted from Tropp, B.E. (2008) [6].

The secondary, tertiary, and quaternary structures of a protein are stabilized by a delicate balance of weak non-covalent forces such as hydrogen bonds, ionic, hydrophobic and van der Waals interactions, which allow the proteins to assume different configurations on the performance of their activities and in the interaction with other compounds (see Figure 1.1.2). Some proteins can also stabilise their tertiary structures by strong covalent disulphide bonds between different spots of the same polypeptide chain or between two chains for quaternary

structure stabilization (see Figure 1.1.2). Therefore, the protein structure is the greater component influencing its properties and consequently its functionality. The variety of the AAs' physicochemical properties (polarity, acidity, basicity, aromaticity, size, conformational flexibility, capability to cross-linking, hydrogen bonding, and chemical reactivity) controls the immeasurable properties that a protein can have and its three-dimensional structure. In its turn, the folding of the protein into the three-dimensional structure conformation dictates the interaction with other compounds, defines the biological activity of proteins, and highly depends on the forces that hold it together [1,6,8].

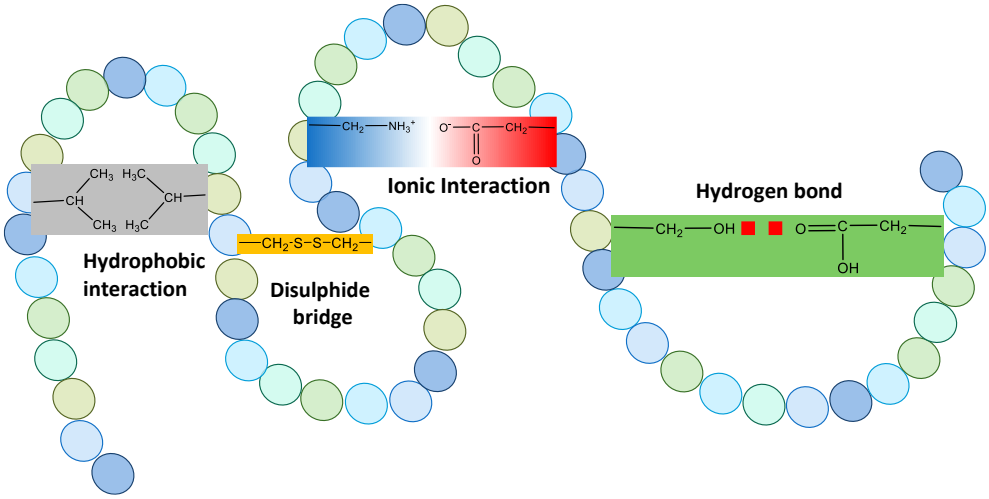

Figure 1.1.2 Forces between the amino acid residues of the polypeptide chain that define the three-dimensional structure of a protein and control its stabilization.

Some properties of the proteins are very useful for their classification since not all their characteristics are predictable from the analysis of the AAs frequency, composing the polypeptide chain. The solubility in different aqueous solvents is useful to understand the protein's nature. It is expected that proteins with more hydrophilic residues are more soluble in aqueous solutions, whereas a decrease in solubility should indicate a more hydrophobic protein. However, this property will mainly depend on the type of AAs located on the surface of the protein, which means that the conditions of the solvent (polarity, ionic strength, pH, and salt concentration) will have a key role in its solubilization. Typically, the hydrophobic groups of the AAs are concealed in the core of the protein, and the hydrophilic groups are exposed to the solvent. Thus, the relative abundance of the ionizable AAs on the surface (acidic and basic residues) and the pH of the solvent will dictate the net charge of the protein. This is given by the isoelectric point (pI) that corresponds to the pH where the protein's net charge is zero. When the pH of the solvent is lower than the isoelectric point of a protein, the charge of the surface is positive. A pH value higher than the pI results in a negative net charge. When the pH of the solution is close to the pI, the solubility of the protein reaches its minimum and it

can precipitate in the solvent. This will dictate the type of interactions of the protein with the compounds in the surrounding [7].

Another important characteristic of the proteins is the highly structural instability, especially in non-native conditions, which makes protein stabilization a very challenging topic due to the unique characteristics of each system. The processes involving the production of recombinant proteins or the extraction of native biomolecules from biological matrices for usage in several applications, such as therapeutic proteins as biopharmaceuticals or plant-based proteins for the food industry, comprehend very stressful environmental conditions. Moreover, the stability of the protein must be ensured during the several processes of purification that are used to provide profitable and safe products and throughout the time of storage that they can experience depending on the field of application. Beyond that, several proteins, principally the ones used for medicinal purposes, are pharmacokinetic and pharmacodynamically unstable due to the significant modifications of the environment in the administration routes of a pharmaceutical. Therefore, a protein can be exposed to abrupt variations in temperature, pH values, mechanical stresses, chemical denaturants (organic solvents, urea, and detergents), and protein concentrations [2,9,10]. Moreover, proteins in solution are highly affected by water, which strongly impacts the flexibility and stability of the three-dimensional structure. The water creates a hydration shell surrounding the protein, which comprehends a critical part in its biological activity, conferring plasticity to the structure, mostly controlled by the polar interactions, and contributing to the interaction with other substances (easing the conformational changes necessary to the biocatalytic processes).

All these factors can have a destabilization effect on the folded state of the protein, compromising its function and leading to the unfolding of the three-dimensional structure through the disruption of the intramolecular non-covalent interactions. The unfolding/denaturation of proteins alters their characteristics and usually causes the loss of biological activity if the extent of the damage is very profound. In some cases, the process can be completely reversible, and the protein refolds to its native state by lowering the temperature, removing the denaturant, or getting the proper physiological conditions [7]. There are several mechanisms in the cellular machinery to control and prevent the misfolding or incorrect folding of the proteins. When those mechanisms fail and the unfolding of the proteins occurs, there is more propensity to form aggregates that can accumulate in the human organs and be the cause of several diseases such as Alzheimer's, Parkinson's, and type II diabetes, among others [11]. On the other hand, the aggregation of proteins also hinder their applications, especially in the development of drug products, causing immunogenicity and several side effects [12]. Therefore, the search for mechanisms to prevent the unfolding and aggregation of the proteins is in the spotlight of protein research.

The proteins can be used in an immeasurable plethora of applications in different fields. Two main applications will be undercover in this work to understand their current situation: (i) the extraction and separation processes of proteins; and (ii) drug delivery systems of therapeutic proteins. The extraction of proteins is an essential process that must be executed to allow the study of the physiological properties of a protein (such as size, charge, shape, and function) and to further enable their application in the potential areas. Native proteins must be extracted from natural sources, for instance, conserved tissues, cells, virus particles, food waste, plants, insects, and algae, among others, while the synthetic ones must be extracted from the cells and media where they are produced. Normally, the disruption of the cell walls is the first step taken to extract the proteins, through several methods like detergent lysis, shearing force, use of low ionic salt (salting out), rapid changes in pressure, and others. However, these processes must guarantee the proper conditions for ensuring the stability of these biomolecules' structure after their extraction, such as low temperature, buffer media to avoid sharp pH changes, purity of the solvents, and the presence of protein denaturants. Moreover, complex processes of purification and separation are needed without compromising the activity of the proteins, as well as they need to be resistant to long storage periods [13]. Currently, the elevated tendency for a protein-based everyday diet has encouraged the food industry to the development of efficient, low-cost, and eco-friendly technologies for the extraction and separation of proteins. Different types of techniques have been used in the food industry for the extraction of proteins from animal and plant-based sources. Examples of extraction methods currently used are aqueous two-phase systems, subcritical water extraction, enzyme-assisted extraction, cell disruption techniques such as microwave-, ultrasound-, high hydrostatic pressure-assisted extractions, pulsed electric field, and high voltage electrical discharge. Therefore, all these techniques have been opening new opportunities for the use of more sustainable techniques in the extraction field of proteins. Nevertheless, most of the research on these techniques is in the early stages and their economic and sustainable impact must be undergone on an industrial scale [14].

The use of therapeutic proteins for the development of highly valuable biopharmaceuticals is another line of protein application that constitutes one of the greatest achievements in modern medicine. The therapeutic proteins can be used for five general biological endings depending on their pharmacological activity: (i) replacement of a protein that has its production diminished or anomalous; (ii) extension of the expression of a pre-existing protein; (iii) offer a therapeutic entity with a new functionality; (iv) restriction of other molecule or organism; and (v) delivery of other substances, such as drugs, other proteins, among others. Therapeutic proteins can be classified as antibody-based drugs, Fc fusion proteins, anticoagulants, blood factors, bone morphogenetic proteins, engineered protein

scaffolds, enzymes, growth factors, hormones, interferons, interleukins, and thrombolytics. The current therapeutic entities are mostly based on recombinant proteins and several of them are in clinical trials or were already approved for the treatment of cancers, immune and inflammatory disorders, infections, diabetes, and other diseases [15]. Therapeutic proteins are usually delivered to the organism by several administration routes such as subcutaneous, intravenous, and intramuscular injections, oral, nasal, pulmonary, rectal, and ocular routes. All of them present downsides in their utilization, such as pain, aggressive side effects, instability and short half-lives of the protein entities, low absorption by the tissues, rapid clearance of proteins, low bioavailability, and others. To overcome some of these difficulties, high dosages of biopharmaceuticals are administrated which can result in immunogenicity and cytotoxicity issues for vulnerable patients. Moreover, the interactions with the excipients used in the formulations of these biopharmaceuticals, the storage conditions, the process of manufacture, resultant impurities and the genetic characteristics of the patient can influence the stability of the structural conformation of the therapeutic proteins, hindering their biological activity [16–20]. These factors challenge the usage of these biopharmaceuticals, and a solution to protect the protein entities must be found. The development of drug delivery systems (DDSs) has been under the spotlight to unravel these problems and improve the safety and efficacy of therapeutic proteins. The DDSs aid to prevent the enzymatic degradation of the proteins, enhancing the circulation period in the bloodstream, controlling the release of the pharmaceutical in the proximity of the site of action, and diminishing the issues related to the immunogenicity and cytotoxicity associated with the administration of high dosages. Different strategies have been investigated to be used as DDSs for protein pharmaceuticals that include chemical and physical carriers. There are: (i) the lipid-based nanocarriers that include liposomes, lipid nanoparticles and emulsions; (ii) the polymeric-based nanocarriers such as nanoparticles, nano-micelles, dendrimers, hydrogels, and nanoemulsions; (iii) inorganic nanomaterials like mesoporous silica, hydroxyapatite, layered double hydroxides, lanthanide particles, gold and magnetic nanoparticles, carbon-based nanostructures, quantum dots; (iv) cell-penetrating peptides; (v) protein-based DDSs such as silk-like particles, elastin-like proteins, collagen, gelatin, and albumin; (vi) polyphenol-based systems; (vii) surfactant-based nanoemulsions; (viii) virus-like particles; among others. Some of these strategies are used in combination to enhance their feasibility. Despite the huge number of available technologies to formulate DDSs for protein entities, none has reached their full potential, and very few have been used at a clinical level. Furthermore, several barriers must be defeated before reaching that point [18,21–24].

1.2 Ionic liquids

Ionic Liquids (ILs) are alternative solvents that have been in the spotlight of green and sustainable chemistry as a solution for replacing harmful volatile organic solvents. These compounds have been widely used in the chemical industry due to the imposition of environmental directives and legislation to regulate the emissions of organic toxic compounds [25]. ILs are salts that have a low melting temperature, commonly close to or lower than 100ºC, whereas much of them are molten at room temperature. They are recognized as "designer-solvents" due to the versatility of choosing the ions that composed their structure. The number of organic cations and organic or inorganic anions that can constitute ILs is immensurable, which allows designing a given IL to a specific ending. Figure 1.2.1 shows some cations and anions that usually compose the structure of conventional ILs. This figure reflects the highest advantage of using ILs because their physicochemical and thermodynamic properties can be tuned by selecting the most suitable ions or even functionalizing them with specific groups. Therefore, these compounds are acknowledged for having negligible vapour pressure, high chemical and thermal stability, low flammability, and tunable properties such as viscosity, density, ionic conductivity, polarity, surface tension, toxicity, and many others [26–29].

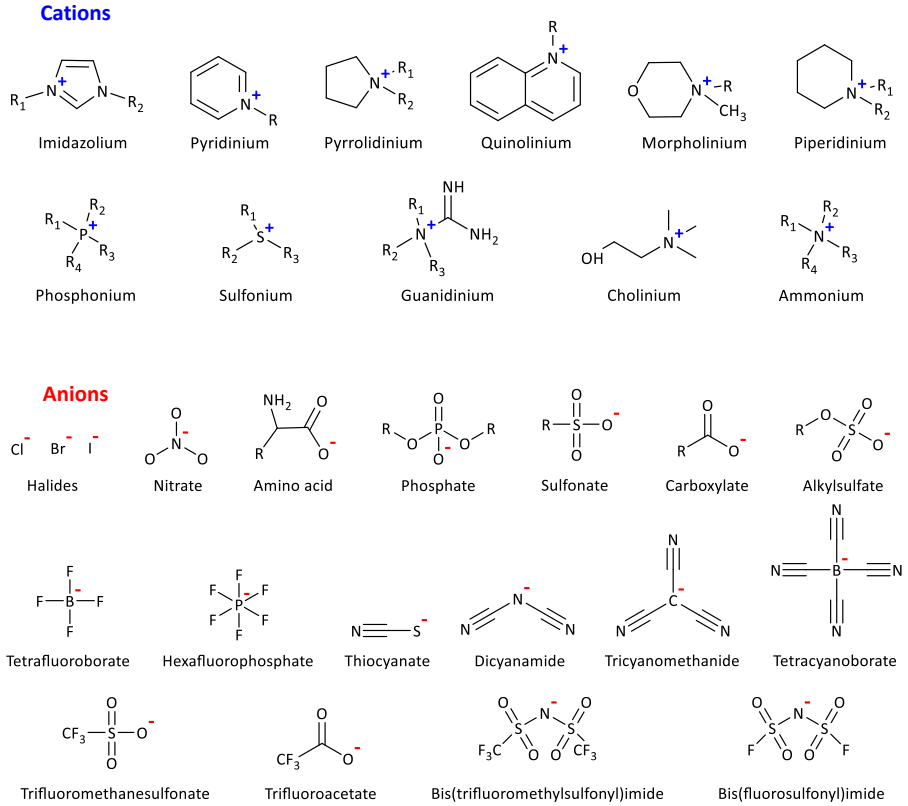

Figure 1.2.1 Cations and anions that commonly compose the structure of ionic liquids.

The ionic nature of ILs has an important influence on their structural properties and their intramolecular and intermolecular interactions. The ions are characterized by their lower density and higher delocalized charge, interacting through strong coulombic interactions. Moreover, the cations and anions are associated through other fragile and collaborative interactions like hydrogen bonding along with van der Waals interactions from their side chains, which determines the liquid structure of the ILs. The ILs composed of aromatic ions also establish π-π interactions. Therefore, all these intramolecular interactions result in a strong ionic aggregation, structural heterogeneity, and consequently nanosegregated polar and non-polar domains. The charged moieties of the cation and anion contribute to the formation of the polar domains, whereas the non-polar domains consist of the hydrophobic side chains. The combination of the non-covalent intermolecular interactions confers to ILs an extraordinary structural organization, being recognized as supramolecular fluids that have enhanced solubilization power, allowing the interaction of polar, non-polar and dipolar solutes with the different nanodomains. Thus, along with their properties, the microstructural organization of the ILs can be highly tuned depending on the size and type of alkyl chains of either ion [30–32].

The task-specific characteristics of ILs permit their application in uncountable fields [33–35]. The usage of ILs has grown mainly due to the promising non-harmful and non-toxic nature, being classified mostly as "greener", ease of recovery and recyclability compounds, mainly due to the low vapour pressure. However, ILs can have considerable water miscibility, which can be prejudicial for the environment in case of accidental leakage, being considered persistent contaminants in wastewater. The transferability of ILs from academia to the industrial scale has increased this risk and ignited the awareness of their environmental impact, increasing the research on their relative toxicology and biodegradability. Besides, the demand for task-specific compounds boosted their production, which in some cases does not agree with the green chemistry principles. Moreover, the high chemical and thermal stability made some of the ILs poorly biodegradable, which brought problems regarding the persistence of these compounds in the environment. When evaluating the full life cycle of an IL, toward the synthesis, application, and degradation, very few can be considered green compounds [36–39]. As expected, there is a strong structure-toxicity relationship that will define the environmental impact of ILs, and their wide structural variety can hinder the study of their toxicity and biodegradability. Although it is difficult to generalize the structure-toxicity related influence on the toxicity of ILs, some structural features have shown more incisive effects: (i) the augmented hydrophobicity by the presence of longer alkyl side chains which increases the toxicity; (ii) the aromatic cations demonstrated more toxicity when compared to non-aromatic ones; (iii) the stability and lipophilicity of the anion; (iii) the nature

of the ions that when derived from natural sources are more innocuous (*e.g.* cholinium cations and amino acid-based anions); (iv) self-aggregative systems have shown a reduction on the toxicity; (v) the functionalization of either ion, that beneficiates from the insertion of more hydrophilic groups to decrease the toxicity (e.g. hydroxyl and ether groups); (vi) long aliphatic chains nature-derived (*e.g.* vegetable oils) have low toxicity; (vii) hydrophilic anions have fewer toxicity effects when compared with hydrophobic and fluorine-based ones [36–39]. Nevertheless, the effect of the anion is not fully comprehended, especially because most of the studies are focused on the variation of the cation and its effects on toxicity.[1] Therefore, the literature already gives an important overview of which structural characteristics should be selected to mitigate the environmental impact of ILs. Though, the toxicity and biodegradability must always be studied and considered before their introduction in the market and industries as a task-specific material.

1.3 Biological applications of ionic liquids

ILs are usually classified into three generations depending on their physical and chemical properties. The third and last generation shed light on the formulation of ILs with biological activities (*e.g.,* antifungal, antibacterial and antiviral agents) where the usage of biodegradable and natural ions assumed a predominant position and has conducted the application of ILs toward biological applications [40,41].

In the biological and biotechnological fields, ILs have been used: (i) as solvents for dissolution and regeneration of synthetic and natural polymer-based materials (*e.g.,* proteins, DNA) that are employed in biomaterials processing; (ii) as ILs-based hybrid materials (*e.g.*, hydrogels, films, membranes, fibres, particles, etc.) in conjunction with several biopolymers; (iii) as stabilizers for macromolecules preservation such as DNA, RNA and proteins, to diminish their chemical and physical degradation and aggregation in the production and/or extraction processes, during storage; and (iv) in the food and bioproducts industries for the development of biofuels from vegetable oils and biomass, surfactant and solubility agents, antimicrobial agents, lubricants, food analysis, enzymatic activity inductor, extractions processes and treatment of food waste.

Moreover, ILs are useful tools in the biomedical, biomedicine and pharmaceutical applications: (i) as components of drug formulations to increase the solubility and permeability of active pharmaceutical ingredients (APIs), their bioavailability and solve the polymorphism issues of some drugs; (ii) in the development and design of drug delivery systems of APIs and therapeutic macromolecules (proteins, DNA); (iii) as a solvent, polymerization media, polymer processing, plasticizers, stability agents, permeation

enhancers, formulation components; (iv) as API-ILs, including the API in the structure of the IL, which improves the solubility and bioavailability of the drug and have several clinical applications; (v) in tissue engineering as platforms for the development of artificial muscles and skin, matrices and scaffolds for tissue repairing, among others; (vi) in cancer therapy for the production of biosensors, pharmaceuticals, drug delivery as a carrier, adjuvant or API; (vii) as an antimicrobial agent to inhibit the growth of bacteria, fungus, and virus; (viii) as biosensors for monitorization of biomarkers that have high clinical diagnostic relevance and biomedical parameters like temperature, pH, movement, position, force or deformation); (ix) in chemical applications of pharmacy such as synthesis of drugs, detectors on biomedical analytical techniques (electrophoresis, chromatography, spectroscopy); and (x) as nanocarriers for antibacterial usages, gene transfection, and drug delivery and release [40–45].

In the last years, much work must be done to understand the complex mechanisms of the interactions between protein-IL. Nevertheless, the literature reports that the ILs character and the protein surface (hydrophobic, hydrophilic and/or amphiphilic) are determinants for the protein-IL interactions, as exemplified in Figure 1.3.1. In aqueous solutions, a more density of cations is usually encountered on the protein surface compared to the number of anions, independently of the polarity of the charged residues. This behaviour can be motived by the propensity of the conventional anions for hydrogen bonding with the molecules of water. Therefore, the charged moieties of the ILs will compete with the water molecules to interact with the charged residues of the protein surface. The insertion of hydrophobic counterparts to the structures of ILs increases the dispersion interactions with the hydrophobic residues on the protein surface. The hydrophilic moieties of the ILs tend to establish hydrogen bonds and strong Coulombic interactions with the protein surface. When the ILs ions have stronger interactions with water rather than the surface of the protein, the water is eliminated from the surface of the protein which can be favourable or detrimental for the solubility of the protein, depending on their biological activity and structural conformation. Hence, the type of protein-IL interactions and the competition of the ILs molecules towards the water on the surface of the protein will define the solubility and stability of the proteins and will have a direct influence on the applicability of ILs in the protein field [46–50].

ILs find wide applicability in the protein field, for example: (i) in protein stability and solubility; (ii) in protein crystallization processes; (iii) in biocatalytic processes, aiding the reaction of enzymes; (iv) in the proteomics analysis; (v) in the production of smart materials like films, membranes and ion gels; (vi) in biopharmaceutical field as adjuvants or carriers of drug delivery systems of therapeutic proteins and enhancers of vaccines formulations; and (vii) in the separation and extraction of proteins with IL-based systems using several techniques such as aqueous-biphasic systems, liquid-liquid extraction, three-phase

partitioning, microemulsion and micellar systems, solid-phase extraction, and solid-liquid extractions [48–54]. In summary, the application of ILs in the protein field is highly dependent on the study of the protein-IL interactions. Then, these mechanisms have to be studied individually due to the high tailor ability of ILs and the wide variety of proteins.

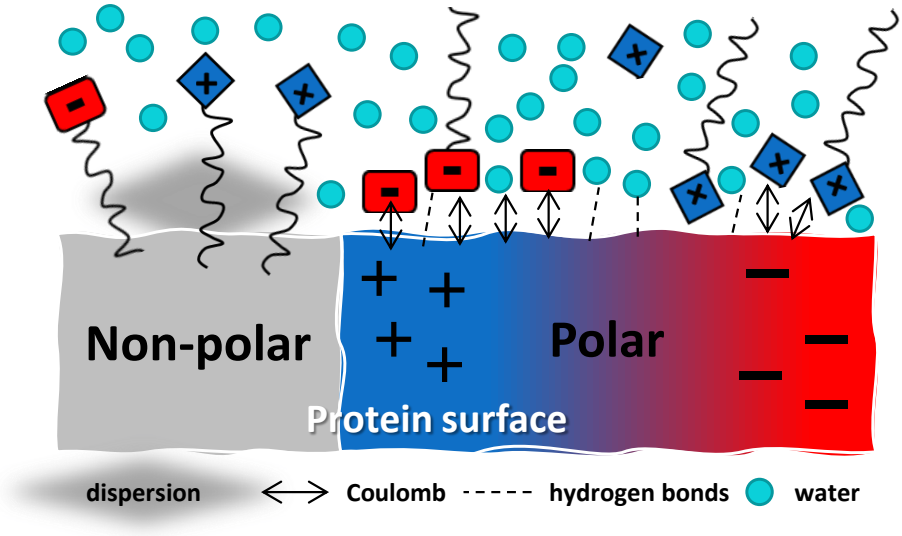

Figure 1.3.1 Representation of the possible interactions that can occur between ionic liquids and the surface of a protein. Adapted from Schröder, C. (2017) [48].

1.4 Surface-active ionic liquids

Water is the more sustainable and safer solvent, being widely used as media in different fields. Several ILs are insoluble in water, as in the case of many conventional organic solvents. Then this behaviour can hinder their application. Aiming to find alternatives for solving water immiscibility concerns, a thrilling family of ILs has been highlighted: the surface-active ionic liquids (SAILs). They are classified as amphiphilic compounds, usually bearing long alkyl side chains in anion and/or cation and behaving as surfactants (see Figure 1.4.1). Depending on the hydrophilicity and lipophilicity, SAILs can form different self-assembled aggregates, micelles or reverse micelles (see Figure 1.4.1). The formation of the self-assembled aggregates is characterized by the critical aggregation concentration (CAC) that corresponds to the maximum concentration where occurs the formation of large aggregates. When the aggregates have a micellar shape, the CAC is currently known as critical micellar concentration (CMC). Therefore, these compounds are described by the high surface activity in-between the air-water interface. The combination of water and SAILs brings several advantages to the application of ILs in their endings, decreasing the amount of needed IL and reducing the price, toxicity and viscosity of the solution and increasing the safety, hydrogen-bonding capacity, and solvation properties tuneability [55–57].

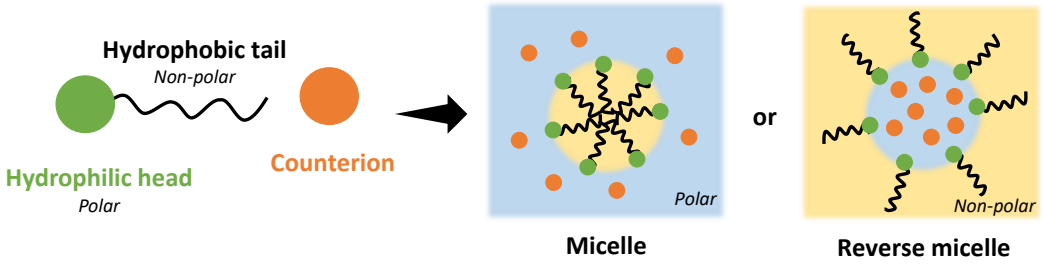

Figure 1.4.1 Amphiphilic structure of the surface-active ionic liquids and the two main types of self-assembled structures that can be formed depending on the polarity of the solvent: micelles and reverse micelles. Adapted from Buettner, C.S. *et al.* (2022) [55].

The aggregation behaviour of SAILs is highly influenced by the structural features of their ions. SAILs with long alkyl chains in the cation usually present higher surface activity and tend to aggregate into smaller micelles than the standard surfactants. Another class of SAILs, the dicationic ILs, with two charged head groups and two hydrophobic chains present even more surface activity than the monocationic SAILs. The addition of aromatic groups on the side chain also increases surface activity. The functional group of a SAIL can also be modified to contain the counterion on the side chain, denominated zwitterionic surfactants, which results in neutral charged and improved surface activity. The functionalization of the side chains with cleavable moieties is usually used to increase the biodegradability of SAILs and has shown positive effects in the enhancement of the surface activity, such as adding hydroxyl, esters, and amide groups to the long alkyl chains. In the cationic SAILs, the anion performs a critical role in the neutralization of the IL charge which eases the micelle formation and is associated with the degree of hydrophobicity, polarization, and hydration of the anion. There is a smaller number of studies concerning the addition of the alkyl chains in the anion. Nevertheless, they have shown lower CMC values, when compared with the identical cationic SAILs or conventional surfactants [55–58].

The toxicity, biodegradability and environmental impact of the SAILs is the most current concern that can hamper their usage. It is inherent to the structure of SAILs where highly hydrophobic groups increase the toxicity of ILs, once the increment of the lipophilicity eases the power to solubilize the phospholipid membranes of the cells of the organisms, causing membrane disruption and consequently cell death. Notably, several alternatives have been investigated in the direction of producing more biocompatible SAILs through the insertion of groups based on natural sources, such as amino acid residues or the long aliphatic chains from oil plants, and the functionalization of the alkyl chains with cleavable groups, which creates discontinuity and eases the biodegradation of these compounds [56].

1.5 Applications of surface-active ionic liquids in the protein field

The improved properties of SAILs, compared to the conventional ILs and surfactants, make them excellent candidates for protein applications. The possibility to design task-specific and environmentally friendly SAILs has increased the interest in using them for the stability, solubility, separation, and extraction of proteins as well as the development of delivery systems for therapeutical proteins. About 150 papers are yielded from the search in the Web of Science database using the keywords "surface active", "ionic liquid", and "protein" which highlights the significance that SAILs are starting to have in the protein field. The most important works are reviewed in this section to infer the investigation status of SAIL-protein systems.

Most of the articles found in the literature concerning proteins and SAILs are related to the bovine serum albumin (BSA) protein, which is a widely used negative charged model protein. The studies show that the interactions of SAILs ([C_8C_1Im]Cl, [C_4C_1Im][C_8SO_4], [$C_1CO_2C_2C_1Im$][$C_{12}SO_4$], [$C_1CO_2C_2C_1pyr$][$C_{12}SO_4$], [C_8C_1Im][$C_{12}SO_4$], [N_{2228}]Br, [$N_{1112(OH)}$][Lau] and [$N_{1112(OH)}$][Pal]) with BSA are mainly hydrophobic, electrostatic, and hydrogen-bonding, and can cause unfolding of the protein at lower concentrations of SAILs and stabilization of the protein above the CMC, demonstrating a high influence from the concentration of the SAIL and their ions structure [59–63]. Other SAILS ([C_nC_1Im][BF_4], n=2, 4, 6, and 8, [NBEA][Lau] and [TBEA][Lau]) bind to the BSA, inducing conformational alterations that can lead to unfold and/or denaturation of the protein [64–66]. Delivery vehicles of different natures and compositions were tested using SAILs ([C_8C_1Im]Br, [N_{11116}][AOT], [N_{11Bz16}][AOT], [$C_{16}C_1Im$][AOT], [$C_{12}C_1Im$][AOT], [C_8C_1Im][AOT], [$C_{10}C_1Im$]Cl, [$ProC_3$][LS], [$C_{12}C_1Im$]Cl; [$C_{12}AC_1Im$]Cl and [$C_{12}EC_1Im$]Cl), successfully stabilizing the secondary structure of BSA [67–71].

Another protein highly explored with SAILs is a positively charged protein model, the lysozyme (LYS). The binding of SAILs ([C_{12}-4,$C_{12}Im$]Br_2, [C_4C_1Im][C_8SO_4], [N_{1888}][$N(CF_2SO_2)_2$], [C_8C_1Im]Cl, and [$C_{12}C_1Im$]DBS) to this protein also showed structural destabilization of the protein through different interactions, which is influenced by the SAIL concentration, pH of the solution, and other factors [62,72–75]. Others SAILs ([$C_{10}C_1Im$]Cl, [C_4C_nIm]Br, n = 4, 8, [C_8C_1Im]DBS, ([$N_{1112(OH)}$][Sar], [$N_{1112(OH)}$][Doc], and [Caf][AOT]) have a positive effect on the stability, activity and prevention of protein aggregation [75–80].

The literature search also yielded some works related to the use of SAILs and cytochrome C (Cyt C), which is an important protein in the field of biological membranes, since is found naturally attached to the membrane of the mitochondria. As for the other

proteins, there are SAILs ([$N_{1112(OH)}$][AOT], [$C_{18}C_1$Im]Cl) that have a high stabilization effect on the Cyt C, and enhance its activity [81,82], whereas in other cases ([$C_{16}C_1$Im]Cl and [C_4C_1Im][C_8SO_4]) the opposite behaviour is found [83–85], depending mostly on the SAIL concentration and the type of protein-SAIL binding.

A smaller number of works have dedicated their attention to other remarkable proteins, such as (i) protein β-casein, which can self-assemble into aggregates with the SAIL [C_8C_1Im]Br [86]; (ii) α-chymotrypsin enzyme, which is negatively affected by the increment of the alkyl side chain of [C_nC_1Im][BF_4], n=12, 14 and 16 [87]; (iii) azurin that is destabilized by the [C_8C_1Im]Cl [88]; (iv) β-lactoglobulin that in one hand can be stabilized by [$C_{12}C_1$Im]Br and [C_6C_1Im][$C_{12}SO_4$], depending on the interactions and SAIL concentration, and in the other hand was successfully complexed with different SAILs ([$C_{12}C_1$Im]Cl, [$C_{12}AC_1$Im]Cl, [$C_{12}EC_1$Im]Cl and [$C_{12}C_1$Im][C_8SO_4]) for the search of feasible self-assembling systems [89]; (v) hemoglobulin, the main component of red blood cells, that shows at lower concentration of [C_6C_1Im][$C_{12}SO_4$] formation of strong protein-SAIL complexes, and SAILs like [$C_{12}C_1$Im]Cl, [$C_{16}C_1$Im]Cl and [C_4C_1Im][C_8SO_4], unfolds and denatures this protein [90,91]; (vi) lipase, where SAILs based on menthol ([$C_4C_{1(men)}$Im]Cl, [$C_8C_{1(men)}$Im]Cl, [$C_{14}C_{1(men)}$Im]Cl and [$N_{118(men)}$]Cl) were used as substrates for the catalytic activity of this protein [92]; (vii) insulin, using biocompatible SAILs ([$N_{1112(OH)}$][FAs]) to the formulation of microemulsions for its transdermal delivery [93]; (viii) human serum albumin that is disrupted by the presence of [C_4C_1Im][C_8SO_4] [94]; and (ix) green fluorescent protein that was efficiently extracted by [C_nC_1Im]Cl n=8, 10, 12, 14, 16, [N_{11110}]Cl, [N_{11112}]Br, [N_{11114}]Br, [C_{16}py]Cl, and [P_{44414}]Cl from *Escherichia coli* cells for downstream process applications [95].

Other contributions have studied the behaviour of SAILs with more than one protein showing: (i) the prevention of aggregation of BSA and human serum using [C_nC_1Im]Cl, n=8, 12, 16 SAILs [96]; (ii) the different interactions that can occur between LYS and BSA in the presence of [$C_{12}C_1$Im]Br [97]; the development of liquid crystal sensor using gemini or zwitterionic SAILs ([C_n-s-C_nIm]Br_2; s =2, n = 6, 8, 10, 12, 16; n = 12, s =2, 4, 6, 10) for identification of positively and negatively charged proteins, using BSA, LYS and trypsin as model proteins [98]; (iii) the application of mesoporous silica nanospheres (based on the cations $[N_{11116}]^+$, $[N_{11112}]^+$, $[N_{111010}]^+$, and anions Cl^-, $[BF_4]^-$ and $[C_1CO_2]^-$) with a moderate to a good loading capacity of lipase and insulin proteins [99]; the development of aqueous micellar two-phase systems for the extraction of human serum albumin and immunoglobulin G from expired human plasma with [$N_{1112(OH)}$][$C_{13}CO_2$], [$N_{11121(C7H7)}$]Br, [P_{44414}]Cl and [$C_{14}C_1$Im]Cl SAILs [100].

Even though much work has been developed on the use of SAILs in the protein field, most of the papers are focused on SAILs with a high environmental impact and the course of

future studies must be driven to the synthesis of SAILs with low toxicity characteristics, avoiding the long alkyl chains. Moreover, most of the contributions are concerning the stabilization and interaction effects of SAILs in the proteins, which are of great relevance to guiding the selection of the best SAILs structural features to provoke a specific effect on the protein. Nevertheless, few works are dedicated to the study of protein extraction and formulation of protein delivery systems using SAILs. Beyond that, the library of proteins studied with SAILs should be improved to have a wider understanding of the possible interactions between SAILs and proteins.

1.6 Objectives and thesis outline

The main goal of the present thesis is the study of the interactions between proteins and a promising family of SAILs, the fluorinated ionic liquids (FILs), to allow their usage as alternative tools for the extraction and separation processes of proteins and protein delivery systems. To achieve the application of FILs in the biological field, the first step was the overview of the literature on the known characteristics of FILs: the physicochemical properties of the pure compounds, the phase equilibria behaviour of FILs mixtures with other compounds, the environmental impact of FILs and their potential applications (Chapter 2). Moreover, aiming to facilitate the characterization of FILs thermophysical properties, it was applied the soft-Statistical Associating Fluid Theory Equation of State (soft-SAFT EoS) for modelling FILs and their mixtures robustly and feasibly, taking into consideration their different structural features (Chapter 3). Furthermore, the behaviour of FILs in aqueous solutions is of critical importance for the application in biological applications and was studied in this thesis through experimental and theoretical tools to have new insights into the self-aggregation behaviour of FILs (Chapter 4). Finally, the feasibility of FILs for the development of systems to extract, separate and deliver proteins was proven by investigating the FILs-protein interactions using different biomolecules such as lysozyme, B1 immunoglobulin binding domain of streptococcal protein G (GB1), *Bacillus Subtilis* lipase A (BSLA), and Interferon-alpha 2b (IFN-α 2b) (Chapter 5). This thesis constitutes an immeasurable contribution to the future application of FILs in the biomedical and biological fields.

1.7 Scientific outputs

The work developed in this thesis has resulted in the following publications:

1. **Margarida L. Ferreira**, Nicole S.M. Vieira, Ana L.S. Oliveira, João M.M. Araújo, Ana B. Pereiro, Disclosing the potential of fluorinated ionic liquids as interferon-alpha 2b delivery systems, *Nanomaterials* 12 (2022) 1851. DOI: 10.3390/nano12111851

2. **Margarida L. Ferreira**, Ana S.D. Ferreira, João M.M. Araújo, Eurico J. Cabrita, Ana B. Pereiro, The impact of fluorinated ionic liquids aggregation in the interactions with proteins, *Fluid Phase Equilibria* 559 (2022) 113488. DOI: 10.1016/j.fluid.2022.113488

3. **Margarida L. Ferreira**, Nicole S.M. Vieira, Paulo J. Castro, Lourdes F. Vega, João M.M. Araújo, Ana B. Pereiro, Understanding the phase and solvation behavior of fluorinated ionic liquids, *Journal of Molecular Liquids* 359 (2022) 119285. DOI: 10.1016/j.molliq.2022.119285

4. **Margarida L. Ferreira**, João M.M. Araújo, Lourdes F. Vega, Ana B. Pereiro, Understanding the absorption of fluorinated gases in fluorinated ionic liquids for recovering purposes using Soft-SAFT, *Journal of Chemical & Engineering Data* 67 (2022) 1951-1963. DOI: 10.1021/acs.jced.1c00984

5. Nicole S.M. Vieira, **Margarida L. Ferreira**, Paulo J. Castro, João M.M. Araújo, Ana B. Pereiro, Fluorinated ionic liquids as task-specific materials: An overview of current research. In: Murshed, S.M.S. (ed). *Ionic Liquids - Thermophysical Properties and Applications*, London, IntechOpen, 2021. DOI: 10.5772/intechopen.96336

6. **Margarida L. Ferreira**, Nicole S.M. Vieira, João M.M. Araújo, Ana B. Pereiro, Unveiling the influence of non-toxic fluorinated ionic liquids aqueous solutions in the encapsulation and stability of lysozyme, *Sustainable Chemistry* 2 (2021) 149-166. DOI: 10.3390/suschem20100101

7. **Margarida L. Ferreira**, João M.M. Araújo, Lourdes F. Vega, Fèlix Llovell, Ana B. Pereiro, Functionalization of fluorinated ionic liquids: A combined experimental-theoretical study, *Journal of Molecular Liquids* 302 (2020) 112489. DOI: 10.1016/j.molliq.2020.112489

8. **Margarida L. Ferreira**, Fèlix Llovell, Lourdes F. Vega, Ana B. Pereiro, João M.M. Araújo, Systematic study of the influence of the molecular structure of fluorinated ionic

liquids on the solubilization of atmospheric gases using a soft-SAFT based approach, *Journal of Molecular Liquids* 294 (2019) 111645. DOI: 10.1016/j.molliq.2019.111645

9. **Margarida L. Ferreira**, João M.M. Araújo, Ana B. Pereiro, Lourdes F. Vega, Insights into the influence of the molecular structure of fluorinated ionic liquids on their thermophysical properties. A soft-SAFT based approach, *Physical Chemistry Chemical Physics* 21 (2019) 6362-6380. DOI: 10.1039/C8CP07522K

Another publication that was not included in this thesis but has been published during the thesis project is:

Ismail I.I. Alkhatib, **Margarida L. Ferreira**, Carlos G. Alba, Daniel Bahamon, Fèlix Llovell, Ana B. Pereiro, João M.M. Araújo, Mohammad R.M. Abu-Zahra, Lourdes F. Vega, Screening of ionic liquids and deep eutectic solvents for physical CO_2 absorption by soft-saft using key performance indicators, *Journal of Chemical & Engineering Data* 65 (2020) 5844-5861. DOI: 10.1021/acs.jced.0c00750

The work developed in this thesis was also presented at several international conferences in the form of **4 papers in Conference Proceedings** with Copyright, **9 oral communications,** and **8 poster communications**.

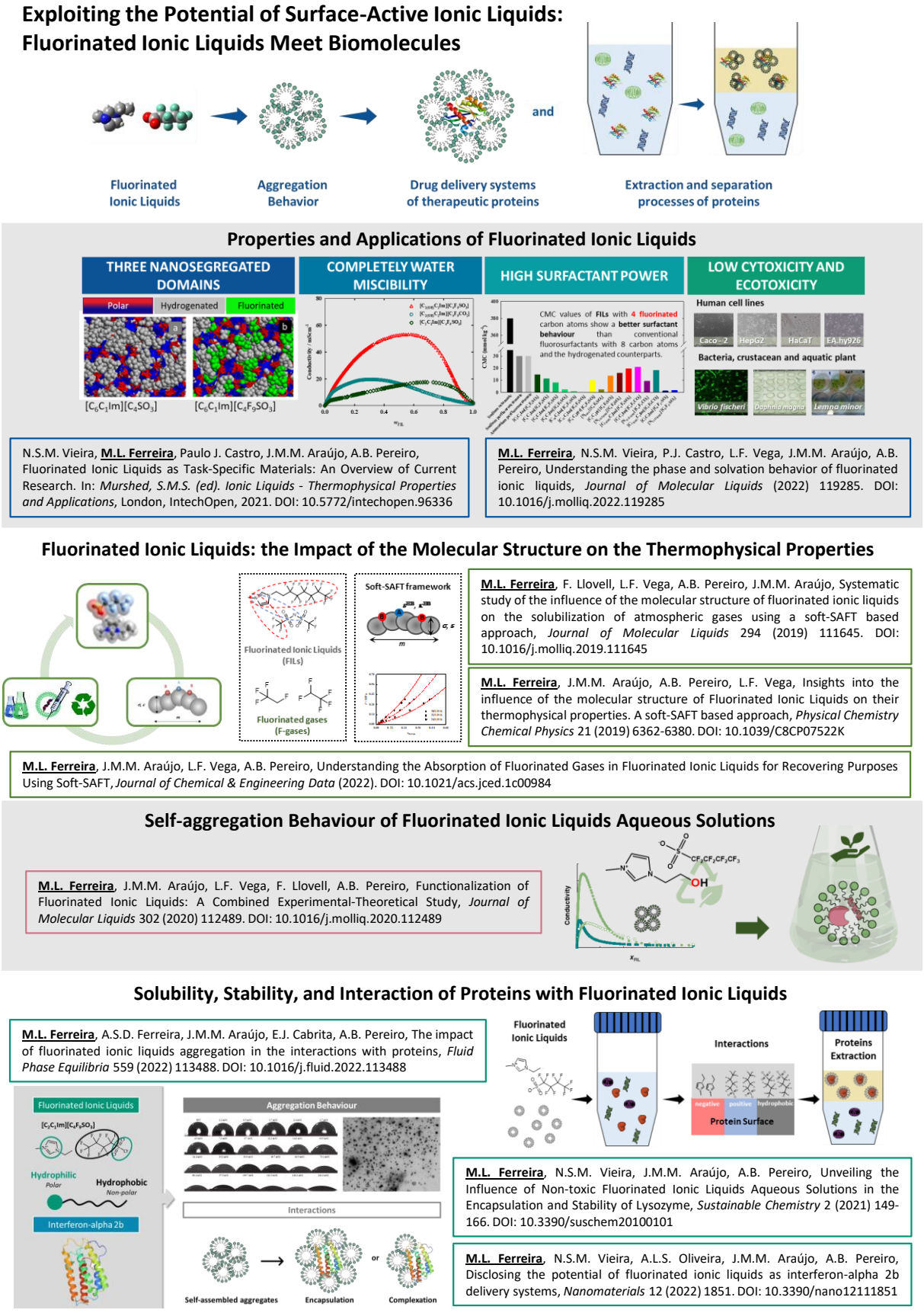

Figure 1.7.1 Schematic representation of the thesis outline, including the relevant publications.

1.8 References

1. Whitford, D. *Proteins: Structure and Function*; John Wiley & Sons: London, UK, 2005;
2. Dingermann, T. Recombinant Therapeutic Proteins: Production Platforms and Challenges. *Biotechnol J* **2008**, *3*, 90–97, doi:10.1002/biot.200700214.
3. Choi, J.M.; Han, S.S.; Kim, H.S. Industrial Applications of Enzyme Biocatalysis: Current Status and Future Aspects. *Biotechnol Adv* **2015**, *33*, 1443–1454, doi:10.1016/j.biotechadv.2015.02.014.
4. Kapoor, S.; Rafiq, A.; Sharma, S. Protein Engineering and Its Applications in Food Industry. *Crit Rev Food Sci Nutr* **2017**, *57*, 2321–2329, doi:10.1080/10408398.2014.1000481.
5. Lazar, G.A.; Marshall, S.A.; Plecs, J.J.; Mayo, S.L.; Desjarlais, J.R. Designing Proteins for Therapeutic Applications. *Curr Opin Struct Biol* 2003, *13*, 513–518.
6. Tropp, B.E. *Molecular Biology: Genes to Proteins*; 4th ed.; Jones and Bartlett Publishers: Burlington, MA, USA, 2008; ISBN 978-0-7637-8663-2.
7. Butler, L. Protein Structure and Properties. *J Am Oil Chem Soc* **1971**, *48*, 101–106, doi:10.1007/BF02545729.
8. Voet, D.; Voet, J.G. *Biochemistry*; 4th ed.; Wiley: New York, 2005; ISBN 978-0-470-57095-1.
9. Butreddy, A.; Janga, K.Y.; Ajjarapu, S.; Sarabu, S.; Dudhipala, N. Instability of Therapeutic Proteins — An Overview of Stresses, Stabilization Mechanisms and Analytical Techniques Involved in Lyophilized Proteins. *Int J Biol Macromol* **2021**, *167*, 309–325, doi:10.1016/j.ijbiomac.2020.11.188.
10. Hamada, H.; Arakawa, T.; Shiraki, K. Effect of Additives on Protein Aggregation. *Curr Pharm Biotechnol* **2009**, *10*, 400–407, doi:10.2174/138920109788488941.
11. Dobson, C.M. Protein Misfolding, Evolution and Disease. *Trends Biochem Sci* **1999**, *24*, 329–332, doi:10.1016/S0968-0004(99)01445-0.
12. Wang, W.; Nema, S.; Teagarden, D. Protein Aggregation-Pathways and Influencing Factors. *Int J Pharm* 2010, *390*, 89–99.
13. Tan, S.C.; Yiap, B.C. DNA, RNA, and Protein Extraction: The Past and the Present. *J Biomed Biotechnol* 2009, *2009*.
14. Franca-Oliveira, G.; Fornari, T.; Hernández-Ledesma, B. A Review on the Extraction and Processing of Natural Source-Derived Proteins through Eco-Innovative Approaches. *Processes* 2021, *9*.
15. Voynov, V.; Caravella, J.A. *Therapeutic Proteins*; Voynov, V., Caravella, J.A., Eds.; Humana Press: Totowa, NJ, 2012; Vol. 899; ISBN 978-1-61779-920-4.
16. Zaman, R.; Islam, R.A.; Ibnat, N.; Othman, I.; Zaini, A.; Lee, C.Y.; Chowdhury, E.H. Current Strategies in Extending Half-Lives of Therapeutic Proteins. *Journal of Controlled Release* 2019, *301*, 176–189.
17. Dingman, R.; Balu-Iyer, S. v. Immunogenicity of Protein Pharmaceuticals. *J Pharm Sci* 2019, *108*, 1637–1654.
18. Raeisi Estabragh, M.A.; Bami, M.S.; Ohadi, M.; Banat, I.M.; Dehghannoudeh, G. Carrier-Based Systems as Strategies for Oral Delivery of Therapeutic Peptides and Proteins: A Mini-Review. *Int J Pept Res Ther* 2021, *27*, 1589–1596.
19. Akash, M.S.H.; Rehman, K.; Tariq, M.; Chen, S. Development of Therapeutic Proteins: Advances and Challenges. *Turkish Journal of Biology* **2015**, *39*, 343–358, doi:10.3906/biy-1411-8.
20. Schuster, J.; Koulov, A.; Mahler, H.C.; Detampel, P.; Huwyler, J.; Singh, S.; Mathaes, R. In Vivo Stability of Therapeutic Proteins. *Pharm Res* 2020, *37*.

21. Torres-Vanegas, J.D.; Cruz, J.C.; Reyes, L.H. Delivery Systems for Nucleic Acids and Proteins: Barriers, Cell Capture Pathways and Nanocarriers. *Pharmaceutics* **2021**, *13*, doi:10.3390/pharmaceutics13030428.
22. Nie, T.; Wang, W.; Liu, X.; Wang, Y.; Li, K.; Song, X.; Zhang, J.; Yu, L.; He, Z. Sustained Release Systems for Delivery of Therapeutic Peptide/Protein. *Biomacromolecules* 2021, *22*, 2299–2324.
23. Moncalvo, F.; Martinez Espinoza, M.I.; Cellesi, F. Nanosized Delivery Systems for Therapeutic Proteins: Clinically Validated Technologies and Advanced Development Strategies. *Front Bioeng Biotechnol* 2020, *8*.
24. Bolhassani, A. Improvements in Chemical Carriers of Proteins and Peptides. *Cell Biol Int* **2019**, *43*, 437–452, doi:10.1002/cbin.11108.
25. Clarke, C.J.; Tu, W.C.; Levers, O.; Bröhl, A.; Hallett, J.P. Green and Sustainable Solvents in Chemical Processes. *Chem Rev* **2018**, *118*, 747–800, doi:10.1021/acs.chemrev.7b00571.
26. Zhang, S.; Sun, N.; He, X.; Lu, X.; Zhang, X. Physical Properties of Ionic Liquids: Database and Evaluation. *J Phys Chem Ref Data* 2006, *35*, 1475–1517.
27. Ohno, H. Functional Design of Ionic Liquids. *Bull Chem Soc Jpn* **2006**, *79*, 1665–1680, doi:10.1246/bcsj.79.1665.
28. Aparicio, S.; Atilhan, M.; Karadas, F. Thermophysical Properties of Pure Ionic Liquids: Review of Present Situation. *Ind Eng Chem Res* **2010**, *49*, 9580–9595, doi:10.1021/ie101441s.
29. Fabre, E.; Murshed, S.M.S. A Review of the Thermophysical Properties and Potential of Ionic Liquids for Thermal Applications. *J Mater Chem A Mater* 2021, *9*, 15861–15879.
30. Canongia Lopes, J.N.A.; Pádua, A.A.H. Nanostructural Organization in Ionic Liquids. *Journal of Physical Chemistry B* **2006**, *110*, 3330–3335, doi:10.1021/jp056006y.
31. Wang, Y.L.; Li, B.; Sarman, S.; Mocci, F.; Lu, Z.Y.; Yuan, J.; Laaksonen, A.; Fayer, M.D. Microstructural and Dynamical Heterogeneities in Ionic Liquids. *Chem Rev* 2020, *120*, 5798–5877.
32. Marullo, S.; D'Anna, F.; Rizzo, C.; Billeci, F. Ionic Liquids: "Normal" Solvents or Nanostructured Fluids? *Org Biomol Chem* 2021, *19*, 2076–2095.
33. Kaur, G.; Kumar, H.; Singla, M. Diverse Applications of Ionic Liquids: A Comprehensive Review. *J Mol Liq* **2022**, *351*, doi:10.1016/j.molliq.2022.118556.
34. Singh, S.K.; Savoy, A.W. Ionic Liquids Synthesis and Applications: An Overview. *J Mol Liq* 2020, *297*.
35. Greer, A.J.; Jacquemin, J.; Hardacre, C. Industrial Applications of Ionic Liquids. *Molecules* 2020, *25*.
36. Cho, C.W.; Pham, T.P.T.; Zhao, Y.; Stolte, S.; Yun, Y.S. Review of the Toxic Effects of Ionic Liquids. *Science of the Total Environment* 2021, *786*.
37. Beil, S.; Markiewicz, M.; Pereira, C.S.; Stepnowski, P.; Thöming, J.; Stolte, S. Toward the Proactive Design of Sustainable Chemicals: Ionic Liquids as a Prime Example. *Chem Rev* **2021**, *121*, 13132–13173, doi:10.1021/acs.chemrev.0c01265.
38. Wei, P.; Pan, X.; Chen, C.Y.; Li, H.Y.; Yan, X.; Li, C.; Chu, Y.H.; Yan, B. Emerging Impacts of Ionic Liquids on Eco-Environmental Safety and Human Health. *Chem Soc Rev* 2021, *50*, 13609–13627.
39. Gonçalves, A.R.P.; Paredes, X.; Cristino, A.F.; Santos, F.J.V.; Queirós, C.S.G.P. Ionic Liquids—a Review of Their Toxicity to Living Organisms. *Int J Mol Sci* 2021, *22*.
40. Egorova, K.S.; Gordeev, E.G.; Ananikov, V.P. Biological Activity of Ionic Liquids and Their Application in Pharmaceutics and Medicine. *Chem Rev* 2017, *117*, 7132–7189.
41. Correia, D.M.; Fernandes, L.C.; Fernandes, M.M.; Hermenegildo, B.; Meira, R.M.; Ribeiro, C.; Ribeiro, S.; Reguera, J.; Lanceros-Méndez, S. Ionic Liquid-Based Materials for Biomedical Applications. *Nanomaterials* 2021, *11*.

42. Gandhewar, N.; Shende, P. Ionic Liquids: A State of the Art for Biomedical Applications. *Ionics (Kiel)* 2021, *27*, 3715–3728.
43. Curreri, A.M.; Mitragotri, S.; Tanner, E.E.L. Recent Advances in Ionic Liquids in Biomedicine. *Advanced Science* 2021, *8*.
44. Toledo Hijo, A.A.C.; Maximo, G.J.; Costa, M.C.; Batista, E.A.C.; Meirelles, A.J.A. Applications of Ionic Liquids in the Food and Bioproducts Industries. *ACS Sustain Chem Eng* 2016, *4*, 5347–5369.
45. Pedro, S.N.; Freire, C.S.R.; Silvestre, A.J.D.; Freire, M.G. The Role of Ionic Liquids in the Pharmaceutical Field: An Overview of Relevant Applications. *Int J Mol Sci* 2020, *21*, 1–50.
46. Patel, R.; Kumari, M.; Khan, A.B. Recent Advances in the Applications of Ionic Liquids in Protein Stability and Activity: A Review. *Appl Biochem Biotechnol* 2014, *172*, 3701–3720.
47. Zhao, H. Protein Stabilization and Enzyme Activation in Ionic Liquids: Specific Ion Effects. *Journal of Chemical Technology and Biotechnology* 2016, *91*, 25–50.
48. Schröder, C. Proteins in Ionic Liquids: Current Status of Experiments and Simulations. *Top Curr Chem* 2017, *375*.
49. Harada, L.K.; Pereira, J.F.B.; Campos, W.F.; Silva, E.C.; Moutinho, C.G.; Vila, M.M.D.C.; Oliveira, J.M.; Teixeira, J.A.; Balcão, V.M.; Tubino, M. Insights into Protein-Ionic Liquid Interactions Aiming at Macromolecule Delivery Systems. *J Braz Chem Soc* 2018, *29*, 1983–1998.
50. Bento, R.M.F.; Almeida, C.A.S.; Neves, M.C.; Tavares, A.P.M.; Freire, M.G. Advances Achieved by Ionic-Liquid-Based Materials as Alternative Supports and Purification Platforms for Proteins and Enzymes. *Nanomaterials* **2021**, *11*, doi:10.3390/nano11102542.
51. Zhao, Q.; Chu, H.; Zhao, B.; Liang, Z.; Zhang, L.; Zhang, Y. Advances of Ionic Liquids-Based Methods for Protein Analysis. *TrAC - Trends in Analytical Chemistry* 2018, *108*, 239–246.
52. Schindl, A.; Hagen, M.L.; Muzammal, S.; Gunasekera, H.A.D.; Croft, A.K. Proteins in Ionic Liquids: Reactions, Applications, and Futures. *Front Chem* 2019, *7*.
53. Uddin, M.; Basak, D.; Hopefl, R.; Minofar, B. *Potential Application of Ionic Liquids in Pharmaceutical Dosage Forms for Small Molecule Drug and Vaccine Delivery System*; 2020; Vol. 23;.
54. Ventura, S.P.M.; Gonçalves, A.M.M.; Sintra, T.; Pereira, J.L.; Gonçalves, F.; Coutinho, J.A.P. Designing Ionic Liquids: The Chemical Structure Role in the Toxicity. *Ecotoxicology* **2013**, *22*, 1–12, doi:10.1007/S10646-012-0997-X.
55. Buettner, C.S.; Cognigni, A.; Schröder, C.; Bica-Schröder, K. Surface-Active Ionic Liquids: A Review. *J Mol Liq* **2022**, *347*, 118160, doi:10.1016/j.molliq.2021.118160.
56. Kharazi, M.; Saien, J.; Asadabadi, S. Review on Amphiphilic Ionic Liquids as New Surfactants: From Fundamentals to Applications. *Top Curr Chem* 2022, *380*.
57. Dib, N.; Lépori, C.M.O.; Correa, N.M.; Silber, J.J.; Falcone, R.D.; García-Río, L. Biocompatible Solvents and Ionic Liquid-Based Surfactants as Sustainable Components to Formulate Environmentally Friendly Organized Systems. *Polymers (Basel)* **2021**, *13*, doi:10.3390/polym13091378.
58. el Seoud, O.A.; Keppeler, N.; Malek, N.I.; Galgano, P.D. Ionic Liquid-Based Surfactants: Recent Advances in Their Syntheses, Solution Properties, and Applications. *Polymers (Basel)* 2021, *13*.
59. Singh, T.; Bharmoria, P.; Morikawa, M.A.; Kimizuka, N.; Kumar, A. Ionic Liquids Induced Structural Changes of Bovine Serum Albumin in Aqueous Media: A Detailed Physicochemical and Spectroscopic Study. *Journal of Physical Chemistry B* **2012**, *116*, 11924–11935, doi:10.1021/jp303609h.
60. Wang, X.; Liu, J.; Sun, L.; Yu, L.; Jiao, J.; Wang, R. Interaction of Bovine Serum Albumin with Ester-Functionalized Anionic Surface-Active Ionic Liquids in Aqueous Solution: A Detailed Physicochemical and Conformational Study. *Journal of Physical Chemistry B* **2012**, *116*, 12479–12488, doi:10.1021/jp307516a.

61. Bharmoria, P.; Rao, K.S.; Trivedi, T.J.; Kumar, A. Biamphiphilic Ionic Liquid Induced Folding Alterations in the Structure of Bovine Serum Albumin in Aqueous Medium. *Journal of Physical Chemistry B* **2014**, *118*, 115–124, doi:10.1021/jp4102042.
62. Satish, L.; Millan, S.; Sasidharan, V.V.; Sahoo, H. Molecular Level Insight into the Effect of Triethyloctylammonium Bromide on the Structure, Thermal Stability, and Activity of Bovine Serum Albumin. *Int J Biol Macromol* **2018**, *107*, 186–193, doi:10.1016/j.ijbiomac.2017.08.157.
63. Panda, S.; Kundu, K.; Basaiahgari, A.; Singh, A.P.; Senapati, S.; Gardas, R.L. Aggregation Behaviour of Biocompatible Choline Carboxylate Ionic Liquids and Their Interactions with Biomolecules through Experimental and Theoretical Investigations. *New Journal of Chemistry* **2018**, *42*, 7105–7118, doi:10.1039/c8nj00336j.
64. Paul, B.K.; Ganguly, A.; Guchhait, N. Deciphering the Interaction of a Model Transport Protein with a Prototypical Imidazolium Room Temperature Ionic Liquid: Effect on the Conformation and Activity of the Protein. *J Photochem Photobiol B* **2014**, *133*, 99–107, doi:10.1016/j.jphotobiol.2014.03.007.
65. Thoppil, A.A.; Chennuri, B.K.; Gardas, R.L. Insights into the Structural Changes of Bovine Serum Albumin in Ethanolammonium Laurate Based Surface Active Ionic Liquids. *J Mol Liq* **2019**, *290*, doi:10.1016/j.molliq.2019.111229.
66. Islam, M.M.; Barik, S.; Sarkar, M. Probing the Interactions of 1-Alkyl-3-Methylimidazolium Tetrafluoroborate (Alkyl = Octyl, Hexyl, Butyl, and Ethyl) Ionic Liquids with Bovine Serum Albumin: An Alkyl Chain Length-Dependent Study. *Journal of Physical Chemistry B* **2019**, *123*, 1512–1526, doi:10.1021/acs.jpcb.8b10795.
67. Gehlot, P.S.; Rao, K.S.; Bharmoria, P.; Damarla, K.; Gupta, H.; Drechsler, M.; Kumar, A. Spontaneous Formation of Multiarchitecture Vesicles of [C8mim]Br + [Na]DBS in Aqueous Medium: Synergic Interplay of Electrostatic, Hydrophobic, and π-π Stacking Interactions. *Journal of Physical Chemistry B* **2015**, *119*, 15300–15309, doi:10.1021/acs.jpcb.5b09850.
68. Banerjee, C.; Roy, A.; Kundu, N.; Banik, D.; Sarkar, N. A New Strategy to Prepare Giant Vesicles from Surface Active Ionic Liquids (SAILs): A Study of Protein Dynamics in a Crowded Environment Using a Fluorescence Correlation Spectroscopic Technique. *Physical Chemistry Chemical Physics* **2016**, *18*, 14520–14530, doi:10.1039/c5cp07225e.
69. Zhang, N.; Hu, X.; Guan, P.; Du, C.; Li, J.; Qian, L.; Zhang, X.; Ding, S.; Li, B. Preparation of Protein Imprinted Microspheres Using Amphiphilic Ionic Liquid as Stabilizer and Emulsifier via Miniemulsion Polymerization. *Chemical Engineering Journal* **2017**, *317*, 356–367, doi:10.1016/j.cej.2017.02.066.
70. Kundu, K.; Singh, A.P.; Panda, S.; Singh, V.; Gardas, R.L.; Senapati, S. Study on the Conformation of Entrapped Protein inside the Reverse Micellar Confinement Based on the Amino Acid Derived Ionic Liquid. *ChemistrySelect* **2018**, *3*, 4768–4776, doi:10.1002/slct.201800918.
71. Singh, G.; Kaur, M.; Kang, T.S.; Aswal, V.K. Aqueous Colloidal Systems of Bovine Serum Albumin and Functionalized Surface Active Ionic Liquids for Material Transport. *RSC Adv* **2020**, *10*, 7073–7082, doi:10.1039/c9ra05549e.
72. Maurya, J.K.; Mir, M.U.H.; Singh, U.K.; Maurya, N.; Dohare, N.; Patel, S.; Ali, A.; Patel, R. Molecular Investigation of the Interaction between Ionic Liquid Type Gemini Surfactant and Lysozyme: A Spectroscopic and Computational Approach. *Biopolymers* **2015**, *103*, 406–415, doi:10.1002/bip.22647.
73. Mandal, B.; Mondal, S.; Pan, A.; Moulik, S.P.; Ghosh, S. Physicochemical Study of the Interaction of Lysozyme with Surface Active Ionic Liquid 1-Butyl-3-Methylimidazolium Octylsulfate [BMIM] [OS] in Aqueous and Buffer Media. *Colloids Surf A Physicochem Eng Asp* **2015**, *484*, 345–353, doi:10.1016/j.colsurfa.2015.07.052.

74. Bisht, M.; Kumar, A.; Venkatesu, P. Analysis of the Driving Force That Rule the Stability of Lysozyme in Alkylammonium-Based Ionic Liquids. *Int J Biol Macromol* **2015**, *81*, 1074–1081, doi:10.1016/j.ijbiomac.2015.09.036.
75. Rather, M.A.; Dar, T.A.; Singh, L.R.; Rather, G.M.; Bhat, M.A. Structural-Functional Integrity of Lysozyme in Imidazolium Based Surface Active Ionic Liquids. *Int J Biol Macromol* **2020**, *156*, 271–279, doi:10.1016/j.ijbiomac.2020.04.033.
76. Kumari, M.; Dohare, N.; Maurya, N.; Dohare, R.; Patel, R. Effect of 1-Methyl-3-Octyleimmidazolium Chloride on the Stability and Activity of Lysozyme: A Spectroscopic and Molecular Dynamics Studies. *J Biomol Struct Dyn* **2017**, *35*, 2016–2030, doi:10.1080/07391102.2016.1204946.
77. Kumari, M.; Singh, U.K.; Beg, I.; Alanazi, A.M.; Khan, A.A.; Patel, R. Effect of Cations and Anions of Ionic Liquids on the Stability and Activity of Lysozyme: Concentration and Temperature Effect. *J Mol Liq* **2018**, *272*, 253–263, doi:10.1016/j.molliq.2018.09.075.
78. Kaur, M.; Singh, G.; Kaur, A.; Sharma, P.K.; Kang, T.S. Thermally Stable Ionic Liquid-Based Microemulsions for High-Temperature Stabilization of Lysozyme at Nanointerfaces. *Langmuir* **2019**, *35*, 4085–4093, doi:10.1021/acs.langmuir.9b00106.
79. Singh, G.; Kaur, M.; Singh, D.; Kesavan, A.K.; Kang, T.S. Antimicrobial Colloidal Complexes of Lysozyme with Bio-Based Surface Active Ionic Liquids in Aqueous Medium. *Journal of Physical Chemistry B* **2020**, *124*, 3791–3800, doi:10.1021/acs.jpcb.0c00339.
80. Singh, G.; Kaur, M.; Kaur, H.; Kang, T.S. Synthesis and Complexation of a New Caffeine Based Surface Active Ionic Liquid with Lysozyme in Aqueous Medium: Physicochemical, Computational and Antimicrobial Studies. *J Mol Liq* **2021**, *325*, doi:10.1016/j.molliq.2020.115156.
81. Bharmoria, P.; Trivedi, T.J.; Pabbathi, A.; Samanta, A.; Kumar, A. Ionic Liquid-Induced All-α to α + β Conformational Transition in Cytochrome c with Improved Peroxidase Activity in Aqueous Medium. *Physical Chemistry Chemical Physics* **2015**, *17*, 10189–10199, doi:10.1039/c4cp06044j.
82. Li, Z.; Guan, P.; Hu, X.; Ding, S.; Tian, Y.; Xu, Y.; Qian, L. Preparation of Molecularly Imprinted Mesoporous Materials for Highly Enhancing Adsorption Performance of Cytochrome C. *Polymers (Basel)* **2018**, *10*, doi:10.3390/polym10030298.
83. Mondal, S.; Das, B. A Study on the Interaction of Horse Heart Cytochrome c with Some Conventional and Ionic Liquid Surfactants Probed by Ultraviolet-Visible and Fluorescence Spectroscopic Techniques. *Spectrochim Acta A Mol Biomol Spectrosc* **2018**, *198*, 278–282, doi:10.1016/j.saa.2018.03.026.
84. Singh, U.K.; Kumari, M.; Patel, R. Dynamics of Cytochrome c in Surface Active Ionic Liquid: A Study of Preferential Interactions towards Denaturation. *J Mol Liq* **2018**, *268*, 840–848, doi:10.1016/j.molliq.2018.07.116.
85. Singh, U.K.; Kumari, M.; Wani, F.A.; Parray, M. ud din; Saraswat, J.; Venkatesu, P.; Patel, R. Refolding of Acid Denatured Cytochrome c by Anionic Surface-Active Ionic Liquid: Choice of Anion Plays Key Role in Refolding of Proteins. *Colloids Surf A Physicochem Eng Asp* **2019**, *582*, doi:10.1016/j.colsurfa.2019.123872.
86. Liu, Y.; Yang, L.; Mao, H.; Guo, R. Comparative Studies on the Interaction of [C4mim]Br, and [C8mim]Br with β-Casein Micelles. *Colloids Surf A Physicochem Eng Asp* **2014**, *441*, 581–588, doi:10.1016/j.colsurfa.2013.10.012.
87. Calderón, C.; Contreras, R.; Campodónico, R. Surfactant-Mediated Enzymatic Superactivity in Water/Ionic Liquid Mixtures, Evaluated on a Model Hydrolytic Reaction Catalyzed by α-Chymotrypsin. *J Mol Liq* **2019**, *283*, 522–531, doi:10.1016/j.molliq.2019.03.106.

88. Acharyya, A.; Digiuseppi, D.; Stinger, B.L.; Schweitzer-Stenner, R.; Vaden, T.D. Structural Destabilization of Azurin by Imidazolium Chloride Ionic Liquids in Aqueous Solution. *Journal of Physical Chemistry B* **2019**, *123*, 6933–6945, doi:10.1021/acs.jpcb.9b04113.
89. Chabba, S.; Vashishat, R.; Mahajan, R.K. Characterization of Interactions between β-Lactoglobulin with Surface Active Ionic Liquids in Aqueous Medium. *J Mol Liq* **2018**, *259*, 134–143, doi:10.1016/j.molliq.2018.03.020.
90. Vashishat, R.; Chabba, S.; Mahajan, R.K. Surface Active Ionic Liquid Induced Conformational Transition in Aqueous Medium of Hemoglobin. *RSC Adv* **2017**, *7*, 13041–13052, doi:10.1039/c7ra00075h.
91. Mondal, S.; Banerjee, A.; Das, B. Spectroscopic and Interfacial Investigation on the Interaction of Hemoglobin with Conventional and Ionic Liquid Surfactants. *J Mol Liq* **2020**, *301*, doi:10.1016/j.molliq.2020.112450.
92. Blesic, M.; Nimal Gunaratne, H.Q.; Nockemann, P.; McCarron, P.; Seddon, K.R. Controlled Fragrance Delivery in Functionalised Ionic Liquid-Enzyme Systems. *RSC Adv* **2013**, *3*, 329–333, doi:10.1039/c2ra22500j.
93. Islam, M.R.; Uddin, S.; Chowdhury, M.R.; Wakabayashi, R.; Moniruzzaman, M.; Goto, M. Insulin Transdermal Delivery System for Diabetes Treatment Using a Biocompatible Ionic Liquid-Based Microemulsion. *ACS Appl Mater Interfaces* **2021**, *13*, 42461–42472, doi:10.1021/acsami.1c11533.
94. Paul, B.K. Unveiling the Thermodynamic Signature Underlying the Interaction of Human Serum Albumin with Sub-Micellar Concentrations of a Surface Active Ionic Liquid. *J Mol Liq* **2020**, *318*, doi:10.1016/j.molliq.2020.114078.
95. Martins, M.; Ooi, C.W.; Neves, M.C.; Pereira, J.F.B.; Coutinho, J.A.P.; Ventura, S.P.M. Extraction of Recombinant Proteins from Escherichia Coli by Cell Disruption with Aqueous Solutions of Surface-Active Compounds. *Journal of Chemical Technology and Biotechnology* **2018**, *93*, 1864–1870, doi:10.1002/jctb.5596.
96. Kundu, S.; Banerjee, C.; Sarkar, N. Inhibiting the Fibrillation of Serum Albumin Proteins in the Presence of Surface Active Ionic Liquids (SAILs) at Low PH: Spectroscopic and Microscopic Study. *Journal of Physical Chemistry B* **2017**, *121*, 7550–7560, doi:10.1021/acs.jpcb.7b03457.
97. Cao, C.; Zhou, Z.L.; Zheng, L.; Huang, Q.L.; Du, F.P. Dilational Rheology of Different Globular Protein with Imidazolium-Based Ionic Liquid Surfactant Adsorption Layer at the Decane/Water Interface. *J Mol Liq* **2017**, *233*, 344–351, doi:10.1016/j.molliq.2017.02.121.
98. Tian, T.; Kang, Q.; Wang, T.; Xiao, J.; Yu, L. Alignment of Nematic Liquid Crystals Decorated with Gemini Surfactants and Interaction of Proteins with Gemini Surfactants at Fluid Interfaces. *J Colloid Interface Sci* **2018**, *518*, 111–121, doi:10.1016/j.jcis.2018.02.027.
99. Guncheva, M.; Dimitrov, M.; Ossowicz, P.; Janus, E. Tetraalkylammonium Acetates and Tetraalkylammonium Tetrafluoroborates as New Templates for Room-Temperature Synthesis of Mesoporous Silica Spheres. *Journal of Porous Materials* **2018**, *25*, 935–943, doi:10.1007/s10934-017-0505-z.
100. Vicente, F.A.; Bairos, J.; Roque, M.; Coutinho, J.A.P.; Ventura, S.P.M.; Freire, M.G. Use of Ionic Liquids as Cosurfactants in Mixed Aqueous Micellar Two-Phase Systems to Improve the Simultaneous Separation of Immunoglobulin G and Human Serum Albumin from Expired Human Plasma. *ACS Sustain Chem Eng* **2019**, *7*, 15102–15113, doi:10.1021/acssuschemeng.9b03841.

CHAPTER 2

PROPERTIES AND APPLICATIONS OF FLUORINATED IONIC LIQUIDS

2.1 Introduction

Perfluorocarbons (PFCs) consist of a large group of man-made chemicals available worldwide in many different fields since the 1940s. The numerous applications of PFCs in different areas rely on their distinctive physical and chemical characteristics (water and oil repellence, thermal and chemical stability, surfactant behaviour, low polarity, weak intermolecular interactions, and reduced surface tension), highly fomented by the fluor-carbon moiety [1,2]. These compounds are widespread in consumers' life through plastics, fire retardants, dyes, surfactants, polymers, and pharmaceuticals, among others [3,4]. Benign PFCs have been used in the development of biomedical applications, such as emulsions [5,6], imaging agents [7,8], biocompatible lubricants [9], oxygen therapeutics [10], pulmonary delivery agents [11], and theranostic agents [12]. On the other hand, perfluoroalkyl acids (PFAs) and fluorinated greenhouse gases (F-gases) belong to a class of persistent chemicals, widely used in industrial and commercial products [13]. Due to their high global warming potential (GWP), long atmospheric lifetime, persistency, and mobility these compounds have been found in several contaminated sites [14], including water, soils, biota, and food [15–17]. Major concerns about their toxicity and bioaccumulation limit their use and encourage their replacement [18].

In the last decades, ionic liquids have emerged as new engineering solvents. The application of these compounds has aroused in many different subjects, including catalysis, electrochemistry, extraction and separation processes, pharmaceutical, and biomedical applications [19]. This massive use of ILs is supported by their unique thermophysical properties and limitlessness combinations between anions and cations. Their title of "green solvents" is corroborated by an almost negligible vapour pressure at room temperature and reduced flammability [20,21]. Additionally, the increased research about the cytotoxicity and environmental toxicity of these compounds reinforces that their possible harmful behaviour is dependent on the cation-anion tested combination [22]. Due to their complexity and variety, ILs have been categorized in several families according to either their properties or their applications [23].

This chapter is focused on the use of a less explored ILs family, the fluorinated ionic liquids, defined as ILs with fluorine tags equal to or longer than four carbon atoms. The fluorinated tags can create one nanosegregated domain distinct from polar and non-polar (hydrogenated) [24–26]. FILs combine the exceptional properties of conventional ILs (high thermal stability, negligible vapour pressure, reduced flammability, and greener potential) with the greatest properties of traditional PFCs (chemical and biological inertness, reduced surface tension and increased surfactant behaviour). In contrast to the low solubility and

toxicity intrinsic to many highly fluorinated compounds, some novel FILs have been designed with completely water miscibility [27,28] and negligible toxicity [29–31], furthering their use in the more green engineering process and biomedical applications. In spite of these outstanding properties, scarce information is available in the literature and research is mainly focused on their synthesis and characterization [32], electrochemical properties [33], gas solubilities [34], and application as reaction media [35]. The study of phase equilibria of FILs mixed with other substances such as other ILs, conventional solvents (water, organic solvents, fuels, hydrocarbons, etc.), and solutes (gases, salts, biomolecules, among others) is of great importance from a technological point of view [36–44]. Of particular interest are studies concerning phase equilibria of FILs with other substances leading to separation and extraction processes, which can be applied in the most diverse areas, from the chemical to the pharmaceutical and biomedical industries [45,46].

Aiming to understand the physicochemical, thermophysical, and toxicity properties of FILs and their potential as task-specific materials for biological applications, this chapter gathers a review of the literature for a thorough analysis of the pure FILs and their behaviour with other substances. The chapter is divided into two main sections.

The first section (2.2) highlights the improved physicochemical characteristics of the pure FILs when compared to the traditional ionic liquids and perfluoro surfactants, such as density, viscosity, ionicity, surface tension, and others. Moreover, the properties of FILs in water are also overviewed, underlining the enhanced aggregation behaviour of these surfactant compounds. In addition, the work related to the toxicity and biodegradability of these compounds was also evaluated in this section. Finally, the possible industrial applications of FILs were analysed focusing on their potential in biomedical applications, such as artificial gas carries and drug delivery systems, as well as solvents for separations in engineering processes.

The second section (2.3) overviews the last two decades of research on the phase equilibria behaviour of FILs, concerning vapour-liquid, liquid-liquid and solid-liquid equilibria. First, it was considered the studies relating to gas solubility performance of FILs, the application of membranes to improve gas absorption in FILs, and the use of modelling tools to accelerate the application of FILs in gas capture and separation processes. Therefore, the liquid-liquid equilibria of FILs in water and with perfluoroalkanes were evaluated in this work, together with the solid-liquid equilibria of solid FILs in water and the eutectic behaviour found in mixtures of solid FILs. This section allowed the understanding of how the structural features of FILs can influence their phase equilibria behaviour, which is of vital importance to design and developing task-specific FILs for a particular application, from the industrial to biomedical fields.

With the work developed in this chapter, it was possible to have a clear idea of the best properties of FILs that can benefit their usage in the biomedical and biological areas, allowing the selection of the structural features composing the FILs used in the next steps of this thesis.

This chapter is adapted from the following publications:

Section 2.2

Nicole S.M. Vieira, **Margarida L. Ferreira**, Paulo J. Castro, João M.M. Araújo, Ana B. Pereiro, Fluorinated Ionic Liquids as Task-Specific Materials: An Overview of Current Research. In: Murshed, S.M.S. (ed). *Ionic Liquids - Thermophysical Properties and Applications*, London, IntechOpen, 2021. DOI: 10.5772/intechopen.96336

The author of this thesis contributed to this section by writing part of the original manuscript, specifically the sections related to the properties of pure FILs and their mixtures with water and their application as artificial gas carriers. The author also contributed to the production of the graphical contents of the section, such as figures and tables.

Section 2.3

Margarida L. Ferreira, Nicole S.M. Vieira, Paulo J. Castro, Lourdes F. Vega, João M.M. Araújo, Ana B. Pereiro, Understanding the phase and solvation behavior of fluorinated ionic liquids, *Journal of Molecular Liquids* 359 (2022) 119285. DOI: 10.1016/j.molliq.2022.119285

The author of this thesis has written most of the original draft of the manuscript, specifically the abstract, introduction, gas solubility in FILs (excepting the parts concerning the fluorinated gases), molecular modelling of gas solubility in FILs, discussion, and conclusion sections. The author also contributed to the production of the graphical contents of the book chapter, such as figures and tables.

2.2 Fluorinated ionic liquids as task-specific materials: an overview of current research

This section covers the main assets of FILs, namely their thermophysical and structural properties, aggregation and surfactant behaviour, cytotoxicity, acute ecotoxicity and biodegradation. Additionally, a more detailed approach throughout the application of FILs as task-specific materials in several areas comprises the analysis of a series of works. It is evidenced by the progress of FILs either in biomedical applications or engineering separation processes.

2.2.1 Properties of fluorinated ionic liquids

The characterization of FILs properties and the influence of the different cation/anion combinations on these properties is still critical to head these specific materials to the potential applications. FILs have enhanced properties due to the nanosegregated structuring into three different domains, one polar and two non-polar (hydrogenated and fluorinated), making them an alternative solvent with new improved mechanisms of solubilization of different compounds (see Figure 2.2.1) [24–26]. The manipulation of the nanosegregation behaviour and intra and intermolecular interactions of FILs allows the control of thermal and thermophysical properties, toxicity, solubility capacity or hydrophobicity of FILs.

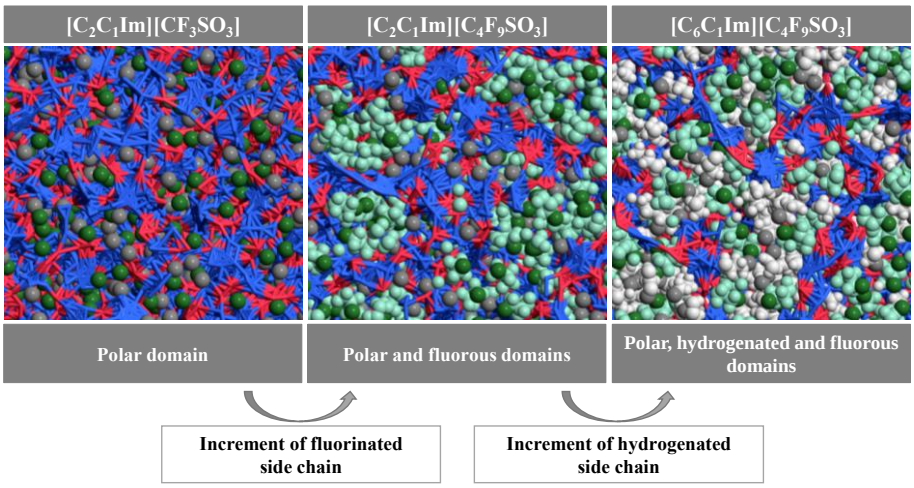

Figure 2.2.1 Formation of three nanosegregated domains of $[C_2C_1Im][CF_3SO_3]$ and $[C_2C_1Im][C_4F_9SO_3]$ and $[C_6C_1Im][C_4F_9SO_3]$ FILs. The red and blue sticks represent negative and positive charges, indicating the segregated polar network in the three ILs. The green space-filled areas represent the fluorinated domains. The grey space-filled areas indicate the segregated hydrogenated moieties. Adapted from Vieira, N.S.M. *et al.* (2015) [47].

In this section, it is emphasized how the formation of the new fluorinated domain and the structural features influence the properties of FILs. The properties of FILs, such as melting point, thermal stability, density, viscosity, refractive index, ionic conductivity, and surface

tension are discussed along with the FILs' self-aggregation behaviour in aqueous solutions. A close sight of the biocompatibility of FILs by examining their toxicological and biodegradability properties is also included for discussion.

2.2.1.1 Thermophysical properties

2.2.1.1.1 Phase behaviour and thermal properties

The phase behaviour of pure FILs is determined by the melting, solid-solid and glass transitions while the thermal stability is defined by the decomposition temperatures. These properties are determinant to define the liquid range of application, allowing a wisely choice of fluid for a specific task. Several works include the thermal characterization of the FILs depicted in Table 2.2.1. In the case of FILs where the formation of three domains occurs, due to long enough hydrogenated (up to 6 carbons) and fluorinated (up to 4 carbons) chains (Figure 2.2.1), a rich phase behaviour is found, with a high number of solid-solid transitions. This indicates the ability of FILs domains to rearrange into different structures until the complete melting, proving the high influence of the nanosegregation [26,48].

The different structural features of FILs can impact the melting and decomposition temperatures, and much work has been done to find trends to design FILs with tuned thermal properties [29,47–52]. The melting and decomposition temperature of several FILs can be found in Table 2.2.2. In the case of the $[C_nC_1Im][C_4F_9SO_3]$ FILs family, it was found that the increment of the cationic hydrogenated chain increases the melting temperature and decreases the decomposition temperature. The increase of the anionic fluorinated chain also raises the melting point. However, the thermal stability is maintained constant at a considerable high temperature [47,50]. Moreover, FILs based on $[C_nF_{2n+1}SO_3]^-$ anions have a much higher thermal stability than ILs conjugated with $[C_nF_{2n+1}CO_2]^-$ anions [47,49,51]. The type of cation and its functionalization also has a great influence on both thermal properties, and careful analysis must be performed when choosing a FIL for a specific ending [26,29,47–49,51].

Table 2.2.1 Structure and nomenclature of the ions constituting the FILs and of the F-gases studied for absorption in FILs and deep eutectic solvents, prepared with the illustrated perfluorinated acids.

Cations structure	
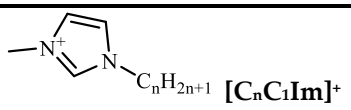 **$[C_nC_1Im]^+$** n = 2, 4, 6, 8, 10 and 12 1-Alkyl-3-methylimidazolium	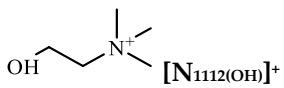 **$[N_{1112(OH)}]^+$** (2-Hydroxyethyl)trimethylammonium
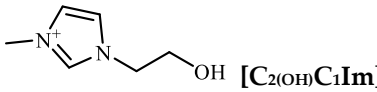 **$[C_{2(OH)}C_1Im]^+$** 1-(2-Hydroxyethyl)-3-methylimidazolium	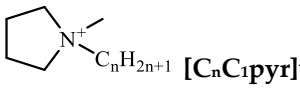 **$[C_nC_1pyr]^+$** n = 2 and 4 1-Alkyl-1-methylpyrrolidinium

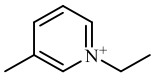
[C2C1py]+
1-Ethyl-3-methylimidazolium

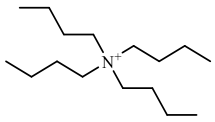
[N4444]+
Tetrabutylammonium

Anions structure	F-gases
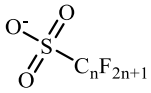 **[CnF2n+1SO3]−** n = 1, 4 and 8 Perfluoroalkyl sulfonate	 **R-32** Difluoromethane
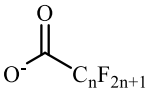 **[CnF2n+1CO2]−** n = 4 and 8 Perfluoroalkyl carboxylate	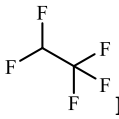 **R-125** Pentafluoroethane
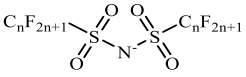 **[N(CnF2n+1SO2)2]−** n = 1 and 4 Bis(perfluoroalkylsulfonyl)imide	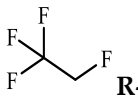 **R-134a** 1,1,1,2-Tetrafluoroethane
Perfluorinated acids	
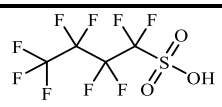 **[C4F9SO3H]** Nonafluoro-1-butanesulfonic acid	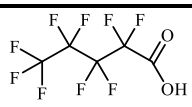 **[C4F9CO2H]** n-Perfluoropentanoic acid

The FILs based on long fluorinated chains (*e.g.* $[N(C_4F_9SO_2)_2]^-$) have a very high melting temperature, automatically reducing the liquid operating range. Eutectic mixtures of FILs can be the solution to solve this handicap. The evaluation of the solid-liquid phase behaviour of binary mixtures of FILs showed a high decline of the melting temperature to values close to or below room temperature [53]. This does not only increase the liquid range of FILs but also expands the tuneability of neat FILs.

Table 2.2.2 Thermophysical and thermodynamic properties of fluorinated ionic liquids at 298.15 K and atmospheric pressure: melting temperature, T_m; decomposition temperature, T_{onset}; density, ρ; viscosity, η; and surface tension, γ.

	T_m [K]	T_{onset} [K]	ρ [g·cm^{-3}]	η [m·Pas^{-1}]	γ [mN·m^{-1}]
			[CnC1Im][C4F9SO3]		
n=2	293 [a]	627 [a]	1.547 [a]	163.0 [a]	25.14 [d,*]
n=4	286 [b]	638 [b]	1.460 [b]	307.3 [b]	22.83 [d,*]
n=6	297 [c]	627 [c]	1.392 [c]	401.7 [c]	21.36 [d,*]
n=8	308 [c]	621 [c]	1.338 [c]	374.6 [c]	20.57 [d,*]
n=10	307 [b]	627 [b]	1.310 [b]	597.1 [b]	22.05 [d,*]
n=12	311 [a,*]	617 [a,*]	1.247 [a,*]	280.9 [a,*]	23.42 [d,*]
			[C4F9SO3]−		
[C2C1py]+	278 [c]	629 [c]	1.515 [c]	201.8 [c]	26.35 [e]

$[N_{4444}]^+$	327 [c]	587 [c]	1.234 [c]	15319 [c]	22.77 [e,**]
$[C_4C_1pyr]^+$	364 [f]	632 [f]			
$[N_{1112(OH)}]^+$	436 [e]	609 [e]			
$[C_{2(OH)}C_1Im]^+$	251 [g]	559 [g]	1.620 [g]	831.6 [g]	
			$[C_4F_9CO_2]^-$		
$[C_2C_1Im]^+$	278 [a]	392 [a]	1.487 [a]	107.5 [a]	
$[C_8C_1Im]^+$	297 [a]	399 [a]	1.292 [a]	307.9 [a]	
$[C_{2(OH)}C_1Im]^+$	295 [g]	433 [g]	1.541 [g]	712.8 [g]	
$[C_2C_1py]^+$	275 [e]	392 [e]	1.454 [e]	147.1 [e]	26.83 [e]
			$[C_8F_{17}SO_3]^-$		
$[N_{4444}]^+$	255 [c]	385 [c]	1.317 [c]	6690 [c]	21.98 [e]
$[C_2C_1Im]^+$	368 [a]	616 [a]			
			$[N(C_4F_9SO_2)_2]^-$		
$[C_2C_1pyr]^+$	428 [e]	619 [e]			
$[C_4C_1pyr]^+$	371 [e]	639 [e]			
$[N_{1112(OH)}]^+$	303 [e,*]	622 [e,*]	1.674 [e,*]	947.1 [e,*]	25.04 [e,*]

Experimental data was obtained * at 313.15 K and ** at 333.15 K. Experimental data from [a]Vieira, N.S.M *et al.*(2015); [b] Pereiro, A.B. *et al.* (2017); [c] Pereiro, A.B. *et al.* (2013); [d] Luís, A. *et al.* (2016); [e]Vieira, N.S.M *et al.*(2016); [f] Ferreira, M.L. *et al.* (2017); [g] Ferreira, M.L. *et al.* (2020). [29,47–49,51]

2.2.1.1.2 Density, transport properties, free volume, and surface tension

Density, transport, free volume, and surface tension properties have high relevance in the biomedical field as well as in the separation and extraction processes for industrial proposes [29,54]. The structural features of FILs can determine the density, as can be seen in Table 2.2.2. While the increment of the fluorinated chains increases FILs density, the opposite behaviour is found for the increment of the hydrogenated side chain. The carboxylate anions show a lower density compared with the sulfonate anions. The functionalization of imidazolium cation with a hydroxyl group has shown an increment in density. The cation nature widely affects the density, and each family must be analysed case by case to infer the applicability of each FIL. The characterization of FILs viscosity, and consequently of their fluidity, was studied in several works, and some of the results can be found in Table 2.2.2. The results indicate that FILs with longer aliphatic and fluorinated chains increase the viscosity. The FILs composed of $[C_nF_{2n+1}SO_3]^-$ anions also present high viscosity compared with the $[C_nF_{2n-1}CO_2]^-$ anions. The nature of the FIL cation affects tremendously the viscosity. In the case of bulkier cations, a lower fluidity is found. The addition of a hydroxyl group in imidazolium cations increases the cohesive forces resulting in more viscous fluids [29,47,49–51].

The ionic conductivity has great importance, especially when correlating the molar conductivity with the fluidity obtaining the ionicity of FILs. The ionicity is evaluated by the Walden plot where FILs are classified depending on the distance to an ideal electrolyte. The ionicity can result in information on the formation of aggregates between ions due to lower

mobility [55]. The analysis of the results shows that the increment of the cationic aliphatic and the anionic fluorinated chains decreases the ionicity, diverging from the ideal behaviour. The free volume has high relevance to FILs suitability as enhanced solvents of gases or other compounds with low molecular weight [56]. The relation between refractive index and density allows the calculation of molar free volume effects, evaluating the available space for the dissolution of gases. Therefore, the increase of both hydrogenated and fluorinated chains and bulkier cations rises the molar free volume values [56].

The surface tension of FILs is the property that most differs from the conventional ILs, in which the cation's nature has a predominant influence on this property. The values of surface tension for some FILs can be found in Table 2.2.2. The surface tension of the $[C_nC_1Im][C_4F_9SO_3]$ family showed the lowest values existing in the overall ILs literature. The increment of the hydrogenated chain decreases the surface tension up to the lowest value, found for the $[C_8C_1Im][C_4F_9SO_3]$. The further increase of FILs aliphatic chain resulted in higher values of surface tension, revealing a global behaviour marked by a bowl-shaped trend. The addition of a fluorinated domain in FILs induces a competition with the aliphatic domain to protrude the interface, which dramatically changes the values of surface tension. As long as the hydrogenated chain increases to $[C_8C_1Im]^+$, a rearrangement in the organization between the non-polar domains happens, allowing both to protrude through the top layer. After $[C_8C_1Im]^+$, the aliphatic chain is much larger than the fluorinated chain, and occupies more space at the interface, increasing the values of surface tension. In the case of quaternary ammonium-based FILs, it was shown that they have lower values of surface tension compared with pyridinium cation. In FILs based on ammonium, the increment of the fluorinated chain deeply decreases the surface tension [49,52,57].

The FILs properties can be tuned by choosing the cation, anion, length of side chains and functionalization of cation, increasing the possibilities of designing the best task material. The complete determination of these properties is a complex assignment, requiring a lot of costs and time. To ease this task, theoretical models can be applied to predict their characteristics. An effort has been done in this direction obtaining several models that accurately reproduce the FILs properties of the neat FILs and the mixtures with gases and aqueous solutions [50,51,58].

2.2.1.2 Aggregation and surfactant behaviour

The behaviour of FILs in aqueous solutions is enhanced in comparison with the PFCs and conventional ILs. Non-toxic FILs based on imidazolium, pyridinium (with short aliphatic chains) and cholinium cations conjugated with the $[C_4F_9SO_3]^-$ anion were used to study the self-aggregation behaviour. These compounds are completely miscible in water at all ranges

of concentrations studied in the conductivity profile. The same behaviour was later found for imidazolium-FILs functionalised with a hydroxyl group and some examples are represented in Figure 2.2.2a. The liquid + liquid equilibria of binary systems FIL + water was also analysed to study the solubility of water. The increment of the aliphatic chain in the $[C_nC_1Im][C_4F_9SO_3]$ family increases the solubility of water in the FIL-rich phase [27,28,51,59,60].

The water-rich region was selected to determine the critical aggregation concentrations (CACs) of several FILs. $[C_2C_1Im][C_4F_9SO_3]$ showed three different transitions related to the formation of distinct aggregates. These aggregates were evaluated and associated with different self-assembled structures. These stable self-assembled structures can be the greatest contribution to the full miscibility of FILs in water. Figure 2.2.2b represents the values of the first CAC, the so-called critical micelle concentration (CMC) of FILs and conventional surfactants [61–63]. All the FILs show much lower CMC and FILs with only four carbon atoms have greater aggregation power than the conventional surfactants with eight carbon atoms. The increment of the hydrogenated chain in the $[C_nC_1Im][C_4F_9SO_3]$ family decreases the CMC value, promoting the formation of more, bulkier and better-packed structures. The longer fluorinated chains also decrease the CMC values. However, the growth of both nonpolar chains hinders the solubility in water. The pyridinium and tetrabutylammonium cations show slightly lower CMC values compared with imidazolium, cholinium or pyrrolidinium cations.

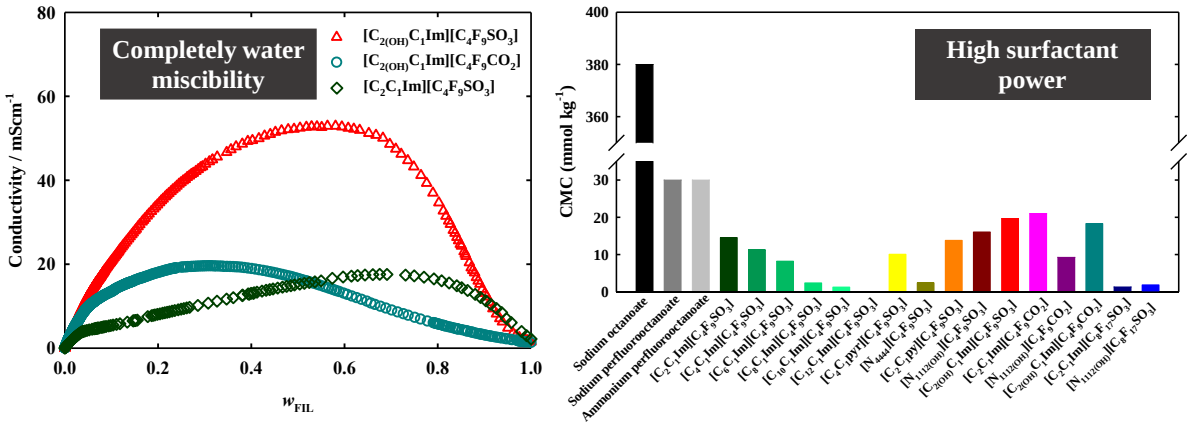

Figure 2.2.2 a) Complete conductivity profile of FILs in water at 298.15 K and b) the values of critical micellar concentrations of PFCs (grey bars) and hydrogenated (black bar) surfactants (Szajdzinska-Pietek, E. *et al.* (2000); González-Pérez, A. *et al.* (2004); López-Fontán, J.L. *et al.* (2004).) [61–63] and of the FILs (coloured bars) (Pereiro, A.B. *et al.* (2015); Teixeira, F.S. *et al.* (2015); Ferreira, M.L. *et al.* (2020); Vieira, N.S.M. *et al.* (2019)) [27,28,51,59,60].

The FILs behaviour in water was also inferred in the FIL-rich phase by investigating the hydrogen-bonding ability and polarizability through Kamlet-Taft parameters. The results indicate that increasing the fluorinated chain restricts the impact of adding water into ILs, keeping the hydrogen bond acceptance ability constant. This result indicates that the rich aggregation of FILs promotes the aggregation of water in a bulky polar network. The water

aggregates expand and drive to the proximity of the polar nanosegregated domains of the FILs due to the higher repulsion of the fluorinated counterparts [59].

2.2.1.3 Cytotoxicity, ecotoxicity and biodegradation

Cytotoxicity, partition properties, acute ecotoxicity and biodegradation are key parameters to assess the health and environmental risks of these FILs. Knowledge about structure-toxicity relationships is of great interest for the design of biocompatible and greener FILs. The design of these new compounds aims to surpass the persistency, bioaccumulation, and toxicity drawbacks of PFCs [2,4,13,18].

This section provides a critical review of the cytotoxicity in different human cell lines: human colon carcinoma cells (Caco-2), human hepatocellular carcinoma cells (HepG2), human umbilical vein cell line (EA.hy926), and spontaneously immortalized human keratinocyte cell line (HaCaT), representing the risks associated to different routes of biomedical administration. Cytotoxicity screenings, with 4 h and 24 h exposure, were performed in these cell lines. For short-chain based-FILs, such as $[C_2C_1Im][C_4F_9SO_3]$ and $[C_2C_1py][C_4F_9SO_3]$, the overall reduced toxicity can be justified by their high hydrophilicity and surfactant performance. In HaCaT cells, lower EC_{50} values were obtained for both FILs mentioned before and these results can be associated with the intrinsic properties of this cell line. Higher biocompatibility was attained with the cholinium cation conjugated with the $[C_4F_9SO_3]^-$ anion, due to the non-aromaticity and symmetry of this cation, which is also an essential nutrient for cell growth [29,31,64,65]. Similar behaviour was reported for several cholinium alkanoates [66,67]. The non-aromatic and symmetric $[N_{4444}]^+$ as well as the alicyclic pyrrolidinium cations, conjugated with the $[C_4F_9SO_3]^-$ anion, maintain the cellular viability in Caco-2, HepG2 and EA.hy926 cells. The elongation of the imidazolium hydrogenated alkyl chain length from $[C_2C_1Im]^+$ up to $[C_{12}C_1Im]^+$ prompts the decrease of the cellular viability in the Caco-2 cell line, as depicted in Figure 2.2.3a. This effect on cellular viability can be due to the presence of delocalized charges or due to the increment of lipophilicity which enhances the disruption of the cell wall [31,68]. A more pronounced decay in the cellular viability is observed with the increment of the anionic fluorinated side chain length. This effect was noticed for the variation of $[C_4F_9SO_3]^-$ to $[C_8F_{17}SO_3]^-$ or $[N(C_4F_9SO_2)_2]^-$ anions, combined with imidazolium, cholinium and ammonium-based cations [29]. The fluorinated elongation on carboxylate-based anions also engenders a significant reduction of the cellular viability in different cell lines [67]. The increment of the fluorinated domain also enhances the FILs lipophilicity and the delocalization of the charge, which is traduced in a higher permeation of the cell membranes. Inside the cell compartment, free fluoride ions are formed by hydrolytic cleavage, which can interfere with the cellular mechanisms leading to cell death [31,69]. Furthermore, hemolytic tests reveal that

red blood cell lysis only occurs at high FIL concentrations. Herein, the lowest hemolytic rates were achieved with both imidazolium and pyridinium cations conjugated with the perfluoropentanoate anion. Although the limited FILs solubility in the tested medium hampers a proper analysis of the effect of the hydrogenated and fluorinated side chain elongation, it was clear by the profiles achieved that the hemolysis accomplished higher levels in long chain-based FILs at similar or reduced concentrations than short chain-based ones [29,31,70,71].

The increment of the lipophilicity as a result of the elongation of both hydrogenated and fluorinated alkyl side chains was confirmed through the 1-octanol/water partition coefficients ($P_{o/w}$) of different FILs. As depicted in Figure 2.2.3b, the $P_{o/w}$ increases with the increment of the hydrogenated side chain length from $[C_2C_1Im]^+$ to $[C_8C_1Im]^+$. This increment is associated with a greater lipophilic behaviour, caused by stronger van der Waals interactions between the FIL alkyl side chain and the hydrophobic region of the organic solvent, promoting their solubility in the organic media. This elongation also decreases the polarity and the acidity of these compounds, and consequently their interaction with water media. The increment on the anion core from $[C_4F_9SO_3]^-$ to $[C_8F_{17}SO_3]^-$ has a more pronounced effect on the partition properties, as illustrated in Figure 2.2.3b. These results were associated with enhanced solubility in lipophilic solvents endorsed by the fluorinated moiety. Finally, the partition properties of both $[C_2C_1Im][C_4F_9SO_3]$ and $[C_2C_1py][C_4F_9SO_3]$ are quite similar due to the highly acidic methylene groups in the constitutive rings. Nevertheless, the partition properties of the studied FILs indicate that they do not accumulate or concentrate in the environment [31,72,73].

An environmental hazard assessment is also essential in the context of sustainability and green chemistry. An ecotoxicological screening to evaluate the impact of FILs in the aquatic environment was performed on the marine bacterium *Vibrio fischeri*, crustacean *Daphnia magna*, and *Lemna minor* plant. This screening was made in aquatic species owing to the selected FILs unique water miscibility. Briefly, all tested FILs present a reduced ecotoxicity for the mentioned species. The EC_{50} values indicate that FILs based on the imidazolium cation conjugated with $[C_4F_9SO_3]^-$ anion are more toxic than FILs based on other cations conjugated with the same anion. The $[C_4F_9CO_2]^-$ anion is also less toxic than the sulfonate equivalent, except for the hydroxylated based imidazolium cations in *Daphnia magna* and *Lemna minor*. Even so, the $[C_4F_9SO_3]^-$based anion is less toxic than the bis(trifluoromethylsulfonyl)imide ($[N(CF_3SO_2)_2]^-$) anion for both *Vibrio fischeri* and *Daphnia magna* [30,65]. Furthermore, both cholinium and hydroxylated imidazolium cations are the least toxic of the three aquatic species [66]. The functionalization of the imidazolium cation decreases the lipophilicity of these compounds and consequently decreases their overall toxicity. Finally, it must be stated

that based on *Daphnia magna* and *Lemna minor* EC_{50} values and accordingly to the "Globally Harmonized System of Classification and Labelling of Chemicals", these FILs do not need to be categorized in terms of acute aquatic hazards. It must be noticed that both cytotoxicity and ecotoxicity results are highly dependent on the target organisms and exposure times, then different species and long-term effects of these compounds must be accessed prior to a large-scale application [30,31,67].

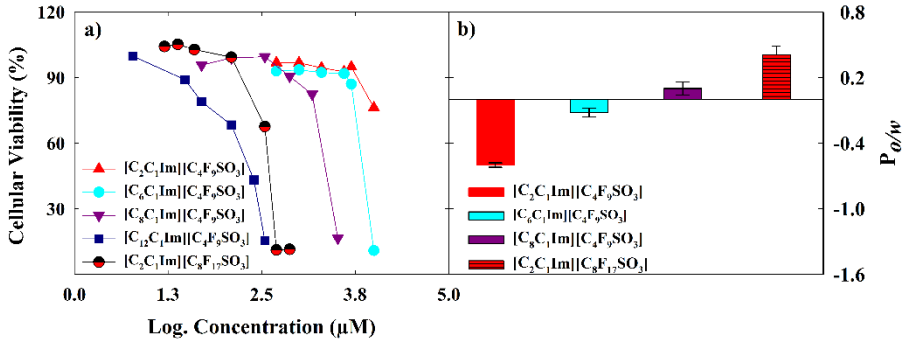

Figure 2.2.3 a) Cellular viability for imidazolium-based FILs with the increment of hydrogenated and fluorinated alkyl side chain length; b) effect of the hydrogenated and fluorinated alkyl side chain length on the 1-octanol/water partition coefficient ($P_{o/w}$) of imidazolium-based FILs. Adapted from Vieira, N.S.M. *et al.* (2019) [31].

Besides, FILs conjugated with the perfluoropentanoate anion generally induce less toxicity than the sulfonate equivalent. For the Gram-negative *Pseudomonas stutzeri*, the inhibition of the bacterial growth was only achieved at very high FIL concentrations, the cholinium cation was shown to be the least toxic, especially when conjugated with the perfluoropentanoate anion, and the increment of either hydrogenated or fluorinated alkyl generated more ecotoxic FILs [30].

The microbial degradation of some FILs showed that short chain-based imidazolium FILs are highly resistant to biodegradation, even with the incorporation of hydroxyl groups. A certain biodegradability occurred in the short-chained pyridinium-based FIL, associated with the oxidation of the alkyl side chain. However, some variability is associated with the biodegradation of these cations that must be associated with the differences in microbial compositions involved in the degradation process. The higher degrees of biodegradation obtained with the cholinium-based FILs are only related to the cation core degradation that retains 75% of the oxidizable carbon [30,74,75]. To overcome the high resistance associated with these compounds, removal or degradation alternative routes must be studied. According to these published results, a proper combination between cations and short-chained fluorinated anions may result in biocompatible FILs with the potential to be biodegradable by alternative routes. Even though the strong C-F bonds present in the anions make FILs highly inert compounds, on one hand, the resistance to biotic and abiotic degradation raises concerns

about their persistence in the environment and on other hand their degradation can generate even more toxic intermediate compounds [30]. Therefore, strategies to overcome the lack of biodegradability of FILs must be found to enable the usage of FILs in their potential applications. These biocompatible FILs can support the application of FILs as task-specific materials in a broad range of applications, from biomedical to reaction media in industrial processes.

2.2.2 Applications of fluorinated ionic liquids

2.2.2.1 Biomedical applications

2.2.2.1.1 Artificial gas carriers

The need for new products to replace the blood transfusions appeared at the beginning of the 21st century because of cross-infection derived from the human immunodeficiency virus (HIV). The lack of safety and trust allied with the severe shortages and increased demand for blood supplies have contributed to the search for an ideal artificial gas carrier (AGC). PFCs-based emulsions are among the substances under clinical trials used to substitute the red blood cells in critical situations such as acute blood loss [3,76]. However, the PFCs have several handicaps that can restrict their usage as AGCs, such as high vapour pressures and poor solubility in water. With the aim to solve these limitations, FILs appeared as a solution to replace the PFCs fully or partially in AGC emulsions. Different works have been developed to infer this prospect. The results show the possibility to design FILs with complete water miscibility, which solves one of the greatest handicaps. The study of phase equilibria between FILs and two PFCs, perfluorodecalin and perfluorooctane, indicated that the enthalpic contributions are larger than the entropic contributions, which results in a favourable process of solvation of PFCs by FILs. The high surfactant behaviour of FILs is also a huge advantage because it enables the stabilization of AGC emulsions, which can be favourable to reducing the usage of excipients and enhancing the solubilization of the respiratory gases. The reduced cytotoxicity and ecotoxicity determined for FILs with the characteristics above-mentioned strengths the possible use of these compounds in the biomedical field. The greatest aspect that spurs the use of FILs as potential substitutes for PFCs in AGC emulsions is their higher ability to solubilize oxygen, carbon dioxide and nitrogen, compared to the conventional fluorine-containing ILs and with PFCs. However, the formulation of an emulsion with high efficacy and the implementation of tests on physiological safety and other health studies must be carried out before applying FILs [27,28,51,77–79].

2.2.2.1.2 Drug delivery systems

Although there are several studies dealing with ILs for the solubilisation and stabilization of proteins, dissolution of low soluble active pharmaceutical ingredients (APIs), and development of drug formulations and delivery systems, the application of FILs in this field of pharmaceutical development is quite unexplored [64,80–83]. Our research group initiated a pioneering research line to use FILs as drug delivery systems (DDSs) [84–86]. These novel biocompatible carriers can overcome the problems associated with proteins administration (*e.g.* sensibility to environmental conditions, short-half lives in the bloodstream, structural conformation and hydrophobic/hydrophilic nature that hamper the in vivo delivery) [87,88] and their traditional delivery platforms (low stability, uncontrolled release, and low encapsulation efficiency) [89]. FIL-based DDSs have been shown the potential to increase the safety and effectiveness of the therapeutic biomolecules, reducing the dosage needed and enabling a time and site-specific release. The application of FILs as DDSs and stabilizing agents was firstly evaluated for two different model proteins, lysozyme, and bovine serum albumin (BSA) [87,88].

Lysozyme is a protein with antiviral, antitumor and immunological properties, whereas BSA is involved in organism homeostasis and the transport of several components essential for several vertebrates' body functioning [90,91]. For these applications, FILs based on imidazolium, pyridinium and cholinium cations, conjugated with $[C_4F_9SO_3]^-$ and $[C_4F_9CO_2]^-$ anions were selected due to biocompatibility and improved surfactant behaviour. The tested FILs concentrations cover values above and below their CMCs values (Figure 2.2.2b). Concentrations above CMC were chosen due to their ability to self-assembling in micellar structures that can be used to protect, encapsulate, and deliver the therapeutic proteins. The stability of both proteins in the presence of FILs was determined based on the variations observed in the melting temperature of the biomolecules. The stability of lysozyme is not significantly affected by the incorporation of FILs, and only a slight decrease was achieved with $[C_2C_1py][C_4F_9CO_2]$ with a minor reduction of 2% in the melting temperature of the protein. However, for BSA the melting temperature increases for all tested FILs concentrations, suggesting a stabilization of the protein. These distinct results indicate a specific interaction between FILs and each tested protein. The differences in the interactions of the two biomolecules with FILs were also supported by structural studies. Both circular dichroism (CD) and Fourier transformed infrared spectroscopy results suggest no substantial lysozyme structural modifications in the presence of cholinium and $[C_2C_1Im][C_4F_9SO_3]$ FILs, respectively. For BSA, a slight increment in molar ellipticity and α-helical content, followed by a β-sheet and random coil reduction, observed in CD results, indicate a stabilization of the secondary structure, and a more compact state of the protein with $[N_{1112(OH)}][C_4F_9SO_3]$.

Furthermore, in the presence of FILs, the biological activity of lysozyme increased, even at concentrations where the encapsulation of the protein inside the micelles occurs. Although there are differences in the interactions between the two different proteins and the FILs, the stability, activity, and secondary structure of biomolecules are not negatively impacted by the selected fluorinated compounds [84,85,92].

The aggregation behaviour of different FILs was analysed in the protein medium. No significant variations were achieved in the FILs self-aggregation process in aqueous solutions. To prove the encapsulation of lysozyme in the aggregates of FILs, the self-assembled structures were studied through dynamic light scattering (DLS). As illustrated in Figure 2.2.4a, an encapsulation of the protein at a concentration of approximately twice the FILs CMC (1.2% v/v) is expected based on the disappearance of the intensity peak of lysozyme (~4nm). This encapsulation is driven by the fluorinated surfactant core of the FILs since the lysozyme characteristic peak remains present for the non-surfactant ILs. This encapsulation was indorsed spectrophotometrically with the concentration of lysozyme in the solution being reduced with the addition of 1.2% v/v $[C_2C_1Im][C_4F_9SO_3]$. Moreover, the FIL-protein aggregates became more stable after 24h and a maximum stabilization was verified after 96h. The lysozyme encapsulation in $[C_2C_1Im][C_4F_9SO_3]$ was also evidenced, illustrated in Figures 2.2.4b and 2.1.4c.

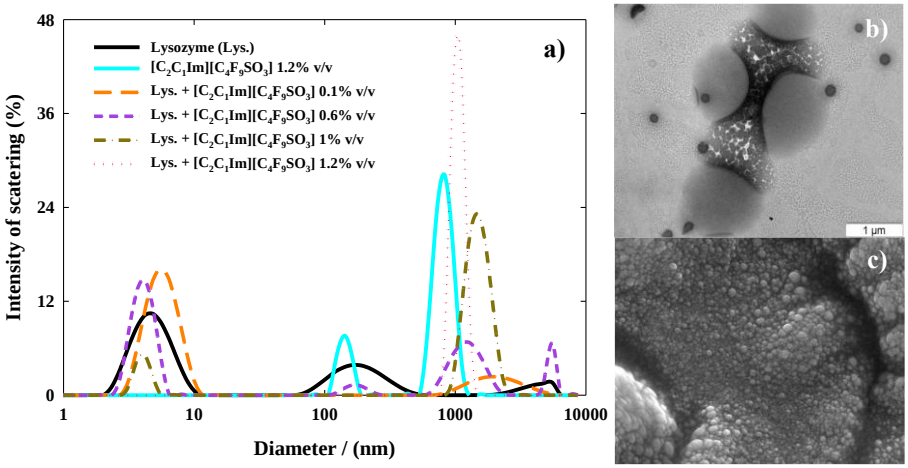

Figure 2.2.4 a) DLS spectra of lysozyme in buffered medium upon the addition of $[C_2C_1Im][C_4F_9SO_3]$ at several concentrations; b) TEM image of $[C_2C_1Im][C_4F_9SO_3]$ 1.2% v/v with lysozyme; c) SEM image of $[C_2C_1Im][C_4F_9SO_3]$ 1.2% v/v with lysozyme. Adapted from Alves, M. *et al.* (2017) [84,85].

Figure 2.2.4b depicts the solution of lysozyme with 1.2% v/v of $[C_2C_1Im][C_4F_9SO_3]$ analysed by transmission electron microscopy (TEM), where an external darker counter surrounding the aggregates of FILs is associated with the heavier elements present in the anion, in contrast to the lighter grey shades of the lysozyme. Moreover, the micellar sizes obtained by TEM are similar to the hydration diameters measured by DLS. A qualitative analysis through scanning

electron microscopy (SEM), Figure 2.2.4c, reveals an external surface of the solution containing lysozyme with 1.2% v/v of $[C_2C_1Im][C_4F_9SO_3]$ similar to the FILs blank solution depicted in Alves, M. *et al.* (2017) [84,85,92].

The interaction and the encapsulation between $[C_2C_1Im][C_4F_9SO_3]$ and BSA were proved through isothermal titration calorimetry (ITC). BSA interacts with the $[C_2C_1Im][C_4F_9SO_3]$ monomers causing conformational changes, as well as hydrogen bonding and hydrophobic interactions. The aggregation of $[C_2C_1Im][C_4F_9SO_3]$ in buffer determined by conductimetry was also supported by the ITC measurements. However, ITC indicates that the interaction between BSA and FIL is stronger than the FIL self-aggregation. A different interaction between BSA and the FIL aggregates, not identified in the conductivity measurements, strongly supports the encapsulation of this protein inside the FILs aggregates.[1]

After the first proof of concept dealing with the encapsulation of lysozyme inside the FIL aggregates, the optimal incubation temperature of the protein for 24h was determined at 4˚C without a significant loss of protein activity. The encapsulation efficiencies of lysozyme in both $[C_2C_1Im][C_4F_9SO_3]$ and $[C_2C_1py][C_4F_9SO_3]$ at 1.8% v/v (3 times higher than CMC) range from 69.4 to 83.4%, values similar or higher than the obtained with other traditional platforms. This lysozyme remains encapsulated up to 12h post-incubation at 4˚C, without significant losses of biological activity. This longer retention of the biomolecule inside the FILs aggregates can be caused by the high stability of the fluorinated counterpart of the IL, as well as by the interaction between FIL and protein. Furthermore, the biomolecule release was accomplished after the application of several external stimuli. With the increment of temperature up to 37˚C, simulating the average body temperature, lysozyme is completely released from the aggregated structures after 6h. This complete release was also achieved after the exposure to an ultrasound bath with a frequency of 80 kHz for 1h. This approach can be applied for a site-specific and controlled delivery of therapeutic proteins through FILs based DDS. Furthermore, within the same time frame at 42˚C, the protein released range from 57% and 39% to $[C_2C_1Im][C_4F_9SO_3]$ and $[C_2C_1py][C_4F_9SO_3]$ based DDS, respectively, suggesting that under a pathological condition the protein can be released at some relevant extent after 1h post-administration. The biological activity of the released protein remains above 50% for all the tested scenarios, except for the release after 12h at 37 ˚C. Then, biocompatible FILs can be designed to encapsulate different therapeutic proteins with good levels of encapsulation efficiencies promoting a site-specific and thermoresponsive release under different external stimuli. The differences in the effect of FILs in both lysozyme and BSA support the need to further study the interactions of these fluorinated compounds with other therapeutic biomolecules prior to the design of the DDS [86].

2.2.3 Conclusions

In this section, the application of FILs as task-specific materials was fully described to be employed in both biomedical and engineering separation processes. The characteristic fluorinated domain and the different ions' structural features prove to have a dominant effect on the thermophysical and thermodynamic properties of FILs. Moreover, FILs have great surfactant behaviour and complete miscibility in water systems. The design of biocompatible and eco-friendly FILs without comprising their surfactant behaviour was demonstrated which ultimate the applicability of FILs as enhanced materials compared with PFCs and conventional fluorinated ILs.

The applicability of biocompatible FILs for biomedical applications was demonstrated by their great power to solubilize respiratory gases, supporting their use as artificial gas carriers. Additionally, the interaction and the encapsulation of different proteins in FIL aggregates, without comprising the biological features of the biomolecules, also represents an advance in the application of FILs to pharmaceutical development. Finally, FILs exhibit great ability to be used individually, or in the development of materials to be further applied to the separation and recovery of F-gases, essentially due to their great free volume and gas-FIL enhanced interactions. To conclude, the discussion offered by this section highlights the identification of FILs as a novel and endless tool for the design of materials and processes whereas their fluorinated nanosegregated domain in combination with their ionic nature can provide unique features.

2.3 Understanding the phase and solvation behaviour of fluorinated ionic liquids

This section covers the most significant literature regarding the phase equilibria of FILs with other substances obtained by experimental and modelling approaches. The work is divided into four major sections. First, an overview of the FILs' exceptional properties that differentiate them from the conventional ILs and traditional fluorinated compounds is presented. Then, the vapour-liquid equilibria (VLE) of different gases with FILs are analysed in three main groups: (i) the direct measurement of the solubility of gases, such as carbon dioxide (CO_2), oxygen (O_2), nitrogen (N_2), hydrogen (H_2), and F-gases, in FILs; (ii) the use of membranes as a platform to improve the absorption of gases in FILs; and (iii) the use of molecular modelling approaches to predict the VLE behaviour of gas + FILs systems. The section also includes the few works found in the literature related to the liquid-liquid equilibria (LLE) and solid-liquid equilibria (SLE) behaviour of FILs, which have high significance for their potential applications. The last section focuses on the analysis and discussion of the main findings related to the phase behaviour of FILs, and the remaining challenges associated with the experimental and theoretical studies of these systems. The nomenclatures and structures of the compounds included in this work can be found in Table 2.3.1.

Table 2.3.1 Structure and nomenclatures of the cations and anions composing the ionic liquids, the fluorinated gases, and the perfluorocarbons mentioned in this study.

Cations	
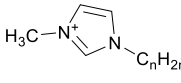 **$[C_nC_1Im]^+$** n = 2, 4, 5, 6, 8, 10, 12 1-alkyl-3-methylimidazolium	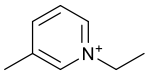 **$[C_2C_1py]^+$** 1-ethyl-3-methylpyridinium
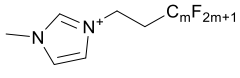 **$[C_2(C_mF_{2m+1})C_1Im]^+$** m = 4, 6 1-methyl-3-ethyl(perfluoroalkyl)imidazolium	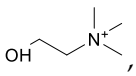 , **$[N_{1112(OH)}]^+$** Cholinium
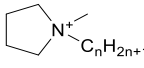 **$[C_nC_1pyr]^+$**, n = 2,4 N-alkyl-N-methylpyrrolidinium	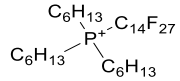 **$[P_{66614}]^+$** Trihexyltetradecylphosphonium
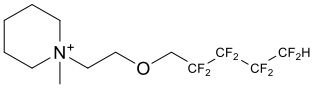 **$[C_{2(O)1(4F)}C_1pip]^+$** N-((2,2,3,3,4,4,5,5-octafluoropentoxy)ethyl)-N-methylpiperidinium	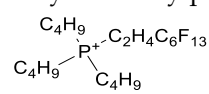 **$[P_{4442(6F)}]^+$** Tributyl-(3,3,4,4,5,5,6,6,7,7,8,8,8-tridecafluorooctyl)-phosphonium
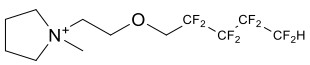 **$[C_{2(O)1(4F)}C_1pyr]^+$**	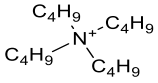 **$[N_{4444}]^+$**

N-((2,2,3,3,4,4,5,5-octafluoropentoxy)ethyl)-N-methylpyrrolidinium 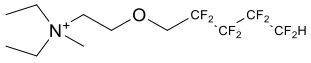 **$[N_{2212(O)1(4F)}]^+$** N,N-diethyl-N-methyl-N-((2,2,3,3,4,4,5,5-octafluoropentoxy)ethyl)-N-ammonium	Tetrabutylammonium 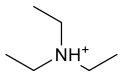 **$[N_{0222}]^+$** Triethylammonium
Anions	
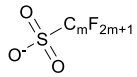 **$[C_mF_{2m+1}SO_3]^-$**, m = 1, 4, 6, 8 Perfluoroalkylsulfonate	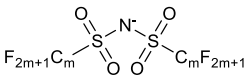 **$[N(C_mF_{2m+1}SO_2)_2]^-$** m = 1, 2, 4 Bis(perfluoroalkylsulfonyl)imide
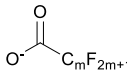 **$[C_mF_{2m+1}CO_2]^-$**, m = 4, 7, 8 Perfluoroalkylcarboxylate	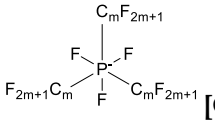 **$[C_mFAP]^-$**, m = 2, 4 Tris(perfluoroalkyl)trifluorophosphate
 **$[BF_4]^-$** Tetrafluoroborate	 **$[PF_6]^-$** Hexafluorophosphate
 **$[SCN]^-$** Thiocyanate	 **$[C_1CO_2]^-$** Acetate
Fluorinated Gases	
 **R-32 (CH_2F_2)** Difluoromethane	 **R-14 (CF_4)** Tetrafluoromethane
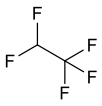 **R-125 (C_2HF_5)** Pentafluoroethane	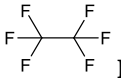 **R-116 (C_2F_6)** Hexafluoroethane
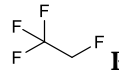 **R-134a ($C_2H_2F_4$)** 1,1,1,2-Tetrafluoroethane	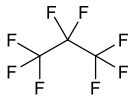 **R-218 (C_3F_8)** Octafluoropropane
 **R-23 (CHF_3)** Trifluoromethane	 **R-143a ($C_2H_3F_3$)** 1,1,1-Trifluoroethane
 **R-152a ($C_2H_4F_2$)** 1,1-Difluoroethane	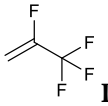 **R-1234yf ($C_3H_2F_4$)** 2,3,3,3-Tetrafluoropropene
Perfluorocarbons	
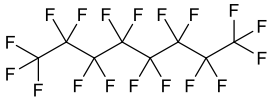 **C_8F_{18}** Perfluorooctane	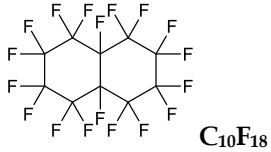 **$C_{10}F_{18}$** Perfluorodecalin

2.3.1 Gas solubility in fluorinated ionic liquids

2.3.1.1 Solubility of carbon dioxide in fluorinated ionic liquids

One of the main features of FILs is their ability to solubilize gases, and a great amount of work has focused on the solubility of CO_2 in FILs as a way to capture it, given its relevance in the context of reducing CO_2 emissions. Baltus *et al*. were the first to report the solubility of CO_2 in the $[C_2(C_6F_{13})C_1Im][N(CF_3SO_2)_2]$. A Henry constant ($H_C$) of 0.45 ± 0.1 MPa was obtained at 298.15 K [93], and later corrected to 0.6 ± 0.1 MPa [94]. Muldoon *et al*. later measured the solubility of CO_2 in $[C_2(C_4F_9)C_1Im][N(CF_3SO_2)_2]$ and obtained a H_C almost five times greater than that obtained by Baltus and co-workers for $[C_2(C_6F_{13})C_1Im][N(CF_3SO_2)_2]$, showing that an increment in 2 carbons of the fluorinated side chain of an imidazolium cation highly favoured the solubility of CO_2 (lower value of H_C). Muldoon *et al*. measured solubility in $[C_2(C_6F_{13})C_1Im][N(CF_3SO_2)_2]$ obtaining a H_C value of 2.73 ± 0.02 MPa at 298.15 K, which is close to the value for $[C_2(C_4F_9)C_1Im][N(CF_3SO_2)_2]$, 2.84 ± 0.01 MPa (see Figure 2.3.1) [95]. Hou *et al*. also determined the absorption and diffusivity of CO_2 in $[C_2(C_4F_9)C_1Im][N(CF_3SO_2)_2]$ obtaining a H_C of 3.1 ± 0.2 MPa at 298.15 K [96]. As can be seen in Figure 2.3.1, this value is identical to the results obtained by Muldoon *et al.* agreeing within 4%. Later on, Almantariotis *et al.* [97] measured the CO_2 uptake by $[C_2(C_6F_{13})C_1Im][N(CF_3SO_2)_2]$ resulting in a H_C value near to the one obtained by Muldoon and co-workers, agreeing in 3% (Figure 2.3.1). The large difference in the H_C obtained from different authors derives from the use of different experimental methods; hence, care must be taken when selecting the method.

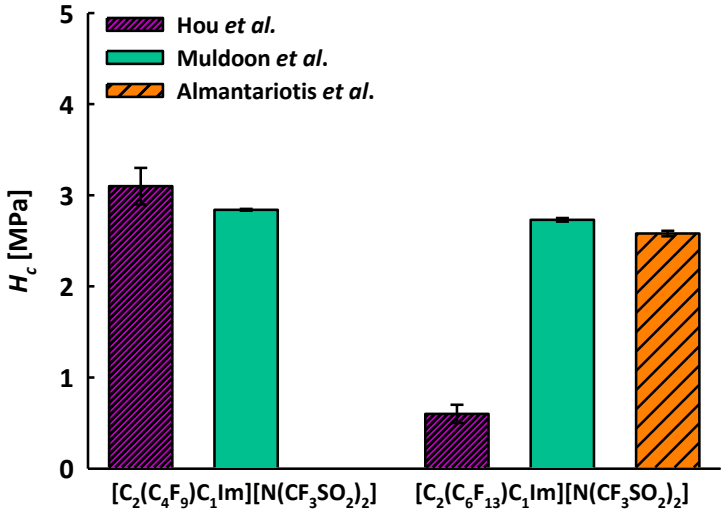

Figure 2.3.1 Comparison of H_C for CO_2 in FILs with cationic fluorinated tags at 298 K. The values of $[C_2(C_4F_9)C_1Im][N(CF_3SO_2)_2]$ are from Hou, Y. and Baltus, R.E. (2007) [96], and for $[C_2(C_6F_{13})C_1Im][N(CF_3SO_2)_2]$ from Muldoon, M.J. *et al.* (2007) and Almantariotis, D. *et al.* (2010) [95,97].

Therefore, the introduction of a fluorinated alkyl chain in the imidazolium cation increases the ability to absorb CO_2. However, it reaches a point where an increment of the fluorinated tag does not significantly increase the uptake of CO_2 by FILs. It is important to point out that the comparison with analogous non-fluorinated FILs demonstrated that the presence of a fluorinated side chain significantly increases the solubility of CO_2. Almantariotis *et al.* used molecular simulations to explain the molecular mechanism of solvation of FILs, concluding that CO_2 is solvated near the charged domains, but also close to the cationic fluorinated chain, increasing the areas of absorption [97].

As depicted in Figure 2.3.2, the solubility of CO_2 in $[C_2(C_4F_9)C_1Im][N(CF_3SO_2)_2]$, $[C_2(C_6F_{13})C_1Im][N(CF_3SO_2)_2]$, $[C_4C_1Im][C_7F_{15}CO_2]$, $[C_5C_1Im][C_4FAP]$, and $[C_4C_1Im][C_4F_9SO_3]$ at 333.15 K [95,98,99], is similar for all the FILs, with $[C_5C_1Im][C_4FAP]$ presenting the highest solubilization capacity, followed by the FILs with fluorinated cations. The FILs with less ability to solubilize CO_2 are the ones with linear fluorinated anions. The FIL with a bulky anion showed higher CO_2 solubilization capacity than the ones with linear anions, indicating that the number and disposition in the space of the fluorine atoms are two factors influencing the gas solubility. It is important to underline the similarity of the values for $[C_4C_1Im][C_7F_{15}CO_2]$ and $[C_4C_1Im][C_4F_9SO_3]$, which can indicate that the sulfonate functional group might have a positive effect on the solubility of CO_2 or the fluorinated chain with seven carbons diminish the solubility of CO_2.

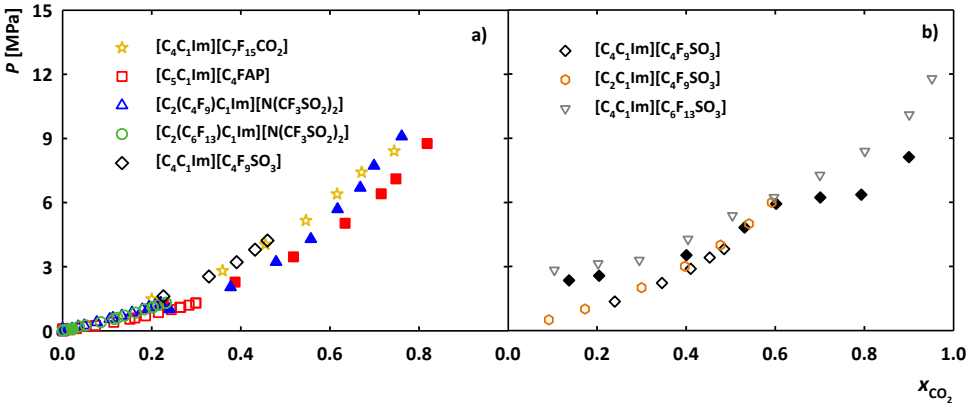

Figure 2.3.2 Solubility data (from literature) of CO_2 in FILs at a) 333.15 K and b) 313.15K. The stars, squares, and upward-pointing triangles up refer to the work of Muldoon, M.J. *et al.* (2007), where two techniques were used for high (filled symbols) and low (empty symbols) pressures. The empty circles refer to the data of Muldoon, M.J. *et al.* (2007) and the filled circles of Almantariotis, D. *et al.* (2010). The empty diamonds represent the data of Zhou, L. *et al.* (2014) and the filled diamonds of Hong, S.K. *et al.* (2016). The hexagons and downward-pointing triangles are from Watanabe, M. *et al.* (2016) and Hong, S.K. *et al.* (2014), respectively [95,97,99,100].

In order to show the effect of increasing the linear fluorinated chain of the anion on the CO_2 solubility, Figure 2.3.2b, showcases a comparison between the solubility of CO_2 in

$[C_2C_1Im][C_4F_9SO_3]$, $[C_4C_1Im][C_4F_9SO_3]$, and $[C_4C_1Im][C_6F_{13}SO_3]$ [98–101]. While the increment of the hydrogenated chain from 2 carbon atoms ($[C_2C_1Im][C_4F_9SO_3]$) to 4 carbon atoms ($[C_4C_1Im][C_4F_9SO_3]$) does not change CO_2 solubility, the increment of the fluorinated alkyl chain of the anion from 4 carbon atoms ($[C_4C_1Im][C_4F_9SO_3]$) to 6 carbon atoms ($[C_4C_1Im][C_6F_{13}SO_3]$) slightly reduces the gas solubility. Therefore, similarly to the cations, there is a point at which the increase of fluorination content of the anion does not favour the solubility of CO_2. This behaviour was also observed by Raveendran and Wallen [102] when studying the solubility of CO_2 in fluorocarbons using computational methods, and discussed by Muldoon *et al.*, inferring that an optimum density of fluorine atoms is required to have an ideal CO_2-philicity [95].

2.3.1.2 Solubility of oxygen, nitrogen, and hydrogen in fluorinated ionic liquids

To the best of our knowledge, only three works reported the direct solubility of O_2, N_2, and H_2 in FILs. Watanabe *et al.* measured the solubility of these three gases in $[C_4C_1Im][C_4F_9SO_3]$ at 323.15 K, as presented in Figure 2.3.3a. $[C_4C_1Im][C_4F_9SO_3]$ has a higher affinity to O_2, followed by N_2 and H_2, with selectivity values (determined from the H_C for each gas) for the separation of CO_2/O_2, CO_2/N_2, and CO_2/H_2 of 8, 6, and 22, respectively. These results highlight this FIL as a great candidate for gas capture and separation processes [101].

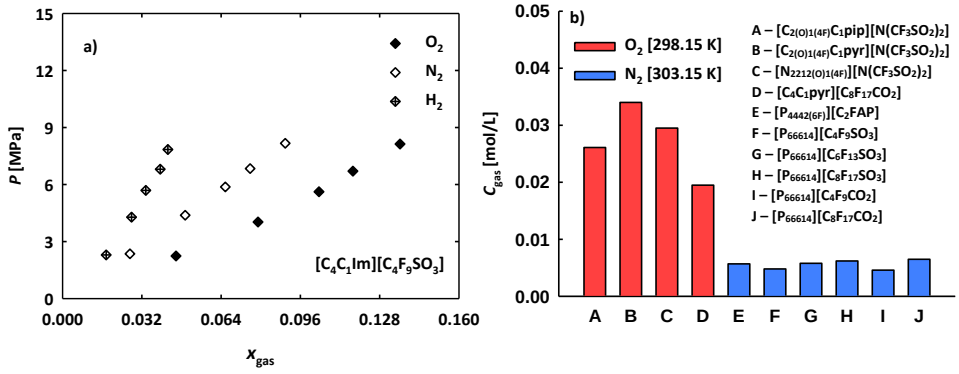

Figure 2.3.3 Solubility of O_2, N_2, and H_2 in FILs at a) 323.15 K from Watanabe, M. *et al.* (2016) [101] and b) atmospheric pressure from Vanhoutte, G. *et al.* (2018) and Kang, C.S. *et al.* (2018) [103,104].

Vanhoutte *et al.* studied the solubility of O_2 at 298.15 K in FILs based on $[C_{2(O)1(4F)}C_1pip]^+$, $[C_{2(O)1(4F)}C_1pyr]^+$, and $[N_{2212(O)1(4F)}]^+$) cations and on the $[N(CF_3SO_2)_2]^-$ anion, as well as in $[C_4C_1pyr][C_8F_{17}CO_2]$ (Figure 2.3.3b). The fluorination was shown to significantly increase the solubility of O_2, being five times higher than that of the corresponding non-fluorinated IL. Moreover, the solubility of O_2 is higher in the FIL based on $[C_{2(O)1(4F)}C_1pyr]^+$, followed by $[N_{2212(O)1(4F)}]^+$ and $[C_{2(O)1(4F)}C_1pip]^+$. The FIL $[C_4C_1pyr][C_8F_{17}CO_2]$ has the lowest O_2 absorption [103]. Kang *et al.* measured the N_2 solubility in phosphonium-based FILs at 303.15

K (Figure 2.3.3b) and observed that increases by incrementing the anionic fluorinated chain: $[C_4F_9SO_3]^-$ < $[C_6F_{13}SO_3]^-$ < $[C_8F_{17}SO_3]^-$ and $[C_4F_9CO_2]^-$ < $[C_8F_{17}CO_2]^-$. This increment is more significant from $[C_4F_9SO_3]^-$ to $[C_6F_{13}SO_3]^-$ than from $[C_6F_{13}SO_3]^-$ to $[C_8F_{17}SO_3]^-$. The same can be concluded by the similar uptake of N_2 by $[P_{4442(6F)}][C_2FAP]$ (with a cationic fluorinated chain of 6 carbons atoms and a bulky fluorinated anion) and $[P_{66614}][C_6F_{13}SO_3]$ [104].

2.3.1.3 Solubility of fluorinated greenhouse gases in fluorinated ionic liquids

As mentioned, most of the studies on gas solubilization in FILs have focused on CO_2. However, the investigation of less common greenhouse gases, such as fluorinated gases, is still scarce, although clearly relevant. These F-gases have high GWP and their emission into the atmosphere must be avoided. Most of the research on the absorption of HFCs, such as R-32, R-125, R-134a, R-23, R-143a, and R-152a, in ILs, is focused on imidazolium- and pyridinium-based ILs containing the anions $[BF_4]^-$, $[PF_6]^-$, $[N(CF_3SO_2)_2]^-$, and $[CF_3SO_3]^-$[105–114]. Additionally, some authors have focused on phosphonium-based ILs [115,116]. These studies showed that the hydrogen–fluorine interactions established between the ILs and the HFCs lead to different solubilization degrees in each IL-HFC pair. A positive correlation was found between the presence of fluorine atoms in the cations and anions of the ILs and the solubilization of F-gases, at least up to a certain fluorination degree [34,117–119]. Additionally, the chain length/volume and dipole moment of F-gases, which are related to their structures and fluorination degree, was also shown to strongly affect solubilization [120]. By changing the constitution of each IL and the operational conditions (*e.g.*, temperature and pressure) it is possible to develop separation processes where the solubilization of one gas is favoured in relation to other gases in a mixture, hence, increasing the selectivity. Therefore, ILs have been investigated for the separation of azeotropic HFC refrigerant mixtures, such as R-410A (50 *wt* % R-125 + 50 *wt* % R-32) [121] and of blends of HFCs with other gases [109].

Regarding FILs investigation for the solubilization of F-gases, Sosa and co-workers compared the solubilization of the HFCs R-32, R-125, and R-134a in imidazolium-based ILs containing $[C_1CO_2]^-$, $[CF_3SO_3]^-$, and $[N(CF_3SO_2)_2]^-$ anions with that obtained in imidazolium- and pyridinium-based FILs containing $[C_4F_9CO_2]^-$ and $[C_4F_9SO_3]^-$ anions. Their work demonstrated the relevance of the fluorination of the anions of FILs and the nanosegregated domains for the establishment of FIL-gas interactions and increasing gas solubility [121].

To circumvent the unfavourable properties of some FILs, such as the toxicity, poor biodegradability, high viscosity, high melting temperature of those with long fluorinated alkyl side chains, and high production costs, deep eutectic solvents are emerging as an alternative. Despite having different chemical properties from the ones of ILs, they share some physical properties such as high tuneability, low vapour pressure, and non-flammability [122]. Some

authors have studied the solubility of HFCs in DES prepared from ILs, but no higher solubilities were determined when compared with the corresponding ILs. Nevertheless, Castro and co-workers prepared new DES by mixing FILs with high melting points, based on cholinium, imidazolium, or tetrabutylammonium cations, with 4-carbon perfluoroalkyl acids, showing the advantages of the properties of FILs in the liquid state at a wider range of temperatures for the solubility of a variety of HFCs compared to traditional ionic liquids [123].

2.3.1.4 Molecular modelling of gas solubility in fluorinated ionic liquids

The great diversity of ILs that can be synthesized by different cation/anion combinations and by different functionalization makes their fully experimental characterization almost an impossible task. This has urged the use of theoretical tools to predict and model ILs to fasten the determination of their properties and the characterization of their mixtures. A rising number of publications have been released concerning the implementation of theoretical methods to carry out the characterization of the behaviour of different gases in ILs and DESs [36,37,41,105,124–127]. In this section, we focused our attention on the works that have been published related to FILs.

Almantariotis *et al.* carried out molecular simulations of $[C_2(C_6F_{13})C_1Im][N(CF_3SO_2)_2]$, searching for a solvation mechanism to explain the solubilization of CO_2 [97]. Sistla *et al.* computed the solubility parameters of several FILs through molecular simulations. The prediction of 210 ILs solubility parameters was obtained and compared with the ones of CO_2, concluding that the fluorinated anions and phosphonium cations favour the capture and separation of CO_2 [125].

Atomistic force field methods are of great relevance to clarifying the molecular features and local structure of ILs, elucidating mechanisms of ILs behaviour that sometimes cannot be explained by experimental methods. However, it is a time-consuming approach and other tools based on correlative methods, hybrid quantum chemical/statistical thermodynamics, and molecular-based equations approaches have gained importance. Recently, Liu *et al.* proposed an ionic polarity index parameter based on quantum chemical methods to correlate the CO_2 solubility in ILs. The authors presented a useful strategy to pre-screen possible cations and anions to design ILs with high CO_2-philicity [128]. Several works have focused, with the support of modelling approaches, on the development of technologies to mitigate the environmental impact of F-gases. A COSMO-based/Aspen Plus methodology was successfully employed to evaluate the performance of $[C_2C_1Im][C_4F_9SO_3]$, $[C_2C_1Im][C_8F_{17}SO_3]$, $[C_2C_1Im][C_4F_9CO_2]$, $[C_2C_1Im][N(C_4F_9SO_2)_2]$, $[C_2C_1py][C_4F_9SO_3]$, $[C_2(C_6F_{13})C_1Im][N(CF_3SO_2)_2]$ and $[C_2(C_6F_{13})C_1Im][N(C_2F_5SO_2)_2]$ as HFCs (R-32 and R-134a) absorbents in a commercial packing column at process scale. ILs with shorter fluorinated chains were demonstrated to

have the best thermodynamic performance for HFC capture. The longer FILs have a higher viscosity, which results in lower efficiencies because the process is controlled by mass transfer kinetics [129]. Moreover, the absorption of F-gases in FILs [121] and on DESs based on mixtures of FILs and perfluorinated acids [123] has been successfully correlated with the non-random two-liquid (NRTL) model, allowing the implementation of simulation studies for the development of new separation processes.

Equations of state (EoS) have been established as one of the most used ways to predict the phase behaviour of gases in FILs. Hong and co-workers have used two classical cubic EoS, the Peng-Robinson EoS and the Soave-Redlich-Kwong EoS, to correlate the VLE data of CO_2 in $[C_4C_1Im][C_4F_9SO_3]$ and $[C_4C_1Im][C_6F_{13}SO_3]$ [98,100]. Zhou *et al.* employed the Krichevsky-Kasarnovsky equation to correlate the experimental data of CO_2, O_2, N_2, and H_2 solubility in the FIL $[C_4C_1Im][C_4F_9SO_3]$ [99]. Watanabe *et al.* used the Sanchez-Lacombe EoS to correct the buoyancy effects at high pressures of experimental data of $[C_2C_1Im][C_4F_9SO_3]$ with a CO_2 gas system [101]. Among the most used EoS are the molecular-based SAFT approaches, based on Statistical Mechanics, which explicitly consider structural details of the ILs, including the molecular size, shape, and hydrogen bonding formation in the formulation of the equation. The soft-SAFT EoS, proposed by Blas and Vega, has been applied in the description of gas behaviour in FILs and DESs [130,131]. Ferreira *et al.* showed a comprehensive analysis of several FILs studied in literature by using soft-SAFT, predicting their CO_2 solubility [58]. Soft-SAFT EoS has also been used to predict the solubilities of atmospheric gases (CO_2, N_2, and O_2) in pyridinium and imidazolium-based FILs conjugated with the $[C_4F_9CO_2]^-$ and $[C_4F_9SO_3]^-$ anions [77]. These works allowed the finding of FILs structural features that favour the solubilization of those gases, using a limited amount of experimental data. Alkhatib *et al.* have successfully applied the soft-SAFT EoS to the screening of potential ILs, including some FILs such as $[C_nC_1Im][C_4F_9SO_3]$, n = 2,4, and DESs for CO_2 capture by assessing their performance in terms of key process indicators, such as cyclic working capacity, enthalpy of desorption, and CO_2 diffusion coefficient. It was concluded that the majority of ILs have superior performance to capture CO_2 compared with DES [127]. Jovell *et al.* employed the soft-SAFT framework to model the solubility of F-gases, such as R134a, in FILs and DESs based on PFAs [120]. Finally, Ferreira et al. also successfully used the soft-SAFT EoS to infer the solubility of F-gases such as HFCs (R-32, R-125, R-134a) and PFCs (R-14, R-116, R-218) in FILs with different anionic and cationic fluorinated chains [132].

2.3.1.5 Gas separation processes using fluorinated ionic liquids-based membranes

Ionic liquid-based membranes present improved properties for their application in gas separation processes, as has been recently reviewed by Friess *et al.* Despite the great advantages of using FILs-based membranes for separation processes, they are still poorly explored. Given their relevance, and in order to avoid repetition, in this section, we focus on FILs-based membrane platforms studied for the separation of CO_2, F-gases, and other gases, not considered in reference [133]. Most works are related to gas permeability and selectivity in supported ionic liquid membranes (SILMs), prepared by impregnating a small amount of FIL into a porous membrane. Bara *et al.* were the first ones to apply FILs ($[C_2(C_4F_9)C_1Im][N(CF_3SO_2)_2]$ and $[C_2(C_6F_{13})C_1Im][N(CF_3SO_2)_2]$) into a SILMs configuration, determining the permeation of CO_2, O_2, N_2, and CH_4. at 296 K [134]. Soon after, Pereiro *et al.* studied the single gas permeability, diffusivity, and solubility of CO_2, O_2, N_2, CH_4, C_2H_6, C_3H_8, C_3H_6, CF_4, C_2F_6, and C_3F_8 in $[N_{4444}][C_8F_{17}SO_3]$- and $[C_2C_1py][C_4F_9SO_3]$-based SILMs at 294 K [79]. Gouveia *et al.* assessed the permeation, diffusion, and solubility of CO_2 and N_2 in $[C_2C_1Im][C_4F_9SO_3]$-based SILM at 293 K. All these permeabilities results are represented in Figure 2.3.4a. $[C_2C_1py][C_4F_9SO_3]$ shows the highest permeation for all gases except O_2). Interestingly, when comparing the permeation of CO_2 in SILMs based on $[C_2C_1py][C_4F_9SO_3]$ and $[C_2C_1Im][C_4F_9SO_3]$, the latter has a permeation 28 times lower than the former, showing that the cation has a huge influence on the permeation of CO_2. Moreover, the fluorination of SILMs is only beneficial for gas permeation until a certain point, similar to what is observed for pure FILs. $[C_2C_1py][C_4F_9SO_3]$ shows higher permeation for almost all gases compared with the $[N_{4444}][C_8F_{17}SO_3]$ and the permeation of CO_2, O_2, N_2 and CH_4 is higher for $[C_2(C_4F_9)C_1Im][N(CF_3SO_2)_2]$ than $[C_2(C_6F_{13})C_1Im][N(CF_3SO_2)_2]$ (Figure 2.3.4a) [135].

The ideal permselectivities of some systems are represented in Figure 2.3.4b. The FILs containing a fluorinated cation have a higher selectivity for the separation of CO_2/N_2 and CO_2/CH_4, and therefore are of interest to be used in the separation of CO_2 from industrial flue gases and natural gas. Regarding the F-gases separation performance, $[N_{4444}][C_8F_{17}SO_3]$ has the highest efficiency and thus is useful for the development of technologies to mitigate climate change.

Sood *et al.* studied proton conducting ionic liquids (PCILs), such as $[N_{0222}][C_4F_9SO_3]$ and $[N_{0222}][C_8F_{17}SO_3]$, as dopants of Nafion® membranes. The permeabilities of H_2 and O_2, studied at 293.15 K, using the doped membranes were identical. The authors found out that the FILs form crystalline domains, which sharply increased the gas permeability. This is a result of the diffusion paths formed in the interface between the crystalline PCIL domains and the membrane [136].

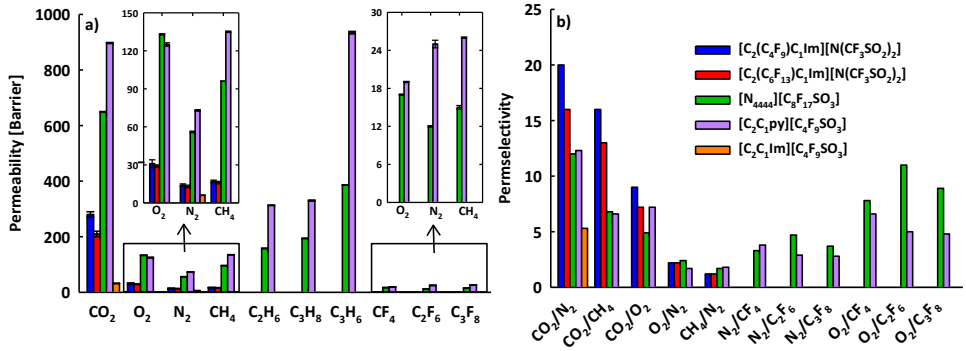

Figure 2.3.4 Comparison of literature data of a) permeability and b) ideal permselectivity of SILMs based on FILs. Adapted from Bara, J.E. *et al.* (2009), Pereiro, A.B *et al.* (2013), Gouveia, A.S. *et al.* (2017) and Sood, R. *et al.* (2015) [79,134–136].

Recently, experimental data were collected for the first time regarding the gas permeation properties of HFCs commonly blended with other HFCs or with hydrofluoroolefins (HFOs) [137]. Polymeric membranes functionalized with ILs, the so-called composite ionic liquid–polymer membranes (CILPMs), started to be investigated as an advantageous technology for the separation of HFC blends and of HFC/HFO blends used for refrigeration applications. Pebax membranes functionalized with the ILs $[C_2C_1Im][SCN]$ and $[C_2C_1Im][BF_4]$ were tested for the separation of the refrigerant R-410A (a near-azeotropic system of the HFCs R-32 and R-125), showing improvement in the permeability towards R-32 and of the R-32/R-125 selectivity, relatively to the neat polymer membranes [138]. Additionally, CILPMs were prepared by functionalizing Pebax membranes with $[C_2C_1Im][SCN]$, $[C_2C_1Im][BF_4]$, $[C_2C_1Im][CF_3SO_3]$, and $[C_2C_1Im][N(CF_3SO_2)_2]$ and were tested for the solubility and permeation of R-32, R-134a, and the HFO R-1234yf. In this study, the CILPM based on $[C_2C_1Im][BF_4]$ showed higher permeability towards the HFCs R-32 and R-134a compared to the HFO R-1234yf, demonstrating to be useful for the separation of HFC/HFO blends [139]. Furthermore, Pebax membranes were functionalized with the so-called ioNanofluids, a suspension of exfoliated graphene nanoplatelets in the FIL $[C_2C_1py][C_4F_9SO_3]$, and used for the separation of the R-410A refrigerant, showing enhanced gas permeation relative to the neat membranes [140].

2.3.2 Liquid-liquid and solid-liquid fluorinated ionic liquids phase equilibria

Recently, efforts are being made to evaluate the liquid-liquid equilibria and solid-liquid equilibria, of several families of FILs with water, perfluorocarbons, as well as with other FILs. A summary of the main contributions is presented here.

2.3.2.1 Liquid + liquid equilibria of fluorinated ionic liquids with water

The impact of the hydrogenated alkyl chain length increment from 1-butyl-3-methylimidazolium to 1-dodecyl-3-methylimidazolium ($[C_nC_1Im]^+$; n = 4, 6, 8, 10, 12) in FILs containing the $[C_4F_9SO_3]^-$ anion on the phase equilibria is illustrated in the phase diagrams depicted in Figure 2.3.5. The systems show a classic LLE behaviour in which temperature has a small impact on the solubility increment. In the presence of the $[C_4F_9SO_3]^-$ anion, the solubility of water in the FIL-rich-phase increases with lengthier hydrogenated alkyl chains [28,60]. The increment of the hydrogenated alkyl chain length induces a better phase separation since it increases the nanosegregation of the nonpolar regions that impels the water aggregates to the polar region of the IL [26,59]. As illustrated in Figure 2.3.5, the solubility of FILs in the water-rich-phase is very small and it decreases with the increment of the hydrogenated content up to an alkyl chain of C_6/C_8 in the imidazolium-based FILs, due to the increment of their hydrophobic behaviour. The opposite behaviour was noticed for $[C_{10}C_1Im][C_4F_9SO_3]$ and $[C_{12}C_1Im][C_4F_9SO_3]$ and can be explained by their higher surfactant behaviour and different structural arrangement that lead to an increased solubility in water, caused by a competition between the nonpolar domains of FILs (hydrogenated and fluorinated domains) [28,52,60].

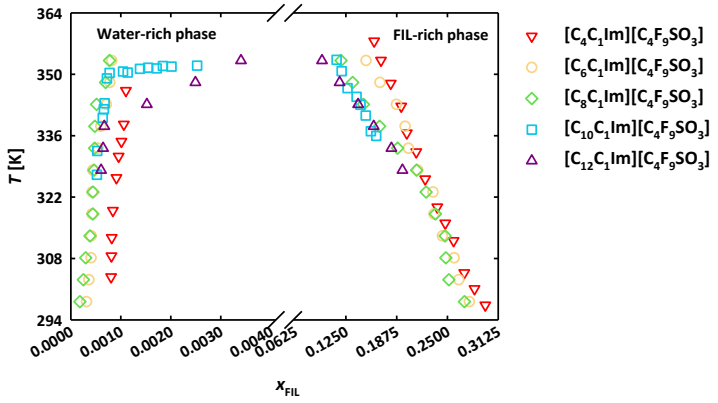

Figure 2.3.5 Liquid-liquid phase diagrams for binary mixtures of $[C_nC_1Im][C_4F_9SO_3]$ + water as a function of FIL molar fraction. Adapted from Teixeira, F.S. *et al.* (2015) and Vieira, N.S.M. *et al.* (2019) [28,60].

Based on the solubility data obtained from the LLE experiments, several thermodynamic properties were determined to better understand the solvation mechanism of the FIL-water systems, including standard molar Gibbs energy ($\Delta_{sol}G_m^0$), standard molar enthalpy ($\Delta_{sol}H_m^0$) and standard molar entropy ($\Delta_{sol}S_m^0$) of solution [141–143]. These parameters explain the transfer of one molecule of solute to a theoretical dilute ideal solution and were calculated for all studied systems. In FIL + water systems, the solubility of water was

linearly correlated with temperature. The calculated molar enthalpies of water in this class of imidazolium-based FILs show that the solubilization process of water in FILs is endothermic. Furthermore, the increment of the hydrogenated alkyl chain length also increases the values of these parameters, and major entropic contributions to the solution process were observed for the dodecyl-based cation. This behaviour can be associated with the higher free volume and surfactant behaviour of the longer chain-based FILs that might boost the solubility of the water in this FIL [28,29,60]. Additionally, the thermodynamic standard properties of solution and solvation, proposed by the standard state model of Ben-Naim, decrease with the increase of the alkyl side chain length of the imidazolium-based FILs [28,29,60]. Under the conditions established by Ben-Naim, the Gibbs free energy of solvation is negative, indicating a spontaneous and favourable solvation process, mainly induced by enthalpic contributions. Additionally, the results suggest that spontaneous solvation is caused by the existence of interactions between water and FILs [141–143].

2.3.2.2 Liquid + liquid equilibria of perfluorocarbons with fluorinated ionic liquids

Martinho *et al.* studied the phase behaviour of several families of FILs with traditional PFCs, perfluorooctane (C_8F_{18}), and perfluorodecalin ($C_{10}F_{18}$). The phase diagrams depicted in Figure 2.3.6 show the classic LLE behaviour, with higher solubilities associated with the increment of temperature. The low solubility of the FILs in both $C_{10}F_{18}$ and C_8F_{18}-rich phases is observed; however, the solubility in the PFC-rich phase was only determined at one point, corresponding to lower FIL compositions [28,29,60]. The lack of data for higher compositions is due to the high vapour pressure and boiling temperature of the PFCs, which limits a temperature rise until the point in which only one phase is observed. The solubility of $C_{10}F_{18}$ in the studied FILs increased accordingly to the following trend: $[C_2C_1py][C_4F_9SO_3]$ < $[C_6C_1Im][C_4F_9SO_3]$ < $[C_8C_1Im][C_4F_9SO_3]$ < $[N_{4444}][C_4F_9SO_3]$ < $[N_{4444}][C_8F_{17}SO_3]$, whereas for C_8F_{18} the solubility in $[C_8C_1Im][C_4F_9SO_3]$ is higher than in $[N_{4444}][C_4F_9SO_3]$.

The increment of solubility associated with higher hydrogenated alkyl chains observed in the water-FIL binary systems was also observed for both PFCs in imidazolium-based FILs, but more pronounced in the case of C_8F_{18}. Yet, the highest solubility of C_8F_{18} and $C_{10}F_{18}$ occurred for $[N_{4444}]^+$ when conjugated with $[C_8F_{17}SO_3]^-$. In this case, the temperature plays a significant role since up to 323.15 K the solubility is superior for C_8F_{18}, whereas for higher temperatures the behaviour shift, and the solubility is higher for $C_{10}F_{18}$. The most pronounced difference between the solubility of PFCs was achieved with $[C_8C_1Im][C_4F_9SO_3]$ in which the solubility of C_8F_{18} was always superior to that of $C_{10}F_{18}$ [78].

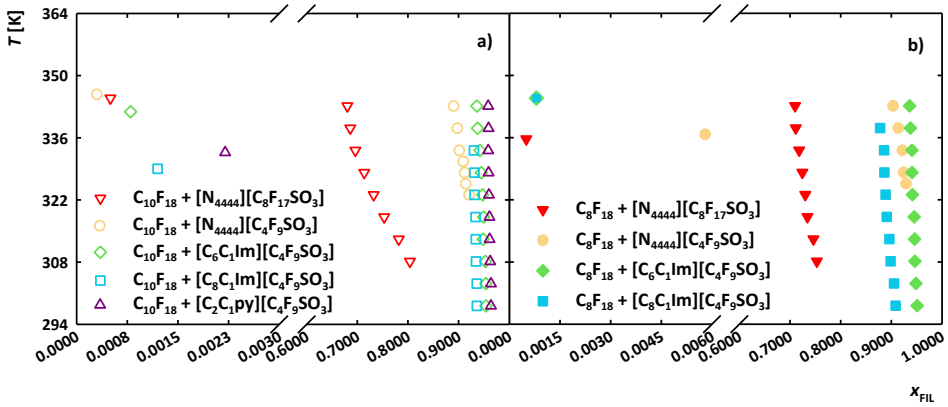

Figure 2.3.6 Liquid-liquid phase diagrams for binary mixtures of a) perfluorodecalin + FILs and b) perfluooctane + FILs as function of FIL molar fraction. Adapted from Martinho, S. *et al.* (2013) [78].

Several thermodynamic parameters can be determined from the LLE diagram depicted in Figure 2.3.6, as detailed in the previous section. In all binary systems, the solubility of PFCs in the FILs-rich phase was linearly correlated with temperature and the molar enthalpies of solution for both PFCs in all tested FILs indicate that their solubilization is an endothermic process. As noticed for FIL-water binary systems, the increment of the hydrogenated alkyl chain length increases the values of these thermodynamic parameters, with the major entropic contribution to the solution process found for the ammonium-based FILs This can be associated with the higher free volume of the ammonium cation in comparison to the imidazolium and pyridinium cations, which also leads to a higher solubility of the PFCs [78].

According to the conditions proposed by Ben-Naim, the Gibbs free energy of solvation is always negative, resulting in a spontaneous and favoured solvation process, for which the main contributions are enthalpic. The local standard enthalpies of solvation indicate that pyridinium and imidazolium-based FILs interact strongly with the PFCs in comparison with the ammonium-based FILs. Since the entropic contribution cannot be neglected, these results imply that the spontaneous solvation is mainly caused by the strong chemical F-F interactions, the rigid organic fluorine (C-F···F-C) bond between FILs anions and PFCs, and the hydrogen bonding interactions (C-H···F-C) between the FILs cations and the PFCs [78,144–147].

2.3.2.3 Solid + liquid equilibria of fluorinated ionic liquids with water

The solubility of solid FILs in water is essential to define the operational concentration ranges for any industrial application. To our knowledge, the only study available in the literature is the study performed by Teixeira *et al.* for $[C_4C_1pyr]^+$ and $[N_{4444}]^+$ cations both conjugated with the $[C_4F_9SO_3]^-$ anion was studied. Remarkably, the solubility equilibrium took 24 h and 22 days to be achieved for $[C_4C_1pyr][C_4F_9SO_3]$ and $[N_{4444}][C_4F_9SO_3]$, respectively. The solubility at 298.15 K increases in the following order: $[N_{4444}]^+$ (0.0035 in mass fraction) <

$[C_4C_1pyr]^+$ (0.0206 in mass fraction). The pyrrolidinium-based FIL has the highest solubility due to its larger alkyl chain length and localized positive charge, whereas the high degree of symmetry of the ammonium cation difficult its solubility in water [28].

2.3.2.4 Solid + liquid equilibria of binary mixtures of fluorinated ionic liquids

Besides their unique properties, some FILs have limitations regarding industrial applications, related to their high melting temperatures, fomented by their fluorinated region. To overcome this situation, eutectic mixtures based on different FILs and fluorine-containing ILs have been investigated [148]. Although the advantages of these mixtures are notable, the number of studied combinations is very scarce, and the complexity of the observed phase behaviour is notorious. The solid-liquid equilibria of these binary mixtures studied by Teles *et al*. revealed the existence of three distinct SLE behaviour. The distinct phase diagrams elucidate the complex behaviour of FILs mixtures. A quasi-ideal behaviour, with a eutectic profile, was determined, with eutectic points over the room temperature, and with partial miscibility close to neat FILs. A negative deviation from the ideal behaviour was also observed, in accordance with the formation of a solid solution. A very distinct phase behaviour was observed by the same authors for $[C_4C_1pyr][N(C_4F_9SO_2)_2]$ + $[C_2C_1pyr][N(C_4F_9SO_2)_2]$ with total miscibility in the solid phase. Herein, the melting temperature of $[C_2C_1pyr][N(C_4F_9SO_2)_2]$ is reduced by the addition of $[C_4C_1pyr][N(C_4F_9SO_2)_2]$. This continuous solid solution profile occurs due to the size similarity between the two cations. The solid phase structure was supported by the X-ray diffraction, suggesting the incorporation of $[C_2C_1pyr][N(C_4F_9SO_2)_2]$ in the crystalline structure of $[C_4C_1pyr][N(C_4F_9SO_2)_2]$ [53].

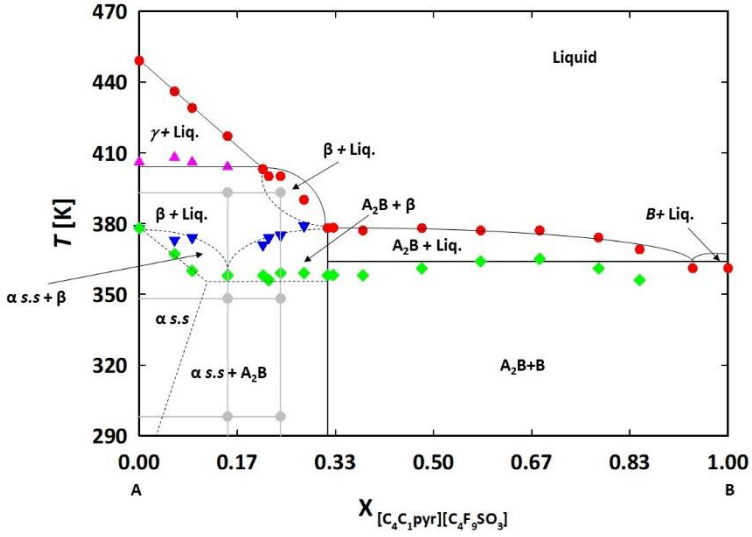

Figure 2.3.7 Solid-liquid phase diagram from the $x[C_4C_1pyr][N(C_4F_9SO_2)_2]$ + (1 - x)$[N_{1112(OH)}][C_4F_9SO_3]$, temperature versus mole fraction of $[C_4C_1pyr][N(C_4F_9SO_2)_2]$. Solid–liquid transition (●), eutectoic and eutectic thermal transitions (◆), and solid-solid transitions (▼) and (▲), obtained by DSC. Solid and

dashed lines correspond to the interpretation of the diagram. Figure adapted from Teles, A.R.R. *et al.* (2016) [53].

Another very complex behaviour was observed with the presence of several polymorphs in the cholinium-based FIL systems. As depicted in Figure 2.3.7, this complex system presents: i) an intermediate compound, identified as A_2B; ii) a region, identified as α *s.s*, indicating a limited solubility of the polymorph, α, and the intermediate A_2B; iii) solid-solid phase transitions between the polymorphs β and γ at 400 K; and iv) an eutectoid reaction after the cooling step of polymorph β, revealing the existence of a solid-solid transition, from the solid polymorph β to the two solid phases correspondent to α *s.s* + A_2B [53].

2.3.3 Findings and remaining challenges of FILs phase equilibria determination

As inferred from the previous sections, most of the FILs phase equilibria studies have focused on gas solubility measurements or modelling, with few works dealing with liquid-liquid and solid-liquid equilibria.

Key main conclusions extracted from these studies are that the FILs present a high capacity to i) solubilize gases due to their surfactant nature; ii) obtain three domains involved in the interaction with solutes; and iii) have a rigid molecular backbone that forms large cavities to accommodate solutes. The presence of perfluoroalkyl chains either in the cation and/or in the anion promotes the solubility of gases, such as CO_2 and HFCs, with the solubility capacity being proportional to the size of the chain until a certain number of carbons (between 6 and 8 carbons atoms in the cases reported). Solubility power is also promoted by the presence of bulky anions, probably as a result of the generation of a structural asymmetry that provides more space to accommodate gas molecules. In the case of F-gases, the volume of the chains and their dipole moment also contribute to the solubilization process.

Despite promoting gas solubility, fluorine atoms may have negative effects on toxicity and biodegradability, as stated in section 2.2.3, and therefore a fine tune of the fluorine content of FILs is needed to increase the benefits/risks ratio. Some new strategies can be followed to increase their biodegradability, such as i) inserting specific chemical groups (such as esters, amides, hydroxyl, and carboxyl groups) in between the fluorinated chains; and ii) the use of more biodegradable cations, such as cholinium, conjugated with appropriate anions (with up to four carbon perfluorinated chains, for example). The combination of the cholinium cation with the perfluoropentanoate anion has enabled the design of a FIL with negligible toxicity, completely miscible in water, and improved biodegradability [30,60,70].

As highlighted in this work, the use of theoretical tools to predict gas solubility in FILs has been of great relevance to advance in the use of these compounds for several applications.

Molecular simulations have provided insights into the mechanisms of solvation and the determination of solubility parameters, easing the study of the gas-philicity of a great number of FILs structural features. Other methods based on correlative and hybrid quantum chemical/statistical thermodynamics approaches, such as the COSMO-based/Aspen Plus and NRTL models, have been successfully implemented. These models capture the behaviour of the absorption of GHGs in different FILs, facilitating the development of separation processes. In this topic, equations of state can be highlighted as the most used method to predict the phase behaviour of gases in FILs. Different equations have been applied and have allowed the computation of these complex systems with good agreement with experimental data. The molecular-based soft-SAFT equation of state stands out as the most used equation and is a promising tool to accelerate the actual implementation of FILs for gas solubility applications. The robust and simple way in which the interaction of these complex systems with gases can be modelled enables the accurate prediction of the vapour-liquid behaviours. Additionally, this tool can capture the influence of the structural features of FILs and enables the search for properties that favour the solubilization of gases, such as CO_2 and HFCs. The theoretical models show great benefit to the study of phase behaviour, and more time should be invested in this topic to envisage new ILs for gas solubility and other applications.

Considering the high impact of some GHGs on the environment and living organisms, the use of FILs with low toxicity, improved biodegradability, high adsorption capacity, and high selectivity may have a positive environmental impact, with clear benefits when compared to other sustainable options with lower efficiency. In this context, the development of smart and sustainable technologies based on FILs must be considered. For example, as stated in this section, the combination of FILs with membrane technologies would allow reducing the amounts of FILs needed and increase efficiency, with clear environmental and economic benefits. Other approaches can also be taken to bypass some properties of FILs that hamper their efficient application, such as their viscosity. Therefore, the use of FILs-based eutectic mixtures may be considered.

Three main factors have been shown to influence the LLE behaviour of FILs in water, such as their water miscibility, high surfactant behaviour, and the presence of three nanosegregated domains. The increment of the hydrogenated chain in the $[C_nC_1Im][C_4F_9SO_3]$ family increases the solubility of water in the FIL-rich phase. The reverse is found for the water-rich phase; solubility decreases with the increase of the hydrogenated chain up to a certain number of carbon atoms. The further increment of the hydrogenated chain leads to a rearrangement between the nanosegregated domains and consequently to an increase in the solubility of the FIL in water. The study of FILs phase behaviour with traditional PFCs highlights that FILs have very low solubility in the PFCs-rich phase. The larger hydrogenated

and fluorinated chains increase the solubility of PFCs in the FILs-rich phase. However, the determination of FILs solubility in the PFC-rich phase is hindered by the high vapour pressure and boiling point of the PFCs which severely limits the possible temperature working range. The solid-liquid equilibria behaviour of solid FILs in water shows the influence of the cation in solubility. FILs having bulkier content of fluorine tend to have shorter liquid ranges and the increment of this interval has huge relevance in their industrial applications. The study of the solid-liquid equilibria of FILs mixtures revealed that they can assume a liquid form in a wider interval of temperatures.

The phase diagrams of FILs mixtures are very challenging to determine and evaluate due to the large number of different behaviours found in the few works studied in the literature, which hinders the studies on them. Therefore, it is extremely important to further study the liquid-liquid and solid-liquid equilibria of FILs, not only to learn how the fluorination affects their behaviour but also to progress in the study of FILs mixtures, creating new opportunities for applications. Moreover, the use of theoretical tools should greatly benefit the still unexplored area of study of LLE and SLE of the highly surfactant FILs with different solvents. The promising applications would vastly benefit from exploring more theoretical methods that can ease the screening of FILs complex properties. Therefore, studies concerning the phase behaviour of FILs with compounds that have significant value in the environmental, biomedical, and chemical industries, such as GHGs gases, industrial solvents, pharmaceuticals, refrigerants, etc. are still needed.

2.3.4 Conclusions and perspectives

In the last two decades, a vast amount of work has been produced on the phase equilibria of FILs, mostly focused on gas solubility. These studies show that the fluorine content of FILs, up to a certain length, impacts positively the absorption of different gases. However, fluorinated chains with more than 6 carbons do not compensate for the increased toxicity of these FILs. In this sense, outstanding contributions have been published on modelling FILs + gases VLE, showing that this is a powerful method to decrease the time of screening a vast amount of FILs, being highly accurate and useful when only scarce experimental data is available.

The LLE of FILs showed that they have a rich phase behaviour in the presence of water. They can be designed to be totally miscible and to have a high aggregation behaviour in water, making them enhanced surfactant compounds through an appropriate balance between the hydrogenated and fluorinated side chain length. The LLE of PFCs with FILs show that the mechanism of solvation depends on the length of the fluorinated and hydrogenated chain, and the temperature. Finally, the SLE of FILs mixtures show that different FILs combinations can

be tested and introduced as viable options for industrial processes, namely for the substitution of environmentally dangerous compounds, such as methanol or toluene. The formation of eutectic mixtures, which allows FILs to be in a liquid state at a wider temperature range has been already reported, which is also a great advantage for several industrial applications. However, more work should be done to apply the benefits of this approach to different commercial processes.

The three-nanosegregated domains of FILs are responsible for most of their final performance. In this work, a detailed analysis has been provided on the impact of both cation and anion nature, as well as hydrogenated and fluorinated side chain length in many properties, which directly influences the formation and size of the nanosegregated domains Then, this work demonstrated a structure-activity relationship between FILs structure and properties, easing a future FIL design accordingly to the final application and enabling the manipulation of their properties, such as thermal and thermophysical properties, surface tension, surfactant behaviour, cytotoxicity, and ecotoxicity.

The design of FILs with high surfactant power and aggregation behaviour, enabling the formation of self-assembled structures, total miscibility in water, negligible cytotoxicity and ecotoxicity, and ease of regeneration favours their application in fields where greener and biocompatible substances are required. FILs are a sustainable solution for gas capture and separation processes, and for biomedical purposes where the immiscibility of PFCs in water is a major drawback, such as artificial gas carriers and drug delivery systems.

Considering the great potential of using FILs for gas capture and separation processes, greater efforts must be taken regarding the development of FIL-based membranes to ease the capture and separation of GHGs gases as well as the design and optimization of processes involving them as well as the development of scale-up strategies of promising FILs to facilitate the transfer of these systems from laboratory to industrial scale. On the fundamental side, studies regarding ions dissociation to infer in the phase equilibria of FILs with water and other solvents are still missing in the literature and should be carried out to assess their possible role in the performance of FILs for this application.

The selection of biocompatible FILs for biomedical applications is a subject of growing interest. Several FILs with different structures and properties can be designed resulting in specific interactions of FILs with different biomolecules. Therefore, it is of high importance to study FILs interactions with biomolecules. It is also imperative to advance in the studies concerning the development of stable formulations based on FILs and biomolecules. These delivery platforms can be undertaken by inferring the phase equilibria of FILs with excipients of great relevance in the pharma industry. Moreover, must be initiated *in vivo* studies of FILs formulations, opening the possibility of the use of FILs as biomaterials.

In conclusion, the detailed study of FILs phase equilibria is a key first step to optimising their use for applications where the changes in phase behaviour are critical. The exceptional tuneability of FILs makes them optimal candidates for the design of alternative and sustainable solutions for almost unlimited applications. Therefore, the study of FILs is an area with great potential and key advances are expected in the next years.

2.4 References

1. Berger, R.; Resnati, G.; Metrangolo, P.; Weber, E.; Hulliger, J. Organic Fluorine Compounds: A Great Opportunity for Enhanced Materials Properties. *Chem Soc Rev* **2011**, *40*, 3496–3508, doi:10.1039/C0CS00221F.
2. European Environment Agency *Emerging Chemical Risks in Europe – PFAS*; 2019;
3. Castro, C.I.; Briceno, J.C. Perfluorocarbon-Based Oxygen Carriers: Review of Products and Trials. *Artif Organs* **2010**, *34*, 622–634, doi:10.1111/J.1525-1594.2009.00944.X.
4. Tsai, W.T.; Chen, H.P.; Hsien, W.Y. A Review of Uses, Environmental Hazards and Recovery/Recycle Technologies of Perfluorocarbons (PFCs) Emissions from the Semiconductor Manufacturing Processes. *J Loss Prev Process Ind* **2002**, *15*, 65–75, doi:10.1016/S0950-4230(01)00067-5.
5. Melich, R.; Zorgani, A.; Padilla, F.; Charcosset, C. Preparation of Perfluorocarbon Emulsions by Premix Membrane Emulsification for Acoustic Droplet Vaporization (ADV) in Biomedical Applications. *Biomed Microdevices* **2020**, *22*, doi:10.1007/S10544-020-00504-5.
6. Choi, M.; Park, S.; Park, K.; Jeong, H.; Hong, J. Nitric Oxide Delivery Using Biocompatible Perfluorocarbon Microemulsion for Antibacterial Effect. *ACS Biomater Sci Eng* **2019**, *5*, 1378–1383, doi:10.1021/ACSBIOMATERIALS.9B00016.
7. Choi, H.; Choi, W.; Kim, J.; Kong, W.H.; Kim, K.S.; Kim, C.; Hahn, S.K. Multifunctional Nanodroplets Encapsulating Naphthalocyanine and Perfluorohexane for Bimodal Image-Guided Therapy. *Biomacromolecules* **2019**, *20*, 3767–3777, doi:10.1021/ACS.BIOMAC.9B00842.
8. Fernandes, D.A.; Kolios, M.C. Near-Infrared Absorbing Nanoemulsions as Nonlinear Ultrasound Contrast Agents for Cancer Theranostics. *J Mol Liq* **2019**, *287*, doi:10.1016/J.MOLLIQ.2019.04.125.
9. Badv, M.; Alonso-Cantu, C.; Shakeri, A.; Hosseinidoust, Z.; Weitz, J.I.; Didar, T.F. Biofunctional Lubricant-Infused Vascular Grafts Functionalized with Silanized Bio-Inks Suppress Thrombin Generation and Promote Endothelialization. *ACS Biomater Sci Eng* **2019**, *5*, 6485–6496, doi:10.1021/ACSBIOMATERIALS.9B01062.
10. Kohlhauer, M.; Boissady, E.; Lidouren, F.; de Rochefort, L.; Nadeau, M.; Rambaud, J.; Hutin, A.; Dubuisson, R.M.; Guillot, G.; Pey, P.; et al. A New Paradigm for Lung-Conservative Total Liquid Ventilation. *EBioMedicine* **2020**, *52*, doi:10.1016/J.EBIOM.2019.08.026.
11. Courrier, H.M.; Vandamme, T.F.; Krafft, M.P. Reverse Water-in-Fluorocarbon Emulsions and Microemulsions Obtained with a Fluorinated Surfactant. *Colloids Surf A Physicochem Eng Asp* **2004**, *244*, 141–148, doi:10.1016/J.COLSURFA.2004.06.003.
12. Zhu, J.; Wang, Z.; Xu, X.; Xu, M.; Yang, X.; Zhang, C.; Liu, J.; Zhang, F.; Shuai, X.; Wang, W.; et al. Polydopamine-Encapsulated Perfluorocarbon for Ultrasound Contrast Imaging and Photothermal Therapy. *Mol Pharm* **2020**, *17*, 817–826, doi:10.1021/ACS.MOLPHARMACEUT.9B01070.
13. Lindstrom, A.B.; Strynar, M.J.; Libelo, E.L. Polyfluorinated Compounds: Past, Present, and Future. *Environ Sci Technol* **2011**, *45*, 7954–7961, doi:10.1021/ES2011622.
14. Bakker, J.; Reihlen, A.; Meura, L.; Camboni, M.; Goldenman, G.; Lietzmann, J. *Study for the Strategy for a Non-Toxic Environment of the 7th Environment Action Programme.*; 2017;
15. Gyllenhammar, I.; Berger, U.; Sundström, M.; McCleaf, P.; Eurén, K.; Eriksson, S.; Ahlgren, S.; Lignell, S.; Aune, M.; Kotova, N.; et al. Influence of Contaminated Drinking Water on Perfluoroalkyl Acid Levels in Human Serum - A Case Study from Uppsala, Sweden. *Environ Res* **2015**, *140*, 673–683, doi:10.1016/J.ENVRES.2015.05.019.

16. Naile, J.E.; Khim, J.S.; Wang, T.; Chen, C.; Luo, W.; Kwon, B.O.; Park, J.; Koh, C.H.; Jones, P.D.; Lu, Y.; et al. Perfluorinated Compounds in Water, Sediment, Soil and Biota from Estuarine and Coastal Areas of Korea. *Environmental Pollution* **2010**, *158*, 1237–1244, doi:10.1016/J.ENVPOL.2010.01.023.
17. Noorlander, C.W.; van Leeuwen, S.P.J.; te Biesebeek, J.D.; Mengelers, M.J.B.; Zeilmaker, M.J. Levels of Perfluorinated Compounds in Food and Dietary Intake of PFOS and PFOA in the Netherlands. *J Agric Food Chem* **2011**, *59*, 7496–7505, doi:10.1021/JF104943P.
18. Lindstrom, A.B.; Strynar, M.J.; Libelo, E.L.; Field, J.A. Guest Comment: Perfluoroalkyl Acid Focus Issue. *Environ Sci Technol* **2011**, *45*, 7951–7953, doi:10.1021/ES202963P.
19. Rogers, R.D.; Seddon, K.R. Ionic Liquids - Solvents of the Future? *Science (1979)* **2003**, *302*, 792–793, doi:10.1126/SCIENCE.1090313.
20. Earle, M.J.; Esperança, J.M.S.S.; Gilea, M.A.; Lopes, J.N.C.; Rebelo, L.P.N.; Magee, J.W.; Seddon, K.R.; Widegren, J.A. The Distillation and Volatility of Ionic Liquids. *Nature* **2006**, *439*, 831–834, doi:10.1038/NATURE04451.
21. Plechkova, N. v.; Seddon, K.R. Applications of Ionic Liquids in the Chemical Industry. *Chem Soc Rev* **2008**, *37*, 123–150, doi:10.1039/B006677J.
22. Egorova, K.S.; Ananikov, V.P. Toxicity of Ionic Liquids: Eco(Cyto)Activity as Complicated, but Unavoidable Parameter for Task-Specific Optimization. *ChemSusChem* **2014**, *7*, 336–360, doi:10.1002/CSSC.201300459.
23. Lei, Z.; Chen, B.; Koo, Y.M.; Macfarlane, D.R. Introduction: Ionic Liquids. *Chem Rev* **2017**, *117*, 6633–6635, doi:10.1021/ACS.CHEMREV.7B00246.
24. Pereiro, A.B.; Araújo, J.M.M.; Esperança, J.M.S.S.; Rebelo, L.P.N. Chapter 4. Surfactant Fluorinated Ionic Liquids. In; 2017; Vol. 4, pp. 79–102.
25. Tindale, J.J.; Na, C.; Jennings, M.C.; Ragogna, P.J. Synthesis and Characterization of Fluorinated Phosphonium Ionic Liquids. *Can J Chem* **2007**, *85*, 660–667, doi:10.1139/V07-035.
26. Pereiro, A.B.; Pastoriza-Gallego, M.J.; Shimizu, K.; Marrucho, I.M.; Lopes, J.N.C.; Piñeiro, M.M.; Rebelo, L.P.N. On the Formation of a Third, Nanostructured Domain in Ionic Liquids. *Journal of Physical Chemistry B* **2013**, *117*, 10826–10833, doi:10.1021/JP402300C.
27. Pereiro, A.B.; Araújo, J.M.M.; Teixeira, F.S.; Marrucho, I.M.; Piñeiro, M.M.; Rebelo, L.P.N. Aggregation Behavior and Total Miscibility of Fluorinated Ionic Liquids in Water. *Langmuir* **2015**, *31*, 1283–1295, doi:10.1021/LA503961H.
28. Teixeira, F.S.; Vieira, N.S.M.; Cortes, O.A.; Araújo, J.M.M.; Marrucho, I.M.; Rebelo, L.P.N.; Pereiro, A.B. Phase Equilibria and Surfactant Behavior of Fluorinated Ionic Liquids with Water. *Journal of Chemical Thermodynamics* **2015**, *82*, 99–107, doi:10.1016/j.jct.2014.10.021.
29. Pereiro, A.B.; Araújo, J.M.M.; Martinho, S.; Alves, F.; Nunes, S.; Matias, A.; Duarte, C.M.M.; Rebelo, L.P.N.; Marrucho, I.M. Fluorinated Ionic Liquids: Properties and Applications. *ACS Sustain Chem Eng* **2013**, *1*, 427–439, doi:10.1021/SC300163N.
30. Vieira, N.S.M.; Stolte, S.; Araújo, J.M.M.; Rebelo, L.P.N.; Pereiro, A.B.; Markiewicz, M. Acute Aquatic Toxicity and Biodegradability of Fluorinated Ionic Liquids. *ACS Sustain Chem Eng* **2019**, *7*, 3733–3741, doi:10.1021/ACSSUSCHEMENG.8B03653.
31. Vieira, N.S.M.; Bastos, J.C.; Rebelo, L.P.N.; Matias, A.; Araújo, J.M.M.; Pereiro, A.B. Human Cytotoxicity and Octanol/Water Partition Coefficients of Fluorinated Ionic Liquids. *Chemosphere* **2019**, *216*, 576–586, doi:10.1016/j.chemosphere.2018.10.159.
32. Prikhod'ko, S.A.; Shabalin, A.Yu.; Shmakov, M.M.; Bardin, V. v.; Adonin, N.Yu. Ionic Liquids with Fluorine-Containing Anions as a New Class of Functional Materials: Features of the Synthesis, Physicochemical Properties, and Use. *Russian Chemical Bulletin* **2020**, *69*, 17–31, doi:10.1007/s11172-020-2719-5.

33. Tong, B.; Chen, X.; Chen, L.; Zhou, Z.; Peng, Z. Engineering Solid Electrolyte Interphase in Lithium Metal Batteries by Employing an Ionic Liquid Ether Double-Solvent Electrolyte with Li[(CF3SO2)(n-C4F9SO2)N] as the Salt. *ACS Appl Energy Mater* **2018**, *1*, 4426–4431, doi:10.1021/ACSAEM.8B00821.
34. Lepre, L.F.; Andre, D.; Denis-Quanquin, S.; Gautier, A.; Pádua, A.A.H.; Costa Gomes, M. Ionic Liquids Can Enable the Recycling of Fluorinated Greenhouse Gases. *ACS Sustain Chem Eng* **2019**, *7*, 16900–16906, doi:10.1021/acssuschemeng.9b04214.
35. Rufino-Felipe, E.; Valdés, H.; Germán-Acacio, J.M.; Reyes-Márquez, V.; Morales-Morales, D. Fluorinated N-Heterocyclic Carbene Complexes. Applications in Catalysis. *J Organomet Chem* **2020**, *921*, doi:10.1016/J.JORGANCHEM.2020.121364.
36. Lei, Z.; Dai, C.; Chen, B. Gas Solubility in Ionic Liquids. *Chem Rev* **2014**, *114*, 1289–1326, doi:10.1021/cr300497a.
37. Mellein, B.R.; Scurto, A.M.; Shiflett, M.B. Gas Solubility in Ionic Liquids. *Curr Opin Green Sustain Chem* **2021**, *28*, 100425, doi:10.1016/j.cogsc.2020.100425.
38. Shiflett, M.B.; Maginn, E.J. The Solubility of Gases in Ionic Liquids. *AIChE Journal* **2017**, *63*, 4722–4737, doi:10.1002/AIC.15957.
39. Marsh, K.N.; Boxall, J.A.; Lichtenthaler, R. Room Temperature Ionic Liquids and Their Mixtures - A Review. *Fluid Phase Equilib* **2004**, *219*, 93–98, doi:10.1016/J.FLUID.2004.02.003.
40. Freire, M.G.; Santos, L.M.N.B.F.; Fernandes, A.M.; Coutinho, J.A.P.; Marrucho, I.M. An Overview of the Mutual Solubilities of Water-Imidazolium-Based Ionic Liquids Systems. *Fluid Phase Equilib* **2007**, *261*, 449–454, doi:10.1016/J.FLUID.2007.07.033.
41. Vega, L.F.; Vilasecaa, O.; Llovell, F.; Andreua, J.S. Modeling Ionic Liquids and the Solubility of Gases in Them: Recent Advances and Perspectives. *Fluid Phase Equilib* **2010**, *294*, 15–30, doi:10.1016/J.FLUID.2010.02.006.
42. Maia, F.M.; Calvar, N.; González, E.J.; Carneiro, A.P.; Rodriguez, O.; Macedo, E.A. Modeling of Ionic Liquid Systems: Phase Equilibria and Physical Properties. *Ionic Liquids - New Aspects for the Future* **2013**, doi:10.5772/51812.
43. Yuksel Orhan, O. Effects of Various Anions and Cations in Ionic Liquids on CO2 Capture. *J Mol Liq* **2021**, *333*, doi:10.1016/J.MOLLIQ.2021.115981.
44. Safarov, J.; Abdullayeva, G.; Bashirov, M.; Tuma, D.; Bashirov, R. The Ionic Liquid 1-Ethyl-3-Methylimidazolium Methanesulfonate Revisited: Solubility of Carbon Dioxide over an Extended Range of Temperature and Pressure. *J Mol Liq* **2021**, *333*, doi:10.1016/J.MOLLIQ.2021.115920.
45. Pereiro, A.B.; Araújo, J.M.M.; Esperança, J.M.S.S.; Marrucho, I.M.; Rebelo, L.P.N. Ionic Liquids in Separations of Azeotropic Systems - A Review. *Journal of Chemical Thermodynamics* **2012**, *46*, 2–28, doi:10.1016/J.JCT.2011.05.026.
46. Domańska, U. Experimental Data of Fluid Phase Equilibria- Correlation and Prediction Models: A Review. *Processes* **2019**, *7*, doi:10.3390/PR7050277.
47. Vieira, N.S.M.; Reis, P.M.; Shimizu, K.; Cortes, O.A.; Marrucho, I.M.; Araújo, J.M.M.; Esperança, J.M.S.S.; Lopes, J.N.C.; Pereiro, A.B.; Rebelo, L.P.N. A Thermophysical and Structural Characterization of Ionic Liquids with Alkyl and Perfluoroalkyl Side Chains. *RSC Adv* **2015**, *5*, 65337–65350, doi:10.1039/C5RA13869H.
48. Ferreira, M.L.; Pastoriza-Gallego, M.J.; Araújo, J.M.M.; Canongia Lopes, J.N.; Rebelo, L.P.N.; M Piñeiro, M.; Shimizu, K.; Pereiro, A.B. Influence of Nanosegregation on the Phase Behavior of Fluorinated Ionic Liquids. *Journal of Physical Chemistry C* **2017**, *121*, doi:10.1021/acs.jpcc.7b00516.
49. Vieira, N.S.M.; Luís, A.; Reis, P.M.; Carvalho, P.J.; Lopes-Da-Silva, J.A.; Esperança, J.M.S.S.; Araújo, J.M.M.; Rebelo, L.P.N.; Freire, M.G.; Pereiro, A.B. Fluorination Effects on the

Thermodynamic, Thermophysical and Surface Properties of Ionic Liquids. *Journal of Chemical Thermodynamics* **2016**, *97*, 354–361, doi:10.1016/j.jct.2016.02.013.

50. Pereiro, A.B.; Llovell, F.; Araújo, J.M.M.; Santos, A.S.S.; Rebelo, L.P.N.; Piñeiro, M.M.; Vega, L.F. Thermophysical Characterization of Ionic Liquids Based on the Perfluorobutanesulfonate Anion: Experimental and Soft-SAFT Modeling Results. *ChemPhysChem* **2017**, *18*, 2012–2023, doi:10.1002/CPHC.201700327.
51. Ferreira, M.L.; Araújo, J.M.M.; Vega, L.F.; Llovell, F.; Pereiro, A.B. Functionalization of Fluorinated Ionic Liquids: A Combined Experimental-Theoretical Study. *J Mol Liq* **2020**, *302*, doi:10.1016/j.molliq.2020.112489.
52. Luís, A.; Shimizu, K.; Araújo, J.M.M.; Carvalho, P.J.; Lopes-da-Silva, J.A.; Canongia Lopes, J.N.; Rebelo, L.P.N.; Coutinho, J.A.P.; Freire, M.G.; Pereiro, A.B. Influence of Nanosegregation on the Surface Tension of Fluorinated Ionic Liquids. *Langmuir* **2016**, *32*, 6130–6139, doi:10.1021/acs.langmuir.6b00209.
53. Teles, A.R.R.; Correia, H.; Maximo, G.J.; Rebelo, L.P.N.; Freire, M.G.; Pereiro, A.B.; Coutinho, J.A.P. Solid-Liquid Equilibria of Binary Mixtures of Fluorinated Ionic Liquids. *Physical Chemistry Chemical Physics* **2016**, *18*, 25741–25750, doi:10.1039/C6CP05372F.
54. Gupta, S.; Olsont, J.D. Industrial Needs in Physical Properties. *Ind Eng Chem Res* **2003**, *42*, 6359–6374, doi:10.1021/IE030170V.
55. Ueno, K.; Tokuda, H.; Watanabe, M. Ionicity in Ionic Liquids: Correlation with Ionic Structure and Physicochemical Properties. *Physical Chemistry Chemical Physics* **2010**, *12*, 1649–1658, doi:10.1039/B921462N.
56. Tariq, M.; Forte, P.A.S.; Gomes, M.F.C.; Lopes, J.N.C.; Rebelo, L.P.N. Densities and Refractive Indices of Imidazolium- and Phosphonium-Based Ionic Liquids: Effect of Temperature, Alkyl Chain Length, and Anion. *Journal of Chemical Thermodynamics* **2009**, *41*, 790–798, doi:10.1016/j.jct.2009.01.012.
57. Santos, C.S.; Baldelli, S. Gas-Liquid Interface of Room-Temperature Ionic Liquids. *Chem Soc Rev* **2010**, *39*, 2136–2145, doi:10.1039/B921580H.
58. Ferreira, M.L.; Araújo, J.M.M.; Pereiro, A.B.; Vega, L.F. Insights into the Influence of the Molecular Structures of Fluorinated Ionic Liquids on Their Thermophysical Properties. A Soft-SAFT Based Approach. *Physical Chemistry Chemical Physics* **2019**, *21*, doi:10.1039/c8cp07522k.
59. Bastos, J.C.; Carvalho, S.F.; Welton, T.; Canongia Lopes, J.N.; Rebelo, L.P.N.; Shimizu, K.; Araújo, J.M.M.; Pereiro, A.B. Design of Task-Specific Fluorinated Ionic Liquids: Nanosegregation versus Hydrogen-Bonding Ability in Aqueous Solutions. *Chemical Communications* **2018**, *54*, 3524–3527, doi:10.1039/C8CC00361K.
60. Vieira, N.S.M.; Bastos, J.C.; Hermida-Merino, C.; Pastoriza-Gallego, M.J.; Rebelo, L.P.N.; Piñeiro, M.M.; Araújo, J.M.M.; Pereiro, A.B. Aggregation and Phase Equilibria of Fluorinated Ionic Liquids. *J Mol Liq* **2019**, *285*, 386–396, doi:10.1016/j.molliq.2019.04.086.
61. Szajdzinska-Pietek, E.; Wolszczak, M. Time-Resolved Fluorescence Quenching Study of Aqueous Solutions of Perfluorinated Surfactants with the Use of Protiated Luminophore and Quencher. *Langmuir* **2000**, *16*, 1675–1680, doi:10.1021/LA990981X.
62. González-Pérez, A.; Ruso, J.M.; Prieto, G.; Sarmiento, F. Apparent Molar Quantities of Sodium Octanoate in Aqueous Solutions. *Colloid Polym Sci* **2004**, *282*, 1133–1139, doi:10.1007/S00396-003-1047-2.
63. López-Fontán, J.L.; Sarmiento, F.; Schulz, P.C. The Aggregation of Sodium Perfluorooctanoate in Water. *Colloid Polym Sci* **2005**, *283*, 862–871, doi:10.1007/S00396-004-1228-7.

64. Araújo, J.M.M.; Florindo, C.; Pereiro, A.B.; Vieira, N.S.M.; Matias, A.A.; Duarte, C.M.M.; Rebelo, L.P.N.; Marrucho, I.M. Cholinium-Based Ionic Liquids with Pharmaceutically Active Anions. *RSC Adv* **2014**, *4*, 28126–28132, doi:10.1039/C3RA47615D.
65. Ventura, S.P.M.; Gonçalves, A.M.M.; Sintra, T.; Pereira, J.L.; Gonçalves, F.; Coutinho, J.A.P. Designing Ionic Liquids: The Chemical Structure Role in the Toxicity. *Ecotoxicology* **2013**, *22*, 1–12, doi:10.1007/S10646-012-0997-X.
66. Petkovic, M.; Ferguson, J.L.; Gunaratne, H.Q.N.; Ferreira, R.; Leitão, M.C.; Seddon, K.R.; Rebelo, L.P.N.; Pereira, C.S. Novel Biocompatible Cholinium-Based Ionic Liquids—Toxicity and Biodegradability. *Green Chemistry* **2010**, *12*, 643–664, doi:10.1039/B922247B.
67. Patinha, D.J.S.; Tomé, L.C.; Florindo, C.; Soares, H.R.; Coroadinha, A.S.; Marrucho, I.M. New Low-Toxicity Cholinium-Based Ionic Liquids with Perfluoroalkanoate Anions for Aqueous Biphasic System Implementation. *ACS Sustain Chem Eng* **2016**, *4*, 2670–2679, doi:10.1021/ACSSUSCHEMENG.6B00171.
68. Gal, N.; Malferarri, D.; Kolusheva, S.; Galletti, P.; Tagliavini, E.; Jelinek, R. Membrane Interactions of Ionic Liquids: Possible Determinants for Biological Activity and Toxicity. *Biochim Biophys Acta Biomembr* **2012**, *1818*, 2967–2974, doi:10.1016/J.BBAMEM.2012.07.025.
69. Kumar, R.A.; Papaïconomou, N.; Lee, J.-M.; Salminen, J.; Clark, D.S.; Prausnitz, J.M. In Vitro Cytotoxicities of Ionic Liquids: Effect of Cation Rings, Functional Groups, and Anions. *Environ Toxicol* **2009**, *24*, 388–395, doi:10.1002/tox.20443.
70. Ferreira, M.L.; Vieira, N.S.M.; Araújo, J.M.M.; Pereiro, A.B. Unveiling the Influence of Non-Toxic Fluorinated Ionic Liquids Aqueous Solutions in the Encapsulation and Stability of Lysozyme. *Sustainable Chemistry* **2021**, *2*, 149–166, doi:10.3390/suschem2010010.
71. Vieira, N.S.M.; Oliveira, A.L.S.; Araújo, J.M.M.; Gaspar, M.M.; Pereiro, A.B. Ecotoxicity and Hemolytic Activity of Fluorinated Ionic Liquids. *Sustainable Chemistry* **2021**, *2*, 115–126, doi:10.3390/SUSCHEM2010008.
72. Lungwitz, R.; Strehmel, V.; Spange, S. The Dipolarity/Polarisability of 1-Alkyl-3-Methylimidazolium Ionic Liquids as Function of Anion Structure and the Alkyl Chain Length. *New Journal of Chemistry* **2010**, *34*, 1135–1140, doi:10.1039/B9NJ00751B.
73. Kim, M.; Li, L.Y.; Grace, J.R.; Yue, C. Selecting Reliable Physicochemical Properties of Perfluoroalkyl and Polyfluoroalkyl Substances (PFASs) Based on Molecular Descriptors. *Environmental Pollution* **2015**, *196*, 462–472, doi:10.1016/J.ENVPOL.2014.11.008.
74. Docherty, K.M.; Dixon, J.K.; Kulpa, C.F. Biodegradability of Imidazolium and Pyridinium Ionic Liquids by an Activated Sludge Microbial Community. *Biodegradation* **2007**, *18*, 481–493, doi:10.1007/S10532-006-9081-7.
75. Zhang, C.; Wang, H.; Malhotra, S. v.; Dodge, C.J.; Francis, A.J. Biodegradation of Pyridinium-Based Ionic Liquids by an Axenic Culture of Soil Corynebacteria. *Green Chemistry* **2010**, *12*, 851–885, doi:10.1039/B924264C.
76. Busch, M.P.; Kleinman, S.H.; Nemo, G.J. Current and Emerging Infectious Risks of Blood Transfusions. *J Am Med Assoc* **2003**, *289*, 959–962, doi:10.1001/JAMA.289.8.959.
77. Ferreira, M.L.; Llovell, F.; Vega, L.F.; Pereiro, A.B.; Araújo, J.M.M. Systematic Study of the Influence of the Molecular Structure of Fluorinated Ionic Liquids on the Solubilization of Atmospheric Gases Using a Soft-SAFT Based Approach. *J Mol Liq* **2019**, *294*, doi:10.1016/j.molliq.2019.111645.
78. Martinho, S.; Araújo, J.M.M.; Rebelo, L.P.N.; Pereiro, A.B.; Marrucho, I.M. (Liquid + Liquid) Equilibria of Perfluorocarbons with Fluorinated Ionic Liquids. *Journal of Chemical Thermodynamics* **2013**, *64*, 71–79, doi:10.1016/J.JCT.2013.04.019.

79. Pereiro, A.B.; Tomé, L.C.; Martinho, S.; Rebelo, L.P.N.; Marrucho, I.M. Gas Permeation Properties of Fluorinated Ionic Liquids. *Ind Eng Chem Res* **2013**, *52*, 4994–5001, doi:10.1021/IE4002469.
80. Egorova, K.S.; Gordeev, E.G.; Ananikov, V.P. Biological Activity of Ionic Liquids and Their Application in Pharmaceutics and Medicine. *Chem Rev* 2017, *117*, 7132–7189.
81. Marrucho, I.M.; Branco, L.C.; Rebelo, L.P.N. Ionic Liquids in Pharmaceutical Applications. *Annu Rev Chem Biomol Eng* **2014**, *5*, 527–546, doi:10.1146/ANNUREV-CHEMBIOENG-060713-040024.
82. Fujita, K.; MacFarlene, D.R.; Forsyth, M.; Yoshizawa-Fujita, M.; Murata, K.; Nakamura, N.; Ohno, H. Solubility and Stability of Cytochrome c in Hydrated Ionic Liquids: Effect of Oxo Acid Residues and Kosmotropicity. *Biomacromolecules* **2007**, *8*, 2080–2086, doi:10.1021/BM070041O.
83. Moniruzzaman, M.; Tamura, M.; Tahara, Y.; Kamiya, N.; Goto, M. Ionic Liquid-in-Oil Microemulsion as a Potential Carrier of Sparingly Soluble Drug: Characterization and Cytotoxicity Evaluation. *Int J Pharm* **2010**, *400*, 243–250, doi:10.1016/J.IJPHARM.2010.08.034.
84. Alves, M.; Vieira, N.S.M.; Rebelo, L.P.N.; Araújo, J.M.M.; Pereiro, A.B.; Archer, M. Fluorinated Ionic Liquids for Protein Drug Delivery Systems: Investigating Their Impact on the Structure and Function of Lysozyme. *Int J Pharm* **2017**, *526*, 309–320, doi:10.1016/j.ijpharm.2017.05.002.
85. Alves, M.M.S.; Araújo, J.M.M.; Martins, I.C.; Pereiro, A.B.; Archer, M. Insights into the Interaction of Bovine Serum Albumin with Surface-Active Ionic Liquids in Aqueous Solution. *J Mol Liq* **2021**, *322*, 114537, doi:10.1016/J.MOLLIQ.2020.114537.
86. Vieira, N.S.M.; Castro, P.J.; Marques, D.F.; Araújo, J.M.M.; Pereiro, A.B. Tailor-Made Fluorinated Ionic Liquids for Protein Delivery. *Nanomaterials* **2020**, *10*, 1–16, doi:10.3390/NANO10081594.
87. Ibraheem, D.; Elaissari, A.; Fessi, H. Administration Strategies for Proteins and Peptides. *Int J Pharm* **2014**, *477*, 578–589, doi:10.1016/J.IJPHARM.2014.10.059.
88. Dai, C.; Wang, B.; Zhao, H. Microencapsulation Peptide and Protein Drugs Delivery System. *Colloids Surf B Biointerfaces* **2005**, *41*, 117–120, doi:10.1016/J.COLSURFB.2004.10.032.
89. Mishra, H.; Chauhan, V.; Kumar, K.; Teotia, D. A Comprehensive Review on Liposomes: A Novel Drug Delivery System. *Journal of Drug Delivery and Therapeutics* **2018**, *8*, 400–404, doi:10.22270/jddt.v8i6.2071.
90. Bujacz, A. Structures of Bovine, Equine and Leporine Serum Albumin. *Acta Crystallogr D Biol Crystallogr* **2012**, *68*, 1278–1289, doi:10.1107/S0907444912027047.
91. Abeyrathne, E.D.N.S.; Lee, H.Y.; Ahn, D.U. Egg White Proteins and Their Potential Use in Food Processing or as Nutraceutical and Pharmaceutical Agents-A Review. *Poult Sci* **2013**, *92*, 3292–3299, doi:10.3382/PS.2013-03391.
92. Geng, F.; Zheng, L.; Liu, J.; Yu, L.; Tung, C. Interactions between a Surface Active Imidazolium Ionic Liquid and BSA. *Colloid Polym Sci* **2009**, *287*, 1253–1259, doi:10.1007/S00396-009-2085-1.
93. Baltus, R.E.; Culbertson, B.H.; Dai, S.; Luo, H.; DePaoli, D.W. Low-Pressure Solubility of Carbon Dioxide in Room-Temperature Ionic Liquids Measured with a Quartz Crystal Microbalance. *Journal of Physical Chemistry B* **2004**, *108*, 721–727, doi:10.1021/JP036051A.
94. Baltus, R.E.; Counce, R.M.; Culbertson, B.H.; Luo, H.; DePaoli, D.W.; Dai, S.; Duckworth, D.C. Examination of the Potential of Ionic Liquids for Gas Separations. *Sep Sci Technol* **2005**, *40*, 525–541, doi:10.1081/SS-200042513.
95. Muldoon, M.J.; Aki, S.N.V.K.; Anderson, J.L.; Dixon, J.K.; Brennecke, J.F. Improving Carbon Dioxide Solubility in Ionic Liquids. *J Phys Chem B* **2007**, *111*, 9001–9009, doi:10.1021/jp071897q.
96. Ying, H.; Baltus, R.E. Experimental Measurement of the Solubility and Diffusivity of CO 2 in Room-Temperature Ionic Liquids Using a Transient Thin-Liquid-Film Method. *Ind Eng Chem Res* **2007**, *46*, 8166–8175, doi:10.1021/IE070501U.

97. Almantariotis, D.; Gefflaut, T.; Pádua, A.A.H.; Coxam, J.Y.; Costa Gomes, M.F. Effect of Fluorination and Size of the Alkyl Side-Chain on the Solubility of Carbon Dioxide in 1-Alkyl-3-Methylimidazolium Bis(Trifluoromethylsulfonyl) Amide Ionic Liquids. *Journal of Physical Chemistry B* **2010**, *114*, 3608–3617, doi:10.1021/JP912176N.
98. Hong, S.K.; Park, Y.K. Measurement and Correlation of Vapor-Liquid Equilibria for a Binary System Containing 1-Butyl-3-Methylimidazolium Tridecafluorohexylsulfonate and Carbon Dioxide. *Korean Journal of Chemical Engineering* **2016**, *33*, 260–264, doi:10.1007/S11814-015-0127-6.
99. Zhou, L.; Fan, J.; Shang, X. CO2 Capture and Separation Properties in the Ionic Liquid 1-n-Butyl-3-Methylimidazolium Nonafluorobutylsulfonate. *Materials* **2014**, *7*, 3867–3880, doi:10.3390/MA7053867.
100. Hong, S.K.; Park, Y.K.; Pore, D.M. Experimental Determination and Prediction of Phase Behavior for 1-Butyl-3-Methylimidazolium Nonafluorobutyl Sulfonate and Carbon Dioxide. *Korean Journal of Chemical Engineering* **2014**, *31*, 1656–1660, doi:10.1007/S11814-014-0097-0.
101. Watanabe, M.; Kodama, D.; Makino, T.; Kanakubo, M. CO2 Absorption Properties of Imidazolium Based Ionic Liquids Using a Magnetic Suspension Balance. *Fluid Phase Equilib* **2016**, *420*, 44–49, doi:10.1016/J.FLUID.2015.12.055.
102. Raveendran, P.; Wallen, S.L. Exploring CO2-Philicity: Effects of Stepwise Fluorination. *Journal of Physical Chemistry B* **2003**, *107*, 1473–1477, doi:10.1021/JP027026S.
103. Vanhoutte, G.; Hojniak, S.D.; Bardé, F.; Binnemans, K.; Fransaera, J. Fluorine-Functionalized Ionic Liquids with High Oxygen Solubility. *RSC Adv* **2018**, *8*, 4525–4530, doi:10.1039/C7RA13403G.
104. Kang, C.S.M.; Zhang, X.; Macfarlane, D.R. Synthesis and Physicochemical Properties of Fluorinated Ionic Liquids with High Nitrogen Gas Solubility. *Journal of Physical Chemistry C* **2018**, *122*, 24550–24558, doi:10.1021/ACS.JPCC.8B07752.
105. Shiflett, M.B.; Yokozeki, A. Solubility and Diffusivity of Hydrofluorocarbons in Room-Temperature Ionic Liquids. *AIChE Journal* **2006**, *52*, 1205–1219, doi:10.1002/AIC.10685.
106. Shiflett, M.B.; Yokozeki, A.; Knapp, J.P. Process for the Separation of Fluorocarbons Using Ionic Liquids, US7964760B2. 2007.
107. Shiflett, M.B.; Harmer, M.A.; Junk, C.P.; Yokozeki, A. Solubility and Diffusivity of 1,1,1,2-Tetrafluoroethane in Room-Temperature Ionic Liquids. *Fluid Phase Equilib* **2006**, *242*, 220–232, doi:10.1016/J.FLUID.2006.01.026.
108. Shiflett, M.B.; Yokozeki, A. Binary Vapor-Liquid and Vapor-Liquid-Liquid Equilibria of Hydrofluorocarbons (HFC-125 and HFC-143a) and Hydrofluoroethers (HFE-125 and HFE-143a) with Ionic Liquid [Emim][Tf2N]. *J Chem Eng Data* **2008**, *53*, 492–497, doi:10.1021/JE700588D.
109. Asensio-Delgado, S.; Pardo, F.; Zarca, G.; Urtiaga, A. Vapor-Liquid Equilibria and Diffusion Coefficients of Difluoromethane, 1,1,1,2-Tetrafluoroethane, and 2,3,3,3-Tetrafluoropropene in Low-Viscosity Ionic Liquids. *J Chem Eng Data* **2020**, *65*, 4242–4251, doi:10.1021/ACS.JCED.0C00224.
110. Morais, A.R.C.; Harders, A.N.; Baca, K.R.; Olsen, G.M.; Befort, B.J.; Dowling, A.W.; Maginn, E.J.; Shiflett, M.B. Phase Equilibria, Diffusivities, and Equation of State Modeling of HFC-32 and HFC-125 in Imidazolium-Based Ionic Liquids for the Separation of R-410A. *Ind Eng Chem Res* **2020**, *59*, 18222–18235, doi:10.1021/ACS.IECR.0C02820.
111. Ren, W.; Scurto, A.M.; Shiflett, M.B.; Yokozeki, A. Phase Behavior and Equilibria of Ionic Liquids and Refrigerants: 1-Ethyl-3-Methyl-Imidazolium Bis(Trifluoromethylsulfonyl)Imide ([EMIm][Tf 2N]) and R-134a. *ACS Symposium Series* **2009**, *1006*, 112–128, doi:10.1021/BK-2009-1006.CH006.

112. Liu, X.; He, M.; Lv, N.; Qi, X.; Su, C. Vapor–Liquid Equilibrium of Three Hydrofluorocarbons with [HMIM][TF2N]. *J Chem Eng Data* **2015**, *60*, 1354–1361, doi:10.1021/je501069b.
113. Liu, X.; He, M.; Lv, N.; Qi, X.; Su, C. Solubilities of R-161 and R-143a in 1-Hexyl-3-Methylimidazolium Bis(Trifluoromethylsulfonyl)Imide. *Fluid Phase Equilib* **2015**, *388*, 37–42, doi:10.1016/j.fluid.2014.12.026.
114. Dong, L.; Zheng, D.; Sun, G.; Wu, X. Vapor-Liquid Equilibrium Measurements of Difluoromethane + [Emim]OTf, Difluoromethane + [Bmim]OTf, Difluoroethane + [Emim]OTf, and Difluoroethane + [Bmim]OTf Systems. *J Chem Eng Data* **2011**, *56*, 3663–3668, doi:10.1021/JE2005566.
115. Liu, X.; Lv, N.; Su, C.; He, M. Solubilities of R32, R245fa, R227ea and R236fa in a Phosphonium-Based Ionic Liquid. *J Mol Liq* **2016**, *218*, 525–530, doi:10.1016/j.molliq.2016.02.041.
116. Sousa, J.M.M.V.; Granjo, J.F.O.; Queimada, A.J.; Ferreira, A.G.M.; Oliveira, N.M.C.; Fonseca, I.M.A. Solubility of Hydrofluorocarbons in Phosphonium-Based Ionic Liquids: Experimental and Modelling Study. *Journal of Chemical Thermodynamics* **2014**, *79*, 184–191, doi:10.1016/J.JCT.2014.08.001.
117. Shiflett, M.B.; Harmer, M.A.; Junk, C.P.; Yokozeki, A. Solubility and Diffusivity of Difluoromethane in Room-Temperature Ionic Liquids. *J Chem Eng Data* **2006**, *51*, 483–495, doi:10.1021/JE050386Z.
118. Ren, W.; Scurto, A.M. Phase Equilibria of Imidazolium Ionic Liquids and the Refrigerant Gas, 1,1,1,2-Tetrafluoroethane (R-134a). *Fluid Phase Equilib* **2009**, *286*, 1–7, doi:10.1016/J.FLUID.2009.07.007.
119. Lepre, L.F.; Pison, L.; Otero, I.; Gautier, A.; Dévemy, J.; Husson, P.; Pádua, A.A.H.; Costa Gomes, M. Using Hydrogenated and Perfluorinated Gases to Probe the Interactions and Structure of Fluorinated Ionic Liquids. *Physical Chemistry Chemical Physics* **2019**, *21*, 8865–8873, doi:10.1039/C9CP00593E.
120. Jovell, D.; B. Gómez, S.; Zakrzewska, M.E.; Nunes, A.V.M.; Araújo, J.M.M.; Pereiro, A.B.; Llovell, F. Insight on the Solubility of R134a in Fluorinated Ionic Liquids and Deep Eutectic Solvents. *J Chem Eng Data* **2020**, *65*, 4956–4969, doi:10.1021/acs.jced.0c00588.
121. Sosa, J.E.; Ribeiro, R.P.P.L.; Castro, P.J.; Mota, J.P.B.; Araújo, J.M.M.; Pereiro, A.B. Absorption of Fluorinated Greenhouse Gases Using Fluorinated Ionic Liquids. *Ind Eng Chem Res* **2019**, *58*, 20769–20778, doi:10.1021/ACS.IECR.9B04648.
122. García, G.; Aparicio, S.; Ullah, R.; Atilhan, M. Deep Eutectic Solvents: Physicochemical Properties and Gas Separation Applications. *Energy and Fuels* **2015**, *29*, 2616–2644, doi:10.1021/EF5028873.
123. Castro, P.J.; Redondo, A.E.; Sosa, J.E.; Zakrzewska, M.E.; Nunes, A.V.M.; Araújo, J.M.M.; Pereiro, A.B. Absorption of Fluorinated Greenhouse Gases in Deep Eutectic Solvents. *Ind Eng Chem Res* **2020**, *59*, 13246–13259, doi:10.1021/acs.iecr.0c01893.
124. Pelaquim, F.P.; Barbosa Neto, A.M.; Dalmolin, I.A.L.; Costa, M.C. da Gas Solubility Using Deep Eutectic Solvents: Review and Analysis. *Ind Eng Chem Res* **2021**, *60*, 8607–8620, doi:10.1021/ACS.IECR.1C00947.
125. Sistla, Y.S.; Jain, L.; Khanna, A. Validation and Prediction of Solubility Parameters of Ionic Liquids for CO 2 Capture. *Sep Purif Technol* **2012**, *97*, 51–64, doi:10.1016/J.SEPPUR.2012.01.050.
126. Alkhatib, I.I.I.; Bahamon, D.; Llovell, F.; Abu-Zahra, M.R.M.; Vega, L.F. Perspectives and Guidelines on Thermodynamic Modelling of Deep Eutectic Solvents. *J Mol Liq* **2020**, *298*, 112183, doi:10.1016/j.molliq.2019.112183.
127. Alkhatib, I.I.I.; Ferreira, M.L.; Alba, C.G.; Bahamon, D.; Llovell, F.; Pereiro, A.B.; Araújo, J.M.M.; Abu-Zahra, M.R.M.; Vega, L.F. Screening of Ionic Liquids and Deep Eutectic Solvents for

Physical CO2 Absorption by Soft-SAFT Using Key Performance Indicators. *J Chem Eng Data* **2020**, *65*, doi:10.1021/acs.jced.0c00750.

128. Liu, X.; O'Harra, K.E.; Bara, J.E.; Turner, C.H. Solubility Behavior of CO2 in Ionic Liquids Based on Ionic Polarity Index Analyses. *Journal of Physical Chemistry B* **2021**, *125*, 3665–3676, doi:10.1021/ACS.JPCB.1C01508.
129. Sosa, J.E.; Santiago, R.; Hospital-Benito, D.; Costa Gomes, M.; Araújo, J.M.M.; Pereiro, A.B.; Palomar, J. Process Evaluation of Fluorinated Ionic Liquids as F-Gas Absorbents. *Environ Sci Technol* **2020**, *54*, 12784–12794, doi:10.1021/ACS.EST.0C05305.
130. Blas, F.J.; Vega, L.F. Thermodynamic Behaviour of Homonuclear and Heteronuclear Lennard-Jones Chains with Association Sites from Simulation and Theory. *Mol Phys* **1997**, *92*, 135–150, doi:10.1080/002689797170707.
131. Blas, F.J.; Vega, L.F. Prediction of Binary and Ternary Diagrams Using the Statistical Associating Fluid Theory (SAFT) Equation of State. *Ind Eng Chem Res* **1998**, *37*, 660–674, doi:10.1021/ie970449+.
132. Ferreira, M.L.; Araújo, J.M.M.; Vega, L.F.; Pereiro, A.B. Understanding the Absorption of Fluorinated Gases in Fluorinated Ionic Liquids for Recovering Purposes Using Soft-SAFT. *J Chem Eng Data* **2022**, acs.jced.1c00984, doi:10.1021/ACS.JCED.1C00984.
133. Friess, K.; Izák, P.; Kárászová, M.; Pasichnyk, M.; Lanč, M.; Nikolaeva, D.; Luis, P.; Jansen, J.C. A Review on Ionic Liquid Gas Separation Membranes. *Membranes (Basel)* **2021**, *11*, 97, doi:10.3390/membranes11020097.
134. Bara, J.E.; Gabriel, C.J.; Carlisle, T.K.; Camper, D.E.; Finotello, A.; Gin, D.L.; Noble, R.D. Gas Separations in Fluoroalkyl-Functionalized Room-Temperature Ionic Liquids Using Supported Liquid Membranes. *Chemical Engineering Journal* **2009**, *147*, 43–50, doi:10.1016/J.CEJ.2008.11.021.
135. Gouveia, A.S.L.; Tomé, L.C.; Lozinskaya, E.I.; Shaplov, A.S.; Vygodskii, Y.S.; Marrucho, I.M. Exploring the Effect of Fluorinated Anions on the CO2/N2 Separation of Supported Ionic Liquid Membranes. *Physical Chemistry Chemical Physics* **2017**, *19*, 28876–28884, doi:10.1039/C7CP06297D.
136. Sood, R.; Iojoiu, C.; Espuche, E.; Gouanvé, F.; Mendil-Jakani, H.; Lyonnard, S. Influence of Different Perfluorinated Anion Based Ionic Liquids on the Intrinsic Properties of Nafion®. *J Memb Sci* **2015**, *495*, 445–456, doi:10.1016/j.memsci.2015.07.006.
137. Pardo, F.; Zarca, G.; Urtiaga, A. Separation of Refrigerant Gas Mixtures Containing R32, R134a, and R1234yf through Poly(Ether-Block-Amide) Membranes. *ACS Sustain Chem Eng* **2020**, *8*, 2548–2556, doi:10.1021/acssuschemeng.9b07195.
138. Pardo, F.; Zarca, G.; Urtiaga, A. Effect of Feed Pressure and Long-Term Separation Performance of Pebax-Ionic Liquid Membranes for the Recovery of Difluoromethane (R32) from Refrigerant Mixture R410A. *J Memb Sci* **2021**, *618*, 118744, doi:10.1016/j.memsci.2020.118744.
139. Pardo, F.; Gutiérrez-Hernández, S. v.; Zarca, G.; Urtiaga, A. Toward the Recycling of Low-GWP Hydrofluorocarbon/Hydrofluoroolefin Refrigerant Mixtures Using Composite Ionic Liquid–Polymer Membranes. *ACS Sustain Chem Eng* **2021**, *9*, 7012–7021, doi:10.1021/acssuschemeng.1c00668.
140. Pardo, F.; Gutiérrez-Hernández, S. v.; Hermida-Merino, C.; Araújo, J.M.M.; Piñeiro, M.M.; Pereiro, A.B.; Zarca, G.; Urtiaga, A. Integration of Stable Ionic Liquid-Based Nanofluids into Polymer Membranes. Part II: Gas Separation Properties toward Fluorinated Greenhouse Gases. *Nanomaterials* **2021**, *11*, 582, doi:10.3390/nano11030582.
141. Adkins, C.J. *Equilibrium Thermodynamics*; 3rd ed.; Cambridge University Press: Cambridge, UK, 1983; ISBN 052125445.

142. Freire, M.G.; Carvalho, P.J.; Santos, L.M.N.B.F.; Gomes, L.R.; Marrucho, I.M.; Coutinho, J.A.P. Solubility of Water in Fluorocarbons: Experimental and COSMO-RS Prediction Results. *J Chem Thermodyn* **2010**, *42*, 213–219, doi:10.1016/j.jct.2009.08.005.
143. Duce, C.; Tiné, M.R.; Lepori, L.; Matteoli, E. Thermodynamic Study of Perfluorohexane+ether Mixtures. *Fluid Phase Equilib* **2008**, *269*, 59–68, doi:10.1016/j.fluid.2008.04.021.
144. Ben-Naim, A. On the Evolution of the Concept of Solvation Thermodynamics. *J Solution Chem* **2001**, *30*, 475–487, doi:10.1023/A:1010304732665.
145. Ben-Naim, A. *Molecular Theory of Solutions*; Oxford : New York, 2006;
146. Cavallo, G.; Metrangolo, P.; Milani, R.; Pilati, T.; Priimagi, A.; Resnati, G.; Terraneo, G. The Halogen Bond. *Chem Rev* **2016**, *116*, 2478–2601, doi:10.1021/acs.chemrev.5b00484.
147. Panini, P.; Chopra, D. Understanding of Noncovalent Interactions Involving Organic Fluorine. In; Springer-Verlag: Berlin Heidelberg , 2015; pp. 37–67.
148. Kunze, M.; Jeong, S.; Paillard, E.; Winter, M.; Passerini, S. Melting Behavior of Pyrrolidinium-Based Ionic Liquids and Their Binary Mixtures. *The Journal of Physical Chemistry C* **2010**, *114*, 12364–12369, doi:10.1021/jp103746k.

CHAPTER 3

MODELLING FLUORINATED IONIC LIQUIDS: THE IMPACT OF THE MOLECULAR STRUCTURE ON THE THERMOPHYSICAL PROPERTIES

3.1 Introduction

Ionic liquids (ILs) have emerged as a new and innovative class of alternative green solvents for industrial applications that have high environmental, health, or safety issues [1–3]. The remarkable physical and chemical properties of ILs empower their use in numerous fields, from chemistry to biology [4]. The versatility of ILs applications has arisen from the fact that they can be designed with specific properties, by varying both the cation and the anion, or through the introduction of a specific functional group on the cation and/or anion [5]. A sheer number of available ILs higher than 10^{18} (including their binary and ternary mixtures) have been predicted, which results in the constant emergence of novel ILs families. This provides a massive number of possibilities for scientific innovation and, subsequently, the number of publications in the field has grown exponentially in the last years [6]. However, this rapid growth has not been followed by the undeniable requirement to understand the physicochemical properties and thermodynamic behaviour of ILs, whereas the experimental work to perform a fully physicochemical characterization takes a huge amount of resources, costs and time, hindering their use in new technologies. An alternative approach to characterize them would be by using equations of state (EoS), however, due to the complex behaviour of these systems, most classical equations fail in describing their behaviour.

Among these novel compounds, fluorinated ionic liquids (FILs) have recently started to be explored and attained special attention as an alternative in areas where highly fluorinated compounds (FCs) are used. They can combine the best properties of highly FCs (inert compounds with extremely low surface tension, high capacity to dissolve gases and ability to rearrange into stable self-assembled supramolecular and colloidal systems), with those of ILs (almost null vapour pressure, easiness in recovering and recycling, non-flammability and tuneable properties) [7–9]. The FILs can form a new nano-segregated, fluorinated domain, asides from the polar and hydrogenated domains that occur in the non-fluorinated ILs. This structural feature allows the formation of three distinct solvation regions, converting FILs into "*3-in-1*" solvents [10–13]. These three domains can assume different arrangements greatly affecting their phase behaviour, playing an important role in the tuneable thermodynamic properties of FILs for the desired application [14,15]. Exceptional properties have been found for these systems, for example, they can have an amphiphilic behaviour which improves their self-aggregation and therefore, make them enhanced surfactants, as well as their capacity to reduce the impact of the addition of water upon the IL's H-bond acceptance ability. FILs with short alkyl chains in the cation have surprisingly shown: (i) total miscibility in water and stable self-assembled structures were found in an aqueous medium; (ii) and the potential to make constant their hydrogen bond acceptance

ability [16–21]. Moreover, the study of FILs binary mixtures showed lower melting points (regarding the pure FILs), expanding thus their application range which allowed to obtain a wider amount of solvents that can be liquid at temperatures close to or below room temperature [22]. Along with these exceptional properties, FILs are of high interest as new cleaner compounds to replace totally or partially the harmful FCs that are used for instance in components of pharmaceuticals, fire retardants, insecticides, lubricants, polymers, refrigerants, and surfactants [23]. Beyond these applications, FILs can play a meaningful role as a potential tool in biomedical applications such as artificial blood substitutes, liquid ventilation, imaging agents, intravenous formulations [8,16,24–26], and more recently as drug delivery systems for biomolecules [27].

The complexity of FILs emphasizes the need for reliable, systematic, fast, and economical methodologies to understand and predict their physicochemical and structural properties. Therefore, several efforts have been made in recent years to develop modelling tools to predict the properties of ILs and mixtures with other ILs or other compounds in a systematic way, to increase their actual implementation in the desired applications [28,29]. Different modelling approaches have been proposed, from those based on empirical (regressions) methodologies to the theoretical (predictive) ones, such as molecular simulations (MS) and equations of state (EoS) [30–32]. MS has played an important role in the characterization of ILs, mainly in the study of the local structure, the solubility of compounds and transport properties [14,15,33–37]. Despite the success and undeniable interest in using MS as a powerful predictive approach, the generation of new force fields to allow the search for new potential ILs and the estimation of ILs properties by molecular simulations remains a complex and lengthy task. Therefore, MS is not yet an ordinary tool for the design of new processes and products in this field, nor for screening purposes before selecting the right IL for a potential application. Consequently, the use of EoS, which are relatively simple models that provide reliable and faster calculations, stands as one of the most promising alternatives for describing the thermophysical properties of ILs in a fast and still accurate manner. Recent developments in statistical thermodynamics and molecular-based EoSs, in which the structural information of the molecules is built from their inception and their parameters have physical meaning, have been applied to ILs with great success [31,32].

Of special interest are those based on the SAFT EoS (from the Statistical Associating Fluid Theory) proposed by Chapman *et al*. [38–40] based on Wertheim's first-order thermodynamic perturbation theory [41–44]. Among them, soft-SAFT [45,46] has been extensively used for the prediction of thermophysical properties of ILs, including pure ILs density, transport, interfacial and derivative properties and phase equilibria of their mixtures with water, gases, and also with other ILs, in excellent agreement with experimental data

[29,47–60]. Following the pioneering work of Andreu and Vega, most of the SAFT models of ILs contemplate the cation and anion in a coarse grain approach as a single molecule, explicitly considering the contribution of the hydrogen-bonding interactions present in ILs as associative forces [48,49]. Vega and co-workers have successfully applied soft-SAFT to several ILs families, being the more meaningful ones for this work those modelling ILs with fluorinated anions [29,47–60]

In this chapter soft-SAFT EoS [45,46] was used to characterize the FILs properties and allow the design and development of FILs with the best characteristics for biological applications. For that, the soft-SAFT EoS was used to model and characterize FILs with promising characteristics for biomedical applications. The modelling of the FILs was performed using knowledge of previous studies, information on the charge delocalization of the FILs and experimental data from the literature. Therefore, the soft-SAFT modelling was used to effectively predict the properties of the pure FILs, such as density and surface tension. To ensure the validity of these new models, the soft-SAFT was used to predict the thermodynamic behaviour of FILs in the presence of different gases (systems with sufficient available data), and a very good agreement was achieved, indicating the robustness of the soft-SAFT approach.

FILs are much more complex compounds when compared with traditional ILs. Aiming to facilitate and reduce the amount of experimental data necessary to model FILs within the soft-SAFT framework, a thorough analysis of the already modelled FILs present in the literature was performed. A total of 38 FILs models were considered, paying special attention to the structural features of FILs and the physical meaning of the soft-SAFT parameters. This careful analysis has allowed the development of a systematic methodology to build new transferable molecular models for FILs and describe their behaviour and of their mixtures. The methodology was validated by predicting the thermophysical and derivative properties of pure FILs and their behaviour with different solutes (gases, alcohols, water), demonstrating the high predictive capabilities of soft-SAFT EoS. Then, FILs can be modelled intuitively and robustly regarding the process of parametrization when limited experimental data are available.

To extend and confirm the validity of these transferable models, FILs, that were not modelled by soft-SAFT EoS yet were chosen from the literature. This theoretical tool allowed their characterization and successfully captured the behaviour of the FILs with fluorinated gases, to allow a comparison with the predictions obtained by soft-SAFT EoS.

Therefore, the soft-SAFT EoS allows the characterization of the pure FILs and the behaviour of their complex mixtures with other compounds, showing a highly predictive ability to describe the behaviour of these complex systems in a faster and more robust way.

This chapter has allowed the improvement of a feasible tool to accelerate the study of the physical and chemical properties of very complex systems, aiding the selection of the best structural features of FILs to use in the biological field.

This chapter is adapted from the following publications:

Section 3.3

Margarida L. Ferreira, Fèlix Llovell, Lourdes F. Vega, Ana B. Pereiro, João M.M. Araújo, Systematic study of the influence of the molecular structure of fluorinated ionic liquids on the solubilization of atmospheric gases using a soft-SAFT based approach, *Journal of Molecular Liquids* 294 (2019) 111645. DOI: 10.1016/j.molliq.2019.111645

Section 3.4

Margarida L. Ferreira, João M.M. Araújo, Ana B. Pereiro, Lourdes F. Vega, Insights into the influence of the molecular structure of Fluorinated Ionic Liquids on their thermophysical properties. A soft-SAFT based approach, *Physical Chemistry Chemical Physics* 21 (2019) 6362-6380. DOI: 10.1039/C8CP07522K

Section 3.5

Margarida L. Ferreira, João M.M. Araújo, Lourdes F. Vega, Ana B. Pereiro, Understanding the Absorption of Fluorinated Gases in Fluorinated Ionic Liquids for Recovering Purposes Using Soft-SAFT, *Journal of Chemical & Engineering Data* 67 (2022) 1951-1963. DOI: 10.1021/acs.jced.1c00984

3.2 The soft-SAFT equation of state

The soft-SAFT EoS [45,46] is a variant of SAFT using the Lennard-Jones (LJ) as the reference fluid, that successfully provides the thermophysical properties and phase behaviour of complex molecules and their mixtures in good agreement with experimental data. The main advantage of this approach is that the different molecular effects on a system, like the molecular shape and association, can be independently quantified, providing a separate contribution to the energy of the system. The soft-SAFT approach has been showing great results in the description of pure ILs and their mixtures with liquid and gas solutes [29,47–60]. The equation has the ability to explicitly account for strong short-range directional forces, such as hydrogen bonding effects, from Wertheim's first-order perturbation theory [41–44], and to account for the van der Waals interactions, through a LJ reference term [45,46]. It is expressed as a sum of microscopic contributions to the total Helmholtz free energy of the system (Equation 3.2.1):

$$A^{res} = A - A^{id} = A^{ref} + A^{chain} + A^{assoc} + A^{polar} \qquad 3.2.1$$

where A^{res} is the residual Helmholtz free energy and A^{id} corresponds to the ideal contribution. Subsequently, A^{ref} refers to the contributions to the free energy due to the monomer-monomer repulsive and attractive (dispersion) interactions, A^{chain} to the formation of chains and A^{assoc} to the site-site intermolecular association, respectively. Soft-SAFT uses a Lennard-Jones (LJ) intermolecular potential as reference term, considering simultaneously the repulsive and dispersive contributions of the monomers that constitute the chain. The accurate EoS of Johnson *et al*. [61] is used to calculate the contribution of the LJ intermolecular potential. The extension of the equation to mixtures is performed by applying the van der Waals one-fluid theory with the modified Lorentz-Berthelot combining rules (Equations 3.2.2 and 3.2.3):

$$\sigma_{ij} = \eta_{ij}\left(\frac{\sigma_{ii} + \sigma_{jj}}{2}\right) \qquad 3.2.2$$

$$\varepsilon_{ij} = \xi_{ij}\left(\varepsilon_{ii}\varepsilon_{jj}\right)^{1/2} \qquad 3.2.3$$

where η_{ij} and $\xi_{ij}$are the size and energy binary parameters, respectively, accounting for size and energy asymmetries between the different compounds in the mixture. These values become unity when the equation is used in a predictive approach from the pure component parameters. However, η_{ij} and ξ_{ij} can be fitted to phase equilibrium binary data to improve the description of some mixtures.

A total of five parameters are used to define each molecule of an associating fluid: the chain length, m; the segment diameter, σ; the dispersive energy between the segments, ε, and

two more parameters that consider the associating interactions of the model, the site-site association energy, ε^{HB} and the site-site bonding volume of association, κ^{HB}.

A multipolar term (A^{polar}) can be explicitly included, as an additional term to Equation 3.2.1, to treat the polarity of molecules, such as carbon dioxide, accounting for the quadrupole−quadrupole or dipole-dipole interactions. This methodology requires the inclusion of an effective quadrupole moment, Q (c·m²) for the case of CO_2. The extension of this method into chain fluids assumes that the polar moments are well-localized on certain segments of the chain [62]. As consequence, a fraction x_p is defined as the fraction of the molecule affected by the quadrupole, while the value of x_p is fixed. The value of Q is fitted to experimental data, along with the rest of soft-SAFT molecular parameters, but its value is restricted within the range of experimental values.

The chain and association terms of the equation derive directly from Wertheim's first-order thermodynamic perturbation theory (TPT1) and can be directly applied to mixtures [41–44]. If the mixture studied is composed of two associating fluids, like ILs and F-gases, the association energy ($\varepsilon^{HB}_{\alpha\beta,\,ij}$) and volume ($\kappa^{HB}_{\alpha\beta,\,ij}$) parameters of the binary system must be calculated by the following rules:

$$\kappa^{HB}_{\alpha\beta,\,ij}=\left(\frac{\sqrt[3]{\kappa^{HB}_{\alpha\beta,\,ii}}+\sqrt[3]{\kappa^{HB}_{\alpha\beta,\,jj}}}{2}\right)^{3} \qquad 3.2.4$$

$$\varepsilon^{HB}_{\alpha\beta,\,ij}=\sqrt{\varepsilon^{HB}_{\alpha\beta,\,ii}\varepsilon^{HB}_{\alpha\beta,\,jj}} \qquad 3.2.5$$

The soft-SAFT model and corresponding software are readily available for phase equilibria calculations, and hence, solubility calculations, by imposing the equality of chemical potential of each component in the coexisting phases at fixed temperature and pressure, to satisfy chemical, thermal and mechanical stability. As the model is explicitly formulated in terms of temperature, density, and phase composition, the fugacity method is applied by equating chemical potential and pressure at a fixed temperature as:

$$\mu_i^I(T,\rho^I,x^I) = \mu_i^{II}(T,\rho^{II},x^{II}) \qquad 3.2.6$$

$$P^I(T,\rho^I,x^I) = P^I(T,\rho^{II},x^{II}) \qquad 3.2.7$$

An extended version of soft-SAFT EoS has been used to calculate the surface tension of FILs, by coupling it with the Density Gradient Theory (DGT) [63–65]. In the DGT approach, the local Helmholtz free energy density is calculated through the expansion of a Taylor series around the free energy density term (a_0) of the homogeneous fluid at the local density, to the

second order, that is, to the second derivative of the profile with respect to the distance from the interface, which is given by Equation 3.2.8:

$$A = \int \left[a_0(\rho) + \sum_i \sum_j \frac{1}{2} c_{ij} \nabla\rho_i \nabla\rho_j \right] d^3r \qquad 3.2.8$$

where $a_0(\rho)$ is the Helmholtz free energy density of the homogeneous fluid at the local density ρ_0. $\nabla\rho_x$ represents the local gradient in the density of a given component x, while the parameter c_{ij} represents the direct correlation function, known as the influence parameter. It is assumed that this parameter is temperature independent and obtained by fitting to experimental or molecular simulation interfacial tension data.

The soft-SAFT EoS methodology has been already extensively described in the literature, and the reader is referred to previous works for further details [31,50,60,66–68].

3.3 Systematic study of the influence of the molecular structure of fluorinated ionic liquids on the solubilization of atmospheric gases using a soft-SAFT based approach

In the current section, the thermophysical properties and the phase behaviour with carbon dioxide, nitrogen and oxygen of seven ILs (five FILs and two fluoro-containing ILs) have been studied using a combined experimental-theoretical approach in order to select the best ionic liquid to enhance gas solubility. The compounds investigated are based on four anions (perfluorobutanesulfonate ($[C_4F_9SO_3]^-$), perfluoropentanoate ($[C_4F_9CO_2]^-$), trifluoromethanesulfonate ($[CF_3SO_3]^-$) and trifluoroacetate ($[CF_3CO_2]^-$) combined with imidazolium ($[C_nC_1Im]^+$, n = 2 and 4) and pyridinium ($[C_2C_1py]^+$) cations. Taking advantage of the transferability of soft-SAFT models and parameters already proven, models previously obtained with soft-SAFT [47,48,54] have been transferred for the FILs investigated in this work, for which there were no soft-SAFT models developed. Thus, the density and surface tension of the pure FILs have been calculated and compared with experimental data in order to validate these models. Subsequently, the solubility of CO_2, N_2 and O_2 in the ILs depicted in Table 3.3.1 have been predicted with soft-SAFT and compared with experimental data.

3.3.1 Soft-SAFT molecular models

The accurate prediction of ILs thermodynamic properties through the soft-SAFT framework depends on the selection of a reliable and simplified coarse-grained model that describes the main physical features of ILs. In earlier studies, [48,50,51,54] ILs have been modelled as single chain molecules with the cation and the anion together by assuming a low ionic character, due to the formation of short-lived ion pairs [69–71]. In addition, a specific number of associating sites were considered to mimic the highly anisotropic interactions between the counterions.

For this purpose, molecular simulations and quantum information can be used as a guide [48–52,54,55,72]. For the case of ILs with similar structural features or charge delocalization, the association schemes can be transferred, as has been done in previous works [47,51]. Overall, associating molecules as ILs [48,49] have been modelled by the definition of five molecular parameters: monomers chain length, m; monomer diameter, σ; van der Waals energy between the monomers, ε; and site-site association energy and bonding-volume, $\varepsilon^{HB}$and the κ^{HB}, respectively. The first three parameters describe the molecules as homonuclear chains, composed of monomers that interact according to a certain van der Waals energy value and occupy a molecular volume (represented by $m\sigma^3$). The last two parameters

mimic the highly directional short-range forces such as hydrogen bonding, by including square-well spheres embedded into the core of the LJ segments (see Figure 3.3.1).

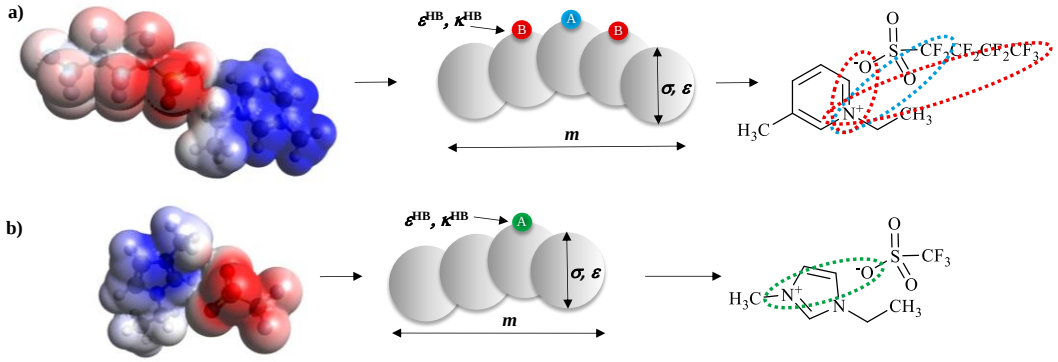

Figure 3.3.1 Electrostatic potential (blue stands for positive and red for negative charges), soft-SAFT molecular model and respective scheme of association for a) $[C_2C_1py][C_4F_9SO_3]$, $[C_2C_1Im][C_4F_9CO_2]$ and $[C_2C_1py][C_4F_9CO_2]$, all described by a 3-site model; and b) $[C_2C_1Im][CF_3SO_3]$ and $[C_2C_1Im][CF_3CO_2]$, both described by 1-site scheme of association.

In this work, seven different ILs (nomenclature and chemical structures depicted in Table 3.3.1) have been selected to study the solubility of CO_2, N_2 and O_2. First, the structures of $[C_2C_1py][C_4F_9SO_3]$, $[C_2C_1Im][C_4F_9CO_2]$, $[C_2C_1py][C_4F_9CO_2]$, $[C_2C_1Im][CF_3SO_3]$ and $[C_2C_1Im][CF_3CO_2]$ have been energy-minimized by using the molecular mechanisms Universal Force Field (UFF) [73]. Subsequently, the electrostatic potential surfaces for these ILs have been obtained by using the MMFF94 force field (see Figure 3.3.1) [74]. The quantum chemical calculations have been performed by using the open-source software Avogadro (version 1.2.0) [75]. In previous work, the model of $[C_nC_1Im][C_4F_9SO_3]$ FILs family was chosen through the guidance of quantum chemical calculations that disclose the electrostatic potential. A highly negative delocalized charged area was identified, suggesting that more than one association site is needed to mimic the FILs interactions [47]. Using the aforementioned information and considering that the FILs herein studied have a similar charge distribution (see Figure 3.3.1a), the 3-site associating scheme that has been used to model $[C_2C_1Im][C_4F_9SO_3]$ and $[C_4C_1Im][C_4F_9SO_3]$ has been transferred to $[C_2C_1py][C_4F_9SO_3]$, $[C_2C_1Im][C_4F_9CO_2]$ and $[C_2C_1py][C_4F_9CO_2]$. This model is defined by three associating sites, one associating site of type *A*, representing the main interactions of the fluorine atoms with the cation, and two sites of type *B* on behalf of the delocalized charge due to the surrounding fluorine atoms and the oxygen atoms of the anion. Only *A*–*B* interactions between different FIL molecules are allowed (see Figure 3.3.1a).

Table 3.3.1 Chemical structure and respective acronyms of the studied ionic liquids.

IL Designation	Chemical Structure
1-Ethyl-3-methylimidazolium perfluorobutanesulfonate **[C_2C_1Im][$C_4F_9SO_3$]**	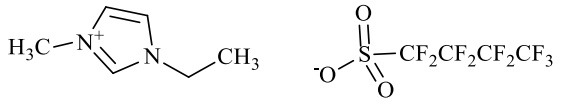
1-Butyl-3-methylimidazolium perfluorobutanesulfonate **[C_4C_1Im][$C_4F_9SO_3$]**	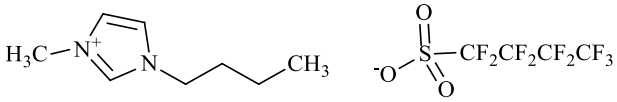
1-Ethyl-3-methylpyridinium perfluorobutanesulfonate **[C_2C_1py][$C_4F_9SO_3$]**	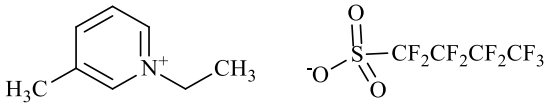
1-Ethyl-3-methylimidazolium perfluoropentanoate **[C_2C_1Im][$C_4F_9CO_2$]**	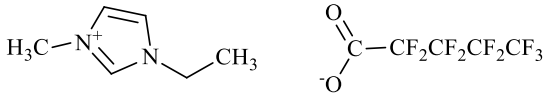
1-Ethyl-3-methylpyridinium perfluoropentanoate **[C_2C_1py][$C_4F_9CO_2$]**	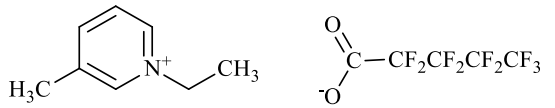
1-Ethyl-3-methylimidazolium trifluoromethanesulfonate **[C_2C_1Im][CF_3SO_3]**	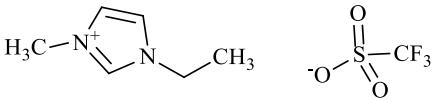
1-Ethyl-3-methylimidazolium trifluoroacetate **[C_2C_1Im][CF_3CO_2]**	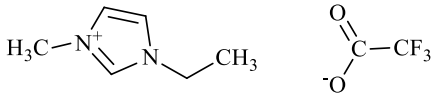

The [C_2C_1Im][CF_3SO_3] and [C_2C_1Im][CF_3CO_2] ILs have already been studied in our previous work [76]. The 3-site associating scheme fails into describing the thermodynamic behaviour of these ILs. As depicted in Figure 3.3.1b, these ILs have an electrostatic potential much more centred, and the delocalization of charges is lower. This is due to the quasi-spherical shape of $[CF_3SO_3]^-$ and $[CF_3CO_2]^-$ anions, which is very similar to the behaviour described by the ILs based on $[BF_4]^-$ and $[PF_6]^-$ anions [48,54]. Therefore, these ILs have been described with a 1-associating site scheme as shown in Figure 3.3.1b where site *A* stands for the interactions between the oxygen atoms with the cation. Only *A*-*A* interactions are allowed between the different ILs molecules, so this site has a dual positive-negative nature.

The studied atmospheric gases (CO_2, N_2 and O_2) have been already modelled in previous studies, and models and parameters were used in a transferable manner in this work. Briefly, CO_2 and N_2 have been modelled as LJ chains with a quadrupole. The quadrupolar interactions are taken into account through the molecular parameter x_p which was fixed to 1/3 for CO_2 and 1/2 for N_2, representing the number of segments in those molecules that may momentarily contain the quadrupole, and Q, the quadrupolar moment. In the case of the O_2 model, the quadrupole moment has not been explicitly considered [51,67,77]. More details on

these models can be found elsewhere [31,58]. The respective molecular parameters for these three gases and the values of *Q* are reported in Table 3.3.2.

Table 3.3.2 Molecular weight and molecular parameters of carbon dioxide, nitrogen, and oxygen.[1]

	$\mathbf{M_w}$ [g mol^{-1}]	m	σ [Å]	ε/k_B [K]	Q [C·m^2]	x_p
CO_2	44.01	1.571	3.184	160.2	4.4×10^{-40}	⅓
N_2	28.01	1.205	3.384	89.16	1.2×10^{-40}	½
O_2	32.00	1.168	3.198	111.5	–	–

3.3.2 Results and discussion

3.3.2.1 Thermodynamic properties of fluorinated ionic liquids

FILs based on perfluorobutanesulfonate ($[C_4F_9SO_3]^-$) and perfluoropentanoate ($[C_4F_9CO_2]^-$) anions and fluoro-containing ILs based on trifluoromethanesulfonate ($[CF_3SO_3]^-$) and trifluoroacetate ($[CF_3CO_2]^-$) anions, conjugated with imidazolium ($[C_nC_1Im]^+$, n = 2 and 4) and pyridinium ($[C_2C_1py]^+$) cations (see Table 3.3.1) have been selected to study the solubilization of CO_2, N_2 and O_2. Three novel molecular models have been defined with soft-SAFT EoS for $[C_2C_1py][C_4F_9SO_3]$, $[C_2C_1Im][C_4F_9CO_2]$ and $[C_2C_1py][C_4F_9CO_2]$ FILs (see Section 3.3.2), implementing a transferability methodology recently proposed [76]. The procedure allows assembling FIL models with high predictive capabilities in an intuitive way regarding the process of parametrization from the molecular structure, allowing one to characterize the thermophysical behaviour of FILs when limited experimental data are available.

After the definition of the association schemes, a set of molecular parameters has to be obtained for each FIL by fitting temperature-density experimental data at atmospheric pressure [8,12,19]. Considering the quasi-linear behaviour of the experimental data, the five molecular parameters adjustment allows a huge number of combinations with good agreement with these data. Therefore, taking advantage of the transferability and physical basis of the soft-SAFT approach, and in order to reduce the number of combinations, several assumptions have been made to obtain molecular parameters describing the right physical trends of FILs properties, taking into account their structural features. These successive assumptions are based on physical arguments, previous experience, and the transferability of soft-SAFT molecular parameters for similar families [31,58].

Two major assumptions have been made for the definition of the molecular models of the $[C_2C_1py][C_4F_9SO_3]$, $[C_2C_1Im][C_4F_9CO_2]$ and $[C_2C_1py][C_4F_9CO_2]$ FILs. First, the same value for the chain molecular parameter, m, has been kept for the FILs based on pyridinium and imidazolium cations conjugated with the same anion (due to the similarity in the chemical structure and size, see Table 3.3.1). Thus, the size differences can be taken into account by the segment diameter parameter, σ. Second, the site-site association energy (ε^{HB}) and volume (κ^{HB}) have been transferred from $[C_nC_1Im][C_4F_9SO_3]$ FILs family [47]. This last hypothesis

assumes that the association interactions are independent of the cation and the anion functional group. The differences between FILs, regarding van der Waals energy, have been fully considered by the optimization of ε parameter. Thus, σ and ε are the two, out of five parameters, obtained by fitting to temperature-density experimental data at atmospheric pressure [47]. Subsequently, the molecular parameters set, that provided a good description of density data (see Figure 3.3.2), have been used to calculate the surface tension of the FILs for which there are available experimental data, $[C_2C_1py][C_4F_9SO_3]$ and $[C_2C_1py][C_4F_9CO_2]$ (see Figure 3.3.3) [19]. The fluoro-containing ILs, $[C_2C_1Im][CF_3SO_3]$ and $[C_2C_1Im][CF_3CO_2]$, which have been modelled in our previous work, have small and spherical anions, with a very localized charge (see Figure 3.3.1b), as the case of imidazolium-based ILs conjugated with $[BF_4]^-$ and $[PF_6]^-$ anions [76]. Therefore, the five molecular parameters of $[C_3C_1Im][BF_4]$ and $[C_4C_1Im][BF_4]$ [48,54] have been directly transferred to $[C_2C_1Im][CF_3SO_3]$ and $[C_2C_1Im][CF_3CO_2]$, respectively, without performing any fitting. The density and solubility of carbon dioxide have been calculated for these two ILs in good agreement with experimental data [47]. Looking for the chemical structure of these ILs, the addition of a carbon into the hydrogenated side chain of the cation of $[C_3C_1Im][BF_4]$ and $[C_4C_1Im][BF_4]$, compensates for the size difference between $[C_2C_1Im][CF_3SO_3]$ and $[C_2C_1Im][CF_3CO_2]$ anions functional groups. In addition, the calculation of surface tension for the $[C_2C_1Im][CF_3SO_3]$ and $[C_2C_1Im][CF_3CO_2]$ ILs is presented in Figure 3.3.3. The excellent agreement with experimental data emphasizes the robustness of soft-SAFT in the transferability of molecular parameters (see Figure 3.3.3).

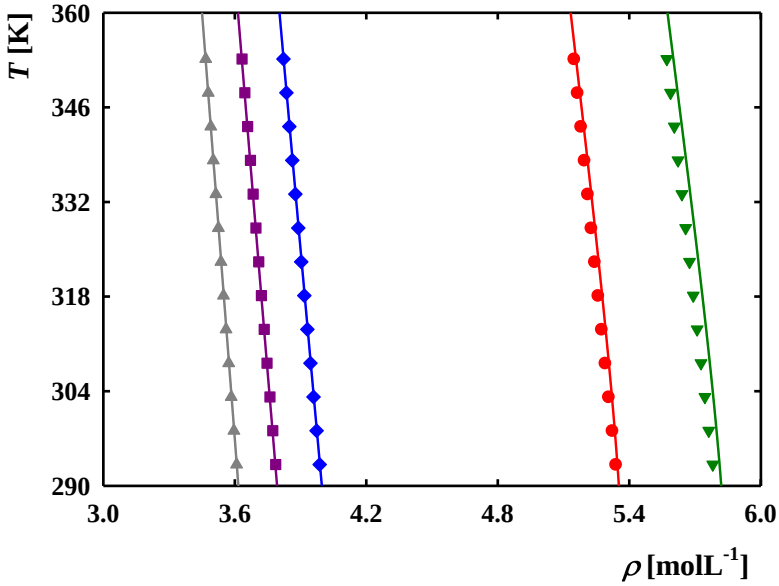

Figure 3.3.2 Temperature-density diagram for the studied ionic liquids at atmospheric pressure. Symbols represent experimental data from literature [8,12,19] (red ●, $[C_2C_1Im][CF_3SO_3]$; green ▼, $[C_2C_1Im][CF_3CO_2]$; blue ♦, $[C_2C_1Im][C_4F_9CO_2]$; grey ▲, $[C_2C_1py][C_4F_9SO_3]$; purple ■, $[C_2C_1py][C_4F_9CO_2]$) and the lines are the soft-SAFT calculations.

As has been mentioned in Section 3.2, the DGT procedure involves an additional influence parameter, *c*, which is fitted to experimental surface tension data [19,78,79]. Table 3.3.3 shows the values for this parameter, which is in the range of values that have been found for similar ILs [47]. Using this parameter, good agreement with experimental data for the $[C_2C_1py][C_4F_9SO_3]$ and $[C_2C_1py][C_4F_9CO_2]$ FILs with available surface tension-temperature experimental data (absolute average deviations (AAD) of less than 0.8%, within the experimental uncertainty) have been attained. Moreover, the right slope of the surface tension curve indicates an accurate balance between association and dispersive energies in the model. Therefore, a final set of molecular parameters has been selected for the three FILs (see Table 3.3.4) which shows an excellent description of the density-temperature diagram (see Figure 3.3.2) with AAD less than 0.02% and surface tensions (see Figure 3.3.3).

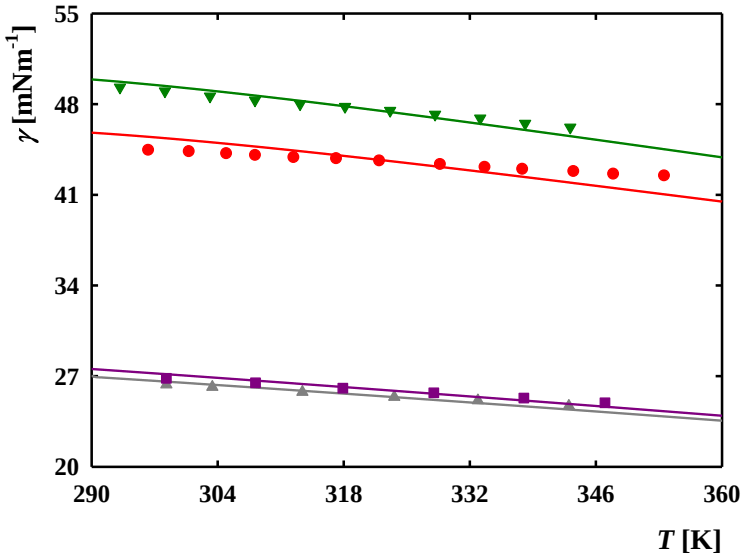

Figure 3.3.3 Surface tensions of the studied ionic liquids at atmospheric pressure. Symbols represent experimental data from literature[1] (red ●, $[C_2C_1Im][CF_3SO_3]$; green ▼, $[C_2C_1Im][CF_3CO_2]$; grey ▲, $[C_2C_1py][C_4F_9SO_3]$; purple ■, $[C_2C_1py][C_4F_9CO_2]$) and the lines are the soft-SAFT calculations.

For the $[C_2C_1Im][CF_3SO_3]$ and $[C_2C_1Im][CF_3CO_2]$ ILs, the description of the density (see Figure 3.3.2) could be slightly improved if at least one of the parameters had been optimized. However, the five molecular parameters transferred from $[C_3C_1Im][BF_4]$ and $[C_4C_1Im][BF_4]$, respectively, already give excellent results without further fitting, underlining the robustness of the soft-SAFT approach [76]. Furthermore, the surface tension calculations also show very good agreement with experimental data with AAD of less than 1.5%, within the experimental uncertainty (see Table 3.3.3 and Figure 3.3.3).

The molecular parameters m, σ and ε, can be directly correlated to size, volume, and energy of the ILs chemical structure, with $m\sigma^3$ representing the volume and $m\varepsilon$ standing for the van der Waals energy between ILs molecules. In Figure 3.3.4, the correlation of $m\sigma^3$ and

$m\varepsilon$ with the molecular weight of the five ILs has been plotted. In both cases, there is a clear linear increment of volume and energy with the molecular weight. Figure 3.3.2 shows that the density increases in the following order: $[C_2C_1py][C_4F_9SO_3]$ < $[C_2C_1Im][C_4F_9CO_2]$ < $[C_2C_1py][C_4F_9CO_2]$ < $[C_2C_1Im][CF_3SO_3]$ < $[C_2C_1Im][CF_3CO_2]$, while the exact inverse trend have been found for $m\sigma^3$ regression (see Figure 3.3.4). This result supports the accuracy of the molecular parameters to describe the physical features and thermodynamic properties of these ILs.

Table 3.3.3 Optimized influence parameter for the surface tension, *c*, for the ionic liquids studied in this work.

	M_w [g mol^{-1}]	T range [K]	c x 10^{19} [J m^5 mol^{-2}]	AAD [%]
$[C_2C_1py][C_4F_9SO_3]$	421.28	298.30 – 343.00 [19]	9.609	0.631
$[C_2C_1py][C_4F_9CO_2]$	385.23	298.30 – 347.00 [78]	9.161	0.726
$[C_2C_1Im][CF_3SO_3]$	260.24	296.28 – 353.56 [78]	0.126	1.522
$[C_2C_1Im][CF_3CO_2]$	224.18	293.15 – 343.15 [79]	0.125	0.743

Table 3.3.4 Molecular weight, molecular parameters, and absolute average density (AAD) for the densities of the ionic liquids studied in this work.

	M_w [g mol^{-1}]	m	σ [Å]	ε/k_B [K]	ε^{HB}/k_B [K]	κ^{HB} [Å^3]	AAD [%]
$[C_2C_1Im][C_4F_9SO_3]$[a]	410.31	7.320	3.816	343.4	3850	2250	-
$[C_4C_1Im][C_4F_9SO_3]$[a]	438.31	7.685	3.919	349.4	3850	2250	-
$[C_2C_1py][C_4F_9SO_3]$	421.28	7.320	3.889	359.4	3850	2250	0.019
$[C_2C_1Im][C_4F_9CO_2]$	374.21	7.233	3.762	338.8	3850	2250	0.008
$[C_2C_1py][C_4F_9CO_2]$	385.23	7.233	3.836	349.2	3850	2250	0.005
$[C_2C_1Im][CF_3SO_3]$[b]	260.24	4.495	4.029	420.0	3450	2250	-
$[C_2C_1Im][CF_3CO_2]$[b]	224.18	4.225	3.998	417.1	3450	2250	-

Molecular parameters from reference [a]Pereiro, A.B. *et al.* (2017) and [b]Ferreira, M.L. *et al.* (2019) [47,76].

3.3.2.2 Solubility of atmospheric gases in ionic liquids

The main goal of this work is to study the solubility of CO_2, N_2 and O_2 in the selected ILs listed in Table 3.3.1, for which a molecular model and molecular parameters of the ILs have been provided in the previous section. The solubility has been calculated at atmospheric pressure and reference temperatures, 298.15 K (room temperature) and 310.15 K (average human body temperature). Several comparisons have been made in order to understand how the chemical structure of ILs influences the solubility of atmospheric gases, analysing the influence of the cation and anion and their structural features, such as hydrogenated cationic and fluorinated anionic alkyl chains.

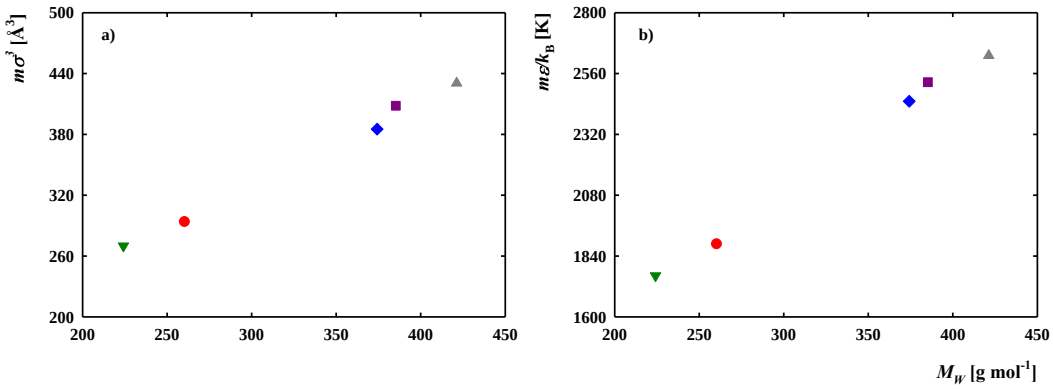

Figure 3.3.4 Trends between ionic liquids molecular weight (M_w) and molecular volume and energy soft-SAFT parameters, where a) $m\sigma^3$ represents the volume and b) $m\varepsilon$ stands for van der Waals energy of the ILs molecules. Symbols correspond to: red ●, $[C_2C_1Im][CF_3SO_3]$; green ▼, $[C_2C_1Im][CF_3CO_2]$; blue ♦, $[C_2C_1Im][C_4F_9CO_2]$; grey ▲, $[C_2C_1py][C_4F_9SO_3]$; purple ■, $[C_2C_1py][C_4F_9CO_2]$.

3.3.2.2.1 Validation of molecular parameters for binary mixtures

In the scope of this study, the ILs molecular parameters must predict the properties of the pure compounds and the properties of the binary IL + atmospheric gas mixtures. Thus, it is important not only to have insights into the solubilization power of ILs but also to corroborate the molecular parameters' capability to characterise the binary IL + atmospheric gas systems. In molecular-based equations, the deviations from the ideal behaviour due to energy and size differences between the molecules of the compounds in a mixture can be accounted for by the energy (ξ) and size (η) binary parameters (see Section 3.2). These parameters can be fitted to experimental data when an exact agreement is imperative. For qualitative results, using the equation as a predictive approach, the values of these binary parameters become unity, showing if the molecular equation captures the non-ideal behaviour of the mixture. In this work, all calculations have been done in a predictive manner or, when needed, using an energy binary parameter, ξ (see Equation 3.2.3), fitted at an isotherm and used in a predictive manner at other temperatures. Experimental data are only available in literature for the following systems: $[C_2C_1Im][C_4F_9SO_3]$ + CO_2 at 313.15 K; $[C_4C_1Im][C_4F_9SO_3]$ + CO_2 at 293.15, 303.15, 313.15, 323.15, 333.15 and 343.15 K; $[C_4C_1Im][C_4F_9SO_3]$ + O_2 at 323.15; $[C_4C_1Im][C_4F_9SO_3]$ + N_2 at 323.15; $[C_2C_1Im][CF_3SO_3]$ + CO_2 at 303.2, 313.2, 323.2, 333.2 and 343.2 K; $[C_2C_1Im][CF_3CO_2]$ + CO_2 at 298.1, 323.1 and 348.1 K. Figures 3.3.5 and 3.3.6 show the solubility for the abovementioned systems that has been calculated using soft-SAFT.

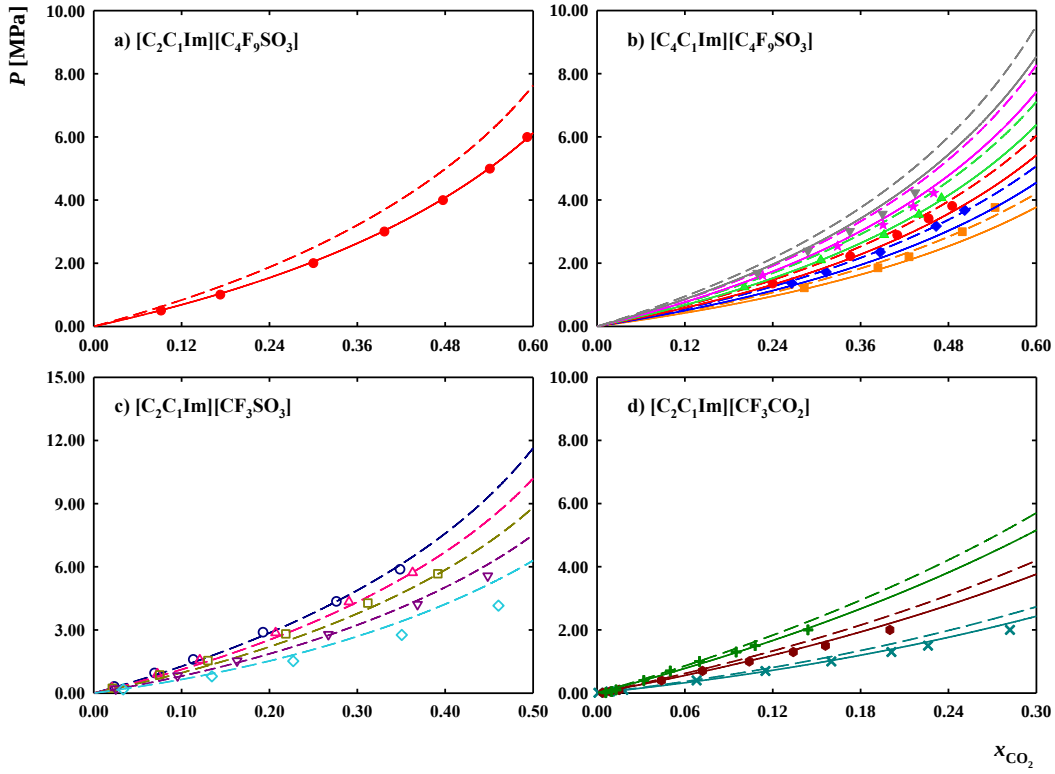

Figure 3.3.5 Solubility of CO_2 at atmospheric pressure in: a) $[C_2C_1Im][C_4F_9SO_3]$ at 313.15 K; b) $[C_4C_1Im][C_4F_9SO_3]$ at 293.15 K (orange ■), 303.15 K (blue ♦), 313.15 K (red ●), 323.15 K (green ▲), 333.15 K (pink ★) and 343.15 K (grey ▼); c) $[C_2C_1Im][CF_3SO_3]$ at 303.2 K (light blue ◇), 313.2 K (purple ▽), 323.2 K (dark yellow □), 333.2 K (dark pink △) and 343.2 K (dark blue ○); and d) $[C_2C_1Im][CF_3CO_2]$ at 298.1 K (dark cyan x), 323.1 K (dark red ●) and 348.1 K (dark green +). The dashed lines represent pure predictions from soft-SAFT (the binary parameter ξ=1.0) and the solid lines represent the calculations using the ξ value fitted to experimental data from literature, represented by symbols [80–83].

The dashed lines represent the calculations when the binary parameter ξ has been kept at unity. The solid lines represent the calculations done using the ξ value fitted to literature data.[1] Globally, the theoretical results show a good agreement with experimental data from the literature. For the $[C_2C_1Im][CF_3SO_3]$ + CO_2 system (see Figure 3.3.5c), only the dashed line has been depicted because the predictive approach quantitatively represented the literature data and no fitting of ξ is required. From the fitting procedure the following ξ binary parameters have been obtained: 1.020 for the system $[C_2C_1Im][C_4F_9SO_3]$ + CO_2 (Figure 3.3.5a); 1.011 for the system $[C_4C_1Im][C_4F_9SO_3]$ + CO_2 (Figure 3.3.5b); 1.010 for the system $[C_2C_1Im][CF_3CO_2]$ + CO_2 (Figure 3.3.5d); 0.875 for the system $[C_4C_1Im][C_4F_9SO_3]$ + O_2 (Figure 3.3.6a); 0.975 for the system $[C_4C_1Im][C_4F_9SO_3]$ + N_2 (Figure 3.3.6b).

This parameter characterizes the binary system, and it is independent of the temperature. It is interesting to remark that for all CO_2 and N_2 mixtures, the ξ binary parameter remains very close to unity, indicating that the prediction of the equation using a geometric combining rule provides quite accurate results, slightly underpredicting the

solubility of CO_2 and overpredicting the solubility of N_2. However, the binary parameter of O_2 has a lower value, so a prediction would severely overpredict the solubility. This fact has been observed previously when describing the solubility of O_2 in other solvents with SAFT and it can be a consequence of the specific strong interactions between O_2 and the IL. In a coarse grain approach these types of interactions can be considered in different ways: implicitly, just including them in the binary parameter, as in the current study, or explicitly, for example, considering a cross-association between O_2 and the solvent, as in the work of Dias *et al.* [67].

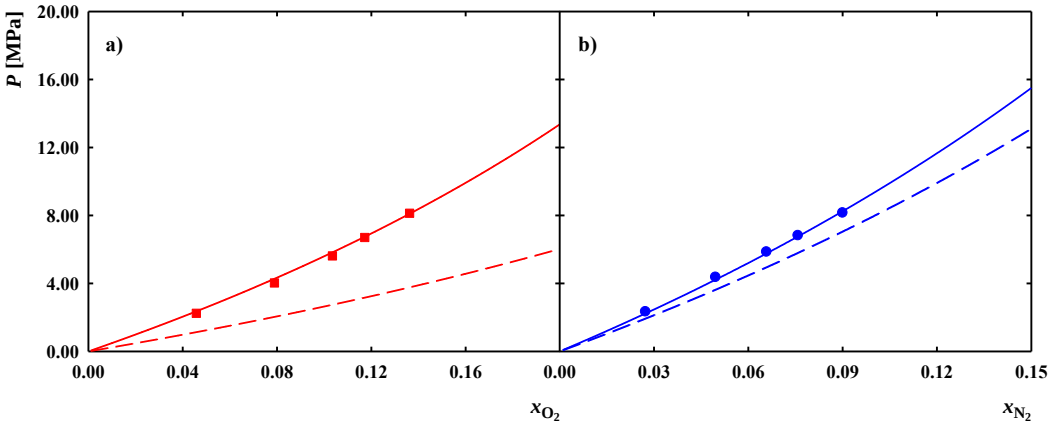

Figure 3.3.6 Solubility of O_2 and N_2 at atmospheric pressure and 323.15 K in the FIL $[C_4C_1Im][C_4F_9SO_3]$. Lines as in Figure 3.3.5. Symbols represent experimental data from the literature [67].

3.3.2.2.2 *Effect of the cation and the cationic hydrogenated chain length on the solubility of atmospheric gases*

Given the robustness of the approach and taking into account the molecular information that soft-SAFT contains, we present next a study showing the effect of the cation and the cationic hydrogenated side chain length in the solubility of atmospheric gases. The following three comparisons have been studied: $[C_2C_1Im]^+$ versus $[C_2C_1py]^+$ for the $[C_4F_9SO_3]$- and $[C_4F_9CO_2]$-based FILs; $[C_2C_1Im]^+$ versus $[C_4C_1Im]^+$ for the $[C_4F_9SO_3]$-based FILs. This comparison has been carried out using the solubility calculations of the systems FILs + atmospheric gases through the predictive approach ($\xi = 1$), as illustrated in Figure 3.3.7.

Figures 3.3.7a and 3.3.7b show the solubility of the mixtures FILs + CO_2. For the $[C_4F_9SO_3]$-based FILs (Figure 3.3.7a), the results indicate that the solubility of CO_2 decreases as the temperature increases for the three FILs. Thus, it is necessary to apply less pressure at lower temperatures to reach the same gas composition absorbed by the FIL. Further, the increasing CO_2 solubility trend is as follow, $[C_2C_1Im]^+ < [C_2C_1py]^+ < [C_4C_1Im]^+$. The increment of hydrogenated side chain length ($[C_2C_1Im]^+$ versus $[C_4C_1Im]^+$) increases the solubility of CO_2, and the pyridinium-based FIL ($[C_2C_1Im]^+$ versus $[C_2C_1py]^+$) presents a higher solubilization of CO_2. A similar behaviour has been observed for the $[C_4F_9CO_2]$-based FILs, $[C_2C_1Im]^+$ versus $[C_2C_1py]^+$ (see Figures 3.3.7b). The solubility of CO_2 is higher in the $[C_2C_1py][C_4F_9CO_2]$ FIL,

and the solubility decreases as the temperature increases. A comparable behaviour in the FILs + O_2 systems has been observed. The O_2 solubility trends follow the same order of CO_2 for all the $[C_4F_9SO_3]$- and $[C_4F_9CO_2]$-based FILs (see Figures 3.3.7c and 3.3.7d, respectively). Also, the solubility of O_2 decreases as the temperature increases.

Regarding the solubility of N_2 in the $[C_4F_9SO_3]$- and $[C_4F_9CO_2]$-based FILs, similar tendencies have been observed (see Figures 3.3.7e and 3.3.7f, respectively). Contrarily, there are no significant differences in the N_2 solubility with the temperature increase. Briefly, the comparison between $[C_2C_1Im]^+$, $[C_4C_1Im]^+$ and $[C_2C_1py]^+$ cations using the soft-SAFT approach reveals that (i) FILs with longer cationic hydrogenated chain present higher solubilization of atmospheric gases, and that (ii) the solubility of the atmospheric gases is higher in the pyridinium-based FILs.

3.3.2.2.3 *Effect of the anion and the anionic fluorinated chain length on the solubility of atmospheric gases*

The anion and anionic fluorinated chain length effect have been also studied using a similar approach as in Section 3.3.3.1.2. A comparison between $[C_4F_9SO_3]^-$, $[C_4F_9CO_2]^-$, $[CF_3SO_3]^-$ and $[CF_3CO_2]^-$ anions, conjugated with $[C_2C_1Im]^+$ and $[C_2C_1py]^+$ cations, have been performed to verify the capacity of these ILs to solubilize atmospheric gases. Figures 3.3.8a and 3.3.8b illustrate the solubility of CO_2 in imidazolium- ($[C_nC_1Im]^+$, n = 2 and 4) and pyridinium- ($[C_2C_1py]^+$) based ILs CO_2, respectively. The increasing CO_2 solubility trend in $[C_nC_1Im]$-based ILs is as follow: $[CF_3CO_2]^- < [CF_3SO_3]^- < [C_4F_9CO_2]^- < [C_4F_9SO_3]^-$. The $[C_4F_9CO_2]$- and $[C_4F_9SO_3]$-based FILs present higher solubilization of CO_2. The solubility of CO_2 is higher in the $[C_nC_1Im]$-based ILs conjugated with sulfonate anions than in carboxylate anions (see Figure 3.3.8a). A similar trend concerning the sulfonate versus carboxylate anions has been verified for the $[C_2C_1py]$-based FILs (see Figure 3.3.8b). In all ILs, the solubility of CO_2 decreases as the temperature increases. A comparable behaviour in the ILs + O_2 systems has been observed, and consequently, the O_2 solubility trends follow the same order of CO_2 for all the previous ILs (see Figures 3.3.8c and 3.3.8d). Likewise, the solubility of O_2 decreases as the temperature increases.

The solubility of N_2 in all the previous ILs presents similar trends to the solubility of CO_2 and O_2 (see Figures 3.3.8e and 3.3.8f). Contrarily, the solubility of N_2 is independent of temperature for the longer anionic fluorinated chains ($[C_4F_9CO_2]$- and $[C_4F_9SO_3]$-based FILs). Though, the solubility of N_2 decreases as the temperature increases for the shorter anionic fluorinated chains ($[CF_3CO_2]$- and $[CF_3SO_3]$-based ILs). In summarizing, the comparison between $[CF_3CO_2]^-$, $[CF_3SO_3]^-$, $[C_4F_9CO_2]^-$ and $[C_4F_9SO_3]^-$ anions discloses that (i) ILs with longer fluorinated chains present higher solubilization of atmospheric gases, and that (ii) the

solubility of the atmospheric gases is higher in the ILs conjugated with sulfonate anions than carboxylate anions.

3.3.3 Conclusions

In this work, a theoretical approach has been used as a tool to obtain insights into the solubility of atmospheric gases in fluoro-containing ionic liquids and fluorinated ionic liquids. The molecular models of the $[C_nC_1Im][C_4F_9SO_3]$ family from previous contributions have been transferred to other FILs ($[C_2C_1py][C_4F_9SO_3]$, $[C_2C_1Im][C_4F_9CO_2]$ and $[C_2C_1py][C_4F_9CO_2]$). The needed molecular parameters have been optimized, restricted to several assumptions to account for the structure and basic physical features of these compounds, finding a good agreement with experimental data in all cases. The models and parameters accurately describe the density and surface tension data of the pure ILs. This approach enables the prediction of the solubility of atmospheric gases in ILs, with the need for one binary interaction parameter, close to unity, in some cases. It has been verified that all the studied ILs display a high potential to solubilize atmospheric gases, being the $[C_4C_1Im][C_4F_9SO_3]$ and $[C_2C_1py][C_4F_9SO_3]$ FILs the ones presenting the higher solubilization capability.

Overall, this work proves the robustness of the soft-SAFT equation for the characterization of the thermodynamic properties of fluoro-containing ionic liquids and fluorinated ionic liquids and their mixtures with atmospheric gases using limited experimental data. Specifically, the results that have been obtained herein highlight the power of this theoretical approach as an accurate tool to obtain results in a faster and simplified way, allowing the study of FILs as potential candidates to replace, partially or totally, the use of PFCs in different industrial and biomedical applications.

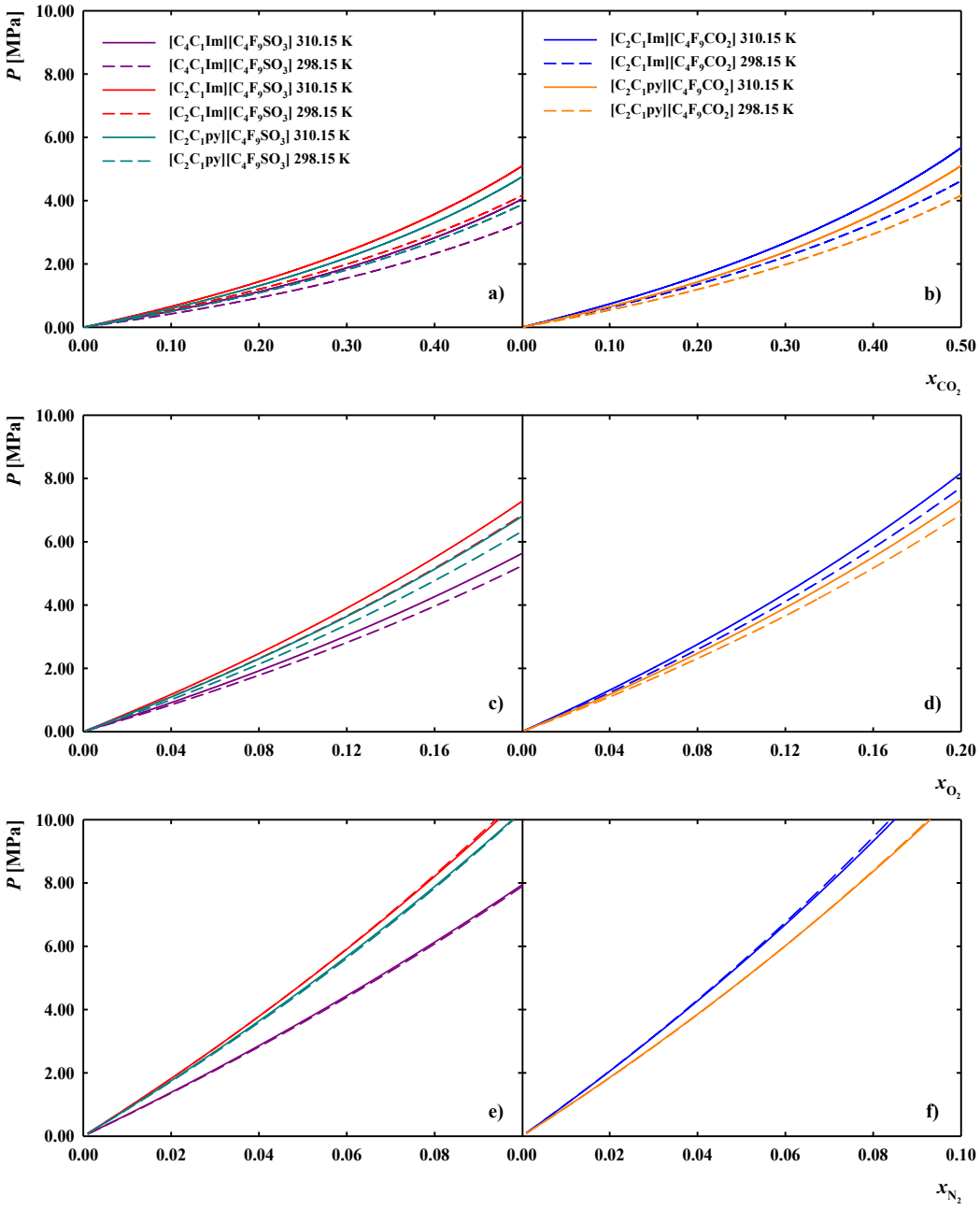

Figure 3.3.7 Effect of the cation and the cationic hydrogenated chain length in the solubility of atmospheric gases in FILs at atmospheric pressure where: a) $[C_4F_9SO_3]$- and b) $[C_4F_9CO_2]$-based FILs with CO_2; c) $[C_4F_9SO_3]$- and d) $[C_4F_9CO_2]$-based FILs with O_2, and e) $[C_4F_9SO_3]$- and f) $[C_4F_9CO_2]$-based FILs with N_2. The solid lines represent the calculations at 310.15 and dashed lines at 298.15 K. In c) the dashed red line and solid cyan line are overlapped.

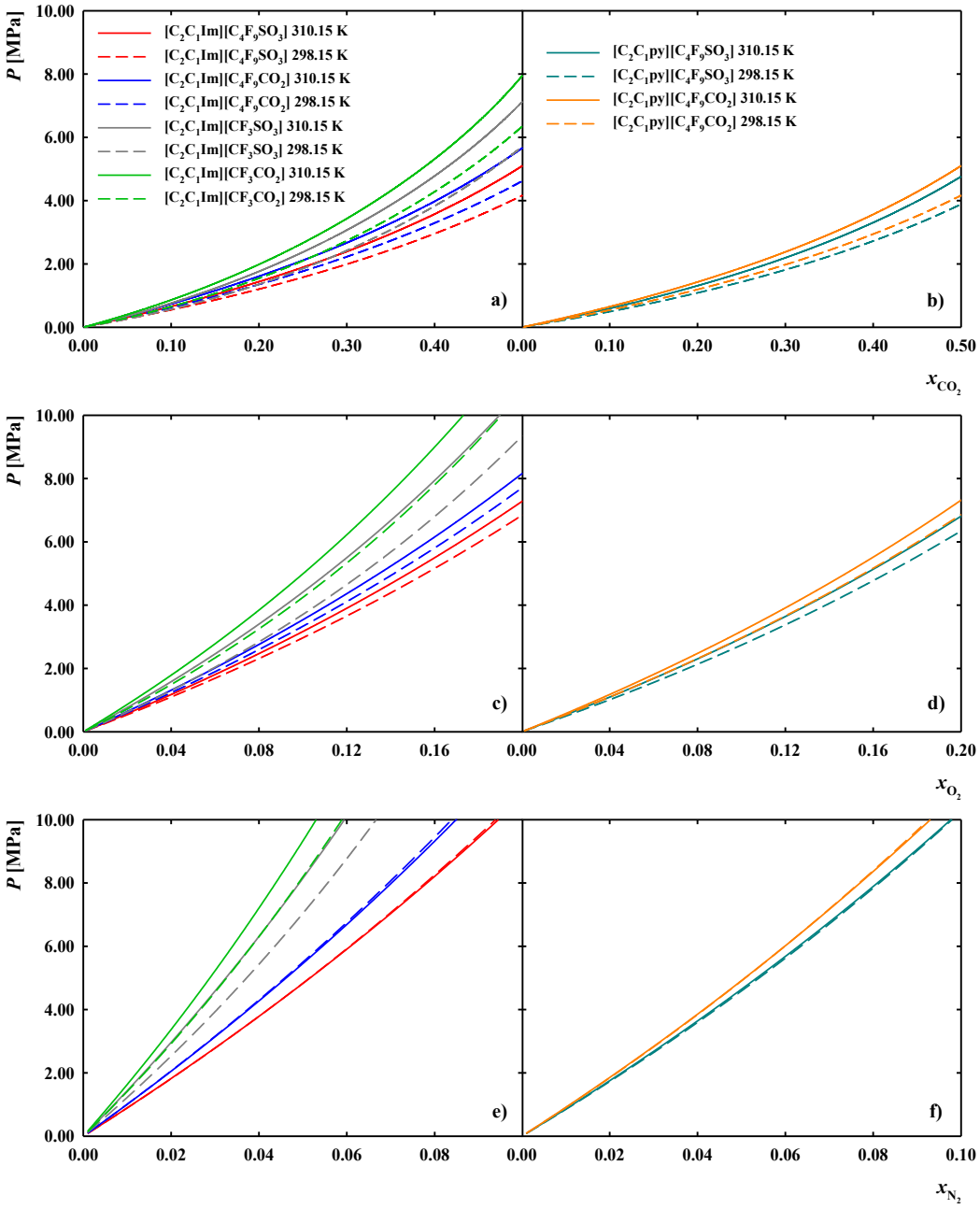

Figure 3.3.8 Effect of the anion and the anionic fluorinated chain length in the solubility of atmospheric gases in FILs at atmospheric pressure where: a) [C_2C_1Im]- and b) [C_2C_1py]-based ILs with CO_2; c) [C_2C_1Im]- and d) [C_2C_1py]-based ILs with O_2; and e) [C_2C_1Im]- and f) [C_2C_1py]-based ILs with N_2. The solid lines represent the calculations at 310.15 and dashed lines at 298.15 K. In d) the dashed orange line and solid cyan line are overlapped, and in e) the dashed green line and solid grey line are overlapped.

3.4 Insights into the influence of the molecular structure of Fluorinated Ionic Liquids on their thermophysical properties. A soft-SAFT based approach

Building on the success of the previous studies, this work aims to provide novel insights into the influence of the FILs structural features on the soft-SAFT transferability approach, on the robustness of the molecular models and on the macroscopic FILs thermodynamic properties. We first provide an overview of the methodology used to build FILs molecular models, exploiting the parameterization and transferability approaches applied in soft-SAFT. A detailed comparison between the parametrization of families based on different fluorinated anions is performed, seeking for new information regarding the robustness of the equation calculations from the molecular structure of the FILs. Pyridinium and imidazolium based ILs conjugated with different fluorinated anions such as $[N(CF_3SO_2)_2]^-$, $[CF_3SO_3]^-$, $[CF_3CO_2]^-$, $[C_4F_9SO_3]^-$ and $[C_4F_9CO_2]^-$ were selected for this purpose. The approach is used to build models for three ILs not included in the parametrization procedure: $[C_2C_1Im][N(C_2F_5SO_2)_2]$, $[C_4C_1Im][N(C_2F_5SO_2)_2]$ and $[C_4C_1py][CF_3SO_3]$, showing good predictions with respect to available experimental data, validating the proposed methodology and the robustness of using the structural information to construct the models. The systematic study allows the establishment of guidelines to build new FILs models in the future in a faster and efficient way, ensuring that the model can accurately represent the physical features of the different structures.

3.4.1 Soft-SAFT molecular models

3.4.1.1 Molecular models of fluorinated ionic liquids with soft-SAFT

The first step before applying soft-SAFT to experimental systems is to propose a coarse-grain molecular model of the compounds. The proposed models for ILs assume that they are characterized by dispersion forces, specific steric interactions and the formation of short-lived ion pairs which reduce the ionic character of these compounds [29,47–60,84]. Thus, ILs are modelled in soft-SAFT as single chains where the anions and cations are considered to be associated as ion pairs or ionic clusters in the bulk liquid state, taking into account experimental and theoretical studies (see Figure 3.4.1) [69–71,85]. Besides, specific associating sites are defined to mimic the short range and highly directional attractive interactions between the counterions. The number of association sites and the association schemes have to be defined a priori. This is usually done through the guidance of quantum chemical

calculations, molecular simulation results, experimental spectroscopic data, and previous works [69–71,85].

The $[C_nC_1Im][N(CF_3SO_2)_2]$ series was one of the first ILs families containing fluorinated anions described by soft-SAFT. ILs were modelled as a homonuclear chain like molecules with three association sites. The number of sites was chosen on the basis of the delocalization of the anion electric charge, due to the presence of the oxygen groups, enhancing the ability to interact with the surrounding cations. Consequently, one associating site *A*, which represents the nitrogen atom interactions with the cation, and two *B* sites representing the delocalized charge due to the oxygen molecules on the anion, were defined, being only *AB* interactions allowed between the different IL molecules (see Figures 3.4.1a and 3.4.1b). This model was validated by calculating the thermophysical properties of pure ILs like density, vapour pressure, interfacial tension, and isothermal compressibility as well as ILs mixtures and solubilities of alcohols and water in ILs, providing excellent agreement with experimental data in all cases [50].

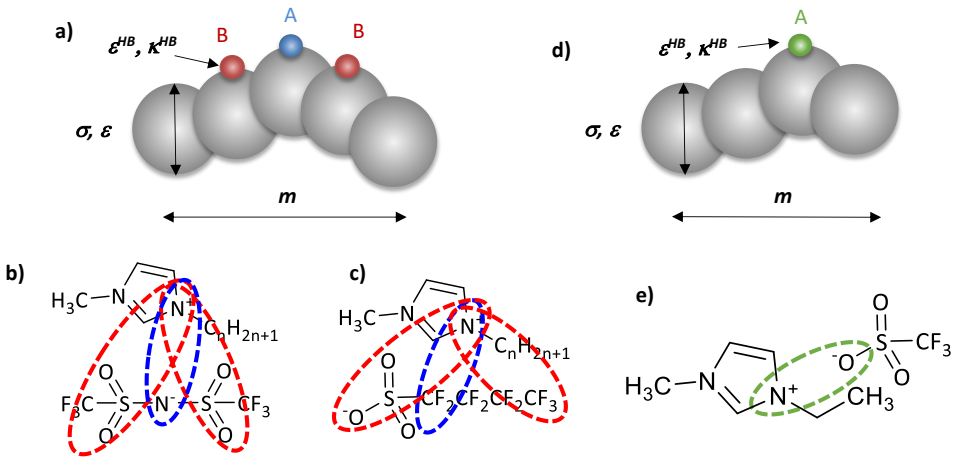

Figure 3.4.1 Sketch of the interactions used to model the FILs families within the soft-SAFT approach. The three association schemes are represented as follows: positive – blue; negative – red and one association scheme is represented as green. a) 3-Sites coarse grain model used in soft-SAFT for b) $[C_nC_1Im][N(CF_3SO_2)_2]$ family. The same scheme is used for $[C_nC_1py][N(CF_3SO_2)_2]$ and $[C_npy][N(CF_3SO_2)_2]$, $[C_4C_1Im][CF_3SO_3]$ and $[C_4C_1Im][CF_3CO_2]$ FILs; c) association scheme for $[C_nC_1Im][C_4F_9SO_3]$, also used for $[C_2C_1py][C_4F_9SO_3]$, $[C_2C_1Im][C_4F_9CO_2]$ and $[C_2C_1py][C_4F_9CO_2]$ FILs. d) 1-Site coarse grain model for e) $[C_2C_1Im][CF_3SO_3]$ and $[C_2C_1Im][CF_3CO_2]$ FILs.

The same three sites associating model was successfully used to study the $[C_nC_1py][N(CF_3SO_2)_2]$ and $[C_npy][N(CF_3SO_2)_2]$ families. These ILs have a charge distribution similar to those of $[C_nC_1Im][N(CF_3SO_2)_2]$, where the same association scheme can be attributed (see Figures 3.4.1a and 3.4.1b). The model was applied to calculate the thermophysical properties of pure ILs, such as density, surface tension and isothermal compressibility as well as the solubility of carbon dioxide, sulphur dioxide and water in excellent agreement with available experimental data. A similar approach was used for the $[C_4C_1Im][CF_3SO_3]$ and

$[C_4C_1Im][CF_3CO_2]$ ILs. The association scheme was transferred from $[C_nC_1Im][N(CF_3SO_2)_2]$, considering three associating sites. For $[C_4C_1Im][CF_3SO_3]$, site *A* also stands for the oxygen atom interactions with the cation, however, the two *B* sites represent the delocalized charge due to the oxygen atoms. Analogously, three association sites were considered for $[C_4C_1Im][CF_3CO_2]$, where *A* represents the oxygen atom interactions with the cation and the two sites *B* stand for the oxygen and fluorine atoms, with only *AB* interactions allowed between different ILs molecules (Figure 3.4.1c). The models were validated by calculating the density of pure ILs and the water activity coefficients [51]. No soft-SAFT published models are available for $[C_2C_1Im][CF_3SO_3]$ and $[C_2C_1Im][CF_3CO_2]$. In this work we have applied two models for them, a three site associating model, as for the previous FILs mentioned in this section, and a one site associating model, as for the $[C_nC_1Im][BF_4]$ [48,54] and $[C_nC_1Im][PF_6]$ [49] (see Figures 3.4.1d and 3.4.1e). The one site model was used considering that the shape of $[CF_3SO_3]^-$ and $[CF_3CO_2]^-$ is quasi-spherical, with a very localized charge, similar to the case of $[BF_4]^-$ and $[PF_6]^-$. Results for these two models are discussed in the next section. Recently, soft-SAFT models were proposed for the $[C_nC_1Im][C_4F_9SO_3]$ family using quantum chemical calculations for the charge distribution and a three-site model, as in the case of $[C_nC_1Im][N(CF_3SO_2)_2]$. One associating site, *A*, stands for the main interactions of the fluorine atom with the cation, whereas two *B* sites represent the delocalized charge owing to the surrounding fluorine atoms and the oxygen atoms of the anion. Only *AB* interactions between different FIL molecules were allowed (Figure 3.4.1c). The density, viscosity and surface tension of the pure FILs were accurately calculated. Furthermore, this model was successfully transferred to other FILs such as $[C_2C_1py][C_4F_9SO_3]$, $[C_2C_1Im][C_4F_9CO_2]$ and $[C_2C_1py][C_4F_9CO_2]$ preserving the association scheme (Figure 3.4.1c). The density, surface tension and solubility of carbon dioxide, oxygen and nitrogen were calculated in good agreement with experimental data [47,60].

In summary, the reported fluorinated ionic liquids modelled with soft-SAFT that have bulky hydrogenated chains and fluorinated anions preserve the same three-site association scheme model and successfully reproduce experimental data. This indicates that the three association sites give enough degrees of freedom to account for all the interactions between the functional group of the anion with the cation and the charge delocalization caused either by the oxygen atoms present in the anion functional group or by the presence of fluorine atoms in the anion (in the case of larger fluorinated side chains). FILs with short fluorinated and hydrogenated chains length ($[C_2C_1Im][CF_3SO_3]$ and $[C_2C_1Im][CF_3CO_2]$) have been studied with soft-SAFT for the first time in this work, using two different association schemes, the performance of these approaches is discussed in the forthcoming sections.

3.4.1.2 Soft-SAFT parametrization of fluorinated ionic liquids and physical trends

All the FILs molecular structures studied in this work, together with their nomenclatures, are reported in Table 3.4.1. The studied FILs are composed of imidazolium and pyridinium cations with different hydrogenated alkyl chain lengths, conjugated with fluorinated anions ($[N(CF_3SO_2)_2]^-$, $[CF_3SO_3]^-$, $[CF_3CO_2]^-$, $[C_4F_9SO_3]^-$ and $[C_4F_9CO_2]^-$).

Table 3.4.1 Chemical structure and respective acronyms of the studied fluorinated ionic liquids.

Fluorinated Ionic Liquid Designation	Chemical Structure
1-Alkyl-3-methylimidazolium trifluoroacetate **[C_nC_1Im][CF_3CO_2] with n = 2 or 4**	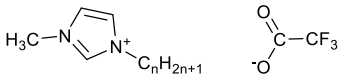
1-Ethyl-3-methylimidazolium perfluoropentanoate **[C_2C_1Im][$C_4F_9CO_2$]**	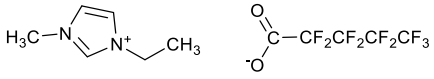
1-Ethyl-3-methylpyridinium perfluoropentanoate **[C_2C_1py][$C_4F_9CO_2$]**	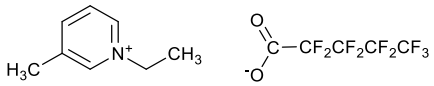
1-Butyl-3-methylpyridinium trifluoromethanesulfonate **[C_4C_1py][CF_3SO_3]**	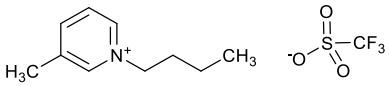
1-Ethyl-3-methylpyridinium perfluorobutanesulfonate **[C_2C_1py][$C_4F_9SO_3$]**	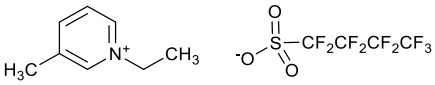
1-Alkyl-3-methylimidazolium perfluorobutanesulfonate **[C_nC_1Im][$C_4F_9SO_3$] with n = 2, 4, 6, 8, 10 or 12**	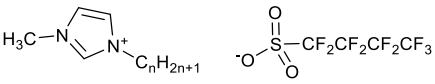
1-Alkyl-3-methylimidazolium trifluoromethanesulfonate **[C_nC_1Im][CF_3SO_3] with n = 2 or 4**	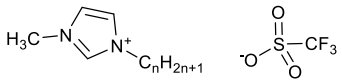
1-Alkyl-3-methylimidazolium bis(trifluoromethylsufonyl)imide **[C_nC_1Im][$N(CF_3SO_2)_2$] with n = 1-10, 12 or 14**	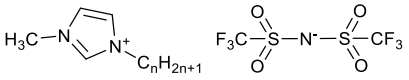
1-Alkyl-3-methylpyridinium bis(trifluoromethylsulfonyl)imide **[$C_nC_1$py][$N(CF_3SO_2)_2$] with n = 2-4, 6 or 8**	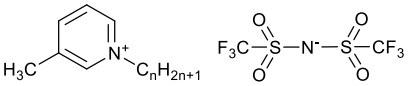
1-Alkylpyridinium bis(trifluoromethylsulfonyl)imide **[$C_n$py][$N(CF_3SO_2)_2$] with n = 2-6, 8, 10 or 12**	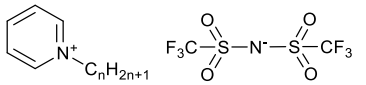
1-Alkyl-3-methylimidazolium bis(perfluoroethylsulfonyl)imide **[C_nC_1Im][$N(C_2F_5SO_2)_2$] with n = 2 or 4**	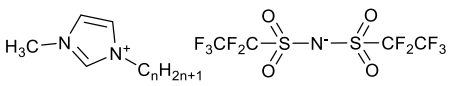

Once the association scheme is selected, the next step in using soft-SAFT to study the FILs experimental systems is to parametrize a set of molecular parameters, usually by fitting available temperature-density experimental data at atmospheric pressure, although other available properties such as high-pressure data, heat capacities or isothermal compressibility, to mention some, can also be used, as explained in the next section. Care must be taken so that the values capture the physical trends consistent with the structure of the molecules related to the size, energy, and specific molecular interactions. The optimization of the five parameters

(the chain length, m; the segment diameter, σ; the dispersive energy between segments, ε, the site–site association energy and volume parameters, ε^{HB} and κ^{HB}, respectively) can be challenging from a numerical perspective, as a high number of possible combinations with small deviations from the experimental data are possible. Therefore, it is important to guide the optimization based on physical information in order to reduce the number of solutions and use soft-SAFT as transferable as possible. In this work, we first compiled all published soft-SAFT molecular parameters for the different FILs, searching for trends and possible inconsistencies. All parameters for the different families are summarized in Table 3.4.2.

The comparison between the studied families shows a major difference regarding the association parameters of $[C_nC_1py][N(CF_3SO_2)_2]$ and $[C_npy][N(CF_3SO_2)_2]$. The association parameters of $[C_nC_1Im][N(CF_3SO_2)_2]$ family were fixed at 3450 K for ε^{HB}/k_B and 2250 Å^3 for κ^{HB} [50]. In the case of pyridinium-based ionic liquids families, the ε^{HB}/k_B and κ^{HB} were fixed at 1550 K and 2020 Å^3, respectively [51]. When all the ILs are compared, these values appear as "outliers" regarding those of other families, as illustrated in Figures 3.4.2 and 3.4.3. Searching for consistency and building robust models, in this work we have transferred the association parameters of $[C_nC_1Im][N(CF_3SO_2)_2]$ to the $[C_nC_1py][N(CF_3SO_2)_2]$ and $[C_npy][N(CF_3SO_2)_2]$ families. The m and σ molecular parameters were preserved from those values previously obtained for the pyridinium-based ionic liquids. However, the ε value was re-parametrized (see Table 3.4.2). The differences in the performance between the parameters previously published and the new ones versus experimental density-temperature data are depicted in Figure 3.4.4. Figures 3.4.4a and 3.4.4b stand for $[C_nC_1py][N(CF_3SO_2)_2]$ and $[C_npy][N(CF_3SO_2)_2]$ ILs families, respectively, where *set 1* represents the parameters previously published (solid lines) [51] and *set 2* corresponds to the optimized parameters in this work (dashed lines). In both families, there is an improvement in the agreement between the experimental data [86–93] and soft-SAFT results obtained with *set 2*. This result is also sustained by the decrease of the average absolute deviation (ADD < 0.07%) for almost all ILs (see Table 3.4.2), except for $[C_8C_1py][N(CF_3SO_2)_2]$, for which only one value of density experimental data is available in the literature.

Table 3.4.2 Symbols, molecular weight, soft-SAFT molecular parameters from literature and reparametrized, correlations of molecular parameters and absolute average deviation (AAD) for the densities of all ionic liquids studied in this work.

Symbol	Ionic Liquid	M_w [g mol^{-1}]	m	σ [Å]	ε/k_B [K]	$m\sigma^3$ [Å^3]	$m\varepsilon/k_B$ [K]	ε^{HB}/k_B [K]	κ^{HB} [Å^3]	AAD [%]	REF
★	$[C_2C_1Im][C_4F_9CO_2]$	374.21	7.233	3.762	338.8	385	2451	3850	2250	0.008	[60]
☆	$[C_2C_1py][C_4F_9CO_2]$	385.23	7.233	3.836	349.2	408	2526	3850	2250	0.005	[60]
⊗	$[C_2C_1py][C_4F_9SO_3]$	421.28	7.320	3.889	359.4	431	2631	3850	2250	0.019	[60]
□	$[C_2C_1Im][C_4F_9SO_3]$	410.31	7.320	3.816	343.4	407	2514	3850	2250	0.053	[47]
△	$[C_4C_1Im][C_4F_9SO_3]$	438.31	7.685	3.919	349.4	463	2685	3850	2250	0.033	[47]
○	$[C_6C_1Im][C_4F_9SO_3]$	466.33	8.050	4.006	355.4	518	2861	3850	2250	0.074	[47]
◇	$[C_8C_1Im][C_4F_9SO_3]$	494.42	8.429	4.078	357.4	572	3013	3850	2250	0.017	[47]
▽	$[C_{10}C_1Im][C_4F_9SO_3]$	522.43	8.812	4.126	359.4	619	3167	3850	2250	0.091	[47]
⬡	$[C_{12}C_1Im][C_4F_9SO_3]$	550.48	9.178	4.194	360.2	677	3306	3850	2250	0.036	[47]
✚	$[C_2C_1Im][CF_3SO_3]$	260.24	4.495	4.029	420.0	294	1888	3450	2250	-	This work
✖	$[C_4C_1Im][CF_3SO_3]$	288.29	4.149	4.375	378.0	347	1568	3650	2400	0.116	[57]
▬	$[C_2C_1Im][CF_3CO_2]$	224.18	4.225	3.998	417.1	270	1762	3450	2250	-	This work
▮	$[C_4C_1Im][CF_3CO_2]$	252.33	4.180	4.256	360.7	322	1508	3725	2400	0.016	[57]
⊞	$[C_1C_1Im][N(CF_3SO_2)_2]$	377.29	5.947	3.992	391.1	378	2326	3450	2250	–	[50]
■	$[C_2C_1Im][N(CF_3SO_2)_2]$	391.32	6.023	4.069	394.6	406	2377	3450	2250	–	[50]
⊕	$[C_3C_1Im][N(CF_3SO_2)_2]$	405.33	6.101	4.143	397.0	434	2422	3450	2250	–	[50]
●	$[C_4C_1Im][N(CF_3SO_2)_2]$	419.34	6.175	4.211	399.4	461	2466	3450	2250	–	[50]
⟁	$[C_5C_1Im][N(CF_3SO_2)_2]$	433.35	6.247	4.277	401.8	489	2510	3450	2250	–	[50]
▲	$[C_6C_1Im][N(CF_3SO_2)_2]$	447.36	6.338	4.334	404.2	516	2562	3450	2250	–	[50]
⊕	$[C_7C_1Im][N(CF_3SO_2)_2]$	461.45	6.418	4.395	407.6	545	2616	3450	2250	–	[50]
◆	$[C_8C_1Im][N(CF_3SO_2)_2]$	475.48	6.489	4.45	410.0	572	2660	3450	2250	–	[50]
⛛	$[C_9C_1Im][N(CF_3SO_2)_2]$	489.49	6.575	4.501	411.7	600	2707	3450	2250	–	[50]
▼	$[C_{10}C_1Im][N(CF_3SO_2)_2]$	503.5	6.653	4.551	414.0	627	2754	3450	2250	–	[50]
⊕	$[C_{12}C_1Im][N(CF_3SO_2)_2]$	531.52	6.810	4.645	418.5	683	2850	3450	2250	–	[50]
⬢	$[C_{14}C_1Im][N(CF_3SO_2)_2]$	559.54	6.967	4.731	422.7	738	2945	3450	2250	–	[50]
⬓	$[C_2C_1py][N(CF_3SO_2)_2]$	402.33	6.023	4.125	378.4	423	2279	3450	2250	0.017	This work
◒	$[C_3C_1py][N(CF_3SO_2)_2]$	416.37	6.101	4.194	380.2	450	2320	3450	2250	0.062	This work
◒	$[C_4C_1py][N(CF_3SO_2)_2]$	430.39	6.175	4.257	378.9	476	2340	3450	2250	0.042	This work
◆	$[C_6C_1py][N(CF_3SO_2)_2]$	458.44	6.338	4.375	380.2	531	2410	3450	2250	0.028	This work
⛋	$[C_8C_1py][N(CF_3SO_2)_2]$	486.49	6.489	4.483	402.4	585	2611	3450	2250	0.112	This work
◕	$[C_2py][N(CF_3SO_2)_2]$	388.3	5.947	4.044	368.2	393	2190	3450	2250	0.036	This work
◑	$[C_3py][N(CF_3SO_2)_2]$	402.33	6.023	4.119	378.4	421	2279	3450	2250	0.040	This work
◆	$[C_4py][N(CF_3SO_2)_2]$	416.37	6.101	4.193	378.5	450	2309	3450	2250	0.025	This work
◆	$[C_5py][N(CF_3SO_2)_2]$	430.38	6.175	4.248	378.2	473	2335	3450	2250	0.015	This work
◘	$[C_6py][N(CF_3SO_2)_2]$	444.42	6.247	4.305	379.2	498	2369	3450	2250	0.048	This work
◪	$[C_8py][N(CF_3SO_2)_2]$	472.48	6.418	4.429	386.4	558	2480	3450	2250	0.066	This work
⬢	$[C_{10}py][N(CF_3SO_2)_2]$	500.52	6.575	4.529	382.5	611	2515	3450	2250	0.023	This work
◑	$[C_{12}py][N(CF_3SO_2)_2]$	528.57	6.732	4.622	387.7	665	2610	3450	2250	0.036	This work

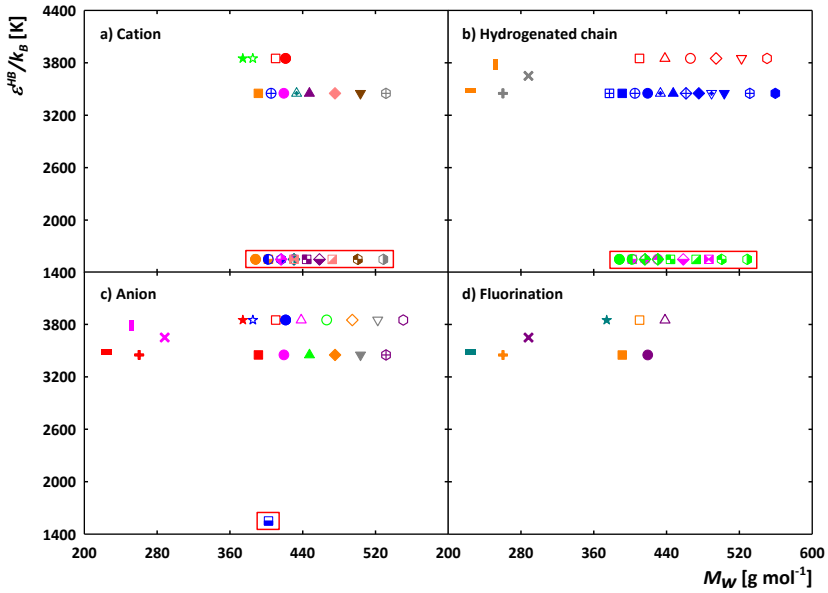

Figure 3.4.2 Values of the association parameter ε^{HB} versus the molecular weight of the studied ionic liquids, where: a) the influence of cations; b) increment of cation hydrogenated alkyl side chain; c) anions; and d) increment of fluorination. The comparisons are grouped by colour. These values illustrate the trends from Oliveira, M.B. *et al.* (2012) [51] before any reparameterization process of $[C_nC_1py][N(CF_3SO_2)_2]$ and $[C_npy][N(CF_3SO_2)_2]$ families. Herein, one can identify the "outliers" values, around 1550 K, highlighted by the red box in the comparisons a), b) and c). Symbols are described in Table 3.4.2.

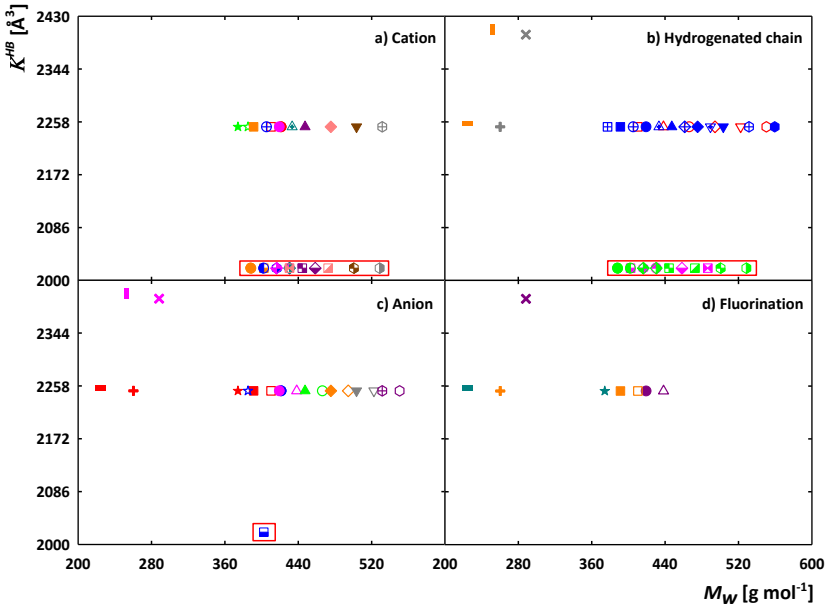

Figure 3.4.3 Values of the association parameter κ^{HB} versus the molecular weight of the studied ionic liquids, where: a) influence of cations; b) increment of cation hydrogenated alkyl side chain; c) anions; and d) increment of fluorination. The comparisons are grouped by colour. These values illustrate the trends from Oliveira, M.B. *et al.* (2012) [51] before any reparameterization process of $[C_nC_1py][N(CF_3SO_2)_2]$ and $[C_npy][N(CF_3SO_2)_2]$ families. Herein, one can identify the "outliers" values, around 2020 Å^3, highlighted by the red box in the comparisons a), b) and c). Symbols are described in Table 3.4.2.

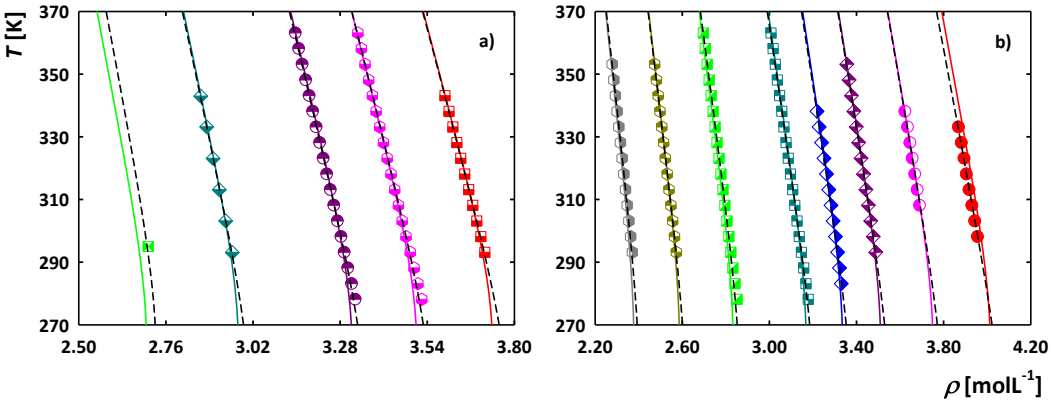

Figure 3.4.4 Temperature versus density diagram at 0.1 MPa for: a) $[C_nC_1py][N(CF_3SO_2)_2]$; and b) $[C_npy][N(CF_3SO_2)_2]$ for different alkyl chains (n = 2, red; n = 3, pink; n = 4, purple; n = 5, blue; n = 6, dark cyan; n = 8, green; n = 10, dark yellow; n = 12, grey). The solid lines represent the calculations obtained with the parameters from Oliveira, M.B. *et al.* (2012) [51] whereas the dashed lines are the results obtained with the parameters optimized in this work. Symbols represent the experimental data [86–90] for each system (see Table 3.4.2 for more details).

For consistency with the previous calculations and with previous work [48,49], we have tested the performance of two association schemes for $[C_2C_1Im][CF_3SO_3]$ and $[C_2C_1Im][CF_3CO_2]$ FILs for predicting the density and carbon dioxide solubility and the results are shown in Figure 3.4.5. Considering a 3-site associating model (Figure 3.4.1a), m, σ and ε were adjusted to density experimental data [12], while association parameters were transferred from $[C_4C_1Im][CF_3SO_3]$ and $[C_4C_1Im][CF_3CO_2]$ ILs. Results from this approach are depicted in Figure 3.4.5b as a dashed-dotted line; the density is not shown in Figure 3.4.5a because it was fitted. As inferred from the figure, those parameters are unable to accurately represent the behaviour of the FILs with carbon dioxide. Taking into account the small, spherical size of the anions, a 1-site association scheme was also considered (Figure 3.4.1d), similarly to the imidazolium ionic liquids with $[BF_4]^-$ and $[PF_6]^-$ [48,49]. In this case, the five molecular parameters were directly transferred from $[C_3C_1Im][BF_4]$ and $[C_4C_1Im][BF_4]$ to $[C_2C_1Im][CF_3CO_2]$ and $[C_2C_1Im][CF_3SO_3]$, respectively, without performing any fitting. Figure 3.4.5a shows excellent agreement between the density experimental data [12] and soft-SAFT predictions.

Regarding the CO_2 solubility, (Figure 3.4.5b) very good agreement is obtained for $[C_2C_1Im][CF_3CO_2]$ for the available experimental data 323.1 K [94]. The overall behaviour of the solubility of CO_2 in $[C_2C_1Im][CF_3SO_3]$ is also well captured, although higher deviations from experimental data (324.15 K) [95] are observed at high CO_2 concentrations. Note that these are pure predictions from the transferred parameters, and much better agreement can be obtained if any of the parameters of the pure FILs were fitted to experimental data. Also notice that the 1-site model better captures the shape of the experimental solubility data than the 3-

sites model, even though the latter gives good solubility predictions at low CO_2 concentrations. By direct transfer of the soft-SAFT parameters, we were able to describe two FILs, without any adjustment to experimental data, emphasising the robustness of the models. The final molecular parameters used for all FILs studied in this work are provided in Table 3.4.2.

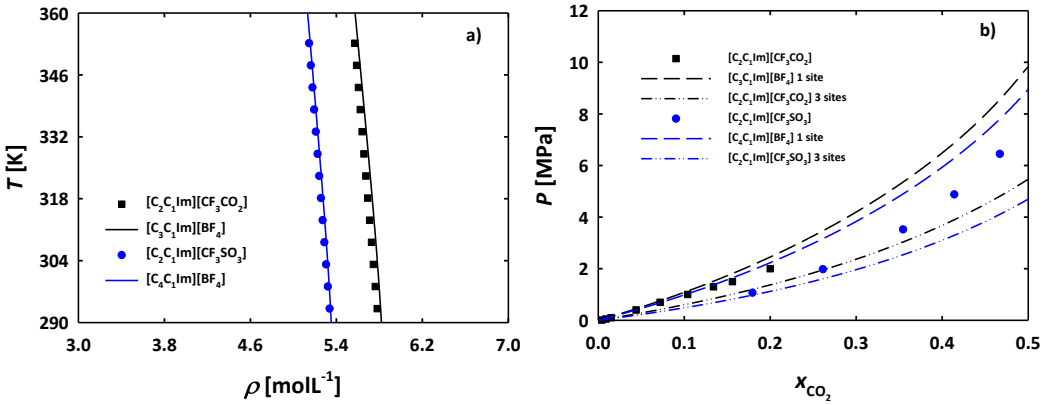

Figure 3.4.5 a) Density-temperature diagram at atmospheric pressure of $[C_2C_1Im][CF_3CO_2]$ and $[C_2C_1Im][CF_3SO_3]$ FILs calculated by the direct transference of soft-SAFT five parameters from $[C_3C_1Im][BF_4]$ and $[C_4C_1Im][BF_4]$, respectively (solid lines represent the calculations with the parameters from Table 3.4.2). b) Solubility of carbon dioxide in $[C_2C_1Im][CF_3CO_2]$ (at 323.1 K) and $[C_2C_1Im][CF_3SO_3]$ (at 324.15 K) FILs, with the 3- (dashed dot-dot lines) and 1-site (dashed lines, calculations with parameters from Table 3.4.2) association schemes. Symbols represent experimental data [12,94,95].

3.4.2 Results and discussion

In this section, we focus on analysing the influence of the cation, the cation hydrogenated alkyl side chain length, the anion, and the fluorination of the anion on some of the physicochemical properties of these compounds, in a systematic way. All the molecular structures are reported in Table 3.4.1.

We first performed a study to obtain insights into the influence of different cations, with a fixed anion, on the thermophysical properties of the families, and how this is reflected in the molecular parameters of soft-SAFT. This is called Strategy 1 or ST1 (see Table 3.4.3). The cations considered were $[C_nC_1Im]^+$, $[C_nC_1py]^+$ and $[C_npy]^+$, all of them with the same hydrogenated alkyl side chain length. Strategy 2 (ST2 in Table 3.4.3) focused on the influence of the cations hydrogenated side chain length (for different cations) and the anions studied in ST1. The following homologous families were studied in ST2: $[C_nC_1Im][C_4F_9SO_3]$, $[C_nC_1Im][CF_3SO_3]$, $[C_nC_1Im][CF_3CO_2]$, $[C_nC_1Im][N(CF_3SO_2)_2]$, $[C_nC_1py][N(CF_3SO_2)_2]$, $[C_npy][N(CF_3SO_2)_2]$.

Table 3.4.3 Strategy of the several comparisons carried out in this work.

ST1 - Influence of the cation	*Anions*
$[C_2C_1Im]^+$	$[C_4F_9SO_3]^-$ or $[C_4F_9CO_2]^-$
$[C_2C_1py]^+$	$[C_4F_9SO_3]^-$ or $[C_4F_9CO_2]^-$
$[C_nC_1Im]^+$, $[C_nC_1py]^+$ or $[C_npy]^+$, n = 2,3,4,6,8	$[N(CF_3SO_2)_2]^-$
$[C_nC_1Im]^+$ or $[C_npy]^+$, n = 5, 10, 12	$[N(CF_3SO_2)_2]^-$
ST2 - Influence of the cation hydrogenated side chain	
$[C_nC_1Im]^+$, n = 2, 4, 6, 8, 10, 12	$[C_4F_9SO_3]^-$
$[C_nC_1Im]^+$, n = 2, 4	$[CF_3SO_3]^-$
$[C_nC_1Im]^+$, n = 2, 4	$[CF_3CO_2]^-$
$[C_nC_1Im]^+$, n = 1-10, 12, 14	$[N(CF_3SO_2)_2]^-$
$[C_nC_1py]^+$, n = 2, 3, 4, 6, 8	$[N(CF_3SO_2)_2]^-$
$[C_npy]^+$, n = 2-6, 8, 10, 12	$[N(CF_3SO_2)_2]^-$
ST3- Influence of the anion	*Cations*
$[C_4F_9SO_3]^-$, $[C_4F_9CO_2]^-$, $[CF_3SO_3]^-$, $[CF_3CO_2]^-$ or $[N(CF_3SO_2)_2]^-$	$[C_2C_1Im]^+$
$[C_4F_9SO_3]^-$, $[CF_3SO_3]^-$, $[CF_3CO_2]^-$ or $[N(CF_3SO_2)_2]^-$	$[C_4C_1Im]^+$
$[C_4F_9SO_3]^-$, $[C_4F_9CO_2]^-$ or $[N(CF_3SO_2)_2]^-$	$[C_2C_1py]^+$
$[C_4F_9SO_3]^-$ or $[N(CF_3SO_2)_2]^-$	$[C_nC_1Im]^+$, n = 6, 8, 10, 12
ST4- Influence of the anion fluorination	
$[C_4F_9CO_2]^-$ or $[CF_3CO_2]^-$	$[C_2C_1Im]^+$
$[C_4F_9SO_3]^-$, $[CF_3SO_3]^-$ or $[N(CF_3SO_2)_2]^-$	$[C_nC_1Im]^+$ n = 2, 4

To investigate the influence of the anion, the cation with a given hydrogenated side chain length was fixed and the anions replaced. The anions studied were $[C_4F_9SO_3]^-$, $[C_4F_9CO_2]^-$, $[CF_3SO_3]^-$, $[CF_3CO_2]^-$ and $[N(CF_3SO_2)_2]^-$ (ST3 in Table 3.4.3). Finally, to study the influence of the anion fluorination, two different comparisons were made (see ST4 in Table 3.4.3). First, the cation was fixed and the anion iterated considering anions with different structural features, such as $[C_4F_9SO_3]^-$, $[CF_3SO_3]^-$ and $[N(CF_3SO_2)_2]^-$, investigating the effect of incrementing the number of fluorine atoms in the anion. Secondly, we studied the effect of increasing the linear fluorinated side chain on the molecular parameters optimization, considering the variation of *n* and *m* in FILs based on $[C_nF_mSO_3]^-$ and $[C_nF_mCO_2]^-$ anions.

3.4.2.1 Fluorinated ionic liquids structural features and molecular parameters in soft-SAFT

The features of the specific cation, the cation hydrogenated alkyl side chain length, anion and the fluorination of the anion will be reflected in the values found for the molecular and association parameters. The *m* and σ molecular parameters are directly related to the size

and volume of the groups making the ILs, while $m\sigma^3$ represents the volume and $m\varepsilon$ the energy of the ILs molecules. Previous soft-SAFT works show that m, $m\sigma^3$ and $m\varepsilon$ correlate with the molecular weight for regular chemical families; the association parameters are generally independent of the molecular weight of the compounds, except for very short chains [47,51,53,60]. This is due to the fact that hydrogen bonding forces are localized and of very short range. We have used this approach here, keeping the same association parameters for each IL family (see Table 3.4.2 and Figures 3.4.2 and 3.4.3) and having m, σ and ε correlated with the molecular weight. This enables the equation with predictive power allowing the prediction of thermophysical properties for other members of the same family for which no experimental data is available.

3.4.2.1.1 Effect of the cation

Once the molecular parameters were assessed and good results obtained versus experimental data, we can use them as a designing tool, checking for trends. Hence, we first show how the characteristics of different cations in the ILs families are captured by the soft-SAFT parameters (ST1 in Table 3.4.3) and their influence on the thermophysical properties. Figure 3.4.6a depicts the comparison among the *m* parameter of the ILs with different cations, versus their molecular weight. The trend $[C_npy]^+ < [C_nC_1py]^+ \approx [C_nC_1Im]^+$ is explained due to the lack of a methyl group in the aromatic ring of $[C_npy]^+$ cation. It is also observed that differences in the *m* values between the compared cations are very small. From this, it is inferred that the cation is not a structural feature highly influencing the overall length of the ILs, represented by the *m* parameter. Furthermore, the value of *m* can be transferred from pyridinium to imidazolium cations, when the cations are conjugated with the same anion because the only deviations that can be found are related to the anion. The size parameter σ, Figure 3.4.6b, shows similar values for most of the FILs with the same cations, increasing as the molecular weight of the ILs increases, the values following the trend $[C_npy]^+ < [C_nC_1Im]^+ < [C_nC_1py]^+$. The regression for the molecular volume of the molecules ($m\sigma^3$), represented in Figure 3.4.6c, linearly increases with the molecular weight. As inferred from this figure, the differences in the molecular volume of FILs based on pyridinium and imidazolium are almost negligible. The energy parameter ε is represented in Figure 3.4.6d versus the molecular weight. Different trends can be found for the different considered ILs. In the case of the cations conjugated with the linear fluorinated anions, the trend is $[C_nC_1Im]^+ < [C_nC_1py]^+$. However, for the ILs based on branched anions, the general trend is $[C_npy]^+ \approx [C_nC_1py]^+ < [C_nC_1Im]^+$. Only in cases where the hydrogenated chain is composed by 2 and 8 carbons, the energy parameter follows the trend $[C_npy]^+ < [C_nC_1py]^+ < [C_nC_1Im]^+$. These differences can be justified by the role of this parameter in capturing the molecular energy, as it accounts for most of the

differences in energy when the association parameters are kept constant, as happens in this case. Once again, it is important to bear in mind that there is only one value for the experimental density of $[C_8C_1py][N(CF_3SO_2)_2]$ available in the literature. The same trends are observed for $m\varepsilon$ (Figure 3.4.6e).

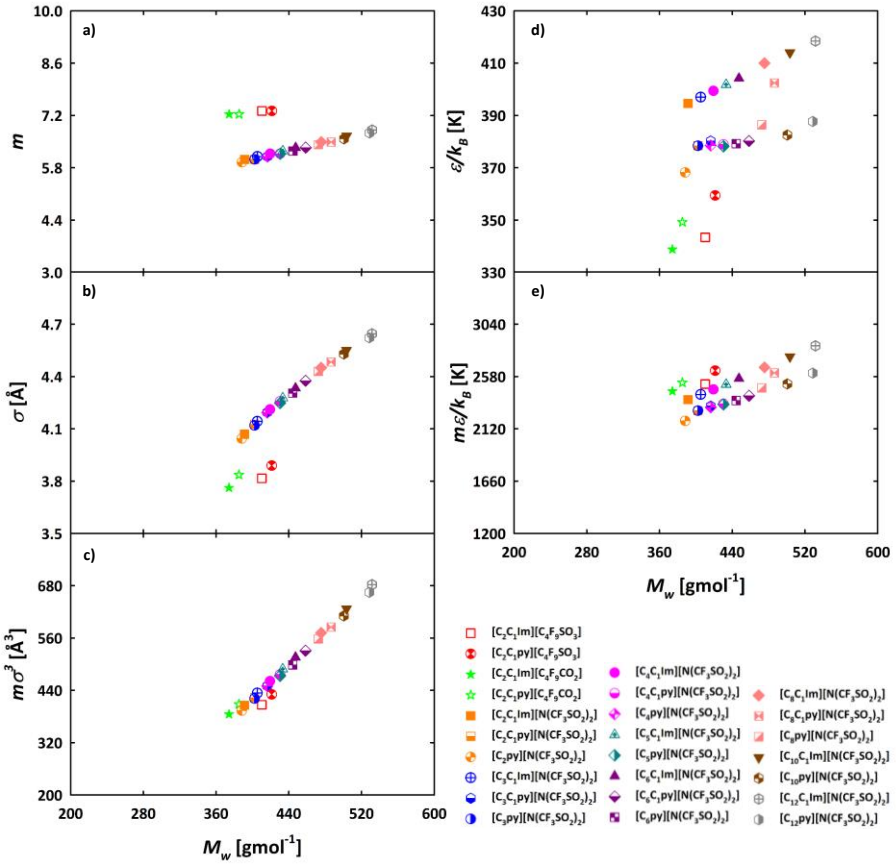

Figure 3.4.6 Molecular parameters values *versus* molecular weight for FILs with different cations, where: a) m parameter; b) σ parameter; c) $m\sigma^3$ correlation of the volume of the molecules (anion + cation); d) ε parameter; and e) $m\varepsilon$ is a correlation representing the van der Waals energy of the molecules (anion + cation). The comparisons are grouped by colour.

As mentioned, the values of the association parameters are kept constant, being the energy and volume of association for $[C_2py][N(CF_3SO_2)_2]$, $[C_2C_1py][N(CF_3SO_2)_2]$ and $[C_2C_1Im][N(CF_3SO_2)_2]$ 3450 K and 2250 Å^3, respectively (see Table 3.4.2). We will discuss now how these molecular trends are reflected in the macroscopic behaviour of the systems using soft-SAFT to calculate them. As an initial verification, the $[C_2C_1Im][C_4F_9SO_3]$ and$[C_2C_1Im][N(CF_3SO_2)_2]$ FILs were selected to predict the density-pressure diagram and the solubility of carbon dioxide (Figure 3.4.7).

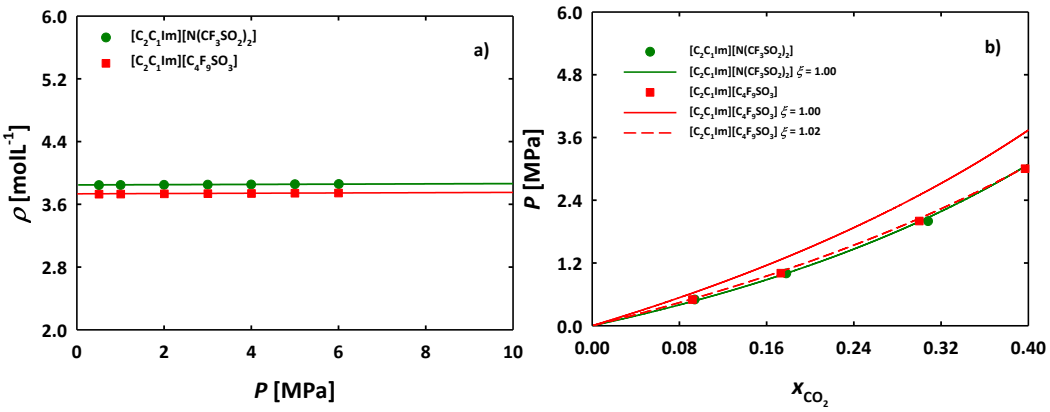

Figure 3.4.7 Validation of soft-SAFT predictions for $[C_2C_1Im][N(CF_3SO_2)_2]$ and $[C_2C_1Im][C_4F_9SO_3]$ thermodynamic properties. a) High-pressure density at 313.15 K; and b) Carbon dioxide solubility in these FILs at 313.15 K. Symbols represents experimental data [80]. The solid lines denote predictions obtained with soft-SAFT with the parameters provided in Table 3.4.2. In b) the dashed lines stand for the calculations with the binary parameter ξ adjusted to data for the $[C_2C_1Im][C_4F_9SO_3]$ IL.

The soft-SAFT calculations were assessed with available experimental data. Figure 3.4.7a shows that soft-SAFT predictions (calculated from the molecular parameters of the pure fluid) are in excellent agreement with high-pressure density experimental data for the two FILs. The solubility of CO_2 in the FILs is depicted in Figure 3.4.7b. Predictions for the solubility of CO_2 in $[C_2C_1Im][N(CF_3SO_2)_2]$ are in excellent agreement with the experimental data. For the case of $[C_2C_1Im][C_4F_9SO_3]$ some deviations from experimental data are observed, this is mainly due to the large differences between the van der Waals energies of carbon dioxide and the FILs molecules. Thus, the correct behaviour is accurately described when a binary parameter ξ is fitted (see Figure 3.4.7b) [80]. However, as we are searching for trends, calculations with pure component parameters can be used to distinguish the effect of the cation on these properties considering the pure component parameters capture the behaviour.

We present the next soft-SAFT predictions for the effect of the cation on high-pressure densities and the solubility of CO_2 in FILs. Although we have calculated these properties for all the FILs depicted in Figure 3.4.6, at 313.15K, we have selected to represent only some of them for easier visualization. Figure 3.4.8a shows the density-pressure diagram, and the solubility of carbon dioxide is depicted in Figure 3.4.8b for the selected FILs.

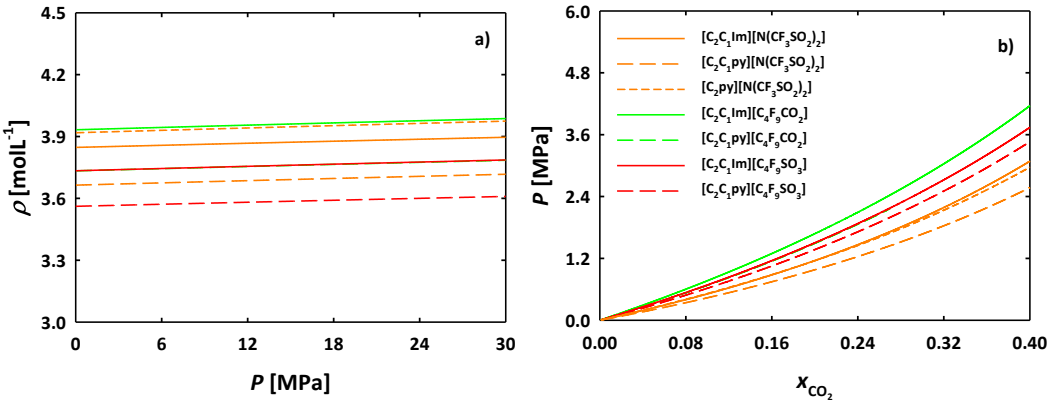

Figure 3.4.8 Influence of FILs cation on the thermodynamic properties of selected FILs. a) Prediction of high-pressure density at 313.15 K; and b) Predictions of carbon dioxide solubility in FILs at 313.15 K. The green dashed line, $[C_2C_1py][C_4F_9CO_2]$, overlaps with the red solid line, $[C_2C_1Im][C_4F_9SO_3]$). The lines represent predictions obtained with soft-SAFT with the parameters represented in Figure 3.4.6 and Table 3.4.2.

ILs with a hydrogenated alkyl side chain of two carbons conjugated with $[N(CF_3SO_2)_2]^-$, $[C_4F_9CO_2]^-$ and $[C_4F_9SO_3]^-$ anions were chosen for this purpose. The density at high pressures shows the tendency: $[C_nC_1py]^+ < [C_nC_1Im]^+ < [C_npy]^+$, being independent of the anion. These results are consistent with the physical trends observed in the molecular parameters. As the density is related to the volume occupied by the molecules, the exact inverse tendency ($[C_npy]^+ < [C_nC_1Im]^+ < [C_nC_1py]^+$) can be found in the regression $m\sigma^3$ (see Figure 3.4.6c), supporting the accuracy of the molecular parameters for describing the physical features of these FILs.

The predicted solubility of carbon dioxide in these FILs, (see Figure 3.4.8b), follows the tendency $[C_npy]+ \approx [C_nC_1Im]^+ < [C_nC_1py]^+$. The free volume is related to the solubility of low molecular weight solutes (such as carbon dioxide) and the density. Previous studies have shown that the increment of the free volume allows a better accommodation of gas molecules [8,47], hence increasing the gas solubility. This evidence is clear for cases where the solubilization process happens through a physical mechanism. The free volume is inversely proportional to the density, which means that compounds with a lower density have a higher free volume available. This is the behaviour observed in this case, where the ILs with lower density have a higher solubilization power of carbon dioxide [12,94,95].

Hence, in summary, based on the discussed results, FILs containing the cations $[C_npy]^+$, $[C_nC_1Im]^+$ and $[C_nC_1py]^+$ have similar molecular length and association energy, mainly differing in molecular volume and van der Waals interactions. As a consequence, the same values of the molecular parameters related to the molecular length, m, and association, ε^{HB} and κ^{HB} can be used for $[C_npy]^+$, $[C_nC_1Im]^+$ and $[C_nC_1py]^+$ cations-based FILs, while only

the group size and energy parameters, σ and ε, need to be fitted to experimental data (see Table 3.4.4).

Table 3.4.4 Summary of the transferability analysis of the molecular parameters, where *T* indicates the parameters that can be transferred and *F* the parameters that have to be fitted to experimental data, regarding the different structural features of the studied ionic liquids. $[C_nC_1Im][CF_3SO_3]$ and $[C_nC_1Im][CF_3CO_2]$ are not included here. See text for details.

Parameter	Cation (ST1)		Hydrogenated chain (ST2)		Anion (ST3)		Fluorinated chain (ST4)	
	T	F	T	F	T	F	T	F
m	✓			✓		✓		✓
σ [Å]		✓		✓		✓		✓
ε/k_B [K]		✓	✓			✓		✓
ε^{HB}/k_B [K]	✓		✓			✓		✓
κ^{HB} [Å^3]	✓		✓			✓		✓

3.4.2.1.2 Effect of the cation hydrogenated side chain

We present the next results for FILs in which the hydrogenated side chain length varies, the molecular parameters associated with this, and the influence of the structure on selected thermodynamic properties.

We first consider three $[N(CF_3SO_2)_2]^-$ -based ILs families conjugated with the $[C_nC_1Im]^+$, $[C_nC_1py]^+$ and $[C_npy]^+$ cations, all of them with hydrogenated chains (see Table 3.4.3, ST2). Taking into account that the type and strength of the association of these families should be very similar, the association parameters were kept constants for all members of the three families, assuming that the increment of the cation hydrogenated chain does not influence the localized association.

As for the other three parameters, in the case of $[C_nC_1Im][N(CF_3SO_2)_2]$, m, $\sigma$and ε were fitted to density data and correlated with the molecular weight (M_w) by:

$$m = 0.0056M_w + 3.8337 \quad (3.4.1)$$

$$m\sigma^3 = 1.9733M_w + 366.33 \text{ (Å}^3\text{)} \quad (3.4.2)$$

$$m\varepsilon/k_B = 3.3986M_w + 1043.3 \text{ (K)} \quad (3.4.3)$$

These correlations, together with the constant association parameters, enable the prediction of the thermodynamic behaviour of other members of the series, not included in the fitting procedure [50]. In addition, considering the similarity between the chemical structure of $[C_nC_1Im][N(CF_3SO_2)_2]$ and $[C_nC_1py][N(CF_3SO_2)_2]$ FILs, the chain length value m was transferred from imidazolium- to the pyridinium- based ILs with the same cation alkyl chains length (*i.e.*, $m_{[C_2C_1py][N(CF_3SO_2)_2]} = m_{[C_2C_1Im][N(CF_3SO_2)_2]}$). For the $[C_npy][N(CF_3SO_2)_2]$ family, the transferability was not direct due to the lack of a methyl group in the aromatic ring, conversely, the m values were transferred corresponding to $[C_{n-1}C_1Im]^+$ (*e.g.*, $m_{[C_3py][N(CF_3SO_2)_2]} =$

$m_{[C_2C_1Im][N(CF_3SO_2)_2]}$). As the m parameter was transferred from the imidazolium family, the correlation of Equation 3.4.1 is also effective for the pyridinium families in a predictive manner. Regarding the σ size parameter, two different correlations were found for each pyridinium family to account for the small deviations in molecular volume between both families. Equation 3.4.4 stands for $[C_nC_1py][N(CF_3SO_2)_2]$ and Equation 3.4.5 represents $[C_npy][N(CF_3SO_2)_2]$ [51].

$$m\sigma^3 = 1.9345M_w + 357.92\ (\text{Å}^3) \quad 3.4.4$$

$$m\sigma^3 = 1.9205M_w + 349.81\ (\text{Å}^3) \quad 3.4.5$$

Notice that ε parameter for the pyridinium families with the $[N(CF_3SO_2)_2]^-$ anion was reparametrized in this work to allow the association parameters to be transferred between families (see Table 3.4.2), as all differences in energy are now implicitly included in this parameter.

We studied next to the imidazolium cations with different anions: $[CF_3SO_3]^-$, $[CF_3CO_2]^-$ and $[C_4F_9SO_3]^-$. The FILs $[C_nC_1Im][CF_3SO_3]$ and $[C_nC_1Im][CF_3CO_2]$ (n= 2, 4), were modelled with different associations schemes. For C2 FILs the molecular and association parameters were transferred from the $[C_nC_1Im][BF_4]$ [48,54] family (see Figure 3.4.5) using a 1-site association scheme, while parameters for C4 were adjusted to experimental data in previous work [53]. Although there is not enough available experimental for these ILs families to correlate them with the molecular weight (only C2 and C4 are available; see Table 3.4.3, ST2), it can be seen that the molecular volume and molecular energy of these two families are smaller than for the others, mainly as a consequence of their lower molecular weight (see Figure 3.4.9).

Pereiro *et al.* modelled the $[C_nC_1Im][C_4F_9SO_3]$ FILs family, where the five molecular parameter values were fitted to temperature-density experimental data at atmospheric pressure. The association parameters of $[C_nC_1Im][C_4F_9SO_3]$ were kept constant for the whole family [47], obtaining linear correlations with the molecular weight for m, σ and ε:

$$m = 0.01330M_w + 1.857 \quad 3.4.6$$

$$m\sigma^3 = 1.911M_w + 375.4\ (\text{Å}^3) \quad 3.4.7$$

$$m\varepsilon/k_B = 5.664M_w + 203.2\ (\text{K}) \quad 3.4.8$$

In summary, as far as the hydrogenated chain length of the cation is concerned, we can conclude that for the alkanes and alkanol families [71,96], m, σ and ε linearly correlate with the molecular weight (Equations 3.4.1 to 3.4.8), while the association parameters are independent of the cation hydrogenated side chain length, being their values constant for all the series members.

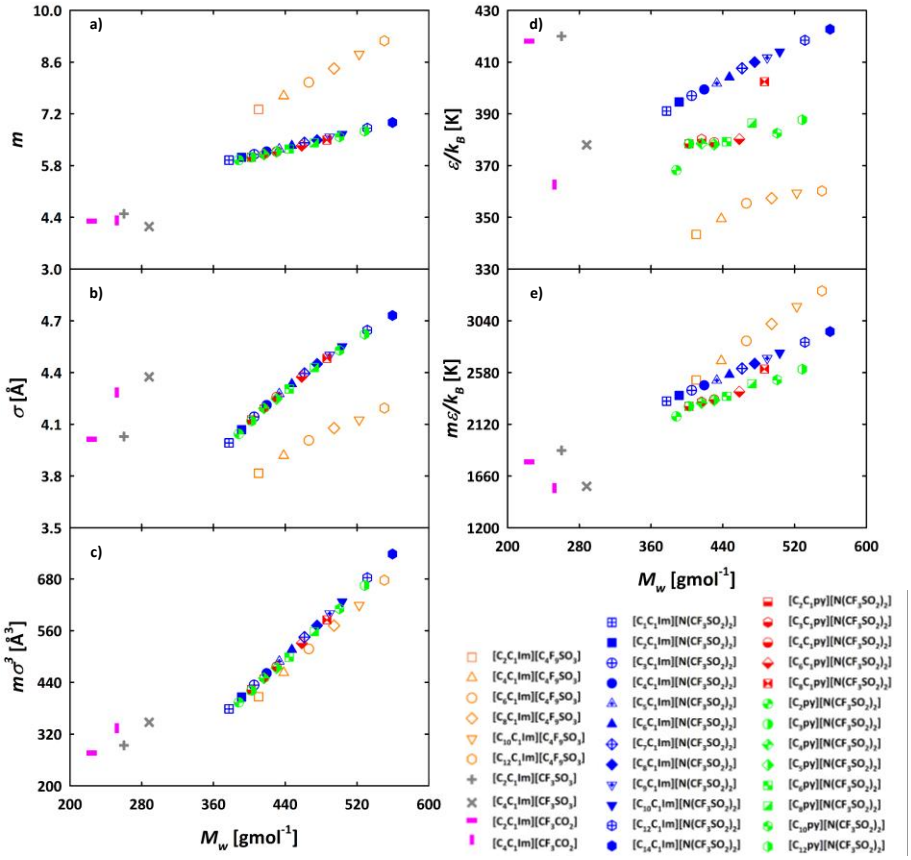

Figure 3.4.9 Molecular parameters values versus molecular weight for FILs with different hydrogenated alkyl side chains in the cation, where: a) m parameter; b) σ parameter; c) $m\sigma^3$ is a correlation of the volume of the molecules (anion + cation); d) ε/k_B parameter; and e) $m\varepsilon/k_B$ is a correlation representing the van der Waals energy of the molecules (anion + cation). The comparisons are grouped by colour.

In previous studies the van der Waals energy parameter, ε, was usually fitted to experimental data and not transferred between families, carrying most of the molecular energetic differences among FILs families. However, a closer look into the parameters provided in Table 3.4.2 shows that for the $[C_nC_1py][N(CF_3SO_2)_2]$ and $[C_npy][N(CF_3SO_2)_2]$ families the value of ε was kept constant for the whole family. For other families, the values of ε are quite similar (see Figure 3.4.9), except for the case of FILs with short, fluorinated chains. Based on this fact we took one step forward into building transferable models and fixed the ε value for each family, not including $[C_nC_1Im][CF_3SO_3]$ and $[C_nC_1Im][CF_3CO_2]$ (only two members of each family are available). The ε parameter was fixed at an intermediate value between those obtained for each member of the family and the density-temperature diagrams were calculated for each ILs family. Results are presented in Figure 3.4.10, with the following optimized values for each family: a) $[C_nC_1Im][N(CF_3SO_2)_2]$ with ε/k_B = 406 K; b) $[C_nC_1Im][C_4F_9SO_3]$ with ε/k_B = 355 K; c) $[C_nC_1py][N(CF_3SO_2)_2]$; and d) $[C_npy][N(CF_3SO_2)_2]$ with ε/k_B = 380 K. The solid lines represent the calculations with the parameters depicted on Table 3.4.2 and the dashed lines stand for the calculations with the optimized fixed ε values for each

family (Figure 3.4.10). The overall agreement between the experimental data [8,47,86–93,97,98] and the two types of calculations is excellent. For the outermost members, the calculations with the fixed energy parameter are slightly allocated. However, the differences are not significant, and it can be stated that by fixing the ε value along the ILs families included in this work, the calculations provide a good representation of the experimental data, leading to the conclusion that this parameter can be fixed along with a FIL family.

Taking advantage of the transferability of the models we have studied the influence of the cation hydrogenated alkyl side chain on the thermodynamic properties of FILs and the results are presented in Figure 3.4.11 for the $[C_nC_1Im][N(CF_3SO_2)_2]$ family as an example. This family is the one with more studied FILs; the same thermophysical behaviour was found in the other FILs families. The high-pressure density diagram is depicted in Figure 3.4.11a showing that the density decreases as the hydrogenated alkyl side chain length increases. This agrees with the linear correlation of $m\sigma^3$, the molecular volume (see Figure 3.4.9c), which has the inverse behaviour, increasing as the hydrogenated side chain length increases. For the solubility of carbon dioxide in these FILs, it is observed that the solubility increases as the hydrogenated side chain increases (see Figure 3.4.11b).

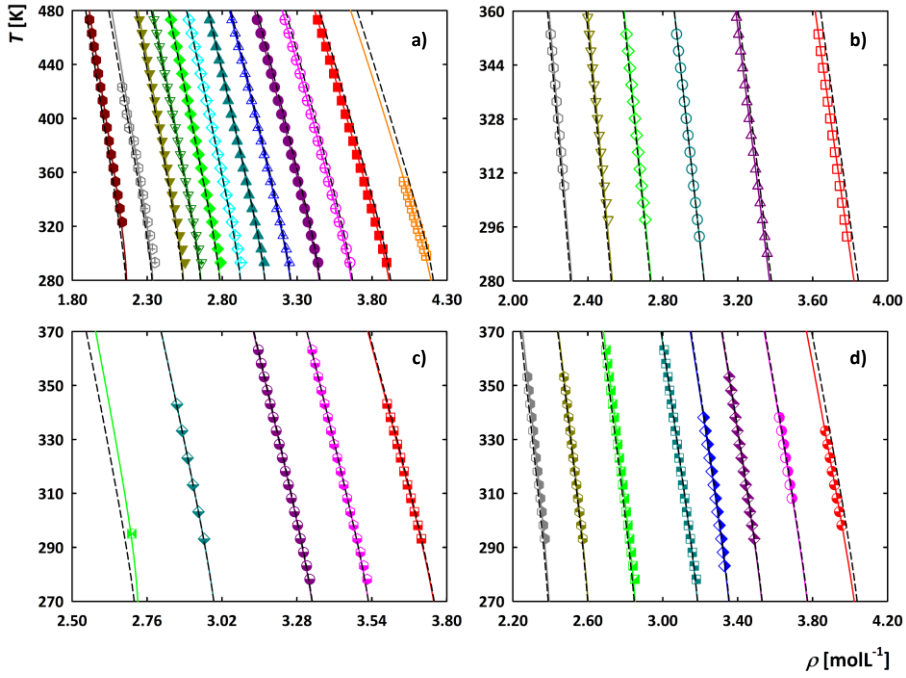

Figure 3.4.10 Temperature *versus* density diagrams at 0.1 MPa for: a) $[C_nC_1Im][N(CF_3SO_2)_2]$; b) $[C_nC_1Im][C_4F_9SO_3]$; c) $[C_nC_1py][N(CF_3SO_2)_2]$; and d) $[C_npy][N(CF_3SO_2)_2]$. The colour code is for the alkyl chain length of the cation: n=1, orange; n=2, red; n=3, pink; n=4, purple; n=5, blue; n=6, dark cyan; n=7, light cyan; n=8, light green; n=9, dark green; n=10, dark yellow; n=12, grey; n=14, dark red. The solid lines represent the calculations obtained with the optimized ε parameter for each IL (Table 3.4.2), and the dashed lines illustrate the calculations with the fixed ε/k_B parameter for each family at: a) 406 K, b) 355 K, c) and d) 380 K. Symbols represent the experimental data [8,47,86–93,97,98].

This result can also be related to the free volume between the molecules (the increment of the alkyl chain corresponds to an increase in the free volume). This behaviour is directly related to the increment of the asymmetry between the FILs molecules [12]. Again, the molecular parameters accurately capture the physical features of the FILs families.

In summary, it has been observed that the hydrogen bonding of these FILs is independent of the length of the hydrogenated alkyl chain of the cation, and the corresponding ε^{HB} and κ^{HB} parameters can be transferred between FILs families. It has also been observed that the van der Waals energy parameter can be kept constant within a family, while m and σ are different for each member of the family, and they need to be fitted to experimental data, showing a good correlation with the molecular weight (see Table 3.4.4). This implies that most of the differences between members of the studied FILs are related to their size and molecular volumes.

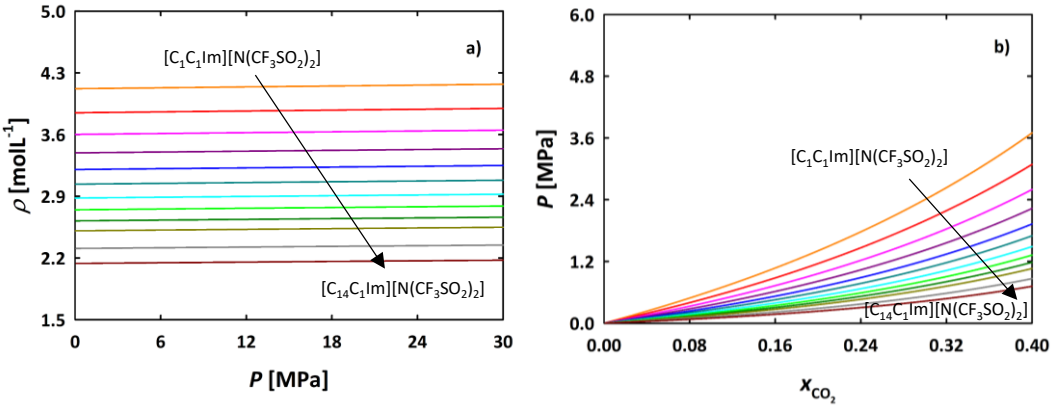

Figure 3.4.11 Influence of the FILs cation hydrogenated side chain in a) high-pressure density at 313.15 K; and b) carbon dioxide solubility in FILs at 313.15 K. The lines represent predictions obtained with soft-SAFT with the parameters represented in Figure 3.4.9 and Table 3.4.2. The colour code is for the alkyl chain length: n=1, orange; n=2, red; n=3, pink; n=4, purple; n=5, blue; n=6, dark cyan; n=7, light cyan; n=8, light green; n=9, dark green; n=10, dark yellow; n=12, grey; n=14, dark red.

3.4.2.1.3 Effect of the anion

In a similar manner as for the cations, we have studied several FILs with a given cation and different anions, comparing the values of the molecular parameters versus their molecular weight (see Figure 3.4.12) and the corresponding effect on selected thermodynamic properties (ST3 in Table 3.4.3 and Figure 3.4.13). As shown in Figure 3.4.12a, the length of the ILs depends on the anions considered. Accordingly, the value of m increases in the following order: $[CF_3CO_2]^-$ ≈ $[CF_3SO_3]^-$ < $[N(CF_3SO_2)_2]^-$ < $[C_4F_9CO_2]^-$ ≈ $[C_4F_9SO_3]^-$ for the same cation. This tendency is not linear with the increment of the molecular weight. However, it can be related to the structure of the anions, where a linear fluorinated chain (*e.g.* $[C_4F_9SO_3]^-$) has a higher m contrarily to the anion with branched fluorinated chains (*e.g.* $[N(CF_3SO_2)_2]^-$). It is clear that the

sulfonate and carboxylate functional groups do not have an influence on the overall length of the ILs considered. These behaviours justify the deviations found in the cation (see Figure 3.4.9), emphasising that those results are accurate only when the cations are conjugated with the same anion.

The differences in the anion are clearly captured by the σ size parameter as displayed in Figure 3.4.12b. However, the tendency is quite the reverse from those of m results, where $[C_4F_9CO_2]^- < [C_4F_9SO_3]^- < [N(CF_3SO_2)_2]^- < [CF_3CO_2]^- \approx [CF_3SO_3]^-$. Furthermore, the difference in size between the sulfonate and carboxylate functional groups is well captured by the σ parameter. Figure 3.4.12c shows the $m\sigma^3$ correlation with the following trend: $[CF_3CO_2]^- \approx [CF_3SO_3]^- < [C_4F_9CO_2]^- < [C_4F_9SO_3]^- \approx [N(CF_3SO_2)_2]^-$. The volume of a FIL conjugated with $[C_4F_9SO_3]^-$ or $[N(CF_3SO_2)_2]^-$ anion is similar, even $[C_4F_9SO_3]^-$ has a high number of fluorine atoms and a slightly different M_w. This similarity can be explained by the structure of each IL family (see Table 3.4.1). The $[C_4F_9SO_3]^-$ anion has a linear structure with higher m and lower σ values. On the contrary, the $[N(CF_3SO_2)_2]^-$ anion has two symmetric branched chains with shorter chain length, m, but it is composed of bulkier groups, hence with higher σ values.

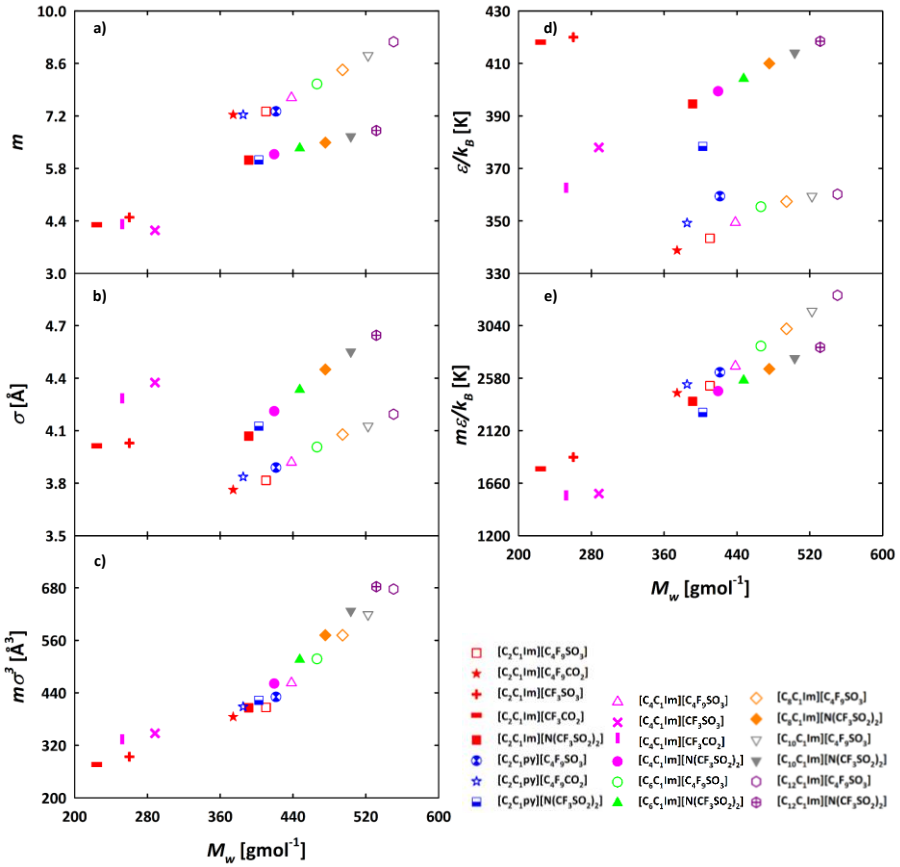

Figure 3.4.12 Molecular parameters values *versus* molecular weight for FILs with different anions, where: a) m parameter; b) σ parameter; c) $m\sigma^3$ is a correlation of the volume of the molecules (anion + cation); d) ε/k_B parameter; and e) $m\varepsilon/k_B$ is a correlation representing the van der Waals energy of the molecules (anion + cation). The comparisons are grouped by colour.

Therefore, they seem to occupy very similar volumes, even though they have completely different structures. Else, the main structural difference between the volumes of $[CF_3CO_2]^-$ and $[CF_3SO_3]^-$ is the addition of an oxygen atom. Figure 3.4.12d depicts the ε values for FILs with different anions. The values of ε follow the trend $[C_4F_9CO_2]^-$ < $[C_4F_9SO_3]^-$ < $[CF_3CO_2]^-$ < $[CF_3SO_3]^-$ < $[N(CF_3SO_2)_2]^-$, for C4 FILs and $[C_4F_9CO_2]^-$ < $[C_4F_9SO_3]^-$ < $[N(CF_3SO_2)_2]^-$ < $[CF_3CO_2]^-$ ≈ $[CF_3SO_3]^-$ for C2 FILs. Both trends are not linear with the M_w but reflect the intermolecular interactions of the different ILs. The trend found for $m\varepsilon$ regression (shown in Figure 3.4.12e) is the following: $[CF_3CO_2]^-$ ≈ $[CF_3SO_3]^-$ < $[N(CF_3SO_2)_2]^-$ < $[C_4F_9CO_2]^-$ ≈ $[C_4F_9SO_3]^-$.

As mentioned in the previous section, the association parameter κ^{HB} for FILs with different anions is kept constant while ε^{HB} varies. It follows the tendency: $[N(CF_3SO_2)_2]^-$ (3450 K) < $[C_4F_9CO_2]^-$ = $[C_4F_9SO_3]^-$ (3850 K) (see Table 3.4.2), except for $[CF_3SO_3]^-$ and $[CF_3CO_2]^-$, which have different ε^{HB} values depending on if they are C2 (3450 K) or C4 (3650 K, $[CF_3SO_3]^-$ and 3725 K, $[CF_3CO_2]^-$) FILs, due to the different association schemes, as explained in section 2.3. It is concluded that ILs with a linear fluorinated chain have a higher value of the energy of association than the corresponding IL with a branched fluorinated chain. Interestingly, we have observed that the volume of association can be kept constant for all the FILs investigated (κ^{HB} = 2250 Å^3), except for $[C_4C_1Im][CF_3SO_3]$ and $[C_4C_1Im][CF_3CO_2]$, where the value of κ^{HB} is 2400 Å^3. This exception can be attributed to the relatively short length of the $[CF_3SO_3]^-$- and $[CF_3CO_2]^-$-based ILs, allowing stronger association due to the absence of steric effects.

The calculated thermodynamic properties of the different anions conjugated with the $[C_2C_1Im]^+$ cation are discussed next, being the only comparison involving all the anions studied in this work. Figure 3.4.13a illustrates the density of the different ILs at high pressures. It follows the tendency: $[C_4F_9SO_3]^-$ < $[N(CF_3SO_2)_2]^-$ < $[C_4F_9CO_2]^-$ < $[CF_3SO_3]^-$ < $[CF_3CO_2]^-$. This trend is similar to the inverse of the $m\sigma^3$ trend ($[CF_3CO_2]^-$ < $[CF_3SO_3]^-$ < $[C_4F_9CO_2]^-$ < $[C_4F_9SO_3]^-$ ≈ $[N(CF_3SO_2)_2]^-$), as expected. Hence, the molecular parameters correctly capture the relation between the density and volume. Notice that the density of the ILs with heavier anions is very similar and lower than the ones with shorter anions.

The influence of the different anions on the solubility of carbon dioxide in FILs is depicted in Figure 3.4.13b, following the tendency: $[CF_3CO_2]^-$ < $[CF_3SO_3]^-$ < $[C_4F_9CO_2]^-$ < $[C_4F_9SO_3]^-$ < $[N(CF_3SO_2)_2]^-$. This implies that the solubilisation power for carbon dioxide is higher for anions with bulkier fluorinated chains, given a clear indication of the design of ILs for this specific application.

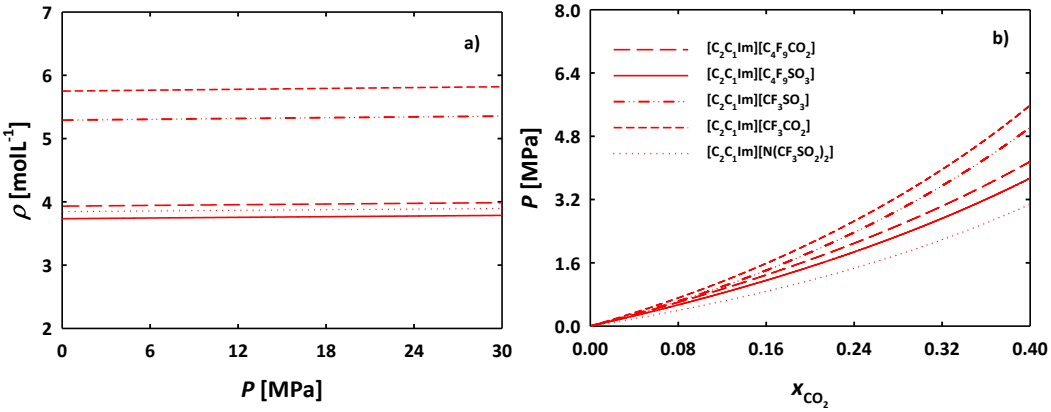

Figure 3.4.13 Influence of the FILs anion in a) high-pressure density at 313.15 K; and b) carbon dioxide solubility in FILs at 313.15 K. The lines represent predictions obtained from soft-SAFT with the parameters provided in Figure 3.4.12 and Table 3.4.2.

3.4.2.1.4 Effect of the anion fluorination

Results regarding the anion fluorination are quite similar to those of the anions discussed in the preceding subsection. The number of fluorine atoms and the length of the fluorinated side chain of the anion is considered in this study (ST4 in Table 3.4.3). The comparison related to the number of fluorine atoms and the chain length m is presented in Figure 3.4.14a, showing that $[CF_3SO_3]^-$ < $[N(CF_3SO_2)_2]^-$ < $[C_4F_9SO_3]^-$. Therefore, the increment of the fluorine atoms in the anion demands a higher m value (linear tendency with the increment of M_w), as expected, given the size of the fluorine atoms. As previously discussed, branched anions have m lower values than linear anions with an equivalent number of atoms. It is also observed that anions with linear fluorinated chains follow the trend $[CF_3CO_2]^-$ < $[C_4F_9CO_2]^-$, where longer chains have higher M_w and corresponding larger m values. As in the previous cases, the inverse trend is found for the σ parameter regarding the anion fluorination: $[C_4F_9SO_3]^-$ < $[N(CF_3SO_2)_2]^-$ < $[CF_3SO_3]^-$ and $[C_4F_9CO_2]^-$ < $[CF_3CO_2]^-$ (see Figure 3.4.14b). The effect of the anion fluorination in the $m\sigma^3$ correlation (see Figure 3.4.14c) is similar to that observed for the anion comparisons of the previous subsection (ST3): $[CF_3SO_3]^-$ < $[C_4F_9SO_3]^-$ ≈ $[N(CF_3SO_2)_2]^-$, highlighting that ILs with a similar number of atoms have similar molecular volume. The same happens for the increment of fluorination for the linear anions: $[CF_3CO_2]^-$ < $[C_4F_9CO_2]^-$. In the case of the ε parameter, the trend is $[C_4F_9SO_3]^-$ < $[N(CF_3SO_2)_2]^-$ < $[CF_3SO_3]^-$ (except for C4 FILs, see Figure 3.4.14d of ESI†). It is also observed that the increase of the fluorinated side chain length decreases the overall van der Waal energy, implying lower values of the ε parameter: $[C_4F_9CO_2]^-$ < $[CF_3CO_2]^-$. These results suggest that for the coarse grain models used for the FILs in this work, the energy of interaction between the groups (monomers integrating the chains) of a short chain is greater than in a longer or bulkier chain. This tendency implies that the energy parameter value is larger for anions with a higher

number of fluorine atoms. For the $m\varepsilon$ correlation (Figure 3.4.14e) versus M_w, the tendency found for the addition of fluorine atoms to the anions is $[CF_3SO_3]^-$ < $[N(CF_3SO_2)_2]^-$ < $[C_4F_9SO_3]^-$ and also $[CF_3CO_2]^-$ < $[C_4F_9CO_2]^-$. This regression is highly influenced by the anion fluorination, where the higher values are found for the FILs with nine fluorine atoms. Notice that all the ILs depicted in Figure 3.4.14a are described by the same molecular weight correlation. In regard to ε^{HB}/k_B and the fluorination effects, the trend is $[N(CF_3SO_2)_2]^-$ (3450 K) ≤ $[CF_3SO_3]^-$ (C2, 3450 K; C4, 3650 K) < $[C_4F_9SO_3]^-$ (3850 K) and $[CF_3CO_2]^-$ (C2, 3450 K; C4, 3725 K) < $[C_4F_9CO_2]^-$ (3850 K). As was already seen, the only feature affecting this energy parameter is the structure of the anions. A linear fluorinated chain can have a higher or similar value of energy between the ILs molecules association compared to a branched fluorinated chain. The increment of the fluorinated linear chain rises the associating energy. The κ^{HB} value is transferable into the different anions, as in the case of $[N(CF_3SO_2)_2]^-$, $[C_4F_9SO_3]^-$ (2250 Å^3) and C2 based FILs with shorter fluorinated chain. However, the anions with short fluorinated chains based on C4 ($[C_4C_1Im][CF_3SO_3]^-$ and $[C_4C_1Im][CF_3CO_2]^-$) have a higher value of associating volume (2400 Å^3).

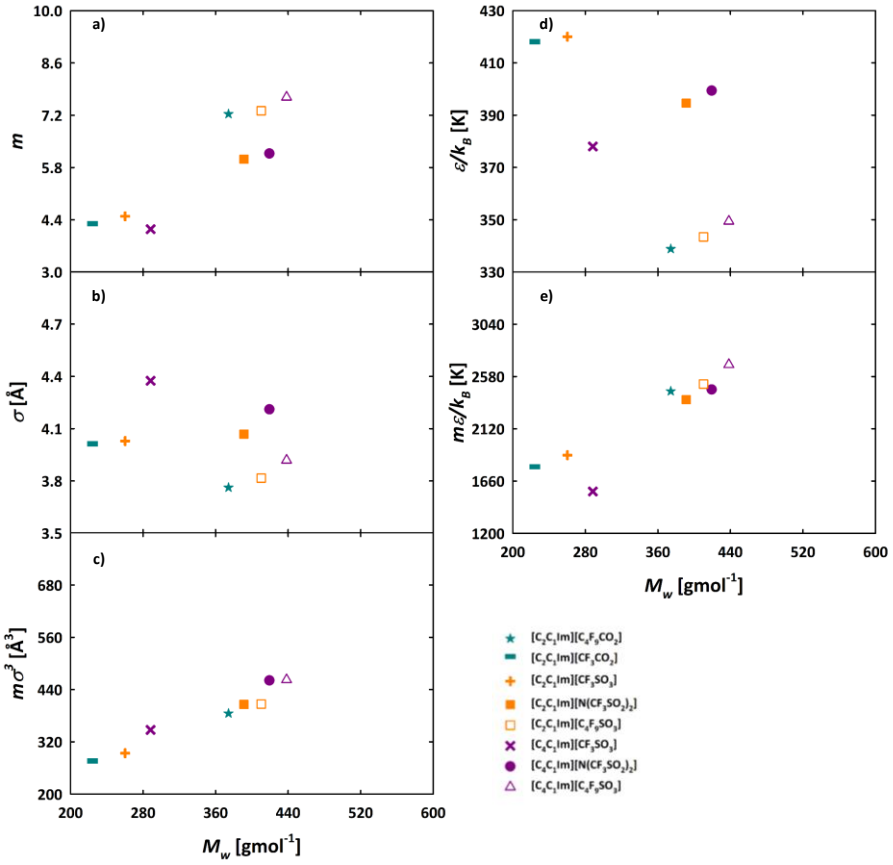

Figure 3.4.14 Molecular parameters values *versus* molecular weight for FILs with different anion fluorination, where: a) m parameter; b) σ parameter; c) $m\sigma^3$ is a correlation of the volume of the molecules (anion + cation); d) ε/k_B parameter; and e) $m\varepsilon/k_B$ is a correlation representing the van der Waals energy of the molecules (anion + cation). The comparisons are grouped by colour.

Figure 3.4.15 depicts the influence of the anion fluorination on the high-pressure density of the pure FILs at 313.15 K and the solubility of carbon dioxide in FILs at 313.15 K. The density, illustrated in Figure 3.4.15a, varies in the following order: $[C_4F_9SO_3]^-$ < $[N(CF_3SO_2)_2]^-$ < $[CF_3SO_3]^-$; decreasing as the chain length increases. This tendency is inversely proportional to the $m\sigma^3$ result, with the parameters accurately describing the physical features of the ILs molecules. In the case of carbon dioxide solubilisation, as previously observed for different anions (ST3), the FILs with bulkier fluorinated chains have a greater solubilisation power, followed by the branched fluorinated chains and at last the shorter linear fluorinated chains (see Figure 3.4.15b). This behaviour is a direct consequence of increasing the number of fluorine atoms and the length of the linear fluorinated chain.

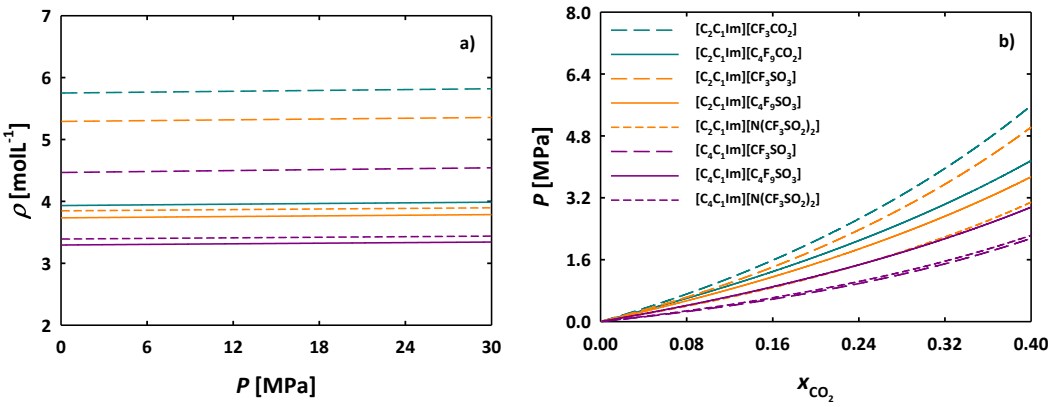

Figure 3.4.15 Influence of the FILs anion fluorination in: a) high-pressure density at 313.15 K; and b) carbon dioxide solubility in FILs at 313.15 K. Lines are predictions from soft-SAFT with parameters represented in Figure 3.4.14 and Table 3.4.2.

3.4.2.2 Validity of the transferability approach for prediction purposes

In order to validate the robustness of the parameters and the approach for prediction purposes, we selected some FILs not included in the previous discussions to be modelled with the soft-SAFT framework and compare its accuracy to experimental data. For this purpose we selected two FILs from $[C_nC_1Im][N(C_2F_5SO_2)_2]$ ILs family, where n = 2 and 4, and $[C_4C_1py][CF_3SO_3]$, taking advantage of the experimental data available in the literature [80,99–104]. The $[C_nC_1Im][N(C_2F_5SO_2)_2]$ ILs family as a fluorinated anion is different from those of the ILs studied in the previous section. The anion of the $[C_4C_1py][CF_3SO_3]$ IL was studied in the previous sections, however, in this particular case, it is conjugated with a different cation. Besides, this IL has an anion with a short, fluorinated chain which has a behaviour quite different from the other ILs. For consistency, a 3-site association model was used (see Figure 3.4.1a).

Selected thermodynamic properties of the pure FILs and solubilities of carbon dioxide, methanol and water in the FILs were calculated in a predictive manner and compared with

the available experimental data. The molecular models of carbon dioxide (CO_2), methanol (CH_3OH) and water (H_2O) were transferred from previous works. Carbon dioxide was modelled as a Lennard-Jones (LJ) chain, where quadrupolar interactions were taken into account with the molecular parameter x_p fixed to 1/3 (representing the number of segments in those molecules that may momentarily contain the quadrupole) [51]. Methanol was modelled as a homonuclear chainlike molecule with two association sites embedded off-centre in one of the LJ segments to mimic the hydroxyl group interactions. One *A* site stands for the lone pair of electrons on the oxygen atom and one *B* site represents the H atom. Only *A*-*B* interactions were allowed for the pure component [72,105]. Water was modelled as a single spherical LJ monomer (m_{H2O} = 1) with four association sites: two *e* sites (negative, corresponding to the lone pairs of the oxygen electrons) and two *H* type sites (positive, corresponding to the hydrogen atoms). Only *e*-*H* bonding was allowed. These four association sites preserve the tetrahedral geometry of the compound [96]. The values of the respective molecular parameters for the three compounds are summarized in Table 3.4.5 for completeness.

Table 3.4.5 Molecular weight and molecular parameters of carbon dioxide, methanol and water used in this work.

Compound	M_w [g mol^{-1}]	m	σ [Å]	ε/k_B [K]	ε^{HB}/k_B [K]	κ^{HB} [Å^3]	Q (C m^2)	x_p	REF
CO_2	44.01	1.571	3.184	160.2	–	–	4.4×10^{-40}	1/3	[51]
CH_3OH	32.04	1.491	3.375	220.4	3213	4847	–	–	[72,105]
H_2O	18.01	1.000	3.154	365.0	2388	2932	–	–	[96]

The validation process of the transferability of the parameters started with $[C_2C_1Im][N(C_2F_5SO_2)_2]$. Three different approaches to optimize the molecular parameters of this FIL were performed. The first approach (approach 1) was focused on the analysis of the number of fluorine atoms in the FIL anion, independently of their distribution. In this case, the $[C_4F_9SO_3]^-$ anion, with a similar number of fluorine atoms, was chosen and a direct transfer of parameters from the $[C_2C_1Im][C_4F_9SO_3]$ FIL molecular parameters to $[C_2C_1Im][N(C_2F_5SO_2)_2]$ was intended and results compared to density-temperature data of $[C_2C_1Im][N(C_2F_5SO_2)_2]$ available in the literature [80]. The results are represented in Figure 3.4.16 as a black line, very far from the experimental data. From the knowledge learned about the influence of the different molecular features on the molecular parameters (discussed in the previous sections) it was decided to fit σ parameter to density data, while the other four molecular parameters were directly transferred from $[C_2C_1Im][C_4F_9SO_3]$ (see Table 3.4.6, set A). An excellent agreement with the experimental values was achieved in this case (Figure 3.4.16, red solid line, overlapped by green solid line) with an AAD of 0.017%. However, the previous approach implies fitting to experimental data, even though it is only for one parameter. In a second approach (approach 2), searching for pure predictions, we focused on the symmetry of the

anion branched fluorinated side chain, as it has been shown to have an important effect on parameterization. Thus, it was considered that the anion structural features can be characterized by the presence of only 5 fluorine atoms, since the two side chains are a mirror of each other (see Table 3.4.1). A member of the $[C_nC_1Im][N(CF_3SO_2)_2]$ series with a longer hydrogenated chain capable of compensating for the presence of 2 additional fluorine atoms (considering the symmetry of the anions, $[N(CF_3SO_2)_2]^-$ = 3 fluorine atoms versus $[N(C_2F_5SO_2)_2]^-$ = 5 fluorine atoms) was chosen in this case. In terms of size, one fluorine atom is approximately 1.5 times larger than a hydrogen atom [12]. Therefore, 3 hydrogen atoms are needed to have approximately 2 fluorine atoms. With this strategy in mind, the molecular parameters of $[C_5C_1Im][N(CF_3SO_2)_2]$ (Table 3.4.2) were directly transferred to $[C_2C_1Im][N(C_2F_5SO_2)_2]$ FIL. Results with this set are presented in Figure 3.4.16 as a green line.

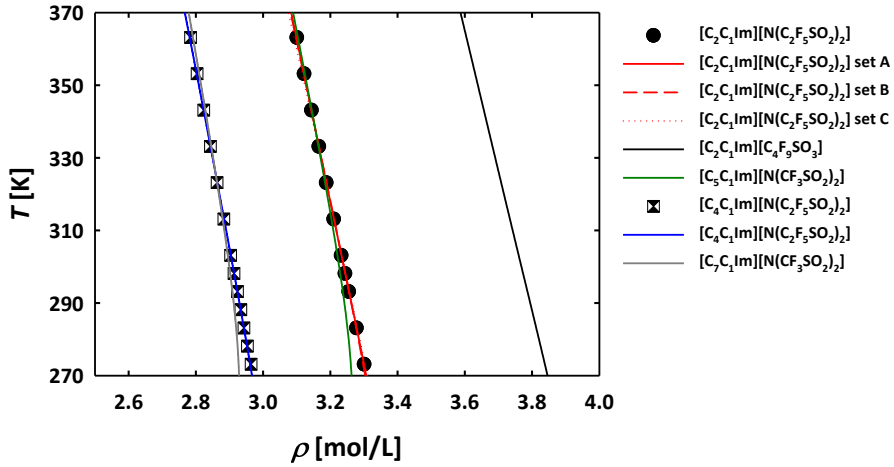

Figure 3.4.16 Temperature-density diagram of $[C_2C_1Im][N(C_2F_5SO_2)_2]$ and of $[C_4C_1Im][N(C_2F_5SO_2)_2]$ at atmospheric pressure. Lines represent the soft-SAFT calculations, where the three red lines and solid blue line are the calculations obtained with the optimized sets of parameters (see Table 3.4.6) and black, green, and grey lines are the calculations with the parameters directly transferred from other ILs. The three red lines and the green line overlap. Symbols are the experimental data [80,101].

The predictions show very good agreement with experimental data, having only a small deviation in the lower temperatures range. This is an outstanding result, showing that a direct transfer of the parameters, taking into consideration the molecular features of the equivalent ILs allows a good agreement with experimental data, without any fitting. Of course, excellent agreement in the whole range of temperatures can be achieved if the experimental data is used to fit some of the parameters. For instance, results fitting σ and ε while transferring the other three parameters from $[C_5C_1Im][N(CF_3SO_2)_2]$ are shown in Figure 3.4.16 as a red dashed line, with parameters provided in Table 3.4.6 as set B. In all cases used in the previous section, only temperature-density data was used in the fitting or to assess the transferred parameters. In order to check the sensitivity of the parameters and their performance to the data used to estimate them, a third approach was used (approach 3). In

this approach, high-pressure density and isothermal compressibility data were used, simultaneously, to fit σ and ε, while also transferring the other four molecular parameters from $[C_5C_1Im][N(CF_3SO_2)_2]$ (see Table 3.4.6, set C). Results with this set of parameters are presented in Figure 3.4.16 as a dotted red line, overlapping with those obtained from sets A and B.

Table 3.4.6 Molecular weight, molecular parameters, and density absolute average deviation (AAD) from the fitting procedure of the ionic liquids modelled in this work. The references correspond to the density experimental data used in the fitting or assessment approach.

Ionic Liquid	M_w [g mol^{-1}]	m	σ [Å]	ε/k_B [K]	$m\sigma^3$ [Å^3]	$m\varepsilon/k_B$ [K]	ε^{HB}/k_B [K]	κ^{HB} [Å^3]	AADρ [%]	REF
$[C_2C_1Im][N(C_2F_5SO_2)_2]$ set A	491.32	7.320	4.013	343.4	473	2514	3850	2250	0.0168	
$[C_2C_1Im][N(C_2F_5SO_2)_2]$ set B	491.32	6.247	4.240	354.8	476	2216	3450	2250	0.0386	[80]
$[C_2C_1Im][N(C_2F_5SO_2)_2]$ set C	491.32	6.247	4.225	337.1	471	2106	3450	2250	0.010	
$[C_4C_1Im][N(C_2F_5SO_2)_2]$	519.39	6.418	4.356	356.0	530	2285	3450	2250	0.0341	[100]
$[C_4C_1py][CF_3SO_3]$	299.31	4.149	4.457	378.0	347	1568	3650	2400	0.0521	[104]

A comparison of the performance of the four sets of parameters for $[C_2C_1Im][N(C_2F_5SO_2)_2]$ FIL at high pressure and isothermal compressibility data is presented in Figure 3.4.17. Note results for sets A and B (red full and dashed lines) and those obtained from approach 2 (green line) are pure predictions, while set C from approach 3 was fitted to these data. As inferred from the figure, sets A, B and C (see Table 3.4.6) give similar results for the high pressure-density data, in excellent agreement with experimental data [80]. The set directly transferred from $[C_5C_1Im][N(CF_3SO_2)_2]$ (green line) also shows good agreement, the soft-SAFT calculations give the correct slope, with a deviation from data near to 4.6% (considering the range 3.1-3.3 mol·L^{-1} of density).

The high-pressure density experimental data[1] was used to calculate a derivative property, isothermal compressibility (k_T), using the Tait equation.[2] The corresponding isothermal compressibility data is represented in Figure 3.4.17 using symbols, while the soft-SAFT calculations are represented by lines. Set C, fitted to this data, is the one providing the best results, with an AAD% of 0.6. Predictions from the other three sets are also shown in the figure; although they capture the correct slope, none of them is able to quantitatively reproduce the derived experimental data, being the ones from set B (red dashed line) the closest, with an AAD% of 14%. This behaviour has been observed in previous SAFT works in which the molecular parameters fitted to vapour equilibria data do not quantitatively predict second derivative properties, such as the isothermal compressibility or heat capacities [99,106]. It is important to emphasize that the derivative properties are more sensitive to errors in both, the experimental data and the values of the parameters.

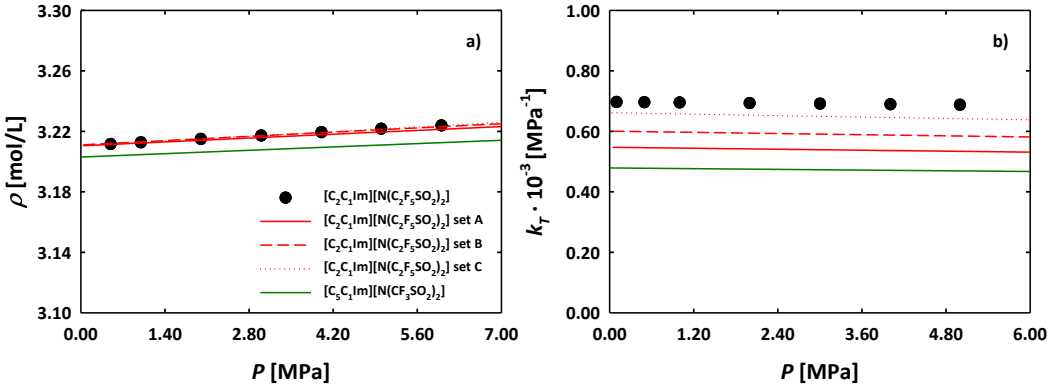

Figure 3.4.17 Thermodynamic properties of FIL $[C_2C_1Im][N(C_2F_5SO_2)_2]$. a) Pressure-density diagram at 313.15 K (red lines overlap) and b) isothermal compressibility at 313.15 K. Lines correspond to the soft-SAFT calculations, where the three red lines are the calculations obtained with the optimized sets of parameters (see Table 3.4.6) and the green line the calculation with the parameters directly transferred from the indicated IL. Symbols are the experimental data.[1] In b) the data was calculated using the Tait equation [50,107,108].

Predictive results using these four sets of parameters for the calculation of the solubility of carbon dioxide in $[C_2C_1Im][N(C_2F_5SO_2)_2]$ and the density of FIL + methanol binary system are presented in Figure 3.4.18, as compared to available experimental data. The predicted solubility of carbon dioxide in $[C_2C_1Im][N(C_2F_5SO_2)_2]$ is depicted in Figure 3.4.18a where calculations with the four sets are compared to available experimental data [80]. No specific association interactions between the ILs and the CO_2 are considered in this case, as it corresponds to physical absorption. It can be observed that set A gives excellent agreement with experimental data, while sets B and C, and parameters transferred from $[C_5C_1Im][N(CF_3SO_2)_2]$ give the correct trend, but slightly overestimate the solubility of CO_2 in $[C_2C_1Im][N(C_2F_5SO_2)_2]$. It is important to remark that these calculations are complete predictions from the pure component parameters of the ILs and CO_2. Furthermore, the calculation shown as a green line has been obtained with parameters transferred from other families of ILs. It is also interesting to observe that the set of parameters obtained by including two sets of experimental data (set C) gives the same level of predictions as those obtained fitting only temperature-density data (B). This reinforces the robustness of the soft-SAFT equation, and the procedure presented herein to predict/describe the thermodynamic properties of pure compounds and mixtures, even in the absence of experimental data. Taking advantage of the available experimental data, the density of the binary system $[C_2C_1Im][N(C_2F_5SO_2)_2]$ + methanol was also calculated and the results are presented in Figure 3.4.18b. Soft-SAFT calculations with the four sets show excellent agreement with the experimental data [100], supporting the outstanding predictive power of this tool for binary systems (the red lines and the green line all overlap in agreement with the data).

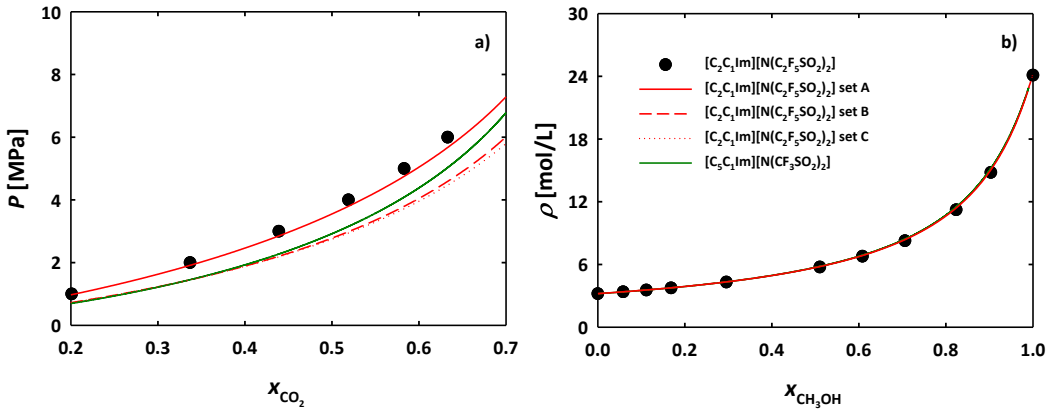

Figure 3.4.18 Predictions of some properties of $[C_2C_1Im][N(C_2F_5SO_2)_2]$. a) Carbon dioxide solubility at 313.15 K; and b) density of IL + methanol binary system at 313.15 K. Lines represent the soft-SAFT predictions, where the red lines are the calculations obtained with optimized sets of parameters (see Table 3.4.6) and the green line is from the set of parameters directly transferred from the indicated IL (approach 2). See text for details. All soft-SAFT calculations overlap in figure b). Symbols are the experimental data [80,100].

The validity of the approach was also assessed with the $[C_4C_1Im][N(C_2F_5SO_2)_2]$ IL. Following approach 2, taking into account the symmetry of the anion branched fluorinated side chain, the direct transfer of the $[C_7C_1Im][N(CF_3SO_2)_2]$ molecular parameters to $[C_4C_1Im][N(C_2F_5SO_2)_2]$ was applied and the density-pressure diagram was calculated. Results are presented in Figure 3.4.16, corresponding to the grey line, in very good agreement with experimental data [101]. As in the case of $[C_2C_1Im][N(C_2F_5SO_2)_2]$, slightly deviations are observed at low temperatures. Optimization of the σ and ε parameters with the density-temperature data was also performed, transferring the other three parameters (see Table 3.4.6). Results with this optimized set are represented in Figure 3.4.16 as a blue line, now in excellent agreement with the data. No further properties were studied due to the absence of experimental data, the accuracy of the model is expected to be similar to the one obtained for the $[C_2C_1Im][N(C_2F_5SO_2)_2]$ systems.

The procedure developed in this work and the predictive power of the equation were also tested for the $[C_4C_1py][CF_3SO_3]$ and compared to available experimental data. This IL have a similar structure to $[C_4C_1Im][CF_3SO_3]$. Therefore, the direct transfer of the molecular parameters from $[C_4C_1Im][CF_3SO_3]$ to $[C_4C_1py][CF_3SO_3]$ was applied and calculations were performed with soft-SAFT in a predictive manner. Results are depicted in Figure 3.4.19a, where the calculated density-temperature diagram is compared with experimental data of $[C_4C_1py][CF_3SO_3]$ [102]. The orange dashed line represents the calculations using parameters directly transferred from $[C_4C_1Im][CF_3SO_3]$, showing a deviation from experimental data but with the right slope. Taking into account the results obtained from the analysis of the cation effect on the molecular parameters, the σ and ε parameters were optimized by fitting to the

density-temperature experimental data (see Table 3.4.6). The results are presented in Figure 3.4.19a as a full solid orange line, in excellent agreement with experimental data.

The surface tension of $[C_4C_1py][CF_3SO_3]$ was also calculated with the optimized set of molecular parameters (see Table 3.4.6). This property requires the fitting of experimental data [104] to the influence parameter, *c*, while the input value from soft-SAFT is the density. As the correct density is obtained only with the optimized set, this was the one used for the surface tension calculations. The optimized *c* value was 1.839×10^{-18} Jm^5mol^{-2} with an AAD of 0.579%. The results show an accurate agreement with experimental data, as illustrated in Figure 3.4.19b. The two sets of parameters were used to predict the density of the $[C_4C_1py][CF_3SO_3]$ + water binary system. Both sets show very good agreement to experimental data [103], without any fitting to binary data (Figure 3.4.19c), showing that the leading interactions in this mixture are the hydrogen bonding formation and the length of the molecules.

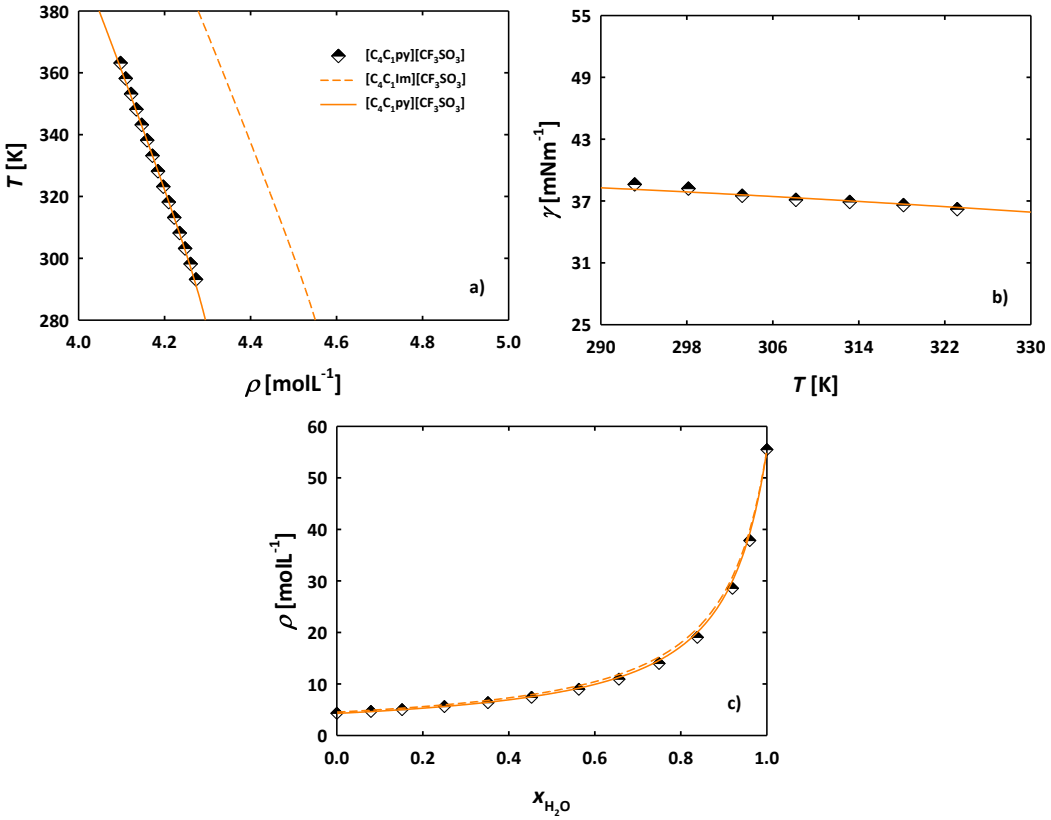

Figure 3.4.19 Thermodynamic properties of the FIL $[C_4C_1py][CF_3SO_3]$: a) temperature-density diagram at atmospheric pressure; b) surface tension of $[C_4C_1py][CF_3SO_3]$ at atmospheric pressure and c) density of the $[C_4C_1py][CF_3SO_3]$ + water binary system at 288.15 K. Lines represent the soft-SAFT predictions, where solid lines are the calculations obtained with the optimized set of parameters and dashed lines are the parameters directly transferred from $[C_4C_1Im][CF_3SO_3]$. Symbols are the experimental data taken from literature [102–104].

3.4.3 Conclusions

We have presented a compilation of all FILs studied with the soft-SAFT EoS, focusing on the influence that the molecular feature of the anions and cations have on selected thermophysical properties, and how this is captured by the model. A procedure to transfer molecular parameters in a systematic and intuitive manner has been developed to model fluorinated ionic liquids within the soft-SAFT framework, searching for a design tool. The FILs families with branched and longer fluorinated chains in the anion preserved the same 3-site association scheme model to mimic the hydrogen bonds of these systems. Hence, three association sites provide enough degrees of freedom to represent the interactions between the anions and cations and the delocalization of the charge due to the presence of oxygen atoms in the anion functional groups and/or the fluorine atoms of the anion side chains. Furthermore, the analysis of the validation process for each model shows that the thermophysical properties should be calculated, not only for the pure systems but also for binary mixtures. Thus, the model accurately reproduces the main interactions with other ILs or other potential solutes. The FILs with short, fluorinated chains were modelled by 3-site and 1-site association schemes, due to FILs with short hydrogenated and fluorinated chains assuming a spherical shape, like the $[BF_4]^-$ and $[PF_6]^-$ anions, and preliminary results show a better performance of the 1-site model in this case.

A throughout analysis of the parameters leads to several conclusions regarding the key attributes of the ionic liquid's structural features as captured by the soft-SAFT coarse grain models. For instance, the comparisons between the chain length m and σ size parameters show that the chain length values can be transferred from pyridinium to imidazolium cations when they are conjugated with the same anion. In the same manner, differences in group size and volume should be carried out using the σ parameter, fitting it to the density-temperature data of the corresponding ILs. Both parameters (m and σ) linearly correlate with the molecular weight for each ILs family, allowing calculations of ILs not included in the fitting procedure. The anion is the structural feature that has a higher influence on the molecular length and group size of the ILs. The m parameter increases linearly with the increase of the number of fluorine atoms and the fluorinated side chain length, while the σ parameter has an inverted trend.

The van der Waals energy parameter of the groups making the chain, ε, has different values depending on the studied FILs. It has been observed that the same value can be used for all members of the same family, making it transferable within the family. The molecular van der Waals energy, represented by the $m\varepsilon$ correlation, shows a linear trend with increasing the cation hydrogenated chain length, and it is highly influenced by the anion fluorination. The highest $m\varepsilon$ values are found for the FILs with nine fluorine atoms.

Finally, regarding the association parameters, it is concluded that only the anion has a direct effect on the associating energy. A linear fluorinated chain has a higher energy of association value than a branched fluorinated chain. Besides, the associating energy increases with the increase of the fluorinated linear chain length. The effect of the anion and the cation features on the association volume is less noticeable. Its value is transferable between different FILs with different anions, except for those with short, fluorinated chains, as the associating volume increases because of the lack of steric effects. In conclusion, the anions and their fluorination are the main structural features that can influence the five soft-SAFT molecular parameters.

The learnings from the analysis relating the molecular features of the FILs to the soft-SAFT molecular parameters were used to model other ILs not included in the approach, in order to check the robustness of the procedure and the transferability power of the FILs models. $[C_2C_1Im][N(C_2F_5SO_2)_2]$, $[C_4C_1Im][N(C_2F_5SO_2)_2]$ and $[C_4C_1py][CF_3SO_3]$ ILs were used for this purpose. The study shows that it is possible to obtain very good agreement with experimental data for the thermophysical properties of these FILs without fitting any parameter, just from the inspection of the molecular features of the ILs to be modelled, transferring the parameters from similar ILs previously parametrized.

Overall, this work proves the robustness of the soft-SAFT equation for modelling FILs with different molecular features and allows for building reliable ILs models with high predictive capabilities in a more intuitive way regarding the process of optimization and parametrization. It also allows the molecular approach to be used as a designing tool where the influence of the different molecular features can be investigated searching for trends in mixtures, such as the solubility of gases or mixture density data. The approach will permit optimization of resources and time spent, between the selections of potential ILs for a new application to the actual implementation. However, an extra effort is still needed to obtain enough reliable data for a handful of ILs and mixtures to further assess the accuracy of the models.

3.5 Understanding the absorption of fluorinated gases in fluorinated ionic liquids for recovering purposes using soft-SAFT

In spite of the highlighted relevance, few works have focused so far on the determination of F-gases absorption by FILs. Sosa et al. have determined the solubility of several HFCs in FILs containing perfluorobutanesulfonate and perfluoropentanoate anions, showing the importance of the fluorine content and nanosegregated domains in the absorption of F-gases [109]. Lepre and co-workers have studied the behaviour of a HFC and different PFCs in the presence of FILs with cationic perfluoroalkyl chains with six carbon atoms, obtaining a positive correlation between the presence of cationic fluorine content and the solubilization of F-gases [110,111]. Castro et al. and Jovell et al. successfully studied the solubilization of HFCs in FILs and deep eutectic solvents (DESs) based on mixtures of FILs and perfluoroalkyl acids [112,113].

The use of models able to predict the absorption of F-gases by FILs is of great importance to accelerate their actual implementation. Different tools can be used for this purpose, such as molecular simulation approaches, correlative methods, and equations of state [31,114–117]. Pereiro and co-workers have contributed to the development of new technologies to alleviate the environmental impact of F-gases with the support of modelling approaches such as the COSMO-based/Aspen Plus methodology and Non-Random Two-Liquid (NRTL) models [109,112]. The soft-SAFT EoS, proposed by Blas and Vega [45,46], extensively used to study the gas solubility in complex systems, including ILs and DES.[31,47,48,50,60,77,113,117–123], has also been used to describe the solubility of selected F-gases in ILs [66–68]. Of particular interest to this contribution is the recent work by Albà *et al*. [121], modelling FILs for selectively separating hydrofluoroolefins (HFOs) from HFCs from the azeotropic blend R513A. Jovell *et al.* [113], have also used soft-SAFT to model the solubility of R134a in FILs and DES based on perfluoroalkyl acid, but much work remains to be done. Building on previous works, in this contribution we apply the soft-SAFT framework to predict the solubility of selected F-gases in FILs, searching for trends between their molecular structure and their final performance.

3.5.1 Methodology

The soft-SAFT EoS [45,46] is a well-known version of the original SAFT EoS [38–40], widely used for the description of complex systems. Literature corroborates soft-SAFT as a great tool to accurately provide the properties and phase behaviour of ILs and their mixtures

with other substances like water, gases, and/or other ILs in good agreement with experimental data, and more details are found in Section 3.2 of this work.

Different thermodynamic parameters were considered and determined in the work, to further extract information on the interactions between the F-gases and the FILs, and hence, their solubility. This includes Henry constants, enthalpy and entropy of dissolution, and the Hildebrand solubility parameter. The Henry constants (*H*c) were determined from the diagram of the pressure versus gas composition at two different temperatures. The values of *H*c were obtained in the range of low gas composition (0.01 to 0.05 $x_{\text{F-gas}}$) corresponding to the infinite dilution of each VLE of FIL + F-gas as described by Equation 3.5.1.

$$H_{\text{C}} = \lim_{x_{\text{F-gas}} \to 0} \left(\frac{P}{x_{\text{F-gas}}} \right) \qquad 3.5.1$$

The enthalpy ($\Delta_{\text{dis}}H$) and entropy ($\Delta_{\text{dis}}S$) of dissolution were also considered in this work to obtain information on the strength of the interactions and the degree of order of the F-gases dissolved in the FILs, respectively.[1] These two thermodynamic parameters were calculated by Equations 3.5.2 and 3.5.3.

$$\Delta_{\text{dis}}H = R \left| \frac{\Delta \ln H_C}{\Delta\, 1/T} \right|_{x_{\text{id}}}^{\infty} \qquad 3.5.2$$

$$\Delta_{\text{dis}}S = -R \left| \frac{\Delta \ln H_C}{\Delta \ln T} \right|_{x_{\text{id}}}^{\infty} \qquad 3.5.3$$

where T is the temperature of the system and x_{id} is the molar composition of the F-gas dissolved in the FIL at infinite dilution.

Finally, the Hildebrand solubility parameter (δ_{H}) was determined for each FIL and each F-gas. This parameter is obtained through the square root of the ratio between the energy of vaporization ($\Delta_{\text{vap}}U$) and the molar volume (v) as represented in Equation 3.5.4.

$$\delta_{\text{H}} = \sqrt{\frac{\Delta_{\text{vap}}U}{v}} = \sqrt{\frac{\Delta_{\text{vap}}H - \text{R}T}{v}} \qquad 3.5.4$$

The $\Delta_{\text{vap}}U$ can be obtained through the enthalpy of vaporization ($\Delta_{\text{vap}}H$) as indicated in Equation 3.5.4. Therefore, the $\Delta_{\text{vap}}H$ was determined in this work by predicting the vapour pressure of the pure systems, as indicated in Equation 3.5.5.

$$\Delta_{\text{vap}}H = -R \left| \frac{\Delta \ln P}{\Delta 1/\text{T}} \right| \qquad 3.5.5$$

3.5.2 Results and discussion

The solubility of different F-gases in FILs has been studied in this work using soft-SAFT in order to extract insights into the relationship between the molecular structure and the solvation performance of these FILs. The selected F-gases are three PFCs (R-14, R-116, and R-218) and three HFCs (R-32, R-125, and R-134a), whose chemical structures, contain from 2 to 8 fluorine atoms, are provided in Table 3.5.1. Besides, five FILs were chosen: two very similar ILs, (1) $[C_2C_1Im][C_4F_9SO_3]$ and (2) $[C_2C_1Im][C_4F_9CO_2]$, just replacing SO_3 in the anion in (1) by CO_2 in the anion of (2); (3) $[C_2C_1py][C_4F_9SO_3]$, containing the same anion as (1) but changing the cation, (4) $[C_2(C_6F_{13})C_1Im][N(CF_3SO_2)_2]$ and (5) $[C_2(C_6F_{13})C_1Im][N(C_2F_5SO_2)_2]$ both with very bulky cations compared to (1)-(3) and in which the only difference between them is the number of fluorine atoms in the anion. Their nomenclature and structures can also be found in Table 3.5.1.

Table 3.5.1 Structure and nomenclatures of the cations and anions composing the ionic liquids, and the fluorinated gases studied in this work.

Cations	Anions
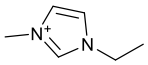 $[C_2C_1Im]^+$ 1-Ethyl-3-methylimidazolium	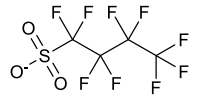 $[C_4F_9SO_3]^-$ Perfluorobutanesulfonate
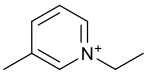 $[C_2C_1py]^+$ 1-Ethyl-3-methylpyridinium	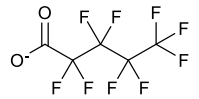 $[C_4F_9CO_2]^-$ Perfluoropentanoate
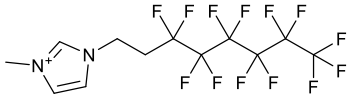 $[C_2(C_6F_{13})C_1Im]^+$ 1-(3,3,4,4,5,5,6,6,7,7,8,8,8-Tridecafluorooctyl)-3-methylimidazolium	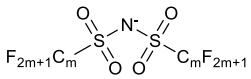 $[N(C_mF_{2m+1}SO_2)_2]^-$, m = 1, 2 Bis(perfluoroalkylsulfonyl)imide
Fluorinated Gases	
 R-32 (CH_2F_2) Difluoromethane	 R-14 (CF_4) Tetrafluoromethane
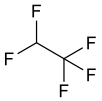 R-125 (C_2HF_5) Pentafluoroethane	 R-116 (C_2F_6) Hexafluoroethane
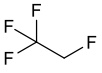 R-134a ($C_2H_2F_4$) 1,1,1,2-Tetrafluoroethane	 R-218 (C_3F_8) Octafluoropropane

3.5.2.1 Soft-SAFT coarse-grained molecular models and parameterization

Soft-SAFT characterizes the fluids by a coarse-grained model that must mimic the principal structural features and interactions of the fluids. As mentioned, non-associating molecules are defined by three molecular parameters (m, σ and ε). For associating fluids, an association scheme must be delineated by selecting the number of association sites, defining the type of association that can occur between those sites, and characterizing them with two parameters, one representing the energy of the association sites (ε^{HB}) and the other one related to the volume of association (κ^{HB}). The models of F-gases considered in this work have been already established within the soft-SAFT framework and are used here in a transferable manner, without any refinement [67,68,118]. PFCs are modelled as non-associating homonuclear chains [66]. In the soft-SAFT approach, HFCs can be modelled as polar fluids (where the dipolar interactions are explicitly taken into account), or as associating fluids, where the dipolar interactions are considered in an implicit manner through the association term [124]. In this work, HFCs were modelled as associating molecules by adding two association sites (one negative and the other positive) to the homonuclear chainlike model, to mimic the dipolar interactions from the fluorine electronegativity. This model was chosen for consistency with previous works, where it was successfully used to describe the thermodynamic properties of HFCs, including the behaviour with other ILs with the soft-SAFT approach. The molecular and association parameters of HFCs recently reparametrized [66,68,113,118] have been used in this work and they are provided in Table 3.5.2 for completeness.

Table 3.5.2 Molecular weight, soft-SAFT molecular parameters of fluorinated ionic liquids and fluorinated gases from literature and optimized in this work, and the respective absolute average deviation (AAD) of the density experimental data [66,68,113,118].

Substance	M_w [g·mol^{-1}]	m	σ [Å]	ε/k_B [K]	ε^{HB}/k_B [K]	κ^{HB} [Å^3]	AAD [%]	REF
Ionic Liquids								
$[C_2C_1Im][C_4F_9CO_2]$	374.21	7.233	3.762	338.8	3850	2250		[60]
$[C_2C_1Im][C_4F_9SO_3]$	410.31	7.320	3.816	343.4	3850	2250		[47]
$[C_2C_1py][C_4F_9SO_3]$	421.28	7.320	3.889	359.4	3850	2250		[60]
$[C_{11}C_1Im][N(CF_3SO_2)_2]$	517.55	6.732	4.595	416.3	3450	2250		[50]
$[C_{14}C_1Im][N(CF_3SO_2)_2]$	559.54	6.967	4.731	422.7	3450	2250		[50]
$[C_2(C_6F_{13})C_1Im][N(CF_3SO_2)_2]$	709.34	6.518	4.595	343.7	3450	2250	0.013	This work
$[C_2(C_6F_{13})C_1Im][N(C_2F_5SO_2)_2]$	809.36	6.690	4.731	339.4	3450	2250	0.007	This work
Fluorinated Gases								
R-32 (CH_2F_2)	52.02	1.321	3.529	144.4	1708	24050		[118]
R-125 (C_2HF_5)	120.02	1.392	4.242	148.8	1685	24050		[118]
R-134a ($C_2H_2F_4$)	102.03	1.392	4.166	166.6	1862	24050		[68]
R-14 (CF_4)	88.00	1.000	4.217	190.1	–	–		[67]
R-116 (C_2F_6)	138.01	1.392	4.342	204.5	–	–		[67]
R-218 (C_3F_8)	188.02	1.776	4.399	214.7	–	–		[67]

In soft-SAFT, ILs are modelled as associating chain molecules, considering the anion and the cation as an ion pair due to the reduced ionic character consequence of specific steric interactions, dispersion forces, and formation of short-lived ion pairs [31,50,60,113,118]. The reader is referred to previous work for more details on modelling FILs within the soft-SAFT framework [76]. The soft-SAFT coarse-grain models of $[C_2C_1Im][C_4F_9SO_3]$, $[C_2C_1Im][C_4F_9CO_2]$ and $[C_2C_1py][C_4F_9SO_3]$ FILs [47,60] already available in the literature were used in this work in a transferable manner. They were modelled with a three-site association scheme: one site named *A* to represent the interactions between the cation and anion and two sites *B* to account for the delocalization of charge due to the fluorinated alkyl chains. Only *AB* interactions are allowed in these models. The molecular and association parameters are in Table 3.5.2.

Conversely, $[C_2(C_6F_{13})C_1Im][N(CF_3SO_2)_2]$ and $[C_2(C_6F_{13})C_1Im][N(C_2F_5SO_2)_2]$ were modelled for the first time in this work. For consistency, the scheme of association for $[C_2(C_6F_{13})C_1Im][N(CF_3SO_2)_2]$ and $[C_2(C_6F_{13})C_1Im][N(C_2F_5SO_2)_2]$ was transferred from the $[C_nC_1Im][N(CF_3SO_2)_2]$ series [66]. Three association sites were included to describe the FIL interactions (one site *A* and two sites *B*) where only *AB* contacts are allowed: *A* site represents the interactions between the cation and the anionic nitrogen atom and the *B* sites are on behalf of the delocalized charge of the anion resulting from the oxygen groups. The approach for obtaining the molecular and association parameters consisted of transferring and optimizing the soft-SAFT parameters through the careful analysis of the FILs structural features [76]. The structures of both $[C_2(C_6F_{13})C_1Im][N(CF_3SO_2)_2]$ and $[C_2(C_6F_{13})C_1Im][N(C_2F_5SO_2)_2]$ FILs were evaluated in order to find a member of the $[C_nC_1Im][N(CF_3SO_2)_2]$ series similar in size and volume. The additional fluorine atoms were considered by choosing and transferring all the parameters of a member of $[C_nC_1Im][N(CF_3SO_2)_2]$ with longer hydrogenated chains, taking into account that one fluorine atom is approximately 1.5 times larger than a hydrogen atom [16]. Therefore, the molecular parameters of $[C_{11}C_1Im][N(CF_3SO_2)_2]$ and $[C_{14}C_1Im][N(CF_3SO_2)_2]$[4] (see Table 3.5.2) were directly transferred to $[C_2(C_6F_{13})C_1Im][N(CF_3SO_2)_2]$ and $[C_2(C_6F_{13})C_1Im][N(C_2F_5SO_2)_2]$, respectively, without any adjustment to experimental data. The densities at atmospheric pressure were calculated with the soft-SAFT parameters of $[C_{11}C_1Im][N(CF_3SO_2)_2]$ and $[C_{14}C_1Im][N(CF_3SO_2)_2]$ and compared with the experimental data [109,111] of $[C_2(C_6F_{13})C_1Im][N(CF_3SO_2)_2]$ and $[C_2(C_6F_{13})C_1Im][N(C_2F_5SO_2)_2]$, respectively, (see Figure 3.5.1, dashed lines) showing good agreement with the available data.

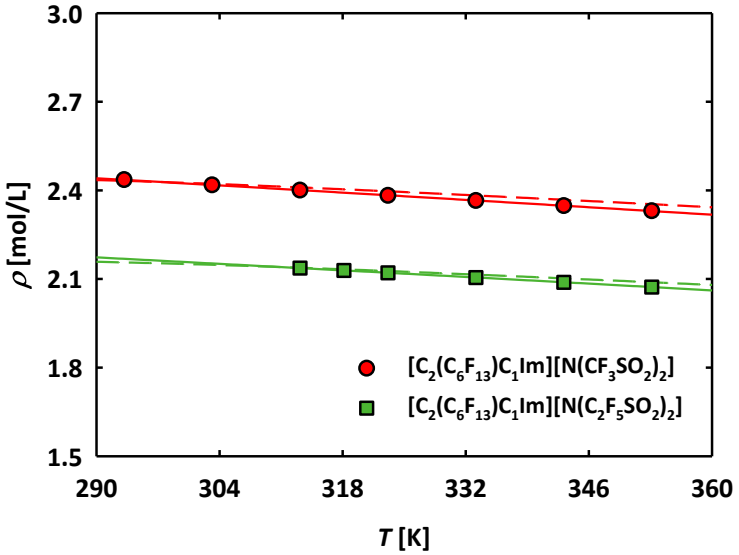

Figure 3.5.1 Density-temperature diagram of the $[C_2(C_6F_{13})C_1Im][N(CF_3SO_2)_2]$ and $[C_2(C_6F_{13})C_1Im][N(C_2F_5SO_2)_2]$ FILs. Experimental data (symbols) taken from the literature [110,111]. The solid lines represent soft-SAFT with optimized parameters obtained by fitting the m and ε molecular parameters, where the dashed lines were obtained by using soft-SAT with transferred parameters from $[C_{11}C_1Im][N(CF_3SO_2)_2]$ and $[C_{14}C_1Im][N(CF_3SO_2)_2]$ [66] systems. See text for details.

With the aim to correct the differences in size/volume and energy between the $[C_2(C_6F_{13})C_1Im][N(CF_3SO_2)_2]$ and $[C_2(C_6F_{13})C_1Im][N(C_2F_5SO_2)_2]$ and the ILs of $[C_nC_1Im][N(CF_3SO_2)_2]$ series (n=11 and 14), the association parameters and the molecular parameter σ were directly transferred from $[C_nC_1Im][N(CF_3SO_2)_2]$ series (n=11 and 14) and fixed at the same value, whereas the parameters m and ε were adjusted to experimental data.[2] These parameters are listed in Table 3.5.2, identified as $[C_2(C_6F_{13})C_1Im][N(CF_3SO_2)_2]$ and $[C_2(C_6F_{13})C_1Im][N(C_2F_5SO_2)_2]$ parameters. The density calculated with this new set of molecular parameters is in slightly better agreement with the experimental data as represented by the solid lines in Figure 3.5.1. The absolute average deviation (AAD) from density data, also provided in Table 3.5.2, is small in all cases.

In summary, molecular models of $[C_2(C_6F_{13})C_1Im][N(CF_3SO_2)_2]$ and $[C_2(C_6F_{13})C_1Im][N(C_2F_5SO_2)_2]$ FILs were proposed using transferable parameters and a holistic approach, by using the methodology previously established [60], providing excellent agreement with available experimental data, further corroborating the robustness of the methodology. Once all soft-SAFT models are defined and parameterized, the next step is to study the solubility of F-gases in FILs, as discussed in the following section.

3.5.2.2 Solubility of fluorinated gases in fluorinated ionic liquids.

The selection of the systems for this study was based on the availability of experimental data from the literature, as well as the different molecular structures, in order to extract information about the influence of the molecular structure on the solubility behaviour.

As already mentioned, Sosa *et al*. [109] studied the solubility of HFCs (R-32, R-125 and R-134a) in $[C_2C_1Im][C_4F_9SO_3]$, $[C_2C_1Im][C_4F_9CO_2]$ and $[C_2C_1py][C_4F_9SO_3]$. Soon after, Jovell et al. [113] used soft-SAFT EoS to assess the solubility of R134a in these three FILs. Lepre and co-workers determined experimentally the absorption of the HFC R-134a and of the perfluoroalkanes R-14, R-116 and R-218 in $[C_2(C_6F_{13})C_1Im][N(CF_3SO_2)_2]$ and $[C_2(C_6F_{13})C_1Im][N(C_2F_5SO_2)_2]$ [110,111].

In this work, we assess the ability of soft-SAFT to predict the solubility of the F-gases in these ILs. Therefore, for studying the solubilities of R-32 and R-125 in $[C_2C_1Im][C_4F_9SO_3]$, $[C_2C_1Im][C_4F_9CO_2]$ and $[C_2C_1py][C_4F_9SO_3]$, for consistency, we have used the same approach previously done for R-134a solubility in these FILs [113]. Given the non-ideality of the mixtures, two binary parameters were needed to accurately reproduce the experimental data. The η parameter (Equation 3.5.2), taking into account the different volumes of the groups, was transferred from the study of the solubility of R-134a in the selected ILs [113] fixed to 1.049, while the ξ energy parameter (Equation 3.5.3) was fitted for each F-gas/ILs pair to have the best representation of the experimental data (see Table 3.5.3). Notice that for $[C_2(C_6F_{13})C_1Im][N(CF_3SO_2)_2]$ and $[C_2(C_6F_{13})C_1Im][N(C_2F_5SO_2)_2]$ only one binary parameter (ξ) was needed for all the studied gases, keeping η equal to one (see Table 3.5.3). For the case of HFCs with FILs, the best results were obtained with values of the binary energy parameter greater than one, except for R-134a. The opposite behaviour was found for perfluoroalkanes, with values of ξ smaller than 1. These results revealed that the interaction of the HFCs, polar fluids, with the FILs, is stronger than those of the pure fluids, whereas, for the perfluoroalkanes, the opposite is found. This behaviour was previous observed when studying the solubility of F-gases and other gases in ILs [60,113,118]. Notice that no specific interactions, other than the Lorentz-Berthelot mixing rules for the LJ monomers (Equations 3.2.2 and 3.2.3) and the calculated average of the cross-association between the HFCs and the FILs (Equations 3.2.4 and 3.2.5), have been considered in the mixtures, which may be too simple for the complex interactions existing between the HFCs and perfluoroalkanes with the FILs.

Table 3.5.3 Binary energy interaction parameter values, ξ and η, for binary mixtures of F-gases with FILs.

FILs	F-gas	ξ	η	REF
$[C_2C_1Im][C_4F_9CO_2]$	R-32 (CH_2F_2)	1.141	1.049	This work
	R-125 (C_2HF_5)	1.234	1.049	This work

	R-134a ($C_2H_2F_4$)	1.146	1.049	[113]
	R-32 (CH_2F_2)	1.141	1.049	This work
$[C_2C_1Im][C_4F_9SO_3]$	R-125 (C_2HF_5)	1.214	1.049	This work
	R-134a ($C_2H_2F_4$)	1.140	1.049	[113]
	R-32 (CH_2F_2)	1.161	1.049	This work
$[C_2C_1py][C_4F_9SO_3]$	R-125 (C_2HF_5)	1.238	1.049	This work
	R-134a ($C_2H_2F_4$)	1.157	1.049	[113]
	R-134a ($C_2H_2F_4$)	1.060	1.000	This work
$[C_2(C_6F_{13})C_1Im][N(CF_3SO_2)_2]$	R-14 (CF_4)	0.850	1.000	This work
	R-116 (C_2F_6)	0.900	1.000	This work
	R-218 (C_3F_8)	0.930	1.000	This work
	R-134a ($C_2H_2F_4$)	1.040	1.000	This work
$[C_2(C_6F_{13})C_1Im][N(C_2F_5SO_2)_2]$	R-14 (CF_4)	0.830	1.000	This work
	R-116 (C_2F_6)	0.890	1.000	This work
	R-218 (C_3F_8)	0.930	1.000	This work

The solubilities of R-32 and R-125 in $[C_2C_1Im][C_4F_9SO_3]$, $[C_2C_1Im][C_4F_9CO_2]$ and $[C_2C_1py][C_4F_9SO_3]$ were calculated at 303.15 K, and results can be found in Figure 3.5.2, compared to those of R-134a absorption in the same FILs from reference,[2] for comparative purposes. As inferred from the figure, soft-SAFT calculations for all HFCs are very accurate compared to experimental data. It also observed that the three FILs have a similar ability to absorb the R-32, R-125, and R-134a in the studied range of pressures, inferring that the leading molecular interactions are similar in all cases. The solubility of R-134a in $[C_2(C_6F_{13})C_1Im][N(CF_3SO_2)_2]$ and in $[C_2(C_6F_{13})C_1Im][N(C_2F_5SO_2)_2]$ FILs, obtained by soft-SAFT and compared to experimental results, is illustrated in Figure 3.5.3. The ξ parameter was adjusted to the intermediate temperature (323.15 K) and used to predict the solubilities at 303.15 and 343.15 K. For both FILs, a good agreement was found for all the studied temperatures, showing the robustness of the soft-SAFT model. As expected, the increment of temperature impairs the solubility of R-134a in both FILs, while when comparing both FILs, the increment of the fluorine content in the anion does not significantly affect the solubility of R-134a, having similar behaviour.

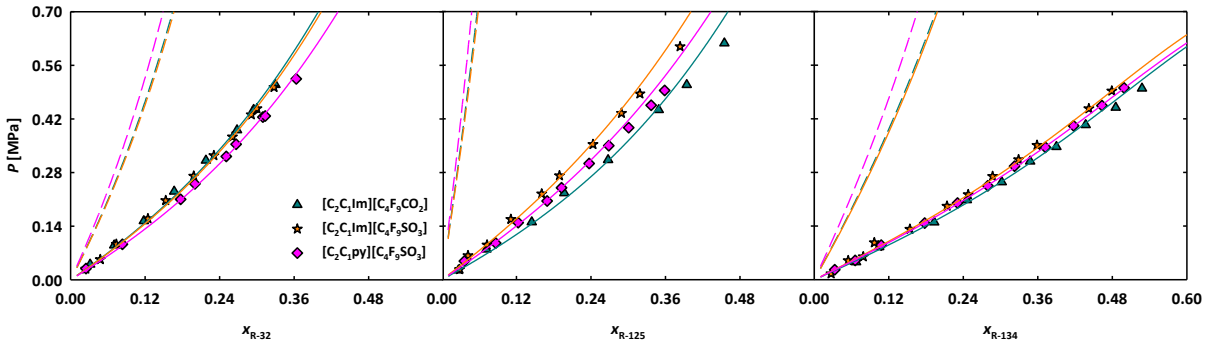

Figure 3.5.2. Solubility of a) R-32, b) R-125 and c) R-134a gases in $[C_2C_1Im][C_4F_9SO_3]$, $[C_2C_1Im][C_4F_9CO_2]$ and $[C_2C_1py][C_4F_9SO_3]$. The symbols represent the experimental data [109] and the lines of the soft-SAFT calculations. The calculations in c) are from literature [113], and are shown here for comparative purposes.

Finally, Figure 3.5.4 shows the absorption of the linear perfluoroalkanes (R-14, R-116, and R-218) in the FILs $[C_2(C_6F_{13})C_1Im][N(CF_3SO_2)_2]$ and $[C_2(C_6F_{13})C_1Im][N(C_2F_5SO_2)_2]$ at 0.07 MPa, with soft-SAFT calculations showing good agreement with experimental data by using a ξ parameter for each F-gas/IL pair (see Table 3.5.3). It is observed that both FILs have the same ability to solubilize the studied gases, increasing in the following order: R-14 < R-116 < R-218. Higher temperatures also decrease the solubilities of these gases, which is more pronounced in the case of R-218.

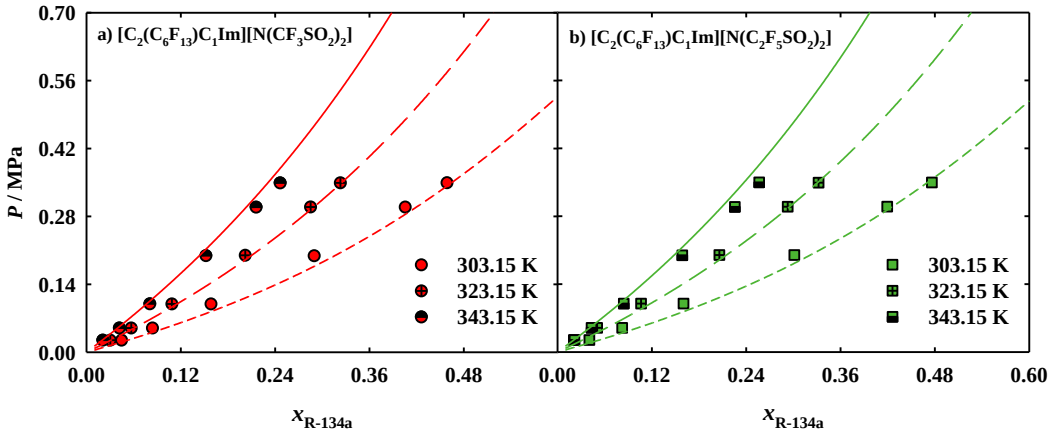

Figure 3.5.3 Solubility of R-134a in $[C_2(C_6F_{13})C_1Im][N(CF_3SO_2)_2]$ and $[C_2(C_6F_{13})C_1Im][N(C_2F_5SO_2)_2]$. Symbols represent the experimental data [111] and lines the soft-SAFT calculations.

3.5.2.3 Influence of the structural features of fluorinated ionic liquids in the absorption of fluorinated gases.

Once the model and parameters of FILs and F-gases are obtained and validated with experimental data, they can be used to predict the properties of these systems at other thermodynamic conditions (e.g., pressure and temperature) in a reliable manner, as they do not depend on the conditions at which they were fitted. In this way, it is possible to obtain relevant information on how the structural features of these complex systems can affect the absorption performance and highlight the best characteristics of FILs that favour the solubility of F-gases. With this aim in mind, the diagrams of solubility of the six F-gases in the five FILs were calculated using soft-SAFT with two different approaches: (i) varying the temperature in the range of 300 to 400 K and at constant atmospheric pressure (see Figure 3.5.5) and (ii) changing the pressure between 0 and 3 MPa, at the constant temperatures of 343.15 and 303.15 K (Figure 3.5.6). Please, notice that the goal of these calculations is not to provide quantitative predictions (as there is no experimental data available for some of these systems to compare to), but to explore the trends for all cases following the same approach; in order to do this, the binary parameters (ξ and η) were set to unity in all cases.

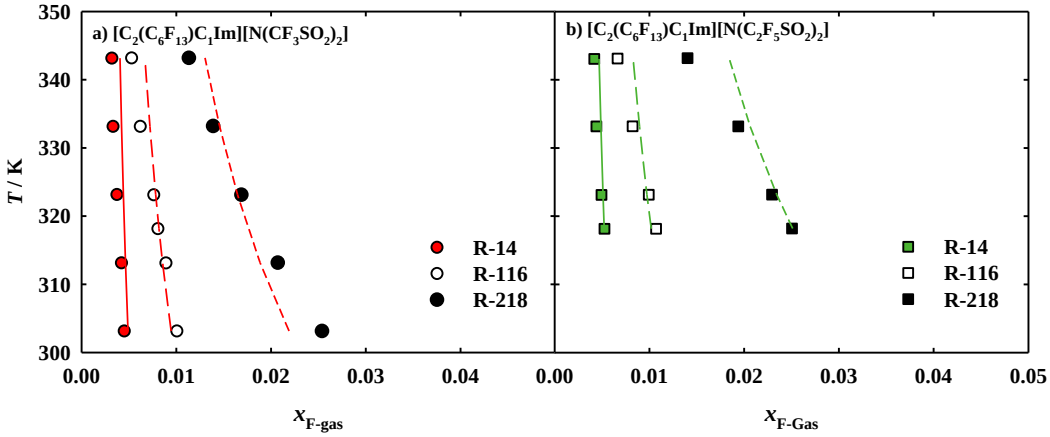

Figure 3.5.4 Solubility of R-14, R-116 and R-128 in $[C_2(C_6F_{13})C_1Im][N(CF_3SO_2)_2]$ and $[C_2(C_6F_{13})C_1Im][N(C_2F_5SO_2)_2]$. The symbols represent the experimental data [110] and the lines are the soft-SAFT calculations from this work.

Results presented in Figure 3.5.5 show that the decrease in temperature favours the absorption of all gases by the FILs, as expected. This behaviour is more pronounced in the systems with $[C_2(C_6F_{13})C_1Im][N(CF_3SO_2)_2]$ and $[C_2(C_6F_{13})C_1Im][N(C_2F_5SO_2)_2]$ FILs. The absorption of the six F-gases in $[C_2C_1Im][C_4F_9SO_3]$, $[C_2C_1Im][C_4F_9CO_2]$ and $[C_2C_1py][C_4F_9SO_3]$ is very similar when comparing to each other. Only a minor decrease in solubility of R-32, R-125, and R-134a is found for $[C_2C_1py][C_4F_9SO_3]$, indicating that the imidazolium cation has better absorption power (see Figures 3.5.5a to 3.5.5c). No significant difference is found when comparing the functional group of $[C_4F_9SO_3]^-$ and $[C_4F_9CO_2]^-$ anions. Some higher values are found for the case of R-32 and R-134a absorption in these three FILs (Figures 3.5.5a and 3.5.5c) when compared to the remaining F-gases. The solubility of the F-gases in the $[C_2C_1Im][C_4F_9SO_3]$, $[C_2C_1Im][C_4F_9CO_2]$ and $[C_2C_1py][C_4F_9SO_3]$ FILs is significantly lower than the values found for $[C_2(C_6F_{13})C_1Im][N(CF_3SO_2)_2]$ and $[C_2(C_6F_{13})C_1Im][N(C_2F_5SO_2)_2]$. This behaviour indicates that the presence of a perfluoroalkyl chain in the imidazolium cation and the bulkier anion favours the absorption of these gases when compared with FILs that have anionic and linear perfluoroalkyl chains. Moreover, in all cases, the $[C_2(C_6F_{13})C_1Im][N(C_2F_5SO_2)_2]$ shows a superior solubility of F-gases than the $[C_2(C_6F_{13})C_1Im][N(CF_3SO_2)_2]$, indicating that the addition of one carbon to the two anionic symmetric fluorinated chains also contributes to the gas-philicity of the FILs. Both $[C_2(C_6F_{13})C_1Im][N(CF_3SO_2)_2]$ and $[C_2(C_6F_{13})C_1Im][N(C_2F_5SO_2)_2]$ have higher level of absorption of gases having more fluorine atoms. This is showed for HFCs, where the gas absorption has the tendency: R-32 < R-125 < R-134a; and for PFCs where R-14 < R-116 < R-218.

Figure 3.5.6 depicts the influence of the pressure, keeping the temperature constant. In this case, the calculations were executed at two different temperatures, which also gives information on the temperature effect. Results show that the increase in temperature decreases

the solubility of F-gases in the FILs, as expected. However, the increase of pressure has the opposite effect, beneficiating the absorption of all gases. When comparing all the systems at the same temperature, very similar conclusions can be extracted. The $[C_2C_1Im][C_4F_9SO_3]$, $[C_2C_1Im][C_4F_9CO_2]$ and $[C_2C_1py][C_4F_9SO_3]$ have a quite similar behaviour for all systems. In the case of R-32, R-125, and R-134a a more pronounced reduction of gas solubility for the $[C_2C_1py][C_4F_9SO_3]$ is found (Figure 3.5.6a to 3.5.6c). The FILs based on bulkier anions and the imidazolium cation with a perfluoroalkyl side chain have a higher intake of absorbed F-gases compared to the ones based on anionic perfluoroalkyl chains. The increment of one carbon atom from $[C_2(C_6F_{13})C_1Im][N(CF_3SO_2)_2]$ to $[C_2(C_6F_{13})C_1Im][N(C_2F_5SO_2)_2]$ increases the absorption of all studied F-gases. As long as the number of fluorine atoms increases in the structure of the F-gases, the absorption in the $[C_2(C_6F_{13})C_1Im][N(CF_3SO_2)_2]$ and $[C_2(C_6F_{13})C_1Im][N(C_2F_5SO_2)_2]$ also increases.

Therefore, from the results obtained in this work, the ideal FIL for solubilizing F-gas should be designed preferably with an imidazolium cation, and the solubility is promoted if it is functionalized with a perfluoroalkyl side chain. The bulkier anions based on the $[N(C_mF_{2m+1}SO_2)_2]^-$ series have better performance to absorb the studied gases. Finally, the amount of fluorine atoms on the gas also increases their absorption by FILs, another characteristic that must be accounted for when choosing the best structural characteristics of FILs to be used in capturing and recovering F-gases from air conditioning, refrigeration and heat equipment systems.

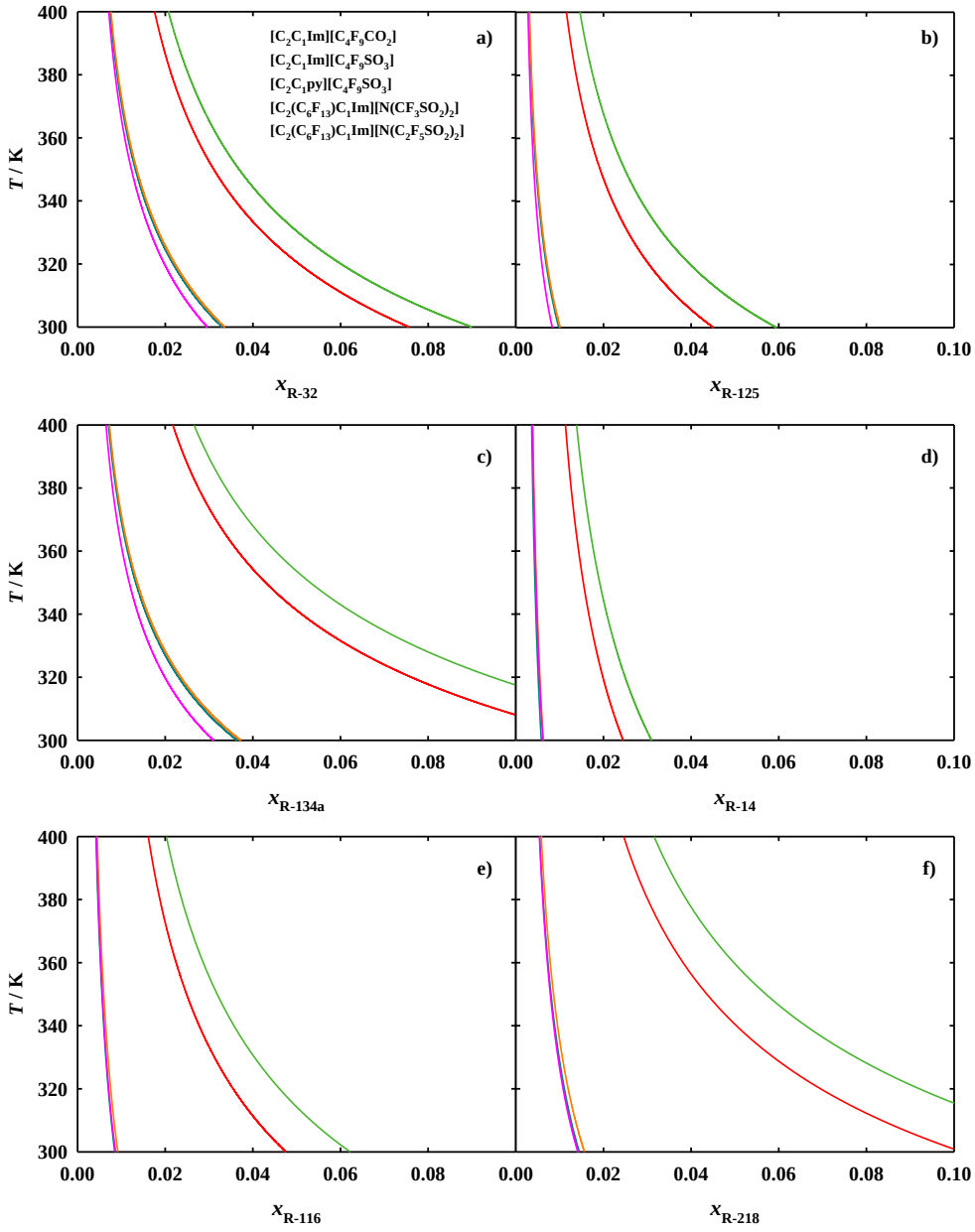

Figure 3.5.5 Effect of the temperature, predicted by soft-SAFT, in the absorption of a) R-32, b) R-125, c) R-134a, d) R-14, e) R-116 and f) R-218 in $[C_2C_1Im][C_4F_9SO_3]$ (cyan), $[C_2C_1Im][C_4F_9CO_2]$ (orange), $[C_2C_1py][C_4F_9SO_3]$ (pink), $[C_2(C_6F_{13})C_1Im][N(CF_3SO_2)_2]$ (red), and $[C_2(C_6F_{13})C_1Im][N(C_2F_5SO_2)_2]$ (green) at atmospheric pressure.

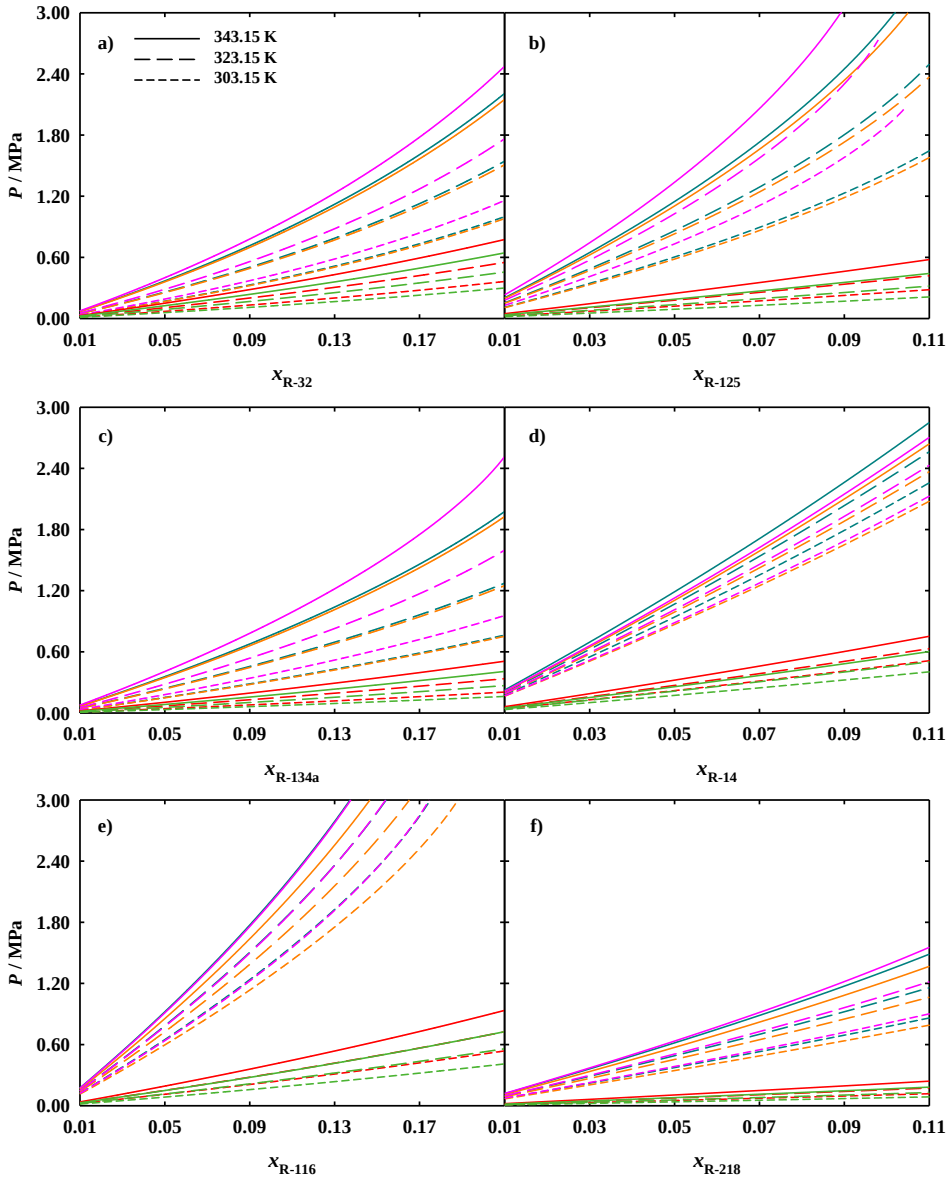

Figure 3.5.6 Effect of the pressure, predicted by soft-SAFT, in the absorption of a) R-32, b) R-125, c) R-134a, d) R-14, e) R-116 and f) R-218 in $[C_2C_1Im][C_4F_9SO_3]$ (cyan), $[C_2C_1Im][C_4F_9CO_2]$ (orange), $[C_2C_1py][C_4F_9SO_3]$ (pink), $[C_2(C_6F_{13})C_1Im][N(CF_3SO_2)_2]$ (red), and $[C_2(C_6F_{13})C_1Im][N(C_2F_5SO_2)_2]$ (green) at two different temperatures (solid lines, 343.15 K, and short dashed lines, 303.15 K).

To further assess the solubility of the F-gases in the FILs, additional thermodynamic properties/parameters were considered and determined in the work, such as Henry constants, enthalpy and entropy of dissolution, and the Hildebrand solubility parameter. Henry's constants were calculated using Equation 3.5.1, which suggests that a smaller value of H_C corresponds to a larger absorption of F-gas by the FIL. The values of Hc for each FIL + F-gas system are provided in Table 3.5.4. Results are consistent with the trends found in the studied solubility diagrams. The H_C values are lower for the lower temperature, indicating higher

solubility of F-gas. In this sense, lower values of *H*c were found to $[C_2(C_6F_{13})C_1Im][N(CF_3SO_2)_2]$ and $[C_2(C_6F_{13})C_1Im][N(C_2F_5SO_2)_2]$ FILs for all F-gases, compared to the higher values obtained to the FILs with linear fluorinated anions and without fluorination in the cation. All FILs show a similar tendency to absorb the studied F-gases, which is: R-14 < R-116 ≈ R-125 < R-218 < R-32 ≈ R134a. Therefore, results indicate that there is not a direct correlation between the fluorine content and the structure of the F-gases with the FILs ability to absorb them, and case by case studies should be performed for each system.

Table 3.5.4 Henry constants (H_C) determine at 303.15 and 343.15 K, and enthalpy ($\Delta_{dis}H$) and entropy ($\Delta_{dis}S$) of dissolution are calculated from the Henry constants for the binary mixtures of F-gases with the FILs.

FILs	**F-gas**	H_C **(MPa)**		$\Delta_{dis}H$	$\Delta_{dis}S$
		343.15 K	303.15 K	[kJ/mol]	[J/mol K]
$[C_2C_1Im][C_4F_9CO_2]$	R-32	7.49	3.46	-16.7	-51.8
	R-125	23.5	12.3	-14.0	-43.4
	R-134a	7.20	3.08	-18.4	-57.0
	R-14	24.1	19.1	-5.0	-15.6
	R-116	18.7	13.1	-7.7	-23.9
	R-218	12.5	7.52	-11.0	-34.1
$[C_2C_1Im][C_4F_9SO_3]$	R-32	7.31	3.39	-16.6	-51.5
	R-125	22.6	11.9	-13.9	-43.0
	R-134a	7.02	3.01	-18.3	-56.8
	R-14	22.4	17.6	-5.2	-16.2
	R-116	17.3	12.1	-7.7	-24.0
	R-218	11.6	6.94	-11.1	-34.5
$[C_2C_1py][C_4F_9SO_3]$	R-32	8.14	3.88	-16.0	-49.7
	R-125	27.5	15.0	-13.1	-40.7
	R-134a	8.25	3.65	-17.6	-54.7
	R-14	22.8	17.9	-5.2	-16.2
	R-116	18.5	12.9	-7.8	-24.2
	R-218	12.8	7.76	-10.8	-33.6
$[C_2(C_6F_{13})C_1Im][N(CF_3SO_2)_2]$	R-32	3.04	1.41	-16.6	-51.5
	R-125	4.98	2.44	-15.4	-47.9
	R-134a	2.12	0.86	-19.5	-60.5
	R-14	6.50	4.43	-8.3	-25.7
	R-116	3.88	2.26	-11.7	-36.3
	R-218	2.12	1.04	-15.4	-47.8
$[C_2(C_6F_{13})C_1Im][N(C_2F_5SO_2)_2]$	R-32	2.54	1.17	-16.8	-52.0
	R-125	3.82	1.83	-15.9	-49.4
	R-134a	1.69	0.67	-20.0	-62.1
	R-14	5.20	3.49	-8.6	-26.8
	R-116	3.01	1.71	-12.2	-37.9
	R-218	1.60	0.77	-15.8	-49.1

The enthalpy ($\Delta_{dis}H$) and entropy ($\Delta_{dis}S$) of dissolution were also considered in this work to obtain information on the strength of the interactions and the degree of order of the

F-gases dissolved in the FILs, respectively [121,125]. These two thermodynamic parameters were calculated by Equations 3.5.2 and 3.5.3 with the values of H_C previously determined at low gas compositions. Values of $\Delta_{dis}H$ and $\Delta_{dis}S$ for each F-gas + FIL system are provided in Table 3.5.4. Results indicate that for $[C_2C_1Im][C_4F_9SO_3]$, $[C_2C_1Im][C_4F_9CO_2]$ and $[C_2C_1py][C_4F_9SO_3]$, the enthalpy and entropy values become more negative, in the order R-14 < R-116 < R-218 < R-125 < R-32 < R134a, whereas for $[C_2(C_6F_{13})C_1Im][N(CF_3SO_2)_2]$ and $[C_2(C_6F_{13})C_1Im][N(C_2F_5SO_2)_2]$ the order is R-14 < R-116 < R-218 ≈ R-125 < R-32 < R134a. A negative enthalpy and a positive entropy favour the dissolution of the F-gas in the FIL. This means that for all cases, R134a has a higher energy of interaction with all the FILs, increasing the absorption of this gas. However, the negative entropy might indicate a condensation of the gas, and this behaviour was also found in the study of F-gases with other ILs [121]. The comparison between FILs shows that $[C_2(C_6F_{13})C_1Im][N(CF_3SO_2)_2]$ and $[C_2(C_6F_{13})C_1Im][N(C_2F_5SO_2)_2]$ have more negative values of enthalpy for almost all gases (except R-32 where similar values were obtained for all FILs) compared to $[C_2C_1Im][C_4F_9SO_3]$, $[C_2C_1Im][C_4F_9CO_2]$ and $[C_2C_1py][C_4F_9SO_3]$, supporting the results previously discussed.

Finally, the solubility parameters of FILs and F-gases calculated from Equation 3.5.4 [126] are provided in Table 3.5.5. It is observed that $[C_2C_1Im][C_4F_9CO_2]$, $[C_2C_1Im][C_4F_9SO_3]$ and $[C_2C_1py][C_4F_9SO_3]$ have very similar values of δ_H, as it happens for $[C_2(C_6F_{13})C_1Im][N(CF_3SO_2)_2]$ and $[C_2(C_6F_{13})C_1Im][N(C_2F_5SO_2)_2]$. Regarding the F-gases, different values are obtained for each of them, with the HFCs showing greater values than the perfluoroalkanes, in general, as a consequence of their polar nature, and hence, higher cohesive energy density.

In principle, a solvent has more ability to solubilize a solute that has a similar value of δ_H. According to the results presented in Table 3.5.5, the $[C_2C_1Im][C_4F_9SO_3]$, $[C_2C_1Im][C_4F_9CO_2]$ and $[C_2C_1py][C_4F_9SO_3]$ FILs have closer values of δ_H than $[C_2(C_6F_{13})C_1Im][N(CF_3SO_2)_2]$ and $[C_2(C_6F_{13})C_1Im][N(C_2F_5SO_2)_2]$ for almost F-gases, except R-14. This should indicate that they have more ability to solubilize these gases. However, as demonstrated by the results discussed earlier in this contribution, the best FILs to solubilize the F-gases are $[C_2(C_6F_{13})C_1Im][N(CF_3SO_2)_2]$ and $[C_2(C_6F_{13})C_1Im][N(C_2F_5SO_2)_2]$. Notice that the Hildebrand parameter is related to the cohesive energy of the pure fluids and it is known to be accurate for non-polar solvents, hence, for the systems investigated in this work, having similar Hildebrand parameters does not necessarily lead to good solubility power, pinpointing on the high complexity of the interactions occurring between the F-gases and FILs, and the polar nature of them.

Table 3.5.5 Hildebrand solubility parameter (δ_H) determined to each FIL and F-gas at 343.15 K.

FIL	δ_H [MPa$^{0.5}$]	F-gas	δ_H [MPa$^{0.5}$]
[C_2C_1Im][$C_4F_9CO_2$]	23.59	R-32	25.85
[C_2C_1Im][$C_4F_9SO_3$]	23.23	R-125	25.63
[C_2C_1py][$C_4F_9SO_3$]	23.30	R-134a	27.88
[$C_2(C_6F_{13})C_1Im$][$N(CF_3SO_2)_2$]	17.51	R-14	18.41
[$C_2(C_6F_{13})C_1Im$][$N(C_2F_5SO_2)_2$]	17.58	R-116	22.31
		R-218	25.00

3.5.3 Conclusions

Soft-SAFT EoS was used in this work to showcase the absorption behaviour of F-gases in FILs. Five different FILs ([C_2C_1Im][$C_4F_9SO_3$], [C_2C_1Im][$C_4F_9CO_2$], [C_2C_1py][$C_4F_9SO_3$], [$C_2(C_6F_{13})C_1Im$][$N(CF_3SO_2)_2$] and [$C_2(C_6F_{13})C1Im$][$N(C_2F_5SO_2)_2$]), three PFCs (R-14, R-116 and R-218) and three HFCs (R-32, R-125 and R-134a) were chosen for this purpose. In order to achieve that goal, [$C_2(C_6F_{13})C_1Im$][$N(CF_3SO_2)_2$] and [$C_2(C_6F_{13})C1Im$][$N(C_2F_5SO_2)_2$] were modelled using soft-SAFT for the first time in this work. The molecular models accurately predict the density of both FILs, evidencing once again the strength of soft-SAFT to modelling FILs in a simple and fast manner.

The solubility of the F-gases in these FILs was successfully captured by soft-SAFT in all cases. The [C_2C_1Im][$C_4F_9SO_3$], [C_2C_1Im][$C_4F_9CO_2$] and [C_2C_1py][$C_4F_9SO_3$] and F-gases have more complex interactions and two binary parameters were needed for a quantitative agreement of the experimental solubility, whereas for [$C_2(C_6F_{13})C_1Im$][$N(CF_3SO_2)_2$] and [$C_2(C_6F_{13})C1Im$][$N(C_2F_5SO_2)_2$], only the energy binary parameter was fitted. Once the parameterization of all systems was concluded, soft-SAFT was used in a systematic manner to extract trends on the influence of the molecular structure of the FILs and F-gases on their absorption behaviour. For this purpose, the solubility of the six F-gases in the five studied FILs was calculated using soft-SAFT exactly at the same thermodynamic conditions. Moreover, the determination of thermodynamic parameters such as Henry constants, enthalpy and entropy of dissolution, and Hildebrand constants were determined with soft-SAFT EoS. As expected, the increment of temperature reduces the absorption of gases, whereas the opposite behaviour is found when increasing the pressure. The FILs with bulkier anions and the perfluoroalkyl side chains in the imidazolium cations showed a higher degree of absorption of all gases, with better results for the F-gases with a higher number of fluorine atoms in their structure. Hence, the interactions between FILs and F-gases fluorinated counterparts play a critical role in the solubility mechanisms as well as the amount of fluorine content in the structure of both systems.

Among the systems studied in this work, $[C_2(C_6F_{13})C1Im][N(C_2F_5SO_2)_2]$ is the most promising FIL for capturing and separating F-gases. However, understanding the solubility is only a first step toward finding the best FILs; other properties of the FILs must be considered to ensure a higher solubility of F-gases. For instance, the addition of carbon atoms in the perfluoroalkyl chains of FILs not only increases the viscosity but also results in more toxic compounds, which can hinder their application in this field. Therefore, a balance must be found between the absorption of F-gases, viscosity, and toxicity obtained when adding a higher number of fluorinated counterparts in the FILs structure, before proceeding to the application of these new systems in the capture and recovery of F-gases. With this in mind, $[C_2(C_6F_{13})C_1Im][N(CF_3SO_2)_2]$ seems an excellent candidate, as it shows a significant absorption performance for all gases while being environmentally friendlier than the other FILs. This work also highlights the need of using robust models as a screening tool to assess different solvents for this application, before embarking on long experimental studies, which can be performed guided by these approaches, hastening the process of moving the FILs from the laboratory to the industrial implementation.

3.6 References

1. Welton, T. Room-Temperature Ionic Liquids. Solvents for Synthesis and Catalysis. *Chem Rev* **1999**, *99*, 2071–2083, doi:10.1021/CR980032T.
2. Earle, M.J.; Seddon, K.R. Ionic Liquids. Green Solvents for the Future. *Pure and Applied Chemistry* **2000**, *72*, 1391–1398, doi:10.1351/pac200072071391.
3. Rogers, R.D.; Seddon, K.R. Ionic Liquids - Solvents of the Future? *Science (1979)* **2003**, *302*, 792–793, doi:10.1126/SCIENCE.1090313.
4. Petkovic, M.; Seddon, K.R.; Rebelo, L.P.N.; Pereira, C.S. Ionic Liquids: A Pathway to Environmental Acceptability. *Chem Soc Rev* **2011**, *40*, 1383–1403, doi:10.1039/C004968A.
5. Plechkova, N. v.; Seddon, K.R. Applications of Ionic Liquids in the Chemical Industry. *Chem Soc Rev* **2008**, *37*, 123–150, doi:10.1039/B006677J.
6. Deetlefs, M.; Fanselow, M.; Seddon, K.R. Ionic Liquids: The View from Mount Improbable. *RSC Adv* **2016**, *6*, 4280–4288, doi:10.1039/C5RA05829E.
7. Castiglione, F.; Moreno, M.; Raos, G.; Famulari, A.; Mele, A.; Appetecchi, G.B.; Passerini, S. Structural Organization and Transport Properties of Novel Pyrrolidinium-Based Ionic Liquids with Perfluoroalkyl Sulfonylimide Anions. *Journal of Physical Chemistry B* **2009**, *113*, 10750–10759, doi:10.1021/JP811434E.
8. Pereiro, A.B.; Araújo, J.M.M.; Martinho, S.; Alves, F.; Nunes, S.; Matias, A.; Duarte, C.M.M.; Rebelo, L.P.N.; Marrucho, I.M. Fluorinated Ionic Liquids: Properties and Applications. *ACS Sustain Chem Eng* **2013**, *1*, 427–439, doi:10.1021/SC300163N.
9. Hollõczki, O.; Macchiagodena, M.; Weber, H.; Thomas, M.; Brehm, M.; Stark, A.; Russina, O.; Triolo, A.; Kirchner, B. Triphilic Ionic-Liquid Mixtures: Fluorinated and Non-Fluorinated Aprotic Ionic-Liquid Mixtures. *ChemPhysChem* **2015**, *16*, 3325–3333, doi:10.1002/CPHC.201500473.

10. Shen, Y.; Kennedy, D.F.; Greaves, T.L.; Weerawardena, A.; Mulder, R.J.; Kirby, N.; Song, G.; Drummond, C.J. Protic Ionic Liquids with Fluorous Anions: Physicochemical Properties and Self-Assembly Nanostructure. *Physical Chemistry Chemical Physics* **2012**, *14*, 7981–7992, doi:10.1039/C2CP40463J.
11. Russina, O.; lo Celso, F.; di Michiel, M.; Passerini, S.; Appetecchi, G.B.; Castiglione, F.; Mele, A.; Caminiti, R.; Triolo, A. Mesoscopic Structural Organization in Triphilic Room Temperature Ionic Liquids. *Faraday Discuss* **2013**, *167*, 499–513, doi:10.1039/C3FD00056G.
12. Vieira, N.S.M.; Reis, P.M.; Shimizu, K.; Cortes, O.A.; Marrucho, I.M.; Araújo, J.M.M.; Esperança, J.M.S.S.; Lopes, J.N.C.; Pereiro, A.B.; Rebelo, L.P.N. A Thermophysical and Structural Characterization of Ionic Liquids with Alkyl and Perfluoroalkyl Side Chains. *RSC Adv* **2015**, *5*, 65337–65350, doi:10.1039/C5RA13869H.
13. Shimizu, K.; Freitas, A.A.; Canongia Lopes, J.N. Structural Characterization of the [CnC1im][C4F9SO3] Ionic Liquid Series: Alkyl versus Perfluoroalkyl Side Chains. *J Mol Liq* **2017**, *226*, 28–34, doi:10.1016/j.molliq.2016.08.014.
14. Pereiro, A.B.; Pastoriza-Gallego, M.J.; Shimizu, K.; Marrucho, I.M.; Lopes, J.N.C.; Piñeiro, M.M.; Rebelo, L.P.N. On the Formation of a Third, Nanostructured Domain in Ionic Liquids. *Journal of Physical Chemistry B* **2013**, *117*, 10826–10833, doi:10.1021/JP402300C.
15. Ferreira, M.L.; Pastoriza-Gallego, M.J.; Araújo, J.M.M.; Canongia Lopes, J.N.; Rebelo, L.P.N.; M Piñeiro, M.; Shimizu, K.; Pereiro, A.B. Influence of Nanosegregation on the Phase Behavior of Fluorinated Ionic Liquids. *Journal of Physical Chemistry C* **2017**, *121*, doi:10.1021/acs.jpcc.7b00516.
16. Pereiro, A.B.; Araújo, J.M.M.; Teixeira, F.S.; Marrucho, I.M.; Piñeiro, M.M.; Rebelo, L.P.N. Aggregation Behavior and Total Miscibility of Fluorinated Ionic Liquids in Water. *Langmuir* **2015**, *31*, 1283–1295, doi:10.1021/LA503961H.
17. Costa Gomes, M.F.; Pádua, A.A.H. Interactions of Carbon Dioxide with Liquid Fluorocarbons. *Journal of Physical Chemistry B* **2003**, *107*, 14020–14024, doi:10.1021/JP0356564.
18. Teixeira, F.S.; Vieira, N.S.M.; Cortes, O.A.; Araújo, J.M.M.; Marrucho, I.M.; Rebelo, L.P.N.; Pereiro, A.B. Phase Equilibria and Surfactant Behavior of Fluorinated Ionic Liquids with Water. *Journal of Chemical Thermodynamics* **2015**, *82*, 99–107, doi:10.1016/j.jct.2014.10.021.
19. Vieira, N.S.M.; Luís, A.; Reis, P.M.; Carvalho, P.J.; Lopes-Da-Silva, J.A.; Esperança, J.M.S.S.; Araújo, J.M.M.; Rebelo, L.P.N.; Freire, M.G.; Pereiro, A.B. Fluorination Effects on the Thermodynamic, Thermophysical and Surface Properties of Ionic Liquids. *Journal of Chemical Thermodynamics* **2016**, *97*, 354–361, doi:10.1016/j.jct.2016.02.013.
20. Luís, A.; Shimizu, K.; Araújo, J.M.M.; Carvalho, P.J.; Lopes-da-Silva, J.A.; Canongia Lopes, J.N.; Rebelo, L.P.N.; Coutinho, J.A.P.; Freire, M.G.; Pereiro, A.B. Influence of Nanosegregation on the Surface Tension of Fluorinated Ionic Liquids. *Langmuir* **2016**, *32*, 6130–6139, doi:10.1021/acs.langmuir.6b00209.
21. Bastos, J.C.; Carvalho, S.F.; Welton, T.; Canongia Lopes, J.N.; Rebelo, L.P.N.; Shimizu, K.; Araújo, J.M.M.; Pereiro, A.B. Design of Task-Specific Fluorinated Ionic Liquids: Nanosegregation versus Hydrogen-Bonding Ability in Aqueous Solutions. *Chemical Communications* **2018**, *54*, 3524–3527, doi:10.1039/C8CC00361K.
22. Teles, A.R.R.; Correia, H.; Maximo, G.J.; Rebelo, L.P.N.; Freire, M.G.; Pereiro, A.B.; Coutinho, J.A.P. Solid-Liquid Equilibria of Binary Mixtures of Fluorinated Ionic Liquids. *Physical Chemistry Chemical Physics* **2016**, *18*, 25741–25750, doi:10.1039/C6CP05372F.
23. *Organofluorine Chemistry*; Banks, R.E., Smart, B.E., Tatlow, J.C., Eds.; Springer US: Boston, MA, 1994; ISBN 978-1-4899-1204-6.

24. Pereiro, A.B.; Tomé, L.C.; Martinho, S.; Rebelo, L.P.N.; Marrucho, I.M. Gas Permeation Properties of Fluorinated Ionic Liquids. *Ind Eng Chem Res* **2013**, *52*, 4994–5001, doi:10.1021/IE4002469.
25. Pereiro, A.B.; Araújo, J.M.M.; Esperança, J.M.S.S.; Marrucho, I.M.; Rebelo, L.P.N. Ionic Liquids in Separations of Azeotropic Systems - A Review. *Journal of Chemical Thermodynamics* **2012**, *46*, 2–28, doi:10.1016/J.JCT.2011.05.026.
26. Martinho, S.; Araújo, J.M.M.; Rebelo, L.P.N.; Pereiro, A.B.; Marrucho, I.M. (Liquid + Liquid) Equilibria of Perfluorocarbons with Fluorinated Ionic Liquids. *Journal of Chemical Thermodynamics* **2013**, *64*, 71–79, doi:10.1016/J.JCT.2013.04.019.
27. Alves, M.; Vieira, N.S.M.; Rebelo, L.P.N.; Araújo, J.M.M.; Pereiro, A.B.; Archer, M. Fluorinated Ionic Liquids for Protein Drug Delivery Systems: Investigating Their Impact on the Structure and Function of Lysozyme. *Int J Pharm* **2017**, *526*, 309–320, doi:10.1016/j.ijpharm.2017.05.002.
28. Dong, L.; Zheng, D.; Sun, G.; Wu, X. Vapor-Liquid Equilibrium Measurements of Difluoromethane + [Emim]OTf, Difluoromethane + [Bmim]OTf, Difluoroethane + [Emim]OTf, and Difluoroethane + [Bmim]OTf Systems. *J Chem Eng Data* **2011**, *56*, 3663–3668, doi:10.1021/JE2005566.
29. Coutinho, J.A.P.; Carvalho, P.J.; Oliveira, N.M.C. Predictive Methods for the Estimation of Thermophysical Properties of Ionic Liquids. *RSC Adv* **2012**, *2*, 7322–7346, doi:10.1039/C2RA20141K.
30. Maginn, E.J. Molecular Simulation of Ionic Liquids: Current Status and Future Opportunities. *Journal of Physics Condensed Matter* **2009**, *21*, doi:10.1088/0953-8984/21/37/373101.
31. Vega, L.F.; Vilasecaa, O.; Llovell, F.; Andreua, J.S. Modeling Ionic Liquids and the Solubility of Gases in Them: Recent Advances and Perspectives. *Fluid Phase Equilib* **2010**, *294*, 15–30, doi:10.1016/J.FLUID.2010.02.006.
32. Gubbins, K.E. Perturbation Theories of the Thermodynamics of Polar and Associating Liquids: A Historical Perspective. *Fluid Phase Equilib* **2016**, *416*, 3–17, doi:10.1016/J.FLUID.2015.12.043.
33. Rey-Castro, C.; Vega, L.F. Transport Properties of the Ionic Liquid 1-Ethyl-3-Methylimidazolium Chloride from Equilibrium Molecular Dynamics Simulation. the Effect of Temperature. *Journal of Physical Chemistry B* **2006**, *110*, 14426–14435, doi:10.1021/JP062885S.
34. Rey-Castro, C.; Tormo, A.L.; Vega, L.F. Effect of the Flexibility and the Anion in the Structural and Transport Properties of Ethyl-Methyl-Imidazolium Ionic Liquids. *Fluid Phase Equilib* **2007**, *256*, 62–69, doi:10.1016/J.FLUID.2006.09.027.
35. Tariq, M.; Carvalho, P.J.; Coutinho, J.A.P.; Marrucho, I.M.; Lopes, J.N.C.; Rebelo, L.P.N. Viscosity of (C2-C14) 1-Alkyl-3-Methylimidazolium Bis(Trifluoromethylsulfonyl)Amide Ionic Liquids in an Extended Temperature Range. *Fluid Phase Equilib* **2011**, *301*, 22–32, doi:10.1016/J.FLUID.2010.10.018.
36. Canongia Lopes, J.N.; Costa Gomes, M.F.; Husson, P.; Pádua, A.A.H.; Rebelo, L.P.N.; Sarraute, S.; Tariq, M. Polarity, Viscosity, and Ionic Conductivity of Liquid Mixtures Containing [C4C1im][NTF2] and a Molecular Component. *Journal of Physical Chemistry B* **2011**, *115*, 6088–6099, doi:10.1021/JP2012254.
37. Shimizu, K.; Almantariotis, D.; Costa Gomes, M.F.; Pádua, A.A.H.; Canongia Lopes, J.N. Molecular Force Field for Ionic Liquids V: Hydroxyethylimidazolium, Dimethoxy-2methylimidazolium, and Fluoroalkylimidazolium Cations and Bis(Fluorosulfonyl)Amide, Perfluoroalkanesulfonylamide, and Fluoroalkylfluorophosphate Anions. *Journal of Physical Chemistry B* **2010**, *114*, 3592–3600, doi:10.1021/JP9120468.
38. Chapman, W.G.; Gubbins, K.E.; Jackson, G.; Radosz, M. SAFT: Equation-of-State Solution Model for Associating Fluids. *Fluid Phase Equilib* **1989**, *52*, 31–38, doi:10.1016/0378-3812(89)80308-5.

39. Chapman, W.G.; Gubbins, K.E.; Jackson, G.; Radosz, M. New Reference Equation of State for Associating Liquids. *Ind Eng Chem Res* **1990**, *29*, 1709–1721, doi:10.1021/IE00104A021.
40. Huang, S.H.; Radosz, M. Equation of State for Small, Large, Polydisperse, and Associating Molecules. *Ind Eng Chem Res* **1990**, *29*, 2284–2294, doi:10.1021/ie00107a014.
41. Wertheim, M.S. Fluids with Highly Directional Attractive Forces. III. Multiple Attraction Sites. *J Stat Phys* **1986**, *42*, 459–476, doi:10.1007/BF01127721.
42. Wertheim, M.S. Fluids with Highly Directional Attractive Forces. IV. Equilibrium Polymerization. *J Stat Phys* **1986**, *42*, 477–492, doi:10.1007/BF01127722.
43. Wertheim, M.S. Fluids with Highly Directional Attractive Forces. II. Thermodynamic Perturbation Theory and Integral Equations. *J Stat Phys* **1984**, *35*, 35–47, doi:10.1007/BF01017363.
44. Wertheim, M.S. Fluids with Highly Directional Attractive Forces. I. Statistical Thermodynamics. *J Stat Phys* **1984**, *35*, 19–34, doi:10.1007/BF01017362.
45. Blas, F.J.; Vega, L.F. Prediction of Binary and Ternary Diagrams Using the Statistical Associating Fluid Theory (SAFT) Equation of State. *Ind Eng Chem Res* **1998**, *37*, 660–674, doi:10.1021/ie970449+.
46. Blas, F.J.; Vega, L.F. Thermodynamic Behaviour of Homonuclear and Heteronuclear Lennard-Jones Chains with Association Sites from Simulation and Theory. *Mol Phys* **1997**, *92*, 135–150, doi:10.1080/002689797170707.
47. Pereiro, A.B.; Llovell, F.; Araújo, J.M.M.; Santos, A.S.S.; Rebelo, L.P.N.; Piñeiro, M.M.; Vega, L.F. Thermophysical Characterization of Ionic Liquids Based on the Perfluorobutanesulfonate Anion: Experimental and Soft-SAFT Modeling Results. *ChemPhysChem* **2017**, *18*, 2012–2023, doi:10.1002/CPHC.201700327.
48. Andreu, J.S.; Vega, L.F. Capturing the Solubility Behavior of CO2 in Ionic Liquids by a Simple Model. *The Journal of Physical Chemistry C* **2007**, *111*, 16028–16034, doi:10.1021/jp074353x.
49. Andreu, J.S.; Vega, L.F. Modeling the Solubility Behavior of CO2, H2, and Xe in [Cn-Mim][Tf2N] Ionic Liquids. *Journal of Physical Chemistry B* **2008**, *112*, 15398–15406, doi:10.1021/JP807484G.
50. Llovell, F.; Valente, E.; Vilaseca, O.; Vega, L.F. Modeling Complex Associating Mixtures with [Cn-Mim][Tf 2N] Ionic Liquids: Predictions from the Soft-SAFT Equation. *Journal of Physical Chemistry B* **2011**, *115*, 4387–4398, doi:10.1021/JP112315B.
51. Oliveira, M.B.; Llovell, F.; Coutinho, J.A.P.; Vega, L.F. Modeling the [NTf2] Pyridinium Ionic Liquids Family and Their Mixtures with the Soft Statistical Associating Fluid Theory Equation of State. *Journal of Physical Chemistry B* **2012**, *116*, 9089–9100, doi:10.1021/JP303166F.
52. Llovell, F.; Vilaseca, O.; Vega, L.F. Thermodynamic Modeling of Imidazolium-Based Ionic Liquids with the [PF 6] - Anion for Separation Purposes. *Sep Sci Technol* **2012**, *47*, 399–410, doi:10.1080/01496395.2011.635625.
53. Oliveira, M.B.; Domínguez-Pérez, M.; Freire, M.G.; Llovell, F.; Cabeza, O.; Lopes-Da-Silva, J.A.; Vega, L.F.; Coutinho, J.A.P. Surface Tension of Binary Mixtures of 1-Alkyl-3-Methylimidazolium Bis(Trifluoromethylsulfonyl)Imide Ionic Liquids: Experimental Measurements and Soft-SAFT Modeling. *Journal of Physical Chemistry B* **2012**, *116*, 12133–12141, doi:10.1021/JP3059905.
54. Llovell, F.; Vega, L.F. Assessing Ionic Liquids Experimental Data Using Molecular Modeling: [Cnmim][BF4] Case Study. *J Chem Eng Data* **2014**, *59*, 3220–3231, doi:10.1021/JE5002472.
55. Pereira, L.M.C.; Oliveira, M.B.; Llovell, F.; Vega, L.F.; Coutinho, J.A.P. Assessing the N2O/CO2 High Pressure Separation Using Ionic Liquids with the Soft-SAFT EoS. *Journal of Supercritical Fluids* **2014**, *92*, 231–241, doi:10.1016/J.SUPFLU.2014.06.005.
56. mac Dowell, N.; Llovell, F.; Sun, N.; Hallett, J.P.; George, A.; Hunt, P.A.; Welton, T.; Simmons, B.A.; Vega, L.F. New Experimental Density Data and Soft-SAFT Models of Alkylimidazolium

([CnC1im]+) Chloride (Cl-), Methylsulfate ([MeSO4]-), and Dimethylphosphate ([Me 2PO4]-) Based Ionic Liquids. *Journal of Physical Chemistry B* **2014**, *118*, 6206–6221, doi:10.1021/JP501619Y.

57. Oliveira, M.B.; Crespo, E.A.; Llovell, F.; Vega, L.F.; Coutinho, J.A.P. Modeling the Vapor–Liquid Equilibria and Water Activity Coefficients of Alternative Refrigerant-Absorbent Ionic Liquid–Water Pairs for Absorption Systems. *Fluid Phase Equilib* **2016**, *426*, 100–109, doi:10.1016/j.fluid.2016.02.017.
58. Vega, L.F.; Llovell, F. Review and New Insights into the Application of Molecular-Based Equations of State to Water and Aqueous Solutions. *Fluid Phase Equilib* **2016**, *416*, 150–173, doi:10.1016/J.FLUID.2016.01.024.
59. Pereira, L.M.C.; Martins, V.; Kurnia, K.A.; Oliveira, M.B.; Dias, A.M.A.; Llovell, F.; Vega, L.F.; Carvalho, P.J.; Coutinho, J.A.P. High Pressure Solubility of CH4, N2O and N2 in 1-Butyl-3-Methylimidazolium Dicyanamide: Solubilities, Selectivities and Soft-SAFT Modeling. *Journal of Supercritical Fluids* **2016**, *110*, 56–64, doi:10.1016/J.SUPFLU.2015.12.006.
60. Ferreira, M.L.; Llovell, F.; Vega, L.F.; Pereiro, A.B.; Araújo, J.M.M. Systematic Study of the Influence of the Molecular Structure of Fluorinated Ionic Liquids on the Solubilization of Atmospheric Gases Using a Soft-SAFT Based Approach. *J Mol Liq* **2019**, *294*, doi:10.1016/j.molliq.2019.111645.
61. Johnson, J.K.; Zollweg, J.A.; Gubbins, K.E. The Lennard-Jones Equation of State Revisited. *Mol Phys* **1993**, *78*, 591–618, doi:10.1080/00268979300100411.
62. Jog, P.K.; Sauer, S.G.; Blaesing, J.; Chapman, W.G. Application of Dipolar Chain Theory to the Phase Behavior of Polar Fluids and Mixtures. *Ind Eng Chem Res* **2001**, *40*, 4641–4648, doi:10.1021/ie010264+.
63. Waals, J.D. van der Thermodynamische Theorie Der Kapillarität Unter Voraussetzung Stetiger Dichteänderung. *Zeitschrift für Physikalische Chemie* **1894**, *13U*, 657–725, doi:10.1515/ZPCH-1894-1338.
64. van der Waals, J.D. The Thermodynamic Theory of Capillarity under the Hypothesis of a Continuous Variation of Density. *J Stat Phys* **1979**, *20*, 200–244, doi:10.1007/BF01011514.
65. Cahn, J.W.; Hilliard, J.E. Free Energy of a Nonuniform System. I. Interfacial Free Energy. *J Chem Phys* **1958**, *28*, 258–267, doi:10.1063/1.1744102.
66. Vilaseca, O.; Llovell, F.; Yustos, J.; Marcos, R.M.; Vega, L.F. Phase Equilibria, Surface Tensions and Heat Capacities of Hydrofluorocarbons and Their Mixtures Including the Critical Region. *J Supercrit Fluids* **2010**, *55*, 755–768, doi:10.1016/j.supflu.2010.10.015.
67. Dias, A.M.A.; Pàmies, J.C.; Coutinho, J.A.P.; Marrucho, I.M.; Vega, L.F. SAFT Modeling of the Solubility of Gases in Perfluoroalkanes. *J Phys Chem B* **2004**, *108*, 1450–1457, doi:10.1021/jp036225o.
68. Albà, C.G.; Vega, L.F.; Llovell, F. A Consistent Thermodynamic Molecular Model of N-Hydrofluoroolefins and Blends for Refrigeration Applications. *International Journal of Refrigeration* **2020**, *113*, 145–155, doi:10.1016/j.ijrefrig.2020.01.008.
69. Urahata, S.M.; Ribeiro, M.C.C. Structure of Ionic Liquids of 1-Alkyl-3-Methylimidazolium Cations: A Systematic Computer Simulation Study. *Journal of Chemical Physics* **2004**, *120*, 1855–1863, doi:10.1063/1.1635356.
70. Morrow, T.I.; Maginn, E.J. Molecular Dynamics Study of the Ionic Liquid 1-n-Butyl-3-Methylimidazolium Hexafluorophosphate. *Journal of Physical Chemistry B* **2002**, *106*, 12807–12813, doi:10.1021/JP0267003.
71. del Pópolo, M.G.; Voth, G.A. On the Structure and Dynamics of Ionic Liquids. *Journal of Physical Chemistry B* **2004**, *108*, 1744–1752, doi:10.1021/JP0364699.

72. Llovell, F.; Vilaseca, O.; Jung, N.; Vega, L.F. Water+1-Alkanol Systems: Modeling the Phase, Interface and Viscosity Properties. *Fluid Phase Equilib* **2013**, *360*, 367–378, doi:10.1016/j.fluid.2013.10.002.
73. Rappé, A.K.; Casewit, C.J.; Colwell, K.S.; Goddard, W.A.; Skiff, W.M. UFF, a Full Periodic Table Force Field for Molecular Mechanics and Molecular Dynamics Simulations. *J Am Chem Soc* **1992**, *114*, 10024–10035, doi:10.1021/JA00051A040.
74. Halgren, T.A. MMFF VII. Characterization of MMFF94, MMFF94s, and Other Widely Available Force Fields for Conformational Energies and for Intermolecular-Interaction Energies and Geometries. *J Comput Chem* **1999**, *20*, 730–748, doi:10.1002/(SICI)1096-987X(199905)20:7<730::AID-JCC8>3.0.CO;2-T.
75. Hanwell, M.D.; Curtis, D.E.; Lonie, D.C.; Vandermeerschd, T.; Zurek, E.; Hutchison, G.R. Avogadro: An Advanced Semantic Chemical Editor, Visualization, and Analysis Platform. *J Cheminform* **2012**, *4*, doi:10.1186/1758-2946-4-17.
76. Ferreira, M.L.; Araújo, J.M.M.; Pereiro, A.B.; Vega, L.F. Insights into the Influence of the Molecular Structures of Fluorinated Ionic Liquids on Their Thermophysical Properties. A Soft-SAFT Based Approach. *Physical Chemistry Chemical Physics* **2019**, *21*, doi:10.1039/c8cp07522k.
77. Pereira, L.M.C.; Oliveira, M.B.; Dias, A.M.A.; Llovell, F.; Vega, L.F.; Carvalho, P.J.; Coutinho, J.A.P. High Pressure Separation of Greenhouse Gases from Air with 1-Ethyl-3-Methylimidazolium Methyl-Phosphonate. *International Journal of Greenhouse Gas Control* **2013**, *19*, 299–309, doi:10.1016/j.ijggc.2013.09.007.
78. Kilaru, P.; Baker, G.A.; Scovazzo, P. Density and Surface Tension Measurements of Imidazolium-, Quaternary Phosphonium-, and Ammonium-Based Room-Temperature Ionic Liquids: Data and Correlations. *J Chem Eng Data* **2007**, *52*, 2306–2314, doi:10.1021/JE7003098.
79. Fang, D.W.; Zhang, F.; Jia, R.; Shan, W. jun; Xia, L. xin; Yang, J. zhen Physicochemical Properties of [Cnmim][TFA] (n = 2, 3, 4, 5, 6) Ionic Liquids. *RSC Adv* **2017**, *7*, 11616–11625, doi:10.1039/C7RA00197E.
80. Watanabe, M.; Kodama, D.; Makino, T.; Kanakubo, M. CO2 Absorption Properties of Imidazolium Based Ionic Liquids Using a Magnetic Suspension Balance. *Fluid Phase Equilib* **2016**, *420*, 44–49, doi:10.1016/J.FLUID.2015.12.055.
81. Zhou, L.; Fan, J.; Shang, X. CO2 Capture and Separation Properties in the Ionic Liquid 1-n-Butyl-3-Methylimidazolium Nonafluorobutylsulfonate. *Materials* **2014**, *7*, 3867–3880, doi:10.3390/MA7053867.
82. Soriano, A.N.; Doma, B.T.; Li, M.H. Carbon Dioxide Solubility in 1-Ethyl-3-Methylimidazolium Trifluoromethanesulfonate. *Journal of Chemical Thermodynamics* **2009**, *41*, 525–529, doi:10.1016/J.JCT.2008.11.001.
83. Shiflett, M.B.; Yokozeki, A. Phase Behavior of Carbon Dioxide in Ionic Liquids: [Emim][Acetate], [Emim][Trifluoroacetate], and [Emim][Acetate] + [Emim][Trifluoroacetate] Mixtures. *J Chem Eng Data* **2009**, *54*, 108–114, doi:10.1021/JE800701J.
84. Weiss, V.C.; Heggen, B.; Müller-Plathe, F. Critical Parameters and Surface Tension of the Room Temperature Ionic Liquid [Bmim][PF6]: A Corresponding-States Analysis of Experimental and New Simulation Data. *Journal of Physical Chemistry C* **2010**, *114*, 3599–3608, doi:10.1021/JP9109282.
85. Marcus, Y.; Hefter, G. Ion Pairing. *Chem Rev* **2006**, *106*, 4585–4621, doi:10.1021/CR040087X.
86. Seoane, R.G.; Corderí, S.; Gómez, E.; Calvar, N.; González, E.J.; MacEdo, E.A.; Domínguez, Á. Temperature Dependence and Structural Influence on the Thermophysical Properties of Eleven Commercial Ionic Liquids. *Ind Eng Chem Res* **2012**, *51*, 2492–2504, doi:10.1021/IE2029255.

87. Oliveira, F.S.; Freire, M.G.; Carvalho, P.J.; Coutinho, J.A.P.; Lopes, J.N.C.; Rebelo, L.P.N.; Marrucho, I.M. Structural and Positional Isomerism Influence in the Physical Properties of Pyridinium NTf2-Based Ionic Liquids: Pure and Water-Saturated Mixtures. *J Chem Eng Data* **2010**, *55*, 4514–4520, doi:10.1021/JE100377K.
88. Deng, Y.; Husson, P.; Delort, A.M.; Besse-Hoggan, P.; Sancelme, M.; Costa Gomes, M.F. Influence of an Oxygen Functionalization on the Physicochemical Properties of Ionic Liquids: Density, Viscosity, and Carbon Dioxide Solubility as a Function of Temperature. *J Chem Eng Data* **2011**, *56*, 4194–4202, doi:10.1021/JE2006743.
89. Ohlin, C.A.; Dyson, P.J.; Laurenczy, G. Carbon Monoxide Solubility in Ionic Liquids: Determination, Prediction and Relevance to HydroformylationElectronic Supplementary Information (ESI) Available: Further Experimental Details. See Http://Www.Rsc.Org/Suppdata/Cc/B4/B401537a/. *Chemical Communications* **2004**, 1070, doi:10.1039/b401537a.
90. Kato, R.; Gmehling, J. Activity Coefficients at Infinite Dilution of Various Solutes in the Ionic Liquids MMIM Methylsulfate, MMIM Methoxyethylsulfate, MMIM Dimethylphosphate, N Ethylpyridinium Bis(Trifluoromethylsulfonyl) Imide and Pyridiniumethoxyethylsulfate (MMIM = 1 Methyl 3 Methylimidazolium). *Fluid Phase Equilib* **2004**, *226*, 37–44, doi:10.1016/J.FLUID.2004.08.039.
91. Liu, Q.S.; Yang, M.; Li, P.P.; Sun, S.S.; Welz-Biermann, U.; Tan, Z.C.; Zhang, Q.G. Physicochemical Properties of Ionic Liquids [C3py][NTf 2] and [C6py][NTf2]. *J Chem Eng Data* **2011**, *56*, 4094–4101, doi:10.1021/JE200534B.
92. Yunus, N.M.; Abdul Mutalib, M.I.; Man, Z.; Bustam, M.A.; Murugesan, T. Thermophysical Properties of 1-Alkylpyridinum Bis(Trifluoromethylsulfonyl)Imide Ionic Liquids. *Journal of Chemical Thermodynamics* **2010**, *42*, 491–495, doi:10.1016/J.JCT.2009.11.004.
93. Liu, Q.S.; Yang, M.; Yan, P.F.; Liu, X.M.; Tan, Z.C.; Welz-Biermann, U. Density and Surface Tension of Ionic Liquids [Cnpy][NTF2] (n = 2, 4, 5). *J Chem Eng Data* **2010**, *55*, 4928–4930, doi:10.1021/JE100507N.
94. Shiflett, M.B.; Yokozeki, A. Binary Vapor-Liquid and Vapor-Liquid-Liquid Equilibria of Hydrofluorocarbons (HFC-125 and HFC-143a) and Hydrofluoroethers (HFE-125 and HFE-143a) with Ionic Liquid [Emim][Tf2N]. *J Chem Eng Data* **2008**, *53*, 492–497, doi:10.1021/JE700588D.
95. Shin, E.K.; Lee, B.C. High-Pressure Phase Behavior of Carbon Dioxide with Ionic Liquids: 1-Alkyl-3-Methylimidazolium Trifluoromethanesulfonate. *J Chem Eng Data* **2008**, *53*, 2728–2734, doi:10.1021/JE8000443.
96. Vega, L.F.; Llovell, F.; Blas, F.J. Capturing the Solubility Minima of N-Alkanes in Water by Soft-SAFT. *Journal of Physical Chemistry B* **2009**, *113*, 7621–7630, doi:10.1021/JP9018876.
97. Krummen, M.; Wasserscheid, P.; Gmehling, J. Measurement of Activity Coefficients at Infinite Dilution in Ionic Liquids Using the Dilutor Technique. *J Chem Eng Data* **2002**, *47*, 1411–1417, doi:10.1021/JE0200517.
98. Tariq, M.; Serro, A.P.; Mata, J.L.; Saramago, B.; Esperança, J.M.S.S.; Lopes, J.N.C.; Rebelo, L.P.N. High-Temperature Surface Tension and Density Measurements of 1-Alkyl-3-Methylimidazolium Bistriflamide Ionic Liquids. *Fluid Phase Equilib* **2010**, *294*, 131–138, doi:10.1016/J.FLUID.2010.02.020.
99. Llovell, F.; Vega, L.F. Prediction of Thermodynamic Derivative Properties of Pure Fluids through the Soft-SAFT Equation of State. *Journal of Physical Chemistry B* **2006**, *110*, 11427–11437, doi:10.1021/JP0608022.
100. Deenadayalu, N.; Bhujrajh, P. Density, Speed of Sound, and Derived Thermodynamic Properties of Ionic Liquids [EMIM]+[BETI]- or ([EMIM]+[CH 3(OCH2CH2)2OSO3] - + Methanol or +

Acetone) at T = (298.15 or 303.15 or 313.15) K. *J Chem Eng Data* **2008**, *53*, 1098–1102, doi:10.1021/JE700648C.

101. Nazet, A.; Sokolov, S.; Sonnleitner, T.; Makino, T.; Kanakubo, M.; Buchner, R. Densities, Viscosities, and Conductivities of the Imidazolium Ionic Liquids [Emim][Ac], [Emim][FAP], [Bmim][BETI], [Bmim][FSI], [Hmim][TFSI], and [Omim][TFSI]. *J Chem Eng Data* **2015**, *60*, 2400–2411, doi:10.1021/ACS.JCED.5B00285.
102. Okuniewski, M.; Paduszyński, K.; Domańska, U. Effect of Cation Structure in Trifluoromethanesulfonate-Based Ionic Liquids: Density, Viscosity, and Aqueous Biphasic Systems Involving Carbohydrates as "Salting-Out" Agents. *J Chem Eng Data* **2016**, *61*, 1296–1304, doi:10.1021/ACS.JCED.5B00931.
103. González, E.J.; Domínguez, Á.; Macedo, E.A. Physical and Excess Properties of Eight Binary Mixtures Containing Water and Ionic Liquids. *J Chem Eng Data* **2012**, *57*, 2165–2176, doi:10.1021/je201334p.
104. Bittner, B.; Wrobel, R.J.; Milchert, E. Physical Properties of Pyridinium Ionic Liquids. *Journal of Chemical Thermodynamics* **2012**, *55*, 159–165, doi:10.1016/J.JCT.2012.06.018.
105. Pàmies, J.P. Bulk and Interfacial Properties of Chain Fluids: A Molecular Modelling Approach., Universitat Rovira i Virgili: Tarragona, Spain, 2004.
106. Oliveira, M.B.; Llovell, F.; Coutinho, J.A.P.; Vega, L.F. New Procedure for Enhancing the Transferability of Statistical Associating Fluid Theory (SAFT) Molecular Parameters: The Role of Derivative Properties. *Ind Eng Chem Res* **2016**, *55*, 10011–10024, doi:10.1021/ACS.IECR.6B02205.
107. Gardas, R.L.; Freire, M.G.; Carvalho, P.J.; Marrucho, I.M.; Fonseca, I.M.A.; Ferreira, A.G.M.; Coutinho, J.A.P. PρT Measurements of Imidazolium-Based Ionic Liquids. *J Chem Eng Data* **2007**, *52*, 1881–1888, doi:10.1021/JE700205N.
108. Dymond, J.H.; Malhotra, R. The Tait Equation: 100 Years On. *Int J Thermophys* **1988**, *9*, 941–951, doi:10.1007/BF01133262.
109. Sosa, J.E.; Ribeiro, R.P.P.L.; Castro, P.J.; Mota, J.P.B.; Araújo, J.M.M.; Pereiro, A.B. Absorption of Fluorinated Greenhouse Gases Using Fluorinated Ionic Liquids. *Ind Eng Chem Res* **2019**, *58*, 20769–20778, doi:10.1021/ACS.IECR.9B04648.
110. Lepre, L.F.; Andre, D.; Denis-Quanquin, S.; Gautier, A.; Pádua, A.A.H.; Costa Gomes, M. Ionic Liquids Can Enable the Recycling of Fluorinated Greenhouse Gases. *ACS Sustain Chem Eng* **2019**, *7*, 16900–16906, doi:10.1021/acssuschemeng.9b04214.
111. Lepre, L.F.; Pison, L.; Otero, I.; Gautier, A.; Dévemy, J.; Husson, P.; Pádua, A.A.H.; Costa Gomes, M. Using Hydrogenated and Perfluorinated Gases to Probe the Interactions and Structure of Fluorinated Ionic Liquids. *Physical Chemistry Chemical Physics* **2019**, *21*, 8865–8873, doi:10.1039/C9CP00593E.
112. Castro, P.J.; Redondo, A.E.; Sosa, J.E.; Zakrzewska, M.E.; Nunes, A.V.M.; Araújo, J.M.M.; Pereiro, A.B. Absorption of Fluorinated Greenhouse Gases in Deep Eutectic Solvents. *Ind Eng Chem Res* **2020**, *59*, 13246–13259, doi:10.1021/acs.iecr.0c01893.
113. Jovell, D.; B. Gómez, S.; Zakrzewska, M.E.; Nunes, A.V.M.; Araújo, J.M.M.; Pereiro, A.B.; Llovell, F. Insight on the Solubility of R134a in Fluorinated Ionic Liquids and Deep Eutectic Solvents. *J Chem Eng Data* **2020**, *65*, 4956–4969, doi:10.1021/acs.jced.0c00588.
114. Lei, Z.; Dai, C.; Chen, B. Gas Solubility in Ionic Liquids. *Chem Rev* **2014**, *114*, 1289–1326, doi:10.1021/cr300497a.
115. Mellein, B.R.; Scurto, A.M.; Shiflett, M.B. Gas Solubility in Ionic Liquids. *Curr Opin Green Sustain Chem* **2021**, *28*, 100425, doi:10.1016/j.cogsc.2020.100425.
116. Shiflett, M.B.; Maginn, E.J. The Solubility of Gases in Ionic Liquids. *AIChE Journal* **2017**, *63*, 4722–4737, doi:10.1002/AIC.15957.

117. Alkhatib, I.I.I.; Bahamon, D.; Llovell, F.; Abu-Zahra, M.R.M.; Vega, L.F. Perspectives and Guidelines on Thermodynamic Modelling of Deep Eutectic Solvents. *J Mol Liq* **2020**, *298*, 112183, doi:10.1016/j.molliq.2019.112183.
118. Asensio-Delgado, S.; Jovell, D.; Zarca, G.; Urtiaga, A.; Llovell, F. Thermodynamic and Process Modeling of the Recovery of R410A Compounds with Ionic Liquids. *International Journal of Refrigeration* **2020**, *118*, 365–375, doi:10.1016/j.ijrefrig.2020.04.013.
119. Llovell, F.; Oliveira, M.B.; Coutinho, J.A.P.; Vega, L.F. Solubility of Greenhouse and Acid Gases on the [C4mim][MeSO4] Ionic Liquid for Gas Separation and CO2 Conversion. *Catal Today* **2015**, *255*, 87–96, doi:10.1016/j.cattod.2014.12.049.
120. Alonso, G.; Gamallo, P.; Sayós, R.; Llovell, F. Combining Soft-SAFT and COSMO-RS Modeling Tools to Assess the CO2–SO2 Separation Using Phosphonium-Based Ionic Liquids. *J Mol Liq* **2020**, *297*, 111795, doi:10.1016/j.molliq.2019.111795.
121. Albà, C.G.; Vega, L.F.; Llovell, F. Assessment on Separating Hydrofluoroolefins from Hydrofluorocarbons at the Azeotropic Mixture R513A by Using Fluorinated Ionic Liquids: A Soft-SAFT Study. *Ind Eng Chem Res* **2020**, *59*, 13315–13324, doi:10.1021/acs.iecr.0c02331.
122. Ojeda, R.M.; Llovell, F. Soft-SAFT Transferable Molecular Models for the Description of Gas Solubility in Eutectic Ammonium Salt-Based Solvents. *J Chem Eng Data* **2018**, *63*, 2599–2612, doi:10.1021/acs.jced.7b01103.
123. Lloret, J.O.; Vega, L.F.; Llovell, F. Accurate Description of Thermophysical Properties of Tetraalkylammonium Chloride Deep Eutectic Solvents with the Soft-SAFT Equation of State. *Fluid Phase Equilib* **2017**, *448*, 81–93, doi:10.1016/j.fluid.2017.04.013.
124. Vega, L.F.; Bahamon, D.; Alkhatib, I.I.I.; Fouad, W.A.; Llovell, F.; Pereira, L.M.C.; Vilaseca, O. How Molecular Modelling Tools Can Help in Mitigating Climate Change. In; 2021; pp. 181–220.
125. Cadena, C.; Anthony, J.L.; Shah, J.K.; Morrow, T.I.; Brennecke, J.F.; Maginn, E.J. Why Is CO2 So Soluble in Imidazolium-Based Ionic Liquids? *J Am Chem Soc* **2004**, *126*, 5300–5308, doi:10.1021/ja039615x.
126. Marciniak, A. The Hildebrand Solubility Parameters of Ionic Liquids—Part 2. *Int J Mol Sci* **2011**, *12*, 3553–3575, doi:10.3390/ijms12063553.

CHAPTER 4

SELF-AGGREGATION BEHAVIOUR OF FLUORINATED IONIC LIQUIDS AQUEOUS SOLUTIONS

4.1 Introduction

The challenge of producing sustainable and green compounds has been one of the greatest efforts of academia and industries, prompting the development of "greener" ionic liquids (ILs). The major attribute of these compounds is the possibility to fine-tune their physicochemical properties by combining different cations and anions or functionalizing their structures, allowing the design of tailor-made ILs for specific applications [1,2].

The growing interest in task-specific ILs has empowered their functionalization through the introduction of functional groups in their structures, such as polar oxygenated features as hydroxyl, ester or ether groups [3]. The addition of polar groups can drastically reduce their cytotoxicity and ecotoxicity, as well as enhance their biodegradability, increasing their sustainability [4–7]. Several works showed that the introduction of a hydroxyl group in the cationic alkyl chain of imidazolium-based ILs decreases the thermal stability and self-aggregation behaviour while increasing the viscosity, density, polarity and hydrophilicity [8–10].

The application of FILs in biomedical and biological applications is completely dependent on their behaviour in aqueous solutions. FILs have improved surfactant behaviour which allows them to behave as SAILs in aqueous solutions due to their amphiphilic nature. The self-aggregation behaviour of FILs can be a great advantage for their use in the protein field, for stabilization, extraction, and delivery of proteins. However, the properties of the structural features of the SAILs that confers the ability to self-assemble are usually associated with toxicity and biodegradability issues. One of the methods that have been used to solve those problems is the insertion of cleavable groups into the hydrogenated chains, to improve the biocompatibility and biodegradability of these compounds.

In this chapter, new imidazolium-based FILs were synthesized with a hydroxyl group at the end of the cationic hydrogenated side chain and characterized through experimental and modelling methods. The main goal was to have insights into the influence of the hydroxyl group on the thermophysical and thermodynamic properties of FILs and their behaviour in aqueous solutions, aiming to have more biodegradable and biocompatible FILs. All the results were compared with the properties of the analogous non-functionalized FILs. The results obtained in this chapter demonstrated that the addition of a hydroxyl group can hinder some of the properties of FILs, for instance, decreasing their self-aggregation behaviour in water, through the raise of the critical aggregation concentrations. However, the comparison of the critical aggregation concentrations of FILs functionalized with the hydroxyl group and the traditional and toxic hydrogenated and fluorinated surfactants has shown that FILs have a significantly improved self-aggregation behaviour and are completely miscible in water. This

will allow the designing and developing of formulations based on FILs, using lower concentrations, and improving biocompatibility, making them promising tools for biological applications.

This chapter is based on the following work:

Margarida L. Ferreira, João M.M. Araújo, Lourdes F. Vega, Fèlix Llovell, Ana B. Pereiro, Functionalization of fluorinated ionic liquids: A combined experimental-theoretical study, *Journal of Molecular Liquids* 302 (2020) 112489. DOI: 10.1016/j.molliq.2020.112489

4.2 Functionalization of fluorinated ionic liquids: a combined experimental-theoretical study

In this work, two imidazolium-based FILs functionalized with a hydroxyl group in the tail of the cationic hydrogenated side chain (named as OH-FILs), conjugated with perfluorobutanesulfonate and perfluoropentanoate anions, were synthesized and characterized. (Table 4.2.1 shows structure and nomenclature). Melting and decomposition temperatures, density, viscosity, refractive index and conductivity were determined for OH-FILs. Moreover, the self-aggregation behaviour, density, viscosity and ionic conductivity profile of OH-FILs in aqueous systems were analyzed. Previous work shows that these OH-FILs have lower acute ecotoxicity than non-functionalized imidazolium and pyridinium-based FILs [4]. Results are discussed in terms of how the hydroxyl group can influence the pure and aqueous mixtures of FILs properties by comparing with the analogous FILs without the hydroxyl group (see Table 4.2.1). Finally, the soft-SAFT EoS was used to build new molecular models for OH-FILs, describing the density and viscosity of the pure and binary systems with a limited amount of experimental information. This theoretical approach allows us to better understand the microscopic behaviour of OH-FILs, predicting the properties under different conditions and corroborating the experimental observations.

Table 4.2.1 Chemical structure and acronyms of the fluorinated ionic liquids cations and anions studied in this work.

Cations structure	Anions structure
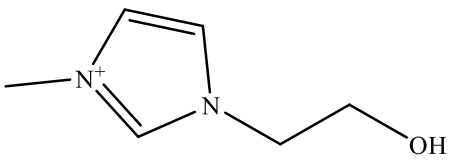 1-(2-hydroxyethyl)-3-methylimidazolium **$[C_{2(OH)}C_1Im]^+$**	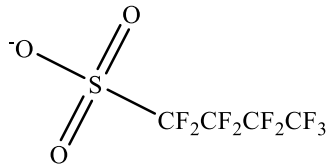 Perfluorobutanesulfonate **$[C_4F_9SO_3]^-$**
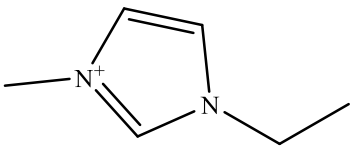 1-ethyl-3-methylimidazolium **$[C_2C_1Im]^+$**	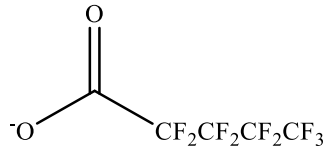 Perfluoropentanoate **$[C_4F_9CO_2]^-$**

4.2.1 Experimental section

4.2.1.1 Materials

1-(2-Hydroxyethyl)-3-methylimidazolium perfluorobutanesulfonate, $[C_{2(OH)}C_1Im][C_4F_9SO_3]$, 98% mass fraction purity, 1-(2-hydroxyethyl)-3-methylimidazolium

perfluoropentanoate, $[C_{2(OH)}C_1Im][C_4F_9CO_2]$, 98% mass fraction purity and 1-ethyl-3-methylimidazolium perfluoropentanoate, $[C_2C_1Im][C_4F_9CO_2]$, 98% mass fraction purity, were synthesized by ion exchange resin method, as developed by Ohno et al. [11] and previously implemented in our lab for these compounds [4,12,13]. The synthesized fluorinated ionic liquids were characterized by ^1H and ^{19}F NMR spectroscopy as well as elemental analysis to check their purity [4,12,13]. Each IL was dried for at least 48 hours immediately prior to its use at 323.15 K under vacuum (4 Pa) and vigorously stirred to ensure the absence of water and volatile substances. The water content of the ILs was less than 100 ppm and was determined by Karl Fisher coulometric titration method (Metrohm 831 KF Coulometer).

4.2.1.2 Methods and Procedures

A differential scanning calorimeter (DSC) from TA Instruments, model Q200, was used to measure the phase transitions of the OH-FILs. The cooling was accomplished by a refrigerator system capable to reach a minimum temperature of 183.15 K. The sample was continuously purged using 50 $mLmin^{-1}$ of dry dinitrogen gas. About 15 mg of each FIL was sealed in an aluminium standard sample pan. Indium, with a melting point of 429.76 K, was used as a standard for the DSC calibration. Samples were all cooled down to 183.15 K and tempered for 30 min. Afterwards, they were heated to different temperatures, leaving a range of 20 K between the last transition and the end of the cycle. The cooling–heating cycles were repeated three times at different scan rates (10 $Kmin^{-1}$, 5 $Kmin^{-1}$ and 1 $Kmin^{-1}$). This scan rate selection guarantees the best delineation and characterization of the several solid-fluid phase transitions of each ionic liquid. The uncertainty of the apparatus was estimated at ± 2 K. Universal Analysis 2000 v.4.5A software (TA Instruments) was used to integrate the calorimetric peaks and determine the solid-solid transition ($T_{s\text{-}s}$) and melting temperatures (T_m).

A thermogravimetric analysis equipment (LABSYS evo TGA from SETARAM) was used to measure the weight loss as a function of the temperature of the OH-FILs. These experiments provide useful information concerning the decomposition temperature of the pure FILs, which is crucial to their application range. The samples were continuously purged using 50 $mLmin^{-1}$ of dry dinitrogen gas. About 20 to 60 mg of FIL was inserted in an aluminium standard sample pan. Samples were heated up to 873.15 K at a scan rate of 1 $Kmin^{-1}$ until complete thermal degradation. The uncertainty of the temperature was ± 1 K. Regarding TGA analysis, the CALISTO PROCESSING software was used to determine the onset (T_{onset}) and start (T_{start}) temperatures (corresponding to the temperatures where the baseline slope changed during heating and the weight loss was less than 1%, respectively).

Density and dynamic viscosity measurements were performed using an automated SVM 3000 Anton Paar rotational Stabinger viscometer-densimeter. The apparatus operated at atmospheric pressure in a range of temperatures from 283.25 to 353.15 K for the pure OH-FILs and from 298.15 to 318.15K for the FILs + water systems. This equipment uses Peltier elements ensuring fast and efficient temperature control with an uncertainty of ± 0.02 K. The uncertainty of the density is better than 2×10^{-4} gcm^{-3}. Regarding the dynamic viscosity, duplicates were performed and the maximum relative standard deviation was observed to be below 1%. The uncertainty of the overall viscosity measurement procedure, which considers the purity and handling of the samples, is estimated to be 2%.

The refractive index was measured by an ABBEMAT 500 Anton Paar automatic refractometer with a resolution of $\pm10^{-6}$. The equipment was calibrated with tetrachloroethylene (provided by the equipment supplier) and verified with Millipore water before each series of measurements. Duplicates were measured in a range of temperatures from 283.15K to 353.15K and the obtained results showed an uncertainty below $\pm 4\times10^{-5}$.

The ionic conductivity was determined using a CDM210 Radiometer Analytical conductometer and a CDC749 electrode. Each sample was introduced in a jacketed glass cell and well stirred during the measurements, ensuring constant temperature. This conductometer provides an alter current of 12 V in the range of study. The use of high frequency alters the current in addition to the platinized electrodes and avoids polarization effects at the surface of the cell electrodes. Sample temperature was thermostated to bath temperature using a platinum resistance thermometer coupled to a Keithley 199 System DMM/Scanner with an uncertainty of ± 0.05 K. The thermometer was calibrated against high accuracy mercury thermometers (0.01 K). In order to carry out ionic conductivity measurements, 1.5 mL of sample were added to the thermostatic cell and vigorously stirred. The cell was closed and flushed with dry nitrogen to ensure a secure seal and prevent humidity. The conductometer was calibrated at each temperature with certified 0.01 D and 0.1 D KCl standard solutions supplied by Radiometer Analytical. The calibration was performed as previously described in the literature [14]. Each conductivity value was determined at least twice, concluding an uncertainty below 1% in absolute value.

4.2.2 Theory

4.2.2.1 Soft-SAFT equation of state

Soft-SAFT uses a Lennard-Jones (LJ) intermolecular potential as a reference term, considering simultaneously the repulsive and dispersive contributions of the fluids molecules. As other SAFT-type equations, it separately accounts for van der Waals interactions and strong short-range directional forces (*e.g.* hydrogen bonding effects) [15,16]. The soft-SAFT EoS

characterizes the fluids as a coarse-grained model, where the molecules are represented by a chain of interconnected spheres with associating sites. As with all the SAFT variants, this equation is expressed by the sum of the microscopic contributions to the residual Helmholtz energy (A^{res}) of the fluid system (Equation 4.2.1):

$$A^{res} = A - A^{id} = A^{ref} + A^{chain} + A^{assoc} \quad 4.2.1$$

A and A^{id} are the total and ideal contributions of Helmholtz free energy; A^{ref} corresponds to the reference term, where the monomer-monomer repulsive and attractive interactions are accounted; the A^{chain} represents the chain term accounting for the formation of the chains; and A^{assoc} is the term that considers the site-site intermolecular association. In the LJ reference term, two molecular parameters characterize the fluid: the segment diameter, σ, and the dispersive energy, ε, between the monomers. The contribution of the reference term is calculated by the LJ EoS of Johnson et al. [17].The extension of this equation to mixtures is performed by the van der Waals one-fluid theory with the modified Lorentz-Berthelot combining rules expressed in Equations 4.2.2 and 4.2.3.

$$\sigma_{ij} = \eta_{ij} \frac{(\sigma_{ii} + \sigma_{jj})}{2} \quad 4.2.2$$

$$\varepsilon_{ij} = \xi_{ij} \sqrt{\varepsilon_{ii} \varepsilon_{jj}} \quad 4.2.3$$

where η_{ij} and ξ_{ij} are binary parameters that account for size and energy asymmetries, respectively, among the different fluids of a mixture. The binary parameters values become unity when the equation is predictively used from the pure component parameters.

The chain and association terms of the equation are directly derived from Wertheim's first-order thermodynamic perturbation theory and are described in detail in the original contributions [18–21]. Regarding the binary system (IL+water) studied in this work, cross-association interactions between the water and IL molecules must be explicitly considered. The association energy and volume parameters of the binary system are calculated using the following combining rules (Equations 4.2.4 and 4.2.5):

$$\kappa^{HB}_{\alpha\beta,\,ij} = \left(\frac{\sqrt[3]{\kappa^{HB}_{\alpha\beta,\,ii}} + \sqrt[3]{\kappa^{HB}_{\alpha\beta,\,jj}}}{2} \right)^3 \quad 4.2.4$$

$$\varepsilon^{HB}_{\alpha\beta,\,ij} = \sqrt{\varepsilon^{HB}_{\alpha\beta,\,ii} \varepsilon^{HB}_{\alpha\beta,\,jj}} \quad 4.2.5$$

where $\kappa^{HB}_{\alpha\beta,\,ij}$ and $\varepsilon^{HB}_{\alpha\beta,\,ij}$ are the association volume and energy, respectively, of the cross-association strength between the associating site α of the molecule i and site β of molecule j.

From all terms of soft-SAFT EoS, a total of five parameters are used to define each fluid: the chain length, m, the segment diameter, σ, the dispersive energy between the segments, ε, and two more parameters that consider the associating interactions of the model, the site-site association energy, ε^{HB}, and the site-site bonding-volume of association, κ^{HB}.

4.2.2.2 Free-volume theory

In this work, the Free-Volume Theory (FVT) [22,23], coupled with the soft-SAFT EoS [24,25], was used in order to describe the viscosity of pure and aqueous mixtures of FILs. This approach expresses the viscosity η (mPa·s^{-1}) of a system as a sum of a dilute gas term, η_0, (where the intermolecular effects are neglected), and a dense liquid term, $\Delta\eta$ (related to the density and the microstructure of the fluid) (Equation 4.2.6):

$$\eta=\eta_0+\Delta\eta \qquad 4.2.6$$

The dilute gas term is typically neglected for molecules with negligible vapour pressure [26], as in the case of FILs. The dense-state term $\Delta\eta$ is obtained through an expression that relates the viscosity to the fluid microstructure. In parallel, this expression is also related to the free space among the molecules, defined as a free-volume fraction through an exponential relation originally proposed by Doolittle [27]. Then, the final expression is represented in Equation 4.2.7:

$$\Delta\eta=L_v\left(0.1P+10^{-4}\alpha\rho^2M_w\right)\sqrt{\frac{10^{-3}M_w}{3Nk_BT}}\ \exp\left[B\left(\frac{10^3P+\alpha\rho^2M_w}{\rho Nk_BT}\right)^{\frac{3}{2}}\right] \qquad 4.2.7$$

The approach includes three parameters related to the structural and energetic properties of the fluid: a (Jm^{3}mol^{-1}kg^{-1}) which describes the proportionality between the energy barrier and the density; B (dimensionless) which corresponds to the free-volume overlap; and L_v (Å) is a length parameter related to the structure of the molecules and the characteristic relaxation time. These parameters are fitted to available experimental viscosity data. The thermodynamic variables, such as the pressure P (MPa), the temperature T (K) and the density ρ (molL^{-1}), are obtained from soft-SAFT.

With the aim to obtain viscosity parameters that accurately describe the pure compounds and mixtures, a robust methodology named Spider-Web [28] was used in this work. This approach allows the connection of the parameters describing the compounds of interest through the simultaneous fitting of FVT parameters to pure compounds and mixtures, assuming the parameters of one compound in a mixture influence the values of the parameters

of the other compounds in that mixture. The extension of the FVT approach to mixtures is done by applying direct compositional rules to the viscosity parameters, in a similar manner as done in the original soft-SAFT + FVT contribution for mixtures [24,25]. The expressions for the parameters are given in Equations 4.2.8 to 4.2.10.

$$B_{\mathrm{mix}} = \sum_{\mathrm{i}} x_{\mathrm{i}} B_{\mathrm{i}} \qquad 4.2.8$$

$$\alpha_{\mathrm{mix}} = \sum_{\mathrm{i}} x_{\mathrm{i}} \alpha_{\mathrm{i}} \qquad 4.2.9$$

$$L\mathrm{v}_{\mathrm{mix}} = \sum_{\mathrm{i}} x_{\mathrm{i}} L\mathrm{v}_{\mathrm{i}} \qquad 4.2.10$$

No fitted binary parameters are added in the viscosity treatment of mixtures. For further details, the reader is referred to the original articles on the FVT implementation into soft-SAFT[1] and the Spider-Web methodology [28].

4.2.2.3 Water molecular model

Water was already modelled in a former work [29], where it was considered as a single spherical Lennard-Jones sphere (m = 1), with an association scheme of 4 associating sites. Two sites of type *H* represent the hydrogen atoms (positive sites) and two sites of type *e* represent the lone pairs of electrons of the oxygen (negative sites). In this model, only *e*–*H* interactions are allowed.

4.2.2.4 Soft-SAFT molecular models

Soft-SAFT accounts for the different molecular effects on a system as separated entities (*e.g.* molecular shape and association), enabling the description of the thermophysical properties and phase behaviour of complex systems like ILs and their mixtures, in a good agreement with experimental data [30–35].

To accurately predict FILs properties through soft-SAFT EoS, a proper coarse-grained model has to be selected to describe the physical features of the FILs structure. This model is based on the assumption of the ILs' intrinsic low ionic character due to the formation of short-lived ion pairs caused by the interactions between the ions, which are characterized through dispersion forces and specific steric interactions [36–38]. Through quantum information, molecular simulation results and previous experience, ILs are modelled as single chain molecules (cation and anion together) with a number of associating sites specified to account for the highly anisotropic interactions between the counterions, such as hydrogen bonding [30–35]. Five molecular parameters must be defined to describe the molecules (chain length,

m, spheres diameter, σ, and dispersive energy, ε, between monomers) and the association scheme (site-site association energy, ε^{HB}, and volume, κ^{HB}).

A methodical study of all FILs parameterized by soft-SAFT EoS underlined the robustness of this approach and disclosed a systematic procedure for modelling FILs. The parameterization is executed through the transference of the parameters between FILs with common cationic or anionic structures, simplifying the screening of similar compounds and their properties with less amount of experimental data [39]. The models of $[C_2C_1Im][C_4F_9SO_3]$ [30] and $[C_2C_1Im][C_4F_9CO_2]$ [31] were previously defined by three associating sites accounting for the counterions interactions and the negative charge delocalization caused by the fluorine and oxygen atoms. We had initially transferred this 3-association scheme to the model of $[C_{2(OH)}C_1Im][C_4F_9SO_3]$ and $[C_{2(OH)}C_1Im][C_4F_9CO_2]$. However, the study of the electrostatic potential surfaces of OH-FILs (see Figure 4.2.1), determined by using the MMFF94 force field [40] and performed through the open-source software Avogadro (version 1.2.0) [41], showed that this association scheme is not suitable. In fact, the addition of the hydroxyl group in the cationic hydrogenated chain contributes to higher charge delocalization and a number of hydrogen bonding interactions between FILs cations. Consequently, a 5-site association scheme was selected: one associating site of type *A* represented the interactions between counterions, two sites of type *B* described the charge delocalization caused by the surrounding fluorines and the oxygens of the anion, and two additional sites were added to account for the hydroxyl group association, where a negative site *C* stands for oxygen and a positive site *D* for hydrogen (Figure 4.2.1). To sum up, only interactions between *A*–*B*, *A*–*C*, *B*–*D* and *C*–*D* are allowed.

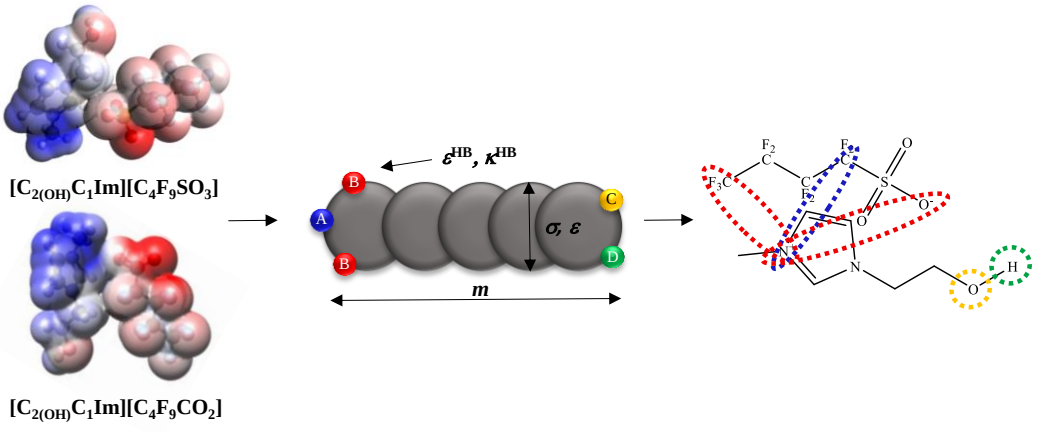

Figure 4.2.1 Sketch of 5-associating sites model used to describe the hydroxyl-containing fluorinated ionic liquids within soft-SAFT framework. Blue and green represents the positive sites and red and yellow corresponds to negative sites.

To guarantee the definition of a suitable model based on the systematic methodology to parameterize FILs [39], several molecular parameters of OH-FILs were transferred from the

FILs-analogous values following some restrictions [30–35] to reduce the parameters degeneracy and improve the transferability. As the anion is the structural feature that has a higher influence on the transferability [39], various parameters for FILs based on the same anion were transferred: the segments chain length, m, and the association parameters, ε^{HB} and κ^{HB}, were directly transferred from $[C_2C_1Im][C_4F_9SO_3]$ [30] and $[C_2C_1Im][C_4F_9CO_2]$ [39] to $[C_{2(OH)}C_1Im][C_4F_9SO_3]$ and $[C_{2(OH)}C_1Im][C_4F_9CO_2]$, respectively. For the two additional associating sites added to represent the interactions of the OH–OH groups, the association strength was transferred from the ethanol model (ε^{HB}/k_B=2388 K and κ^{HB}=2932 Å^3) [42]. Besides, cross-association between OH group and the anion/cation counterparts is allowed (*A–C*, *B–D* interactions). Then, the association strength values were calculated using the combining rules given in Equations 4.2.4 to 4.2.5. The remaining segment diameter, σ, and dispersive energy between segments, ε, for both OH-FILs were obtained by fitting to the experimental density data at atmospheric pressure. The final parameters sets of OH-FILs can be found in Table 4.2.2, as well as those previously published for the analogous FILs [30,39]. The binary mixtures of FILs + water were also studied with soft-SAFT parameters provided in Table 4.2.2 [29]. Cross-association interactions between FILs and water molecules were calculated using combining rules (Equations 4.2.4 to 4.2.5).

Table 4.2.2 Molecular weight, molecular parameters, and absolute average deviation (AAD) for the densities of the studied fluorinated ionic liquids and water.

Substance	M_w [g·mol^{-1}]	m	σ [Å]	ε/k_B [K]	ε^{HB}/k_B [K]	κ^{HB} [Å^3]	AAD [%]
$[C_{2(OH)}C_1Im][C_4F_9SO_3]$	426.26	7.320	3.818	324.0	3850	2250	0.028
$[C_{2(OH)}C_1Im][C_4F_9CO_2]$	390.21	7.233	3.788	328.1	3850	2250	0.046
$[C_2C_1Im][C_4F_9SO_3]$[a]	410.26	7.320	3.816	343.4	3850	2250	0.053
$[C_2C_1Im][C_4F_9CO_2]$[b]	374.21	7.233	3.762	338.8	3850	2250	0.008
Water[c]	18.01	1.000	3.154	365	2388	2932	

Parameters from Pereiro, A.B. *et al.* (2017) for (a); Ferreira, M.L. *et al.* (2019) for (b) and Vega, L.F. *et al.* (2009) for (c) [29,30,39]

4.2.3 Results and discussion

$[C_{2(OH)}C_1Im][C_4F_9SO_3]$ and $[C_{2(OH)}C_1Im][C_4F_9CO_2]$ FILs were synthesized pursuing the functionalization of the analogous FILs, $[C_2C_1Im][C_4F_9SO_3]$ and $[C_2C_1Im][C_4F_9CO_2]$ [13]. The melting point, thermal stability, density, viscosity, refractive index, ionic conductivity, and the calculated fluidity and free volume parameters were studied to experimentally characterize them. The self-aggregation behaviour of OH-FILs in aqueous solutions was obtained by measuring the density and viscosity as well as determining the critical aggregation concentrations (CACs) and the ionization degree of the aggregates. Moreover, the density and viscosity of the pure OH-FILs and the FILs + water systems were characterized with soft-SAFT EoS to better understand the microscopic behaviour of OH-FILs and to corroborate the

experimental observations. This study discloses the influence on the physicochemical properties caused by the addition of a hydroxyl group in FILs since it increases the biocompatibility and enhances their properties to be used in biological applications [4–7]. Consequently, the discussion is focused on two different structural features: (i) the influence induced by introducing a hydroxyl group in the cation structure and (ii) the influence of the anions $[C_4F_9SO_3]^-$ and $[C_4F_9CO_2]^-$ in these properties.

4.2.3.1 Thermal analysis

Thermal properties are crucial to deciding the eligibility of a substance to a specific application because the melting and decomposition temperatures determine the liquid and operative range of FILs. Thus, the onset temperature, T_{onset}, starting temperature, T_{start}, melting temperature, T_m, and glass transition temperature, T_g, for OH-FILs were measured (Table 4.2.3).

Table 4.2.3 Thermal properties of the fluorinated ionic liquids: start temperature, T_{start}; onset temperature, T_{onset}; glass transition, T_g; and melting temperature, T_m.

FIL	$\boldsymbol{T_{start}}$[a] [K]	$\boldsymbol{T_{onset}}$[a] [K]	$\boldsymbol{T_g}$ [K]	$\boldsymbol{T_m}$ [K]
$[C_{2(OH)}C_1Im][C_4F_9SO_3]$	381.36	558.76	211.29	251.46
$[C_{2(OH)}C_1Im][C_4F_9CO_2]$	392.13	432.66	206.88	294.84

In Figure 4.2.2, the T_{onset} versus T_m results were compared with the analogous FILs values previously reported [13]. In order to consider their applicability in biomedical applications, thermal stability must be ensured under 310.15 K (the human body temperature, black line in Figure 4.2.2). FILs with T_m above this value are discarded, preferring those with higher T_{onset} values. All FILs showed a value of T_m lower than 310.15 K, and regarding the influence of the hydroxyl group, OH-FIL conjugated with $[C_4F_9SO_3]^-$ anion has lower T_m and T_{onset} values than with the $[C_2C_1Im]^+$ cation. The opposite behaviour was observed for $[C_4F_9CO_2]^-$ anion, where $[C_{2(OH)}C_1Im]^+$ cation has higher values of T_m and T_{onset}. The anion influence shows that $[C_4F_9SO_3]$-FILs have higher values of T_{onset}. However, T_m is higher for OH-FIL based on $[C_4F_9CO_2]^-$ anion. It can be inferred that both structural features (hydroxyl group and anion) highly influence these thermal properties. Nonetheless, all FILs show an adequate thermal behaviour and the best T range was observed for $[C_{2(OH)}C_1Im][C_4F_9SO_3]$ due to the combination of a low T_m and a high T_{onset}. All FILs have T_m under 298.15K, ensuring thermal stability at room temperature, regarding the compound's handling and storage. Another interesting feature is that both OH-FILs have a T_g (Table 4.2.3), whereas the analogous FILs did not show any T_g in the studied temperature range [13].

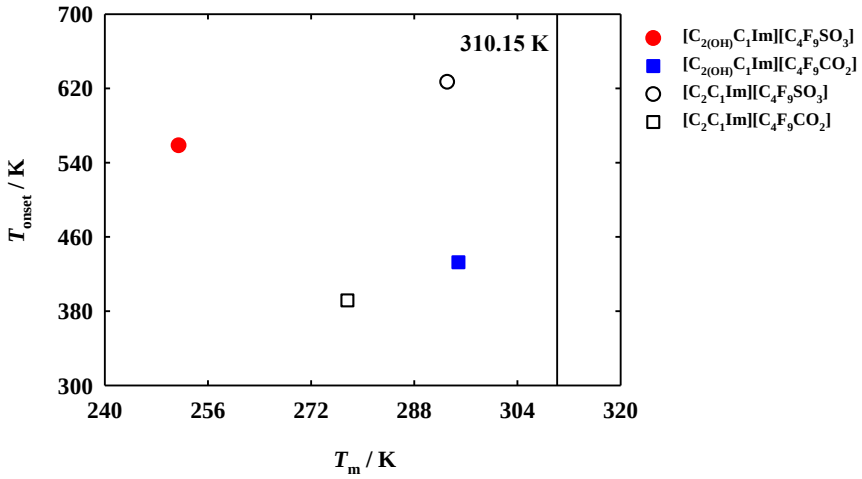

Figure 4.2.2 Decomposition onset temperature versus melting temperature for $[C_{2(OH)}C_1Im][C_4F_9SO_3]$ (red, ●) and $[C_{2(OH)}C_1Im][C_4F_9CO_2]$ (blue, ■) FILs and comparison with $[C_2C_1Im][C_4F_9SO_3]$ (black, ○) and $[C_2C_1Im][C_4F_9CO_2]$ (black, □) literature values [13]. The line indicates the reference temperature of human body, 310.15 K.

4.2.3.2 Thermophysical and transport properties

FILs are tunable compounds and any alteration in their structure allows changes in their thermophysical and transport properties [43]. Then, density, viscosity and conductivity have been analysed. In addition, the refractive index, related to the molar free-volume effects, forces between ILs molecules and their behaviour in solution [44], are also relevant for assessing their application.

4.2.3.2.1 Density and viscosity

The density and viscosity of OH-FILs were measured (Table 4.2.4) and the results are illustrated in Figure 4.2.3. The values previously determined for analogous FILs are also represented for comparative purposes [13]. Figure 4.2.3a shows the density results, where all FILs values linearly decrease when the temperature increases. The same behaviour was found for other FILs in earlier publications [13,45]. The comparison between $[C_{2(OH)}C_1Im]$- and $[C_2C_1Im]$-FILs shows that the hydroxyl group significantly increases the density of the FILs. Besides, the $[C_4F_9SO_3]$-FILs present higher densities than those with the $[C_4F_9CO_2]^-$ anion. Finally, $[C_2C_1Im][C_4F_9CO_2]$ (1.47g·cm^{-3} at 313.15 K) is the FIL with lower density.

Table 4.2.4 Density, ρ, dynamic viscosity, η, refractive index, n_D, and ionic conductivity, k, of the fluorinated ionic liquids as a function of temperature, T.

T [K]	ρ [g·cm^{-3}]	η [mPa·s]	n_D	k [mS·cm^{-1}]
		$[C_{2(OH)}C_1Im][C_4F_9SO_3]$		
283.15	1.6361	3022	1.40040	0.1312
288.15	1.6307	1888	1.39909	0.1916
293.15	1.6254	1242	1.39776	0.2783
298.15	1.6200	831.6	1.39644	0.3849

303.15	1.6146	580.2	1.39512	0.5356
308.15	1.6092	411.4	1.39381	0.7115
313.15	1.6040	301.3	1.39249	0.9325
318.15	1.5987	224.0	1.39118	1.194
323.15	1.5938	170.8	1.38989	1.511
328.15	1.5889	132.0	1.38858	
333.15	1.5839	104.1	1.38727	
338.15	1.5788	83.15	1.38600	
343.15	1.5734	67.47	1.38471	
348.15	1.5677	55.35	1.38343	
353.15	1.5623	46.04	1.38216	
		$[C_{2(OH)}C_1Im][C_4F_9CO_2]$		
283.15	1.5563	2707	1.41083	0.09427
288.15	1.5515	1632	1.40948	0.1449
293.15	1.5462	1099	1.40814	0.2169
298.15	1.5413	712.8	1.40683	0.3151
303.15	1.5361	510.1	1.40548	0.4554
308.15	1.5312	351.3	1.40417	0.6338
313.15	1.5260	264.2	1.40284	0.8613
318.15	1.5211	190.8	1.40152	1.141
323.15	1.5162	149.7	1.40020	1.478
328.15	1.5112	112.6	1.39885	
333.15	1.5068	91.52	1.39752	
338.15	1.5015	71.18	1.39619	
343.15	1.4970	59.58	1.39487	
348.15	1.4919	47.66	1.39355	
353.15	1.4869	40.85	1.39221	

The provided experimental data were used to parameterize the OH-FILs using soft-SAFT EoS, as explained in "soft-SAFT molecular models" Section. The resulting model calculations are plotted as solid lines in Figure 4.2.3a, showing an excellent agreement with experimental data (deviations lower than 0.05%). Soft-SAFT calculations related to the analogous FILs [30] are plotted as dashed lines in Figure 4.2.3a.

In order to verify the consistency and physical meaning of the fitted molecular parameters of the OH-FILs, two correlations of the molecular parameters with the molecular weight (M_w) of FILs were used (Figure 4.2.4). The $m\sigma^3$ refers to a rough approximation of the volume of the ILs individual molecules (volume of each group multiplied by the chain length), while $m\varepsilon$ refers to the energy of the ILs molecules. The $m\sigma^3$ values (Figure 4.2.4a) of $[C_4F_9CO_2]$-FILs have a proportional increment with the M_w, whereas the $[C_4F_9SO_3]$-FILs do not show significant differences. Since the m parameter was transferred from FILs [30,31] to OH-FILs, the volume differences from the addition of the hydroxyl group are considered by the σ parameter (Figure 4.2.4a). The OH-FILs show a higher M_w and a lower $m\varepsilon$ value compared to the analogous FILs,[1] indicating that the addition of the OH group minimizes the inner van der Waals energy of the FILs molecules (Figure 4.2.4b).

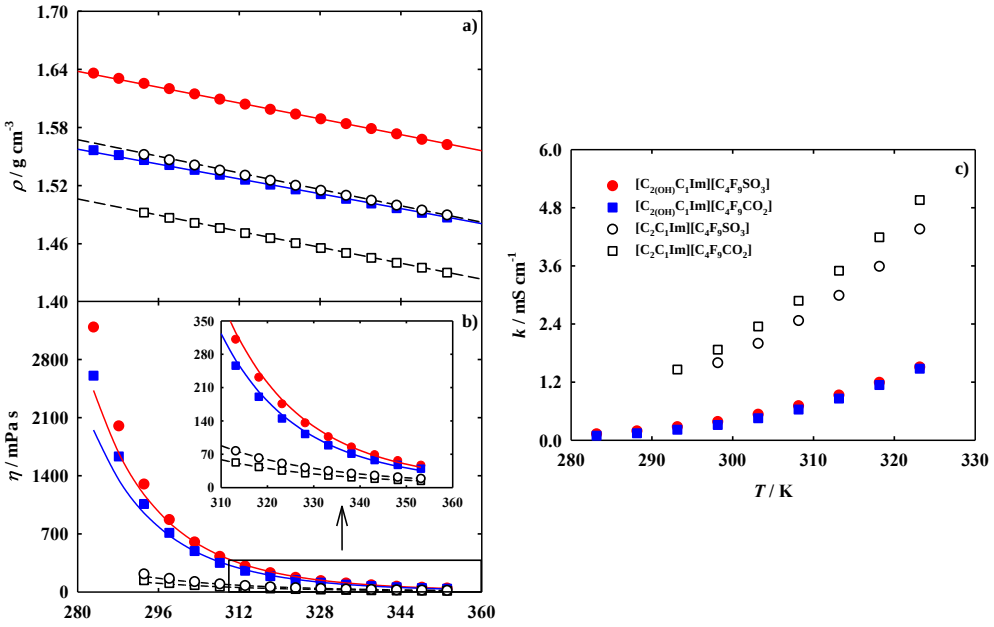

Figure 4.2.3 Density (a), dynamic viscosity (b) and ionic conductivity (c) versus temperature at atmospheric pressure, for the pure FILs studied in this work, ([$C_{2(OH)}C_1Im$][$C_4F_9SO_3$] and [$C_{2(OH)}C_1Im$][$C_4F_9CO_2$]), and for the analogous FILs [13], ([C_2C_1Im][$C_4F_9SO_3$] and [C_2C_1Im][$C_4F_9CO_2$]). The lines in (a) and (b) represent the soft-SAFT calculations (solid lines for OH-FILs and dashed lines for analogous FILs).

In Figure 4.2.3b the viscosity data of OH-FILs and the analogous FILs are plotted [13]. The analysis of these results shows a high dependence and inverse proportionality with temperature. The addition of the hydroxyl group severely increases the viscosity, which can be related to the increment of the cationic interactions [8]. Conversely, the viscosity is higher for [$C_4F_9SO_3$]-FILs than for [$C_4F_9CO_2$]-FILs.

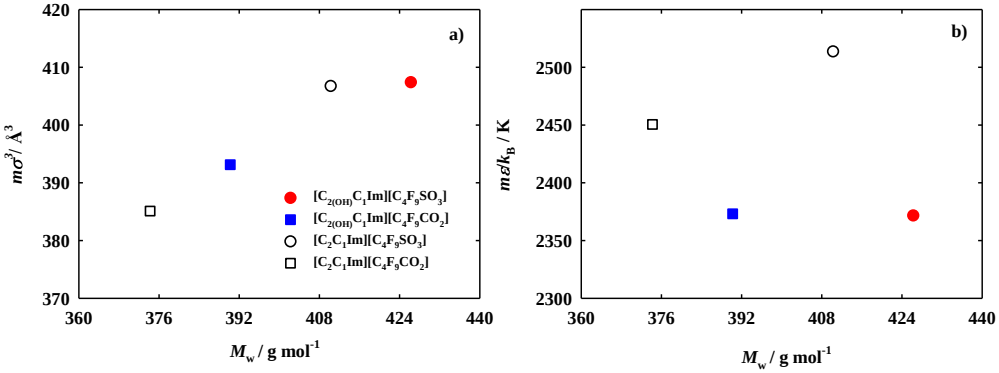

Figure 4.2.4 Correlations $m\sigma^3$ (a) and $m\varepsilon$ (b) with the molecular weight for [$C_{2(OH)}C_1Im$][$C_4F_9SO_3$] and [$C_{2(OH)}C_1Im$][$C_4F_9CO_2$], and for the analogous FILs previously investigated [30], [C_2C_1Im][$C_4F_9SO_3$] and [C_2C_1Im][$C_4F_9CO_2$].

In order to gain molecular insights into the behaviour of the systems, the viscosity data was theoretically characterized by soft-SAFT coupled with FVT [24,25], as described in Section 4.2.3.2. Results are depicted in Figure 4.2.3b where a good agreement with experimental values is observed. Only a small deviation between the two experimental points at the lowest temperatures is found. The FVT parameters are given in Table 4.2.5.

Results of viscosity and density show that OH-FILs and $[C_4F_9SO_3]$-FILs present higher cohesive structures, resulting in more dense and viscous compounds. As expected, higher fluidity is found for non-functionalized FILs with the $[C_4F_9CO_2]^-$ anion.

Table 4.2.5 Optimized characteristic parameters of the free-volume theory and the respective absolute average deviation for the pure fluorinated ionic liquids (set *B*) and their aqueous mixtures (0 to 0.2 x_{FIL}, set *A* and 0.2 to 1.0 x_{FIL}, set *B*) studied in this work. The FVT parameters for pure water are also included [46].

	Set	M_w [g·mol^{-1}]	a [J·m^3·mol^{-1}·kg^{-1}]	$B\times10^3$	$L_v\times10^1$ [Å]	**AAD** η^{pure} [%]	**AAD** η^{mix} [%]
$[C_{2(OH)}C_1Im][C_4F_9SO_3]$	A	426.26	291.8	2.944	1.698	25.4	5.88
	B			4.053	0.143	6.43	14.0
$[C_{2(OH)}C_1Im][C_4F_9CO_2]$	A	390.21	279.6	2.839	4.175	32.6	7.93
	B			4.615	0.142	6.76	21.7
$[C_2C_1Im][C_4F_9SO_3]$	A	410.26	345.9	2.004	1.499	8.25	6.55
	B			2.255	0.769	3.30	8.35
$[C_2C_1Im][C_4F_9CO_2]$	A	374.21	262.0	2.888	2.569	10.0	7.79
	B			3.312	1.261	3.91	8.35
Water		18.01	357.3	1.441	0.218		

4.2.3.2.2 Molar free-volume effects

Refractive index enables the measurement of the electric polarizability of a molecule, providing useful information about the response of the molecules electron distribution to an electric field, which can also be induced by electric interactions with ionic solvents, allowing the study of the internal structure of molecules and their bounded systems [44,47]. Data for OH-FILs regarding the refractive index are presented in Table 4.2.4, showing inverse proportionality with temperature, the same behaviour of the analogous FILs [13]. The results indicate slightly higher values for $[C_{2(OH)}C_1Im][C_4F_9CO_2]$ in comparison with the other FILs.
Considering the importance of defining the ability of FILs to dissolve, the molar free-volume effects were calculated for OH-FILs by Lorentz-Lorentz equation. The Lorentz-Lorentz equation relates the refractive index, n_D, with the electronic polarizability, a_e, and can be expressed in terms of the molar refraction, or molar polarizability, R_m, as follows [13]:

$$R_m = \frac{N_A \alpha_e}{3\varepsilon_0} = \left(\frac{{n_D}^2 - 1}{{n_D}^2 + 2}\right) V_m \qquad 4.2.11$$

where N_A is the Avogadro's constant, ε_0 is the dielectric constant, and V_m is the molar volume. The electronic polarizability can be associated with a spherical molecular radius, considering the molecular refractions a measure of the hardcore molecular volumes, by [44,47]:

$$\alpha_e = 4\pi\varepsilon_0\alpha^3 \qquad 4.2.12$$

Then, the Equation 4.2.12 can be re-written as:

$$n_D - 1 = 3\left(\frac{V_m}{R_m - 1}\right)^{-1} = \left(3\frac{V_m}{f_m}\right) \quad 4.2.13$$

where f_m is the free volume between the FIL molecules, and can be defined by Equation 4.2.14.

$$f_m = (V_m - R_m) \quad 4.2.14$$

The refractive index has a directly proportional relation with molar volume, considering it as the hard-core molecular volume [48,49]. This methodology is only valid when it is assumed that only dispersion forces are present, which is not the case with ILs. However, the relative ratio of the free volume over molar volume, $f_m V_m^{-1}$, can be calculated, given that the dispersion forces of ILs are significant, opposing the common molten salts [13,30,45].

The calculated values of the molar refractions and molar volumes of OH-FILs are listed in Table 4.2.6 and they were also compared with the ones from analogous FILs [13]. The analysis of the molar refractions showed the tendency $[C_2C_1Im][C_4F_9CO_2]$ < $[C_{2(OH)}C_1Im][C_4F_9CO_2]$ < $[C_{2(OH)}C_1Im][C_4F_9SO_3]$ < $[C_2C_1Im][C_4F_9SO_3]$; whereas the molar volumes are $[C_2C_1Im][C_4F_9CO_2]$ ≈ $[C_{2(OH)}C_1Im][C_4F_9CO_2]$ < $[C_{2(OH)}C_1Im][C_4F_9SO_3]$ ≈ $[C_2C_1Im][C_4F_9SO_3]$. The relative ratio of the free volume over molar volume, $f_m V_m^{-1}$, was also calculated in this work[1] (see Table 4.2.6). The analysis of $f_m V_m^{-1}$ indicated that the effect of the anion and of the addition of a hydroxyl group is not significant (with slightly lower ratio values for $[C_{2(OH)}C_1Im][C_4F_9CO_2]$). The increment of the cationic interactions due to the OH group can compact the structure of the OH-FIL, diminishing the free spaces caused by the asymmetric counterions and bulky imidazolium cation of the analogous compounds.

Table 4.2.6 Values of calculated molar volume, V_m, molar refraction, R_m, and the ratio of free volume, f_m, over molar volume as a function of temperature for studied fluorinated ionic liquids as a function of temperature, T.

T [K]	V_m [cm^3·mol^{-1}]	R_m [cm^3·mol^{-1}]	$f_m V_m^{-1}$	V_m [cm^3·mol^{-1}]	R_m [cm^3·mol^{-1}]	$f_m V_m^{-1}$
	$[C_{2(OH)}C_1Im][C_4F_9SO_3]$			**$[C_{2(OH)}C_1Im][C_4F_9CO_2]$**		
283.15	260.54	63.22	0.7574	250.72	62.23	0.7518
288.15	261.40	63.24	0.7581	251.50	62.24	0.7525
293.15	262.25	63.26	0.7588	252.36	62.28	0.7532
298.15	263.12	63.29	0.7595	253.17	62.30	0.7539
303.15	264.00	63.31	0.7602	254.03	62.33	0.7546
308.15	264.90	63.34	0.7609	254.84	62.35	0.7553
313.15	265.75	63.35	0.7616	255.70	62.38	0.7561
318.15	266.63	63.37	0.7623	256.54	62.40	0.7568
323.15	267.45	63.38	0.7630	257.35	62.42	0.7575
328.15	268.28	63.39	0.7637	258.20	62.44	0.7582
333.15	269.13	63.40	0.7644	258.97	62.44	0.7589
338.15	270.00	63.42	0.7651	259.87	62.47	0.7596
343.15	270.92	63.45	0.7658	260.65	62.47	0.7603

348.15	271.90	63.49	0.7665	261.56	62.50	0.7610
353.15	272.84	63.52	0.7672	262.44	62.52	0.7618

4.2.3.2.3 Walden plot

The ionic conductivities of OH-FILs are reported in Figure 4.2.3c and Table 4.2.4. The results show no significant differences between OH-FILs. The addition of the hydroxyl group decreases the ionic conductivity of OH-FILs, which can be related to the decrement of fluidity associated with the polar interactions by cationic OH groups, compacting the structure of the OH-FILs, and diminishing their mobility. Figure 4.2.5 reports the ionicity of the OH-FILs studied and the analogous FILs [13]. This property establishes a relation between the molar conductivity and the fluidity (inverse of viscosity) of a solution using the Walden Plot (Figure 4.2.5). Ionicity provides useful information about transport properties, mobility and the possible formation of aggregates, whose presence decreases the mobility of FILs and increases their viscosity, resulting in an ionic behaviour away from the ideal electrolyte [4,13]. The ionicity of these compounds is mainly controlled by the molar concentration of ions, the charged aggregates, and their mobility in the fluid. Thus, this property is a measure of the formation of aggregates due to the decrease of fluidity and conductivity of a compound. The standard classification of ionic liquids using the Walden plot (Figure 4.2.5a) is pictured by a straight line representing the ideal behaviour corresponding to aqueous KCl solutions (fully dissociated, where the ions have equal mobility). In Figure 4.2.5b, a closer look into the Walden plot shows a linear trend with temperature observed for each pure FIL. The ionicity is very similar for all FILs, with slightly higher values for $[C_4F_9SO_3]$-FILs. The hydroxyl group functionalization does not affect this property.

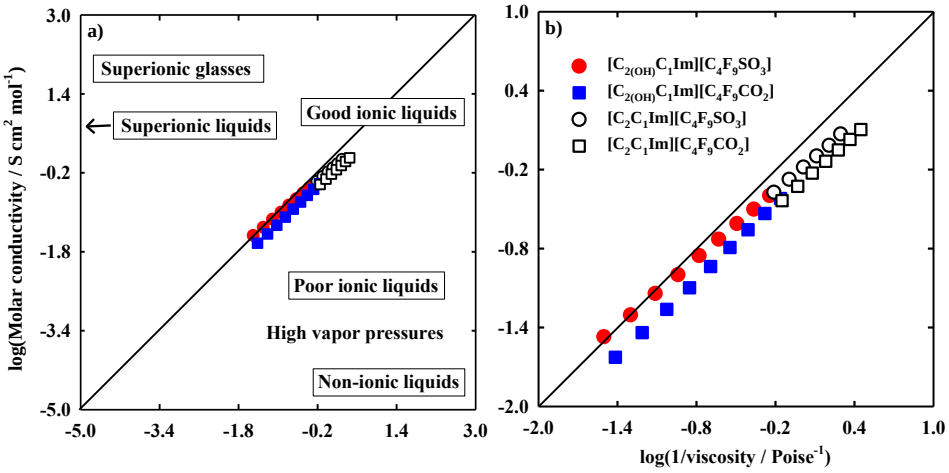

Figure 4.2.5 (a) Classification diagram for ionic liquids based on the Walden plot and (b) a closer look for the pure FILs studied in this work, ($[C_{2(OH)}C_1Im][C_4F_9SO_3]$ and $[C_{2(OH)}C_1Im][C_4F_9CO_2]$), in a temperature range of 283.15-323.15 K and for the analogous FILs,[1] ($[C_2C_1Im][C_4F_9SO_3]$ and $[C_2C_1Im][C_4F_9CO_2]$).

4.2.3.3 Self-aggregation behaviour of fluorinated ionic liquids in aqueous solutions

Knowledge of the self-aggregation behaviour and solvation mechanisms of FILs and how the structural features can affect the organization of the self-assembled components will allow the design of new compounds with improved surfactant power. In this section, the density, viscosity, ionicity and the critical aggregation concentrations (CACs) of FILs + water systems are disclosed. These results elucidate the insight of the OH-FILs self-aggregation mechanism in water and the verification of their usefulness as totally water-miscible fluorinated surfactants.

4.2.3.3.1 Density, viscosity and ionicity

The density and viscosity of the $[C_{2(OH)}C_1Im][C_4F_9SO_3]$, $[C_{2(OH)}C_1Im][C_4F_9CO_2]$ and $[C_2C_1Im][C_4F_9CO_2]$ FILs in aqueous solutions were determined in this work between 298.15 and 318.15 K, whereas the ionic conductivity of OH-FILs was determined at 298.15 K (Table 4.2.7). The results were compared with the previous measurements of $[C_2C_1Im][C_4F_9SO_3]$ + water system [50]. The density and viscosity at 298.15 K are represented in Figure 4.2.6, (the other temperatures are plotted in Figures 4.2.7 and 4.2.8, respectively). As expected, the increment of temperature decreases the density and viscosity of the binary systems. Through the detailed analysis of Figure 4.2.6, the increment of water concentration reduces both properties. The results show the same trends obtained for the pure components, where higher values of density and viscosity are found in OH-FILs and $[C_4F_9SO_3]$-FILs.

Table 4.2.7 Density, ρ, dynamic viscosity, η, and ionic conductivity, k, as function of ionic liquid mass fraction, w_{FIL}, for the binary system $[C_{2(OH)}C_1Im][C_4F_9SO_3]$ + water, $[C_{2(OH)}C_1Im][C_4F_9CO_2]$ + water and $[C_2C_1Im][C_4F_9CO_2]$ + water at 298.15, 308.15 and 318.15 K.

w_{FIL}	ρ [g·cm^{-3}]	η [mPa·s]	k [mS·cm^{-1}]	ρ [g·cm^{-3}]	η [mPa·s]	ρ [g·cm^{-3}]	η [mPa·s]
			$[C_{2(OH)}C_1Im][C_4F_9SO_3]$ + water				
		T = 298.15 K		**T = 308.15 K**		**T = 318.15 K**	
1.0000	1.6200	831.6	0.3295	1.6092	411.4	1.5987	224.0
0.9803	1.5699	255.8	1.163	1.5604	143.5	1.5508	86.79
0.9606	1.5500	133.7	2.414	1.5406	79.56	1.5309	50.53
0.9393	1.5324	87.06	5.166	1.5231	53.85	1.5135	35.36
0.9202	1.5170	63.78	8.497	1.5078	40.61	1.4975	27.37
0.8998	1.5029	50.56	12.63	1.4938	32.80	1.4841	22.44
0.8778	1.4860	38.80	17.44	1.4771	25.70	1.4677	17.91
0.8605	1.4731	32.07	21.30	1.4643	21.60	1.4548	15.23
0.8400	1.4590	27.44	25.79	1.4502	18.72	1.4412	13.38
0.8207	1.4444	23.25	29.81	1.4359	16.05	1.4269	11.56
0.7994	1.4292	19.81	33.93	1.4208	13.84	1.4118	10.06
0.7799	1.4121	16.91	37.35	1.4040	11.95	1.3953	8.758
0.7596	1.3982	14.88	40.49	1.3902	10.63	1.3818	7.860

0.7403	1.3814	12.91	43.10	1.3736	9.290	1.3653	6.929
0.7206	1.3676	11.50	45.36	1.3600	8.343	1.3519	6.233
0.7004	1.3528	10.36	47.26	1.3453	7.606	1.3374	5.755
0.6800	1.3398	9.225	48.80	1.3325	6.796	1.3247	5.164
0.6594	1.3251	8.214	49.99	1.3165	6.106	1.3086	4.670
0.6403	1.3129	7.659	50.80	1.3060	5.727	1.2985	4.423
0.6195	1.2984	6.821	51.40	1.2917	5.130	1.2843	3.976
0.6001	1.2873	6.299	51.74	1.2807	4.757	1.2735	3.702
0.5796	1.2751	5.754	51.91	1.2685	4.364	1.2614	3.417
0.5604	1.2632	5.323	51.90	1.2568	4.069	1.2498	3.204
0.5406	1.2511	4.866	51.77	1.2451	3.728	1.2383	2.950
0.5203	1.2403	4.433	51.53	1.2343	3.394	1.2276	2.675
0.4998	1.2298	4.192	51.18	1.2240	3.247	1.2175	2.584
0.4804	1.2161	3.703	50.78	1.2105	2.867	1.2043	2.274
0.4605	1.2059	3.562	50.29	1.2004	2.782	1.1943	2.227
0.4399	1.1943	3.304	49.70	1.1891	2.597	1.1830	2.096
0.4202	1.1843	3.094	49.05	1.1791	2.420	1.1731	1.975
0.4000	1.1727	2.806	48.29	1.1675	2.200	1.1617	1.770
0.3805	1.1637	2.663	47.45	1.1588	2.104	1.1531	1.719
0.3599	1.1531	2.479	46.42	1.1484	1.972	1.1428	1.601
0.3385	1.1421	2.326	45.20	1.1372	1.847	1.1314	1.517
0.3196	1.1331	2.133	43.98	1.1287	1.689	1.1234	1.381
0.3002	1.1238	2.036	42.57	1.1195	1.632	1.1143	1.344
			$[C_{2(OH)}C_1Im][C_4F_9CO_2]$ + water				
		***T* = 298.15 K**		***T* = 308.15 K**		***T* = 318.15 K**	
1.0000	1.5413	712.8	0.3151	1.5312	351.3	1.5211	190.8
0.9825	1.5206	232.4	0.5299	1.5100	129.6	1.4988	78.31
0.9592	1.5070	131.5	0.9686	1.4966	77.34	1.4857	48.88
0.9395	1.4955	86.61	1.344	1.4853	52.77	1.4745	34.26
0.9200	1.4842	64.40	1.727	1.4741	40.16	1.4635	26.58
0.9007	1.4730	52.21	2.127	1.4631	33.08	1.4526	22.22
0.8805	1.4613	43.87	2.572	1.4515	28.19	1.4412	19.16
0.8585	1.4485	38.12	3.094	1.4389	24.75	1.4288	16.97
0.8189	1.4255	29.64	4.146	1.4162	19.60	1.4064	13.63
0.8018	1.4156	26.76	4.645	1.4064	17.82	1.3967	12.47
0.7789	1.4023	22.47	5.357	1.3933	15.15	1.3838	10.73
0.7598	1.3912	18.85	5.985	1.3824	12.87	1.3730	9.237
0.7217	1.3691	15.01	7.323	1.3605	10.41	1.3515	7.544
0.7000	1.3565	13.43	8.127	1.3481	9.392	1.3392	6.839
0.6789	1.3442	12.37	8.929	1.3360	8.651	1.3273	6.296
0.6592	1.3328	10.72	9.693	1.3247	7.605	1.3162	5.621
0.6415	1.3225	9.674	10.38	1.3146	6.914	1.3061	5.160
0.5997	1.2982	8.234	12.01	1.2906	5.966	1.2825	4.488
0.5811	1.2874	7.621	12.72	1.2800	5.553	1.2720	4.203
0.5611	1.2758	6.800	13.47	1.2685	4.999	1.2607	3.804
0.5405	1.2638	6.180	14.20	1.2567	4.566	1.2491	3.511
0.4997	1.2401	4.983	15.55	1.2333	3.718	1.2260	2.869
0.4793	1.2283	4.621	16.15	1.2217	3.496	1.2145	2.730
0.4591	1.2166	4.350	16.69	1.2101	3.301	1.2031	2.585
0.4189	1.1932	3.672	17.59	1.1870	2.804	1.1804	2.204
0.3988	1.1815	3.288	17.93	1.1755	2.546	1.1690	2.027
0.3800	1.1706	3.099	18.19	1.1648	2.403	1.1584	1.914
0.3416	1.1483	2.723	18.52	1.1427	2.129	1.1367	1.713

0.3015	1.1250	2.373	18.56	1.1197	1.881	1.1140	1.521
			$[C_2C_1Im][C_4F_9CO_2]$ + water				
		***T* = 298.15 K**		***T* = 308.15 K**		***T* = 318.15 K**	
1.0000	1.4868	107.5		1.4762	65.87	1.4659	43.09
0.9799	1.4651	73.58		1.4543	46.89	1.4429	31.80
0.9392	1.4438	36.29		1.4333	24.27	1.4223	17.06
0.8993	1.4229	25.20		1.4128	17.04	1.4020	12.16
0.8806	1.4131	22.43		1.4031	15.23	1.3925	10.88
0.8656	1.4052	20.95		1.3953	14.29	1.3848	10.22
0.8394	1.3915	17.94		1.3818	12.32	1.3715	8.849
0.8189	1.3808	16.31		1.3712	11.24	1.3610	8.101
0.8012	1.3716	14.99		1.3621	10.35	1.3521	7.473
0.7800	1.3605	13.63		1.3512	9.478	1.3413	6.882
0.7612	1.3506	12.96		1.3415	9.041	1.3317	6.582
0.6998	1.3185	10.41		1.3098	7.344	1.3004	5.402
0.6607	1.2981	8.377		1.2896	6.004	1.2806	4.498
0.6197	1.2766	7.229		1.2685	5.224	1.2597	3.927
0.5987	1.2656	6.836		1.2576	4.932	1.2490	3.698
0.5615	1.2461	5.963		1.2384	4.366	1.2301	3.348
0.5201	1.2244	5.301		1.2171	3.921	1.2090	3.013
0.4813	1.2042	4.618		1.1971	3.435	1.1893	2.639
0.4398	1.1824	3.860		1.1756	2.909	1.1682	2.271
0.3998	1.1615	3.365		1.1550	2.574	1.1478	2.036
0.3601	1.1408	2.877		1.1345	2.221	1.1276	1.773
0.3201	1.1198	2.586		1.1139	2.016	1.1073	1.616

In Figure 4.2.6a, the predicted density by soft-SAFT EoS (lines) shows a good agreement with experimental data, although the density is slightly overestimated in the concentration range 0.2-1.0 molar fraction of FIL (x_{FIL}). Though, the qualitative trend is well represented. It is important to stress that no fitting to the binary data was used, being the results a full prediction from the parameters adjusted to the pure FILs data. This empowers the modelling approach to predict other mixture conditions for which no experimental data are available. The calculations related to all ranges of temperatures are represented by the solid lines in Figures 4.2.7 and 4.2.8.

Two approaches were executed in the viscosity description of the FILs + water system using soft-SAFT + FVT [24,25]. Firstly, the Spider-Web methodology [28] (see Section 4.2.3.2) was used to reproduce the viscosity in all FILs composition ranges. However, the calculations did not show good agreement with the experimental data, as depicted in Figure 4.2.9, where the calculations for all FILs at 298.15 K are represented as an example. Looking at the tendency of the experimental data and the change of behaviour in the viscosity before and after a concentration of 0.2, x_{FIL} a second approach was used.

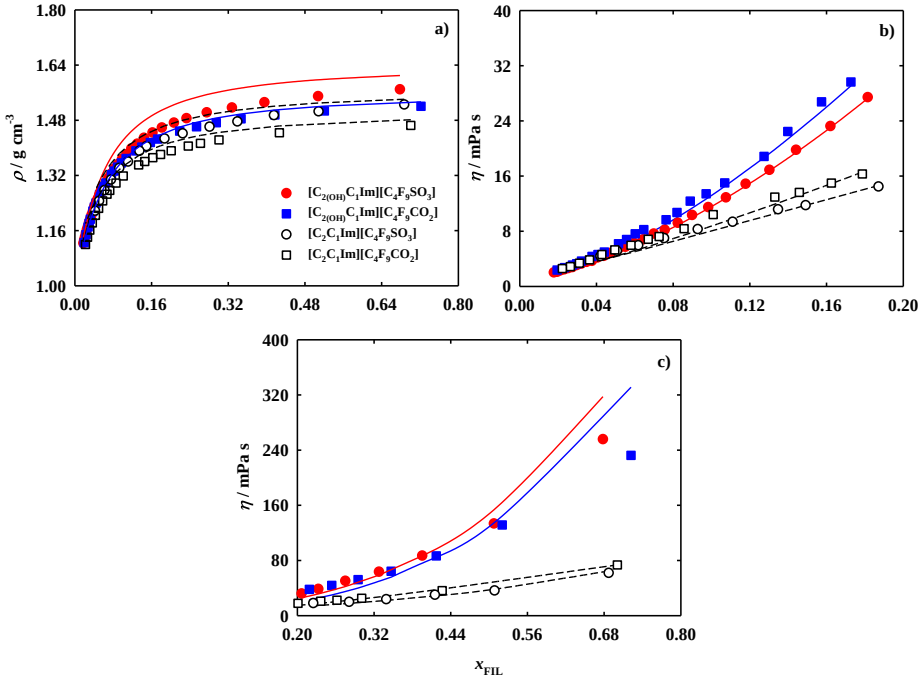

Figure 4.2.6 Density (a) and dynamic viscosity for the x_{FIL} range between 0 to 0.2 (b) and for the x_{FIL} range between 0.2 to 0.8 (c) versus FILs composition for the $[C_{2(OH)}C_1Im][C_4F_9SO_3]$, $[C_{2(OH)}C_1Im][C_4F_9CO_2]$ and $[C_2C_1Im][C_4F_9CO_2]$ determined in this work at 298.15 K, and for $[C_2C_1Im][C_4F_9SO_3]$ [50]. The lines represent the soft-SAFT + FVT calculations (solid lines for OH-FILs and dashed lines for analogous FILs).

The Spider-Web methodology was applied to optimize two sets of FVT parameters characterizing the ranges of 0-0.2 (Figure 4.2.6b) and 0.2-0.8 (Figure 4.2.6c) of x_{FIL} (see FVT parameters in Table 4.2.5). As a consequence, different values of L_v and B were obtained while the α parameter was the same for the whole range of composition for each FIL. The use of two different sets of parameters is not usually executed in the soft-SAFT + FVT approach, but it has been previously used for describing the VLE of water [29], to take into account the anomalous behaviour of the density at low temperatures. In this case, a similar procedure has been considered for the FTV part, as the nanosegregation (applicable to higher concentrations and pure FIL) [51] and the different structuration behaviour of the molecules in aqueous solutions (evident in the range of lower FIL compositions) [50] has a direct impact in the viscosity of the fluid. These structural changes can be considered neither by soft-SAFT theory nor by Free-Volume Theory approach, which are mean-field theories. Moreover, the very sharp decrease of the viscosity of the FILs after the addition of a few amounts of water, which is associated with the mentioned structural changes, is also difficult for the viscosity modelling of water + FILs systems. This highly non-ideal behaviour can hardly be captured by the FVT method, for the reasons already mentioned; more detailed molecular approaches, such as molecular simulations should be used, but they are out of the scope of the current work. As far as the predictive power of the equation is concerned, it is also important to mention that

the extension of the soft-SAFT FVT calculation to mixtures was done without the addition of any binary parameters for the viscosity. A change in the mixing rules, allowing the use of fitting binary parameters, can help to improve the description of aqueous systems [46] but this solution is more related to a less constrained model (with extra parameters) than including a physical interpretation of the behaviour of the mixture.

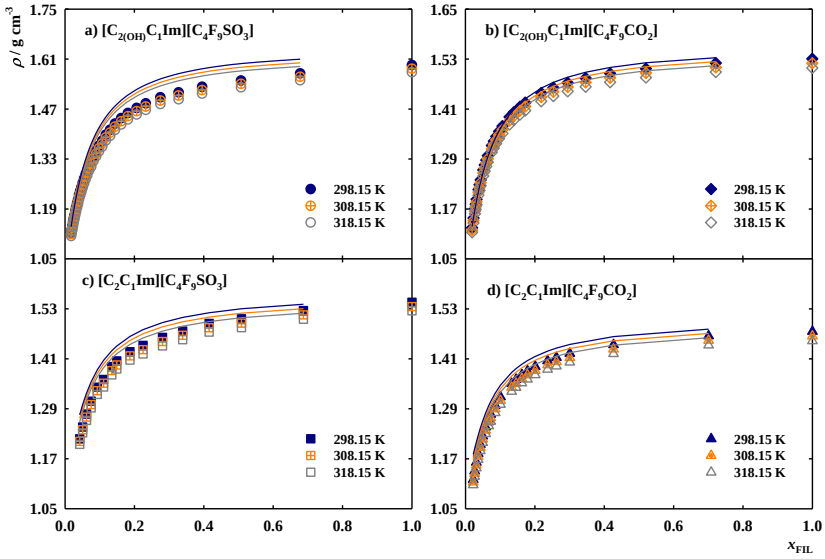

Figure 4.2.7 Density versus FILs composition for the $[C_{2(OH)}C_1Im][C_4F_9SO_3]$, $[C_{2(OH)}C_1Im][C_4F_9CO_2]$ and $[C_2C_1Im][C_4F_9CO_2]$ determined in this work, and for the $[C_2C_1Im][C_4F_9SO_3]$ which was former investigated [46]. Solid lines represent the soft-SAFT predictions.

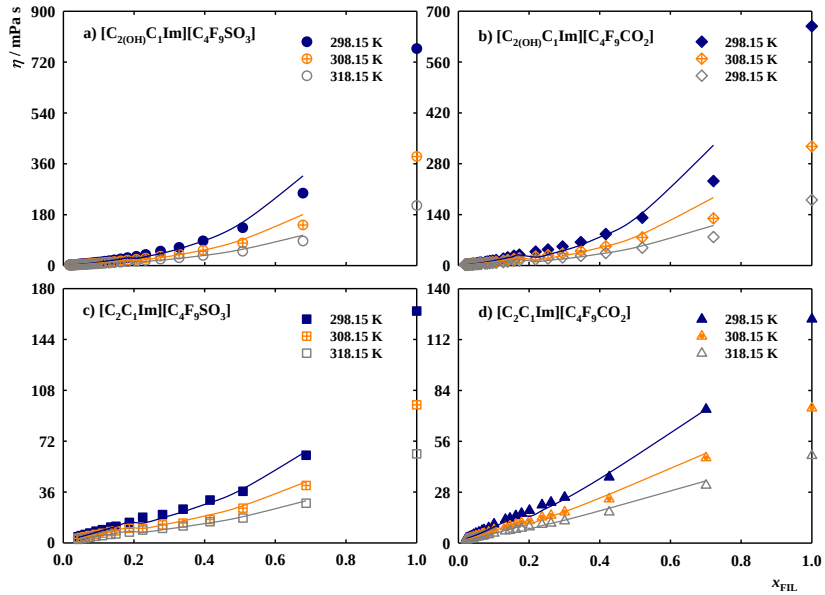

Figure 4.2.8 Dynamic viscosity versus FILs composition for the $[C_{2(OH)}C_1Im][C_4F_9SO_3]$, $[C_{2(OH)}C_1Im][C_4F_9CO_2]$ and $[C_2C_1Im][C_4F_9CO_2]$ determined in this work, and for the $[C_2C_1Im][C_4F_9SO_3]$ which was former investigated [46]. Solid lines represent the soft-SAFT calculations.

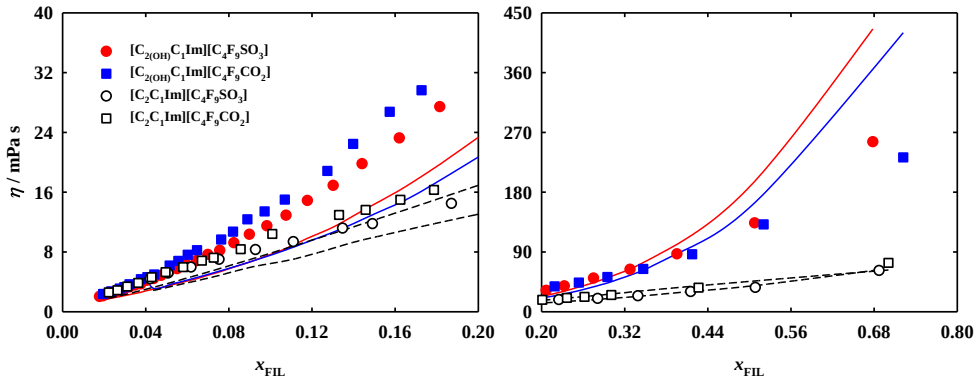

Figure 4.2.9 Dynamic viscosity versus FILs composition for the $[C_{2(OH)}C_1Im][C_4F_9SO_3]$, $[C_{2(OH)}C_1Im][C_4F_9CO_2]$ and $[C_2C_1Im][C_4F_9CO_2]$ at 298.15 K, and for the $[C_2C_1Im][C_4F_9SO_3]$ which was former investigated [50]. The lines represent the soft-SAFT + FVT calculations with a single set of FVT parameters for each mixture optimized for the whole range of compositions, which do not show a good agreement with the experimental data (solid lines for OH-FILs and dashed lines for analogous FILs).

The ionicity of FILs + water systems was obtained in the same way as for the pure systems (see "Walden plot" Section) and represented in Figure 4.2.10. Experimental data for OH-FILs + water ionic conductivity were determined (Table 4.2.7) and compared with the former $[C_2C_1Im][C_4F_9SO_3]$ + water system [50]. The experimental results show that all the three systems have a similar ionicity behaviour (similar vertical distance to the ideal electrolyte line along with each own profile) (Figure 4.2.10).

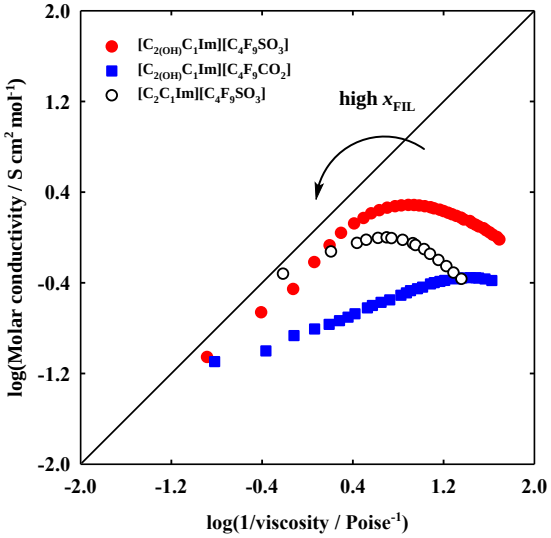

Figure 4.2.10 Walden plot of $[C_{2(OH)}C_1Im][C_4F_9SO_3]$ + water and $[C_{2(OH)}C_1Im][C_4F_9CO_2]$ + water binary systems at 298.15 K. For comparison purposes, the Walden plot of $[C_2C_1Im][C_4F_9SO_3]$ + water system was also included [50]. The arrow indicates the increment of the molar fraction of the FILs in solution.

Interestingly, an increment of ionicity from pure FIL until a maximum at a certain x_{FIL} value is observed. After this value, the ionicity starts to decrease when the x_{FIL} decreases. This

behaviour is more evident in the $[C_4F_9SO_3]$-FILs. The maximum can be related to the extremely high ionic conductivity that will be scrutinized in the next section. The addition of the hydroxyl group (comparing $[C_{2(OH)}C_1Im][C_4F_9SO_3]$ and $[C_2C_1Im][C_4F_9SO_3]$) decreases the "ideal" behaviour (more distance to the ideal electrolyte line) in the region of higher x_{FIL} and increases it in the lower x_{FIL}. Comparing both OH-FILs, the $[C_4F_9SO_3]^-$ anion shows values closer to the "ideal" electrolyte than $[C_4F_9CO_2]^-$. These results indicate the formation of distinct aggregates of FILs in the aqueous solutions. These outcomes will be further supported by the analysis of the complete conductivity profile and CACs of OH-FILs in the next section.

4.2.3.3.2 Critical aggregation concentrations

Amphiphilic molecules aggregate in aqueous solutions depending on the species and the medium. The formation of orientated colloidal aggregates occurs when the concentration of those species with long hydrophobic chains surpasses a certain value. This leads to variation in the physicochemical properties and the narrow ranges of concentrations are known as CACs. According to Philips et al. [52], the first CAC, known as critical micellar concentration (CMC), corresponds to the value of concentration in which a first maximum change in gradient appears when plotting ionic conductivity versus concentration. In this context, measurements of ionic conductivity are usually implemented in ionic micellar studies [50,53,54]. The ionic conductivity of FIL aqueous solutions was measured at 298.15 K for OH-FILs (Figure 4.2.11a) and compared with the analogous FILs [52]. The ionic conductivity data against x_{FIL} are illustrated in Figure 4.2.11a, where full miscibility in water is observed for the complete range of concentration (from pure water to pure FIL) of OH-FILs. Following Philips' definition, [52] already implemented in FILs [50,53,54], the CACs were determined, and values are reported in Table 4.2.8. The analysis of Figure 4.2.11a shows that the gradual addition of FIL to water presents similar tendencies as in the literature, exhibiting two phases: a first step in which the ionic conductivity increases, followed by a second step in which values decrease after reaching a maximum. This is the same behaviour found in the Walden Plots previously discussed. The mentioned increase in ionic conductivity in diluted systems can be explained by the rising number of free ions in the solution. However, at the CAC value, the number and mobility of charge carriers are reduced due to the increase in the aggregate formation and the decrease in fluidity, resulting in a deviation from the linear behaviour [50,53,54].

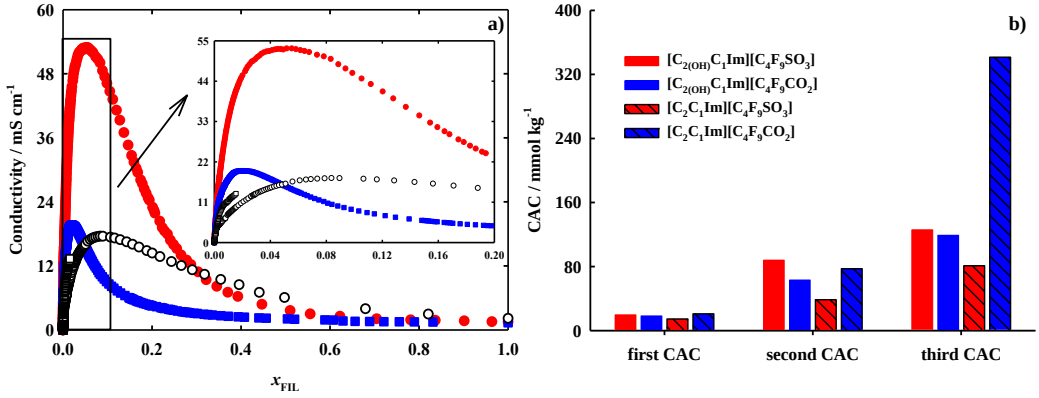

Figure 4.2.11 (a) Conductivity profile of $[C_{2(OH)}C_1Im][C_4F_9SO_3]$ (red, ●) and $[C_{2(OH)}C_1Im][C_4F_9CO_2]$ (blue, ■) in aqueous solution at 298.15 K, determined in this work, and for $[C_2C_1Im][C_4F_9SO_3]$ (black, ○) and $[C_2C_1Im][C_4F_9CO_2]$ (black, □) [52]. (b) Critical aggregation concentration (CAC) values of OH-FILs in aqueous solution at 298.15 K determined in this work and for analogous FILs [52].

Although all the studied FILs have multiple CACs, the most significant change in ionic conductivity behaviour occurs at lower values of x_{FIL}, corresponding to the CMC (Table 4.2.8). Two more transitions were determined at lower x_{FIL}, corresponding to second and third CACs (Table 4.2.8). The changes in the slopes of these plots were analysed according to Phillips definition [52], and compared with the bibliographic values of $[C_2C_1Im][C_4F_9SO_3]$ and $[C_2C_1Im][C_4F_9CO_2]$ [50] (Figure 4.2.11b and Table 4.2.8). The three CACs can be related to the FILs total miscibility in water, indicating the formation of different structures along with the increment of x_{FIL}, concluding that a low x_{FIL} is enough to assemble into colloidal aggregates. From the analysis of the influence of the FILs structural features in the CACs, it is shown in Figure 4.2.11b that the addition of a hydroxyl group: (i) does not significantly affect the CMC values; (ii) increases the second CAC on the case of $[C_4F_9SO_3]$-FILs while does not significantly affect that of the $[C_4F_9CO_2]$-FILs; and (iii) increases the third CAC of $[C_4F_9SO_3]$-FILs and decreases the value of $[C_4F_9CO_2]$-FILs. The $[C_2C_1Im][C_4F_9SO_3]$ shows the best self-aggregation behaviour, with lower values for all three CACs. All FILs studied, with only 4 carbon atoms in the anionic fluorinated tags, have an improved surfactant behaviour compared to the CMC values of the conventional perfluorosurfactants and their hydrogenated counterparts, with fluorine tags of 8 carbons (approximately 30 $mmol.kg^{-1}$ for sodium perfluorooctanoate and ammonium perfluorooctanoate and 380 $mmol.kg^{-1}$ for sodium octanoate) [55–57].

The degree of ionization of the aggregates, represented by α, can be found in Table 4.2.8. This parameter is associated with the charge fraction of the surfactant ions in the micelles, which suffer neutralization through the micelle-bound counterions. It is calculated by the ratio of the slopes of the linear segments above and below the CACs. Even if the surfactant ions are supposedly dissociated in aqueous solutions, the molecules are partly associated with the counterions, enabling the formation of aggregates [50,53]. Therefore, a

lower α value means an improved micelle packaging. Furthermore, the degree of counterion binding/condensed on the micellar surface was also determined, which derives from the degree of ionization as follows:

$$\beta = 1 - \alpha \qquad 4.2.15$$

This β parameter can be correlated with the charge density at the aggregate surface, the aggregate size, and the hydrophobic nature of the counterions.[2] The increment of α values, and consequently decrease of β values, in the first and third transitions (Table 4.2.8, comparison between $[C_{2(OH)}C_1Im][C_4F_9SO_3]$ and $[C_2C_1Im][C_4F_9SO_3]$) proves that the aggregates can lose the packaging in their structures because OH group increases the FILs polarity. The second transition does not have significant changes. This variation is observed in second and third transitions for $[C_{2(OH)}C_1Im][C_4F_9CO_2]$ and $[C_2C_1Im][C_4F_9CO_2]$. On the other hand, $[C_4F_9SO_3]^-$ anion has lower α and higher β values, indicating a better packaging (Table 4.2.8). The standard Gibbs free energy of aggregation, ΔG^0_{agg}, for the ionic surfactants were also determined in this study, and the values are reported in Table 4.2.8. The pseudophase model of micellization was considered by determining the standard Gibbs free energy, ΔG^0_{agg}, for the ionic surfactants by Equation 4.2.16 [58]:

$$\Delta G^0_{agg} = RT(1+\beta)\ln x_{CAC} \qquad 4.2.16$$

where R and T correspond to the universal gas constant and absolute temperature, respectively, and x_{CAC} is the critical aggregation concentration defined in terms of the molar fraction. This parameter stands for the free energy accounted in transferring one mole of surfactant from the aqueous solution to the micellar pseudophase in the aggregates form.[1] When the parameter values are negative, a spontaneous aggregation of the surfactant molecules happens. Furthermore, all OH-FILs show an improved surfactant behaviour compared to the conventional surfactants, demonstrating the possibility to decrease the FILs toxicity, and allowing biodegradability which is the key advantage to use OH-FILs in the biomedical field. All FILs, in all transitions, show that the aggregation behaviour is always spontaneous, with negative ΔG^0_{agg} values. More negative values were found for the non-functionalized FILs, especially for $[C_2C_1Im][C_4F_9SO_3]$, meaning an easy aggregation process for this IL.

Table 4.2.8 Critical aggregation concentrations, CACs, ionization degree, α, and Gibbs free energy of aggregation, ΔG^0_{agg}, of the fluorinated ionic liquids + water systems, determined by conductometry at 298.15 K.

		$[C_{2(OH)}C_1Im][C_4F_9SO_3]$	$[C_{2(OH)}C_1Im][C_4F_9CO_2]$	$[C_2C_1Im][C_4F_9SO_3]$[a]	$[C_2C_1Im][C_4F_9CO_2]$[b]
First CAC	x_{FIL}	0.0004	0.0003	0.0003	0.0004
	mmol·kg^{-1}	19.65	18.32	14.55	20.96
	α	0.91	0.79	0.79	0.87

Second CAC	ΔG^0_{agg} [kJ·mol^{-1}]	-21.4	-24.1	-24.7	-22.1
	x_{FIL}	0.0016	0.0012	0.0007	0.0014
	mmol·kg^{-1}	87.98	63.19	38.54	77.23
	α	0.85	0.80	0.84	0.71
Third CAC	ΔG^0_{agg} [kJ·mol^{-1}]	-18.2	-20.1	-20.8	-20.9
	x_{FIL}	0.0024	0.0022	0.0015	0.0070
	mmol·kg^{-1}	125.8	119.0	81.03	341.4
	α	0.79	0.55	0.29	0.37
Maximum	ΔG^0_{agg} [kJ·mol^{-1}]	-18.1	-21.9	-27.5	-20.0
	x_{FIL}	0.0509	0.0204	0.0867	–
	mmol·kg^{-1}	1312	797	1667	–

Parameters from (a) Pereiro, A.B. *et al.* (2015) and (b) Vieira, N.S.M. *et al.* (2019) [50,53].

4.2.4 Conclusions

The thermodynamic and thermophysical properties of hydroxyl functionalized FILs were determined in this work. Furthermore, the total miscibility and self-aggregation behaviour of OH-FILs + water systems were investigated. Results were compared with the analogous FILs, with the aim to evaluate the influence of adding a hydroxyl group to the structure of the imidazolium cation and how it affects FILs properties. The experimental study was completed with theoretical calculations of the density and viscosity of pure FILs and aqueous mixtures with the soft-SAFT EoS, using a set of transferable parameters in good agreement with the experimental data. This model will allow us to obtain other FILs properties that are not available experimentally.

Overall, the results show an increment in the density and viscosity of the pure OH-FILs and their aqueous mixtures with respect to the non-functionalized FILs, while a decrement in the thermal stability, melting temperature, free volume, ionicity and self-aggregation behaviour is noticed. However, when OH-FILs are compared with the conventional perfluorosurfactants, these novel compounds are of total miscibility in the aqueous systems and show a higher surfactant behaviour. Furthermore, the lower ecotoxicity associated with the increment of the polarity by adding the hydroxyl group to FILs structure can be advantageous for the use of these compounds.

4.3 References

1. Deetlefs, M.; Fanselow, M.; Seddon, K.R. Ionic Liquids: The View from Mount Improbable. *RSC Adv* **2016**, *6*, 4280–4288, doi:10.1039/C5RA05829E.
2. Egorova, K.S.; Gordeev, E.G.; Ananikov, V.P. Biological Activity of Ionic Liquids and Their Application in Pharmaceutics and Medicine. *Chem Rev* 2017, *117*, 7132–7189.
3. Ohno, H. Functional Design of Ionic Liquids. *Bull Chem Soc Jpn* **2006**, *79*, 1665–1680, doi:10.1246/bcsj.79.1665.
4. Vieira, N.S.M.; Stolte, S.; Araújo, J.M.M.; Rebelo, L.P.N.; Pereiro, A.B.; Markiewicz, M. Acute Aquatic Toxicity and Biodegradability of Fluorinated Ionic Liquids. *ACS Sustain Chem Eng* **2019**, *7*, 3733–3741, doi:10.1021/ACSSUSCHEMENG.8B03653.
5. Stolte, S.; Matzke, M.; Arning, J.; Böschen, A.; Pitner, W.R.; Welz-Biermann, U.; Jastorff, B.; Ranke, J. Effects of Different Head Groups and Functionalised Side Chains on the Aquatic Toxicity of Ionic Liquids. *Green Chemistry* **2007**, *9*, 1170–1179, doi:10.1039/B711119C.
6. Stolte, S.; Arning, J.; Bottin-Weber, U.; Müller, A.; Pitner, W.R.; Welz-Biermann, U.; Jastorff, B.; Ranke, J. Effects of Different Head Groups and Functionalised Side Chains on the Cytotoxicity of Ionic Liquids. *Green Chemistry* **2007**, *9*, 760–776, doi:10.1039/B615326G.
7. Coleman, D.; Gathergood, N. Biodegradation Studies of Ionic Liquids. *Chem Soc Rev* **2010**, *39*, 600–637, doi:10.1039/B817717C.
8. Krasovskiy, V.G.; Chernikova, E.A.; Glukhov, L.M.; Kapustin, G.I.; Koroteev, A.A. Effect of Hydroxyl Groups in a Cation Structure on the Properties of Ionic Liquids. *Russian Journal of Physical Chemistry A* **2018**, *92*, 2379–2385, doi:10.1134/S0036024418120245.
9. Liu, X.F.; Dong, L.L.; Fang, Y. Synthesis and Self-Aggregation of a Hydroxyl-Functionalized Imidazolium-Based Ionic Liquid Surfactant in Aqueous Solution. *J Surfactants Deterg* **2011**, *14*, 203–210, doi:10.1007/S11743-010-1234-3.
10. Zhang, S.; Qi, X.; Ma, X.; Lu, L.; Deng, Y. Hydroxyl Ionic Liquids: The Differentiating Effect of Hydroxyl on Polarity Due to Ionic Hydrogen Bonds between Hydroxyl and Anions. *Journal of Physical Chemistry B* **2010**, *114*, 3912–3920, doi:10.1021/JP911430T.
11. Fukumoto, K.; Yoshizawa, M.; Ohno, H. Room Temperature Ionic Liquids from 20 Natural Amino Acids. *J Am Chem Soc* **2005**, *127*, 2398–2399, doi:10.1021/JA043451I.
12. Araújo, J.M.M.; Florindo, C.; Pereiro, A.B.; Vieira, N.S.M.; Matias, A.A.; Duarte, C.M.M.; Rebelo, L.P.N.; Marrucho, I.M. Cholinium-Based Ionic Liquids with Pharmaceutically Active Anions. *RSC Adv* **2014**, *4*, 28126–28132, doi:10.1039/C3RA47615D.
13. Vieira, N.S.M.; Reis, P.M.; Shimizu, K.; Cortes, O.A.; Marrucho, I.M.; Araújo, J.M.M.; Esperança, J.M.S.S.; Lopes, J.N.C.; Pereiro, A.B.; Rebelo, L.P.N. A Thermophysical and Structural Characterization of Ionic Liquids with Alkyl and Perfluoroalkyl Side Chains. *RSC Adv* **2015**, *5*, 65337–65350, doi:10.1039/C5RA13869H.
14. Pereiro, A.B.; Araújo, J.M.M.; Oliveira, F.S.; Bernardes, C.E.S.; Esperança, J.M.S.S.; Canongia Lopes, J.N.; Marrucho, I.M.; Rebelo, L.P.N. Inorganic Salts in Purely Ionic Liquid Media: The Development of High Ionicity Ionic Liquids (HIILs). *Chemical Communications* **2012**, *48*, 3656, doi:10.1039/c2cc30374d.
15. Blas, F.J.; Vega, L.F. Thermodynamic Behaviour of Homonuclear and Heteronuclear Lennard-Jones Chains with Association Sites from Simulation and Theory. *Mol Phys* **1997**, *92*, 135–150, doi:10.1080/002689797170707.

16. Blas, F.J.; Vega, L.F. Prediction of Binary and Ternary Diagrams Using the Statistical Associating Fluid Theory (SAFT) Equation of State. *Ind Eng Chem Res* **1998**, *37*, 660–674, doi:10.1021/ie970449+.
17. Johnson, J.K.; Zollweg, J.A.; Gubbins, K.E. The Lennard-Jones Equation of State Revisited. *Mol Phys* **1993**, *78*, 591–618, doi:10.1080/00268979300100411.
18. Wertheim, M.S. Fluids with Highly Directional Attractive Forces. III. Multiple Attraction Sites. *J Stat Phys* **1986**, *42*, 459–476, doi:10.1007/BF01127721.
19. Wertheim, M.S. Fluids with Highly Directional Attractive Forces. IV. Equilibrium Polymerization. *J Stat Phys* **1986**, *42*, 477–492, doi:10.1007/BF01127722.
20. Wertheim, M.S. Fluids with Highly Directional Attractive Forces. II. Thermodynamic Perturbation Theory and Integral Equations. *J Stat Phys* **1984**, *35*, 35–47, doi:10.1007/BF01017363.
21. Wertheim, M.S. Fluids with Highly Directional Attractive Forces. I. Statistical Thermodynamics. *J Stat Phys* **1984**, *35*, 19–34, doi:10.1007/BF01017362.
22. Allal, A.; Moha-ouchane, M.; Boned, C. A New Free Volume Model for Dynamic Viscosity and Density of Dense Fluids Versus Pressure and Temperature. *Phys Chem Liquids* **2001**, *39*, 1–30, doi:10.1080/00319100108030323.
23. Allal, A.; Boned, C.; Baylaucq, A. Free-Volume Viscosity Model for Fluids in the Dense and Gaseous States. *Phys Rev E* **2001**, *64*, 011203, doi:10.1103/PhysRevE.64.011203.
24. Llovell, F.; Marcos, R.M.; Vega, L.F. Transport Properties of Mixtures by the Soft-SAFT + Free-Volume Theory: Application to Mixtures of n-Alkanes and Hydrofluorocarbons. *Journal of Physical Chemistry B* **2013**, *117*, 5195–5205, doi:10.1021/JP401754R.
25. Llovell, F.; Marcos, R.M.; Vega, L.F. Free-Volume Theory Coupled with Soft-SAFT for Viscosity Calculations: Comparison with Molecular Simulation and Experimental Data. *Journal of Physical Chemistry B* **2013**, *117*, 8159–8171, doi:10.1021/JP401307T.
26. mac Dowell, N.; Llovell, F.; Sun, N.; Hallett, J.P.; George, A.; Hunt, P.A.; Welton, T.; Simmons, B.A.; Vega, L.F. New Experimental Density Data and Soft-SAFT Models of Alkylimidazolium ([CnC1im]+) Chloride (Cl-), Methylsulfate ([MeSO4]-), and Dimethylphosphate ([Me 2PO4]-) Based Ionic Liquids. *Journal of Physical Chemistry B* **2014**, *118*, 6206–6221, doi:10.1021/JP501619Y.
27. Doolittle, A.K. Studies in Newtonian Flow. II. The Dependence of the Viscosity of Liquids on Free-Space. *J Appl Phys* **1951**, *22*, 1471–1475, doi:10.1063/1.1699894.
28. Cané, E.; Llovell, F.; Vega, L.F. Accurate Viscosity Predictions of Linear Polymers from N-Alkanes Data. *J Mol Liq* **2017**, *243*, 115–123, doi:10.1016/j.molliq.2017.08.033.
29. Vega, L.F.; Llovell, F.; Blas, F.J. Capturing the Solubility Minima of N-Alkanes in Water by Soft-SAFT. *Journal of Physical Chemistry B* **2009**, *113*, 7621–7630, doi:10.1021/JP9018876.
30. Pereiro, A.B.; Llovell, F.; Araújo, J.M.M.; Santos, A.S.S.; Rebelo, L.P.N.; Piñeiro, M.M.; Vega, L.F. Thermophysical Characterization of Ionic Liquids Based on the Perfluorobutanesulfonate Anion: Experimental and Soft-SAFT Modeling Results. *ChemPhysChem* **2017**, *18*, 2012–2023, doi:10.1002/CPHC.201700327.
31. Ferreira, M.L.; Llovell, F.; Vega, L.F.; Pereiro, A.B.; Araújo, J.M.M. Systematic Study of the Influence of the Molecular Structure of Fluorinated Ionic Liquids on the Solubilization of Atmospheric Gases Using a Soft-SAFT Based Approach. *J Mol Liq* **2019**, *294*, doi:10.1016/j.molliq.2019.111645.
32. Llovell, F.; Valente, E.; Vilaseca, O.; Vega, L.F. Modeling Complex Associating Mixtures with [Cn-Mim][Tf 2N] Ionic Liquids: Predictions from the Soft-SAFT Equation. *Journal of Physical Chemistry B* **2011**, *115*, 4387–4398, doi:10.1021/JP112315B.

33. Oliveira, M.B.; Llovell, F.; Coutinho, J.A.P.; Vega, L.F. Modeling the [NTf2] Pyridinium Ionic Liquids Family and Their Mixtures with the Soft Statistical Associating Fluid Theory Equation of State. *Journal of Physical Chemistry B* **2012**, *116*, 9089–9100, doi:10.1021/JP303166F.
34. Oliveira, M.B.; Crespo, E.A.; Llovell, F.; Vega, L.F.; Coutinho, J.A.P. Modeling the Vapor–Liquid Equilibria and Water Activity Coefficients of Alternative Refrigerant-Absorbent Ionic Liquid–Water Pairs for Absorption Systems. *Fluid Phase Equilib* **2016**, *426*, 100–109, doi:10.1016/j.fluid.2016.02.017.
35. Llovell, F.; Vega, L.F. Assessing Ionic Liquids Experimental Data Using Molecular Modeling: [Cnmim][BF4] Case Study. *J Chem Eng Data* **2014**, *59*, 3220–3231, doi:10.1021/JE5002472.
36. Urahata, S.M.; Ribeiro, M.C.C. Structure of Ionic Liquids of 1-Alkyl-3-Methylimidazolium Cations: A Systematic Computer Simulation Study. *Journal of Chemical Physics* **2004**, *120*, 1855–1863, doi:10.1063/1.1635356.
37. Morrow, T.I.; Maginn, E.J. Molecular Dynamics Study of the Ionic Liquid 1-n-Butyl-3-Methylimidazolium Hexafluorophosphate. *Journal of Physical Chemistry B* **2002**, *106*, 12807–12813, doi:10.1021/JP0267003.
38. del Pópolo, M.G.; Voth, G.A. On the Structure and Dynamics of Ionic Liquids. *Journal of Physical Chemistry B* **2004**, *108*, 1744–1752, doi:10.1021/JP0364699.
39. Ferreira, M.L.; Araújo, J.M.M.; Pereiro, A.B.; Vega, L.F. Insights into the Influence of the Molecular Structures of Fluorinated Ionic Liquids on Their Thermophysical Properties. A Soft-SAFT Based Approach. *Physical Chemistry Chemical Physics* **2019**, *21*, doi:10.1039/c8cp07522k.
40. Halgren, T.A. MMFF VII. Characterization of MMFF94, MMFF94s, and Other Widely Available Force Fields for Conformational Energies and for Intermolecular-Interaction Energies and Geometries. *J Comput Chem* **1999**, *20*, 730–748, doi:10.1002/(SICI)1096-987X(199905)20:7<730::AID-JCC8>3.0.CO;2-T.
41. Hanwell, M.D.; Curtis, D.E.; Lonie, D.C.; Vandermeerschd, T.; Zurek, E.; Hutchison, G.R. Avogadro: An Advanced Semantic Chemical Editor, Visualization, and Analysis Platform. *J Cheminform* **2012**, *4*, doi:10.1186/1758-2946-4-17.
42. Pàmies, J.P. Bulk and Interfacial Properties of Chain Fluids: A Molecular Modelling Approach., Universitat Rovira i Virgili: Tarragona, Spain, 2004.
43. Zhang, S.; Sun, N.; He, X.; Lu, X.; Zhang, X. Physical Properties of Ionic Liquids: Database and Evaluation. *J Phys Chem Ref Data* 2006, *35*, 1475–1517.
44. Tariq, M.; Forte, P.A.S.; Gomes, M.F.C.; Lopes, J.N.C.; Rebelo, L.P.N. Densities and Refractive Indices of Imidazolium- and Phosphonium-Based Ionic Liquids: Effect of Temperature, Alkyl Chain Length, and Anion. *Journal of Chemical Thermodynamics* **2009**, *41*, 790–798, doi:10.1016/j.jct.2009.01.012.
45. Vieira, N.S.M.; Luís, A.; Reis, P.M.; Carvalho, P.J.; Lopes-Da-Silva, J.A.; Esperança, J.M.S.S.; Araújo, J.M.M.; Rebelo, L.P.N.; Freire, M.G.; Pereiro, A.B. Fluorination Effects on the Thermodynamic, Thermophysical and Surface Properties of Ionic Liquids. *Journal of Chemical Thermodynamics* **2016**, *97*, 354–361, doi:10.1016/j.jct.2016.02.013.
46. Llovell, F.; Vilaseca, O.; Jung, N.; Vega, L.F. Water+1-Alkanol Systems: Modeling the Phase, Interface and Viscosity Properties. *Fluid Phase Equilib* **2013**, *360*, 367–378, doi:10.1016/j.fluid.2013.10.002.
47. May, E.F. Measurement of the Thermodynamic Properties of Single Phases. IUPAC Experimental Thermodynamics, Volume VI. Edited by A. R. H. Goodwin, K. N. Marsh, and W. A. Wakeham. Elsevier: Amsterdam, The Netherlands, 2003. 558 Pp. $US 230. ISBN 0-444-50931-3. *J Chem Eng Data* **2007**, *52*, 662–663, doi:10.1021/je600558y.

48. Deetlefs, M.; Seddon, K.R.; Shara, M. Predicting Physical Properties of Ionic Liquids. *Phys. Chem. Chem. Phys.* **2006**, *8*, 642–649, doi:10.1039/B513453F.
49. Iglesias-Otero, M.A.; Troncoso, J.; Carballo, E.; Romaní, L. Density and Refractive Index in Mixtures of Ionic Liquids and Organic Solvents: Correlations and Predictions. *J Chem Thermodyn* **2008**, *40*, 949–956, doi:10.1016/j.jct.2008.01.023.
50. Pereiro, A.B.; Araújo, J.M.M.; Teixeira, F.S.; Marrucho, I.M.; Piñeiro, M.M.; Rebelo, L.P.N. Aggregation Behavior and Total Miscibility of Fluorinated Ionic Liquids in Water. *Langmuir* **2015**, *31*, 1283–1295, doi:10.1021/LA503961H.
51. Ferreira, M.L.; Pastoriza-Gallego, M.J.; Araújo, J.M.M.; Canongia Lopes, J.N.; Rebelo, L.P.N.; M Piñeiro, M.; Shimizu, K.; Pereiro, A.B. Influence of Nanosegregation on the Phase Behavior of Fluorinated Ionic Liquids. *Journal of Physical Chemistry C* **2017**, *121*, doi:10.1021/acs.jpcc.7b00516.
52. Phillips, J.N. The Energetics of Micelle Formation. *Transactions of the Faraday Society* **1955**, *51*, 561–569, doi:10.1039/TF9555100561.
53. Vieira, N.S.M.; Bastos, J.C.; Hermida-Merino, C.; Pastoriza-Gallego, M.J.; Rebelo, L.P.N.; Piñeiro, M.M.; Araújo, J.M.M.; Pereiro, A.B. Aggregation and Phase Equilibria of Fluorinated Ionic Liquids. *J Mol Liq* **2019**, *285*, 386–396, doi:10.1016/j.molliq.2019.04.086.
54. Teixeira, F.S.; Vieira, N.S.M.; Cortes, O.A.; Araújo, J.M.M.; Marrucho, I.M.; Rebelo, L.P.N.; Pereiro, A.B. Phase Equilibria and Surfactant Behavior of Fluorinated Ionic Liquids with Water. *Journal of Chemical Thermodynamics* **2015**, *82*, 99–107, doi:10.1016/j.jct.2014.10.021.
55. Szajdzinska-Pietek, E.; Wolszczak, M. Time-Resolved Fluorescence Quenching Study of Aqueous Solutions of Perfluorinated Surfactants with the Use of Protiated Luminophore and Quencher. *Langmuir* **2000**, *16*, 1675–1680, doi:10.1021/LA990981X.
56. González-Pérez, A.; Ruso, J.M.; Prieto, G.; Sarmiento, F. Apparent Molar Quantities of Sodium Octanoate in Aqueous Solutions. *Colloid Polym Sci* **2004**, *282*, 1133–1139, doi:10.1007/S00396-003-1047-2.
57. López-Fontán, J.L.; Sarmiento, F.; Schulz, P.C. The Aggregation of Sodium Perfluorooctanoate in Water. *Colloid Polym Sci* **2005**, *283*, 862–871, doi:10.1007/S00396-004-1228-7.
58. Zana, R. Critical Micellization Concentration of Surfactants in Aqueous Solution and Free Energy of Micellization. *Langmuir* **1996**, *12*, 1208–1211, doi:10.1021/LA950691Q.

CHAPTER 5

SOLUBILITY, STABILITY, AND INTERACTION OF PROTEINS WITH FLUORINATED IONIC LIQUIDS

5.1 Introduction

Proteins are macromolecules involved in the most complex processes of living organisms with a high impact on clinical, biomedical, chemical, pharmaceutical, food, cosmetic, textile, and other industries [1–4]. On one hand, protein extraction and purification processes are imperative to enable the analysis of protein individual characteristics such as size, shape, charge, polarity, and function, allowing its application with high levels of purity. However, protein application is hampered by the difficulty in preserving their structural integrity, governed by the fragile equilibrium of disulfide bridges, hydrogen bonds, ionic, and hydrophobic interactions. The minimal variation in their microenvironment, either due to fluctuations in the solvent conditions or the presence of other compounds, can disrupt this delicate balance and affect the protein stability and activity, hindering its usage [5–8]. Therefore, it is impossible to define an ideal system for protein extraction and purification and each process must be studied case by case, which makes the development of new protein-based products a time and cost-consuming task.

On the other hand, in the last decades, the pharmaceutical industry experienced remarkable exponential growth in the approval of new biological therapeutical entities, while the development of traditional small drugs has reached a stagnated phase. The prospect of having biological products for therapeutic endings has revolutionized drug discovery and development, opening unprecedented avenues of research for biopharmaceuticals. These compounds have contributed to the diagnosis and treatment of several diseases where conventional therapies have constantly failed, such as numerous cancers, immune, autoimmune, infections and metabolic diseases, Alzheimer's, HIV, and Parkinson's, along with others [9–12]. Among biopharmaceuticals, therapeutic proteins arise with a vast availability, specific action mode, and impressive characteristics such as high specificity, safety, tolerability, efficiency, and a low prospect of unspecific and drug-drug interaction. These properties made them unique compounds to formulate a huge number of therapeutic protein-based treatments with regulatory and special targeting activity, vaccines, and diagnostics. However, their application in the pharmaceutical industry is limited by their intrinsic properties. Therapeutic proteins are very sensitive to: (i) alterations in the conformation of the structure; (ii) interactions with the excipients on the formulation; (iii) impurities from the process of manufacture; (iv) the storage conditions that can cause degradation or aggregation; (v) the dosage and time needed for therapeutic effect; (vi) the route of administration; and (vii) the genetic characteristics of the patient [13–15]. All these factors hamper the *in vivo* delivery of therapeutic proteins and make them chemical and physically unstable compounds with a short half-life in the bloodstream and consequently

poor bioavailability. This handicap is commonly compensated by the administration of regular dosages or higher amounts of the drug to obtain a therapeutic effect. However, the prolonged exposition to the biopharmaceutical combined with the increased dosages and sensitivity problems outcomes in significant adverse side effects, toxicity, and immunogenicity [16–18]. To overcome these complications, the development of efficient strategies to extend the half-life of therapeutic proteins through the administration routes has been in the spotlight of research. From those strategies, significant advances have been attained using drug delivery systems (DDSs) that aid the control of stability and release of the therapeutic proteins, protecting and maintaining their activity, improving their bioavailability, and guaranteeing their safety. Amongst the different types of DDSs that have been developed, nanocarriers found a ground place as promising tools to circumvent those challenges. They have been demonstrated to be non-invasive, safe, and targeted delivery methods. However, there are still concerns from a biological and technological point of view that limit the usage of these systems, such as low stability, uncontrolled release of proteins, low encapsulation efficiency, expensive costs associated with the formulation and production of these systems, and difficulties on the scale-up of the process. Thus, even though some DDSs are already available in the market, there are still no nanocarriers fully effective and profitable [17,19–23].

FILs have augmented solubilization mechanisms due to their rich aggregation behaviour, and self-assembling in stable structures by means of their amphiphilic character, which can aid their performance as efficient materials for protein extraction, purification and delivery. In this chapter, it was studied the potential of using FILs in protein applications by exploring the protein-FIL interactions and understanding their effect on the solubility, stability, and activity of the proteins, aiming to aid the selection of the best FILs for these biological applications. To a deeper understanding of the self-aggregation behaviour of FILs and how it can be advantageous for protein applications, the first section of this chapter is focused on the determination of the diffusion coefficients of FILs using NMR techniques, obtaining new information on the size and structure of the different aggregates in the complete array of concentration with water. Therefore, the B1 immunoglobulin binding domain of streptococcal protein G, *Bacillus subtilis* lipase A, and interferon-alpha 2b were selected to study the interactions between protein-FIL. From a broad screening of FILs, it was possible to have insights into the structural features contributing to the interaction with the three proteins.

In the second section, the influence of FILs on the stability and activity of a model protein, the lysozyme, was under investigation. For that, firstly, the cytotoxicity of some FILs was tested to evaluate their biocompatibility. Therefore, the interactions lysozyme-FILs and the effect of FILs on the stability and activity of the protein were studied concluding that: (i)

the pre-dominant lysozyme-FIL interaction is the encapsulation of the protein by the self-assembled aggregates of FILs, (ii) the encapsulation efficiency highly depends on the concentration and anion of FIL, and (iii) the encapsulated lysozyme keeps its activity and thermal stability.

To understand the complex protein-FIL interactions and how they depend on the protein characteristics, it was selected a therapeutic protein, the interferon-alpha 2b (IFN-α 2b) which is used for the treatment of cancer, viral infections, and auto-immune diseases. Therefore, the influence of IFN-α 2b in the aggregation behaviour of FILs and the interactions between them were investigated. The results show that the presence of IFN-α 2b influences the aggregation behaviour of FILs and strong interactions between the two compounds occur. IFN-α 2b does not seem to be fully encapsulated by the FILs, as in the previous case. However, the FIL carries IFN-α 2b by the formation of a conjugate that prevents the aggregation of this protein.

This chapter constitutes an important step toward the design and development of FIL-based delivery systems for therapeutic proteins. Furthermore, the results demonstrated the key requirement of individual studies for each type of FIL and protein. The interactions between protein-FIL can be very different and are highly dependent on the properties of the protein.

The chapter is adapted from the following contributions:

Section 5.2

Margarida L. Ferreira, Ana S.D. Ferreira, João M.M. Araújo, Eurico J. Cabrita, Ana B. Pereiro, The impact of fluorinated ionic liquids aggregation in the interactions with proteins, *Fluid Phase Equilibria* 559 (2022) 113488. DOI: 10.1016/j.fluid.2022.113488

Section 5.3

Margarida L. Ferreira, Nicole S.M. Vieira, João M.M. Araújo, Ana B. Pereiro, Unveiling the Influence of Non-toxic Fluorinated Ionic Liquids Aqueous Solutions in the Encapsulation and Stability of Lysozyme, *Sustainable Chemistry* 2 (2021) 149-166. DOI: 10.3390/suschem20100101

Section 5.4

Margarida L. Ferreira, Nicole S.M. Vieira, Ana L.S. Oliveira, João M.M. Araújo, Ana B. Pereiro, Disclosing the potential of fluorinated ionic liquids as interferon-alpha 2b delivery systems, *Nanomaterials* 12 (2022) 1851. DOI: 10.3390/nano12111851

In this work, the author of this thesis has acquired part of the experimental data (except the assays of conductivity of the systems with simulated biological fluids, the STEM with EDS, the DLS and CD spectra) and has written the complete original draft of the manuscript.

5.2 The impact of fluorinated ionic liquids aggregation in the interactions with proteins

In this section we aim to gain a deeper molecular insight into the aggregation behaviour of FILs and how it affects their interactions with proteins, using NMR spectroscopy as the main research tool. We have selected the B1 immunoglobulin binding domain of streptococcal protein G (GB1), *Bacillus subtilis* lipase A (BSLA), and interferon-alpha 2b (IFN-α 2b) as protein models to study their interactions with FILs. GB1 is a highly soluble and stable protein, broadly used in NMR studies and a good model to study protein stability [24,25]. In fact, a recent work regarding ILs and GB1 by HR-MAS NMR using $[C_4C_1Im]Br$ showed that the IL strongly interacted with the α-helical region of this protein [26]. BSLA is a very well-known model protein for the study of lipase mediated biocatalytic processes since it can be easily site-directed mutagenesis engineered to have improved thermostability and catalytic activity in ILs [27–36]. To our knowledge, only two papers report the study of BSLA-ILs interactions but with a very restricted group of ILs and none using surfactant ILs [37,38]. Our final model protein, IFN-α 2b, has antiproliferative, immunomodulation, and antiviral biological activities, being recognized for the treatment of several diseases [39]. This protein has been studied concerning the use of ILs for purification purposes, namely the use of ILs in aqueous two-phase extraction systems, producing high yields of pure protein with low ILs concentration [40].

Since the solubilization power of FILs is related to the presence of different self-assembled structures we have determined the self-diffusion coefficients of one FIL, $[C_2C_1Im][C_4F_9SO_3]$, in the entire range of concentrations in water, to characterize their aggregation behaviour. The results showed valuable information on the hydrodynamic radius of this FIL and its variation when its aggregation behaviour is changed. The interactions of FILs with GB1, BSLA, and IFN-α 2b were also screened to understand if the proteins complex with FILs aggregates. This work discloses the importance of screening protein-IL interactions to identify which structural features of FILs are favourable to those interactions.

5.2.1 Experimental section

5.2.1.1 Materials

1-Ethyl-3-methylimidazolium perfluorobutanesulfonate, $[C_2C_1Im][C_4F_9SO_3]$, ≥97% mass fraction purity; 1-ethyl-3-methylpyridinium perfluorobutanesulfonate, $[C_2C_1py][C_4F_9SO_3]$, 99% mass fraction purity; (2-hydroxyethyl)trimethylammonium perfluorobutanesulfonate, $[N_{1112(OH)}][C_4F_9SO_3]$, >97% mass fraction purity;

tetrabutylammonium perfluorobutanesulfonate, $[N_{4444}][C_4F_9SO_3]$, >98% mass fraction purity; 1-hexyl-3-methylimidazolium perfluorobutanesulfonate, $[C_6C_1Im][C_4F_9SO_3]$, >99% mass fraction purity; 1-methyl-3-octylimidazolium perfluorobutanesulfonate, $[C_8C_1Im][C_4F_9SO_3]$, >99% mass fraction purity and 1-butyl-1-methylpyrrolidinium perfluorobutanesulfonate, $[C_4C_1pyr][C_4F_9SO_3]$, >98% mass fraction purity were provided by IoLiTec GmbH (Heilbronn, Germany). 1-Ethyl-3-methylimidazolium perfluoropentanoate, $[C_2C_1Im][C_4F_9CO_2]$; 1-ethyl-3-methylpyridinium perfluoropentanoate, $[C_2C_1py][C_4F_9CO_2]$; (2-hydroxyethyl)trimethylammonium perfluoropentanoate $[N_{1112(OH)}][C_4F_9CO_2]$; 1-(2-hydroxyethyl)-3-methylimidazolium perfluoropentanoate, $[C_{2(OH)}C_1Im][C_4F_9CO_2]$; 1-(2-hydroxyethyl)-3-methylimidazolium perfluorobutanesulfonate, $[C_{2(OH)}C_1Im][C_4F_9SO_3]$; and tetrabutylphosphonium perfluorobutanesulfonate $[P_{4444}][C_4F_9SO_3]$ were synthesized with a mass fraction purity of ≥98% by the ion exchange resin method previously developed by Fukumoto *et al*. [41] and routinely employed to these FILs [42,43]. The structures and nomenclatures of the FILs are represented in Table 5.2.1. The purity of both commercial and synthesized FILs structure was confirmed by ^1H and ^{19}F NMR and the synthesized FILs were also characterized by elemental analysis. All FILs were dried under vigorous stirring and vacuum (4 Pa) for at least 48 hours at 323.15 K before its usage to assure the complete elimination of any volatile compound remaining from the synthesis procedure. A water content lower than 100 ppm was confirmed by Karl Fisher coulometric titration (Metrohm 831 KF Coulometer) for all FILs.

For the NMR experiments deuterated dimethyl sulfoxide (DMSO-d6), 99,8% D, supplied by Eurisotop, Cambridge Isotope Laboratories, Inc. (Tewksbury, MA, USA), and Milli Q water, provided by the in-house laboratory facilities were used.

The protein assays were performed in Milli Q water and/or in buffers using sodium dihydrogen phosphate anhydrous (NaH_2PO_4, purity ≥99.0%) from Fluka, Honeywell (Charlotte, NC, USA) and sodium acetate anhydrous ($NaH_3C_2O_2$, purity ≥ 99.0%) from Riedel-de-Häen, Honeywell (Charlotte, North Carolina, US). Interferon-alpha 2b, human recombinant, (IFN-α 2b; SRP4595) expressed in *E. coli*, (purity ≥ 98% by SDS-PAGE and HPLC) was supplied by Sigma-Aldrich (Saint Louis, MO, USA). The BCA™ and Micro BCA™ Protein Assay Kits purchased from Thermo Fisher Scientific (Waltham, MA, USA) were used for protein quantification assays. The B1 immunoglobulin binding domain of streptococcal protein G (GB1) and *Bacillus subtilis* Lipase A (BSLA) were expressed and purified by the following methodologies.

Table 5.2.1 Nomenclature and chemical structure of the cations and anions of the fluorinated ionic liquids studied in this work.

Cations	
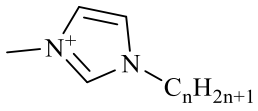 1-Alkyl-3-methylimidazolium $[C_nC_1Im]^+$, n = 2, 6, 8	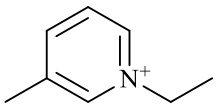 1-Ethyl-3-methylpyridinium $[C_2C_1py]^+$
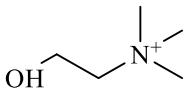 (2-Hydroxyethyl)trimethylammonium $[N_{1112(OH)}]^+$	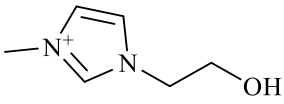 1-(2-Hydroxyethyl)-3-methylimidazolium $[C_{2(OH)}C_1Im]^+$
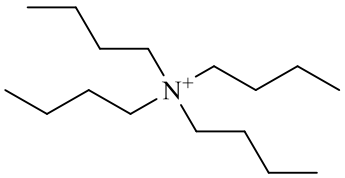 Tetrabutylammonium $[N_{4444}]^+$	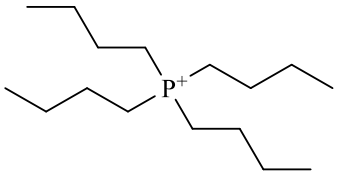 Tetrabutylphosphonium $[P_{4444}]^+$
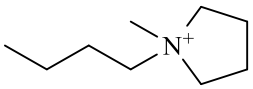 1-butyl-1-methylpyrrolidinium $[C_4C_1pyr]^+$	
Anions	
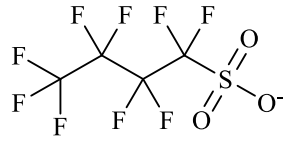 Perfluorobutanesulfonate $[C_4F_9SO_3]^-$	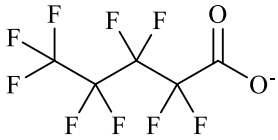 Perfluoropentanoate $[C_4F_9CO_2]^-$

5.2.1.1.1 Heterologous expression and purification of B1 immunoglobulin binding domain of streptococcal protein G

GB1 was expressed and purified similar to the previously described protocol [25]. Briefly, transformed BL21 (DE3) *Escherichia coli* cells were grown and subsequently induced with 0.5 mM isopropyl β-D-1thiogalactopyranoside (IPTG) for approximately 3 hours (until OD_{600}=0.7) in LB containing ampicillin (100 µg/mL) at 37° and 180 rpm. The cells were collected by centrifugation at 6000 rpm for 12 minutes at 4°C. The cells were resuspended in the lysis buffer (10 mM Tris-HCl, 1 mM EDTA, pH 7.5) preheated at 80°C, and left to stabilize at the same temperature for 5 minutes. The lysed cells were cooled in ice and centrifuged at 15 500 rpm for 30 minutes at 4°C. The supernatant was dialyzed (SnakeSkin™, Thermo Scientific, MWCO=3.5 KDa) overnight against 20 mM Tris-HCl, pH 7.5. The dialysed supernatant was purified via anion exchange chromatography using a HiTrap™ (GE Healthcare) and an ÄKTA start protein purification system (GE Healthcare). GB1 was eluted using 20 mM Tris-HCl, 1 M,

pH 7.5 to create a linear gradient of 0 – 400 mM NaCl. Fractions containing the protein were pooled and concentrated in a 3-kDa cut-off ultrafiltration unit (Amicon® Ultra, Merck Millipore) at 5000 rpm at 4ºC. The sample was further purified by size exclusion chromatography (Superdex® 75 10/300 GL column, GE Healthcare) using 20 mM potassium phosphate, 50 mM NaCl, and pH 6.0 as running buffer. The fractions containing protein were pooled and dialyzed against Milli-Q water, frozen and lyophilized.

5.2.1.1.2 Heterologous expression and purification of Bacillus Subtilis Lipase A

The pET21b plasmid vector encoding the BSLA was kindly provided by Prof. Joel Kaar (Colorado University, Boulder, USA). The BSLA with a C-terminal polyhistidine tag was expressed in BL21 DE3 *Escherichia coli* competent cells. The transformed cells were plated on agar containing ampicillin (50 µg/mL) and subsequently expressed following the protocol described by Weltz *et al*. After expression, the cells were harvested by centrifugation at 10 000 rpm for 10 min at 4ºC, resuspended in 50 mM sodium phosphate buffer (pH 7.5), 100 mM NaCl, 5 mM imidazole and 8 M urea and sonicated. The cellular debris was removed by centrifugation 11 000 rpm. The cell lysate was purified by anion exchange chromatography using a nickel affinity column (HiTrap™, GE Healthcare) and an ÄKTA start protein purification system (GE Healthcare). The protein was refolded on-column before linear gradient elution with 50 mM sodium phosphate (pH 7.5), 100 mM NaCl, 350 mM imidazole. Fractions containing BSLA were dialyzed overnight (SnakeSkin™, Thermo Scientific MWCO=3.5 kDa) against 50 mM sodium phosphate, pH 7.50, before concentration in a 7-kDa cut-off ultrafiltration unit (Amicon® Ultra, Merck Millipore) 5000 rpm at 4ºC until a final concentration of 0.7 mg/mL.

5.2.1.2 Nuclear magnetic resonance experiments

The NMR experiments of neat $[C_2C_1Im][C_4F_9SO_3]$ and its aqueous solutions were performed at 298 K using a Bruker Avance III 400 operating at 400.15 MHz for ^{1}H and 376.54 MHz for ^{19}F. The NMR was equipped with two distinct probes: (i) a 5-mm high-resolution BBO probe used for acquisition of ^{1}H and ^{19}F 1D spectra and HOESY experiments and (ii) a diffusion probe Bruker DiffBB to perform the diffusions assays. The probes can generate magnetic field pulsed gradients in the *z*-axis up to 0.54 Tm^{-1} and 17 Tm^{-1}, respectively. Different aqueous $[C_2C_1Im][C_4F_9SO_3]$ solutions were studied in this work, with concentrations chosen according to the critical aggregation concentrations previously determined for this FIL [44]. The solutions were prepared in Milli-Q water and the concentrations are detailed in Table 5.2.2, ranging from the neat FIL to infinite dilution. Subsequently, 0.5 mL of the solutions were

transferred to 5 mm NMR tubes containing a sealed capillary with DMSO-d6, used as an external lock and for chemical shift referencing.

Table 5.2.2 Description of the $[C_2C_1Im][C_4F_9SO_3]$ aqueous solutions concentrations (mass fraction, w_{FIL}), diffusion time (Δ), diffusion gradient length (δ) and gradient strength (g) used in the ^1H and ^{19}F diffusion measurements.

Condition	w_{FIL}	Δ (^1H) [s]	δ (^1H) [s]	g (^1H) [G m^{-1}]	Δ (^{19}F) [s]	δ (^{19}F) [s]	g (^{19}F) [G m^{-1}]
Pure FIL	1.000	0.1	0.002	153 – 42840	0.1	0.002	153 – 61200
		0.8	0.006	153 – 4437	0.4	0.007	153 – 4437
		2.0	0.002	153 – 9180	2.0	0.002	153 – 15300
Between 4th CAC and pure	0.844	0.1	0.002	153 – 12240	0.1	0.002	153 – 18360
		0.8	0.006	153 – 1530	0.4	0.007	153 – 3060
		2.0	0.002	153 – 3060	2.0	0.002	153 – 4590
Above 4th CAC	0.363	0.1	0.002	153 – 9180	0.1	0.002	153 – 13770
		0.8	0.006	153 – 1071	0.4	0.007	153 – 2295
		2.0	0.002	153 – 1836	2.0	0.002	153 – 3060
Between 3rd and 4th CACs	0.038	0.1	0.002	153 – 4590	0.1	0.002	153 – 5355
		0.8	0.006	153 – 612	0.4	0.007	153 – 765
		2.0	0.002	153 – 1071	2.0	0.002	153 – 1224
Between 2nd and 3rd CACs	0.025	0.1	0.002	153 – 3825	0.1	0.002	153 – 4590
		0.8	0.006	153 – 459	0.4	0.007	153 – 612
		2.0	0.002	153 – 918	2.0	0.002	153 – 1071
Between 1st and 2nd CACs	0.011	0.1	0.002	153 – 3825	0.1	0.002	153 – 3825
		0.8	0.006	153 – 459	0.4	0.007	153 – 612
		2.0	0.002	153 – 918	2.0	0.002	153 – 918
Below 1st CAC	0.003	0.1	0.002	153 – 3825	0.1	0.002	153 – 3825
		0.8	0.006	153 – 459	0.4	0.007	153 – 612
		2.0	0.002	153 – 918	2.0	0.002	153 – 918

^{19}F,^{19}F-COSY spectrum was acquired for the more diluted solution (0.003 mass fraction (w_{FIL})) using 8 transients and 16 dummy scans, with a spectral width of 26785 Hz in a total of 2 K data points in F1 and 128 data points in F1 and a relaxation delay of 2 s.

^1H,^{19}F-heteronuclear NOESY (HOESY) data was acquired for the pure $[C_2C_1Im][C_4F_9SO_3]$ by two different approaches, 2D and 1D HOESY. The 2D ^1H,^{19}F-HOESY was acquired using a standard phase sensitive pulse sequence from the spectrometer library, with a mixing time of 0.6 s and a relaxation delay of 2 s. The 16 transients were collected with a spectral window of 8000 Hz and 2K data points in F2 (^1H) and 26730 Hz spectral window and 128 data points in F1 (^{19}F). The selective 1D ^1H,^{19}F-HOESY [45] was obtained by selectively exciting a single each of the four different ^{19}F resonance (−31355, −43929, −46388, −48150 Hz) in independent assays and monitoring the observable ^1H NMR response. All the spectra were acquired using hoesyfhgp1d pulse sequence (Brüker library), with a mixing time of 0.5 s, acquiring 4096 transients, 2 dummy scans, with 32 K data points in a spectral width of 8013 Hz and a relaxation delay of 2 s. The integrals of each proton signal were normalized by the

absolute ratio of the absolute integral from the HOESY and the absolute integral of the ^{1}H spectra and then divided by the amount of fluorine in each carbon atom.

The ^{1}H and ^{19}F diffusion-ordered spectroscopy (DOSY) assays were obtained using the stimulated echo pulse sequence with bipolar quadratic gradient pulse and eddy current delay before the detection (Pulsed Field Gradient Spin Echo - PFGSE) with and without presaturation during relaxation delay [46]. For each of the ^{1}H DOSY experiments, 32 spectra were acquired with 16 K data points, a spectral width of ~4800 Hz, a 1 s relaxation delay, an eddy current delay set to 5 ms, and a gradient delay of 0.2 ms. For the diluted samples (0.025, 0.011, 0.003 w_{FIL}) the diffusion measurements were obtained using the pulse sequence with presaturation and 64 scans, while for the higher concentration samples the number of scans was set to 16 scans. For the ^{19}F diffusion assays 32 spectra were acquired with 64 K data points, a spectral width of ~28400 Hz, a 5 s relaxation delay, an eddy current delay set to 5 ms, and a gradient delay of 0.2 ms. The magnetic field pulsed gradient length (δ), diffusion time (Δ), and gradient strength limits (g) used for the different measurements are detailed in Table 5.2.2. The diffusion decay curve values were obtained through the standard Fourier transform and baseline correction of the F2 dimension using Brüker Topspin software package (version 3.6). The diffusion coefficients were determined by the exponential fitting of the experimental curves in OriginPro 9.0 software. The self-diffusion coefficient (D) is determined from the NMR signal by the Stejskal-Tanner equation [47]:

$$I = I_0 e^{\left[-q^2 D\left(\Delta - \frac{\delta}{3}\right)\right]} \quad 5.2.1$$

where I is the NMR signal dependent on the experimental conditions, I_0 is the NMR signal in the absence of an applied magnetic field, Δ is the diffusion time, and q is the used gradient for the spatial encoding and decoding of the nuclear spin, given by:

$$q = \gamma g \delta \quad 5.2.2$$

where γ is the gyromagnetic ratio of the examined nucleus, g is the gradient strength, and δ is the time during which the gradient is applied. The plot of the decay curves I *versus* $q^2(\Delta - \delta/3)$ allows the calculation of the diffusion coefficient by exponential fitting [48].

5.2.1.3 Viscosity measurements

Dynamic viscosity was measured using an automated SVM 3000 Anton Paar rotational Stabinger viscometer-densimeter. The measurements were performed at 298.15 K for the $[C_2C_1Im][C_4F_9SO_3]$ + water system in a range of 0.3354 to 0.003 w_{FIL}. Each solution was measured in duplicates and the maximum relative standard deviation was observed to be

below 1%. It was considered an error of 2% to cover the uncertainty resulting from the whole procedure (sample purity, low viscosity, and handling).

5.2.1.4 Protein quantification experiments

The concentration of GB1, BSLA, and IFN-α 2b was quantified in the presence of different FILs at variable levels of aggregation. The conditions of the assays are schematically described in Table 5.2.3. After preparing all the solutions of the different FILs in the presence of each protein and the respective blanks for proteins and FILs samples (see Table 5.2.3 for details), the samples were incubated for 24h at 277.15 K. Afterward, the solutions were centrifuged at 277.15 K and 10,000 rpm for 30 minutes. The protein with the FIL aggregates complexation can form structures with enough density difference that allows it to be separated from the solution, as previously demonstrated in other works [49,50]. Therefore, the centrifugation step can separate the amount of protein that is assembled in the FIL aggregates (pellet) from the protein that is free in the solution (supernatant). All the experiments have included a set of samples of known concentrations of each specific protein to obtain a standard curve, which by polynomial fitting allowed the protein quantification on each assayed solution. Thus, 100 µL of each sample, respective blanks, and standard curve solutions were pipetted to U-bottom 96-well plates as well as 100 µL of the colourimetric BCA™ or Micro BCA™ protein assay kits reagents to quantification of the free protein in solution, depending on protein concentration. The percentage of free protein in the solution was calculated by the ratio between the determined protein concentration in each tested solution and the concentration determined on the blank of each protein. The measurements were executed in triplicate with an error within ± 10%.

Table 5.2.3 Summary of the FILs (w_{FIL}) and protein (mg/mL) concentrations screened in this work.

Compounds	**GB1 in water (pH 7)**	**GB1 in 5 mM $NaH_3C_2O_2$ (pH 4.5)**	**BSLA in 50 mM NaH_2PO_4 (pH 7.5)**	**IFN-α 2b in 5 mM NaH_2PO_4 (pH 7.4)**
Proteins (mg/mL)	0.2, 0.3, 0.4, 0.5	0.2	0.2	0.01
$[C_2C_1Im][C_4F_9SO_3]$	0.003, 0.011, 0.025, 0.038, 0.364	0.003, 0.011, 0.025, 0.038, 0.364	0.003, 0.011, 0.025, 0.038, 0.087, 0.174	0.003, 0.011, 0.025, 0.038, 0.087
$[C_2C_1py][C_4F_9SO_3]$			0.012	0.003, 0.009, 0.022, 0.038, 0.087
$[N_{1112(OH)}][C_4F_9SO_3]$	0.045		0.045	0.020
$[N_{4444}][C_4F_9SO_3]$	0.002			
$[P_{4444}][C_4F_9SO_3]$	0.002			
$[C_6C_1Im][C_4F_9SO_3]$				0.006
$[C_8C_1Im][C_4F_9SO_3]$				0.007

$[C_4C_1pyr][C_4F_9SO_3]$		0.002
$[C_{2(OH)}C_1Im][C_4F_9SO_3]$	0.046	0.025
$[C_2C_1Im][C_4F_9CO_2]$	0.078	0.023
$[C_2C_1py][C_4F_9CO_2]$	0.022	0.016
$[N_{1112(OH)}][C_4F_9CO_2]$	0.084	0.010
$[C_{2(OH)}C_1Im][C_4F_9CO_2]$	0.036	0.021

5.2.2 Results and discussion

5.2.2.1 Aggregation behaviour of fluorinated ionic liquids in aqueous solutions

The exceptional properties of FILs grant them unique mechanisms of solvation that can be taken as an advantage to develop new systems for biotechnological applications such as protein extraction and protein delivery systems. The main goal of this work is to obtain insights into the aggregation behaviour of the FILs and their repercussions in terms of the interactions with different proteins to infer the potential of FILs in the biological field. For that, NMR was used since it has been an important tool to obtain molecular insight into the structure and dynamics of complex systems like FILs as well as to assess interactions with proteins. $[C_2C_1Im][C_4F_9SO_3]$ is a FIL with improved surfactant properties and was selected for this work because it has complete miscibility in water at all ranges of concentrations, which is a major advantage when compared with traditional surfactants used in biological applications [20]. The complete miscibility in water can be explained by the formation of stable self-assembled structures water, mostly a result of the contribution of the tensioactive anion $[C_4F_9SO_3]^-$. The aggregation behaviour of $[C_2C_1Im][C_4F_9SO_3]$ is characterized by multiple CACs instead of a single CMC that occurs commonly in the traditional surfactants or other SAILs [51,52]. Different tools, such as surface tension measurements, conductivity titration, and isothermal titration calorimetry (ITC) enabled the identification of four distinct CACs in this FIL, attributed to the formation of different self-assembled structures that vary in size and shape: from monomers to spherical micelles (1st CAC), from spheric to globular micelles (2nd CAC) and from globular to cylindrical or lamellar micelles (3rd CAC). ITC showed an additional transition further appointed as a 4th CAC [44]. As mentioned in the introduction, the molecular dynamics of pure $[C_2C_1Im][C_4F_9SO_3]$ is ruled by the nanosegregation into a polar and a fluorinated domain, since the alkyl side chain of the anion is not long enough to segregate in a hydrogenated domain [53]. Therefore, in this work, NMR experiments will be used to explore $[C_2C_1Im][C_4F_9SO_3]$ self-aggregation behaviour by determining self-diffusion coefficients and by Nuclear Overhauser Effect (NOE) techniques. Figure 5.2.1 shows the structure of $[C_2C_1Im][C_4F_9SO_3]$, as well as the numbering of the different Hydrogen and

Fluorine atoms used for the assignment of NMR spectra, aiming to guide the reader along with the discussion of this work. The assignment of the ^{19}F NMR signals of the anion $[C_4F_9SO_3]^-$ was confirmed by the acquisition of a ^{19}F,^{19}F-COSY (see Figure 5.2.2).

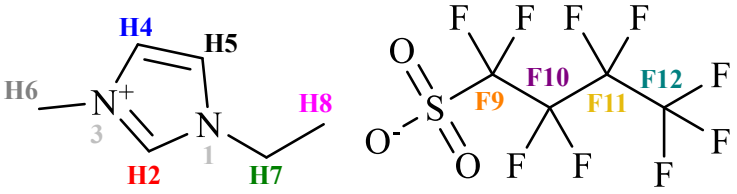

Figure 5.2.1 Structure of 1-ethyl-3-methylimidazolium perfluorobutanesulfonate, $[C_2C_1Im][C_4F_9SO_3]$, with the numbering used for Hydrogen and Fluorine NMR assignment.

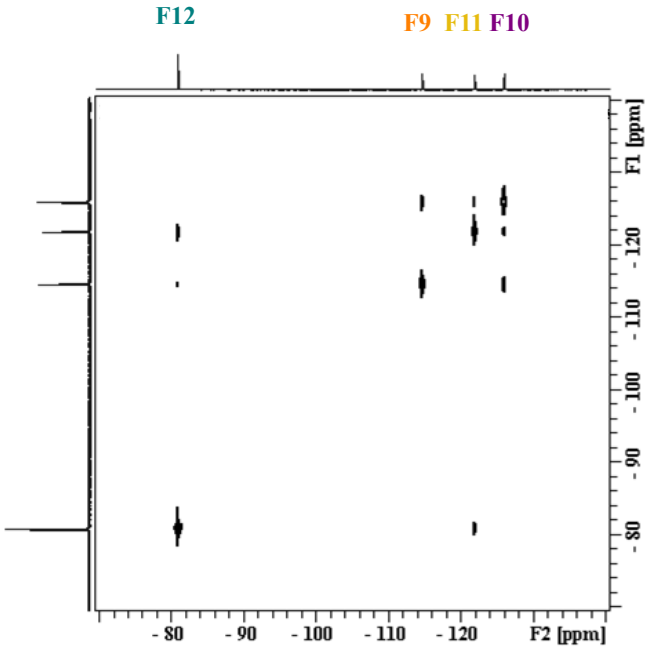

Figure 5.2.2 ^{19}F-^{19}F COSY spectrum of aqueous $[C_2C_1Im][C_4F_9SO_3]$ (0.003 w_{FIL}) recorded at 298 K in a 400.15 MHz spectrometer.

5.2.2.1.1 Self-diffusion coefficients

In order to cover a wide range of $[C_2C_1Im][C_4F_9SO_3]$ mass fractions, and subsequently study the different behaviours of aggregation, six different FIL concentrations were chosen for the diffusion studies: (i) one below the 1st CAC to investigate the behaviour of FIL ions as monomers; (ii) between 1st and 2nd CACs; (iii) between 2nd and 3rd CACs; and (iv) between 3rd and 4th CACs, to have insights about the different self-assembled structures occurring in water; and (v) and (vi) which correspond to concentrations above the 4th CAC in order to cover all the range of FIL mass fraction. Neat FIL was also included in the study for comparison purposes and to understand the interplay of the FIL nanosegregation in its diffusion behaviour. The precise concentration of each solution is presented in Table 5.2.2. As explained in the methodology section, the diffusion coefficients were determined through the

exponential fitting of the decay curves resulting from the DOSY experiments of each solution, acquired in the conditions described in Table 5.2.2. The self-diffusion coefficients were acquired for three different diffusion times both in ^{1}H (100, 800, and 2000 ms) and ^{19}F (100, 400, and 2000 ms) to study the cation $[C_2C_1Im]^+$ and the anion $[C_4F_9SO_3]^-$ diffusion independently (Table 5.2.4). A variation of the self-diffusion coefficient with the increase in diffusion time is indicative either of restricted diffusion (decrease of diffusion coefficient due to an increase in "barriers" to the diffusion as the diffusion time increases) or the existence of exchange between different diffusion domains (increase in diffusion due to an average of the diffusion between different domains as the diffusion time increases). A first observation of the results showed that for all ranges of FIL concentrations and diffusion times, the cation and anion have a monoexponential behaviour identified by a linear dependence of Ln I/I_0 *versus* $[q^2(\Delta-\delta/3)]$ (Figures 5.2.3 and 5.2.4). This behaviour is indicative that if there is an exchange between diffusion domains the exchange rate is extremely fast even for the smallest diffusion time ($k_{exch} >> 100\ s^{-1}$), thus not enabling the detection of different diffusion domains under the current experimental conditions [54,55].

Table 5.2.4 Diffusion coefficients, *D*, determined by ^{1}H and ^{19}F DOSY NMR for the studied solutions of $[C_2C_1Im][C_4F_9SO_3]$ in water at different diffusion times (Δ). Error corresponds to the standard deviation of the different diffusion coefficients in the molecule.

	Diffusion coefficient ($x10^{-10}$ m^2 s^{-1})					
w_{FIL}	**Cation (^{1}H)**			**Anion (^{19}F)**		
	D (Δ=0.1 s)	*D* (Δ=0.8 s)	*D* (Δ=2 s)	*D* (Δ=0.1 s)	*D* (Δ=0.4 s)	*D* (Δ=2 s)
1.00	0.120 ± 0.006	–	0.12 ± 0.01	0.062 ± 0.005	0.060 ± 0.001	0.06 ± 0.01
0.844	0.98 ± 0.01	0.977 ±0.007	1.01 ± 0.01	0.56 ± 0.01	0.54 ± 0.02	0.63 ± 0.01
0.363	2.42 ± 0.03	2.50 ±0.02	2.47 ± 0.01	1.11 ± 0.02	1.10 ± 0.01	1.311 ± 0.004
0.038	5.91 ± 0.02	6.02 ±0.01	5.97 ± 0.01	4.44 ± 0.01	4.362 ± 0.002	4.42 ± 0.01
0.025	7.44 ± 0.01	7.516 ±0.003	7.59 ± 0.01	5.948 ± 0.002	5.960 ± 0.005	6.04 ± 0.02
0.011	7.89 ± 0.02	7.86 ±0.01	7.75 ± 0.01	6.29 ± 0.02	6.244 ± 0.006	6.29 ± 0.01
0.003	8.02 ± 0.01	8.14 ±0.01	8.33 ± 0.04	6.35 ± 0.01	6.410 ± 0.005	6.409 ± 0.003

The change in the diffusion time does not have an impact on the diffusion coefficients of the cation and anion, both for the neat FIL and the aqueous mixtures, consistent with a free diffusion model. This means that the diffusion phenomena can be correlated with the classical diffusion equations.

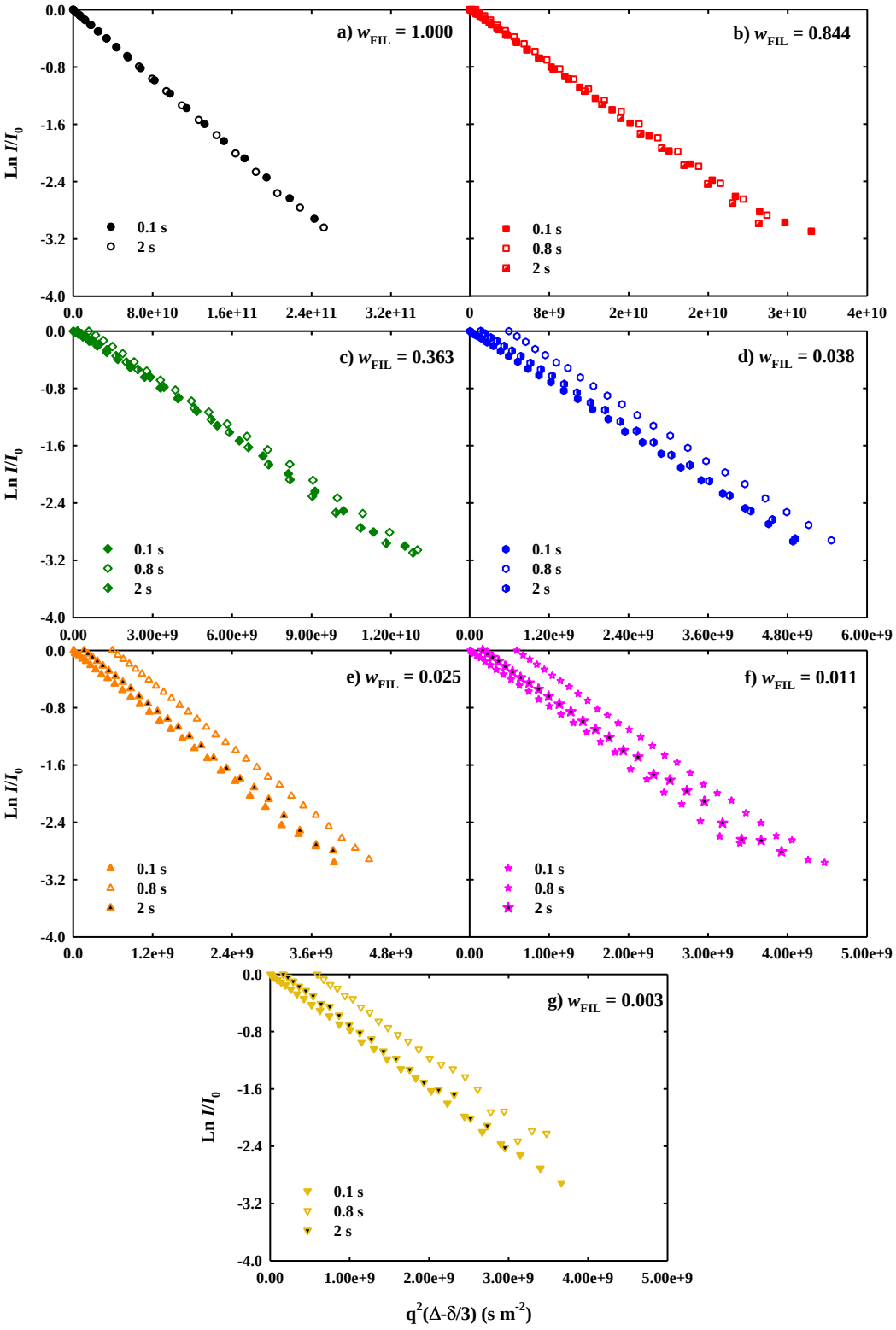

Figure 5.2.3 Plot of the logarithm of ^1H I/I_0 *versus* $q^2(\Delta-\delta/3)$ for different aqueous solutions of $[C_2C_1Im][C_4F_9SO_3]$ used to determine the self-diffusion coefficients of the cation reported in Table 5.2.3. Each symbol represents the different diffusion times (Δ) used in this work. All the values have a cut-off of 5%.

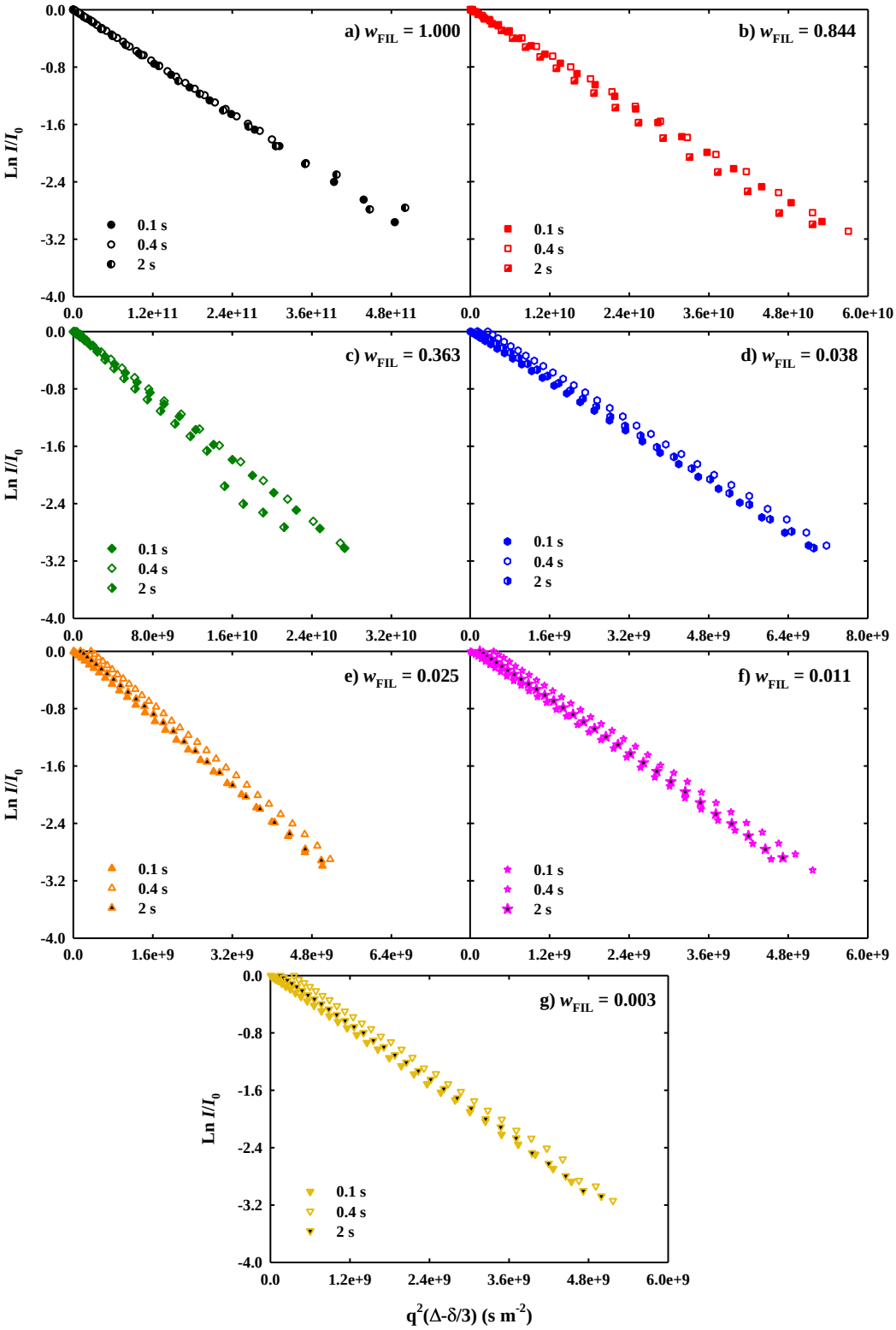

Figure 5.2.4 Plot of the logarithm of ^{19}F I/I_0 *versus* $q^2(\Delta-\delta/3)$ for different aqueous solutions of $[C_2C_1Im][C_4F_9SO_3]$ used to determine the self-diffusion coefficients of the cation reported in Table 5.2.3. Each symbol represents the different diffusion times (Δ) used in this work. All the values have a cut-off of 5%

To analyse the diffusion data analysis in terms of molecular size of $[C_2C_1Im][C_4F_9SO_3]$ and to correlate the results with the rich aggregation behaviour of the FIL, we used the classical Stokes-Einstein (SE) equation to access hydrodynamic radii:

$$D = \frac{k_B T}{f \pi \eta r_H} \qquad 5.2.3$$

Through this equation self-diffusion coefficients (D) are related to the temperature (T), viscosity (η), and hydrodynamic radius (r_H), f is an empirical constant describing the tension between solute and solvent, with a value ranging from 4-6 and k_B is the Boltzmann constant. Since both the viscosity and hydrodynamic radius change with concentration, the viscosity of the solutions in the low FIL mass fraction range (0.34 to 0.003 w_{FIL}) was measured in this work.

The viscosity in the range between (1 to 0.3 w_{FIL}) was previously reported [44]. Both sets are presented in Table 5.2.5. Therefore, the values of viscosity of each solution studied in this work were obtained by fitting a 3rd-degree polynomial function to the experimental data (see Table 5.2.5). The changes in the molecular size in the FIL/water system can be discussed by representing $1/(D \times \eta)$, which is directly proportional to r_H *versus* the mass fraction of FIL (Figure 5.2.5).

From Table 5.2.4 and Figure 5.2.5, we can observe that the cation and anion self-diffusivities are very different for all the concentration ranges. This difference suggests that the cation and the anion in the FIL have a low ion-pairing character, which is consistent with the existence of nanosegregated domains for the cation and the anion as previously stated. For all studied FIL concentration ranges, the cation shows a higher self-diffusion, hence lower molecular size, compared to the anion, reflecting the differences in ion size ($[C_2C_1Im]^+$ has an estimated van der Waals volume of 116 Å^3 while the anion has 158 Å^3) [56].

It is expected that differences in the self-assembled structures will be reflected in the diffusion behaviour of FILs. Starting from the neat FIL, increasing water content, from neat to 0.363 w_{FIL}, we observe an increase in the molecular size of both cation and anion, which is more pronounced for the anion moiety. Below 0.363 w_{FIL} the molecular size of the anion decreases, reaching a plateau for a FIL composition below the 2nd CAC, while the cation experiences a slight molecular size increase in the region between the 3rd and 4th CAC, also reaching a plateau below the 3rd CAC. In the region above the 4th CAC, the steep anion size increase compared with cation is consistent with water competing with the cation for the anion interaction, forming halogen bonds between the fluorines of the anion and the water molecule, creating a preferential water-anion cluster. In this region, a decrease in the water content will decrease the size of the water-anion cluster favouring the formation of nanosegregated domains which are reflected in the lower molecular size closer to neat FIL. An increase in the water content, on the other hand, will break these clusters and lead to the solvation of anion aggregates

between the 4th and the 3rd CAC that will account for the observed size decrease below the 4th CAC and above the 3rd CAC. Below the 3rd CAC, there will be an increase in the population of solvated ions that will dominate the diffusion and contribute to a decrease in the size as observed below the 3rd CAC.

Table 5.2.5 Dynamic viscosity, η, and mass fraction, w_{FIL}, for the binary system $[C_2C_1Im][C_4F_9SO_3]$ + water at 298.15 K.

w_{FIL}	η / mPas	Reference
1.0000	164.1	[44]
0.9804	62.08	[44]
0.9593	36.57	[44]
0.9418	30.35	[44]
0.9212	23.89	[44]
0.8990	20.05	[44]
0.8686	18.18	[44]
0.8440	15.21	[44]
0.8398	14.49	[44]
0.7997	11.78	[44]
0.7801	11.18	[44]
0.7398	9.378	[44]
0.6998	8.315	[44]
0.6496	7.009	[44]
0.5999	5.971	[44]
0.5489	5.165	[44]
0.5001	4.400	[44]
0.3630	3.122	[b]
0.3354	3.030 ± 0.009[a]	This work
0.2000	1.960 ± 0.01[a]	This work
0.1000	1.367 ± 0.008[a]	This work
0.0380	1.174	[b]
0.0384	1.164 ± 0.002[a]	This work
0.025	1.113	[b]
0.0245	1.091 ± 0.003[a]	This work
0.0110	1.055	[b]
0.0109	1.111 ± 0.01[a]	This work
0.0030	1.038 ± 0.02[a]	This work

[a] Standard uncertainties are ± 0.02 mPas; [b] These values were interpolated from fitting the experimental data points to a 3rd degree polynomial function.

The ratio of the diffusion coefficients of the molecules in a solution depends solely on the ratio of the hydrodynamic radius of the probed molecules ($D_{cat}/D_{ani} = r_H^{ani}/r_H^{cat}$). In Figure 5.2.6, the D_{cat}/D_{ani} ratio is plotted as a function of the w_{FIL}. The comparison of the D_{cat}/D_{ani} *versus* w_{FIL} with the ratio of the van der Waals radius (r_{vd}) of the ions gives a better picture of the relative changes discussed before, particularly concerning the formation of anion-water clusters above the 4th CAC. Furthermore, the almost unchanged values at low FIL concentration, with values close to the van der Waals ratio, suggests the existence of a large population of solvated ions and that the cations and anions in the aggregates formed below the 3rd CAC are in fast dynamic equilibrium with the solvated ion, in the diffusion timescale.

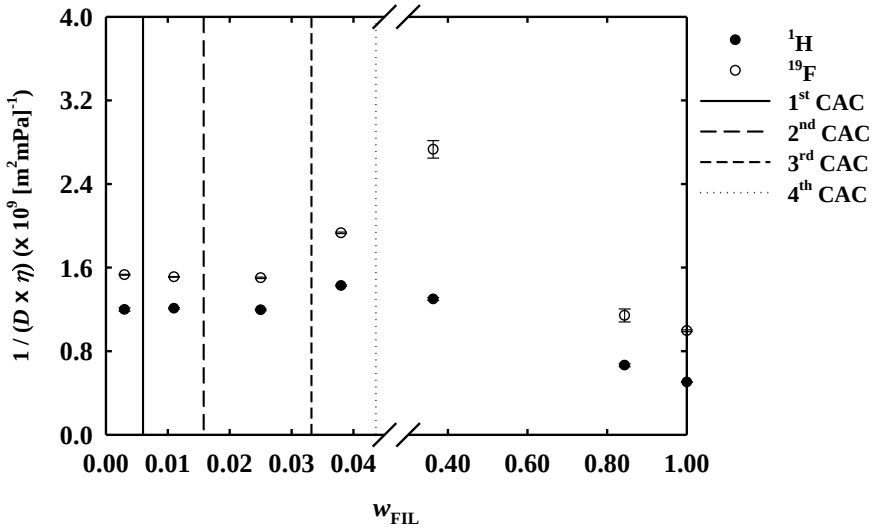

Figure 5.2.5 Plot of $1/(D\times\eta)$ *vs* mass fraction of FIL for $[C_2C_1Im]^+$ (full symbols) and $[C_4F_9SO_3]^-$ (empty symbols). The self-diffusion coefficients used in the determination of $1/(D\times\eta)$ are the average of the D obtained with the different diffusion times (standard deviations are reported). The vertical lines represent the CACs of $[C_2C_1Im][C_4F_9SO_3]$ [44].

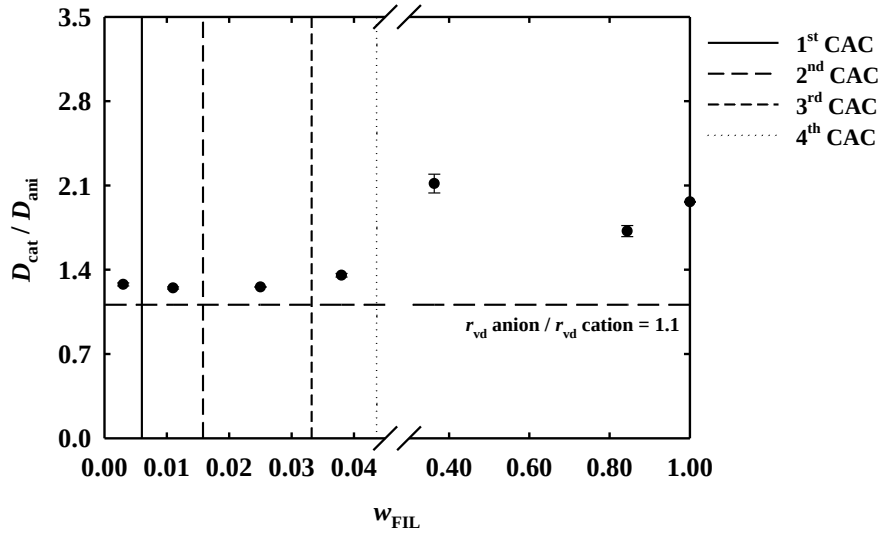

Figure 5.2.6 Ratio between the self-diffusion coefficients of $[C_2C_1Im]^+$ and $[C_4F_9SO_3]^-$. The ratio between the van der Waals radius (r_{vd}) [56] of the anion versus the cation, is represented by the horizontal dashed line. The error bars are included, resulting from the measurement at different diffusion times. The vertical lines represent the CACs of $[C_2C_1Im][C_4F_9SO_3]$ [44].

5.2.2.1.2 Chemical shift perturbation

The changes in the chemical shift of each resonance in the ^{1}H and ^{19}F spectra were also considered in order to get more insight into the aggregation behaviour of $[C_2C_1Im][C_4F_9SO_3]$ in water. The ^{1}H and ^{19}F spectra from where chemical shifts were measured are found in Figures 5.2.7 and 5.2.8, for all studied FIL solutions. Chemical shift differences *versus* IL concentration are plotted in Figure 5.2.9 and were calculated considering as a reference the

chemical shifts of the pure FIL. In concentrated FIL solutions, the proton chemical shift changes should be dominated by FIL-FIL intramolecular interactions while at lower concentrations of FIL it should reflect the establishment of intermolecular interactions with water.

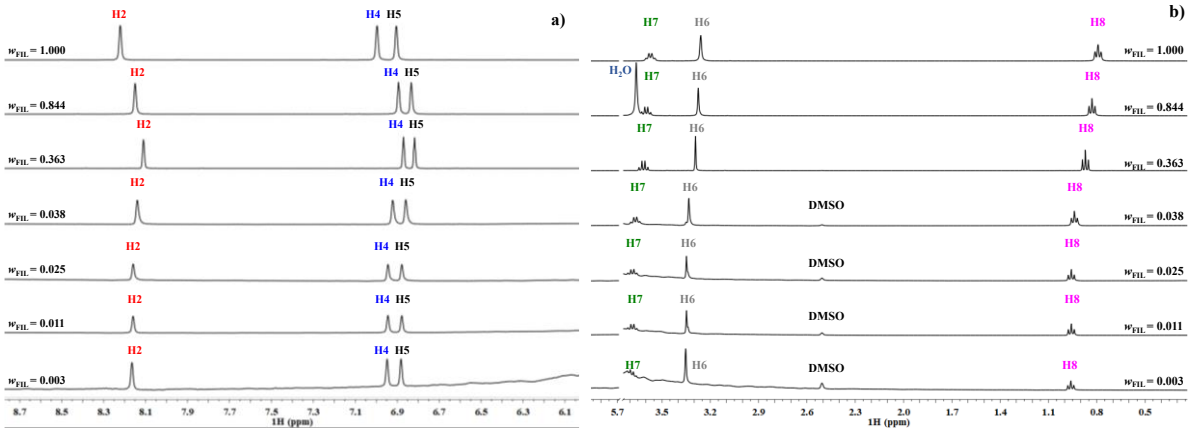

Figure 5.2.7 Effect of concentration on the ^{1}H NMR spectrum of $[C_2C_1Im][C_4F_9SO_3]$ (400.15 MHz, 298 K) where in a) are represented the aromatic protons and in b) the aliphatic protons.

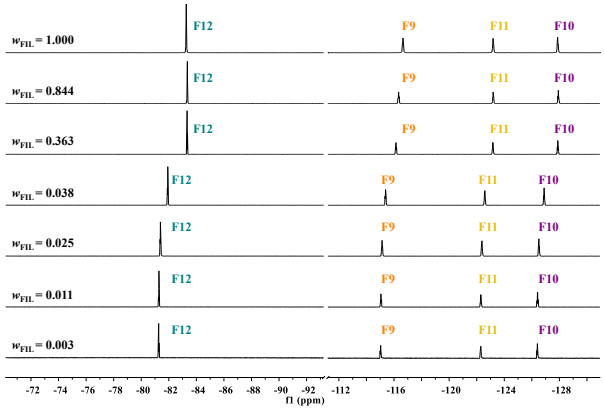

Figure 5.2.8 Effect of concentration on the ^{19}F NMR spectrum of $[C_2C_1Im][C_4F_9SO_3]$ (376.54 MHz, 298 K).

For the cation, Figure 5.2.9a shows that upon the addition of water, the aromatic and aliphatic protons show different behaviour. The aliphatic protons (H6, H7, and H8) always experience a deshielding effect when compared to the neat FIL (downfield shift, higher ppm) which is well pronounced when crossing the composition corresponding to the 4th CAC (particularly for H8) towards the 3rd CAC, beyond this region the addition of water only shifts the aliphatic resonances slightly. The aromatic protons (H2, H4, and H5), on the other hand, first experience a shielding effect (upfield shift, lower ppm) above the 4th CAC, followed by a large deshielding effect when crossing the 4th CAC towards the 3rd CAC, beyond this region they experience a similar deshielding effect as the one observed for the aliphatic protons. For the anion, Figure 5.2.9b, ^{19}F chemical shifts display an overall deshielding effect, but to a different extent for the different fluorine moieties. Above the 4th CAC, the shifts in F10, F11,

and F12 resonances are negligible whereas for F9 it is slightly more pronounced. Similar behaviour to the one observed for the ^{1}H resonances occurs when crossing the 4th CAC towards the 3rd CAC, i.e. a pronounced deshielding effect, which again is more accentuated for F9.

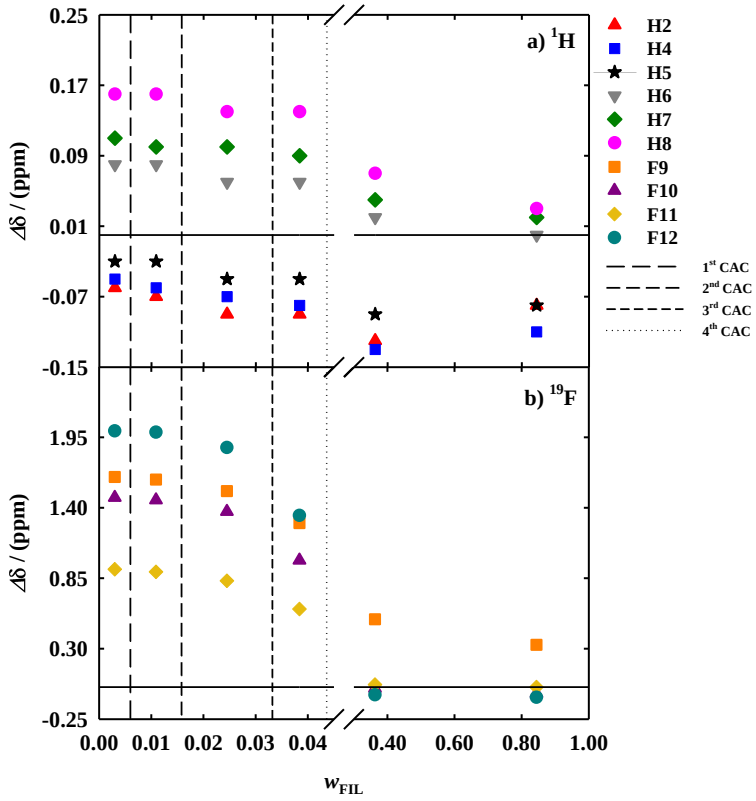

Figure 5.2.9 a) ^{1}H and b) ^{19}F NMR chemical shift deviations of $[C_2C_1Im][C_4F_9SO_3]$ aqueous solutions from the neat FIL. The lines represent the values of the CACs of $[C_2C_1Im][C_4F_9SO_3]$ [44].

Overall, this data is consistent with a dramatic rearrangement of the FIL supramolecular structure when crossing the 4th CAC towards the 3rd CAC. The large deshielding of the resonances observed is indicative of the disruption of large self-assembled structures and water aggregates and the formation of smaller solvated structures where both cation and anion establish stronger interactions with water molecules, in particular hydrogen bonds, that should be responsible for the observed deshielding. The fact that F9 in the anion is the most affected resonance corroborates this conclusion since its proximity to the functional group of the anion directly involved in the establishment of hydrogen bonds with water is expected to be strongly affected. Above the 4th CAC, the chemical shift changes are very small and probably reflect the restructuring of the FIL supramolecular structure to accommodate the water molecules without a major disruption of the polar and fluorinated domains.

Therefore, the chemical shift analysis supports the results obtained in the diffusion studies concerning the different types of structures formed along with the FIL:water composition.

5.2.2.1.3 Intermolecular interactions

In order to get a deeper insight into the interactions between the cation and the anion different heteronuclear Overhauser NMR experiments were performed: 2D $^{1}H,^{19}F$-HOESY and ^{19}F selective 1D proton detected HOESY experiments using neat $[C_2C_1Im][C_4F_9SO_3]$. Efforts were made to obtain results for the solutions of FIL in water, however, the spectra had very low signal-to-noise and the hNOE signals could not be properly quantified or detected. Since it was only possible to obtain hNOE data for a single mixing time the hNOE contacts were analysed qualitatively, concerning its normalized intensity, in terms of the distances between the cation/anion (protons and fluorines). Cross peaks of the 2D $^{1}H,^{19}F$-HOESY (Figure 5.2.10) were integrated and normalized with respect to the number of protons and fluorine atoms (Table 5.2.6) and the hNOE was qualitatively analysed concerning its intensity and occurrence of preferential interactions, as represented in Figure 5.2.11. The results indicate that H2 displays the strongest normalized cross peak intensity with all fluorine groups of the anion and therefore should be in close proximity to the anion, while the other protons of the cation display a relatively lower cross peak intensity, probably due to a relatively higher distance to the anion.

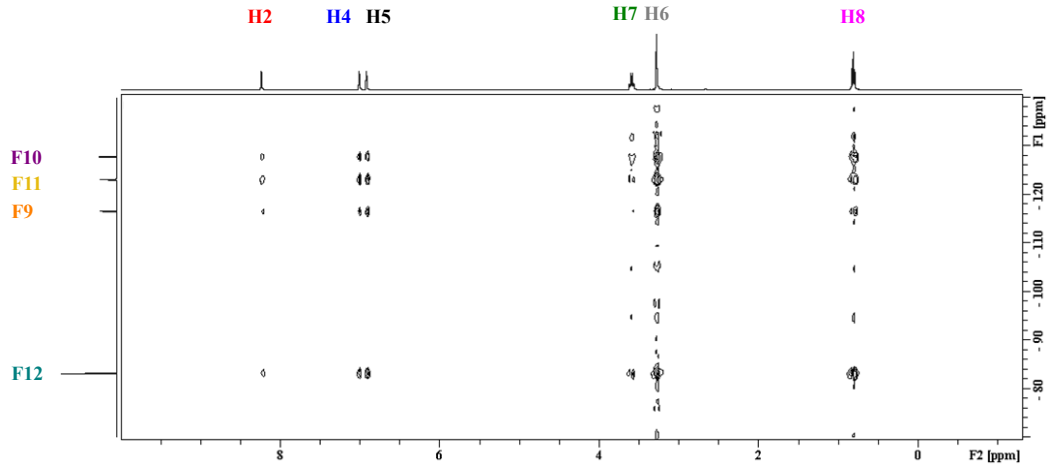

Figure 5.2.10 2D $^{1}H,^{19}F$-HOESY spectrum of neat $[C_2C_1Im][C_4F_9SO_3]$ obtained with a mixing time of 0.6 s at 298 K.

Table 5.2.6 Normalized 2D $^{1}H,^{19}F$-HOESY absolute integrals (in relative intensity units) between the anion and the cation for neat $[C_2C_1Im][C_4F_9SO_3]$ at a mixing time of 0.6 s. The interaction of the protons with a specific F group was used for normalization.

	Absolute Integral Normalized					
w_{FIL}	**H2**	**H4**	**H5**	**H6**	**H7**	**H8**
F9	71.4	23.7	19.0	32.4	*	17.5
F10	76.9	26.8	34.6	46.2	*	41.5
F11	100	30.2	37.4	48.1	*	36.2
F12	64.2	30.5	17.4	39.7	*	23.1

*Signal in the noise level.

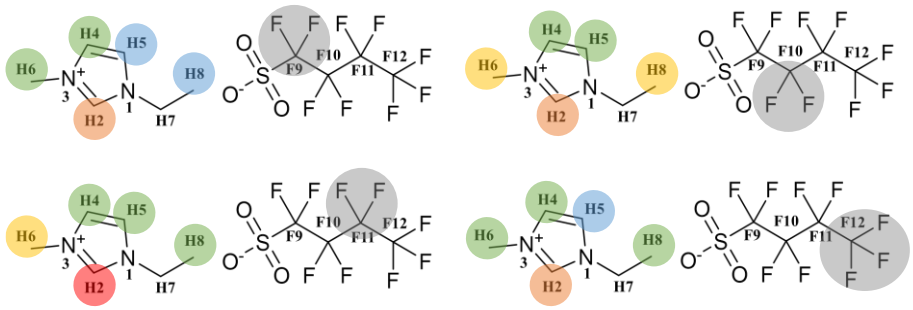

	H2	H4	H5	H6	H7	H8
F9	Strong	Low	Very low	Low	-	Very low
F10	Strong	Low	Low	Medium	-	Medium
F11	Very strong	Low	Low	Medium	-	Low
F12	Strong	Low	Very low	Low	-	Low

100 – 80
80 – 60
60 – 40
40 – 20
20 – 0

Figure 5.2.11 Qualitative analysis of preferential interactions between the molecular groups of neat $[C_2C_1Im][C_4F_9SO_3]$ derived from the 2D $^1H,^{19}F$-HOESY spectra at a mixing time of 0.6 s. The different colours represent the level of relative hNOE taken from Table 5.2.6.

To improve the accuracy of these results and given that the 2D approach yielded cross-peaks with very low intensity, selective 1D $^1H,^{19}F$-HOESY was performed. This method allows time efficiency (better signal-to-noise ratio for the same experimental time) and provides higher proton resolution when compared with the 2D approach [45]. Different selective 1D $^1H,^{19}F$-HOESY were obtained by selective irradiation of each one of the fluorine resonances of the ^{19}F NMR spectra of the anion in different experiments. Therefore, in each experiment, for a given irradiated ^{19}F resonance the feedback corresponds to a 1D hNOE NMR spectrum of the protons, *i.e.* how they respond to the specific irradiation of each fluorine signal. The 1D ^1H-hNOE spectra were integrated and for each experiment, the integral values were corrected for the number of protons and fluorines and normalized (Table 5.2.7). The values were then used, as before, to perform a qualitative analysis of the relative intensity of the hNOE contacts, as represented in Figure 5.2.12.

Table 5.2.7 Normalized selective 1D $^1H,^{19}F$-HOESY absolute integrals (in relative intensity units) between the anion and the cation for neat $[C_2C_1Im][C_4F_9SO_3]$ at a mixing time of 0.5 s. The interaction of the protons with the specific F group was used for normalization.

		Absolute Integral Normalized					
	w_{FIL}	**H2**	**H4**	**H5**	**H6**	**H7**	**H8**
Irradiated Fluorine	**F9**	100	89.9	74.8	58.5	68.2	50.4
	F10	100	94.0	98.8	30.1	75.2	11.2
	F11	100	99.3	98.9	30.3	74.2	11.8
	F12	100	96.5	93.4	29.5	73.4	8.89

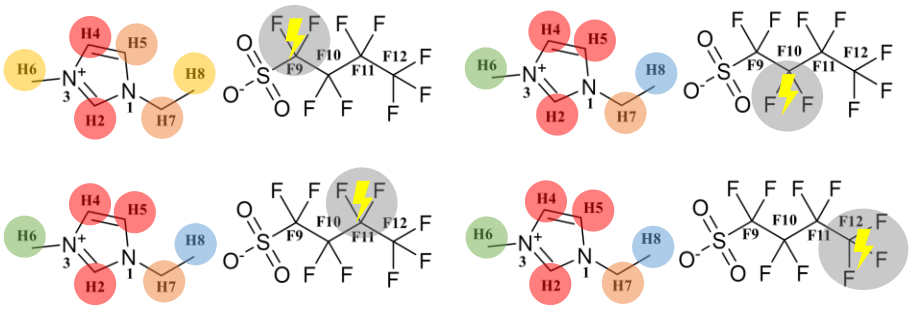

	H2	H4	H5	H6	H7	H8
F9	Very strong	Very strong	Strong	Medium	Strong	Medium
F10	Very strong	Very strong	Very strong	Low	Strong	Very low
F11	Very strong	Very strong	Very strong	Low	Strong	Very low
F12	Very strong	Very strong	Very strong	Low	Strong	Very low

100 – 80
80 – 60
60 – 40
40 – 20
20 – 0

Figure 5.2.12 Qualitative analysis of preferential interactions between the molecular groups of neat $[C_2C_1Im][C_4F_9SO_3]$ derived from the selective 1D $^{1}H,^{19}F$-HOESY spectra at a mixing time of 0.5 s. The different colours represent the level of relative hNOE. The yellow lightning indicates the fluorine irradiated in each experiment.

The results show that, independently of the irradiated fluorine resonance, the protons of the aromatic ring of the cation are the ones that display the highest intensity contacts, which translates in the closest proximity to the anion. Irradiation of F9 also yields a strong relative response from the aliphatic protons. However, as the irradiation frequency shifts from F10 to F12, it becomes apparent that H6, H7, and H8 have weaker hNOE signals, due to a higher distance between these protons and the respective fluorines. These results are in accordance with the FIL nanosegregation behaviour in the pure state. F9 is closer to the aromatic ring protons since it belongs to the CF_2 group which is closer to the polar domain formed by the polar counterparts of both ions. Therefore, the other fluorine moieties are more distant from the polar network, indicating the segregation into a fluorinated domain surrounded by the polar counterparts. Therefore, the 1D selective HOESY was revealed to be an efficient method for a qualitative description of the orientation of these complex systems.

In summary, the aggregation behaviour of FILs is reflected in their properties such as the diffusion coefficients, ^{1}H and ^{19}F chemical shifts, and hNOE contacts. They can be determined and characterized by NMR assays allowing a better understanding of the aggregates that are being formed and the intermolecular interactions established as the concentration of FIL increases.

5.2.2.2 Influence of fluorinated ionic liquids aggregation in protein-FIL interactions

5.2.2.2.1 Model proteins

In previous works, the feasibility of using FILs for protein delivery systems was studied using two proteins, lysozyme, and bovine serum albumin. Biocompatible FILs were chosen, and it was shown that, in a FILs concentration above the 1st CAC, the FIL self-assembled aggregates could encapsulate the proteins. The protein secondary structure was maintained, whereas stability and activity were revealed to be maintained or even improved. Moreover, when subjected to an external stimulus the biomolecules could be released from the FIL aggregates, preserving their structure and activity upon release [49,50,57].

In this work, to gain a deeper insight into the potential use of FILs as extraction systems for proteins, three new proteins were studied: GB1, BSLA, and IFN-α 2b, which have different applications and high biological importance. GB1 is a domain of the protein G with a molecular weight of around 62 kDa and consists of 56 amino acid residues, folded into a four-stranded β-sheet and one α-helix [58,59]. It is known as one of the smallest, most stable globular proteins, having an isoelectric point (pI) close to 4 [60]. In neutral pH, it is highly negatively charged and has a predominantly polar character [61], with a solvent-accessible surface area (SASA) around 3677 Å^2 [62]. BSLA is one of the smallest lipases, with a molecular weight of ~19.8 kDa and composed of 181 amino acid residues. It has a compact globular structure composed of six β-strands in a parallel β-sheet encased by two α-helices on one side and three on the other side, resulting in an α/β hydrolase fold enzyme without a lid domain covering the active site (characteristic of larger lipases) [63]. It has a pI of around 9.3 being its surface at neutral pH positively charged and with a large hydrophobic area exposed to solvent [26] with a total SASA of ~8000 Å^2 [31]. IFN-α 2b is a therapeutic protein used in antiviral and antitumoral pharmaceuticals having huge biopharmaceutical importance. It has a molecular weight of 19.3 kDa and 165 amino acid residues. The fold of this protein comprises a cluster of five α-helices (four assembled in an antiparallel direction creating a left-handed four-helix package) and the conformation is sustained by two disulphide bonds [64]. The pI of the protein is approximately 5.9 [65] indicating that in neutral pH the protein is negatively charged. Information on SASA was not found in the literature for this specific protein, however, information regarding another subtype of IFN-α 2 (IFN-α 2a) which only differs in one amino acid residue from IFN-α 2b, has a SASA of approximately 10000 Å^2 and the contact area is more hydrophobic than hydrophilic [66,67]. Hence, the selected protein models cover a wide structural, solvent availability, and application range.

5.2.2.2.2 Protein quantification in the presence of fluorinated ionic liquids

Following previous works [49,50], we have developed a method to verify if the FILs aggregates form complexes with the selected proteins (GB1, BSLA, and IFN-α 2b) with characteristics that allow, upon centrifugation, to extract the complexed protein from the solution. The selected proteins were screened with several FILs systems in different concentrations and the conditions can be found in Table 5.2.3. The solutions with the protein and FILs were prepared and left to incubate for 24 h and 277.15 K to mimic typical conditions of storage. Afterwards, the solutions were centrifuged. If a pellet was detected, it was separated from the supernatant, resuspended in water/buffer and the protein was quantified (both pellet and supernatant). If no pellet was visually identified, it was considered that the protein remained in the solution and its concentration was determined. For all the assays, control protein samples without the FILs were included as a reference.

In a first approach, GB1 was used at a concentration of 0.2 mg/mL in water, (pH=7) with the FIL $[C_2C_1Im][C_4F_9SO_3]$, probed at diverse concentrations: below 1st CAC, between 1st and 2nd CAC, between 2nd and 3rd CAC, between 3rd and 4th CAC and above the 4th CAC. After centrifugation, and for all samples, the formation of a pellet was not observed, hence, only the protein in the supernatant was quantified. Figure 5.2.13 presents the results, showing that in the presence of this FIL, the protein remains in solution and indicating that GB1 does not strongly interact with the FIL. A slight reduction of protein amount is seen for the concentrations above the 3rd CAC, however, it is not very significant.

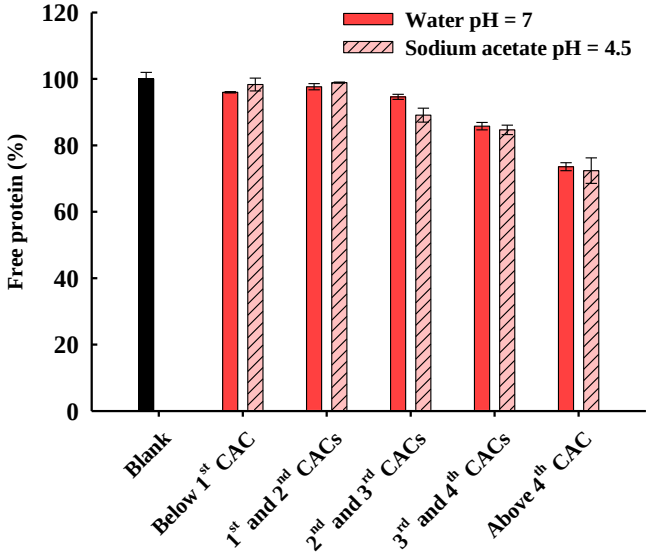

Figure 5.2.13 Quantification of free GB1 (0.2 mg/mL) in solutions of $[C_2C_1Im][C_4F_9SO_3]$ at diverse concentrations and different pH values.

As mentioned above, at pH=7, GB1 is highly negatively charged. This contrasts with lysozyme, which has a pI of approximately 11.4 [68] which, at pH=6.2, is positively charged

and was proven to interact strongly with this FIL [49,50,57]. Since the FIL aggregation is mainly controlled by the anion counterparts, the difference in behaviour observed in GB1 at pH=7 could be related to repulsive interactions between the negative moieties, from the FIL and the GB1, avoiding the formation of the pellet.

In order to understand if the concentration of the protein could induce differences in the interactions with the FIL, the concentration of GB1 was varied from 0.2, 0.3, 0.4, and 0.5 mg/mL while the concentration of $[C_2C_1Im][C_4F_9SO_3]$ was fixed between the 2nd and 3rd CAC. Since there was no influence from the pH the solutions were prepared in water (pH=7). The results are plotted in Figure 5.2.14. The variations for the different protein concentrations are within the experimental error, allowing us to conclude that the concentration of protein is not the determinant factor for the lack of complexation of GB1 with $[C_2C_1Im][C_4F_9SO_3]$.

To try to tune the FIL for this protein, we have selected several FILs with the same anion, given that it is the main structural feature contributing to the self-aggregation behaviour, but with different cations. Choline, tetrabutylammonium, and phosphonium were the selected cations to have a wider screening of different structural features that can contribute to favouring the FILs with GB1 interactions. The choline-based FIL was fixed at a concentration between the 2nd and 3rd CACs because its aggregation behaviour is similar to the $[C_2C_1Im][C_4F_9SO_3]$ [44], and the other two FILs were studied in a concentration 1.5 times the CMC to ensure complete solubility in water [69]. The results are presented in Figure 5.2.15, along with the ones obtained for $[C_2C_1Im][C_4F_9SO_3]$ at a concentration between the 2nd and 3rd CAC for comparison purposes. No significant reduction of protein in the solution was found, leading to the conclusion that none of the studied FILs efficiently complexed with the protein.

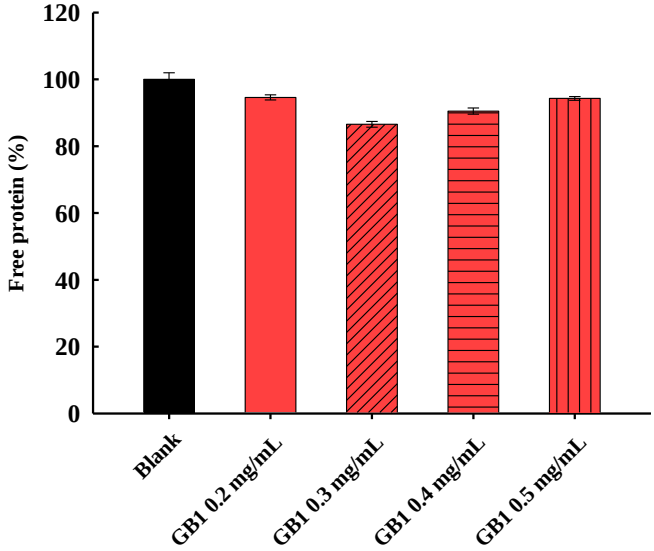

Figure 5.2.14 Quantification of free GB1 at different concentrations in water (pH = 7) and in the presence of $[C_2C_1Im][C_4F_9SO_3]$ between 2nd and 3rd CAC.

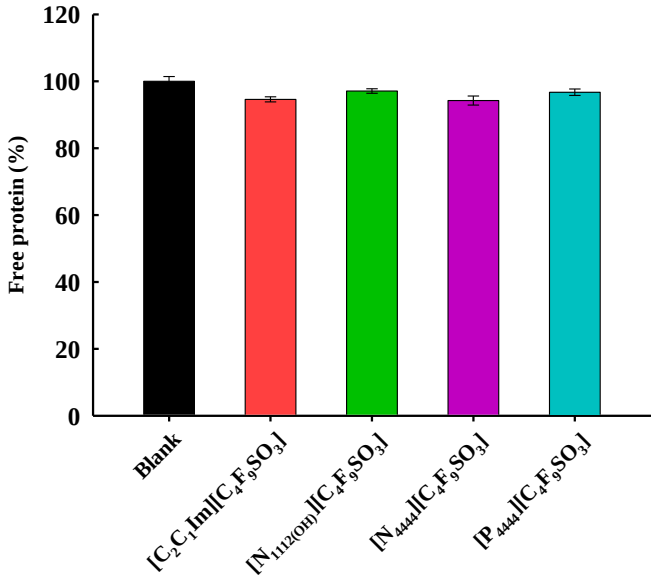

Figure 5.2.15 Quantification of free GB1 (0.2 mg/mL) in water (pH = 7) at the presence of different FILs: $[C_2C_1Im][C_4F_9SO_3]$ and $[N_{1112(OH)}][C_4F_9SO_3]$ between 2nd and 3rd CAC and $[N_{4444}][C_4F_9SO_3]$ and $[P_{4444}][C_4F_9SO_3]$ at 1.5 times the CMC.

BSLA, with a pI around 9.3 and with a large hydrophobic area exposed to solvent with a total SASA of ~8000 Å^2 was then selected to continue with further screenings of FILs. All assays were executed at the optimal pH for the protein (NaH_2PO_4, pH = 7.5). $[C_2C_1Im][C_4F_9SO_3]$ was tested in concentrations below the 1st CAC, between 1st and 2nd, between 2nd and 3rd, between 3rd and 4th CACs, two times and four times the 4th CAC. Other FILs differ in the cation (choline, pyridinium, and hydroxyl functionalized imidazolium) and the anion ($[C_4F_9SO_3]^-$ and $[C_4F_9CO_2]^-$) were also included in the screening to have a broader number of possible FIL + BSLA combinations. These FILs were fixed at concentrations between 2nd and 3rd CAC. BSLA was fixed at a concentration of 0.2 mg/mL as in the case of GB1 (the complete details regarding the concentrations of FILs, buffer, and protein used are depicted in Table 5.2.3). In Figure 5.2.16, the results for the quantification of free protein in solution for all FILs are presented.

For all the studied concentrations of $[C_2C_1Im][C_4F_9SO_3]$ and all the other FILs, with the exception of $[N_{1112(OH)}][C_4F_9CO_2]$, the variations found are almost within the experimental error, indicating that the protein remains in solution and no interactions able to form a complex between the protein and the FIL occur. Therefore, the cation seems not to have a strong influence on the interactions of BSLA with FILs, and these interactions are mainly controlled by the anion. The comparison between the two FILs based on the $[N_{1112(OH)}]^+$ cation shows that slight differences are found for the case of $[C_4F_9CO_2]^-$, compared with $[C_4F_9SO_3]^-$, indicating a slight contribution of the carboxylate functional group to interact with this protein. A slight cation effect can be observed only for the $[C_4F_9CO_2]^-$ anion where a more

polar cation seems to favour the protein-FIL interactions. BSLA is highly hydrophobic and in the tested pH is positively charged as in the case of lysozyme. These two features should be advantageous to promote the interaction with the anionic counterparts of the FILs that also have a strong hydrophobic nature. In fact in the assay with the $[N_{1112(OH)}][C_4F_9CO_2]$ FIL a small decrease in protein concentration was determined, this FIL combines a more polar cation with a hydrophobic anion, and might indicate that a more hydrophobic anion environment is needed to increase the interaction with this protein, while a polar cation is needed to ensure water miscibility. The results point, however, to the existence of other, and less obvious, determinants of protein-FIL interactions than solely the total protein charge and SASA.

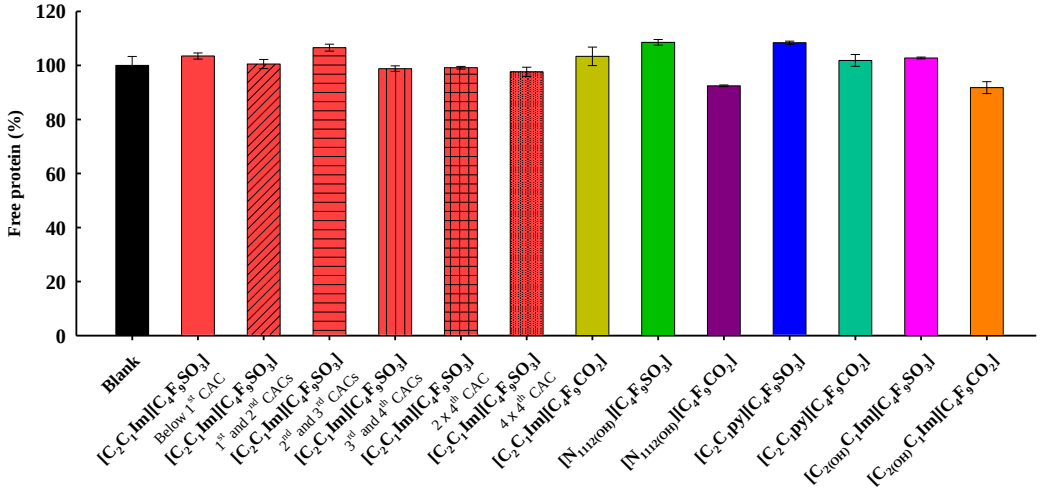

Figure 5.2.16 Quantification of free BSLA (0.2 mg/mL) at the presence of different FILs in 50mM NaH_2PO_4 (pH = 7.5). The $[C_2C_1Im][C_4F_9SO_3]$ was tested at different concentrations whereas the other FILs were tested at a concentration between the 2nd and 3rd CAC.

The last protein model studied was the IFN-α 2b. This protein has high relevance in the biopharmaceutical field and its interaction with FILs might have important applicability. All the experiments were performed in buffered solutions at the optimal pH for IFN-α 2b to assure full activity (NaH_2PO_4, pH = 7.4). The assays were executed with 0.01 mg/mL of IFN-α 2b. The concentration of protein used in the assays was lower than the ones used with GB1 or BSLA since the protein is very unstable and has the tendency to aggregate at higher concentrations. The lower concentration, however, should not be a constraining or favouring factor since, in previous work with lysozyme, it was shown that protein concentrations between 0.04 and 0.2 mg/mL had a negligible effect on the FIL-protein interaction and the extraction results [50]. In the first assay two FILs were screened, $[C_2C_1Im][C_4F_9SO_3]$ and $[C_2C_1py][C_4F_9SO_3]$, at concentrations ranging the self-aggregation behaviour (all the details on concentrations used in this assay are presented in Table 5.2.3). As before, no visual pellet was found for the samples and protein quantification was performed only for the protein in the

solution. Figure 5.2.17 presents the results obtained. No significant differences were found between the FILs and the blank, indicating that no substantial complexation occurs between these FILs and IFN-α 2b.

As in the case of the other studied proteins, several different FILs were selected in order to enlarge the screening possibilities. In this case, FILs based on $[C_2C_1Im]^+$, $[C_2C_1py]^+$, $[C_{2(OH)}C_1Im]^+$ and $[N_{1112(OH)}]^+$ cations and $[C_4F_9SO_3]^-$ and $[C_4F_9CO_2]^-$ anions were used with a concentration fixed between the 2nd and 3rd CAC, and FILs based on $[C_6C_1Im]^+$, $[C_8C_1im]^+$ and $[C_4C_1pyr]^+$ cations and the $[C_4F_9SO_3]^-$ anion were used with a concentration selected to be 1.5 times the CMC due to insolubility in aqueous solution [69].

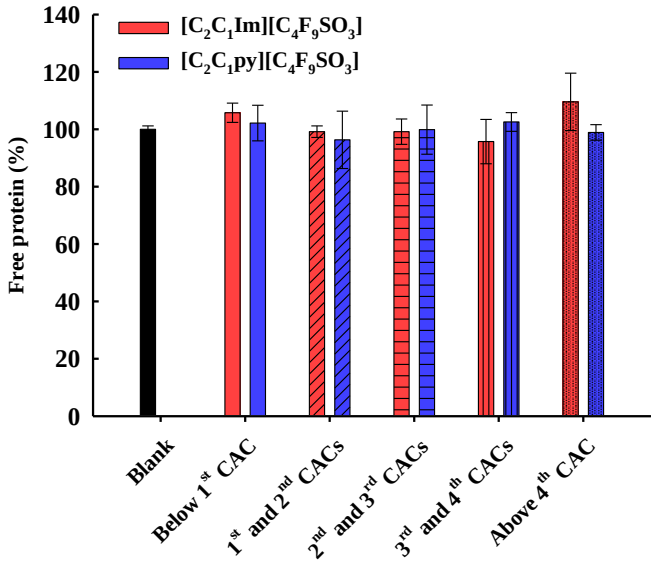

Figure 5.2.17 Quantification of free IFN-α 2b (0.01 mg/mL) at the presence of $[C_2C_1Im][C_4F_9SO_3]$ and $[C_2C_1py][C_4F_9SO_3]$ at different concentrations in 5 mM NaH_2PO_4 (pH = 7.4).

Figure 5.2.18 displays the results of protein quantification for the different FILs used. Analysis of the data shows that in this case some variations are found in the quantity of free protein in the solution. The increment of the hydrogenated alkyl chain in the imidazolium cation, comparing the FILs based on $[C_nC_1Im]^+$ cation with n=2,6,8, does not show significant interactions with IFN-α 2b. The same conclusion is found for the case of $[C_4C_1pyr]^+$ and $[C_2C_1py]^+$ cations when conjugated with the $[C_4F_9SO_3]^-$ anion. Slight differences are found for the case of the FILs based on $[C_{2(OH)}C_1Im]^+$ when compared to the $[C_2C_1Im]^+$, indicating small interactions with the protein, but the anion seems not to influence those interactions. When comparing the FILs conjugated with $[C_2C_1Im]^+$ and $[C_2C_1py]^+$, a more pronounced variation is found for the FILs based on the $[C_4F_9CO_2]^-$ anion. Nevertheless, the most promising FILs are those based on the choline cation, with values very similar to both anions, reinforcing the results obtained with BSLA. However, the extraction efficiency is low because approximately 50% of the protein remains free in the solution. Looking at all of the assays there seems to be

a confirmation of the tendency to increase the extraction efficiency by combining a more polar cation with a more hydrophobic anion, but more studies need to be carried out in order to confirm this trend.

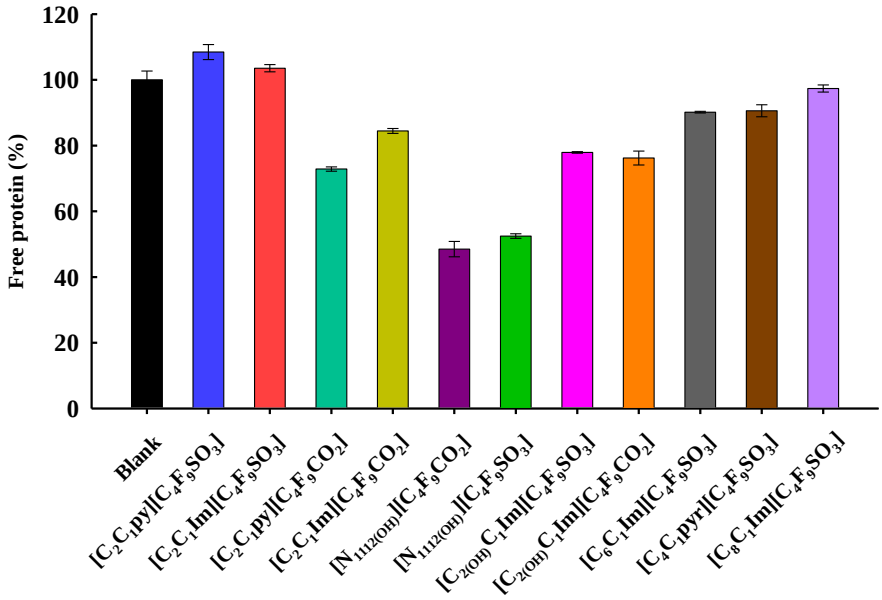

Figure 5.2.18 Quantification of free IFN-α 2b (0.01 mg/mL) at the presence of different FILs at concentrations between the 2nd and 3rd CAC ($[C_2C_1py][C_4F_9SO_3]$, $[C_2C_1Im][C_4F_9SO_3]$, $[C_2C_1py][C_4F_9CO_2]$, $[C_2C_1Im][C_4F_9CO_2]$, $[N_{1112(OH)}][C_4F_9SO_3]$, $[N_{1112(OH)}][C_4F_9CO_2]$, $[C_{2(OH)}C_1Im][C_4F_9SO_3]$ and $[C_{2(OH)}C_1Im][C_4F_9CO_2]$) and 1.5 times the CMC ($[C_6C_1Im][C_4F_9SO_3]$, $[C_8C_1im][C_4F_9SO_3]$ and $[C_4C_1pyr][C_4F_9SO_3]$) in 5mM NaH_2PO_4 (pH = 7.4).

Comparing the SASA of all proteins, there seems to be an influence on the relative surface accessibility of the proteins and their ability to interact with the FILs ($GB1_{SASA}$ < $BSLA_{SASA}$ < IFN-α $2b_{SASA}$) as IFN-α 2b with the highest SASA had the most promising results. However, the results also clearly show that there is no universal FIL for all proteins and that other properties besides the protein charge or SASA must influence the protein-FIL interaction. The most promising results were obtained for the combination of the cholinium cation with a more hydrophobic fluorinated anion, but still with a very low extraction efficiency. Therefore, new FIL structural features must be considered, and most probably proper compounds must be designed to apply in each protein system. The interactions of the proteins with the ILs highly depend on several characteristics of the cations and anions such as polarity, hydrophobicity, the hydrogen-bond capacity of the ILs, and the ILs concentration, as demonstrated in this work. A discussion of the Hofmeister effect might be interesting to understand the influence of the kosmotropicity of the ions in the protein-FIL interactions. However, the Hofmeister effect can only be used to characterize the behaviour of the diluted aqueous solutions of hydrophilic ILs since it was already demonstrated that hydrophobic ILs

do not follow this effect [6]. Therefore, there is a lack of a general theory to explain the Hofmeister effect due to the complex nature of the interactions between ions, water, and protein. This work is an important first step in the direction of screening different structural features of FILs and proteins to envision the formulation of promising systems to allow the use of FILs in biological applications.

5.2.3 Conclusions

In this work, the aggregation behaviour of FILs and the impact that they have on the interactions with proteins were studied. The self-diffusion coefficients of $[C_2C_1Im][C_4F_9SO_3]$ were determined and discussed in terms of the hydrodynamic radius. The results indicated that the molecular size of the FILs increases as long as the concentration rises, indicating the formation of the FIL aggregates. After the 4th CAC, the FIL started to assume a molecular structure governed by the nanosegregation behaviour, and the values became much closer to the pure state. These results were also supported by the chemical shift variation. Moreover, the hNOE experiments on pure FIL showed the proximity of the polar functional groups of the cation and anion to each other and the fluorinated groups are more distant from the polar counterparts, confirming the contribution to the nanosegregation of the FIL. Several FILs were selected to screen their interactions with three different proteins: GB1, BSLA, and IFN-α 2b. Only in the case of IFN-α 2b significant differences in the concentration of free protein in the solution of FIL were found, indicating a stronger interaction with $[N_{1112(OH)}][C_4F_9SO_3]$ and $[N_{1112(OH)}][C_4F_9CO_2]$ FILs. Therefore, the study of the interactions between FILs and IFN-α 2b using NMR techniques should be the next step to have insights at a molecular level with the aim to complete the results discussed in this work. Nevertheless, a widescreen of FILs with different structural features and proteins was obtained in this work. These results constitute a very significant first step to the design of task-specific FILs for protein extraction and separation processes.

5.3 Unveiling the influence of non-toxic fluorinated ionic liquids aqueous solutions in the encapsulation and stability of lysozyme

Lysozyme (Lys) is a small globular protein with 129 amino acid residues, a molecular weight of approximately 14.7 kDa, and a positively charged surface, found in different living organisms and biological fluids. Lys is an enzyme with multifaceted properties which enable its unique antibacterial, antifungal, anti-inflammatory, antitumor, and antihistaminic activities. This enzyme was selected for this study as a model protein due to its vast applicability in biochemical, pharmaceutical, and food industry fields; easy availability due to the high homology of human Lys with hen egg white Lys; and irreversible aggregation which hinders its usage and increases the interest in it as a target of studies in the areas of protein stability, activity, interactions with other compounds, protein-based deliveries, crystallization, and separation processes [70,71].

The superior surface activity of SAILs compared with conventional surfactants allows self-assembly in aqueous solutions into more efficient colloidal systems, such as micelles or vesicles, with greater control of their shape, size, stability, and specific utility. These advantages highlight the substitution of surfactants by SAILs in the protein stability field, successfully demonstrated by some works in the specific case of lysozyme. Bisht et al. reported the influence on structural stability and activity of lysozyme by different ammonium-based ILs, including one that is highly hydrophobic, methyl-trioctylammonium bis(trifluoromethylsulfonyl)imide. This work concluded that the increment of the hydrophobicity decreases the stability and activity of the protein, as well as the increment of IL concentration, for all studied ILs [72]. The same conclusions were found in another work with imidazolium-based ILs [73]. Mandal et al. studied the interactions between 1-butyl-3-methylimidazolium octylsulfate and lysozyme, discovering a destabilizing effect of the IL which highly depends on the variation of the solution pH and the increment of IL concentration added to the solution [74]. Kumari et al. highlighted the binding of 1-methyl-3-octylimidazolium chloride at the active site of lysozyme mainly by hydrophobic interactions, inducing conformational change by reducing the intramolecular hydrogen bond of the enzyme and enhancing the protein activity [75]. In another work, Kumari et al. selected 1-decyl-3-methylimidazolium chloride as an additive to prevent protein aggregation. This IL maintains the conformational and thermal stability of lysozyme at lower concentrations, increasing the activity of the protein with the increment of IL concentration up to a certain concentration [76]. Rather et al. studied the structural-functional integrity of lysozyme in the

presence of two SAILs, 1-octyl-3-methylimidazolium dodecylbenzenesulfonate and 1-dodecyl-3-methylimidazolium dodecylbenzenesulfonate, in the concentration range of critical aggregation concentrations (CACs) and the SAIL saturation concentration of the protein backbone. They found out that this IL is an efficient additive agent for the enhancement of lysozyme stability, increasing its activity and preserving the thermal and conformational stability, while the other studied IL has the opposite behaviour [77]. Singh et al. recently showed in two different works the complexation of lysozyme by binding to bio-based SAILs, allowing the connection of lysozyme molecules to each other and providing enhanced structural stability and antimicrobial activity to the enzyme, depending on the concentration of SAILs and of their distinct interactions with the protein [71,78].

In this work, efforts have been made to find how the structural features of FILs (such as cation, anion, and functionalization of cation) influence the mechanisms of the solubilization and stabilization of lysozyme, which should be granted by the encapsulation of the protein. The cytotoxicity of the studied FILs was firstly determined to ensure biocompatibility. UV–visible spectrophotometry was used as a method of screening the different interactions between FILs and lysozyme. The FILs that significantly altered the lysozyme spectroscopy profile was chosen to determine the encapsulation efficiency by a BCA™ Protein Assay Kit and to study the effect on the bioactivity of the enzyme. Finally, the thermal stability of lysozyme was evaluated by differential scanning calorimetry (DSC) to verify the influence of the mechanism of encapsulation and stabilization of lysozyme by the most efficient FILs. This study proved the greater ability of FILs to enhance the stability and activity of the lysozyme, protecting it from the external factors of its local environment by efficient encapsulation of the protein. Then, it is possible to design compounds with enhanced surface activity, compared to SAILs, but with lower hydrophobic content. This combination bypasses the problems of the highly hydrophobic SAILs where the increment of concentration can have a destabilizing and denaturant effect. In our work, the lysozyme is highly active in concentrations higher than 30% (w/w) of FIL. On one hand, FILs allow a new mechanism of stabilization and protection of the protein by its encapsulation and, on the other hand, extend the range of concentrations where lysozyme is active and stable in the presence of ILs. This work opens doors to the application of FILs in the biopharmaceutical field, as a stabilizer of proteins in all the processes of formulation, production, and storage of new therapeutic products as well as in the administration route of the enzyme as a delivery system.

5.3.1 Materials and experimental methodology

5.3.1.1 Materials

1-Ethyl-3-methylimidazolium perfluoropentanoate, ($[C_2C_1Im][C_4F_9CO_2]$, 98% mass fraction purity); 1-ethyl-3-methylpyridinium perfluoropentanoate, ($[C_2C_1py][C_4F_9CO_2]$, 98% mass fraction purity); (2-hydroxyethyl)trimethylammonium perfluoropentanoate ($[N_{1112(OH)}][C_4F_9CO_2]$, 98% mass fraction purity); 1-(2-hydroxyethyl)-3-methylimidazolium perfluoropentanoate, ($[C_{2(OH)}C_1Im][C_4F_9CO_2]$, 98% mass fraction purity); and 1-(2-hydroxyethyl)-3-methylimidazolium perfluorobutanesulfonate, ($[C_{2(OH)}C_1Im][C_4F_9SO_3]$, 98% mass fraction purity) were synthesized by the ion exchange resin method as previously developed by Fukumoto et al. [41], and implemented in our lab [42,43,53,79]. 1-Ethyl-3-methylimidazolium perfluorobutanesulfonate ($[C_2C_1Im][C_4F_9SO_3]$, ≥97% mass fraction purity) and (2-hydroxyethyl)trimethylammonium perfluorobutanesulfonate ($[N_{1112(OH)}][C_4F_9SO_3]$, >97% mass fraction purity) were supplied by IoLiTec GmbH (Heilbronn, Germany). The synthesized and commercial FILs were characterized by ^{1}H and ^{19}F NMR spectroscopy (NMR spectrometer, Bruker 400 MHz) and the synthesized FILs were checked by elemental analysis for purity determination. All FILs were dried under vigorous stirring and vacuum (4 Pa) for at least 48 hours at 323.15 K prior to usage to guarantee the absence of volatile substances in the synthesis process and a water content lower than 100 ppm, as determined by the Karl Fisher coulometric titration method (Metrohm 831 KF Coulometer). The perfluorobutanesulfonic acid ($C_4F_9SO_3H$, ≥98% mass fraction purity, TCI, Tokyo, Japan) and perfluoropentanoic acid ($C_4F_9CO_2H$, ≥97% mass fraction purity, Fluorochem, Hadfield, UK) were used for comparison purposes in the cytotoxicity assays. The nomenclatures and structures of FILs and fluorinated acids can be found in Table 5.3.1.

For the cytotoxicity assays, two types of human cell lines were used: human colon carcinoma cells (Caco-2, Deutsche Sammlung von Mikroorganismen und Zellkulturen, DSMZ, Germany) and human hepatocellular carcinoma cells (HepG2, European Collection of Cell Culture, ECACC; UK). The cell culture media and supplements were supplied by Gibco (Invitrogen Corporation, UK): RPMI 1640 medium, MEM medium; fetal bovine serum (FBS), L-Glutamine, penicillin-streptomycin solution, MEM nonessential amino acids (MEM-NEAA), sodium pyruvate and trypsin-EDTA solution. The cell viability was determined by a CellTiter 96® AQ_{ueous} One Solution Cell Proliferation Assay from Promega (Madison, WI, USA).

Table 5.3.1 Structures and nomenclatures of fluorinated ionic liquid cations and anions and the fluorinated acids used in the assays.

Cations	
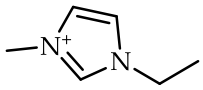 1-Ethyl-3-methylimidazolium **$[C_2C_1Im]^+$**	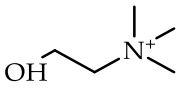 (2-Hydroxyethyl)trimethylammonium **$[N_{1112(OH)}]^+$**
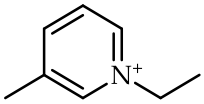 1-Ethyl-3-methylimidazolium **$[C_2C_1py]^+$**	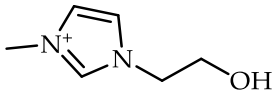 1-(2-Hydroxyethyl)-3-methylimidazolium **$[C_{2(OH)}C_1Im]^+$**
Anions	
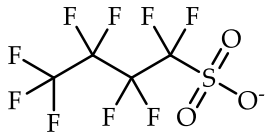 Perfluorobutanesulfonate **$[C_4F_9SO_3]^-$**	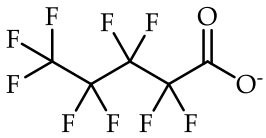 Perfluoropentanoate **$[C_4F_9CO_2]^-$**
Acids	
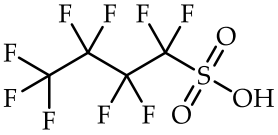 Perfluorobutanesulfonic acid **$C_4F_9SO_3H$**	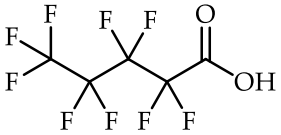 Perfluoropentanoic acid **$C_4F_9CO_2H$**

Lyophilized lysozyme from chicken egg white and *Micrococcus lysodeikticus* lyophilized cells were purchased from Sigma-Aldrich (St. Louis, MO, USA). The potassium dihydrogen phosphate (KH_2PO_4, purity ≥ 99.0%, Fluka, Charlotte, NC, USA) was used as a lysozyme buffer. For encapsulation efficiency assays, the BCA™ Protein Assay Kit was purchased from Thermo Fisher Scientific (Waltham, MA, USA). Milli-Q water was used for buffer preparation.

5.3.1.2 Cytotoxicity assays

The cytotoxicity of FILs ($[C_2C_1Im][C_4F_9CO_2]$, $[C_2C_1py][C_4F_9CO_2]$, $[C_{2(OH)}C_1Im][C_4F_9CO_2]$, $[C_{2(OH)}C_1Im][C_4F_9SO_3]$, and $[N_{1112(OH)}][C_4F_9CO_2]$) and fluorinated acids was tested in two different cell lines: human colon carcinoma cells, Caco-2, and human hepatocellular carcinoma cells, HepG2. The complete details of cell culture maintenance and cytotoxicity assays can be found in previous work [80]. Briefly, the cell lines were cultured and grown with routine maintenance under conditions specific to each type of cell. The stock solutions of FILs were prepared in dimethyl sulfoxide (DMSO) due to the low solubility in the culture medium and then diluted in 0.5% FBS culture medium (up to a maximum of 1% *v/v* DMSO) for a range of FIL concentrations between 500 and 10,000 µM. The FIL solutions were

incubated within each cell line for 24 h, as well as the negative (culture medium with DMSO 1% *v/v*) and the positive control (in 100% *v/v* of DMSO). After the incubation, the medium was removed, and CellTiter 96® Aqueous One Solution Cell Proliferation Assay reagent was added. After 4 h of incubation, the absorbance was measured at 490 nm by a Thermo Scientific Multiskan GO microplate reader (Waltham, MA, USA). Therefore, the cell viability was quantified by the ratio between the measured absorbance of cells that have contact with the FIL and the values of control cells (incubated only in the culture medium). The samples were incubated in three distinct wells and the curves of viability were determined from the average of three independent assays within an experimental error of ±10%.

5.3.1.3 Preparation of solutions for protein assays

The potassium dihydrogen phosphate (KH_2PO_4) was prepared at 66 mM using Milli-Q water (pH = 6.2) and was used as a solvent for all the samples in the studies with lysozyme. For most assays, the lysozyme was studied at a fixed concentration of 0.2 mg/mL, whereas for nano-DSC assays, a concentration of 1 mg/mL of lysozyme was used due to the method sensitivity. The FIL concentrations were chosen according to the specific critical aggregation concentrations (CACs) previously determined for each compound [44,81,82]. The detailed concentrations used for each FIL can be found in Table 5.3.2. In all the assays, the blanks of buffer, lysozyme in buffer, and FILs in buffer were included. All the solutions were prepared, stirred, and left to equilibrate for 30 min following the measurement at 298.15 K, considering this measurement as time zero (0 h). Afterwards, these solutions were incubated at 4 °C for 48 and 96 h and measured after each incubation time (first equilibrating for approximately 30 minutes at room temperature). The incubation temperature was chosen based on previously obtained results, where the ideal activity of lysozyme was found [50,57].

Table 5.3.2. Concentrations of FIL aqueous solutions (mass fraction, w_{FIL}) used in this work.

FILs	Below 1st CAC	1st–2nd CACs	2nd–3rd CACs	3rd–4th CACs	Above 4th CAC
$[C_2C_1Im][C_4F_9SO_3]$	0.0030	0.0109	0.0245	0.0384	0.3636
$[C_2C_1Im][C_4F_9CO_2]$	0.0039	0.0184	0.0784	0.1567	0.3134
$[C_2C_1py][C_4F_9CO_2]$	0.0029	0.0089	0.0222	0.0975	0.3582
$[N_{1112(OH)}][C_4F_9CO_2]$	0.0017	0.0297	0.0843	0.1686	0.3372
$[N_{1112(OH)}][C_4F_9SO_3]$	0.0033	0.0104	0.0447	0.1502	0.3100
$[C_{2(OH)}C_1Im][C_4F_9SO_3]$	0.0042	0.0230	0.0456	0.1072	0.3065
$[C_{2(OH)}C_1Im][C_4F_9CO_2]$	0.0036	0.0159	0.0356	0.0928	0.1788

5.3.1.4 UV–visible spectrophotometry

A double beam UV–vis spectrophotometer, model UV-6300PC, from VWR® (Radnor, PA, USA), was employed for absorbance measurements of the solutions found in Table 5.3.2. A matched pair of quartz cuvettes with a 1 cm path length was used and 400 µL of each sample

were placed in the dried cuvettes and measured in a wavelength range of 190 to 400 nm. For the solutions of lysozyme in buffer and FILs in buffer, the buffer was used as a blank. For the solutions of lysozyme + FILs + buffer, the FILs in buffer solutions were used as blanks in order to follow the profile of the protein. Each sample was recorded at least three times and the absorbance at 280 nm was analysed as well as the overall alterations of the lysozyme profile in the presence of FILs at the different selected concentrations.

5.3.1.5 Encapsulation efficiency

The encapsulation efficiency of lysozyme was determined for $[C_2C_1Im][C_4F_9SO_3]$, $[C_2C_1Im][C_4F_9CO_2]$, $[C_{2(OH)}C_1Im][C_4F_9SO_3]$, and $[C_{2(OH)}C_1Im][C_4F_9CO_2]$ by preparation of the solutions in the concentrations indicated in Table 5.3.2 and as explained in Section 5.3.2.3. After each incubation, the solutions were centrifuged at 4 °C for 30 min at 10,000 rpm. For the concentrations where encapsulation of lysozyme occurred, a white pellet was formed. The pellet corresponded to the encapsulated lysozyme and was separated from the supernatant (free lysozyme in solution) and subsequently resuspended in the same volume of buffer. The protein concentration was determined for both the resuspended pellet and supernatant solutions and for the solutions where no pellet was formed, by adding 100 µL to U-bottom 96-well plates using the colourimetric BCA Protein Assay Kit. A set of samples with known concentrations of lysozyme in a range of 0.004 and 0.24 mg/mL was also prepared and added to the plate as standards. The polynomial fitting of the standard curve was used to determine the final concentration of lysozyme in each solution and the encapsulation efficiency estimated by the ratio of the amount of lysozyme encapsulated to the total amount of lysozyme in the solution. The measurements were taken in triplicate in at least two independent experiments with errors within ±10%. More details of this assay can be found in previous work [50].

5.3.1.6 Lysozyme activity

The influence of FILs on the bioactivity of lysozyme was evaluated and the detailed protocol can be found in previous work [57]. Briefly, the bioactivity was determined by the lytic activity of lysozyme against the cell wall of *Micrococcus lysodeikticus*, changing the turbidity of the bacterial suspension. The absorbance at 450 nm was measured at 298.15 K in U-bottom 96-well plates in a Multiskan GO microplate reader, also from Thermo Fisher Scientific (Waltham, MA, USA). The solutions with $[C_2C_1Im][C_4F_9SO_3]$, $[C_2C_1Im][C_4F_9CO_2]$, $[C_{2(OH)}C_1Im][C_4F_9SO_3]$, and $[C_{2(OH)}C_1Im][C_4F_9CO_2]$ were prepared as described in Section 5.3.2.3 at the concentrations indicated in Table 5.3.2. A solution of *M. lysodeikticus* (substrate) at 0.3 mg/mL was prepared in the protein buffer and left to equilibrate for at least 30 min. The samples were tested before and after the assay of encapsulation efficiency by adding 10 µL of

each tested solution to the wells and, immediately before measurement of absorbance, 100 µL of substrate were added to the wells. The measurements of absorbance were monitored at 30 s intervals for 5 min and taken in triplicate. At least two independent experiments were executed, and the errors were within ±10%. The lysozyme activity was determined through the linear turbidity decline of the plotted absorbances.

5.3.1.7 Differential scanning calorimetry

$[C_2C_1Im][C_4F_9SO_3]$ and $[C_{2(OH)}C_1Im][C_4F_9SO_3]$ samples were prepared as explained in Section 5.3.2.3 and measured only at time zero (0 h). The samples were centrifuged at 4 °C for 30 min at 10,000 rpm, to separate the lysozyme in solution (detected in the supernatant) from the protein interacting with the FIL (detected in the pellet). The pellet was afterwards resuspended with buffer in the same initial volume of solution. The DSC assays were executed by a Nano DSC (TA Instruments, New Castle, DE, USA). The baseline was obtained by filling the cells with the respective reference solution and recorded before the assays. The samples (supernatant and pellet when detected) and references were degassed for 7 min at 20 °C and subsequently measured at a scan rate of 1 °C/min in a temperature range of 20 to 90 °C under a pressure of 3 atm. The software NanoAnalyze (TA Instruments, New Castle, DE, USA) was used to obtain the melting temperature (T_m) of the lysozyme.

5.3.2 Results and discussion

5.3.2.1 Cytotoxicity of fluorinated ionic liquids

The application of FILs in the biopharmaceutical and biomedicine fields is highly dependent on their toxicity and biological properties [83,84]. Information on the correlation between structure and toxicity is imperative to design "greener" FILs. The study of cytotoxicity provides information on the biocompatibility of these compounds with the human body, which has special importance in the administration route of biopharmaceuticals. Few works have focused attention on the cytotoxicity of FILs [80,85,86] and more complementary data are needed. The cytotoxicity of FILs was determined in HepG2 and Caco-2 cell lines, which are *in vitro* models of the liver (HepG2) and intestinal (Caco-2) tissues. These cell lines are widely used in toxicity studies to obtain information on the oral and rectal administration routes of pharmaceuticals [87–89]. The *in vitro* cytotoxicity of $[C_2C_1Im][C_4F_9CO_2]$, $[C_2C_1py][C_4F_9CO_2]$, $[N_{1112(OH)}][C_4F_9CO_2]$, $[C_{2(OH)}C_1Im][C_4F_9CO_2]$, and $[C_{2(OH)}C_1Im][C_4F_9SO_3]$ FILs was determined in this work. These FILs were selected to infer the influence of the anion $[C_4F_9CO_2]^-$ and the functionalization of the cation with a hydroxyl group in the cytotoxicity assay. The cytotoxicity of two fluorinated acids ($C_4F_9SO_3H$ and $C_4F_9CO_2H$), which are the starting reagents used in the synthesis of the FILs, was also

determined for comparison purposes. The cytotoxicity of these acids was already studied in other work, where no significant cytotoxicity was found for a human placental choriocarcinoma cell line [90]. These acids are used as a more biocompatible option to substitute the toxic polyfluoroalkyl acids with longer perfluorinated chains [91]. The cytotoxicity of FILs and fluorinated acids was evaluated in a concentration range of 500 to 10,000 µM for 24 h of exposure time. The cellular viability determined using the CellTiter 96® Aqueous One Solution Cell Proliferation assay can be found in Figure 5.3.1, where Figure 5.3.1a illustrates the results of the Caco-2 cell line and Figure 5.3.1b of the HepG2 cell line.

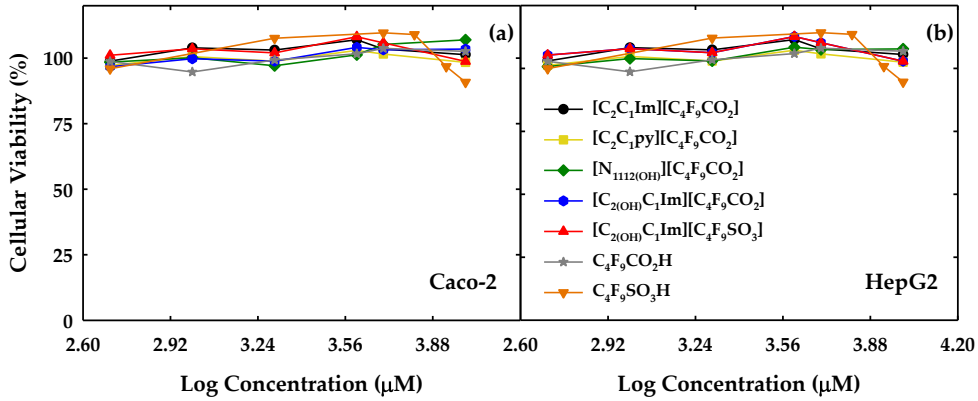

Figure 5.3.1 Cellular viability of FILs and fluorinated acids in (a) Caco-2 and (b) HepG2 cell lines. The lines are a guide for the eye.

The results indicate that none of the compounds shows acute toxicity to both cell lines in the concentration range studied. These results are in concordance with those previously obtained for the homologous FILs composed of $[C_4F_9SO_3]^-$ anion conjugated with short cationic hydrogenated chains [80,85]. Both $[C_4F_9CO_2]^-$ anion and the OH^- group in the cation do not have a negative influence on the cytotoxicity in the studied range of concentrations. Only the fluorinated acid composed of the SO_3^- functional group (orange inverse triangles in Figure 5.3.1) shows a slight decrease in the cellular viability at a concentration close to 10,000 µM. This behaviour is not found for the FIL based on $[C_4F_9SO_3]^-$ anion (red triangles in Figure 5.3.1). The reduced toxicity of all these compounds can be sustained by the complete miscibility in water and high surfactant power. It is well established that the hydrophobic nature of cations and anions is highly related to the higher toxicity of ILs [75,84]. The cations composing the FILs studied here have a lower hydrophobic nature due to the short alkyl chains, which can explain the lower cytotoxicity. Furthermore, the results regarding the fluorinated acids show low cytotoxicity, proving that the anion does not contribute to cytotoxicity in the studied FILs. Therefore, we can design FILs with more hydrophilic cations and fluorinated anions, maintaining their high surfactant power and adding negligible cytotoxicity. This makes them promising candidates to substitute the conventional surfactants, characterized by their high hydrophobic nature and subsequently higher toxicity.

5.3.2.2 Absorption measurements

The absorption measurements by UV–visible spectrophotometry are very useful to obtain insights into the interactions between ILs and proteins. The aromatic amino acids, such as tryptophan, that compose the structure of the proteins are very sensitive to the visible range and are used as spectral probes of protein conformational changes. Lysozyme has six tryptophan residues with a key role in preserving its stability and activity, located in the active site and the hydrophobic core of the protein. Therefore, an absorbance band between 260 and 300 nm with a strong peak around 280 nm characterizes the spectral profile of this enzyme, and any alteration in the spectra can give information on the modifications occurring in the local environment of the characteristic lysozyme tryptophan residues. Usually, these changes are based on the shift to lower or higher wavelength values of the absorbance maximum that can indicate the unfolding of a protein. Several works show an increase or decrease in absorbance intensity in the presence of different families of ILs [72–75,92].

In this work, six different FILs ($[C_2C_1Im][C_4F_9SO_3]$, $[C_2C_1Im][C_4F_9CO_2]$, $[N_{1112(OH)}][C_4F_9SO_3]$, $[N_{1112(OH)}][C_4F_9CO_2]$, $[C_{2(OH)}C_1Im][C_4F_9SO_3]$, and $[C_{2(OH)}C_1Im][C_4F_9CO_2]$) were selected to study their influence on the conformation of lysozyme. The assays were executed at 298.15 K and for three different durations of incubation (0, 24, and 48 h) to infer the influence of time on the FIL–lysozyme interactions. Different CACs can be determined for FILs in aqueous solutions and these CACs indicate the formation of various self-assembled structures. These distinct transitions can be translated into changes in the shape of the self-assembled structures, from monomers to spherical micelles (1st CAC), from spherical to globular micelles (2nd CAC), and from globular to cylindrical or lamellar micelles (3rd CAC). In the case of $[C_2C_1Im][C_4F_9SO_3]$, a 4th CAC was identified by isothermal titration calorimetry. However, the shape of the self-assembled structures in this transition was impossible to characterize by visual or theoretical methods. The formation of these stable aggregates is the main mechanism that controls the total miscibility of these FILs in water [44,81,82]. Therefore, concentrations between the different aggregation transitions of each FIL were selected, to understand how the different self-assembled structures can interact with the lysozyme. The FILs can encapsulate the lysozyme, as previously demonstrated [50,57], by the entrapment of the enzyme inside the self-assembled structures. In this work, the search for the most favourable FIL concentrations, to encapsulate the lysozyme, and the study of the different interactions, are carried out. To ease the analysis and discussion, we categorized the studied concentrations as: (i) below the 1st CAC, where no aggregation is found; (ii) between the 1st and 2nd CACs, the first transition; (iii) between the 2nd and 3rd CAC, the second transition; (iv) between the 3rd and 4th CACs, the third transition; and (v) above the 4th CAC. The exact values of the concentrations used for each FIL are detailed in Table 5.3.2. These assays were executed

by keeping the concentration of lysozyme constant at 0.2 mg/mL. The results are discussed to understand how the structural features of FILs affect the lysozyme conformation by analysing the effect of cation and anion type and the functionalization of the cation with a hydroxyl group, and they can be found in Figure 5.3.2.

Figures 5.3.2a-c illustrate the results of $[C_2C_1Im][C_4F_9SO_3]$–lysozyme assays. As in all the graphs of Figure 5.3.2, the lysozyme in solution is represented by a black dashed line and the coloured solid lines correspond to the different concentrations of the tested FILs, as detailed in Table 5.3.2. The major variations of the lysozyme spectral profile are found for the two concentrations between the 2nd and 3rd and 3rd and 4th CACs. In Figures 5.3.2a-c, the green line (2nd and 3rd CACs) completely loses the conformation and becomes a flat line which, at time zero (0 h), has an increased intensity compared with the lysozyme reference and strongly decreases at 48 and 96 h. This result could be an indication of the encapsulation of lysozyme by $[C_2C_1Im][C_4F_9SO_3]$ due to the complete covering of the lysozyme curve profile. It is not attributed to unfolding because, as previously reported, this process is detected through a shift of the peak absorbance to values around 301 nm [93]. Moreover, the encapsulation of this protein was already proved by this FIL in other works at different concentrations and incubation times.[1] The decrement of absorbance intensity throughout the incubation may indicate a stabilization of the aggregates of FIL in the encapsulation of lysozyme. The same occurs for the concentration between the 3rd and 4th CACs (purple line) but the profile still has some similarities with the lysozyme reference, decreasing the intensity during the incubation. This behaviour could indicate that in this concentration, the FIL does not totally encapsulate the enzyme. The other concentrations do show very slight differences compared with the lysozyme reference, which indicates the presence of the FIL in the local environment and subsequent interactions with the tryptophan residues at the protein surface. A surprising result is the fact that the highest concentration tested, after the 4th CAC, does not alter the lysozyme profile, indicating a turning point in the rearrangement of the FIL structure in these concentrations which does not allow the encapsulation of the protein.

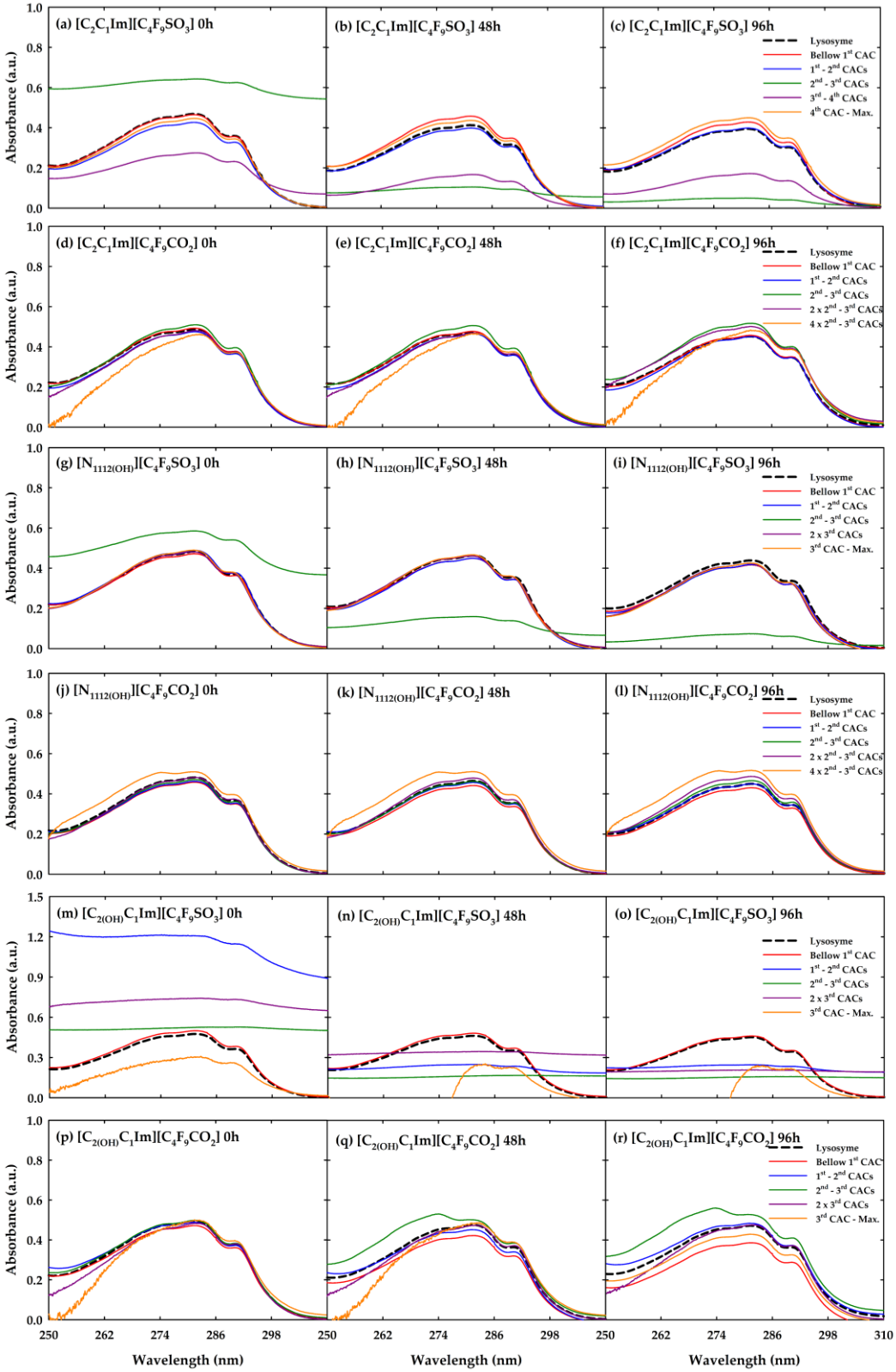

Figure 5.3.2 UV–vis absorption spectra of lysozyme in the different concentrations of FILs studied in this work. The FILs and conditions of incubation are described in each graph.

In the case of $[C_2C_1Im][C_4F_9CO_2]$, the results are illustrated in Figures 5.3.2d-f. Only a slight increment of intensity is found for the 2nd and 3rd CACs at 48 and 96 h and the 3rd and 4th CACs at 96 h. This behaviour indicates that interactions between the surface of lysozyme and FIL are occurring but do not promote enzyme encapsulation or any modification in the overall conformation of the protein. Some spectral noise is found for the highest FIL concentration tested, which could be related to a saturation of the UV–vis signal and subsequently a bad discount of the FIL blank. For the $[N_{1112(OH)}][C_4F_9SO_3]$ FIL (Figures 5.3.2g-i), only the concentration between the 2nd and 3rd CACs shows significant differences compared with the lysozyme reference, with a similar behaviour found in the $[C_2C_1Im][C_4F_9SO_3]$ case. This could be an indication of the encapsulation of lysozyme in this concentration of FIL. No alterations were found to the other concentrations studied. $[N_{1112(OH)}][C_4F_9CO_2]$ (Figures 5.3.2j-l) shows slight alterations, as does the $[C_2C_1Im][C_4F_9CO_2]$ case, which could indicate interactions with the tryptophan residues at the surface without any significant modification of lysozyme conformation.

The $[C_{2(OH)}C_1Im][C_4F_9SO_3]$ is the FIL that has more impact on the spectral profile of lysozyme, as can be seen in Figures 5.3.2m-o. The behaviour of the lysozyme profile in the concentrations between the 1st and 2nd CACs, 2nd and 3rd CACs, and twice the concentration of the 3rd CAC indicates an encapsulation of the enzyme, which seems to stabilize with time. The highest concentration seems to alter the profile in a different way, which could be related to a conformational change of the lysozyme in the presence of FIL. For $[C_{2(OH)}C_1Im][C_4F_9CO_2]$ (Figures 5.3.2p-r), significant differences are only found after 48 and 96 h of incubation and could have been triggered by the changes in the local environment of the protein without significant modifications in its conformation. Only the 2nd and 3rd CAC concentrations have a change in the maximum of absorbance, which is shifted to around 270 nm, possibly indicating a change in lysozyme conformation.

All these results markedly indicate that in terms of anion influence, the FILs based on $[C_4F_9SO_3]^-$ anion have a greater effect on the spectral profile of lysozyme, with a great indication of encapsulation of the protein due to the complete loss of the conformation of the characteristic band. This behaviour is emphasized as the time of incubation increases, possibly indicating a stabilization of the FIL aggregates with the protein. The same is not found for $[C_4F_9CO_2]^-$ anion, which only shows slight increments or decrements of absorbance intensity. Then, there are some interactions between the tryptophan residues on the surface of the protein, but the overall conformation is not highly affected. Looking at the results in terms of cation comparisons, the encapsulation ability grows in the following order: $[N_{1112(OH)}][C_4F_9SO_3]$ > $[C_2C_1Im][C_4F_9SO_3]$ > $[C_{2(OH)}C_1Im][C_4F_9SO_3]$. The results indicate that the functionalization of the cation with a hydroxyl group improves the ability to encapsulate the lysozyme. This is a

surprising result because, as proven in other work [82], the aggregation behaviour of FILs is weakened by the addition of the hydroxyl group. However, they seem to have a higher power of enzyme encapsulation, meaning that the increment of polarity strengthens this mechanism. For the FILs conjugated with the $[C_4F_9CO_2]^-$ anion, the same trend is found, with a greater significant difference in the profile of lysozyme in the presence of $[C_{2(OH)}C_1Im]^+$ cation.

With the aim to verify how the concentration of lysozyme affects the encapsulation ability of the FILs, two concentrations of $[C_2C_1Im][C_4F_9SO_3]$ were selected. One between the 1st and 2nd CACs, where a low influence on the spectral profile was found, and the other between the 2nd and 3rd CACs, where encapsulation of the lysozyme seems to occur. The influence of lysozyme was studied in a range of concentrations between 0.005 and 0.5 mg/mL. The results are depicted in Figure 5.3.3, except for the lowest concentration tested (0.005 mg/L), whose result was not reproducible within the error.

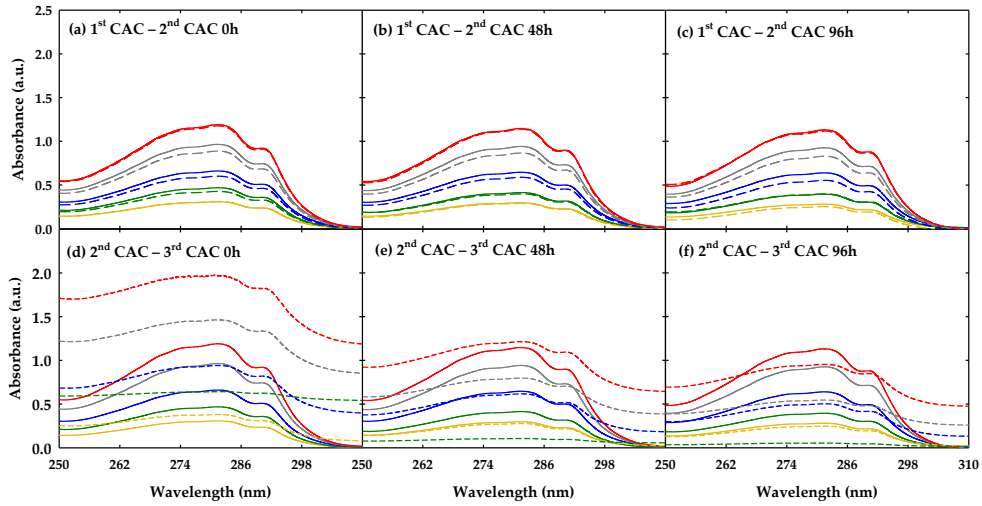

Figure 5.3.3 UV–vis absorption spectra of lysozyme in different concentrations (red, 0.5 mg/mL; grey, 0.3763 mg/mL; blue, 0.2525 mg/mL; green, 0.2000 mg/mL; and yellow, 0.1288 mg/mL) in the presence of $[C_2C_1Im][C_4F_9SO_3]$, where (**a**), (**b**), and (**c**) are the concentrations between 1st and 2nd CAC and (**d**), (**e**), and (**f**) between 2nd and 3rd CACs. The solid lines are the lysozyme reference in each concentration studied and the dashed lines are the solutions with lysozyme and FIL. The duration of incubation is described in each graph.

In Figures 5.3.3a-c, the effect of varying the concentration of lysozyme in the presence of $[C_2C_1Im][C_4F_9SO_3]$ between the 1st and 2nd CACs is shown. The lysozyme profile is slightly altered by the presence of FIL in the concentrations of 0.3763 (grey) and 0.2525 (blue) mg/mL of lysozyme, evidenced by a small decrease in absorbance intensity. This behaviour can be indicative that in these two concentrations of lysozyme, some interactions within the FIL–lysozyme system are promoted but do not lead to substantial modifications of lysozyme conformation. The duration of incubation does not have a meaningful effect. Figures 5.3.3d-f show the assays where the concentration of $[C_2C_1Im][C_4F_9SO_3]$ was fixed at a value between the 2nd and 3rd CAC, in which, in the previous results (Figures 5.3.2a-c), encapsulation of the

protein was found. The lowest concentration of lysozyme (yellow, 0.1288 mg/mL) does not allow the FIL to encapsulate the enzyme, since any significant alterations compared with the reference are found in all incubation times. As explained in the results of Figures 5.3.2a-c, lysozyme at a concentration of 0.2 mg/mL (green lines in Figures 5.3.3d-f) seems to be fully encapsulated by the FIL due to the modification of the characteristic absorbance band to a flat line. If the lysozyme concentration increases, the absorbance band starts to broaden, and some similarities to the shape of the lysozyme reference are visible. This behaviour could mean that the encapsulation of lysozyme by the FIL reaches a level of saturation, and some enzyme is free in the solution. As expected, there is a stabilization of this mechanism throughout the incubation time.

In summary, the results point out that a mechanism of encapsulation of lysozyme can occur in the presence of FIL, which is predominantly promoted by the presence of $[C_4F_9SO_3]^-$ anion. It was also found that the functionalization of the imidazolium cation with a hydroxyl group enhances this mechanism of encapsulation of the protein by the FILs. A longer time of incubation facilitates the stabilization of the FIL aggregates, showing a higher capacity to completely suppress the lysozyme UV–vis band. It was also found that the loading of lysozyme by the FIL self-assembled structures can reach a maximum. With the aim to obtain a better knowledge of this mechanism, the encapsulation efficiency of lysozyme was studied in this work, along with the effect of FILs on its activity and thermal stability and the results are discussed.

5.3.2.3 Encapsulation of lysozyme by fluorinated ionic liquids

The results regarding the UV–vis spectroscopy assays reveal that some of the FILs seem to have the ability of lysozyme encapsulation. Therefore, $[C_2C_1Im][C_4F_9SO_3]$ and $[C_{2(OH)}C_1Im][C_4F_9SO_3]$ were selected to study the encapsulation efficiency of lysozyme due to the larger number of concentrations with this ability. $[C_2C_1Im][C_4F_9CO_2]$ and $[C_{2(OH)}C_1Im][C_4F_9CO_2]$ were also selected as "negative" controls due to the absence of the same behaviour of $[C_4F_9SO_3]^-$-based FILs regarding the spectroscopy results. The same five concentrations of each FIL (Table 5.3.2) were selected to study the encapsulation efficiency of lysozyme. The encapsulation efficiency was evaluated through the centrifugation of the solutions, with the aim to separate the lysozyme encapsulated by the FILs, with the formation of a pellet, from the free lysozyme in the solution that remained in the supernatant. When a pellet was detected, both pellet and supernatant were separated, and the pellet was resuspended in the same volume of buffer solution. The concentration of protein was then measured in both phases, as well as in the solutions where no pellet was detected. The amount of lysozyme in the pellet and supernatant always corresponded to the amount of protein used

for the sample preparation. This indicated that the lysozyme in the pellet was what was entrapped in the self-assembled structures of FILs. The lysozyme in solution at 0.2 mg/mL was also measured by this method and used as a reference to allow the determination of the lysozyme encapsulated by the FILs and for comparison purposes. There was no formation of a pellet after centrifugation of the reference, which emphasizes that the pellet is formed by lysozyme encapsulated in the self-assembled structures. The encapsulation efficiency of each protein concentration was calculated for each FIL-based system and is presented in Table 5.3.3.

Table 5.3.3 Encapsulation efficiency (%) of lysozyme in the different concentrations of FILs.

FILs	Time	Below 1st CAC	1st–2nd CACs	2nd–3rd CACs	3rd–4th CACs	Above 4th CAC
$[C_2C_1Im][C_4F_9SO_3]$	0 h	[1]	[1]	72.1 ± 3.4 [2]	68.7 ± 19.5 [2]	[1]
	48 h			86.3 ± 0.8 [2]		
	96 h			75.5 ± 0.1 [2]		
$[C_{2(OH)}C_1Im][C_4F_9SO_3]$	0 h	[1]	[1]	78.4 ± 3.9 [2]	[1]	[1]
	48 h			80.5 ± 4.4 [2]		
	96 h			82.3 ± 8.5 [2]		

[1] After centrifugation, no pellet was visually detected. [2] Mean values were calculated from two independent assays and their standard deviations.

The results indicate that for the $[C_2C_1Im][C_4F_9SO_3]$ FIL, the formation of a pellet occurs in the concentration between the 2nd and 3rd CACs at the three incubation times. The results are in concordance with the UV–vis spectroscopy data, where a flat line was found for concentrations between the 2nd and 3rd CACs. The encapsulation efficiency of lysozyme by $[C_2C_1Im][C_4F_9SO_3]$ is slightly higher after an incubation time of 48 h. The formation of a pellet was also found between the 3rd and 4th CACs, but only at time zero of incubation and was very difficult to reproduce within the experimental error. These results indicate that the aggregates of FIL in this concentration are not stable enough to maintain the encapsulation of the protein during the incubation. Surprisingly, the formation of a pellet in the solutions with the $[C_{2(OH)}C_1Im][C_4F_9SO_3]$ FIL only arises between the 2nd and 3rd CAC. This was expected to happen in the concentrations between the 1st and 2nd CACs, 2nd and 3rd CACs, and twice the concentration of the 3rd CAC, as shown by the results of UV spectroscopy. However, these results are not reflected by the encapsulation efficiency assay, which probably indicates that the aggregates formed by this FIL in the concentration between the 1st and 2nd CACs, and twice the concentration of the 3rd CAC, have lower stability which does not promote an efficient encapsulation of lysozyme. Regarding the encapsulation efficiency values of the concentration between the 2nd and 3rd CACs, represented in Table 5.3.3, a slight increment is shown with the increment of time. However, the values are within the experimental error, which means no significant relevance. As expected, the two FILs based on $[C_4F_9CO_2]^-$ anion do not encapsulate the lysozyme in any of the studied concentrations.

5.3.2.4 Effect of fluorinated ionic liquids on the bioactivity of lysozyme

The bioactivity of the lysozyme in the presence of FILs was also evaluated in this work. This evaluation has the main objective of understanding the effects of lysozyme encapsulation by FILs on the activity of the enzyme. Furthermore, we want to understand if the FILs that does not encapsulate the protein have an influence on bioactivity. $[C_2C_1Im][C_4F_9SO_3]$ and $[C_{2(OH)}C_1Im][C_4F_9SO_3]$ were selected to study the influence of lysozyme encapsulation, while $[C_2C_1Im][C_4F_9CO_2]$ and $[C_{2(OH)}C_1Im][C_4F_9CO_2]$ were chosen as "negative" controls, as in the case of the encapsulation efficiency results. The solutions studied for the encapsulation efficiency at the same incubation times were submitted to the enzymatic activity assays. The activity of the lysozyme without FIL was used as a reference, considered as 100% of lysozyme activity. In this assay, the samples were also submitted to the centrifugation step, as in the case of encapsulation efficiency, to separate the encapsulated and the free lysozyme in the solutions. The activity of all solutions was measured before and after (samples without formation of pellet; pellet resuspended; supernatant) the step of centrifugation.

Figure 5.3.4 shows the results of the lysozyme activity before the step of centrifugation at the different times of incubation. The most significant alterations of lysozyme activity can be seen in the case of $[C_2C_1Im][C_4F_9SO_3]$ at the concentration between the 3rd and 4th CACs. Surprisingly, a great decrease in activity is found for incubation times of 48 and 96 h. This result indicates that the interactions with the IL in this range of concentrations affect the activity. This behaviour can be translated to a change of the protein conformation that does not enable the protein to reach the substrate. The encapsulation of the protein may not be an explanation for this result since it was concluded that this concentration at both 48 and 96 h of incubation time does not form a pellet. For the other concentrations of this FIL and the other FILs studied, the activity of lysozyme is slightly superior compared with the reference solution. This result is emphasized in the case of $[C_{2(OH)}C_1Im][C_4F_9CO_2]$ at the time zero, where an increment of lysozyme activity to 150% is found. This could indicate that this FIL contributes to better stabilization of the protein, which is reflected in enhanced activity performance. This behaviour was also found in previous works for other families of ILs. The increment of lysozyme activity was attributed to conformational changes in the enzyme structure induced by ILs, stabilizing the integrity of the active site [75,76].

Figure 5.3.5 presents the results regarding the lysozyme activity after the centrifugation of the solutions. As explained in the previous section, only $[C_2C_1Im][C_4F_9SO_3]$ and $[C_{2(OH)}C_1Im][C_4F_9SO_3]$ FILs showed the formation of a pellet. In all concentrations where encapsulation occurs, the activity of lysozyme is preserved and is slightly higher compared with the reference. Therefore, it can be concluded that the encapsulation of lysozyme by the studied FILs can preserve the enzyme bioactivity. Lysozyme, in the presence of the FILs based

on $[C_4F_9CO_2]^-$ anion, also shows good activity values, which are still enhanced by the presence of $[C_{2(OH)}C_1Im][C_4F_9CO_2]$.

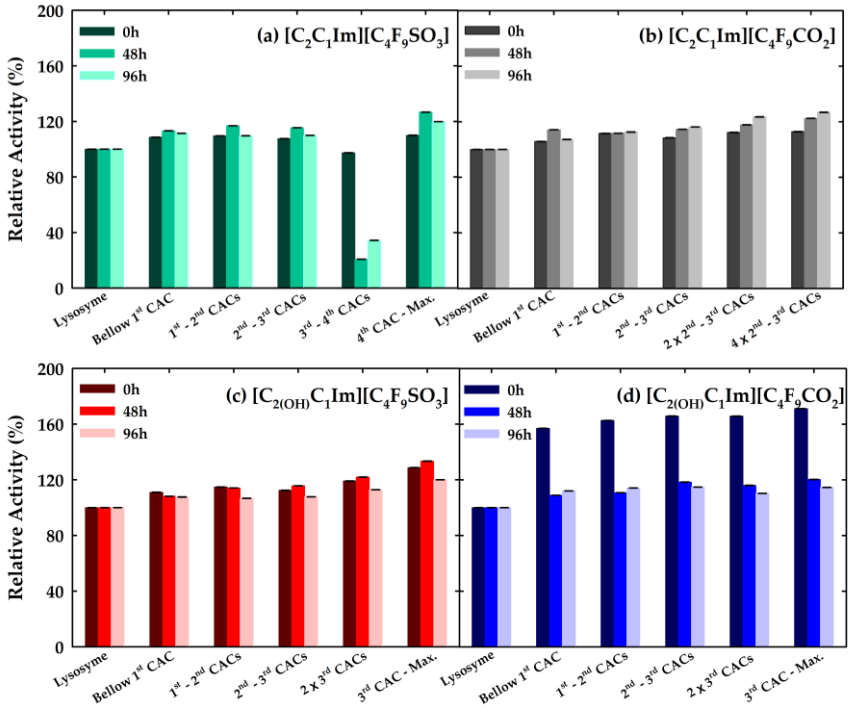

Figure 5.3.4 Relative enzyme activity (%) of lysozyme at different concentrations of FILs before the encapsulation efficiency assays. The FILs and conditions of incubation are described in each graph.

5.3.2.5 Influence of fluorinated ionic liquids on the thermal stability of lysozyme

The thermal stability of lysozyme was studied in this work in the presence and absence of the FILs. The influence of the enzyme encapsulation by FILs was evaluated by the determination of lysozyme melting temperature (T_m), measured in the presence of $[C_2C_1Im][C_4F_9SO_3]$ and $[C_{2(OH)}C_1Im][C_4F_9SO_3]$.

In this study, the concentration of lysozyme was increased to 1 mg/mL due to the apparatus sensitivity. The solutions below the 1st CAC of both FILs were selected to infer the influence of FIL without aggregation behaviour in the lysozyme stability. The concentrations of both FILs that evidenced lysozyme encapsulation in the UV–vis methodology were selected to study the effect of encapsulation on the stability of the enzyme. The solutions were prepared and left to equilibrate for 30 minutes. After that, the solutions were centrifugated and in the cases where the formation of a pellet occurs, it was separated from the supernatant and resuspended in the same volume of buffer. The determined T_m values and the enthalpy (ΔH) of the process of each solution can be found in Table 5.3.4. The T_m characterizes the equilibrium between folded and unfolded states of the protein and is marked by a two-state transition [73,94].

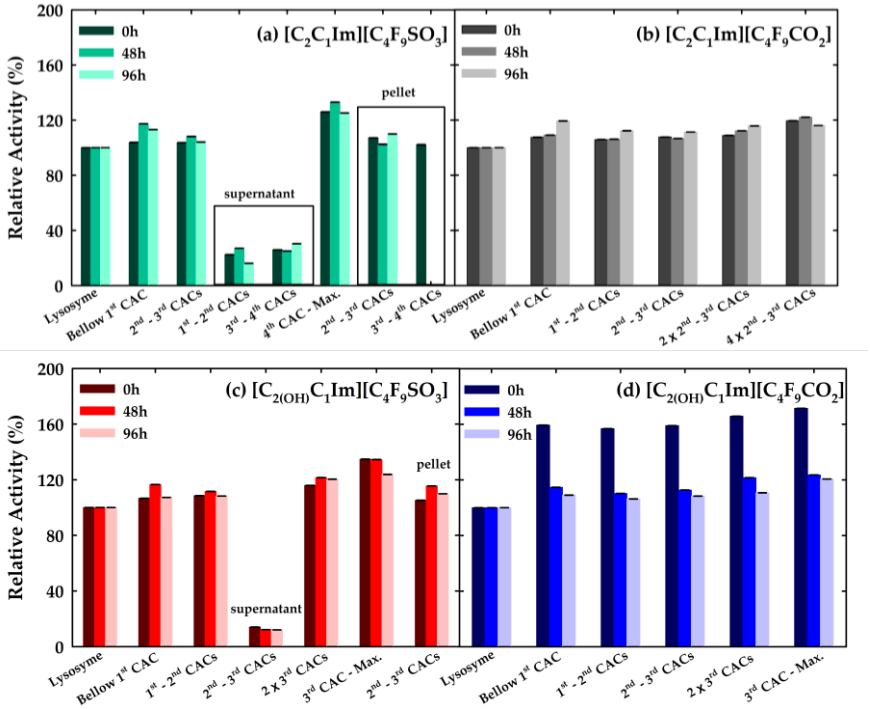

Figure 5.3.5 Relative enzyme activity (%) of lysozyme at different concentrations of FILs after the encapsulation efficiency assays. The FILs and conditions of incubation are described in each graph.

For the case of $[C_2C_1Im][C_4F_9SO_3]$, the concentrations between the 2nd and 3rd and 3rd and 4th CACs were selected to infer their influence on the thermal stability of encapsulated lysozyme. As can be seen in Table 5.3.4, the results indicate that both concentrations maintain the values of lysozyme T_m very close to the reference. However, in the case of the solution below the 1st CAC, where no aggregation of FIL is found, a decrease greater than 3 °C in the T_m and a high decline of the enthalpy is found. This indicates that the encapsulation of the lysozyme by FIL is a favourable mechanism for the enzyme thermal stability. The same behaviour was found for $[C_{2(OH)}C_1Im][C_4F_9SO_3]$, with a difference of almost 7 °C between the T_m of the reference and the concentration below the 1st CAC. Surprisingly, the increment of lysozyme to 1 mg/mL promoted the formation of a pellet in the concentration between the 1st and 2nd CAC, which was not detected in the efficiency encapsulation assays. The concentration between the 2nd and 3rd CAC was also included. For both concentrations, the melting temperature remained very close to the values of the lysozyme reference, indicating a thermal stabilization of the protein by the encapsulation platform. In conclusion, both $[C_2C_1Im][C_4F_9SO_3]$ and $[C_{2(OH)}C_1Im][C_4F_9SO_3]$ show that the encapsulation of lysozyme is useful to thermally stabilize the protein, compared with the case of the concentration of FIL where the aggregation behaviour is not found.

Table 5.3.4 Melting temperature (T_m) and enthalpy (ΔH) of lysozyme in buffer and the presence of different concentrations of FILs.

FILs		0	Below 1st CAC	1st–2nd CACs	2nd–3rd CACs	3rd–4th CACs
$[C_2C_1Im][C_4F_9SO_3]$	T_m [°C]	74.31	70.67	[1]	73.69	72.97
	ΔH [kJ/mol]	526.9	363.1	[1]	458.0	434.6
$[C_{2(OH)}C_1Im][C_4F_9SO_3]$	T_m [°C]	74.31	67.55	73.92	72.42	[1]
	ΔH [kJ/mol]	526.9	337.1	543.2	456.3	[1]

[1] After centrifugation, no pellet was visually detected.

5.3.3 Conclusions

In this work, several FILs were selected to study the influence of their structural features (cation, anion, and functionalization of cation) in the mechanisms of the encapsulation and stabilization of lysozyme. The cytotoxicity of those FILs was studied to ensure biocompatibility with the human body, by selecting two human cell lines (HepG2 and Caco-2), representative of oral and rectal administration routes. The results have indicated that all the studied compounds have negligible cytotoxicity and are appropriate tools to be used in the biological field. UV–visible spectrophotometry was used to infer the different interactions of the FIL–lysozyme system, and the results highlighted that the major differences are found in FIL concentrations able to encapsulate the protein, which is clearly promoted by the presence of $[C_4F_9SO_3]^-$ anion. Some FILs were selected and the encapsulation efficiency was studied, concluding that $[C_2C_1Im][C_4F_9SO_3]$ and $[C_{2(OH)}C_1Im][C_4F_9SO_3]$ efficiently encapsulate the lysozyme at the concentration between the 2nd and 3rd CACs. The activity and thermal stability of lysozyme were determined to understand how encapsulation can affect both properties. The results indicate that the encapsulation by $[C_2C_1Im][C_4F_9SO_3]$ and $[C_{2(OH)}C_1Im][C_4F_9SO_3]$ promotes the activity and thermal stability of lysozyme. Therefore, it was possible to design biocompatible FILs with improved aggregation properties, which enabled the encapsulation of lysozyme, granting enhanced properties to the lysozyme. This makes them promising candidates to be used as stabilizers/additives and/or nanoencapsulation platforms able to preserve the protein stability and activity and consequently can be used in potential applications as therapeutic biopharmaceuticals or biocatalysts.

5.4 Disclosing the potential of fluorinated ionic liquids as interferon-alpha 2b delivery systems

Interferon-alpha 2b (IFN-α 2b) is one of the most relevant therapeutic proteins that has been under research in the past decades. This protein belongs to the class of interferons type I which are cytokines with a key role in the innate immune response [39,95]. Therefore, IFN-α 2b has a highly immunomodulatory response, being used for the treatment of several cancers, viral infections, and auto-immune diseases. It is already approved to be used in the treatment of leukaemia, multiple myeloma, carcinoma, hepatitis B, and C, among others [96–98]. More recently, strong evidence has suggested the use of IFN-α 2b in the mitigation of severe clinical problems caused by COVID-19, such as pneumonia [99,100]. This therapeutic protein is usually administrated subcutaneously and intramuscularly to avoid proteolysis. Nevertheless, alternative routes or new mechanisms must be considered to improve the bioavailability of this protein. IFN-α 2b is very easy to degrade and has a short half-life in the organism (2 to 3 h), being quickly eliminated from the bloodstream. Then, it must be systematically administrated to have a clinical effect, or the dosage must be elevated which results in significant toxicity, triggering severe adverse reactions and limiting its usage in elder and debilitated patients. Therefore, the development of DDSs to provide more efficient and safer IFN-α 2b formulations is of special attention for clinical applications. Several DDSs for transporting IFN-α have been developed such as pegylated forms, liposomes, polymeric micelles, microencapsulation, and nanoencapsulation, along with others. Despite the efforts to search liable DDSs for interferons, none of them was approved for clinical usage in humans, and the research for safer IFN-α 2b formulations must continue [95,96,101,102].

In this work, it was taken the first step in the study of FILs as a tool to stabilize and deliver IFN-α 2b. To obtain insights into the mechanism of FILs solubilization of this specific therapeutic protein, the protein-FIL interactions were under investigation. From the literature, only two works have covered the study of ILs with IFN-α 2b. The first work has studied protein purification by aqueous two-phase systems using ILs as adjuvants [40]. Very recent work has also screened several FILs towards IFN-α 2b to understand which structural features can interact with the protein, obtaining promising results in the ones based on cholinium cation [103]. Therefore, two FILs based on perfluorobutanesulfonate anion ($[C_4F_9SO_3]^-$) conjugated with cholinium and imidazolium cations were selected in this work to obtain insights into protein-FIL interactions. Then, the aggregation behaviour of the FILs was investigated under the presence of IFN-α 2b by: (i) the determination of the critical aggregation concentrations (CACs); (ii) assessment of the surface properties; and (iii) having insights on

the morphology of the FILs self-assembled aggregates using microscopic and spectroscopy methods. Moreover, the interactions of FILs with the IFN-α 2b were studied using different methods such as ultraviolet-visible, fluorescence, and circular dichroism spectroscopies. Finally, the binding of the FILs to IFN-α 2b was also accessed using microscale thermophoresis. The results obtained in this work open new paths in the investigation of DDSs based on FILs to the delivery and stabilization of valuable therapeutic proteins such as IFN-α 2b.

5.4.1 Materials and methods

5.4.1.1 Materials

Interferon-alpha 2b (IFN-α 2b), human recombinant, SRP4595, expressed in E. coli (≥ 98% mass fraction purity by SDS-PAGE and HPLC) was purchased from Sigma-Aldrich (Saint Louis, MO, USA). Different concentrations of the protein were used depending on the sensitivity of each method. The concentrations used are detailed in each method description. Sodium chloride (NaCl, ≥ 99.5% mass fraction purity) from Merck (Darmstadt, Germany), potassium dihydrogen phosphate (KH_2PO_4, ≥ 99.0% mass fraction purity), sodium dihydrogen phosphate anhydrous (NaH_2PO_4, ≥ 99.0% mass fraction purity), hydrochloric acid (HCl) at 0.1 M from Fluka (Charlotte, NC, USA) and Milli-Q water from in-house laboratory facilities were used to buffers preparation. 1-Ethyl-3-methylimidazolium perfluorobutanesulfonate, $[C_2C_1Im][C_4F_9SO_3]$ (≥ 97% mass fraction purity), and (2-hydroxyethyl)trimethylammonium perfluorobutanesulfonate, $[N_{1112(OH)}][C_4F_9SO_3]$ (> 97% mass fraction purity) were provided by IoLiTec GmbH (Heilbronn, Germany). Both FILs were verified by ^1H and ^{19}F NMR spectroscopy (NMR spectrometer, Bruker 400 MHz) and dried under vacuum (4 Pa) and vigorous stirring for at least 48 h at 323.15 K before usage to ensure the absence of volatile substances and a water content lower than 100 ppm, confirmed by the Karl Fisher coulometric titration method (Metrohm 831 KF Coulometer). The nomenclatures and structures of FILs are represented in Table 5.4.1.

Table 5.4.1 The chemical structure and acronyms of the fluorinated ionic liquids studied in this work.

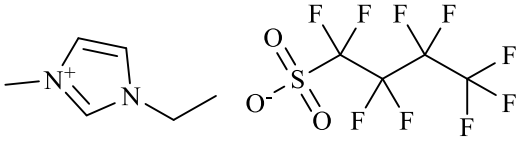	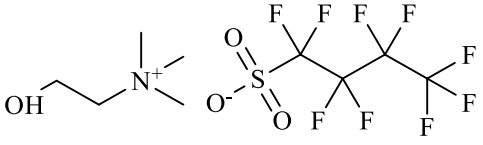
$[C_2C_1Im][C_4F_9SO_3]$ 1-Ethyl-3-methylimidazolium perfluorobutanesulfonate	**$[N_{1112(OH)}][C_4F_9SO_3]$** (2-Hydroxyethyl)trimethylammonium perfluorobutanesulfonate

5.4.1.2 Conductivity titration experiments

The critical aggregation concentrations of $[C_2C_1Im][C_4F_9SO_3]$ were determined by an ionic conductivity titration method in the range of 0 to ~130 mmol kg^{-1} in the presence of different biological simulated fluids and IFN-α 2b. For that, it was utilized a CDM210 conductometer (Radiometer Analytical, Lyon, France) and a CDC749 electrode (Radiometer Analytical, Lyon, France). The electrode was calibrated at 25°C using two standard solutions of 0.1 and 0.01 D KCl (Radiometer Analytical). The standard solutions and samples were measured inside of a glass cell in a thermostated bath at 25°C with constant magnetic stirring. The temperature was maintained and registered using a platinum resistance thermometer attached to a Keithley 199 system DMM/scanner (uncertainty of ± 0.1 °C) from Keithley Instruments (Solon, OH, USA). Six samples of ~130 mmol kg^{-1} $[C_2C_1Im][C_4F_9SO_3]$ were prepared and used to start each system in: (i) 150 mM of NaCl (pH=7.3) to simulate the ionic strength and pH of the bloodstream; (ii) 25 mM of KH_2PO_4 (pH=6.8) to mimic the intestinal fluid; (iii) 100 mM of HCl (pH=1.2) to replicate the gastric fluid; (iv) 150 mM and (v) 5 mM (the two concentrations used in this work, depending on the used method) of NaH_2PO_4 (pH=7.4) as the buffer of IFN-α 2b; and finally (vi) 5 mM of NaH_2PO_4 (pH=7.4) with 10 μg/mL of IFN-α 2b (the mixture of protein with FIL in the buffer of the IFN-α 2b). Each sample was then placed on the cell, stirred, and had the ionic conductivity measured. Afterwards, different amounts of buffer and/or solution of buffer with protein (10 μg/mL of IFN-α 2b) were titrated to the initial solution, stirred, and the ionic conductivity was measured. This experimental procedure was carried out until the ionic conductivity reaches a plateau. After that, a solution of buffer and/or buffer with protein (10 μg/mL of IFN-α 2b) was placed inside the cell and different amounts of a solution with a known concentration of FIL and/or FIL with protein (10 μg/mL of IFN-α 2b) were added to have the complete conductivity profile of each system. The ionic conductivity was measured at least three times before adding more solution and the uncertainty of each measurement was estimated to be less than 1%.

5.4.1.3 Density measurements

The density of $[C_2C_1Im][C_4F_9SO_3]$ + water in a range of 0 to ~730 mM was assessed using an automated SVM 3000 Anton Paar rotational Stabinger viscometer-densimeter. The measurements were performed at atmospheric pressure and 25°C. This apparatus utilizes Peltier elements guaranteeing an uncertainty of ± 0.02°C in the temperature. The density has an uncertainty of 2×10^{-4} g cm^{-3} in-between triplicates.

5.4.1.4 Tensiometry and contact angle goniometry

Several solutions of $[C_2C_1Im][C_4F_9SO_3]$ in the range of 0 to ~240 mM were prepared in 5 mM of NaH_2PO_4 (pH=7.4, buffer of the IFN-α 2b) and in 5 µg/mL of IFN-α 2b with 5 mM of NaH_2PO_4 (pH=7.4). The surface tension of each solution was determined at 25°C by the Du Noüy ring method in a KSV's Sigma 702 Tensiometer (Biolin Scientific, Gothenburg, Sweden). The force tensiometer is equipped with a platinum Du Noüy ring to surface tension measurement and a thermostatic vessel connected to a bath circulator (RW-0535G, Lab. Companion, Korea) for keeping the temperature of the solution constant. 15 mL of each sample were placed in a glass container and left to equilibrate in the thermostatic vessel. After temperature equilibration, the surface tension was measured. The equipment is a standalone-controlled instrument, and the calibration was done with a calibration weight with a known mass before measuring the samples. Each sample was measured five times, and the reported surface tension is the average value with an uncertainty of ± 0.22 mN/m. Each solution was then assessed by a KSV's contact angle goniometer CAM100 (Biolin Scientific, Gothenburg, Sweden). A drop of each solution was placed on a Teflon surface with a Hamilton syringe. This equipment is a PC-controlled instrument, and the tilt was set to 0 degrees at the base of the drop and was recorded for 10 frames with an interval of 1 s. The contact angle is calculated for the left and right sides of the drop and the mean value is the resulting contact angle. At least five different drops of each solution were recorded, and the reported contact angle is the resulting average with an uncertainty of ± 5%.

5.4.1.5 Scanning transmission electron microscopy with energy-dispersive X-ray spectroscopy

The scanning transmission electron microscopy (STEM) with energy-dispersive X-ray spectroscopy (EDS) microanalysis was performed in a Dual-Beam FEI Helios Nanolab microscope, at a working voltage of 15kv with a dark field detector. Three solutions were prepared to measure the blank of the protein, the blank of the FIL and the mixture of protein with FIL in the buffer of the IFN-α 2b: (i) IFN-α 2b at 0.0001 µg/mL in 150 mM of NaH_2PO_4 (pH=7.4); (ii) $[C_2C_1Im][C_4F_9SO_3]$ at 29.2 mM in 150 mM of NaH_2PO_4 (pH=7.4) and (iii) IFN-α 2b at 0.0001 µg/mL with $[C_2C_1Im][C_4F_9SO_3]$ at 29.2 mM in 150 mM of NaH_2PO_4 (pH=7.4). The samples were placed on a 200-mesh copper grid (3 mm diameter). The excess sample was removed using filter paper and samples were dried before measurements.

5.4.1.6 Dynamic light scattering

The dynamic light scattering (DLS) of $[C_2C_1Im][C_4F_9SO_3]$ and $[N_{1112(OH)}][C_4F_9SO_3]$ in the presence of IFN-α 2b was recorded using a Zetasiser Nano Series ZEN3600 (Malvern, U.K.).

The apparatus is equipped with a 633 nm laser and with a non-invasive backscattering technique (173°) used for detection. Stock solutions of FILs and IFN-α 2b were prepared in the buffer of the IFN-α 2b, 150 mM of NaH_2PO_4 (pH=7.4), and filtered with filters with a pore diameter of 0.22 µm. Solutions of FILs+ IFN-α 2b were prepared and adjusted with filtered buffer to final concentrations of 29.3 and 243.8 mM for $[C_2C_1Im][C_4F_9SO_3]$, 29.8 and 248.0 mM for $[N_{1112(OH)}][C_4F_9SO_3]$ and 50 µg/mL of IFN-α 2b. These concentrations were chosen to comprise two different aggregates of each FIL, above the 1st CAC and the 3rd CAC. The solutions were left to equilibrate for 24h at 4°C to promote the interaction of the protein with FILs. Therefore, 20 µL were transferred into a quartz cell of 10 mm pathlength and measured at 25°C.

5.4.1.7 Ultraviolet-visible spectroscopy

Absorbance measurements were performed with a double beam ultraviolet-visible (UV-vis) spectrophotometer (UV-6300PC) from VWR (Radnor, PA, USA). Solutions of $[C_2C_1Im][C_4F_9SO_3]$ (7.3, 26.6, 59.7, 106.3 and 425.1 mM) and $[N_{1112(OH)}][C_4F_9SO_3]$ (8.2, 25.8, 110.8, 192.2 and 384.4 mM) have been prepared in the buffer of the protein, 5 mM of NaH_2PO_4 (pH=7.4), with 20 µg/mL of IFN-α 2b and without the protein (blanks). These concentrations were selected to comprise all the aggregation stages of the FIL: below the 1st CAC, between the 1st and 2nd CACs, 2nd and 3rd CACs, 3rd and 4th CACs and above the 4th CAC. The solutions were prepared, left to equilibrate for 30 min at room temperature, and measured (time 0h). After that, they were incubated at 4°C for 24h to allow the FIL to interact with the protein and measured once again (time 24h). 400 µL of each solution (sample and respective blank) was transferred to a matched pair of quartz cuvettes (10 mm path length) and assessed in a wavelength range in-between 190 and 400 nm. For protein samples, it was used buffer as blank, while for the samples of FIL + protein, the solutions of FIL were used as blank. Each solution was measured at least three times with an error of ± 5%.

5.4.1.8 Fluorescence spectroscopy

The intrinsic fluorescence of IFN-α 2b was determined using a spectrofluorometer Spex Horiba Jobyin-Yvon (Kyoto, Japan) making use of the protein tryptophan residues as intrinsic fluorophores. Several solutions of $[C_2C_1Im][C_4F_9SO_3]$ (2, 3.7, 7.3, 11, 14.6, 26.6, 59.7, 93.6, 221.6, 443.2, 886.4 mM) and $[N_{1112(OH)}][C_4F_9SO_3]$ (2, 4, 8.2, 10.7, 16.1, 25.8, 51.3, 77.1, 110.8, 151.5, 192.2, 288.4, 384.4, 576.6, 768.7 mM) were set in the buffer of the protein, 5 mM of NaH_2PO_4 (pH=7.4), with and without (blanks) the presence of IFN-α 2b (20 µg/mL). The concentrations were chosen to cover the range where the different aggregates of the FILs are formed. Samples, equilibrate for 30 min at room temperature, and 400 µL of each solution were

transferred to a quartz cuvette of 10 mm pathlength and excited at 280 nm, collecting the fluorescence intensity in a wavelength range of 300 to 450 nm. The width of the excitation and emission slit was set to 5 nm for both cases. The spectra of FIL solutions (blanks) were discounted to the spectra of FIL + protein samples to avoid any possible effect of FIL concentration increment in the fluorescence intensity.

5.4.1.9 Circular dichroism spectroscopy

The circular dichroism (CD) spectra were acquired by Chirascan spectropolarimeter (Applied Photophysics, UK) for solutions of IFN-α 2b (100 µg/mL) with $[N_{1112(OH)}][C_4F_9SO_3]$ at 248 mM in the buffer of the protein (150 mM of NaH_2PO_4, pH=7.4). The concentration of FIL was chosen to cover the maximum of FIL that can be used for the studied application. Stock samples of FIL and protein were prepared and filtered through a 0.2 mm filter. Afterwards, they were used to prepare the solutions of protein and protein with FIL at the defined concentrations. Samples were left to equilibrate for 30 min at room temperature and around 230 µL of each sample was moved to a cuvette with 1 mm of path length. CD spectra were expressed in millidegrees and obtained in a range of 200 nm to 260 nm by three consecutive readings at constant temperature (25°C). Spectral deconvolution was executed with K2D3 [104] to allow the estimation of the secondary structure of the protein with and without the presence of FILs.

5.4.1.10 Microscale thermophoresis

IFN-α 2b binding affinity with $[C_2C_1Im][C_4F_9SO_3]$ and $[N_{1112(OH)}][C_4F_9SO_3]$ were determined by microscale thermophoresis (MST) using a Monolith NT.115 (BLUE/RED, NanoTemper Technologies, Munich, Germany). The IFN-α 2b was labelled fluorescently by a protein labelling kit, Alexa Fluor™ 555 (A20174, Invitrogen, Thermofisher Scientific Inc, MA, US), according to instructions from the manufacturer. Several dilution series of 16 samples of 20 µL were prepared in triplicate for each studied system. All the solutions were prepared in the buffer of the protein, 5 mM of NaH_2PO_4 (pH=7.4), and PCR tubes. In the first tube (1 out 16) was added 20 µL of FIL stock solution at twofold the maximum concentration defined for each assay. In the remaining 15 tubes, 10 µL of buffer was added followed by the series dilution of the FIL. Therefore, 10 µL of labelled IFN-α 2b stock solution were added to each tube yielding a final concentration of protein of 2.7 µM. For $[C_2C_1Im][C_4F_9SO_3]$ five maximum concentrations were selected (14, 30, 80, 160, 220 mM), while for $[N_{1112(OH)}][C_4F_9SO_3]$ four maximum concentrations were chosen (15, 35, 70, 375 mM). The selected concentrations cover the range where the distinct CACs are formed in each FIL. The excitation power was determined by a pre-test and set to 20% whereas the MST power was set to medium

(standard). The assays were executed in standard capillaries and triplicates. The results were processed using the MO.Affinity Analysis v2.3 software (NanoTemper Technologies, Munich, Germany).

5.4.2 Results and discussion

5.4.2.1 Influence of interferon-alpha 2b in the aggregation behaviour of fluorinated ionic liquids

FILs have great potential to be used as drug delivery systems of IFN-α 2b due to the rich aggregation behaviour in aqueous solutions which grants improved mechanisms of solvation and complete water miscibility. Therefore, the behaviour of the self-assembled structures of FILs in the presence of IFN-α 2b was disclosed in this work by using different strategies. To begin, the critical aggregation concentrations of FILs aqueous solutions were determined in the presence of different media and IFN-α 2b. In addition, surface properties were accessed by the measurement of the surface tension and contact angles of the FILs aqueous solutions in the presence of IFN-α 2b. Finally, the self-assembled structures of FILs with IFN-α 2b were characterized through scanning transmission electron microscopy and dynamic light scattering.

To study the influence of IFN-α 2b in the aggregates of FILs, it was selected two FILs: $[C_2C_1Im][C_4F_9SO_3]$ and $[N_{1112(OH)}][C_4F_9SO_3]$. These FILs have outstanding surface-active properties, full miscibility in water, and negligible toxicity [105,106]. Both FILs can form different aggregates that were identified by the determination of distinct CACs in water [44]. These self-assembled structures were characterized through different techniques, where different sizes and shapes were determined. The 1st CAC represents the transition from monomers to spherical micelles, the 2nd CAC from spheric to globular micelles, and the 3rd CAC from globular to cylindrical or lamellar micelles [44]. In the case of $[C_2C_1Im][C_4F_9SO_3]$, an extra transition above the 3rd CAC was observed and was identified as a 4th CAC, but no description of the structure shape was made due to experimental limitations [44]. Hence, these FILs have improved aggregation behaviour when compared with the traditional surfactants, which commonly have only one critical micellar concentration (CMC, which in our case we have identified as 1st CAC) [51]. Taking advantage of these different aggregates, in this work, the influence of IFN-α 2b on their behaviour and their proficiency as a drug delivery system for this protein is evaluated.

5.4.2.1.1 Critical aggregation concentrations

To understand the impact of different simulated biological fluids, protein medium, and IFN-α 2b on the aggregation behaviour of FILs, the $[C_2C_1Im][C_4F_9SO_3]$ was selected. This FIL has aggregates very well characterized in pure water [44] and with other biomolecules like BSA and lysozyme [49,50,57]. One way to have this information is through the careful analysis of the FIL conductivity profile which is dependent on the FIL concentration. As mentioned before, $[C_2C_1Im][C_4F_9SO_3]$ has four different CACs, however, only three can be determined using conductometric titration [44]. In this work, it was measured the ionic conductivity of $[C_2C_1Im][C_4F_9SO_3]$ in a concentration range between 0 and 130 mmol kg^{-1} with different simulated biological fluids at 25°C to study the influence of the distinct CACs and consequently on the different FIL aggregates. For that purpose, six different conditions were selected: (i) 150 mM of NaCl (pH=7.3) to mimic the pH and ionic strength of blood; (ii) 25 mM of KH_2PO_4 (pH=6.8) to replicate the intestine environment; (iii) 100 mM of HCl (pH=1.2) to simulate the gastric fluid acidity; (iv) 150 mM and (v) 5 mM of NaH_2PO_4 (pH=7.4) which are both the media/buffer used for IFN-α 2b and the two concentrations used on this work (depending on the method used); and (vi) 10 μg/mL of IFN-α 2b in 5 mM of NaH_2PO_4 (pH=7.4) to understand the influence of the protein in the aggregates of the FIL. The study of the FIL aggregation behaviour in these fluids allows the finding of how the different aggregates can be influenced by the protein and the impact of the possible administration routes mostly used for biopharmaceuticals.

The conductivity profiles determined for all the systems can be found in Figure 5.4.1, as well as the one in water [44] for the comparison proposes. As expected, the value of conductivity is dependent on the concentration of salt and acid, which increments in the following order: water < IFN-α 2b in 5 mM of NaH_2PO_4 (pH=7.4) ≈ 5 mM of NaH_2PO_4 (pH=7.4) < 25 mM of KH_2PO_4 (pH=6.8) < 150 mM of NaH_2PO_4 (pH=7.4) < 150 mM of NaCl (pH=7.3) < 100 mM of HCl (pH=1.2). The higher concentration of salts in the buffers rises the conductivity value, as well as the acidic solution. This behaviour is related to the high number of ions and higher mobility of these ions in the solution which increases the values of conductivity. This profile is typical of surfactants and the formation of aggregates hampers the mobility of the ions that were solvated and/or free in solution after the process of aggregation begins. The same behaviour is not found for the acidic solution, which after a very sharp transition reaches a plateau, and the conductivity is constant along with the increment of FIL concentration. Finally, the systems with and without protein in the same buffer (5 mM of NaH_2PO_4) have similar behaviour.

A thorough analysis of the conductivity profile was proceeded by applying the Phillips definition [107] which studies the change of the slopes of the conductivity curve along with

the variation of FIL concentration. Three different CACs were determined for almost all the studied systems, as previously obtained in water [44], except for the one of $[C_2C_1Im][C_4F_9SO_3]$ in HCl where only one transition was found. The determined CACs values are shown in Table 5.4.2 and Figure 5.4.2a, as well as the ones of water [44] which are used as a reference for the $[C_2C_1Im][C_4F_9SO_3]$ surfactant behaviour in this discussion. Analysing each transition, Figure 5.4.2a shows that the 1st CAC, for the case of the three systems simulating the biological fluids (25 mM KH_2PO_4 (pH=6.8) < 150 mM NaCl (pH =7.3) < 100 mM HCl (pH =1.2)), occurs in a lower concentration of FIL when compared with the reference (water). This behaviour was not found in the case of the systems with the buffer of IFN-α 2b. These CACs values are very close to the one of water and the concentration of NaH_2PO_4 does not significantly affect the 1st CAC. Furthermore, the presence of IFN-α 2b did not impact the value of this 1st CAC, which is very similar to the reference. Therefore, we can conclude that the simulated biological fluids favour the aggregation of $[C_2C_1Im][C_4F_9SO_3]$.

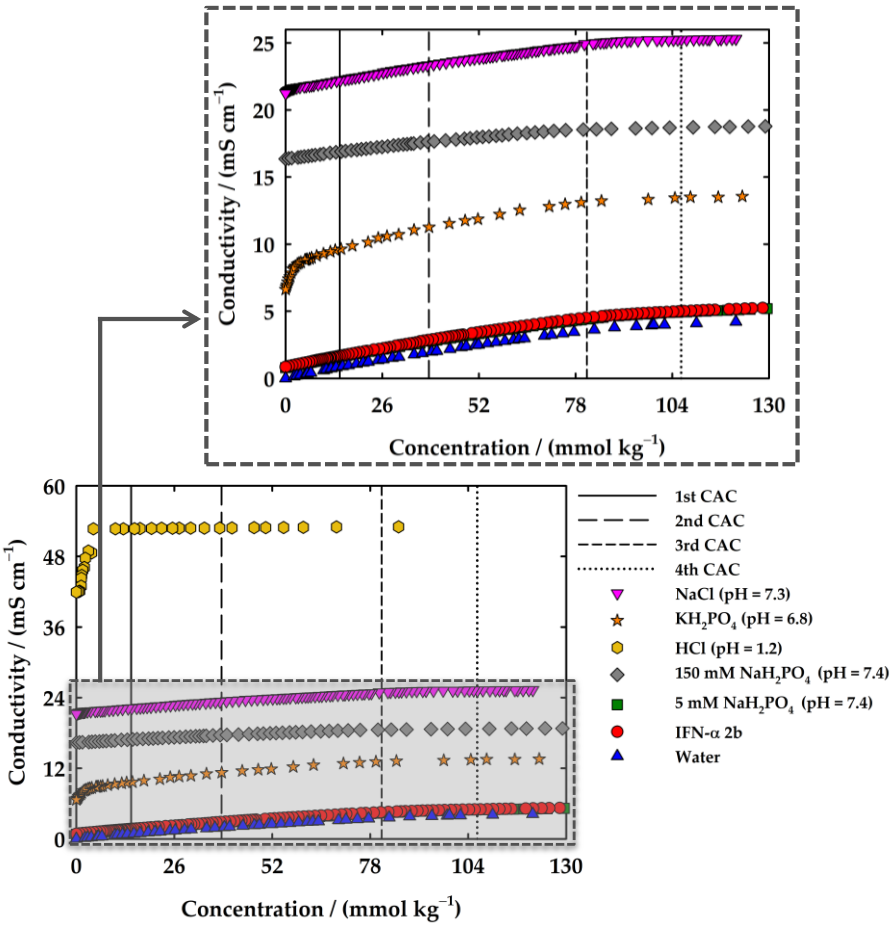

Figure 5.4.1 Conductivity profile of $[C_2C_1Im][C_4F_9SO_3]$ at 25°C from 0 to ~130 mM at different conditions: (i) 150 mM of NaCl at pH=7.3 (pink, ▼); (ii) 25 mM of KH_2PO_4 at pH=6.8 (orange, ★); (iii) 100 mM of HCl at pH 1.2 (yellow, ●); (iv) 150 mM of NaH_2PO_4 at pH 7.4 (grey, ◆); (v) 5 mM of NaH_2PO_4 at pH 7.4 (green, ■); (vi) 5 mM of NaH_2PO_4 at pH 7.4 with 10 µg/mL of IFN-α 2b (red, ●); and (vii)

water (blue, ▲) [44] to comparison purposes. The lines represent the different CACs of $[C_2C_1Im][C_4F_9SO_3]$ in water [44].

Focusing the attention on the second transition, the results indicate two main variations when compared to the water system: (i) there is a slight increment of 2nd CAC and a subsequent impediment on the aggregation for the system with 5 mM of NaH_2PO_4 and with the IFN-α 2b; and (ii) a decrease of 2nd CAC for NaCl (pH =7.3) and 150 mM of NaH_2PO_4 (pH=7.4) indicating an intensification on the aggregation. The system with 25 mM KH_2PO_4 has kept the value very close to the reference and the system with HCl does not show a 2nd CAC, as already mentioned. Finally, in the third transition, there is a decrease in FIL concentration for the systems with 25 mM of KH_2PO_4 (pH=6.8) and 150 mM of NaH_2PO_4 (pH=7.4), indicating that these two conditions boost the aggregation of $[C_2C_1Im][C_4F_9SO_3]$. However. the remaining conditions do not show a significant variation compared to the system in water.

Table 5.4.2 Critical aggregation concentrations, CACs, ionization degree, α, and Gibbs free energy of aggregation, ΔG^0_{agg}, of the systems with $[C_2C_1Im][C_4F_9SO_3]$ determined by conductometry at 25°C.

		150 mM NaCl (pH=7.3)	**25 mM KH_2PO_4 (pH=6.8)**	**100 mM HCl (pH=1.2)**	**150 mM NaH_2PO_4 (pH=7.4)**	**5 mM NaH_2PO_4 (pH=7.4)**	**10 µg/mL IFN-α 2b + 5 mM NaH_2PO_4 (pH=7.4)**	**Water** (a)
First CAC	w_{FIL}	0.0014	0.0008	0.0019	0.0060	0.0056	0.0062	0.0060
	mmol kg^{-1}	3.51	1.99	4.65	14.57	13.75	15.19	14.55
	α	0.14	0.24	0.003	0.85	0.85	0.87	0.79
	ΔG^0_{agg} [kJ mol^{-1}]	-44.6	-44.6	-46.4	-23.4	-23.7	-23.0	-24.7
Second CAC	w_{FIL}	0.0138	0.0158		0.0135	0.0189	0.0179	0.0158
	mmol kg^{-1}	33.69	38.64		32.93	46.13	43.57	38.54
	α	0.75	0.66		0.82	0.85	0.85	0.84
	ΔG^0_{agg} [kJ mol^{-1}]	-22.9	-24.1		-21.6	-20.2	-20.3	-20.8
Third CAC	w_{FIL}	0.0342	0.0293		0.0282	0.0341	0.0342	0.0332
	mmol kg^{-1}	83.46	71.45		68.76	83.13	83.44	81.03
	α	0.17	0.18		0.21	0.34	0.52	0.29
	ΔG^0_{agg} [kJ mol^{-1}]	-29.3	-29.9		-29.5	-26.6	-23.8	-27.5

(a) Data from Pereiro, A.B. *et al.* (2015) [44].

With the aim to obtain additional information on the aggregation behaviour of the $[C_2C_1Im][C_4F_9SO_3]$, the degree of ionization of the aggregates, α, was calculated through the ratio of the slopes of the linear sections over and beneath each CAC. This parameter gives information on the packaging of the aggregates, meaning that a lower value of α indicates that the aggregate is more packed in its structure. From the parameter α, the degree of counterion

binding, β, can be calculated. This parameter is associated with the charge density at the surface, the size, and the hydrophobic nature of the aggregate. It is given by the following equation:

$$\beta = 1 - \alpha \qquad 5.4.1$$

Thus, as much lower is α, higher will be the value of β which is associated with a more packed structure. Then, the counterions will be associated and the polar counterparts will be more compacted due to the larger hydrophobic groups from the tensioactive anion. The α values of the systems studied in this work can be found in Table 5.4.2 and Figure 5.4.2b, like the ones obtained earlier for water [44]. Following the results represented in Figure 5.4.2b, for the 1st CAC, much lower values of α were found for the three simulated biological fluids, when compared to the ones of water, supporting the results former reported. Therefore, these three conditions (NaCl, KH_2PO_4, and HCl) promote the aggregation behaviour of $[C_2C_1Im][C_4F_9SO_3]$ and result in aggregates highly packed than the ones occurring in water. The opposite behaviour was found for the case of solutions with NaH_2PO_4 buffer and IFN-α 2b, where a slight increment of α was noticed. Therefore, the protein and the protein media hinder the aggregation of the FIL, resulting in aggregates with impaired packaging. Moreover, the concentration of NaH_2PO_4 does not affect the packaging of the aggregates, since the calculated α is the same. For the case of 2nd CAC, the NaCl and KH_2PO_4 also show smaller α values compared to water, but this difference is not as strong as in 1st CAC. No significant differences were found between water and the solutions in IFN-α 2b buffer and the one containing the protein. Finally, the 3rd CAC results show a more pronounced result for the case where the IFN-α 2b is present, where a higher value of α was found, indicating that the protein highly disrupts the packing of the aggregates formed in the 3rd CAC.

Another parameter was considered in this study related to the spontaneity of a surfactant to aggregate, given by the standard Gibbs free energy of aggregation, ΔG^0_{agg}. This parameter is provided by the pseudophase model of micellization [108], using the equation:

$$\Delta G^0_{agg} = RT(1+\beta)\ln x_{CAC} \qquad 5.4.2$$

where R is the universal gas constant, T is the absolute temperature and x_{CAC} corresponds to the value of CAC in molar fraction. As long as this parameter is more negative, means that the process of aggregation in the specific CACs is more spontaneous. The values of ΔG^0_{agg}.are illustrated in Table 5.4.2 and Figure 5.4.2c. As expected, the values of the systems with simulated fluids for the case of the 1st CAC are much more negative compared with the reference, supporting the previous conclusions. No significant differences are denoted for the remaining systems. For the second transition, the variations are very small, meaning that the energy spent in the process of aggregation is not highly influenced by the tested conditions.

Similar results are found for the 3rd CAC, excluding the case where the protein is in solution, where the value becomes slightly more positive, indicating an impairment of the FIL aggregation, as previously reported.

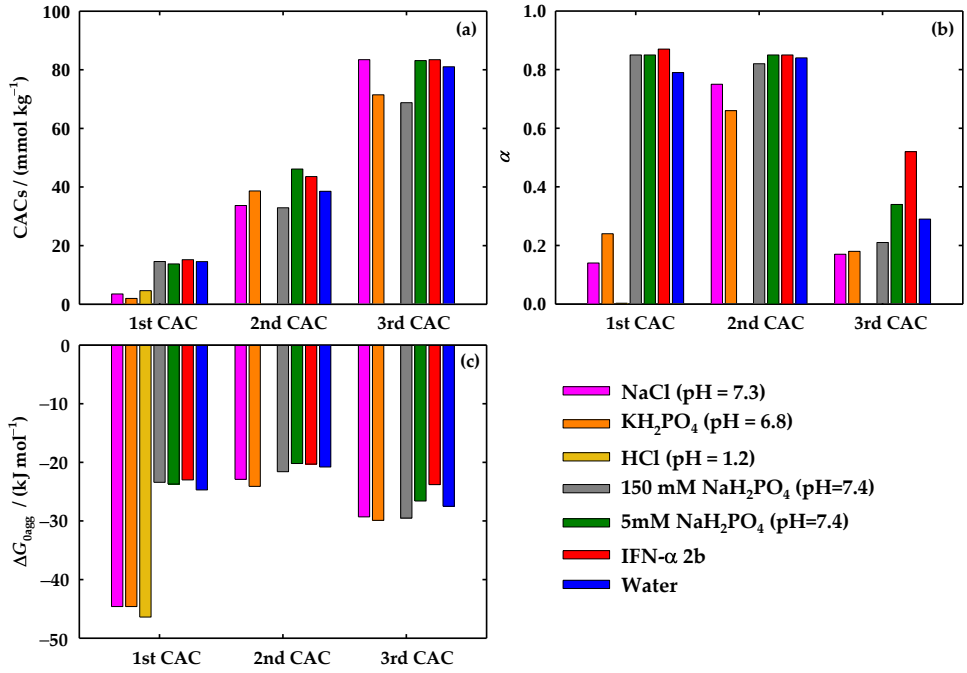

Figure 5.4.2. a) Critical aggregation concentrations (CACs), b) ionization degree (α) and c) Gibbs free energy of aggregation (ΔG^0_{agg}) of $[C_2C_1Im][C_4F_9SO_3]$ at 25°C in different conditions: 150 mM NaCl at pH 7.3 (pink); 25 mM KH_2PO_4 at pH 6.8 (orange); 100 mM HCl at pH 1.2 (yellow); 150 mM of NaH_2PO_4 at pH 7.4 (grey); 5 mM of NaH_2PO_4 pH 7.4 (green); 10 µg/mL mM of IFN-α 2b in 5 mM of NaH_2PO_4 at pH 7.4 (red); and water (blue) [44] to comparison purposes.

In conclusion, the results indicate that the simulated biological fluids (representing the bloodstream strength, gastric and intestinal fluid) improve the aggregation of $[C_2C_1Im][C_4F_9SO_3]$ because the 1st CAC occurs in a lower concentration of FIL, the structure of the aggregates is more packed, and the process of aggregation is more spontaneous when compared with the water + FIL system. This behaviour can be a result of the interactions between the FIL and the ions, increasing the ionic strength of the solution and forcing the molecules of FIL to aggregate sooner. Then, it will allow a reduced amount of FIL to be used in the formulation of drug delivery systems once the aggregation is not impaired in the conditions associated with the routes of administration. Considering the routes of the administration represented by these simulated biological fluids (oral administration: intestinal fluid simulated by 25 mM KH_2PO_4 at pH 6.8 and gastric fluids simulated by 100 mM HCl at pH =1.2; and intravenous administration: bloodstream fluid simulated by 150 mM of NaCl at pH=7.3), it can be chosen a preferential route for the delivery of proteins with this FIL. A drug administrated by the oral route must surpass the gastrointestinal tract until reaching the small

intestine where the drug will be absorbed into the liver and finally enters the bloodstream to be distributed to its site of action, resulting in a lower bioavailability [109]. Consequently, a drug administrated via an intravenous system has full bioavailability since the absorption phase is skipped and lower doses are needed to have a therapeutic effect [109]. Therefore, similar results for the three simulated biological fluids lead to the conclusion that an intravenous administration will be more advantageous to FIL-based delivery systems. On the other hand, no significant influence was found in the case of the system with IFN-α 2b for the first and second CAC. Only in the 3rd CAC is denoted an impairment of the aggregation by the presence of the protein, which might be a result of the protein-FIL interactions or the accommodation of IFN-α 2b in the $[C_2C_1Im][C_4F_9SO_3]$ aggregates.

5.4.2.1.2 Surface properties

For further investigation on the influence of the IFN-α 2b in the aggregation behaviour of FILs, the surface properties of $[C_2C_1Im][C_4F_9SO_3]$ were determined through two methods: (i) the measurement of the surface tension, and (ii) the determination of the contact angles. The surface tension allows the evaluation of the surface activity of the FIL in aqueous solutions. The common behaviour of the surface activity on SAILs is ruled by the adsorption at the air/water interface which reduces the interface energy between both phases. Therefore, the surface tension decreases upon the addition of FIL up to a point where the accumulation of molecules at the interface is completed [110]. This breakpoint is known as the CMC, representing the formation of aggregates. Above the CMC, the value of surface tension is kept constant due to the formation of more aggregates without surface activity For the case of $[C_2C_1Im][C_4F_9SO_3]$, this behaviour was previously found in water, where only one transition, on the surface tension *versus* FIL concentration, was found. In these systems, the perfluoroalkyl chain points towards the inside of the aggregates, keeping the polar functional groups interacting with water [44]. In this work, several independent solutions of $[C_2C_1Im][C_4F_9SO_3]$ in 5 mM of NaH_2PO_4 at pH = 7.4 were prepared and the surface tension was measured. Afterwards, the addition of IFN-α 2b (with a fixed concentration of 5 μg/mL) was carried out for the same systems. To measure the surface tension, the density of the $[C_2C_1Im][C_4F_9SO_3]$ aqueous solutions in water at 25°C was obtained for the diluted region, and the values are described in Table 5.4.3. The density in a range of higher FIL concentrations was previously reported [44] and is also presented in Table 5.4.3.

Figure 5.4.3a represents the results for both systems and an indication of the high purity of the studied solutions is revealed by the lack of a minimum around the breakpoints [110]. In the case of the system in 5 mM of NaH_2PO_4 (pH = 7.4), a very similar behaviour was found when compared with the results previously obtained for $[C_2C_1Im][C_4F_9SO_3]$ in water

[44]. Only one breakpoint was observed, and the CAC and surface tension (γ_{CAC}) values were determined by the linear fitting of the points after and before the breakpoint. This behaviour is very similar to the one of water (see dotted line in Figure 5.4.3a and Table 5.4.4). The transitions corresponding to the 1st and 2nd CAC obtained by conductometric titration are not found in the surface tension profile, while the observed discontinuity reveals a CAC value (81.59 mmol.kg^{-1}) very close to the one of 3rd CAC (80.35 mmol.kg^{-1}) obtained by conductometric titration (see Tables 5.4.2 and 5.4.4).

Table 5.4.3 Density, ρ, and mass fraction, w_{FIL}, for the binary system $[C_2C_1Im][C_4F_9SO_3]$ + water at 25°C.

w_{FIL}	ρ / g·cm^{-3}	Reference
1.0000	1.5458	[44]
0.9804	1.5257	[44]
0.9593	1.5060	[44]
0.9418	1.4949	[44]
0.9212	1.4765	[44]
0.8990	1.4615	[44]
0.8686	1.4421	[44]
0.8398	1.4270	[44]
0.7997	1.4049	[44]
0.7801	1.3914	[44]
0.7398	1.3603	[44]
0.6998	1.3417	[44]
0.6496	1.3081	[44]
0.5999	1.2773	[44]
0.5489	1.2462	[44]
0.5001	1.2177	[44]
0.2989	1.1135	This work
0.1000	1.0353	This work
0.0384	1.0104	This work
0.0245	1.0048	This work
0.0109	0.9994	This work
0.0030	0.9965	This work

The surprising behaviour is found in the system of the $[C_2C_1Im][C_4F_9SO_3]$ with the IFN-α 2b. Four breakpoints were found as observed in Figure 5.4.3a. The CAC and respective γ_{CAC} values are in Table 5.4.4. Three additional transitions occur when compared with the system without the protein, indicating that the IFN-α 2b has a much more active role in the surface activity of the FIL. The 1st breakpoint occurs at a concentration 8 times lower than the 1st CAC determined by conductometric titration. The 2nd and 3rd transitions (6.105 and 21.61 mmol.kg^{-1}, respectively) have values about 2 times smaller when compared with the 1st and 2nd CAC (15.19 and 43.57 mmol.kg^{-1}, respectively). The 4th breakpoint has a similar value to the 3rd CAC

of the FIL (81.59 and 83.44 mmol.kg^{-1}, respectively) as well the CAC and γ_{CAC} values are close to the ones found for the system without protein. These results indicate that the IFN-α 2b decreases the surface tension of the system and promotes the formation of different FIL aggregates at the interface of air/water at a lower FIL concentration. The high influence of the protein on the surface activity of the FILs made the method much more sensitive to alterations in the conformation of the FILs aggregates.

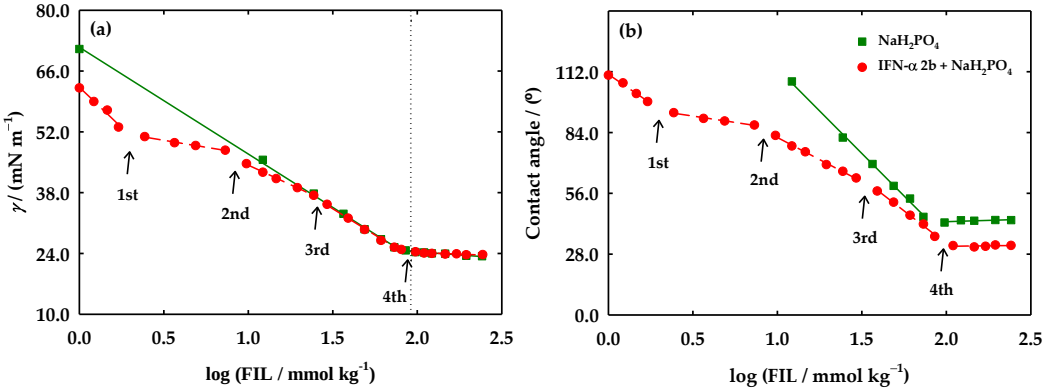

Figure 5.4.3 a) Surface tension and b) contact angles determined at 25°C of $[C_2C_1Im][C_4F_9SO_3]$ aqueous solution in 5 mM NaH_2PO_4 (pH = 7.4) (green, ■) and with 5 µg/mL IFN-α 2b in 5 mM NaH_2PO_4 (pH=7.4) (red, ●). The vertical dotted line in a) represents the value of CAC determined by surface tension in water [44]. The solid and dashed lines represent the fittings to obtain the value of FIL concentration where several breakpoints occurred.

After the evaluation of the CACs, other properties can be taken from the surface tension data. Information on the adsorption occurring in the air/water interface can be determined from the maximum surface excess concentration, Γ_{max}, which is given by the Gibbs adsorption isotherm [111]:

$$\Gamma_{max} = -\frac{1}{2.303nRT}\left(\frac{d\gamma}{d\log C}\right)_T \qquad 5.4.3$$

where n, R, T, and C are the number of species in solution, the universal gas constant, the absolute temperature, and the concentration of FIL, respectively. The n parameter is deduced from the degree of ionization of aggregates, α, as $n = 2 - \alpha$ determined from the conductivity profile of the FIL and assumed to be the same for the surface layer in ionic surfactants [112]. The α value of the 3rd CAC was used to calculate the Γ_{max} of the only transition occurring in $[C_2C_1Im][C_4F_9SO_3]$ in buffer and the 4th breakpoint of the solution with protein. The values of Γ_{max} are expressed in Table 5.4.4 as well as the ones of water for comparison purposes. The Γ_{max} of $[C_2C_1Im][C_4F_9SO_3]$ has the lowest value for the water system, followed by the buffer and finally the solution with protein.

From the Γ_{max} and Avogadro's number (N_A) it can be obtained the minimum area occupied per surfactant molecule at the air/water interface, A_{mim}, as set by:

$$A_{\min} = \frac{10^{18}}{N_A \Gamma_{\max}} \quad 5.4.4$$

Therefore, as bigger is Γ_{max} and subsequently lesser is A_{mim}, the surfactant molecules are rearranged in a denser structure at the solution surface [113]. Therefore, looking for the values of both parameters in Table 5.4.4, the $[C_2C_1Im][C_4F_9SO_3]$ assumes a denser arrangement at the surface in the presence of the protein, given by the highest value of Γ_{max} and lowest value of A_{mim}.

In addition, the parameter that explains the efficacy of a surfactant to reduce the surface tension, Π_{CAC}, was determined, expressing the maximum of surface tension diminution resulting from the dissolution of surfactant molecules. This parameter is determined by the surface tension of the solvent, (γ_0) and the γ_{CAC}, as follows:

$$\Pi_{CAC} = \gamma_0 - \gamma_{CAC} \quad 5.4.5$$

Them, from Π_{CAC}, it was calculated the standard free energy of adsorption, ΔG^0_{ad}, using the following equation [114]:

$$\Delta G^0_{ad} = \Delta G^0_{agg} - \frac{\Pi_{CAC}}{\Gamma_{max}} \quad 5.4.6$$

The results of Π_{CAC} and ΔG^0_{ad} are also reported in Table 5.4.4. When comparing the values of ΔG^0_{ad} with the ones of ΔG^0_{agg}, it is clear that the process of adsorption of the surfactant in the air/water interface is more spontaneous than the process of aggregation due to the more negative values (see Tables 5.4.2 and 5.4.4) for the three systems (water, buffer, protein). Moreover, the previous results are endorsed by the ΔG^0_{ad} parameter, since the less negative value, is found for the case of $[C_2C_1Im][C_4F_9SO_3]$ with IFN-α 2b, indicating that the protein also difficult the adsorption of the FIL in the interface.

Finally, aiming for the disclosure of information on the self-aggregation process and shape of the aggregates, the critical packing parameter, P, was also calculated in this work, as follows [115]:

$$P = \frac{V_0}{A_{\min} l_c} \quad 5.4.7$$

where V_0 and l_c are the volume occupied by the hydrophobic chains in the aggregate core, and the critical chain length, respectively. The structure of the aggregates is defined as spherical when $P \leq 0.33$, cylindrical for $P \leq 0.5$, lamellar when $P \leq 1$ and inverted for $P > 1$ [44]. In summary, it was used a modification of Tanford equations [116] for fluorinated compounds and the critical packing parameter was calculated through the following equations:

$$V_0(\mathrm{nm}^3) = 0.0545 + 0.0380(n_c - 1);\ l_c(\mathrm{nm}) = 0.200 + 0.134(n_c - 1) \qquad 5.4.8$$

$$V_0(\mathrm{nm}^3) = 0.0424 + 0.0416(n_c - 1);\ l_c(\mathrm{nm}) = 0.204 + 0.130(n_c - 1) \qquad 5.4.9$$

where the n_c is the number of carbon atoms in the perfluoroalkyl side chain of the anion. The P values obtained for each system are represented in Table 5.4.4. Analysing the data, the aggregates of $[C_2C_1Im][C_4F_9SO_3]$ assume different conformations in the three systems. For the case of water, the aggregates have a cylindrical shape ($0.33 < P \leq 0.5$). The aggregates of the FIL in 5 mM NaH_2PO_4 (pH = 7.4) have a P very close to 0.5 which is characteristic of cylindrical and lamellar aggregates. The presence of the protein increases the P to values close to 0.7 indicating a lamellar structure of the aggregates. This behaviour might indicate that the aggregates rearrange their structure to accommodate the protein or that the interactions between FIL and IFN-α 2b induce these changes.

Table 5.4.4 Critical aggregation concentration (CAC), surface properties, and critical packing parameters for $[C_2C_1Im][C_4F_9SO_3]$ aqueous solutions determined by the tensiometer and goniometer at 25°C.

		5 mM NaH_2PO_4 (pH=7.4)	**5 µg/mL IFN-α 2b + 5 mM NaH_2PO_4 (pH=7.4)**				**Water[a]**
			Breakpoints				
			1st	**2nd**	**3rd**	**4th**	
Tensiometer	CAC [w_{FIL}]	0.0330	0.0008	0.0025	0.0089	0.0335	0.0375
	CAC [mmol·kg^{-1}]	80.35	1.963	6.105	21.61	81.59	91.39
	γ_{CAC} [mN m^{-1}]	24.6	51.4	48.2	38.3	24.3	24.5
	$10^6\,\Gamma_{max}$ [mol m^{-2}]	3.26	–	–		4.41	2.60
	A_{min} [nm^2]	0.51	–	–		0.38	0.64
	Π_{CAC} [mN m^{-1}]	46.4	–	–		37.8	44.4
	ΔG^0_{ad} [kJ mol^{-1}]	-41.0	–	–		-32.36	-44.5
Critical packing parameters	$P_{eq\ 5.4.8}$ [b]	0.550	–	–		0.7439	0.439
	$P_{eq\ 5.4.9}$ [b]	0.553	–	–		0.7481	0.442
Goniometer	CAC [w_{FIL}]	0.0329	0.0009	0.0030	0.0157	0.0430	–
	CAC [mmol·kg^{-1}]	80.27	2.101	7.288	38.18	104.7	–

(a) Parameters from Pereiro, A.B. *et al.* (2015) [44]; (b) the critical packing parameters were obtained by Equations 5.4.8 and 5.4.9 of the paper.

The study of the contact angles was also carried out in this work. The contact angles are related to the wettability of a surface-active liquid on a solid surface. When a drop of a liquid is placed on a solid surface, the shape of the drop results from the effect of the interfacial tensions between solid (*s*) – water (*w*) – air (*a*). These interfacial tensions are related to the contact angles (θ) by Young's equation [110]:

$$\gamma_{\frac{s}{a}} = \gamma_{\frac{s}{w}} + \gamma_{\frac{w}{a}} \cos\theta \qquad 5.4.10$$

When the drop of a liquid has a contact angle below 90° with the solid, it is established that the liquid wets the surface and is categorized as hydrophilic (*e.g.*, water). When the angle is superior to 90° the liquid is considered hydrophobic and does not wet the solid (*e.g.*, oil).[3] Figure 5.4.3b shows the contact angles calculated to the systems of $[C_2C_1Im][C_4F_9SO_3]$ in 5 mM NaH_2PO_4 (pH = 7.4) and with 5 µg/mL IFN-α 2b in 5 mM NaH_2PO_4 (pH=7.4). A more visual scheme of the behaviour of the drops of each measurement can be found in Figures 5.4.4 and 5.4.5.

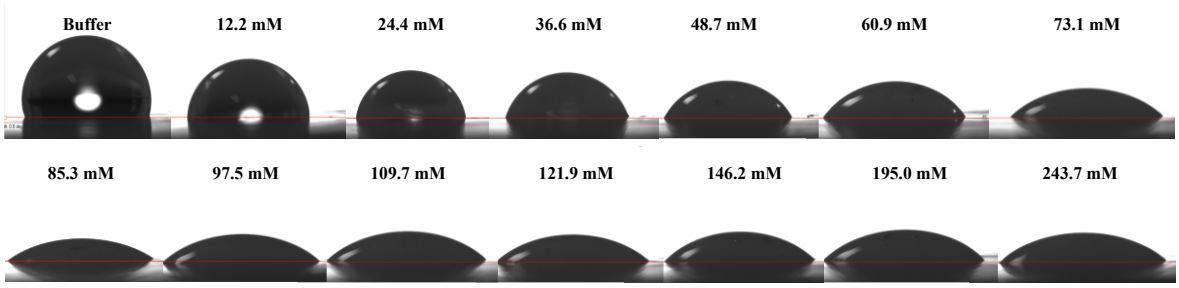

Figure 5.4.4 Drops measured in goniometer at 25°C of $[C_2C_1Im][C_4F_9SO_3]$ aqueous solutions at different concentrations in 5 mM NaH_2PO_4 (pH = 7.4).

The results support the behaviour found for the surface tension measurements. The value of FIL concentration in the breakpoint found for the contact angles (80.27 mmol·kg^{-1}) is very close to the one obtained through the surface tension (80.35 mmol·kg^{-1}) (see Table 5.4.4). For the case of $[C_2C_1Im][C_4F_9SO_3]$ with 5 µg/mL IFN-α 2b system, it was also founded four breakpoints, where the 1st and 2nd transitions have very similar values to the ones obtained with γ, while the 3rd (21.61 (γ) and 38.18 (θ) mmol·kg^{-1}) and 4th (81.59 (γ) and 104.7 (θ) mmol·kg^{-1}) transitions occurred at a higher FIL concentration (see Table 5.4.4). Besides, Figures 5.4.4 and 5.4.5 show a clear decrease in the contact angles with the solid surface with the increment of the FIL concentration. Therefore, the surfactant nature of FILs is characterized by increased wettability.

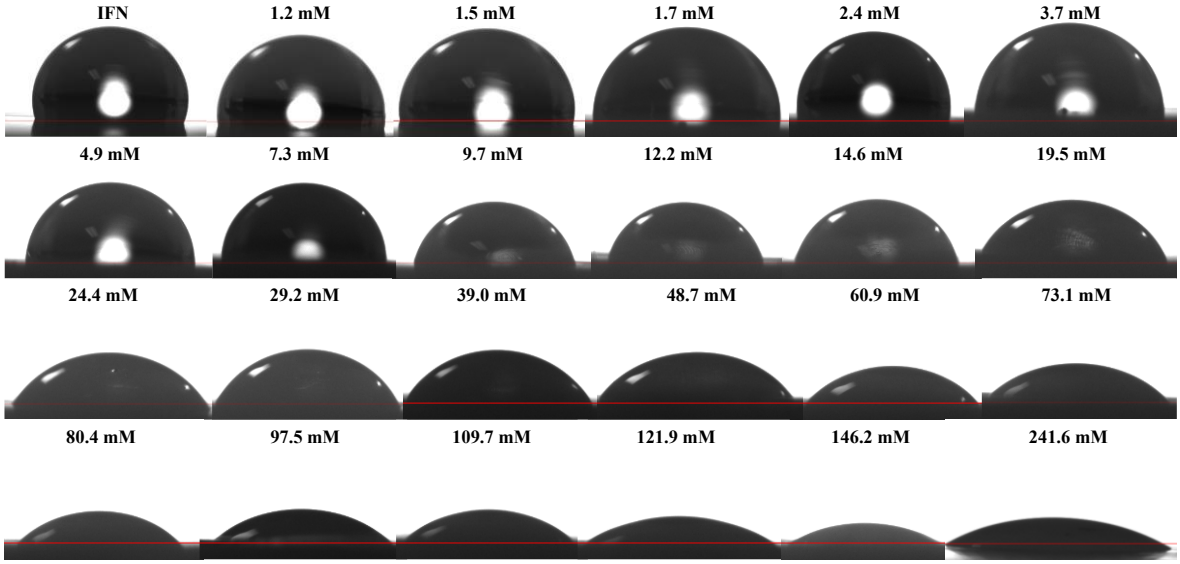

Figure 5.4.5 Drops measured in goniometer at 25°C of $[C_2C_1Im][C_4F_9SO_3]$ aqueous solutions at different concentrations with 5 µg/mL of IFN-α 2b in 5 mM NaH_2PO_4 (pH=7.4).

5.4.2.1.3 Characterization of the self-assembled aggregates

Once the formation of FILs aggregates was determined in the presence of the protein, the characterization of those aggregates was under investigation. First, scanning transmission electron microscopy (STEM) with energy-dispersive X-ray spectroscopy (EDS) was performed to have insight into the size and morphology of $[C_2C_1Im][C_4F_9SO_3]$ aggregates and the impact of IFN-α 2b on them. A concentration above the 1st CAC (approximately two times) of $[C_2C_1Im][C_4F_9SO_3]$ was selected to ensure the formation of FIL aggregates. Three different solutions were prepared: (i) IFN-α 2b at 0.0001 µg/mL; (ii) $[C_2C_1Im][C_4F_9SO_3]$ at 29.2 mM; and c) $[C_2C_1Im][C_4F_9SO_3]$ (29.2 mM) with IFN-α 2b (0.0001 µg/mL). The three samples were prepared in 150 mM NaH_2PO_4 (pH = 7.4). Figure 5.4.6 shows the TEM images obtained for the three solutions on two different scales.

The TEM image of IFN-α 2b is illustrated in Figure 5.4.6a and large dark circles are observed with a size up to around 2 µm, which can indicate that the protein forms large aggregates. In the case of the FIL, Figure 5.4.6b shows considerably smaller dark circles with sizes around 0.05 to 0.7 µm. A comparison with the TEM images of $[C_2C_1Im][C_4F_9SO_3]$ in water (aggregates with sizes around 0.1 to 0.2 µm) [44] shows that the addition of the buffer as dispersant has also an impact on the FIL aggregates with the formation of bigger ones (up to 0.7 µm). These results suggest that the nature of the dispersant plays an important role in the stabilization of the self-assemble structures with an increment of the size in the presence of a buffer. The solution with $[C_2C_1Im][C_4F_9SO_3]$ and IFN-α 2b (Figure 5.4.6c) presents smaller dark circles (around 0.1 to 0.5 µm), and the morphology of the circles seems to change and become more irregular than the circles in the pure compounds. Therefore, an interaction between the

FIL and the protein might justify these differences in size and morphology of the aggregates. This strong interaction between the aggregates of the FIL and the protein can produces complexation between the FIL and the protein, forming aggregates with irregular shapes. This interaction may have positive effects on the stabilization or dispersion of the aggregates of the biomolecule. However, encapsulation of the protein cannot be confirmed by these images.

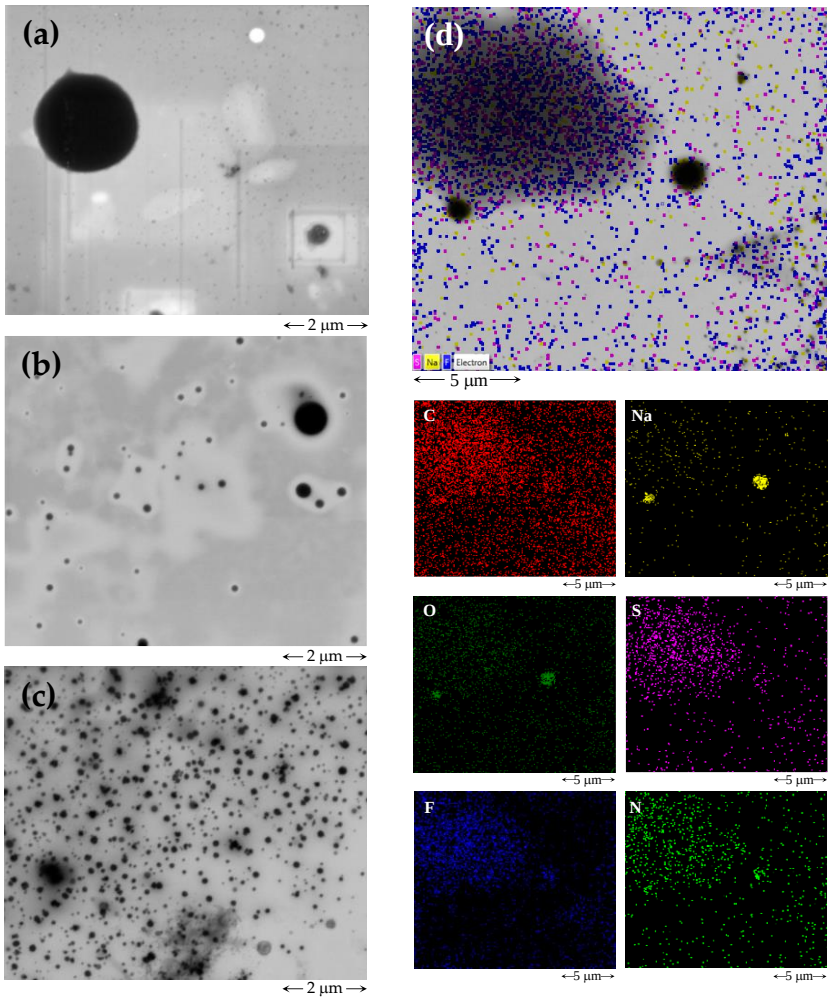

Figure 5.4.6 TEM images of a) IFN-α 2b at 0.0001 µg/mL; b) $[C_2C_1Im][C_4F_9SO_3]$ at 29.2 mM; and c) $[C_2C_1Im][C_4F_9SO_3]$ at 29.2 mM in the presence of IFN-α 2b at 0.0001 µg/mL. d) EDS analysis of $[C_2C_1Im][C_4F_9SO_3]$ with IFN-α 2b at the same conditions. All samples were prepared in 150 mM NaH_2PO_4 (pH = 7.4) and measured at 25°C.

Moreover, the samples were subject to EDS analysis which allowed the elemental analysis of the aggregates, providing images of the distribution of each element present in the aggregate. The IFN-α 2b is constituted by carbon, hydrogen, nitrogen, oxygen, and sulphur, the buffer elements are explicit in its nomenclature, NaH_2PO_4, and the FIL is composed of carbon, hydrogen, nitrogen, sulphur, and fluorine elements. The EDS analysis of IFN-α 2b can be found in Figure 5.4.7 and the elements sodium, oxygen and phosphorus were identified in this solution. The EDS images lead to the conclusion that these elements, predominant in the

buffer structure, are in the darker zones that correspond to the IFN-α 2b aggregates. Then, IFN-α 2b aggregates in a self-assembled structure where an accumulation of the elements of the buffer is identified. There is also the presence of several smaller circles where the buffer elements are concentrated that can be the molecules of protein that do not aggregate or are in a different conformation.

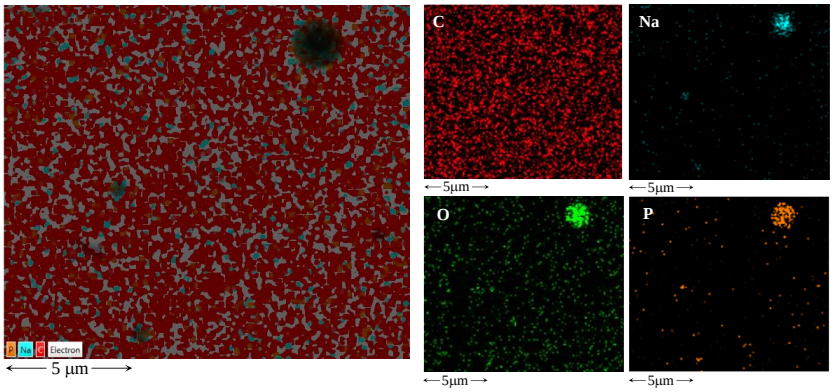

Figure 5.4.7 EDS analysis of IFN-α 2b at 0.0001 µg/mL in 150 mM NaH_2PO_4 measured at 25°C.

Figure 5.4.8 shows the same analysis for the $[C_2C_1Im][C_4F_9SO_3]$ solution. In this case, as expected, the sulphur and fluorine elements of the anion are identified in the areas where the dark circles of FILs aggregates were found. Moreover, the elements of buffer, such as sodium, and oxygen (from FIL and buffer), are more concentrated in the FIL aggregates, leading to the conclusion of a strong effect of the buffer in the FILs aggregates. ~

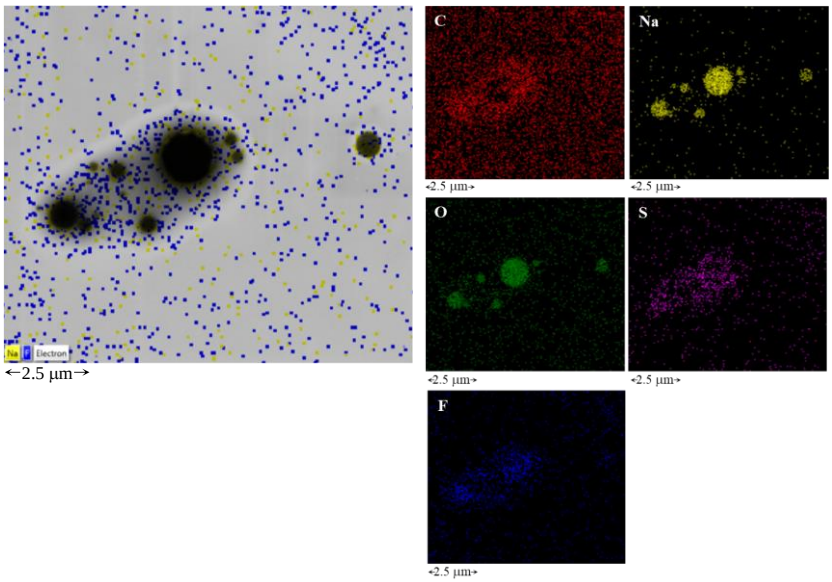

Figure 5.4.8 EDS analysis of $[C_2C_1Im][C_4F_9SO_3]$ at 29.2 mM in 150 mM NaH_2PO_4 measured at 25°C.

The EDS analysis of the mixture $[C_2C_1Im][C_4F_9SO_3]$ with IFN-α 2b is illustrated in Figure 5.4.6d and the results show that the irregular dark circles have a composition similar to both protein and FIL, with a diffusion of the elements of the buffer and the FIL in the dark

spots. In this case, nitrogen analysis was also possible to obtain due to the higher population of this element in the solution (from the protein and FIL). This element is also concentrated in the area that corresponds to the aggregates found in the images. These results support a protein-FIL interaction due to the dispersion of the components of both species focused on the dark spots. Therefore, the dark circles correspond to an aggregate formed by the FIL and the protein, which allows the dispersion of the bigger aggregates formed by the isolated protein.

Dynamic light scattering (DLS) was carried out in this work to further characterize the aggregates of FIL in the presence of the protein IFN-α 2b. This is a useful tool with a non-invasive character that gains access to information on the size of the aggregates. For that, two concentrations of $[C_2C_1Im][C_4F_9SO_3]$ (two times the 1st CAC and above the 3rd CAC) were selected, aiming to understand how the aggregates of the FIL are impacted by the protein. Figures 5.4.9a and 5.4.9b shows the DLS spectra of $[C_2C_1Im][C_4F_9SO_3]$ at 29.3 mM and 243.8 mM, respectively, in 150 mM NaH_2PO_4 at pH = 7.4 with IFN-α 2b at 50 µg/mL. The FIL blanks in each studied concentration and the protein blank are also included in Figures 5.4.9a and 5.4.9b. The characteristic spectrum of the IFN-α 2b (black solid line of Figure 5.4.9) comprises four characteristic peaks that correspond to aggregates of sizes between 8 and 25 nm, 28 and 145 nm, 180 and 1400 nm, and 4000 and 6800 nm. The structural elucidation of the interferon-alpha 2b revealed that this protein exists in crystals as a dimer in the native state. The biological role of the dimer is not fully comprehended, and the literature suggests that this protein is active in a monomer conformation. However, the dimer was associated with a possible inactive storage conformation of the molecule or may have relevance in the biological activity of the protein, once the dimerization is relevant in other types of interferons [64]. The $[C_2C_1Im][C_4F_9SO_3]$ shows two peaks around 80 to 170 nm and 430 to 1000 nm in the concentration two times the 1st CAC and one peak between 2 and 14 nm for the concentration above the 3rd CAC (Figure 5.4.9b). For the samples containing both FIL and IFN-α 2b, the characteristic peaks of the FIL slightly shifted to bigger values (around 95 to 270 nm and 620 to 1970 nm in Figure 5.4.9a). A new peak appears on the spectrum, between 10 and 40 nm, that may correspond to smaller aggregates typical of the protein, with a slight shift in the hydrodynamic diameter. Figure 5.4.9b shows that in the mixture of FIL and protein, the characteristic peak of the $[C_2C_1Im][C_4F_9SO_3]$ is slightly tightened and two new peaks appear on the spectrum between 60 and 615 nm and 2000 and 6200 nm with a very reduced intensity. These new peaks can be associated with the aggregates of the protein either in solution or to another conformation that is a result of the interaction of the FIL with the protein. Therefore, these results endorse the previously obtained, where strong interactions between the FIL and the IFN-α 2b are occurring and have an effect on the aggregates of the FIL.

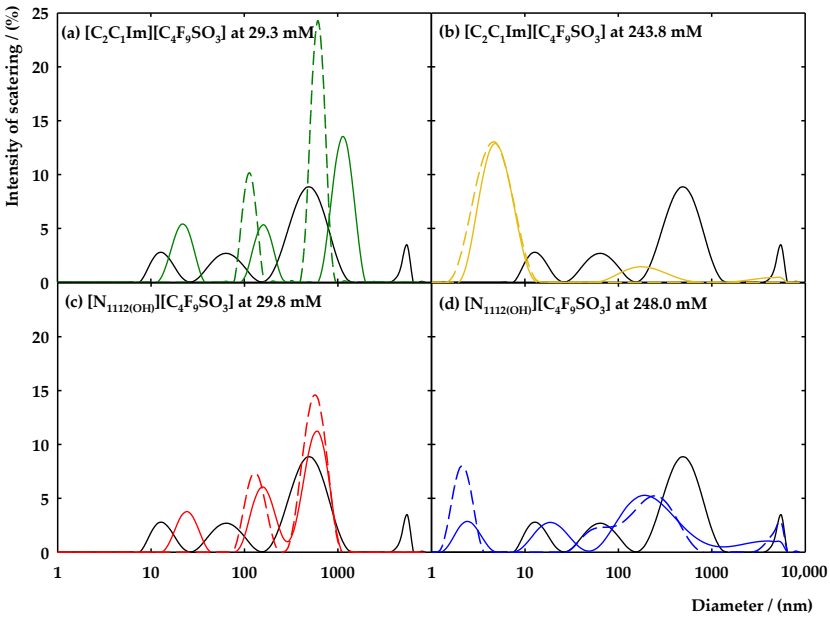

Figure 5.4.9 DLS spectra of IFN-α 2b (50 µg/mL, black solid line) with $[C_2C_1Im][C_4F_9SO_3]$ at: a) 29.3 mM and b) 243.8 mM; and $[N_{1112(OH)}][C_4F_9SO_3]$ at: c) 29.8 mM and d) 248.0 mM. Solid lines represent the samples with protein and FIL and the dashed lines illustrate the FILs blanks. All samples were prepared in 150 mM NaH_2PO_4 at pH = 7.4 and measured at 25°C.

Aiming to seek more evidence into the FIL aggregates behaviour and explore the possibility of encapsulating the IFN-α 2b with those aggregates, $[N_{1112(OH)}][C_4F_9SO_3]$ was also studied by DLS. In recent work, preliminary results pointed out the $[N_{1112(OH)}]^+$ cation as a promotor of interactions between FILs and IFN-α 2b [103]. Therefore, $[N_{1112(OH)}][C_4F_9SO_3]$ concentrations of 29.8 mM and 248 mM were selected to ensure aggregation of this FIL and the results are depicted in Figures 5.4.9c and 5.4.9d. In the case of a concentration two times greater than the 1st CAC (29.8 mM, Figure 5.4.9c), two characteristic peaks are found approximately from 70 to 250 and 290 to 1080 nm, whereas for the case of concentration above the 3rd CAC (248 mM, Figure 5.4.9d) three peaks were recorded in-between 1 and 4 nm, 28 and 825 nm, and 2800 and 6440 nm. Analysing the mixture of $[N_{1112(OH)}][C_4F_9SO_3]$ with IFN-α 2b (see Figure 5.4.9c), the peaks of the FIL have a diminished intensity and there is a small shift of the first peak to values of 85 to 280 nm. Another peak arises in the range of 13 to 44 nm, which does not overlap either with the peaks of the protein or the FIL. However, it might result from the smaller aggregates of the IFN-α 2b that have a change in their hydrodynamic diameter. Figure 5.4.9d also shows that the intensity of the peak of the smaller aggregates of FIL have a decreased intensity and the intermediate peak had suffered a deconvolution in two peaks, shifting to lower values of hydrodynamic diameter. Therefore, an interaction between protein-FIL might be occurring, leading to modifications in the aggregates of FILs. The results are very similar to the ones obtained to $[C_2C_1Im][C_4F_9SO_3]$ (see Figures 5.4.9a and 5.4.9b),

leading to the conclusion that the aggregates of both FILs have very similar interaction with this protein. Therefore, the main structural feature of the FIL controlling this behaviour is the anion. Furthermore, these results support the previously obtain, indicating that the aggregation of the protein is reduced, and smaller aggregates are formed. The FIL aggregates do not completely cover the protein (encapsulation), but DLS results confirm the strong interaction between FILs and IFN-α 2b.

Moreover, the polydispersity index (PdI) was obtained by DLS which determines the heterogeneity of the sample in the function of the size. There are defined international standards organizations (ISOs) for the characterization of nanomaterials based on the PdI, where it is considered that a PdI < 0.05 characterizes monodisperse samples, whereas PdI > 0.7 is characteristic of the polydisperse distribution of the particles (ISO 22,412:2017) [117]. Table 5.4.5 shows the PdI values obtained from the DLS spectra acquisition for each experiment. The analysis of the samples with $[C_2C_1Im][C_4F_9SO_3]$ demonstrates two distinct behaviours: (i) the presence of FIL two times the 1st CAC in the IFN-α 2b increases its poly-dispersity, and decreases the PdI of the FIL aggregates; (ii) in the concentration above the 3rd CAC with IFN-α 2b, the polydispersity is diminished when related with the protein alone and increased for the FIL aggregates. In the case of cholinium cation at lower concentrations, the behaviour is similar to the imidazolium cation. However, for the concentration above the 3rd CAC, the PdI of the solution FIL + protein is always higher than the protein itself and the FIL aggregates. This parameter supports the results previously discussed related to the size of the aggregates.

Table 5.4.5 Polydispersity index (PdI) obtained from DLS measurements in 150 mM NaH_2PO_4 measured at 25°C.

Sample	PDI
50 μg/mL IFNα-2b	0.427
29.3 mM $[C_2C_1Im][C_4F_9SO_3]$	1.000
29.3 mM $[C_2C_1Im][C_4F_9SO_3]$ + 50 μg/mL IFNα-2b	0.630
243.8 mM $[C_2C_1Im][C_4F_9SO_3]$	0.157
243.8 mM $[C_2C_1Im][C_4F_9SO_3]$ + 50 μg/mL IFNα-2b	0.279
29.8 mM $[N_{1112(OH)}][C_4F_9SO_3]$	0.784
29.8 mM $[N_{1112(OH)}][C_4F_9SO_3]$ + 50 μg/mL IFNα-2b	0.628
248.0 mM $[N_{1112(OH)}][C_4F_9SO_3]$	0.543
248.0 mM $[N_{1112(OH)}][C_4F_9SO_3]$ + 50 μg/mL IFNα-2b	0.849

The overall conclusions of this section strengthen the hypothesis of very strong interactions occurring between the selected FILs and the protein IFN-α 2b. This protein has a strong impact on the FILs aggregates, leading to modifications in the aggregation process, surface activity, shape, size, and morphology of those aggregates. These results raise the assumption that a complexation between both molecules is happening and allows the FIL to

disperse the aggregates of the protein by transporting the protein without fully covering the surface of the biomolecule.

5.4.2.2 Interactions of the fluorinated ionic liquids with interferon-alpha 2b

The interactions between the FILs and proteins are of great relevance to understanding the potential of FILs and their application as DDSs of biopharmaceuticals. The stability and activity of proteins depend on a delicate balance between the interactions of the biomolecules with the surroundings, and the addition of FIL can completely alter their conformation and subsequently hinder their function. In this work, it was carried out several efforts to strengthen the knowledge of the interactions between FILs and IFN-α 2b. For that goal, both $[C_2C_1Im][C_4F_9SO_3]$ and $[N_{1112(OH)}][C_4F_9SO_3]$ were selected in a concentration range where the aggregation behaviour plays the key role in their activity. Firstly, it was used several spectroscopy methods to obtain information on protein-FIL interactions by having insights into the structural conformation of the protein, such as UV-vis, fluorescence, and circular dichroism spectroscopies. In the end, the binding affinity between the FILs and IFN-α 2b was accessed by performing microscale thermophoresis.

5.4.2.2.1 Spectroscopy analysis

As a first approach, UV–vis spectrophotometry was used to measure the absorption spectra of the IFN-α 2b. This method follows the behaviour of the chromophores composing the structure of the proteins, such as the amide group of the protein backbone and the aromatic amino acids like tryptophan, tyrosine, and phenylalanine. Therefore, these structural features act as spectral probes of significant perturbations occurring in the local environment of the protein, through their exposure to the solvent. Thus, IFN-α 2b absorption spectra is very similar to most proteins, with a characteristic band between 260 and 300 nm. Any alteration on the profile of this band may indicate a perturbation of the protein chromophores, and consequently the existence of an interaction with a ligand. For example, the coverage of the protein surface by the FIL can be reflected in the absorption spectra by the absence of the characteristic absorption band or reflected in the turbidity of the solution due to the presence of protein-FIL aggregates [49].

Solutions of $[C_2C_1Im][C_4F_9SO_3]$ and $[N_{1112(OH)}][C_4F_9SO_3]$ were prepared in five different concentrations to cover all the aggregation levels: (i) below the 1st CAC (7.3 mM for $[C_2C_1Im]^+$ and 8.2 mM for $[N_{1112(OH)}]^+$) to understand the interplay of the FILs monomers with the protein; (ii) above the 1st CAC (26.6 mM for $[C_2C_1Im]^+$ and 25.8 mM for $[N_{1112(OH)}]^+$); (iii) above the 2nd CAC (59.7 mM for $[C_2C_1Im]^+$ and 110.8 mM for $[N_{1112(OH)}]^+$); (iv) above the 3rd CAC (106.3 mM for $[C_2C_1Im]^+$ and 192.2 mM for $[N_{1112(OH)}]^+$), and (v) above the 4th CAC (425.1 mM for $[C_2C_1Im]^+$

and 384.4 mM for $[N_{1112(OH)}]^+$ where the value of the 4th CAC of $[C_2C_1Im][C_4F_9SO_3]$ was used as a reference for both FILs). The solutions were prepared in 5 mM of NaH_2PO_4 (pH=7.4) with 20 µg/mL of IFN-α 2b. The measurements were made after the preparation of the solutions (time 0h) and after 24h of incubation to increase the contact time between the aggregates of the FIL and the protein. The results can be found in Figures 5.4.10a and 5.4.10b, along with the blank of the protein for comparison purposes. To ease the discussion of the results and the comparison between the studied conditions, the value of absorbance at a wavelength of 280 nm (characteristic band) was represented in Figures 5.4.10c and 5.4.10d.

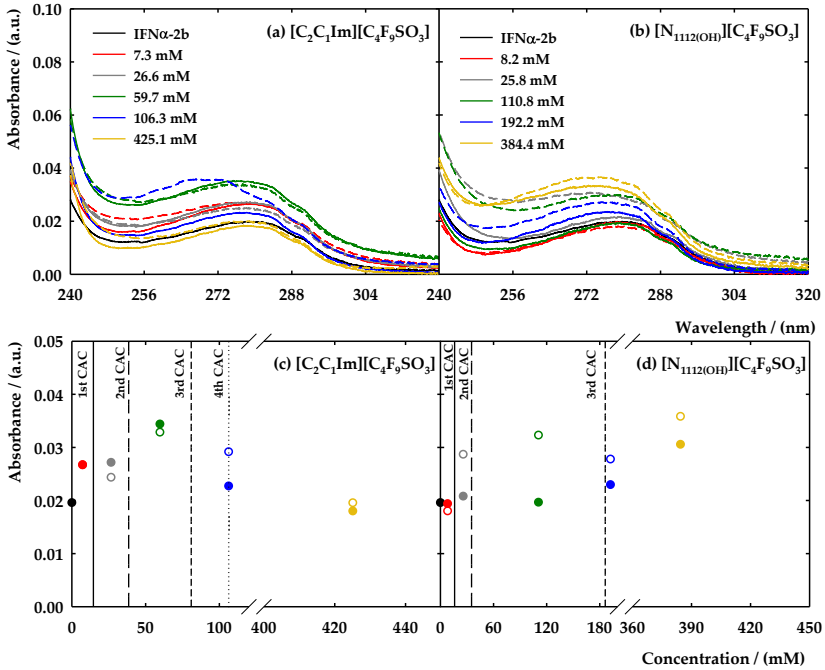

Figure 5.4.10 UV–vis absorption spectra of a) $[C_2C_1Im][C_4F_9SO_3]$ and b) $[N_{1112(OH)}][C_4F_9SO_3]$ with IFN-α 2b at 20 µg/mL (black solid line) at different concentrations. All samples were prepared in 5 mM NaH_2PO_4 (pH = 7.4) and measured at 25°C. In c) and d) are represented the variation of the absorbance at 280nm. The solid lines in a) and b) and full symbols in c) and d) correspond to the measurements at 0h. The dashed lines in a) and b) and the empty symbols in c) and d) correspond to the measurements after 24h of incubation. The colours of the symbols correspond to the colours of the lines.

Figures 5.4.10a and 5.4.10c show the results concerning $[C_2C_1Im][C_4F_9SO_3]$. In almost all concentrations of FIL is perceived a slight increase in the absorbance, when compared to the value of IFN-α 2b. However, this increment was not verified in the most concentrated solution of FIL. Besides, the increment is not proportional to the FIL concentration, which may indicate that the different aggregates do not influence the surroundings of the protein in the same manner. The highest value of Abs_{280nm} is found for the FIL concentration above the 2nd CAC. Comparing the different times of incubation, the results indicate that only in the concentration above the 3rd CAC there is a significant difference in the value of Abs_{280nm} and

is visible a shift of the band towards low values of absorbance. Hence, the most differences are found in the case of the concentrations of FIL above the 2nd and 3rd CAC, enforcing that the aggregates of $[C_2C_1Im][C_4F_9SO_3]$ interact with the IFN-α 2b, boosting the exposition of the chromophores to the solvent. However, in any case, the characteristic band of the protein is reduced or omitted, indicating that the FIL does not cover the chromophores of the protein, and consequently, there is no indication that the protein is being encapsulated by the $[C_2C_1Im][C_4F_9SO_3]$ aggregates.

Analysing the results for $[N_{1112(OH)}][C_4F_9SO_3]$, Figures 5.4.10b and 5.4.10d elucidate the interactions with the IFN-α 2b. A $[C_2C_1Im][C_4F_9SO_3]$-like behaviour is found, where the absorbance of the protein band increases in the presence of the FIL. However, in this case, is proportional to the increment of FIL concentration and is much more evident after the incubation of 24h. The most significant differences are found in the concentrations where the FIL aggregates are formed, reinforcing the assumption of an interaction between the $[N_{1112(OH)}][C_4F_9SO_3]$ aggregates and protein. This interaction also promotes the disclosure of the chromophores to the solvent, increasing the absorbance intensity.

In summary, UV–vis spectrophotometry supports the presence of an interaction between the FILs aggregates and the protein, augmenting the exposition of IFN-α 2b chromophores to the solvent. These results also indicate that $[C_2C_1Im]^+$ and $[N_{1112(OH)}]^+$ cations present similar behaviour, supporting that the anion has the most important role in this interaction. Comparing these results with the ones obtained for lysozyme [49], the protein-FILs interactions have high specificity and depend on the target protein. In this case, there were no significant alterations in the characteristic peak of IFN-α 2b, and the studied solutions do not present turbidity. The FILs aggregates do not seem able to encapsulate the protein, or at least, they do not hide the residues that are studied within this technique.

Another well-established analytical technique to study protein-FIL interactions is fluorescence spectroscopy. The intrinsic fluorescence of the proteins is an outcome of the aromatic residues, where usually the dominant fluorophore is the tryptophan. As observed in the previous section, the tryptophan has an absorption of around 280 nm, and its emission is usually near 340 nm. The emission spectrum of the tryptophan is very sensitive to solvent polarity [118]. Therefore, a shift of the maximum emission towards smaller wavelengths, the so-called blue shift, indicates that the aromatic residue is concealed in the native structure of the protein. A shift of the emission spectrum to longer wavelength values, known as the red shift, indicates an exposition of the tryptophan and is associated with the unfolded state of the protein structure[118]. Consequently, a blue shift of the emission is associated with a productive effect on the structure of the protein, whereas a red shift indicates that the ligand has a destructive impact on the protein's structural features. Besides, the increment or decrease

of the intensity of the emission spectra is related to the amount of exposition of the fluorophores to the solvent.

In this work, the emission spectra of the IFN-α 2b was obtained in a range of 300 to 450 nm and a maximum emission of around 340 nm (Figure 5.4.11). The sample was excited at 280 nm to obtain the maximum emission of the intrinsic fluorescence of the protein. Typically, an excitation of 295 nm is used to selectively excite the tryptophan and avoid the response of other aromatic residues like tyrosine.[1] However, in this case, the goal was to obtain a maximized emission spectrum to avoid issues related to the signal intensity and gather information on the impact and interactions of FIL aggregates with the IFN-α 2b [64].

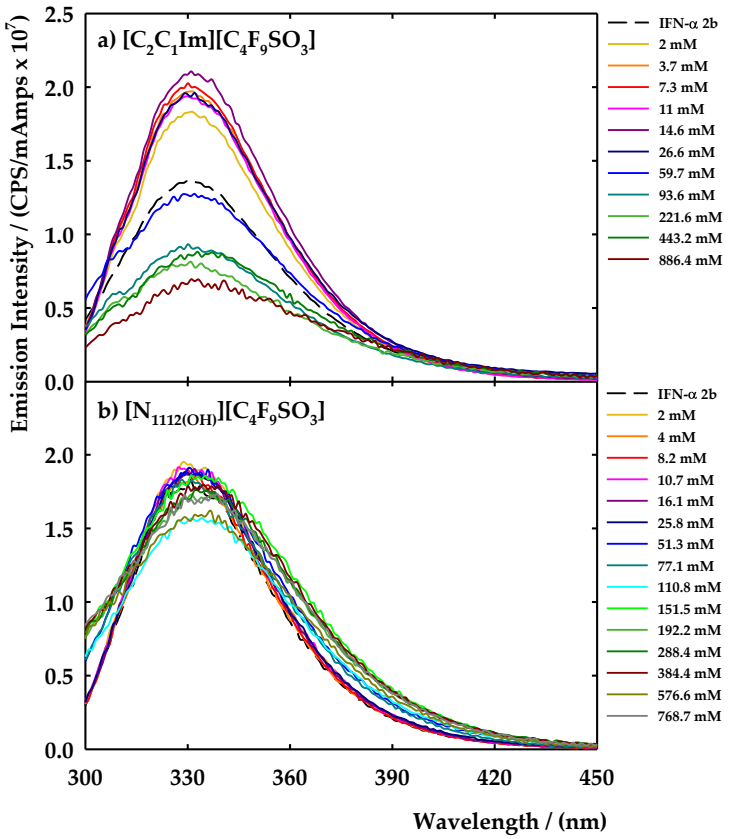

Figure 5.4.11 Fluorescence spectra of IFN-α 2b at 20 µg/mL (black dashed line) with a) $[C_2C_1Im][C_4F_9SO_3]$ and b) $[N_{1112(OH)}][C_4F_9SO_3]$ at different concentrations. All samples were prepared in 5 mM NaH_2PO_4 at pH = 7.4 and measured at 25°C.

Both $[C_2C_1Im][C_4F_9SO_3]$ and $[N_{1112(OH)}][C_4F_9SO_3]$ were selected to study the interactions with IFN-α 2b by fluorescence spectroscopy. Different solutions were prepared and measured in a range of concentrations covering all the aggregation steps of the FIL: (i) four samples below the 1st CAC to seek for interactions between the FILs monomers and the protein; (ii) two samples near and above the 1st CAC; (iii) one above the 2nd CAC; (iv) one above the 3rd CAC, and (v) three above of the 4th CAC for $[C_2C_1Im][C_4F_9SO_3]$. In the case of $[N_{1112(OH)}][C_4F_9SO_3]$, additional samples in-between 2nd and 3rd CAC and above 3rd CAC were measured. The

protein concentration was fixed to 20 µg/mL in all solutions. The emission spectra of all the measured solutions are illustrated in Figure 5.4.11 for $[C_2C_1Im][C_4F_9SO_3]$ and $[N_{1112(OH)}][C_4F_9SO_3]$, respectively. To facilitate the discussion of the results, it was represented in Figures 5.4.12 and 5.4.13 the values of maximum emission intensity and corresponding wavelength (λ_{max}) to have information on the exposition of fluorophores of the protein and which type of interaction the ligands have with the protein, respectively.

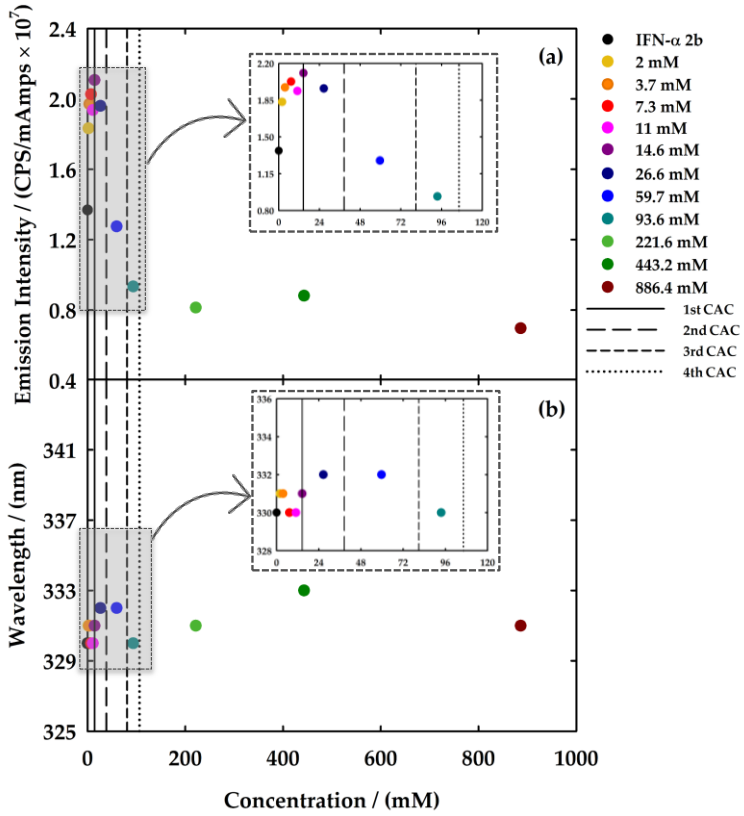

Figure 5.4.12 a) Emission intensity and b) wavelength variation of the maximum of the emission spectra of different concentrations of $[C_2C_1Im][C_4F_9SO_3]$ with IFN-α 2b at 20 µg/mL recorded at 280 nm. All samples were prepared in 5 mM NaH_2PO_4 (pH = 7.4) and measured at 25°C.

Figure 5.4.12 corresponds to the results related to the impact of the variation of the concentration of $[C_2C_1Im][C_4F_9SO_3]$ in the protein emission. In this plot, it is observed two main comportments concerning the intensity of the emission: the presence of FIL in concentrations under the first CAC increases the emission intensity of the IFN-α 2b. After the 1st CAC, a decrease of that intensity to values lower than the spectrum of IFN-α 2b is observed when the FIL concentration is higher. Figure 5.4.12b shows that in the range of concentrations below the 1st CAC, the variations in λ_{max} are between 0 to 1 nm (blue and red shift), and above the 1st CAC are found variations between 0 to 3 nm to a red shift. The results indicate that two different interactions are occurring within this system: (i) first, the FIL monomers interact with the protein and the fluorophores are more exposed to the solvent, and (ii) the aggregation of

the FIL induces a quenching of the emission intensity which might indicate that the interaction with the protein conceals the fluorophores from the solvent. The red shift of λ_{max} does not appear significant, and this FIL does not show a destructive behaviour towards the protein in this range of concentrations.

Figure 5.4.13 reports the results regarding the $[N_{1112(OH)}][C_4F_9SO_3]$ and its influence on the IFN-α 2b emission. In Figure 5.4.13a, it is noticed a distinct behaviour from the $[C_2C_1Im][C_4F_9SO_3]$. Until the concentration above the 2nd CAC, the FIL does not show a considerable influence on the intensity of the emission of IFN-α 2b. Then, there is a slight decrease of the intensity in the concentrations close to the 3rd CAC, and after this transition, the intensity stabilizes once again until the concentration of 384 mM. These variations are very small when compared with the pronounced variations found for the emission intensity of the solutions with $[C_2C_1Im][C_4F_9SO_3]$ (Figure 5.4.12a). However, this comportment is not reflected in Figure 5.4.13b, where much greater differences are found in the λ_{max}. The variation of λ_{max} in the concentrations above the 1st CAC are within 0 and 4 nm and mostly in a blue shift regime, indicating constructive interactions between the $[N_{1112(OH)}][C_4F_9SO_3]$ and IFN-α 2b.

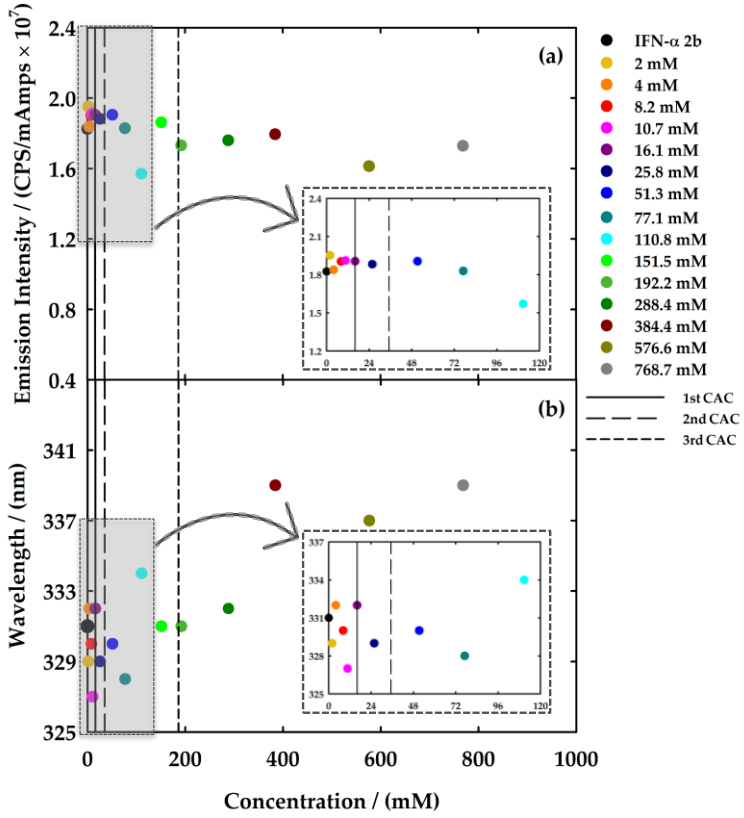

Figure 5.4.13 a) Emission intensity and b) wavelength variation of the maximum of the emission spectra of different concentrations of $[N_{1112(OH)}][C_4F_9SO_3]$ with IFN-α 2b at 20 μg/mL recorded at 280 nm. All samples were prepared in 5 mM NaH_2PO_4 (pH = 7.4) and measured at 25°C.

This behaviour is conserved until 77 mM (above the 2nd CAC), meaning that the FILs aggregates also have a positive interaction with the protein, making its fluorophores assume a tighter conformation regarding the solvent. After that, there is a red shifting of 3 nm in the concentration close to the 3rd CAC, followed by a stabilization of λ_{max}. Finally, in concentrations above 384 mM, there is an interaction with the protein dictated by a red shifting up to 8 nm, meaning that unfolding of the protein might be occurring, completely exposing the fluorophores to the solvent. To sum up, the $[N_{1112(OH)}][C_4F_9SO_3]$ has a very ambiguous behaviour, since in concentrations below the 3rd CAC the interactions are favouring the structure of the protein to a more closed conformation. Between 288 and 384 mM, there is a complete alteration of the behaviour, and the FIL aggregates assume destructive interactions with the protein, leading to its unfolding. Nevertheless, these FIL concentrations are in a much higher range than the ones that must be used in a biomedical approach, and this result does not affect the applicability of this FIL.

Analysing both systems, there was found a decrease in the intensity in the region between ~14mM and ~110mM (above the 1st CAC), more pronounced for $[C_2C_1Im][C_4F_9SO_3]$, which is called the quenching effect. A very well-known equation, the Stern-Volmer, was used to characterize the quenching occurring in this region. This equation characterizes the collisional quenching that can occur when the excited state of the fluorophore is disabled due to the contact with another molecule (quencher), without chemical alteration [118]. Therefore, the collisional quenching is described by:

$$F_0/F = 1 + K[Q] = 1 + k_q\tau_0[Q] \qquad 5.4.11$$

where F_0 and F are the fluorescence intensities of the fluorophore in the absence and presence of the quencher, respectively, K is the Stern-Volmer quenching constant, k_q is the biomolecular quenching constant, τ_0 is the unquenched lifetime, and $[Q]$ is the quencher concentration. The K constants were obtained through the slope of the F_0/F *versus* the quencher concentration, yielding a K of $1.06\text{x}10^{-2}$ mM^{-1} for $[C_2C_1Im][C_4F_9SO_3]$ and $1.95\text{x}10^{-3}$ mM^{-1} for $[N_{1112(OH)}][C_4F_9SO_3]$. This value gives information on the sensitivity of the fluorophore to a quencher. The higher value of K can indicate that the $[C_2C_1Im][C_4F_9SO_3]$ is freer in solution or at the surface of the biomolecule. The lower value of $[N_{1112(OH)}][C_4F_9SO_3]$ can be related to the FIL is more buried in the macromolecule, which is in concordance with the disruption of the protein conformation at higher FIL concentrations. Through the τ_0 of IFN-α 2b (approximately $2.95\text{x}10^{-9}$ s [119]) was possible to obtain the k_q, considering that:

$$K[Q] = k_q\tau_0[Q] \qquad 5.4.12$$

For $[C_2C_1Im][C_4F_9SO_3]$, the value of k_q is 3.59x10^6 mM^{-1}s^{-1} for $[C_2C_1Im]^+$ and 6.61x10^5 mM^{-1}s^{-1} for $[N_{1112(OH)}]^+$. The comparison of these values with the largest possible biomolecular quenching constant for dynamic collision, 2.0× 10^7 mM^{-1}s^{-1} [120], indicates that the quenching is dynamic, and no ground-state complex is formed during quenching process.

Circular dichroism (CD) spectroscopy is the most conventional method used to promptly assess the secondary structure of proteins [121]. In this work, it was used to infer the changes in the secondary structure of IFN-α 2b upon the addition of $[N_{1112(OH)}][C_4F_9SO_3]$. The CD spectrum for $[C_2C_1Im][C_4F_9SO_3]$ was not possible to record due to the imidazolium ring yields very intense signals and consequently is technically unfeasible. Therefore, the CD spectra of IFN-α 2b at 100 µg/mL in 150 mM NaH_2PO_4 (pH = 7.4) and of IFN-α 2b with 248 mM of $[N_{1112(OH)}][C_4F_9SO_3]$ were measured in this work to infer the FIL influence on the protein secondary structure. The selected FIL concentration is above the ones that previously showed potential to unfold the protein in fluorescence spectroscopy studies. The CD spectra were recorded between 200 and 260 nm and are represented in Figure 5.4.14.

The characteristic double minima around 208 and 222 nm are found in both CD spectra, and they almost overlap. The deconvolution of the spectra by the software K2D3 [104] yields a percentage of α helix content of 38.96 and 36.04 and β strand content of 14.71 and 13.63 for the IFN-α 2b and for IFN-α 2b + $[N_{1112(OH)}][C_4F_9SO_3]$, respectively. The literature shows values of α helix content of around 50%, however, the variations in the experimental conditions, apparatus, and software used to deconvolute the secondary structure may justify these differences [122]. Thus, these results sustain the outcomes from the emission spectra, concluding that at this concentration, the interactions between the FIL and the biomolecule do not have a substantial effect on the secondary structure of the IFN-α 2b. This behaviour is maintained for the concentrations of $[N_{1112(OH)}][C_4F_9SO_3]$ equal to or lower than the one here tested.

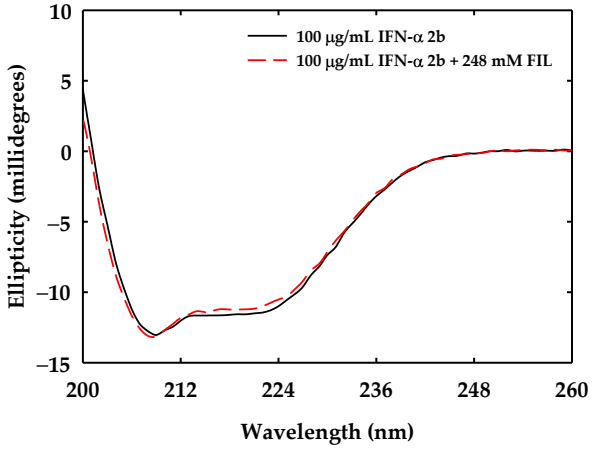

Figure 5.4.14 CD spectra of $[N_{1112(OH)}][C_4F_9SO_3]$ at 248 mM in the presence of IFN-α 2b at 100 µg/mL in 150 mM NaH_2PO_4 (pH = 7.4) and measured at 25°C.

5.4.2.2.2 Binding affinity

Microscale Thermophoresis (MST) is an innovative approach that analyses the movement of fluorescent molecules out of microscopic temperature gradients in very reduced volumes, measuring precise binding events regardless of the size and physical properties of the target molecules. For that, it has been widely used in the detection of binding of biomolecules, like proteins, enzymes, and DNA to small molecules of interest such as ligands, substrates, and liposomes, among others. The binding of a protein to a ligand induces differences in its size, charge, and solvation energy, and these modifications are detected by thermophoresis. Even if that event produces reduced structural modifications, MST can detect the binding due to the induced alterations in the solvation entropy of the molecules, being a very sensitive method. The changes provoked by the binding in the thermophoresis of the fluorescent molecules can be then used to obtain the equilibrium dissociation constant, K_d, by plotting the normalized fluorescence, F_{norm}, of the labelled molecules *versus* the logarithm of the concentration of ligand and fitting the binding curves with the models provided by the software [123,124]. This technique was previously applied in the determination of binding affinity between ILs and lysozyme [125], as well as for inferring the interactions of another type of interferons [126] and other proteins [124,127,128] with different types of ligands.

In this work, a commercial kit was used to fluorescently tag the IFN-α 2b. In the process of labelling, commonly one amine per protein is labelled, statistically distributing the position of the dye. Therefore, the risk of the label impairs with the binding is very low, due to the typical number of lysine residues in proteins [124,127,128]. The $[C_2C_1Im][C_4F_9SO_3]$ and $[N_{1112(OH)}][C_4F_9SO_3]$ were selected to study the binding with the IFN-α 2b. The solutions were prepared with a concentration of IFN-α 2b fixed at 2.7 μM in 5 mM of NaH_2PO_4 (pH=7.4). As explained in the experimental section, in each run of MST, a maximum concentration is chosen, and it will be consecutively diluted in 16 capillaries. Therefore, five different maximum concentrations of $[C_2C_1Im][C_4F_9SO_3]$ were selected to cover the range below the formation of the aggregates and to study the four distinct CACs. Only four maximum concentrations of $[N_{1112(OH)}][C_4F_9SO_3]$ were chosen because this FIL only have three different CACs [44]. These experimental conditions do not allow to study of each phenomenon of aggregation individually above the 1st CAC, once the range of dilutions of the solutions overlaps after this concentration. Thus, the determined dissociation constants K_d for each run that yields binding are being influenced by the several stages of aggregation, which make it impossible to attribute the value to a specific CAC. Nevertheless, the K_d comprise the influence of the different aggregates of a FIL on the binding affinity with IFN-α 2b, and it will be only considered for qualitative analysis. Figure 5.4.15 shows the results for the 9 assays.

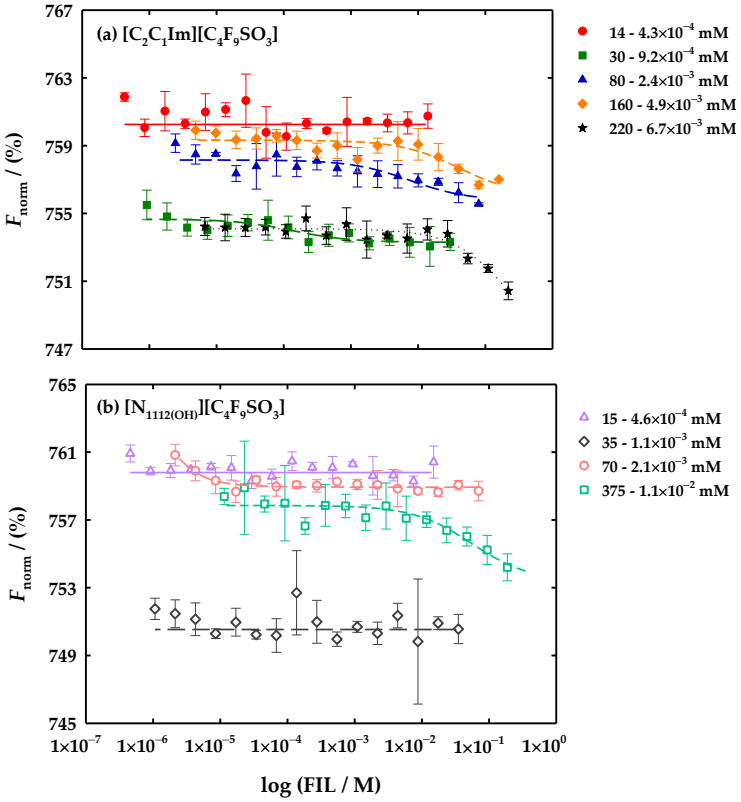

Figure 5.4.15 Dose-response curve from MST of labelled IFN-α at 2.7μM in the presence of different ranges of concentrations of a) $[C_2C_1Im][C_4F_9SO_3]$ and b) $[N_{1112(OH)}][C_4F_9SO_3]$. All the samples were measured in 5 mM NaH_2PO_4 (pH = 7.4) at 25°C. The error bars represent the standard deviations from the triplicate assays.

In the case of $[C_2C_1Im][C_4F_9SO_3]$ (Figure 5.4.15a), it was possible to observe binding between the IFN-α 2b and the FIL in all the runs representing the several stages of aggregation. For the range of concentrations under the 1st CAC, only FIL monomers in aqueous solution, no binding was detected. The $[N_{1112(OH)}][C_4F_9SO_3]$ results, illustrated in Figure 5.4.15b, show that binding only occurs for the runs where concentrations were above the 2nd and 3rd CAC. Therefore, the K_d was determined in the cases where the binding was found, and the results are depicted in Table 5.4.6. The dose-response curves that were fitted for K_d determination are represented in Figure 5.4.16, plotting the fraction bound *versus* the concentration of the ligand. Analysing the results for the case of $[C_2C_1Im][C_4F_9SO_3]$, Figure 5.4.16a shows that the K_d increases as a result of the presence of different types of FILs aggregates in the following order: 1st CAC < 2nd CAC < 3rd CAC < 4th CAC, indicating a decrement of binding affinity between the protein and the FIL aggregates. Therefore, the type of aggregates formed at lower concentrations of FIL has a stronger affinity with this protein. The same behaviour is found in the case of $[N_{1112(OH)}][C_4F_9SO_3]$, represented in Figure 5.4.16b, where an increased K_d is determined for the assay that comprises a higher concentration of FIL. This can also be verified

by the deviation of the typical sigmoidal dose-response to the left, indicating a higher association of the ligand with the target molecule [127,128].

Table 5.4.6 Determined dissociation constants K_d by the analysis of the fitting of the MST dose-curve responses.

FIL	Assay	K_d (mM)
[C_2C_1Im][$C_4F_9SO_3$]	30 – 9.2x10^{-4} mM	0.136 ± 0.117[a]
	80 – 2.4x10^{-3} mM	7.53 ± 5.61[a]
	160 – 4.9x10^{-3} mM	40.5 ± 29.5[a]
	220 – 6.7x10^{-3} mM	263 ± 197[a]
[$N_{1112(OH)}$][$C_4F_9SO_3$]	70 – 2.1x10^{-3} mM	5.97x10^{-4} ± 3.93x10^{-4}[a]
	375 – 1.1x10^{-2} mM	54.7 ± 36.9[a]

[a] These values represent the K_d confidence of the fitting

The comparison between the cations shows that $[N_{1112(OH)}]^+$ has more binding affinity with IFN-α 2b than the $[C_2C_1Im]^+$, demonstrated by the lower K_d values and bigger left shift of the sigmoidal. Nevertheless, the $[C_2C_1Im]^+$ showed a binding affinity with the protein in all stages of aggregation. However, the same behaviour was not verified for $[N_{1112(OH)}]^+$. Then, a higher range of concentrations, and subsequently different types of aggregates, can be used to design a proper system for IFN-α 2b delivery with the imidazolium-based FIL. Furthermore, this behaviour allows the usage of this FIL at lower concentrations, which is highly advantageous from the biomedical perspective. Crossing the results with the ones obtained in the emission analysis of the protein, it can be concluded that the interactions found under the 1st CAC are not so strong as the ones that are occurring above the 1st CAC. Moreover, the stronger affinity of the cholinium cation can explain the unfolding events found for higher concentrations of this FIL (Figure 5.4.13b). The interference of the protein labelling should be ruled out in future studies, using fluorescence-labelling-free techniques, such as isothermal titration calorimetry, to support these results and enabled a more specific study of the binding protein-FIL for each CAC. Nevertheless, this technique has provided valuable information on a strong binding between the aggregates of both studied FILs and IFN-α 2b, supporting the results previously discussed.

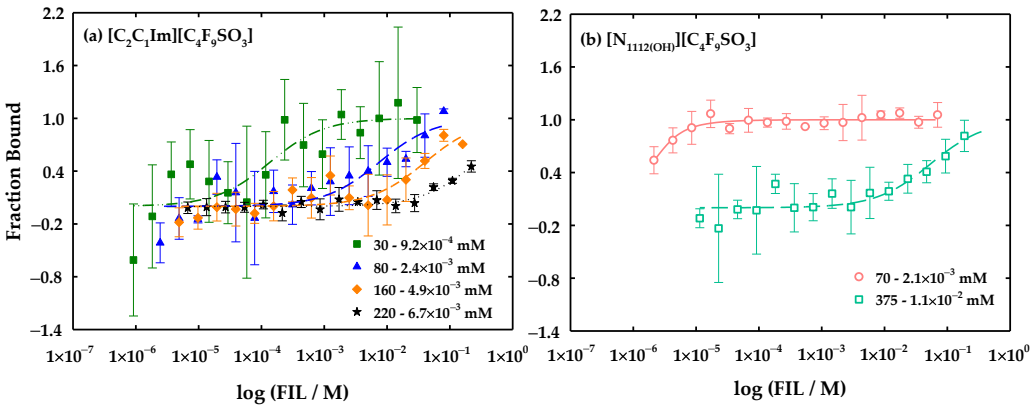

Figure 5.4.16 MST analysis of the interaction between the labelled IFN-α at 2.7μM and the different concentrations of a) $[C_2C_1Im][C_4F_9SO_3]$ and b) $[N_{1112(OH)}][C_4F_9SO_3]$ that yield binding affinity. All the samples were measured in 5 mM NaH_2PO_4 (pH = 7.4) at 25°C. The error bars represent the standard deviations from the triplicate assays.

In conclusion, IFN-α 2b forms a complex (like a conjugate) with the FILs aggregates, that induces changes in the packaging, formation spontaneity, surface activity of the FILs aggregates, and size reduction of the protein aggregates, preventing its aggregation. The significant modifications in the morphology and size of FIL aggregates are most likely occurring due to the spatial adjustment resulting from the presence of IFN-α 2b. Moreover, strong interactions between the FIL aggregates and IFN-α 2b were disclosed using spectroscopy techniques and determining their binding affinity, which are highly dependent on the different types of FIL aggregates and influenced by the nature of the cation.

To the best of our knowledge, there are no studies in the literature that use ILs as delivery systems for this protein. Nevertheless, Castro et al. have used several ILs to increase the efficiency of extraction of IFN-α 2b using several imidazolium-based ILs. The analysis of protein stability also yields prevention of the protein aggregation (no dimers were found) and the secondary structure of IFN-α 2b was not affected by the ILs [40]. Our results also indicate a prevention of the formation of protein aggregates. Therefore, the imidazolium cation seems to have a very positive effect on the stabilization of this specific protein. Looking to other types of compounds near to ILs family of compounds, one work has successfully used deep eutectic solvents based on natural sources for the thermal stabilization of this protein [129] which could be another interesting application for future works.

Finally, the use of FILs can be further tailored for the formulation of efficient delivery systems to transport and stabilize IFN-α 2b. This work constitutes an initial step in the direction of designing proper compounds to enable the encapsulation of IFN-α 2b, as previously obtained for other biomolecules.

5.4.3 Conclusions

In this work, the first step toward the use of FILs as drug delivery systems of the protein IFN-α 2b has been taken. The aggregation behaviour of the $[C_2C_1Im][C_4F_9SO_3]$ and $[N_{1112(OH)}][C_4F_9SO_3]$ was studied to understand how the presence of the IFN-α 2b may alter the formation of aggregates and their properties such as size and morphology. Then, the critical aggregation concentrations of $[C_2C_1Im][C_4F_9SO_3]$ were determined and was concluded that the protein does not impair the formation of the three CACs characteristic of this FIL. The parameters of aggregation have shown that the presence of the protein can alter the packaging of the aggregates and the spontaneity of the process of aggregation, which can indicate an

accommodation of the IFN-α 2b in the FILs aggregates. The surface properties of $[C_2C_1Im][C_4F_9SO_3]$ demonstrated that the IFN-α 2b highly influences the surface activity of this FIL, by the formation of more breaking points in the surface tension and contact angles profiles. Moreover, the critical packing parameters have shown that the conformation of the aggregates is altered in the presence of the protein, demonstrating a close interaction between FIL and protein. The further characterization of the morphology of the FILs aggregates proved that the aggregation of the protein is reduced, and the morphology of FIL aggregates is also modified, supporting that protein and FIL are forming a conjugate.

Finally, the interactions protein-FIL were studied in this work by several spectroscopy techniques. The overall results allow us to conclude that very strong interaction between the FILs aggregates of either $[C_2C_1Im][C_4F_9SO_3]$ and $[N_{1112(OH)}][C_4F_9SO_3]$ and IFN-α 2b are occurring, without altering the secondary structure of the protein. Only in the case of $[N_{1112(OH)}][C_4F_9SO_3]$, an alteration in the structure of the protein was found, but in very high concentrations of FIL, which will not be used in biomedical applications. Furthermore, the determination of binding between protein and FIL has established and supported the complexation and formation of a conjugate that can contribute to the transport of the protein and FILs usage as protein delivery systems. More studies need to be pursued to fully understand the mechanism behind the formation of this complex.

This work represents a first and crucial step for the investigation of the discovery of the interactions between FILs and therapeutic proteins, as well as, the formulation of feasible FILs-based DDSs, opening new avenues for the application of these biomaterials in the pharmaceutical field.

5.5 References

1. Choi, J.M.; Han, S.S.; Kim, H.S. Industrial Applications of Enzyme Biocatalysis: Current Status and Future Aspects. *Biotechnol Adv* **2015**, *33*, 1443–1454, doi:10.1016/j.biotechadv.2015.02.014.
2. Kapoor, S.; Rafiq, A.; Sharma, S. Protein Engineering and Its Applications in Food Industry. *Crit Rev Food Sci Nutr* **2017**, *57*, 2321–2329, doi:10.1080/10408398.2014.1000481.
3. dos Santos, N.V.; de Carvalho Santos-Ebinuma, V.; Pessoa Junior, A.; Pereira, J.F.B. Liquid–Liquid Extraction of Biopharmaceuticals from Fermented Broth: Trends and Future Prospects. *Journal of Chemical Technology and Biotechnology* **2018**, *93*, 1845–1863, doi:10.1002/JCTB.5476.
4. Ding, S.; Zhang, N.; Lyu, Z.; Zhu, W.; Chang, Y.C.; Hu, X.; Du, D.; Lin, Y. Protein-Based Nanomaterials and Nanosystems for Biomedical Applications: A Review. *Materials Today* **2021**, *43*, 166–184, doi:10.1016/j.mattod.2020.11.015.
5. Tan, S.C.; Yiap, B.C. DNA, RNA, and Protein Extraction: The Past and the Present. *J Biomed Biotechnol* 2009, *2009*.
6. Patel, R.; Kumari, M.; Khan, A.B. Recent Advances in the Applications of Ionic Liquids in Protein Stability and Activity: A Review. *Appl Biochem Biotechnol* 2014, *172*, 3701–3720.
7. Schröder, C. Proteins in Ionic Liquids: Current Status of Experiments and Simulations. *Top Curr Chem* 2017, *375*.
8. Zhao, Q.; Chu, H.; Zhao, B.; Liang, Z.; Zhang, L.; Zhang, Y. Advances of Ionic Liquids-Based Methods for Protein Analysis. *TrAC - Trends in Analytical Chemistry* 2018, *108*, 239–246.
9. Berdigaliyev, N.; Aljofan, M. An Overview of Drug Discovery and Development. *Future Med Chem* **2020**, *12*, 939–947, doi:10.4155/fmc-2019-0307.
10. Rasmussen, A.S.B.; Hammou, A.; Poulsen, T.F.; Laursen, M.C.; Hansen, S.F. Definition, Categorization, and Environmental Risk Assessment of Biopharmaceuticals. *Science of The Total Environment* **2021**, *789*, 147884, doi:10.1016/j.scitotenv.2021.147884.
11. Walsh, G. Biopharmaceutical Benchmarks 2018. *Nat Biotechnol* **2018**, *36*, 1136–1145, doi:10.1038/nbt.4305.
12. Kesik-Brodacka, M. Progress in Biopharmaceutical Development. *Biotechnol Appl Biochem* **2018**, *65*, 306–322, doi:10.1002/bab.1617.
13. Voynov, V.; Caravella, J.A. *Therapeutic Proteins*; Voynov, V., Caravella, J.A., Eds.; Humana Press: Totowa, NJ, 2012; Vol. 899; ISBN 978-1-61779-920-4.
14. Akash, M.S.H.; Rehman, K.; Tariq, M.; Chen, S. Development of Therapeutic Proteins: Advances and Challenges. *Turkish Journal of Biology* **2015**, *39*, 343–358, doi:10.3906/biy-1411-8.
15. Schuster, J.; Koulov, A.; Mahler, H.C.; Detampel, P.; Huwyler, J.; Singh, S.; Mathaes, R. In Vivo Stability of Therapeutic Proteins. *Pharm Res* 2020, *37*.
16. Dingman, R.; Balu-Iyer, S. v. Immunogenicity of Protein Pharmaceuticals. *J Pharm Sci* 2019, *108*, 1637–1654.
17. Zaman, R.; Islam, R.A.; Ibnat, N.; Othman, I.; Zaini, A.; Lee, C.Y.; Chowdhury, E.H. Current Strategies in Extending Half-Lives of Therapeutic Proteins. *Journal of Controlled Release* 2019, *301*, 176–189.
18. Tourdot, S.; Hickling, T.P. Nonclinical Immunogenicity Risk Assessment of Therapeutic Proteins. *Bioanalysis* **2019**, *11*, 1631–1643, doi:10.4155/bio-2018-0246.
19. Yin, L.; Yuvienco, C.; Montclare, J.K. Protein Based Therapeutic Delivery Agents: Contemporary Developments and Challenges. *Biomaterials* **2017**, *134*, 91–116, doi:10.1016/j.biomaterials.2017.04.036.

20. Zeb, A.; Rana, I.; Choi, H.-I.; Lee, C.-H.; Baek, S.-W.; Lim, C.-W.; Khan, N.; Arif, S.T.; Sahar, N. us; Alvi, A.M.; et al. Potential and Applications of Nanocarriers for Efficient Delivery of Biopharmaceuticals. *Pharmaceutics* **2020**, *12*, 1184, doi:10.3390/pharmaceutics12121184.
21. Nie, T.; Wang, W.; Liu, X.; Wang, Y.; Li, K.; Song, X.; Zhang, J.; Yu, L.; He, Z. Sustained Release Systems for Delivery of Therapeutic Peptide/Protein. *Biomacromolecules* 2021, *22*, 2299–2324.
22. He, S.; Liu, Z.; Xu, D. Advance in Oral Delivery Systems for Therapeutic Protein. *J Drug Target* **2019**, *27*, 283–291, doi:10.1080/1061186X.2018.1486406.
23. Moncalvo, F.; Martinez Espinoza, M.I.; Cellesi, F. Nanosized Delivery Systems for Therapeutic Proteins: Clinically Validated Technologies and Advanced Development Strategies. *Front Bioeng Biotechnol* 2020, *8*.
24. Phani Kumar, B.V.N.; Reddy, R.R. Interaction of Ionic Liquids with Proteins: NMR Studies of Binding and Dynamics. *Annu Rep NMR Spectrosc* **2020**, *99*, 1–56, doi:10.1016/BS.ARNMR.2019.08.001.
25. Faustino, A.F.; Barbosa, G.M.; Silva, M.; Castanho, M.A.R.B.; da Poian, A.T.; Cabrita, E.J.; Santos, N.C.; Almeida, F.C.L.; Martins, I.C. Fast NMR Method to Probe Solvent Accessibility and Disordered Regions in Proteins. *Sci Rep* **2019**, *9*, doi:10.1038/S41598-018-37599-Z.
26. Warner, L.; Gjersing, E.; Follett, S.E.; Elliott, K.W.; Dzyuba, S. v.; Varga, K. The Effects of High Concentrations of Ionic Liquid on GB1 Protein Structure and Dynamics Probed by High-Resolution Magic-Angle-Spinning NMR Spectroscopy. *Biochem Biophys Rep* **2016**, *8*, 75–80, doi:10.1016/j.bbrep.2016.08.009.
27. Zhou, Y.; Pérez, B.; Hao, W.; Lv, J.; Gao, R.; Guo, Z. The Additive Mutational Effects from Surface Charge Engineering: A Compromise between Enzyme Activity, Thermostability and Ionic Liquid Tolerance. *Biochem Eng J* **2019**, *148*, 195–204, doi:10.1016/j.bej.2018.07.020.
28. Zhao, J.; Jia, N.; Jaeger, K.E.; Bocola, M.; Schwaneberg, U. Ionic Liquid Activated Bacillus Subtilis Lipase A Variants through Cooperative Surface Substitutions. *Biotechnol Bioeng* **2015**, *112*, 1997–2004, doi:10.1002/BIT.25617.
29. Frauenkron-Machedjou, V.J.; Fulton, A.; Zhu, L.; Anker, C.; Bocola, M.; Jaeger, K.E.; Schwaneberg, U. Towards Understanding Directed Evolution: More than Half of All Amino Acid Positions Contribute to Ionic Liquid Resistance of Bacillus Subtilis Lipase A. *ChemBioChem* **2015**, *16*, 937–945, doi:10.1002/CBIC.201402682.
30. Zhao, J.; Frauenkron-Machedjou, V.J.; Fulton, A.; Zhu, L.; Davari, M.D.; Jaeger, K.E.; Schwaneberg, U.; Bocola, M. Unraveling the Effects of Amino Acid Substitutions Enhancing Lipase Resistance to an Ionic Liquid: A Molecular Dynamics Study. *Physical Chemistry Chemical Physics* **2018**, *20*, 9600–9609, doi:10.1039/C7CP08470F.
31. Cui, H.; Pramanik, S.; Jaeger, K.E.; Davari, M.D.; Schwaneberg, U. CompassR-Guided Recombination Unlocks Design Principles to Stabilize Lipases in ILs with Minimal Experimental Efforts. *Green Chemistry* **2021**, *23*, 3474–3486, doi:10.1039/D1GC00763G.
32. el Harrar, T.; Frieg, B.; Davari, M.D.; Jaeger, K.E.; Schwaneberg, U.; Gohlke, H. Aqueous Ionic Liquids Redistribute Local Enzyme Stability via Long-Range Perturbation Pathways. *Comput Struct Biotechnol J* **2021**, *19*, 4248–4264, doi:10.1016/j.csbj.2021.07.001.
33. Pramanik, S.; Dhoke, G. v.; Jaeger, K.E.; Schwaneberg, U.; Davari, M.D. How to Engineer Ionic Liquids Resistant Enzymes: Insights from Combined Molecular Dynamics and Directed Evolution Study. *ACS Sustain Chem Eng* **2019**, *7*, 11293–11302, doi:10.1021/ACSSUSCHEMENG.9B00752.
34. Nordwald, E.M.; Armstrong, G.S.; Kaar, J.L. NMR-Guided Rational Engineering of an Ionic-Liquid-Tolerant Lipase. *ACS Catal* **2014**, *4*, 4057–4064, doi:10.1021/CS500978X.

35. Chado, G.R.; Holland, E.N.; Tice, A.K.; Stoykovich, M.P.; Kaar, J.L. Exploiting the Benefits of Homogeneous and Heterogeneous Biocatalysis: Tuning the Molecular Interaction of Enzymes with Solvents via Polymer Modification. *ACS Catal* **2018**, *8*, 11579–11588, doi:10.1021/ACSCATAL.8B03779.
36. Chado, G.R.; Holland, E.N.; Tice, A.K.; Stoykovich, M.P.; Kaar, J.L. Modification of Lipase with Poly(4-Acryloylmorpholine) Enhances Solubility and Transesterification Activity in Anhydrous Ionic Liquids. *Biomacromolecules* **2018**, *19*, 1324–1332, doi:10.1021/ACS.BIOMAC.8B00176.
37. Sprenger, K.G.; Plaks, J.G.; Kaar, J.L.; Pfaendtner, J. Elucidating Sequence and Solvent Specific Design Targets to Protect and Stabilize Enzymes for Biocatalysis in Ionic Liquids. *Physical Chemistry Chemical Physics* **2017**, *19*, 17426–17433, doi:10.1039/C7CP03013D.
38. Nordwald, E.M.; Plaks, J.G.; Snell, J.R.; Sousa, M.C.; Kaar, J.L. Crystallographic Investigation of Imidazolium Ionic Liquid Effects on Enzyme Structure. *ChemBioChem* **2015**, *16*, 2456–2459, doi:10.1002/CBIC.201500398.
39. Asmana Ningrum, R. Human Interferon Alpha-2b: A Therapeutic Protein for Cancer Treatment. *Scientifica (Cairo)* **2014**, *2014*, 1–8, doi:10.1155/2014/970315.
40. Castro, L.S.; Pereira, P.; Passarinha, L.A.; Freire, M.G.; Pedro, A.Q. Enhanced Performance of Polymer-Polymer Aqueous Two-Phase Systems Using Ionic Liquids as Adjuvants towards the Purification of Recombinant Proteins. *Sep Purif Technol* **2020**, *248*, doi:10.1016/j.seppur.2020.117051.
41. Fukumoto, K.; Yoshizawa, M.; Ohno, H. Room Temperature Ionic Liquids from 20 Natural Amino Acids. *J Am Chem Soc* **2005**, *127*, 2398–2399, doi:10.1021/JA043451I.
42. Vieira, N.S.M.; Luís, A.; Reis, P.M.; Carvalho, P.J.; Lopes-Da-Silva, J.A.; Esperança, J.M.S.S.; Araújo, J.M.M.; Rebelo, L.P.N.; Freire, M.G.; Pereiro, A.B. Fluorination Effects on the Thermodynamic, Thermophysical and Surface Properties of Ionic Liquids. *Journal of Chemical Thermodynamics* **2016**, *97*, 354–361, doi:10.1016/j.jct.2016.02.013.
43. Vieira, N.S.M.; Stolte, S.; Araújo, J.M.M.; Rebelo, L.P.N.; Pereiro, A.B.; Markiewicz, M. Acute Aquatic Toxicity and Biodegradability of Fluorinated Ionic Liquids. *ACS Sustain Chem Eng* **2019**, *7*, 3733–3741, doi:10.1021/ACSSUSCHEMENG.8B03653.
44. Pereiro, A.B.; Araújo, J.M.M.; Teixeira, F.S.; Marrucho, I.M.; Piñeiro, M.M.; Rebelo, L.P.N. Aggregation Behavior and Total Miscibility of Fluorinated Ionic Liquids in Water. *Langmuir* **2015**, *31*, 1283–1295, doi:10.1021/LA503961H.
45. Combettes, L.E.; Clausen-Thue, P.; King, M.A.; Odell, B.; Thompson, A.L.; Gouverneur, V.; Claridge, T.D.W. Conformational Analysis of Fluorinated Pyrrolidines Using 19F-1H Scalar Couplings and Heteronuclear NOEs. *Chemistry - A European Journal* **2012**, *18*, 13133–13141, doi:10.1002/CHEM.201201577.
46. Wu, D.H.; Chen, A.; Johnson, C.S. An Improved Diffusion-Ordered Spectroscopy Experiment Incorporating Bipolar-Gradient Pulses. *J Magn Reson A* **1995**, *115*, 260–264, doi:10.1006/jmra.1995.1176.
47. Stejskal, E.O.; Tanner, J.E. Spin Diffusion Measurements: Spin Echoes in the Presence of a Time-Dependent Field Gradient. *J Chem Phys* **1965**, *42*, 288–292, doi:10.1063/1.1695690.
48. Johnson, C.S. Diffusion Ordered Nuclear Magnetic Resonance Spectroscopy: Principles and Applications. *Prog Nucl Magn Reson Spectrosc* **1999**, *34*, 203–256, doi:10.1016/S0079-6565(99)00003-5.
49. Ferreira, M.L.; Vieira, N.S.M.; Araújo, J.M.M.; Pereiro, A.B. Unveiling the Influence of Non-Toxic Fluorinated Ionic Liquids Aqueous Solutions in the Encapsulation and Stability of Lysozyme. *Sustainable Chemistry* **2021**, *2*, 149–166, doi:10.3390/suschem2010010.

50. Vieira, N.S.M.; Castro, P.J.; Marques, D.F.; Araújo, J.M.M.; Pereiro, A.B. Tailor-Made Fluorinated Ionic Liquids for Protein Delivery. *Nanomaterials* **2020**, *10*, 1–16, doi:10.3390/NANO10081594.
51. Buettner, C.S.; Cognigni, A.; Schröder, C.; Bica-Schröder, K. Surface-Active Ionic Liquids: A Review. *J Mol Liq* **2022**, *347*, 118160, doi:10.1016/j.molliq.2021.118160.
52. Rosen, M.J. Surfactants and Interfacial Phenomena. *Surfactants and Interfacial Phenomena* **2004**, doi:10.1002/0471670561.
53. Vieira, N.S.M.; Reis, P.M.; Shimizu, K.; Cortes, O.A.; Marrucho, I.M.; Araújo, J.M.M.; Esperança, J.M.S.S.; Lopes, J.N.C.; Pereiro, A.B.; Rebelo, L.P.N. A Thermophysical and Structural Characterization of Ionic Liquids with Alkyl and Perfluoroalkyl Side Chains. *RSC Adv* **2015**, *5*, 65337–65350, doi:10.1039/C5RA13869H.
54. Ferreira, A.S.D.; Barreiros, S.; Cabrita, E.J. Probing Sol-Gel Matrices Microenvironments by PGSE HR-MAS NMR. *Magnetic Resonance in Chemistry* **2017**, *55*, 452–463, doi:10.1002/MRC.4427.
55. Cascão, J.; Silva, W.; Ferreira, A.S.D.; Cabrita, E.J. Ion Pair and Solvation Dynamics of [Bmim][BF4] + Water System. *Magnetic Resonance in Chemistry* **2018**, *56*, 127–139, doi:10.1002/MRC.4673.
56. Ue, M.; Murakami, A.; Nakamura, S. A Convenient Method to Estimate Ion Size for Electrolyte Materials Design. *J Electrochem Soc* **2002**, *149*, A1385, doi:10.1149/1.1507593.
57. Alves, M.; Vieira, N.S.M.; Rebelo, L.P.N.; Araújo, J.M.M.; Pereiro, A.B.; Archer, M. Fluorinated Ionic Liquids for Protein Drug Delivery Systems: Investigating Their Impact on the Structure and Function of Lysozyme. *Int J Pharm* **2017**, *526*, 309–320, doi:10.1016/j.ijpharm.2017.05.002.
58. Gallagher, T.; Alexander, P.; Bryan, P.; Gilliland, G.L. Two Crystal Structures of the B1 Immunoglobulin-Binding Domain of Streptococcal Protein G and Comparison with NMR. *Biochemistry* **1994**, *33*, 4721–4729, doi:10.1021/BI00181A032.
59. Gronenborn, A.M.; Filpula, D.R.; Essig, N.Z.; Achari, A.; Whitlow, M.; Wingfield, P.T.; Clore, G.M. A Novel, Highly Stable Fold of the Immunoglobulin Binding Domain of Streptococcal Protein G. *Science (1979)* **1991**, *253*, 657–661, doi:10.1126/science.1871600.
60. Alexander, P.; Orban, J.; Bryan, P.; Fahnestock, S.; Lee, T. Thermodynamic Analysis of the Folding of the Streptococcal Protein Gigg-Binding Domains B1 and B2: Why Small Proteins Tend to Have High Denaturation Temperatures. *Biochemistry* **1992**, *31*, 3597–3603, doi:10.1021/BI00129A007.
61. Lindman, S.; Xue, W.F.; Szczepankiewicz, O.; Bauer, M.C.; Nilsson, H.; Linse, S. Salting the Charged Surface: PH and Salt Dependence of Protein G B1 Stability. *Biophys J* **2006**, *90*, 2911–2921, doi:10.1529/biophysj.105.071050.
62. Ceruso, M.A.; Amadei, A.; Nola, A. di Mechanics and Dynamics of B1 Domain of Protein G: Role of Packing and Surface Hydrophobic Residues. *Protein Science* **2008**, *8*, 147–160, doi:10.1110/PS.8.1.147.
63. van Pouderoyen, G.; Eggert, T.; Jaeger, K.E.; Dijkstra, B.W. The Crystal Structure of Bacillus Subtilis Lipase: A Minimal α/β Hydrolase Fold Enzyme. *J Mol Biol* **2001**, *309*, 215–226, doi:10.1006/jmbi.2001.4659.
64. Radhakrishnan, R.; Walter, L.J.; Hruza, A.; Reichert, P.; Trotta, P.P.; Nagabhushan, T.L.; Walter, M.R. Zinc Mediated Dimer of Human Interferon-α(2b) Revealed by X-Ray Crystallography. *Structure* **1996**, *4*, 1453–1463, doi:10.1016/S0969-2126(96)00152-9.
65. Çorman, M.E.; Armutcu, C.; Özkara, S.; Uzun, L.; Denizli, A. Molecularly Imprinted Cryogel Cartridges for the Specific Filtration and Rapid Separation of Interferon Alpha. *RSC Adv* **2015**, *5*, 45015–45026, doi:10.1039/C5RA07307C.

66. Liu, Y.; Zhu, G.; Shen, Z.; Chen, Y. Sequence Effect of Peptide-Based Materials on Delivering Interferon-α (IFN-α): A Molecular Dynamic Perspective. *Langmuir* **2022**, *38*, 680–688, doi:10.1021/ACS.LANGMUIR.1C02515.
67. Shamloo, A.; Rostami, P.; Mahmoudi, A. PASylation Enhances the Stability, Potency, and Plasma Half-Life of Interferon α-2a: A Molecular Dynamics Simulation. *Biotechnol J* **2020**, *15*, doi:10.1002/BIOT.201900385.
68. Wetter, L.R.; Deutsch, H.F. Immunological Studies on Egg White Proteins. *Journal of Biological Chemistry* **1951**, *192*, 237–242, doi:10.1016/s0021-9258(18)55926-3.
69. Teixeira, F.S.; Vieira, N.S.M.; Cortes, O.A.; Araújo, J.M.M.; Marrucho, I.M.; Rebelo, L.P.N.; Pereiro, A.B. Phase Equilibria and Surfactant Behavior of Fluorinated Ionic Liquids with Water. *Journal of Chemical Thermodynamics* **2015**, *82*, 99–107, doi:10.1016/j.jct.2014.10.021.
70. Callewaert, L.; Michiels, C.W. Lysozymes in the Animal Kingdom. *J Biosci* **2010**, *35*, 127–160, doi:10.1007/S12038-010-0015-5.
71. Singh, G.; Kaur, M.; Singh, D.; Kesavan, A.K.; Kang, T.S. Antimicrobial Colloidal Complexes of Lysozyme with Bio-Based Surface Active Ionic Liquids in Aqueous Medium. *Journal of Physical Chemistry B* **2020**, *124*, 3791–3800, doi:10.1021/acs.jpcb.0c00339.
72. Bisht, M.; Kumar, A.; Venkatesu, P. Analysis of the Driving Force That Rule the Stability of Lysozyme in Alkylammonium-Based Ionic Liquids. *Int J Biol Macromol* **2015**, *81*, 1074–1081, doi:10.1016/j.ijbiomac.2015.09.036.
73. Satish, L.; Rana, S.; Arakha, M.; Rout, L.; Ekka, B.; Jha, S.; Dash, P.; Sahoo, H. Impact of Imidazolium-Based Ionic Liquids on the Structure and Stability of Lysozyme. *Spectroscopy Letters* **2016**, *49*, 383–390, doi:10.1080/00387010.2016.1167089.
74. Mandal, B.; Mondal, S.; Pan, A.; Moulik, S.P.; Ghosh, S. Physicochemical Study of the Interaction of Lysozyme with Surface Active Ionic Liquid 1-Butyl-3-Methylimidazolium Octylsulfate [BMIM] [OS] in Aqueous and Buffer Media. *Colloids Surf A Physicochem Eng Asp* **2015**, *484*, 345–353, doi:10.1016/j.colsurfa.2015.07.052.
75. Kumari, M.; Dohare, N.; Maurya, N.; Dohare, R.; Patel, R. Effect of 1-Methyl-3-Octyleimmidazolium Chloride on the Stability and Activity of Lysozyme: A Spectroscopic and Molecular Dynamics Studies. *J Biomol Struct Dyn* **2017**, *35*, 2016–2030, doi:10.1080/07391102.2016.1204946.
76. Kumari, M.; Singh, U.K.; Beg, I.; Alanazi, A.M.; Khan, A.A.; Patel, R. Effect of Cations and Anions of Ionic Liquids on the Stability and Activity of Lysozyme: Concentration and Temperature Effect. *J Mol Liq* **2018**, *272*, 253–263, doi:10.1016/j.molliq.2018.09.075.
77. Rather, M.A.; Dar, T.A.; Singh, L.R.; Rather, G.M.; Bhat, M.A. Structural-Functional Integrity of Lysozyme in Imidazolium Based Surface Active Ionic Liquids. *Int J Biol Macromol* **2020**, *156*, 271–279, doi:10.1016/j.ijbiomac.2020.04.033.
78. Singh, G.; Kaur, M.; Kaur, H.; Kang, T.S. Synthesis and Complexation of a New Caffeine Based Surface Active Ionic Liquid with Lysozyme in Aqueous Medium: Physicochemical, Computational and Antimicrobial Studies. *J Mol Liq* **2021**, *325*, doi:10.1016/j.molliq.2020.115156.
79. Araújo, J.M.M.; Florindo, C.; Pereiro, A.B.; Vieira, N.S.M.; Matias, A.A.; Duarte, C.M.M.; Rebelo, L.P.N.; Marrucho, I.M. Cholinium-Based Ionic Liquids with Pharmaceutically Active Anions. *RSC Adv* **2014**, *4*, 28126–28132, doi:10.1039/C3RA47615D.
80. Vieira, N.S.M.; Bastos, J.C.; Rebelo, L.P.N.; Matias, A.; Araújo, J.M.M.; Pereiro, A.B. Human Cytotoxicity and Octanol/Water Partition Coefficients of Fluorinated Ionic Liquids. *Chemosphere* **2019**, *216*, 576–586, doi:10.1016/j.chemosphere.2018.10.159.

81. Vieira, N.S.M.; Bastos, J.C.; Hermida-Merino, C.; Pastoriza-Gallego, M.J.; Rebelo, L.P.N.; Piñeiro, M.M.; Araújo, J.M.M.; Pereiro, A.B. Aggregation and Phase Equilibria of Fluorinated Ionic Liquids. *J Mol Liq* **2019**, *285*, 386–396, doi:10.1016/j.molliq.2019.04.086.
82. Ferreira, M.L.; Araújo, J.M.M.; Vega, L.F.; Llovell, F.; Pereiro, A.B. Functionalization of Fluorinated Ionic Liquids: A Combined Experimental-Theoretical Study. *J Mol Liq* **2020**, *302*, doi:10.1016/j.molliq.2020.112489.
83. Kumar, A.; Bisht, M.; Venkatesu, P. Biocompatibility of Ionic Liquids towards Protein Stability: A Comprehensive Overview on the Current Understanding and Their Implications. *Int J Biol Macromol* **2017**, *96*, 611–651, doi:10.1016/J.IJBIOMAC.2016.12.005.
84. Petkovic, M.; Seddon, K.R.; Rebelo, L.P.N.; Pereira, C.S. Ionic Liquids: A Pathway to Environmental Acceptability. *Chem Soc Rev* **2011**, *40*, 1383–1403, doi:10.1039/C004968A.
85. Pereiro, A.B.; Araújo, J.M.M.; Martinho, S.; Alves, F.; Nunes, S.; Matias, A.; Duarte, C.M.M.; Rebelo, L.P.N.; Marrucho, I.M. Fluorinated Ionic Liquids: Properties and Applications. *ACS Sustain Chem Eng* **2013**, *1*, 427–439, doi:10.1021/SC300163N.
86. Patinha, D.J.S.; Tomé, L.C.; Florindo, C.; Soares, H.R.; Coroadinha, A.S.; Marrucho, I.M. New Low-Toxicity Cholinium-Based Ionic Liquids with Perfluoroalkanoate Anions for Aqueous Biphasic System Implementation. *ACS Sustain Chem Eng* **2016**, *4*, 2670–2679, doi:10.1021/ACSSUSCHEMENG.6B00171.
87. García-Lorenzo, A.; Tojo, E.; Tojo, J.; Teijeira, M.; Rodríguez-Berrocal, F.J.; González, M.P.; Martínez-Zorzano, V.S. Cytotoxicity of Selected Imidazolium-Derived Ionic Liquids in the Human Caco-2 Cell Line. Sub-Structural Toxicological Interpretation through a QSAR Study. *Green Chemistry* **2008**, *10*, 508–551, doi:10.1039/B718860A.
88. Matias, A.; Nunes, S.L.; Poejo, J.; Mecha, E.; Serra, A.T.; Madeira, P.J.A.; Bronze, M.R.; Duarte, C.M.M. Antioxidant and Anti-Inflammatory Activity of a Flavonoid-Rich Concentrate Recovered from Opuntia Ficus-Indica Juice. *Food Funct* **2014**, *5*, 3269–3280, doi:10.1039/C4FO00071D.
89. Wilkening, S.; Stahl, F.; Bader, A. Comparison of Primary Human Hepatocytes and Hepatoma Cell Line HepG2 with Regard to Their Biotransformation Properties. *Drug Metabolism and Disposition* **2003**, *31*, 1035–1042, doi:10.1124/DMD.31.8.1035.
90. Gorrochategui, E.; Pérez-Albaladejo, E.; Casas, J.; Lacorte, S.; Porte, C. Perfluorinated Chemicals: Differential Toxicity, Inhibition of Aromatase Activity and Alteration of Cellular Lipids in Human Placental Cells. *Toxicol Appl Pharmacol* **2014**, *277*, 124–130, doi:10.1016/J.TAAP.2014.03.012.
91. Lim, X.Z. Tainted Water: The Scientists Tracing Thousands of Fluorinated Chemicals in Our Environment. *Nature* **2019**, *566*, 26–29, doi:10.1038/D41586-019-00441-1.
92. Singh, U.K.; Kumari, M.; Patel, R. Dynamics of Cytochrome c in Surface Active Ionic Liquid: A Study of Preferential Interactions towards Denaturation. *J Mol Liq* **2018**, *268*, 840–848, doi:10.1016/j.molliq.2018.07.116.
93. Segawa, S. -I; Sugihara, M. Characterization of the Transition State of Lysozyme Unfolding. II. Effects of the Intrachain Crosslinking and the Inhibitor Binding on the Transition State. *Biopolymers* **1984**, *23*, 2489–2498, doi:10.1002/BIP.360231123.
94. Vrikkis, R.M.; Fraser, K.J.; Fujita, K.; MacFarlane, D.R.; Elliott, G.D. Biocompatible Ionic Liquids: A New Approach for Stabilizing Proteins in Liquid Formulation. *J Biomech Eng* **2009**, *131*, doi:10.1115/1.3156810.
95. Paul, F.; Pellegrini, S.; Uzé, G. IFNA2: The Prototypic Human Alpha Interferon. *Gene* **2015**, *567*, 132–137, doi:10.1016/j.gene.2015.04.087.

96. Berraondo, P.; Sanmamed, M.F.; Ochoa, M.C.; Etxeberria, I.; Aznar, M.A.; Pérez-Gracia, J.L.; Rodríguez-Ruiz, M.E.; Ponz-Sarvise, M.; Castañón, E.; Melero, I. Cytokines in Clinical Cancer Immunotherapy. *Br J Cancer* **2019**, *120*, 6–15, doi:10.1038/s41416-018-0328-y.
97. Lin, F.; Young, H.A. Interferons: Success in Anti-Viral Immunotherapy. *Cytokine Growth Factor Rev* **2014**, *25*, 369–376, doi:10.1016/j.cytogfr.2014.07.015.
98. Antonelli, G.; Scagnolari, C.; Moschella, F.; Proietti, E. Twenty-Five Years of Type I Interferon-Based Treatment: A Critical Analysis of Its Therapeutic Use. *Cytokine Growth Factor Rev* **2015**, *26*, 121–131, doi:10.1016/j.cytogfr.2014.12.006.
99. Chkhis, A.; Abdulrazzaq, N.; Mokhtar, S.; al Jasmi, A. al Efficacy of High-Dose Nebulized Interferon α 2b in Severe COVID-19 Pneumonia. *Turk Thorac J* **2021**, *22*, 199–204, doi:10.5152/TurkThoracJ.2021.20255.
100. Yu, J.; Lu, X.; Tong, L.; Shi, X.; Ma, J.; Lv, F.; Wu, J.; Pan, Q.; Yang, J.; Cao, H.; et al. Interferon-α-2b Aerosol Inhalation Is Associated with Improved Clinical Outcomes in Patients with Coronavirus Disease-2019. *Br J Clin Pharmacol* **2021**, *87*, 4737–4746, doi:10.1111/bcp.14898.
101. Ramos, T.I.; Villacis-Aguirre, C.A.; Santiago Vispo, N.; Santiago Padilla, L.; Pedroso Santana, S.; Parra, N.C.; Alonso, J.R.T. Forms and Methods for Interferon's Encapsulation. *Pharmaceutics* **2021**, *13*, 1533, doi:10.3390/pharmaceutics13101533.
102. Fagundes, R.N.; Ferreira, L.E.V.V. de C.; Pace, F.H. de L. Health-Related Quality of Life and Fatigue in Patients with Chronic Hepatitis C with Therapy with Direct-Acting Antivirals Agents Interferon-Free. *PLoS One* **2020**, *15*, e0237005, doi:10.1371/journal.pone.0237005.
103. Ferreira, M.L.; Ferreira, A.S.D.; Araújo, J.M.M.; Cabrita, E.J.; Pereiro, A.B. The Impact of Fluorinated Ionic Liquids Aggregation in the Interactions with Proteins. *Fluid Phase Equilib* **2022**, *559*, doi:10.1016/j.fluid.2022.113488.
104. Louis-Jeune, C.; Andrade-Navarro, M.A.; Perez-Iratxeta, C. Prediction of Protein Secondary Structure from Circular Dichroism Using Theoretically Derived Spectra. *Proteins: Structure, Function, and Bioinformatics* **2012**, *80*, 374–381, doi:10.1002/prot.23188.
105. Vieira, N.S.M.; Ferreira, M.L.; Castro, P.J.; Araújo, J.M.M.; Pereiro, A.B. Fluorinated Ionic Liquids as Task-Specific Materials: An Overview of Current Research. *Ionic Liquids - Thermophysical Properties and Applications* **2021**, doi:10.5772/INTECHOPEN.96336.
106. Ferreira, M.L.; Vieira, N.S.M.; Castro, P.J.; Vega, L.F.; Araújo, J.M.M.; Pereiro, A.B. Understanding the Phase and Solvation Behavior of Fluorinated Ionic Liquids. *J Mol Liq* **2022**, *359*, 119285, doi:10.1016/j.molliq.2022.119285.
107. Phillips, J.N. The Energetics of Micelle Formation. *Transactions of the Faraday Society* **1955**, *51*, 561–569, doi:10.1039/TF9555100561.
108. Zana, R. Critical Micellization Concentration of Surfactants in Aqueous Solution and Free Energy of Micellization. *Langmuir* **1996**, *12*, 1208–1211, doi:10.1021/LA950691Q.
109. Doogue, M.P.; Polasek, T.M. The ABCD of Clinical Pharmacokinetics. *Ther Adv Drug Saf* **2013**, *4*, 5–7, doi:10.1177/2042098612469335.
110. Kharazi, M.; Saien, J.; Asadabadi, S. Review on Amphiphilic Ionic Liquids as New Surfactants: From Fundamentals to Applications. *Top Curr Chem* 2022, *380*.
111. Das, S.; Mondal, S.; Ghosh, S. Physicochemical Studies on the Micellization of Cationic, Anionic, and Nonionic Surfactants in Water–Polar Organic Solvent Mixtures. *J Chem Eng Data* **2013**, *58*, 2586–2595, doi:10.1021/je4004788.
112. Wadekar, M.N.; Boekhoven, J.; Jager, W.F.; Koper, G.J.M.; Picken, S.J. Micellization Behavior of Aromatic Moiety Bearing Hybrid Fluorocarbon Sulfonate Surfactants. *Langmuir* **2012**, *28*, 3397–3402, doi:10.1021/la2047799.

113. Jiao, J.; Dong, B.; Zhang, H.; Zhao, Y.; Wang, X.; Wang, R.; Yu, L. Aggregation Behaviors of Dodecyl Sulfate-Based Anionic Surface Active Ionic Liquids in Water. *J Phys Chem B* **2012**, *116*, 958–965, doi:10.1021/jp209276c.
114. Mahajan, S.; Sharma, R.; Mahajan, R.K. An Investigation of Drug Binding Ability of a Surface Active Ionic Liquid: Micellization, Electrochemical, and Spectroscopic Studies. *Langmuir* **2012**, *28*, 17238–17246, doi:10.1021/la303193n.
115. Israelachvili, J.N.; Mitchell, D.J.; Ninham, B.W. Theory of Self-Assembly of Hydrocarbon Amphiphiles into Micelles and Bilayers. *Journal of the Chemical Society, Faraday Transactions 2* **1976**, *72*, 1525, doi:10.1039/f29767201525.
116. Tanford, C. Micelle Shape and Size. *J Phys Chem* **1972**, *76*, 3020–3024, doi:10.1021/j100665a018.
117. Mudalige, T.; Qu, H.; van Haute, D.; Ansar, S.M.; Paredes, A.; Ingle, T. Characterization of Nanomaterials: Tools and Challenges. In *Nanomaterials for Food Applications*; Elsevier, 2019; pp. 313–353.
118. Lakowicz, J.R. *Principles of Fluorescence Spectroscopy*; Springer US: Boston, MA, 2006; ISBN 978-0-387-31278-1.
119. Nikolaiev, R.; Stepanenko, Y.; Chernykh, S.; Melnichuk, N.; Tkachuk, Z. Conformational, Fluorescence and Energy Parameters of Interferon A2b with Different Forms of Oligoribonucleotides and Adenosine Monophosphate. In Proceedings of the The 1st International Electronic Conference on Pharmaceutics; MDPI: Basel Switzerland, December 1 2020; p. 16.
120. Ware, W.R. Oxygen Quenching of Fluorescence in Solution: An Experimental Study of the Diffusion Process. *J Phys Chem* **1962**, *66*, 455–458, doi:10.1021/j100809a020.
121. Greenfield, N.J. Using Circular Dichroism Spectra to Estimate Protein Secondary Structure. *Nat Protoc* **2006**, *1*, 2876–2890, doi:10.1038/nprot.2006.202.
122. Salmannejad, F.; Nafissi-Varcheh, N. Ectoine and Hydroxyectoine Inhibit Thermal-Induced Aggregation and Increase Thermostability of Recombinant Human Interferon Alfa2b. *European Journal of Pharmaceutical Sciences* **2017**, *97*, 200–207, doi:10.1016/j.ejps.2016.11.014.
123. Jerabek-Willemsen, M.; André, T.; Wanner, R.; Roth, H.M.; Duhr, S.; Baaske, P.; Breitsprecher, D. MicroScale Thermophoresis: Interaction Analysis and Beyond. *J Mol Struct* **2014**, *1077*, 101–113, doi:10.1016/j.molstruc.2014.03.009.
124. Wienken, C.J.; Baaske, P.; Rothbauer, U.; Braun, D.; Duhr, S. Protein-Binding Assays in Biological Liquids Using Microscale Thermophoresis. *Nat Commun* **2010**, *1*, 100, doi:10.1038/ncomms1093.
125. Carvalho, S.F.; Custódio, M.H.; Pereiro, A.B.; Araújo, J.M.M. Towards Enhanced Tunability of Aqueous Biphasic Systems: Furthering the Grasp of Fluorinated Ionic Liquids in the Purification of Proteins. *Journal of Molecular Liquids, submitted* **2022**.
126. Zahradník, J.; Kolářová, L.; Pařízková, H.; Kolenko, P.; Schneider, B. Interferons Type II and Their Receptors R1 and R2 in Fish Species: Evolution, Structure, and Function. *Fish Shellfish Immunol* **2018**, *79*, 140–152, doi:10.1016/j.fsi.2018.05.008.
127. Corin, K.; Baaske, P.; Ravel, D.B.; Song, J.; Brown, E.; Wang, X.; Wienken, C.J.; Jerabek-Willemsen, M.; Duhr, S.; Luo, Y.; et al. Designer Lipid-Like Peptides: A Class of Detergents for Studying Functional Olfactory Receptors Using Commercial Cell-Free Systems. *PLoS One* **2011**, *6*, e25067, doi:10.1371/journal.pone.0025067.
128. Correia, V.G.; Trovão, F.; Pinheiro, B.A.; Brás, J.L.A.; Silva, L.M.; Nunes, C.; Coimbra, M.A.; Liu, Y.; Feizi, T.; Fontes, C.M.G.A.; et al. Mapping Molecular Recognition of B1,3-1,4-Glucans by a Surface Glycan-Binding Protein from the Human Gut Symbiont Bacteroides Ovatus. *Microbiol Spectr* **2021**, *9*, doi:10.1128/Spectrum.01826-21.

129. Lee, M.S.; Lee, K.; Nam, M.W.; Jeong, K.M.; Lee, J.E.; Kim, N.W.; Yin, Y.; Lim, S.Y.; Yoo, D.E.; Lee, J.; et al. Natural Deep Eutectic Solvents as a Storage Medium for Human Interferon-A2: A Green and Improved Strategy for Room-Temperature Biologics. *Journal of Industrial and Engineering Chemistry* **2018**, *65*, 343–348, doi:10.1016/j.jiec.2018.05.005.

CHAPTER 6

CONCLUDING REMARKS AND FUTURE PERSPECTIVES

6.1 General conclusion

The main goal of this dissertation was to study the interactions between FILs and proteins to design and develop efficient biomaterials for use in protein extraction processes and delivery systems. Several steps were executed to cover the main objective of this thesis and were divided into four distinct chapters.

A preliminary analysis of the best FILs characteristics was pursued, yielding that they have enhanced properties when compared to conventional ILs, mainly due to the formation of three nanosegregated domains, which allows enhanced solubilization mechanisms for different solutes. Their behaviour in aqueous solutions is of outstanding importance to biological applications, and they show enhanced surfactant behaviour when compared to conventional surfactants. Using imidazolium, pyridinium with short, hydrogenated chains and cholinium cations, conjugated with anions based on perfluorinated chains of four carbons, it is possible to design: (i) FILs with amphiphilic nature, acting as SAILs in water and self-assembling in stable supramolecular structures; (ii) compounds with complete water miscibility, having different solubilization behaviours depending on the concentration range; and (iii) FILs with negligible cytotoxicity in different cell lines and ecotoxicity in aquatic plants, crustacean and bacteria organisms. All these characteristics make them promising biomaterials to be used in formulations for stabilization, extraction, and/or delivery of proteins.

However, the development of feasible systems for the actual application of FILs is generally hindered by the number of possible combinations of ions composing their structure and granting them unique properties, which makes their characterization a very time and cost task-consuming. In this work, it was developed a methodology that guides the modelling of FILs using the soft-SAFT EoS more systematically and robustly. The careful analysis of the structural features of the FILs and the physical meaning of the soft-SAFT parameters allow the understanding of how these parameters can be transferred from a FIL model to another, obtaining very good approximation with experimental data, without having to use it for parameters fitting. Therefore, several FILs were newly modelled within the soft-SAFT framework, showing very high predictive capabilities and excellent agreement with the experimental data available in the literature. These results have high importance in hastening the selection of task-specific feasible systems for a chosen application. The selection of the experimental data used in this work to validate the soft-SAFT models had taken into account (i) the availability of data in the literature, and (ii) the inclusion of a wide variety of FILs structural features to ensure the robustness of the model to characterise different families of

FILs. This approach will have a highly importance in a wide number of applications of FILs and is not limited to the use of this compounds to biological applications.

The formulation of compounds with improved properties was also included in this thesis. Then, the study of functionalized FILs with a hydroxyl group in the hydrogenated chain was carried out with different experimental techniques and the soft-SAFT EoS approach. The results have shown the high efficiency of soft-SAFT to predict the properties of the FILs in the pure state and the complex systems of FIL+water, reinforcing the importance of using modelling tools to ease the work of researchers and allowing to counteract the lack of experimental data. Moreover, the experimental investigation of the self-aggregation behaviour of the functionalized FILs in water has yielded higher CAC values when compared to the equivalent non-functionalized FILs, indicating a slight disruption in the formation, and packing of the FIL aggregates by the hydroxyl group. Nevertheless, the comparison with the values of CMC of conventional surfactants has shown that the functionalized FILs have an exceptionally superior aggregation behaviour, which leads to the conclusion that is possible to design non-toxic and more biodegradable FILs for use in the protein field.

Finally, the FILs showing the best properties for biological usage were selected and used in the study of solubility, stability, activity, and interactions with different proteins. First, the investigation of the FILs aggregation behaviour using NMR techniques allowed to have new information on the size of the aggregates and their performance, depending on the FIL concentration in aqueous solutions. Moreover, the examination of the interactions, between several FILs and GB1, BSLA and IFN-α 2b proteins, has yielded evidence that the cholinium based-FILs have a higher degree of interactions with the proteins. Moreover, several non-toxic FILs have shown to be able to encapsulate a model protein, the lysozyme, allowing its stabilization inside the aggregates of the FIL, promoting the thermal stability and activity of the protein. This has proved that the FILs can be used in the formulation of materials for entrapping the protein and be used for extraction processes and/or protein delivery systems. Finally, it was selected a therapeutic protein, IFN-α 2b, with high relevance in the treatment of several diseases such as cancer, viral infections, and auto-immune diseases. The assessment of the effect on the FIL aggregates under the presence of the IFN-α 2b has shown that the FIL aggregates strongly interact with the protein, altering their packing, size and morphology and preventing the protein to form aggregates. Additionally, the deeper study of the interactions between FILs-IFN-α 2b leads to the idea that the FIL aggregates are not able to cover the surface of the IFN-α 2b, as occurred in the case of lysozyme. Nonetheless, they form a complex IFN-α 2b that can be used for the extraction and/or delivery of this protein.

In summary, this work has allowed to undercover new information on the interactions between FILs and proteins, which will allow the development of feasible and productive

systems for the protein research by taking advantage of the tuneable properties of FILs, either in the extraction and separation processes of proteins and/or protein delivery systems.

6.2 Future work

The findings obtained in this work have opened new avenues for the development of efficient FIL-based systems for the protein field. However, several steps should be considered until rich the actual applicability of these compounds.

First, the improvement of the modelling tools like soft-SAFT EoS will allow the capture of the behaviour of this complex compounds in aqueous solutions. Therefore, by selecting specific units of proteins, such as amino acids and/or small peptides that have high relevance in their interactions and biological activity will allow the capture of the complex aggregation behaviour of FILs + proteins systems by these models. This will be highly advantageous to accelerate the selection of the best ions combinations of FIL-based biomaterials to obtain task-specific self-assembled structures in aqueous solutions.

Studies using NMR spectroscopy, X-ray methods, molecular dynamic simulations and/or molecular docking may also be highly useful in order to understand the specific sites of the FIL aggregates and the protein residues that are contributing to the interaction, binding and/or encapsulation of the protein, which could be advantageous for the formulation of the FIL-based biomaterials.

In the case of extraction and separation processes, must be pursue studies concerning the use of these systems in the specific potential platforms (*i.e.* aqueous two-phase systems) to have insights into the extraction and separation efficiencies of the FILs. Moreover, the parameters that have high influence in the efficiency of FILs, such as pH, temperature, pressure, concentration, and proportion of the substances used in the technologies must be studied in future work.

Regarding the protein delivery systems, a feasible formulation must be developed and the pharmacokinetic and pharmacodynamic assessment must be undertaken, taking into consideration the bioavailability, route of administration and immunogenicity of the FIL-protein system. Moreover, the evaluation of the efficiency of these systems to do a site-specific and controlled release will be needed to be undertaken, depending on the therapeutic protein used and oriented for a specific disease.

2022 MARGARIDA LOURENÇO FERREIRA

NOVA SCHOOL OF SCIENCE & TECHNOLOGY

2022

MARGARIDA LOURENÇO FERREIRA

EXPLOITING THE POTENTIAL OF SURFACE ACTIVE IONIC LIQUIDS: FLUORINATED IONIC LIQUIDS MEET BIOMOLECULES